A WIND TUNNEL INVESTIGATION OF JETS EXHAUSTING INTO A CROSSFLOW

Volume I

Test Description and Data Analysis

L. B. FRICKE
P. T. WOOLER
H. ZIEGLER

FOREWORD

This report presents the results of one of the efforts expended in performance of Contract F33615-69-C-1602, "V/STOL Aircraft Aerodynamic Prediction Methods Investigation", Project No. 698BT. The work was performed by the Northrop Corporation, Aircraft Division. Sponsored by the Air Force Flight Dynamics Laboratory, Air Force Systems Command, the overall program started in May 1969 and is scheduled to be completed in December 1971. Dr. Peter T. Wooler is the Principal Investigator for the Northrop Corporation. Mr. Robert Nicholson is the Project Engineer for the Air Force.

This report, consisting of four volumes, contains the data generated during low speed wind tunnel testing of a four-foot diameter circular plate model with up to three jets exhausting into a crossflow. The test model, instrumentation, test procedure, and reduction and accuracy of the test data are discussed in this volume. A summary and discussion of the test results are also presented herein. Volumes II, III, and IV contain additional data pertaining to the one-, two-, and three-jet configurations, respectively.

In view of the unusual length of this report (a total of more than 1600 pages), Volumes II, III, and IV are not being as widely distributed as the present volume. Organizations desiring copies of those volumes may obtain them from CFSTI and DDC in addition to AFFDL/FGC, Wright-Patterson AFB, Ohio 45433.

This technical report has been reviewed and is approved.

C. B. WESTBROOK
Chief, Control Criteria Branch
Flight Control Division
Air Force Flight Dynamics Laboratory

ABSTRACT

A low speed wind tunnel test of a four-foot diameter circular plate model with up to three exhausting jets was conducted to determine surface static pressure distributions, jet paths, and jet decay characteristics in the presence of a crossflow. Data were obtained for the one-jet configuration with the jet exiting at a number of angles to the plate and at various velocity ratios and sideslip angles. Two-jet arrangements were tested with the jets exiting normal to the plate for three different spacings between the two jets and at a number of velocity ratios and sideslip angles. Three-jet configuration data were obtained with the jets exiting normal to the plate for a number of velocity ratios and sideslip angles. As a result of this investigation, several conclusions are deduced pertaining to the interaction of multiple jets exhausting into a crossflow.

This report consists of four volumes. The test model, instrumentation, test procedure, and reduction and accuracy of the test data are discussed in this volume. A summary and discussion of the test results are also presented herein. Volumes II, III, and IV contain additional data pertaining to the one-, two-, and three-jet configurations, respectively.

TABLE OF CONTENTS

LIST OF ILLUSTRATIONS

LIST OF ILLUSTRATIONS (Continued)

LIST OF ILLUSTRATIONS (Continued)

LIST OF TABLES

LIST OF SYMBOLS

BETA or β	Angle of Sideslip, Degrees,(See Figure 1)
C_p	Pressure Coefficient, $C_p = (p-p_\infty)/q$
C_{p_t}	Total Pressure Coefficient, $C_{p_t} = \frac{(p_t - p_{t_\infty})}{(p_{t_o} - p_{t_\infty})}$
DELTA J or δ_j	Jet Deflection Angle, Degrees, (See Figure 2)
M	Mach Number
p	Surface Static Pressure, PSF
p_∞	Freestream Static Pressure, PSF
p_a	Atmospheric Pressure, PSF
p_t	Total Pressure, PSF
p_{t_∞}	Freestream Total Pressure, PSF
p_{t_o}	Jet Exit Total Pressure, PSF
Q or q	Freestream Dynamic Pressure, $Q = 1/2\rho U^2$, PSF
QJ or Q_j	Jet Dynamic Pressure, $Q_j = 1/2\rho_j U_{j_o}^2$, PSF
r/d_o	Ratio of Radial Distance to Jet Diameter
U	Freestream Velocity, FPS
U_{j_o}	Jet Exit Velocity, FPS
U/UJ or U/U_j	Effective Velocity Ratio, $U/U_j = \sqrt{Q/Q_j}$
x	Chordwise Coordinate, Inches, (See Figure 1)
y	Spanwise Coordinate, Inches, (See Figure 1)
ρ	Freestream Air Density, Slugs/ft.^{3}
ρ_j	Jet Exit Air Density, Slugs/ft.^{3}

SECTION I

INTRODUCTION

A fundamental problem in the development of methods for predicting the aerodynamic characteristics of lift jet, vectored thrust, and lift fan V/STOL aircraft is that of formulating a mathematical model to estimate the effects of the propulsion system efflux interaction with a crossflow. During the transition flight phase, this efflux is directed at large angles to the freestream flow and has a significant influence on the aircraft aerodynamics as well as the stability and control requirements. Consequently, a considerable amount of research activity, both experimental and analytical, has been devoted to the development of an understanding of this flow problem and also to the development of methods to enable the resulting interference flow fields to be calculated.

Wind tunnel tests of a single jet exhausting at right angles to a flat plate have shown that, in the presence of a crossflow, the jet momentum flow decays at a much greater rate than for the case of the jet exhausting into a static environment (References 1 and 2). Further tests have shown that, for jets exhausting normally to a plate, there are extensive regions of negative pressures on the surface of the plate surrounding the jet (References 3, 4, 5, and 6).

Jet centerline information (usually defined as the position of the maximum total head in the jet) has been obtained for jets exiting at various angles into a crossflow (References 7, 8, and 9) although there does not appear to be data available concerning the surface static pressure distribution for a jet exiting at an angle other than 90° to the surface.

The objectives of the test described in this report were:

1. To generate surface static pressure distribution data for one-jet configurations exiting into a crossflow at large angles to the flow and for various velocity ratios.

2. To generate surface static pressure distribution data for two-jet configurations for a number of jet spacings, velocity ratios, and sideslip angles with the jets exhausting at right angles to the surface.

3. To determine the jet path and jet decay characteristics for one- and two-jet configurations.

4. To obtain surface static pressure distribution data for a three-jet configuration for a number of velocity ratios and sideslip angles.

To achieve these objectives, a low speed wind tunnel test of a four-foot diameter circular plate containing up to three exhausting jets was conducted. The plate contained pressure taps to enable the surface static

pressure distribution to be determined. Jet centerline information and decay characteristics were determined using a total head rake. Further centerline information was obtained using visualization techniques.

This report, consisting of four volumes, contains the data generated during this experimental investigation. The test model, instrumentation, test procedure, and reduction and accuracy of the test data are discussed in this volume. A summary and discussion of the test results are also presented herein. Additional data for the one-, two-, and three-jet configurations are presented in Volumes II, III, and IV, respectively.

SECTION II

TEST FACILITY AND MODEL

The test was conducted in the Northrop 7 x 10 foot low speed wind tunnel. This is a single return, closed throat wind tunnel with an operating static pressure of nominally atmospheric pressure and a mean temperature of nominally 80°F. The jets were powered by the Northrop Auxiliary Air Supply Compressor Sytem.

The model was a four-foot diameter flat plate with a circular planform. It contained up to three one-inch exit diameter nozzles fitted flush with the plate (Figures 1 and 2). The flow through each nozzle could be adjusted separately. The capability of having nozzle deflections in the range $-30° \leq \delta_j \leq +30°$ was included in the model although in this test only Jet 2 (see Figure 2 for numbering system), when operating alone, made use of this capability by using nozzle angles of $\delta_j = -30°$, $-15°$, $0°$, $+15°$, and $+30°$. For multiple jet tests, with various combinations of Jets 1, 2, and 3, δ_j was 0° for all jets. The three nozzles were placed so as to allow two-jet configurations to be tested for spacings between the jets of 2.5, 5.0, and 7.5 inches. When a jet was not operating, its nozzle was replaced by a cover plate. The model with the three 0° nozzles installed is shown in Figure 3. The $\pm 30°$ and $\pm 15°$ nozzles and the cover plates are also shown in Figure 3. The routing of the static pressure tap tubing is shown in Figure 4 and a view of the model installed in the tunnel is shown in Figure 5.

The model was mounted to the tunnel turntable by four 12-inch long standoffs to insure that the plate was outside the tunnel floor boundary layer and also to facilitate nozzle changes. The model could be rotated through sideslip angles of $\pm 90°$ with respect to the mainstream direction.

Flow visualization of the jets was accomplished by injecting water just downstream of the jet air supply manifold. This gave approximately 20 feet of hose from the point of water injection to the point of jet exhaust and insured good mixing of water and air for flow visualization purposes.

SECTION III

INSTRUMENTATION

Jet centerlines and jet decay characteristics were determined by means of a cruciform rake to measure total pressures. This rake, which is illustrated in Figures 6 and 7, could traverse vertically to a height of 20 inches above the plate. The required variation in rake pitch angle of 0° to 90° was obtained by using a serrated disc with a 5° spacing. The rake consisted of an array of 41 total head tubes spanning four inches in each direction. Depending on their magnitude, the pressures were film recorded on either a mercury or water manometer board.

Static pressure taps were located on half of the model surface as shown in Figure 1. Four pressure taps each were located in the Jet 1 cover plate, Jet 1 nozzle, and the Jet 2 0° nozzle. Three pressure taps each were located in the Jet 2 $\pm$15° and $\pm$30° nozzles. The static pressure tap locations, using the coordinate system defined in Figure 1, are shown in Table I. The pressures were film recorded on a vertical alcohol manometer board.

Static pressure taps in each of the jet plenums were employed to monitor the airflow in the jets. These pressures were displayed on a mercury manometer board.

SECTION IV

TEST PROCEDURE

MODEL CHECKOUT

After installation in the tunnel, the static pressure distribution on the model was checked at different tunnel dynamic pressures with the cover plates covering the nozzle exits. A small uniform negative pressure distribution was found to exist over the plate. Due to the sideslip angle requirements in the testing, no attempt was made to eliminate this negative pressure distribution by setting the plate at a negative angle of attack.

JET PROPERTIES

With the jets exhausting into quiescent conditions, the cruciform rake was used to calibrate the static pressure tap in the plenum of each of the three nozzles. This calibration was accomplished for various jet exit Mach Numbers although only two Mach Numbers were utilized during the test. The decay of the jet exhausting into quiescent conditions was measured at six heights above the jet exit plane.

Jet decay and points of maximum total pressure within the jet stream were determined for a number of configurations exhausting into a crossflow. The rake was positioned at a pre-determined location on the plate (based on theoretical predictions) and secured. After the desired operating conditions for both the tunnel and the jet nozzles were obtained, a film recording of the rake pressures, displayed on a mercury or water manometer board, was made.

SURFACE PRESSURES

The jet dynamic pressure and the angle of sideslip of the model could be varied with the wind tunnel in operation. A model change, involving shutdown of the tunnel, was required when different jet configurations were used. For each jet configuration tested, the required jet dynamic pressure was first set using the jet plenum static pressure reading. The tunnel was then turned on to give the desired tunnel dynamic pressure. Surface static pressure distributions were then recorded for a range of sideslip angles, both positive and negative since the model had pressure taps on only one side. The tunnel dynamic pressure was then changed to give a new value for the effective velocity ratio and pressure data were again taken for various sideslip angles. The jets were normally operated with a sonic exit velocity. However, two runs were made with the one-jet configuration operating at a reduced dynamic pressure to verify that the use of the parameter "effective velocity ratio" accounts for both mainstream and jet dynamic pressures. A further four runs were made with Jets 1 and 2 and Jets 1 and 3 using differential thrust levels in the two jets.

FLOW VISUALIZATION

Visualization of the jet flow in the presence of a crossflow was achieved by first adjusting the jet and tunnel dynamic pressures to give the desired test condition. Water was then injected into the jet as required. The amount of water injected was adjusted so as to make the jet visible without substantially influencing the flow characteristics due to the higher relative density of the water.

SECTION V

DATA REDUCTION

JET PROPERTIES

Properties of the jet at the nozzle exit in the static case were reduced in terms of the pressure ratio p_t/p_a.

Data for the jet decay characteristics, both with and without a mainstream, were reduced using the total pressure coefficient function C_{p_t}, where

$$C_{p_t} = \frac{p_t - p_{t_\infty}}{p_{t_o} - p_{t_\infty}} .$$

SURFACE PRESSURES

Surface pressures on the plate were reduced to pressure coefficients, $C_p = \frac{p - p_\infty}{q}$, and plotted against x(Chord) at constant y(span). The pressures measured on the Jet 1 cover plate, at the Jet 1 and Jet 2 nozzles, and at some distant positions from the jet exits, were not plotted. The data for the spanwise stations close to the jets were not faired due to large variations in the pressures for these stations.

SECTION VI

DATA ACCURACY

Manometers were used for determining the tunnel dynamic pressures, jet decay characteristics, and the surface static pressure coefficients as well as for calibrating the jets. Consequently, the accuracy of the data depends primarily on the accuracy of the manometer readings.

The tunnel dynamic pressure, corrected for model blockage, could be measured to within $\pm$0.15 PSF. This represents an error range of 2.0 to 0.2 percent for the wind tunnel dynamic pressure range of 15 PSF to 133 PSF. The jet dynamic pressure, which was nominally 1485 PSF for the majority of the runs, could be measured to within 20 PSF which represents an error or $\pm$1.35 percent. The consequent error which may be expected in the velocity ratio is 2.0 percent at most. Data presented in this report show that errors of this magnitude will not significantly influence jet decay rates, jet centerlines, or surface pressure distributions.

In the determination of the jet properties, using the cruciform rake, a number of possible sources of error exist. The blockage effect due to the presence of the rake in the flow is unknown. However, the close agreement of the centerline and jet decay data with the data of References 1 and 2, where more sophisticated instrumentation was used, suggests that this blockage effect is small. The total head probes comprising the rake were spaced 0.2 inches apart. Thus, a maximum error of 0.2 inches in the position of the jet centerline is indicated although, due to the large number of probes, the actual error is expected to be much less. Changes of flow direction in the vicinity of the jets also could cause some errors in the probe readings near the edge of the jet.

Errors may be expected in the surface pressure coefficient data due to manometer reading errors. The height of fluid in the manometer could be read from film to within 0.05 inch. This indicates errors in pressure coefficients of $\pm$0.015 to $\pm$0.002 for tunnel dynamic pressures ranging from 15 PSF to 133 PSF, respectively. The data in Figures 12 and 13 support these observations.

SECTION VII

RESULTS AND DISCUSSION

The jet configurations and range of parameters for which surface static pressure data were obtained in this investigation are shown in Table II. The configurations and parameters tested for the jet centerline and flow visualization studies are shown in Tables III and IV, respectively.

JET PROPERTIES

The static jet total pressure profiles at the nozzle exit are shown in Figure 8 for a range of exit Mach Numbers. These profiles were obtained using the cruciform rake and hence there are two data points for each value of r/d_o other than zero. The jet decay in the static case is shown in Figure 9. The jet decay for one- and two-jet configurations in a crossflow is shown in Figure 10. The data in Figure 10 were obtained with the jets operating at sonic exit conditions and with the tunnel dynamic pressure adjusted so as to give an effective velocity ratio of 0.125. In the two-jet configurations, the nozzle exits are aligned with respect to the mainstream when $\beta = 0°$.

For the one-jet configuration, the jet exhausting into the crossflow decays more rapidly than the jet exhausting into quiescent conditions. This indicates that a crossflow significantly increases the entrainment by a jet. The jet centerline is in good agreement with data from Reference 2 which resulted from a test with very much lower tunnel and jet dynamic pressures.

For the two-jet configurations, the jet decay for the leading jet appears to be independent of the spacing between the jets. This is indicated by the C_{p_t} = 0.5 and 0.3 contours for the 2.5 and 5.0 diameter spacings and also by the C_{p_t} = 0.05 contour for the 5.0 and 7.5 diameter spacings. The decay of the leading jet is also very similar to the decay for a single jet as may be seen by comparing the C_{p_t} = 0.10 contour for a spacing of 2.5 diameters with the same contour for the one-jet configuration. The centerlines of the leading jets of two-jet configurations are also seen, in Figure 10, to be almost identical to each other and to the centerline for the single jet. Analysis of these data lead to the conclusion that the leading jet in a two-jet configuration behaves independently of the jet spacing.

The decay of the downstream jet in a two-jet configuration is influenced by the presence of the upstream jet with the degree to which it is influenced being a function of the jet spacing. It is observed in Figure 10 that in all cases the downstream jet decays less rapidly than the upstream jet and that this difference in decay rates decreases as the jet spacing increases. This is indicated by the C_{p_t} = 0.3 and 0.5 contours for the 2.5 and 5.0 diameter spacings and by the C_{p_t} = 0.1 and 0.2 contours for the 5.0 and 7.5 diameter spacings.

SURFACE PRESSURES

The model surface static pressure distributions without any of the jets operating and with the cover plates in place are shown in Figure 11. The scatter in the data for the lower tunnel speeds can be attributed to measuring inaccuracies. For the higher speeds the static pressure coefficients are effectively constant with a value of $C_p = -0.04$.

Data were obtained for one-, two-, and three-jet configurations for various test conditions. For the one-jet configuration, data were obtained for the jet deflection angles, δ_j, of 0°, $\pm$15°, and $\pm$30°. The effective velocity ratio was varied between 0.10 and 0.30. For the deflection angles of $\delta_j = 0°$ and -30° data were also obtained employing a lower jet dynamic pressure with the tunnel dynamic pressure also decreased in order to obtain the same effective velocity ratios. In all cases except $\delta_j = 0°$, data were also obtained for a number of sideslip angles.

The effect of changing the jet and tunnel dynamic pressures while keeping the effective velocity ratio the same is shown in Figures 12 and 13. For the lower velocity ratios, although the two sets of data are qualitatively the same, there are some differences between the data due to the less accurate pressure measurements at the low tunnel dynamic pressures. For the higher velocity ratios, changing the jet and tunnel dynamic pressures is seen to have negligible influence on the surface static pressure coefficients. Further evidence to support this observation may be found in Volume II for the case of the one-jet configuration exhausting at $\delta_j = -30°$ into the crossflow.

The effect of changes in the jet deflection angle on the surface static pressure distribution is shown in Figures 14 and 15. These data are for jets exhausting at $\delta_j = \pm 30°$ for a velocity ratio of 0.125 and for various sideslip angles. At $\beta = 0°$, changing δ_j from +30° to -30° results in surface pressures which are predominately increased in magnitude with an upstream shift of the peak values. These results are consistent with the analytical results of Reference 10. Further data for other deflection angles and velocity ratios may be found in Volume II.

Data for the three two-jet configurations at a velocity ratio of 0.125 are presented in Figures 16, 17, and 18. These data illustrate the influence of jet spacing on the pressure distribution for this velocity ratio. For $\beta = 0°$ the magnitude of the peak pressures does not vary significantly. However, the spanwise influence of the downstream jet is much more pronounced for the larger jet spacings. In all cases, as β is increased from 0°, the influence of the downstream jet on the surface static pressure distributions is increased.

Data for velocity ratios of 0.125, 0.20, and 0.30 with Jets 2 and 3 operating are presented in Figures 17, 19, and 20, respectively. In general, an increase in the velocity ratio results in a decrease in the magnitude of the surface pressure coefficients. However, the spanwise pressure coefficients induced by the downstream jet are increased in magnitude as the velocity ratio is increased.

Data for two-jet arrangements with a jet dynamic pressure differential are presented in Figures 21 through 24. In Figures 21 and 22 the jets were spaced 2.5 diameters apart while in Figures 23 and 24 the spacing was 7.5 diameters. For both spacings the peak surface pressure was greatest when the upstream jet was at the higher velocity ratio. Reversing the jet dynamic pressure differential did not appear to significantly influence the spanwise static pressure distribution.

Additional data for the two-jet configurations at other velocity ratios are presented in Volume III.

The surface static pressure distributions for the three-jet configuration with all the jets operating at a velocity ratio of 0.125 are presented in Figure 25. For $\beta = 0°$, as might be expected from the two-jet data, the spanwise pressure distribution appears to be most influenced by the jet furthest downstream. Sideslip increases the influence of the downstream jets as in the two-jet cases. Additional data for the three-jet configuration may be found in Volume IV.

FLOW VISUALIZATION

Photographs of vertical and horizontal scales, with one-inch divisions, were used for the calibration of the flow visualization photographs which are shown in Figure 26.

Jet paths for a single jet at velocity ratios of 0.10 and 0.15 are shown in Figure 27. The jet paths for Jets 1 and 2 when operating at a velocity ratio of 0.125 are shown in Figure 28. With both jets operating, water was injected into Jet 1 (Figure 28(a)), then into both jets 1 and 2 (Figure 28(b)), and then only into Jet 2 (Figure 28(c)). Comparison of Figure 28(a) with the single jet paths of Figure 10 and Figure 30(a) shows that there is greater penetration into the cross flow following intersection with the downstream jet. Comparing Figures 28(a) and 28(b) further suggests that the downstream jet penetrates through the leading jet.

Figure 29 shows the jet paths at a velocity ratio of 0.20 for the same jet configuration shown in Figure 28. The penetration of the upstream jet by the downstream jet is again demonstrated in Figure 29(b).

The jet paths for two-jet configurations spaced 7.5 diameters apart and at a velocity ratios of 0.125, 0.20, and 0.30 are shown in Figures 30, 31, and 32, respectively. For this jet spacing, the downstream jet is

deflected into the stream direction to a greater extent than for the case shown in Figure 28(b). In both cases there is shielding by the leading jet and, consequently, greater penetration by the downstream jet than for the leading jet.

SECTION VIII

CONCLUSIONS

Based on the data presented in this report, it is concluded that:

1. A jet exhausting into a crossflow decays more rapidly than a jet exhausting into a static environment.

2. For a two-jet configuration, with the jet exits aligned in the mainstream direction, the downstream jet decays less rapidly than the upstream jet and this difference in decay rates decreases as the jet spacing increases.

3. The deflection in the stream direction and the decay of the leading jet in a two-jet configuration is independent of the spacing between the jets.

4. The effective velocity ratio is a valid parameter which unifies the jet and mainstream dynamic pressure variables.

5. For a single jet, the deflection of the jet into the cross flow direction results in increased negative pressures on the plate surface.

6. For two-jet configurations, at zero sideslip angle, the negative pressures on the plate increase with increased spacing between the jets. As the sideslip angle is increased from zero, the shielding of the downstream jet is reduced and there is then a greater spanwise influence of the downstream jet on the pressure distribution.

SECTION IX

REFERENCES

1. Jordinson, R., Flow in a Jet Directed Normal to the Wind, British Aeronautical Research Council R&M 3074, 1958.

2. Keffer, J. F., and W. D. Baines, "The Round Turbulent Jet in a Cross Wind," Journal of Fluid Mechanics, Vol. 15, 1963, pp. 481-496.

3. Vogler, R. D., Surface Pressure Distributions Induced on a Flat Plate by a Cold Air Jet Issuing Perpendicularly from the Plate and Normal to a Low-Speed Free-Stream Flow, NASA TN D-1629, 1963.

4. Gelb, G. H., and W. A. Martin, "An Experimental Investigation of the Flow Field About a Subsonic Jet Exhausting into a Quiescent and a Low Velocity Airstream," Canadian Aeronautics and Space Journal, Vol. 12, No. 8, October 1966, pp. 333-342.

5. Bradbury, L. J. S., and W. N. Wood, The Static Pressure Distribution Around a Circular Jet Exhausting Normally from a Plane Wall into an Airstream, RAE Technical Note AERO 2978, August 1968.

6. Wu, J. C., H. M. McMahon, D. K. Mosher, and M. A. Wright, "Experimental and Analytical Investigations of Jets Exhausting into a Deflecting Stream," Journal of Aircraft, Vol. 7, No. 1, January-February 1970.

7. Margarson, R. J., The Path of a Jet Directed at Large Angles to a Subsonic Free Stream, NASA TN D-4919, 1968.

8. Shandorov, G. S., "Calculation of the Axis of a Jet in a Cross Flow," Soviet Aeronautics, Vol. 9, No. 2, 1969, pp. 60-62.

9. Platten, J. L., and J. F. Keffer, Entrainment in Deflected Axisymmetric Jets at Various Angles to the Stream, University of Toronto, Mech. Eng. TP-6808, June 1968.

10. Ziegler, H., and P. T. Wooler, An Analytical Model for the Flow of Multiple Jets into an Arbitrarily Directed Crossflow in Ground Effect, AIAA Paper No. 70-545, May 1970.

TABLE I. STATIC PRESSURE TAP LOCATIONS

TUBE NUMBER	-X	+X	Y
1	17.50	-	0
2	13.50	-	0
3	11.50	-	0
4	9.50	-	0
5	8.50	-	0
6	7.50	-	0
7	6.50	-	0
8	5.50	-	0
9	5.00	-	0
10	2.56	-	0
11	2.45	-	0
12	-	0	0
13	-	0.50	0
14	-	1.00	0
15	-	1.50	0
16	-	2.00	0
17	-	2.50	0
18	-	5.00	0
19	-	5.50	0
20	-	6.50	0
21	-	7.50	0
22	-	8.50	0
23	-	9.50	0
24	-	11.50	0
25	-	13.50	0
26	-	17.50	0
27	5.50	-	0.5
28	5.00	-	0.5
29	2.50	-	0.5
30	-	0	0.5
31	-	0.50	0.5
32	-	1.00	0.5
33	-	1.50	0.5
34	-	2.00	0.5
35	-	2.50	0.5
36	-	5.00	0.5
37	-	5.50	0.5
38	9.50	-	1.00
39	8.50	-	1.00
40	7.50	-	1.00
41	6.50	-	1.00
42	5.50	-	1.00
43	5.00	-	1.00
44	4.50	-	1.00
45	3.00	-	1.00
46	2.50	-	1.00
47	2.00	-	1.00
48	0.50	-	1.00
49	-	0	1.00
50	-	0.50	1.00
51	-	1.00	1.00
52	-	1.50	1.00
53	-	2.00	1.00
54	-	2.50	1.00
55	-	3.00	1.00
56	-	4.50	1.00
57	-	5.00	1.00
58	-	5.50	1.00
59	-	6.50	1.00
60	-	7.50	1.00
61	-	8.50	1.00
62	-	9.50	1.00
63	5.50	-	1.50
64	5.00	-	1.50
65	4.50	-	1.50
66	4.00	-	1.50
67	3.50	-	1.50
68	3.00	-	1.50
69	2.50	-	1.50
70	2.00	-	1.50
71	1.50	-	1.50
72	1.00	-	1.50
73	0.50	-	1.50
74	-	0	1.50
75	-	0.50	1.50
76	-	1.00	1.50
77	-	1.50	1.50
78	-	2.00	1.50
79	-	2.50	1.50
80	-	3.00	1.50
81	-	3.50	1.50
82	-	4.00	1.50
83	-	4.50	1.50
84	-	5.00	1.50
85	-	5.50	1.50
86	9.50	-	2.00
87	8.50	-	2.00
88	7.50	-	2.00
89	6.50	-	2.00
90	5.50	-	2.00
91	4.50	-	2.00
92	3.50	-	2.00
93	2.50	-	2.00
94	1.50	-	2.00
95	0.50	-	2.00
96	-	0.50	2.00
97	-	1.50	2.00
98	-	2.50	2.00
99	-	3.50	2.00
100	-	4.50	2.00
101	-	5.50	2.00
102	-	6.50	2.00
103	-	7.50	2.00
104	-	8.50	2.00
105	-	9.50	2.00
106	8.50	-	3.00
107	6.50	-	3.00
108	4.50	-	3.00
109	3.50	-	3.00
110	2.50	-	3.00
111	1.50	-	3.00
112	0.50	-	3.00
113	-	0.50	3.00
114	-	1.50	3.00
115	-	2.50	3.00
116	-	3.50	3.00
117	-	4.50	3.00
118	-	6.50	3.00
119	-	8.50	3.00
120	11.50	-	4.00
121	8.50	-	4.00
122	6.50	-	4.00
123	4.50	-	4.00
124	3.50	-	4.00
125	2.50	-	4.00
126	1.50	-	4.00
127	0.50	-	4.00
128	-	0.50	4.00
129	-	1.50	4.00
130	-	2.50	4.00
131	-	3.50	4.00
132	-	4.50	4.00
133	-	6.50	4.00
134	-	8.50	4.00
135	-	11.50	4.00
136	7.00	-	6.00
137	5.00	-	6.00
138	3.00	-	6.00
139	1.00	-	6.00
140	-	1.00	6.00
141	-	3.00	6.00
142	-	5.00	6.00
143	-	7.00	6.00
144	17.50	-	8.00
145	7.50	-	8.00
146	2.50	-	7.80
147	-	2.50	7.80
148	-	7.50	8.00
149	-	17.50	8.00
150	17.00	-	14.00
151	6.00	-	14.00
152	-	6.00	14.00
153	-	17.00	14.00
154	6.00	-	20.00
155	-	6.00	20.00
156	4.45	-	0
157	3.04	-	0
158	1.91	-	0.26
159	0.61	-	0.26
160	4.24	-	0.50
161	3.25	-	0.50
162	1.58	-	0.64
163	1.00	-	0.64
156	4.41	-	0.26
157	3.11	-	0.26
160	4.03	-	0.64
161	3.50	-	0.64

TABLE II. TEST CONFIGURATIONS AND CONDITIONS FOR SURFACE PRESSURE MEASUREMENTS

Jet Nos.	Jet Δ	U/U_j	β
(2)	±30, ±15, 0	.10,.125,.15, .20,.25,.30	0,±10,±20,±30 ±40,±90
(2,3),(1,3), (1,2) (1, 2, 3)	0	.10,.125,.15, .20,.25,.30	0,±5,±10,±15, ±20,±30,±40, ±50,±70,±90
(1,3) (1,2)	0	(.215/.15), (.15/.215)	0,±10,±20,±30, ±40,±90

TABLE III. TEST CONFIGURATIONS AND CONDITIONS FOR JET CENTERLINE MEASUREMENTS

Jet Nos.	Jet Δ	U/U_j	β
(2),(1,2),(2,3) (1,3)	0	.125	0
(1,3)	0	.20	0

TABLE IV. TEST CONFIGURATIONS AND CONDITIONS FOR FLOW VISUALIZATION

Jet Nos.	Jet Δ	U/U_j	β
(1)	0	.1,.125,.15	0
(2,3)	0	.125,.20,.30	0,10,20,30
(1,3)	0	.125,.20,.30	0,10,20,30
(1,2)	0	.125,.20,.30	0,10,20,30

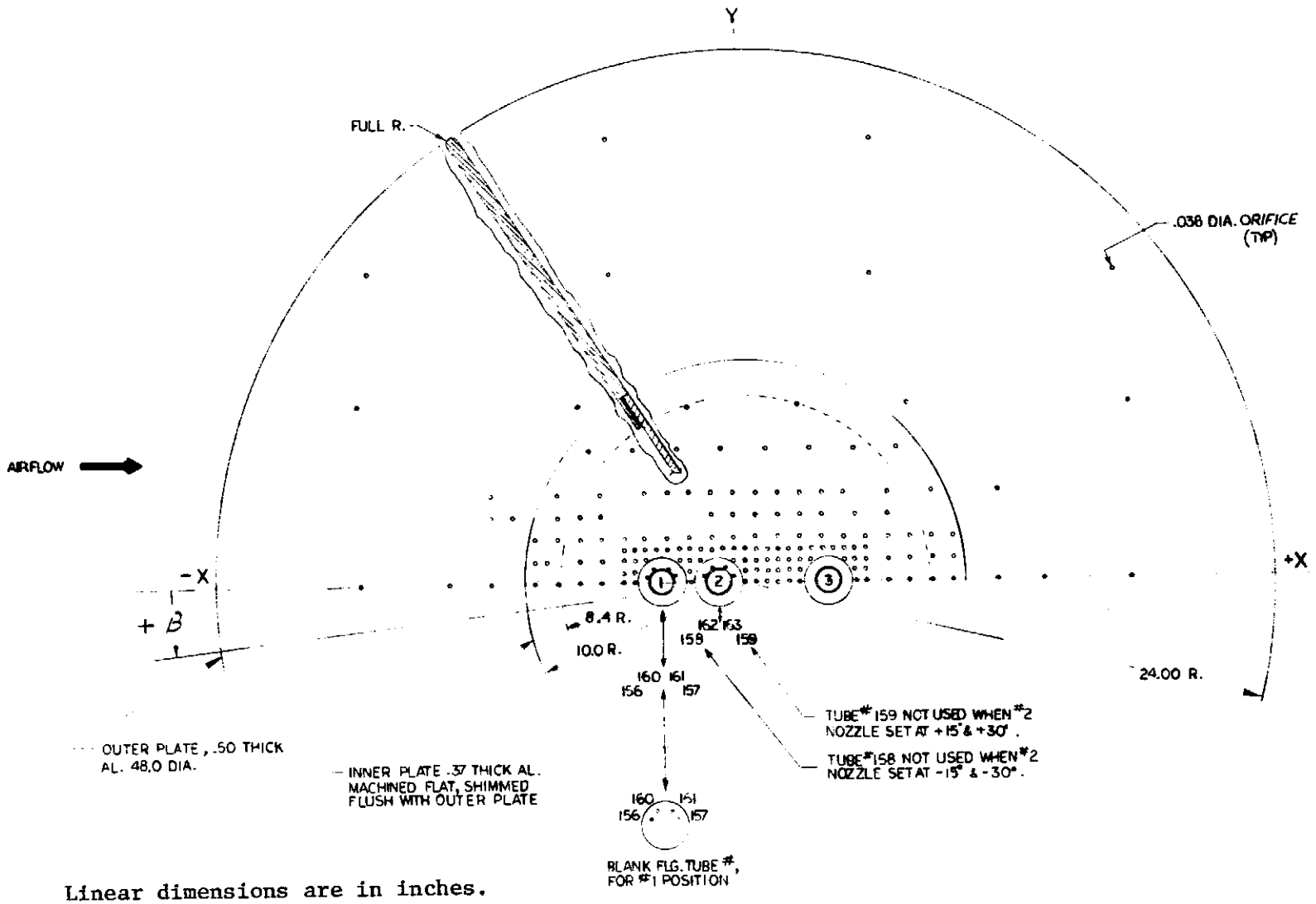

Linear dimensions are in inches.

FIGURE 1. FLAT PLATE MODEL DETAILS

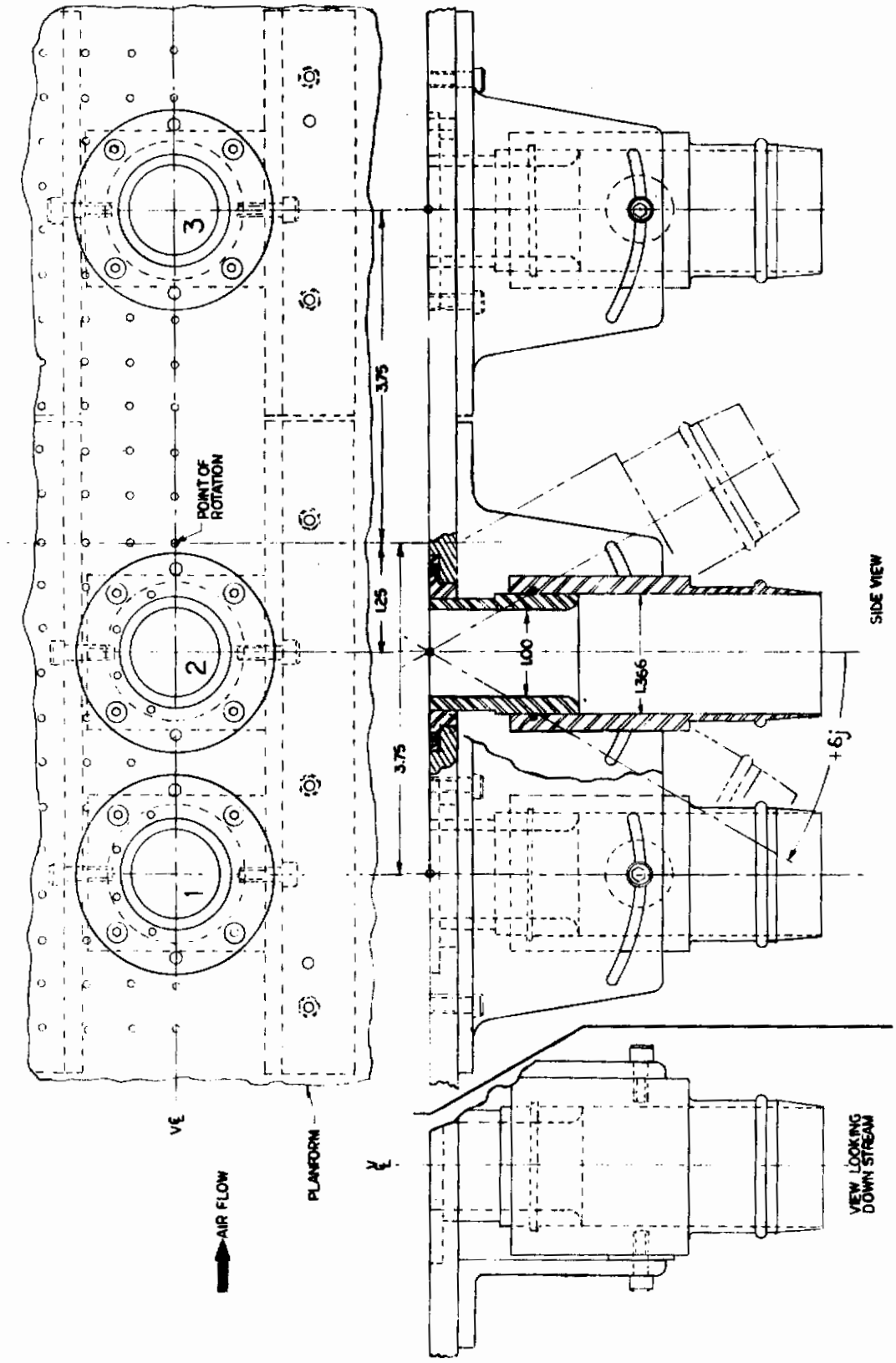

Linear dimensions are in inches.

FIGURE 2. NOZZLE ASSEMBLY DETAILS

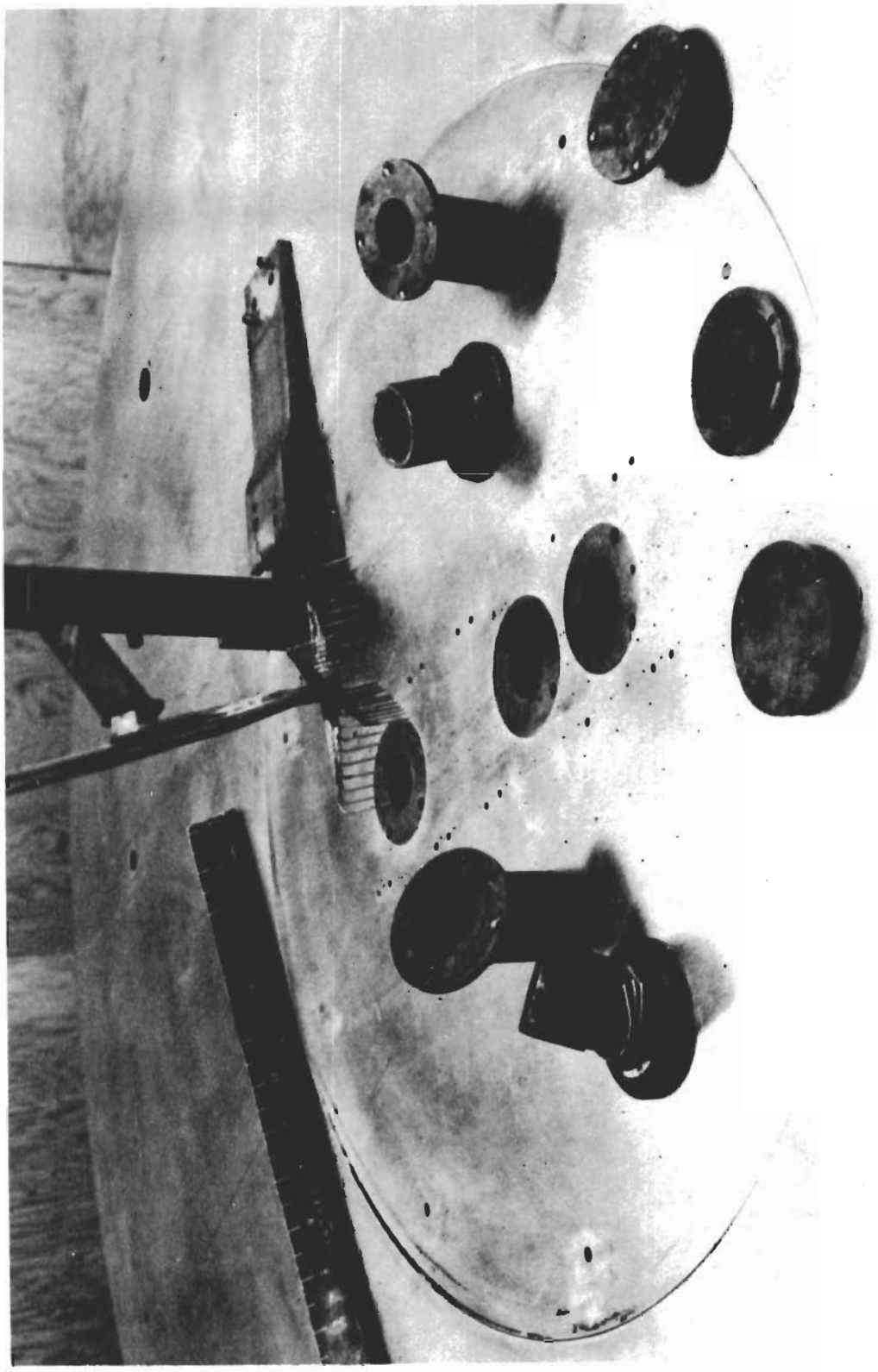

FIGURE 3. FLAT PLATE MODEL WITH NOZZLES, COVER PLATES AND CRUCIFORM RAKE

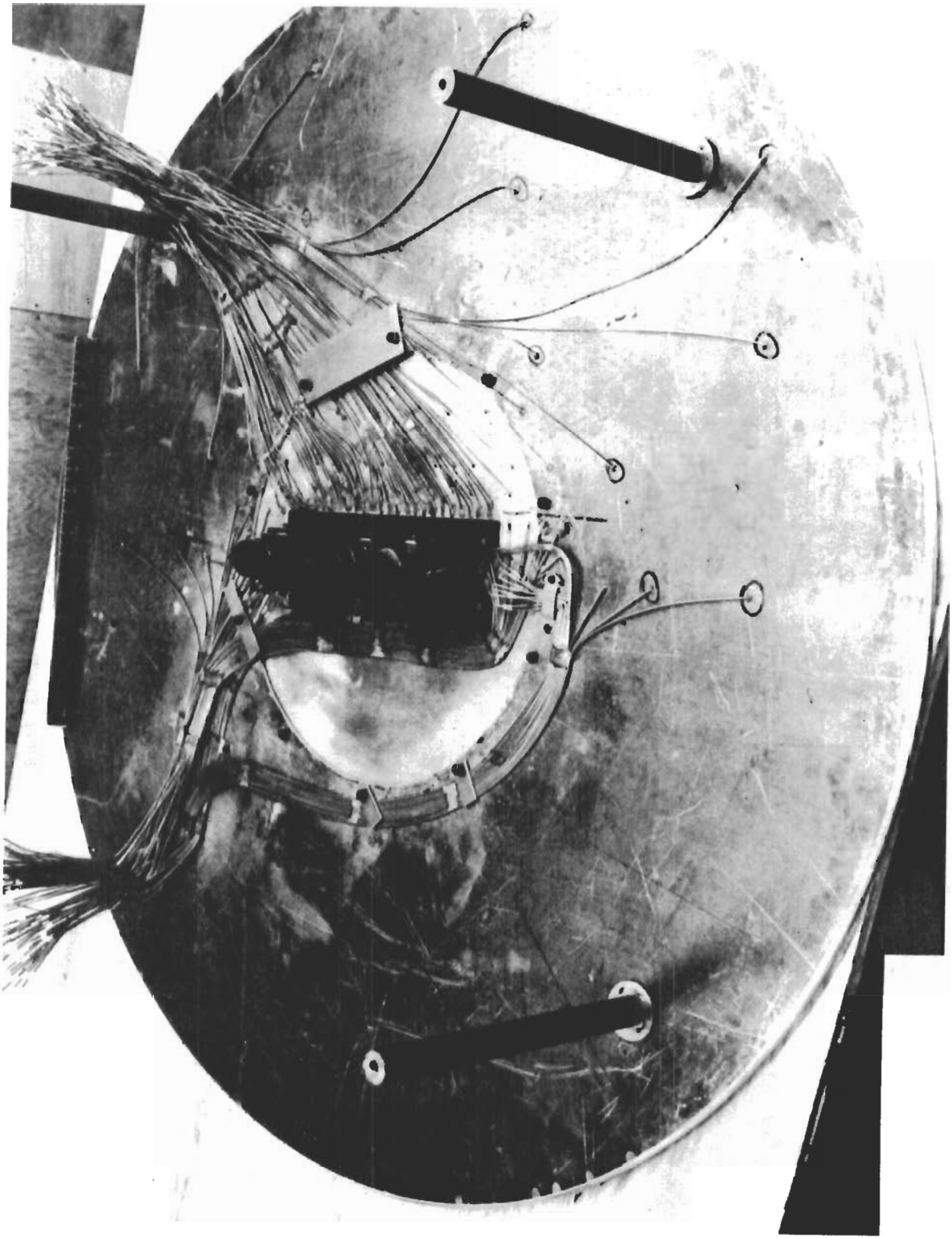

FIGURE 4. BOTTOM VIEW OF FLAT PLATE MODEL

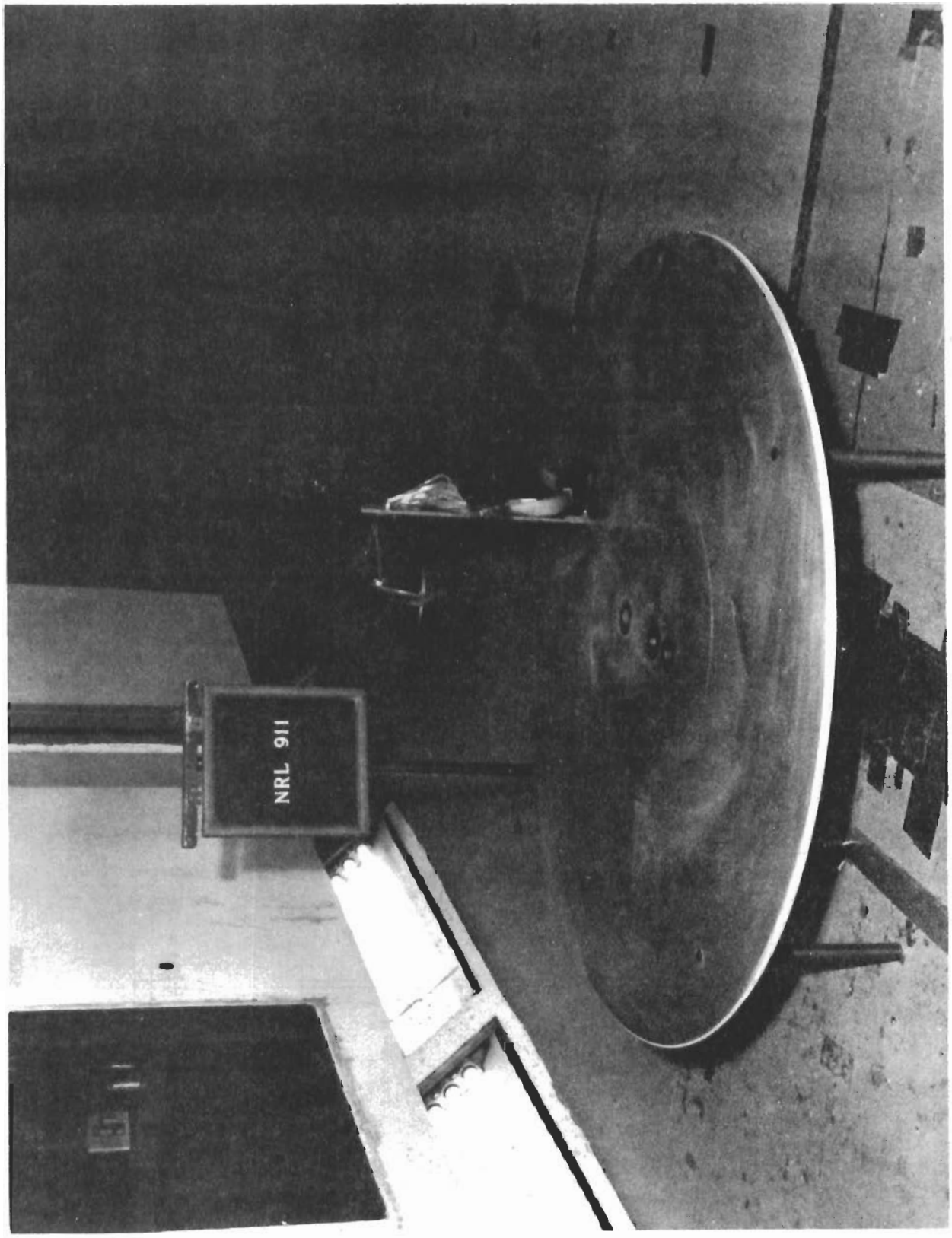

FIGURE 5. FLAT PLATE MODEL INSTALLED IN NORTHROP 7 x 10 FOOT TUNNEL

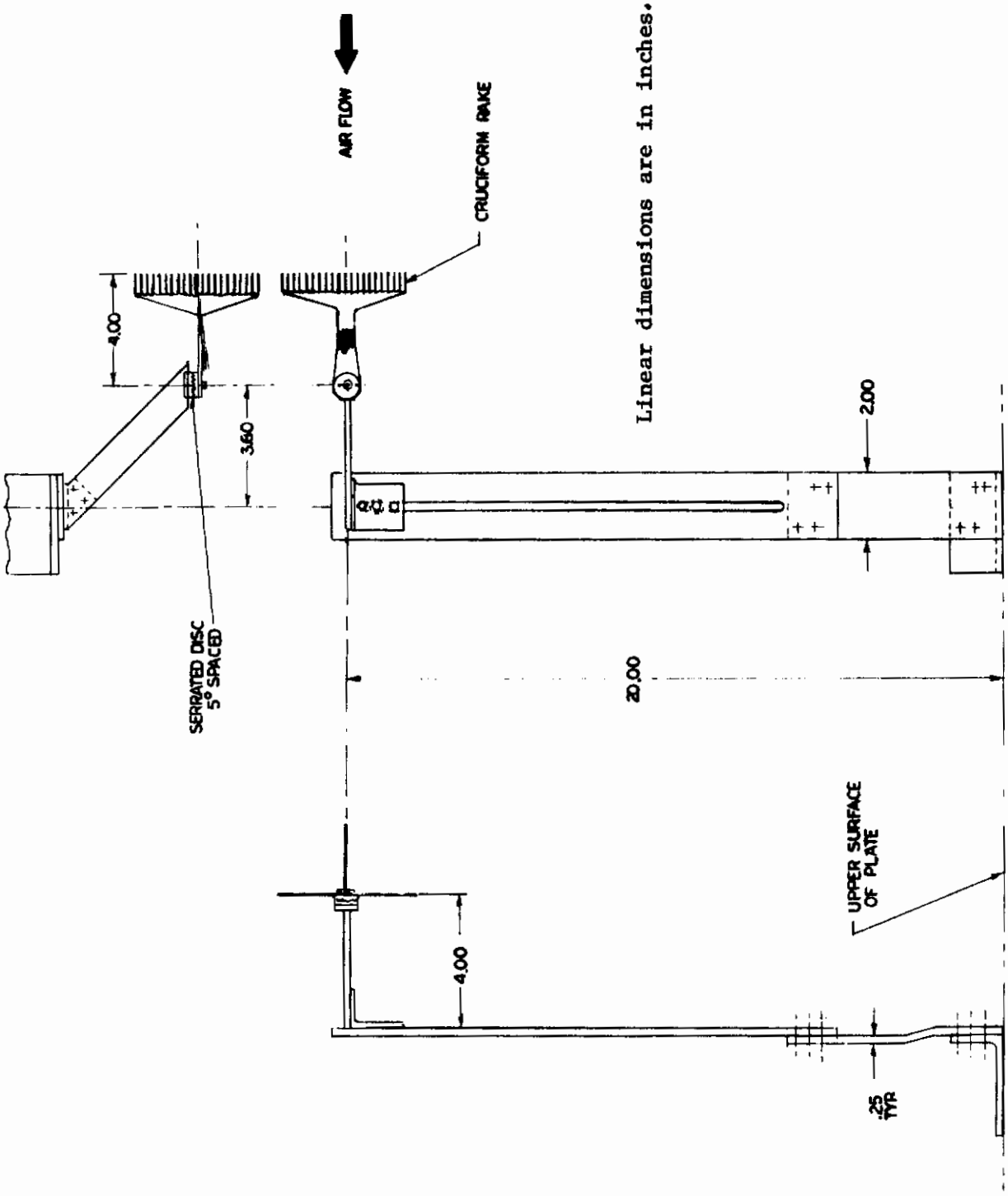

FIGURE 6. CRUCIFORM RAKE SUPPORT STAND

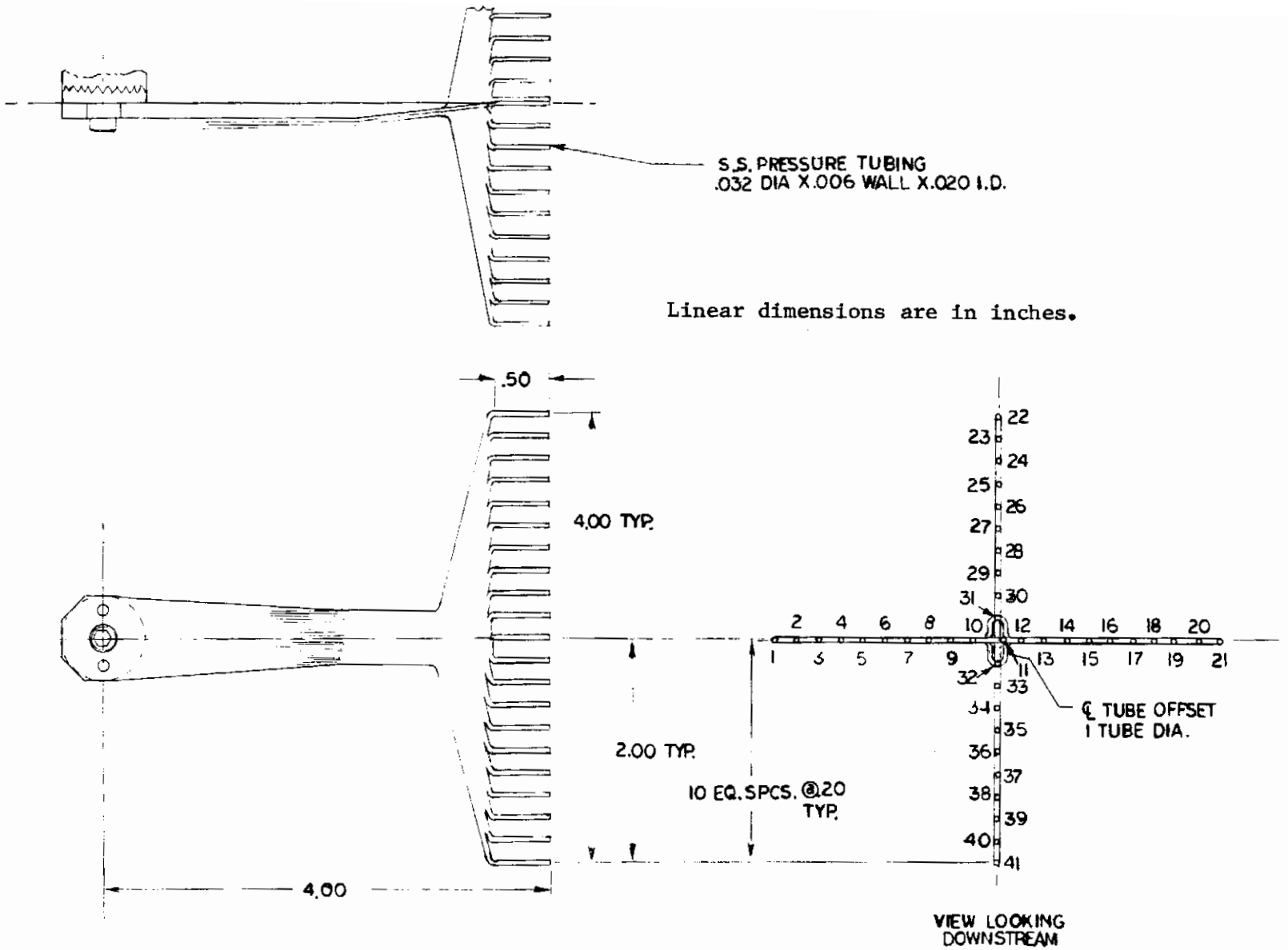

FIGURE 7. CRUCIFORM RAKE DETAILS

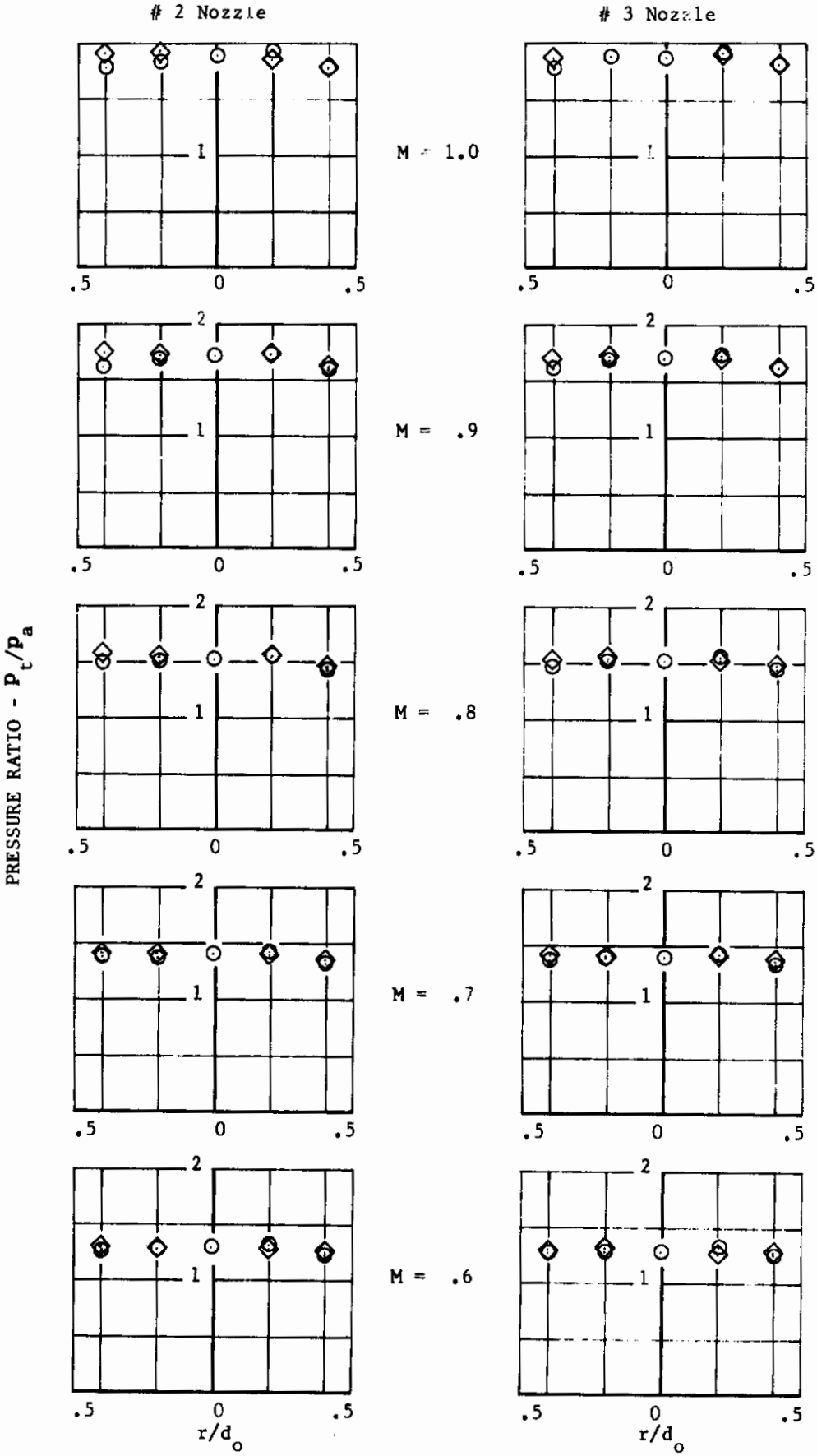

FIGURE 8. STATIC JET PRESSURE PROFILES AT JET EXIT

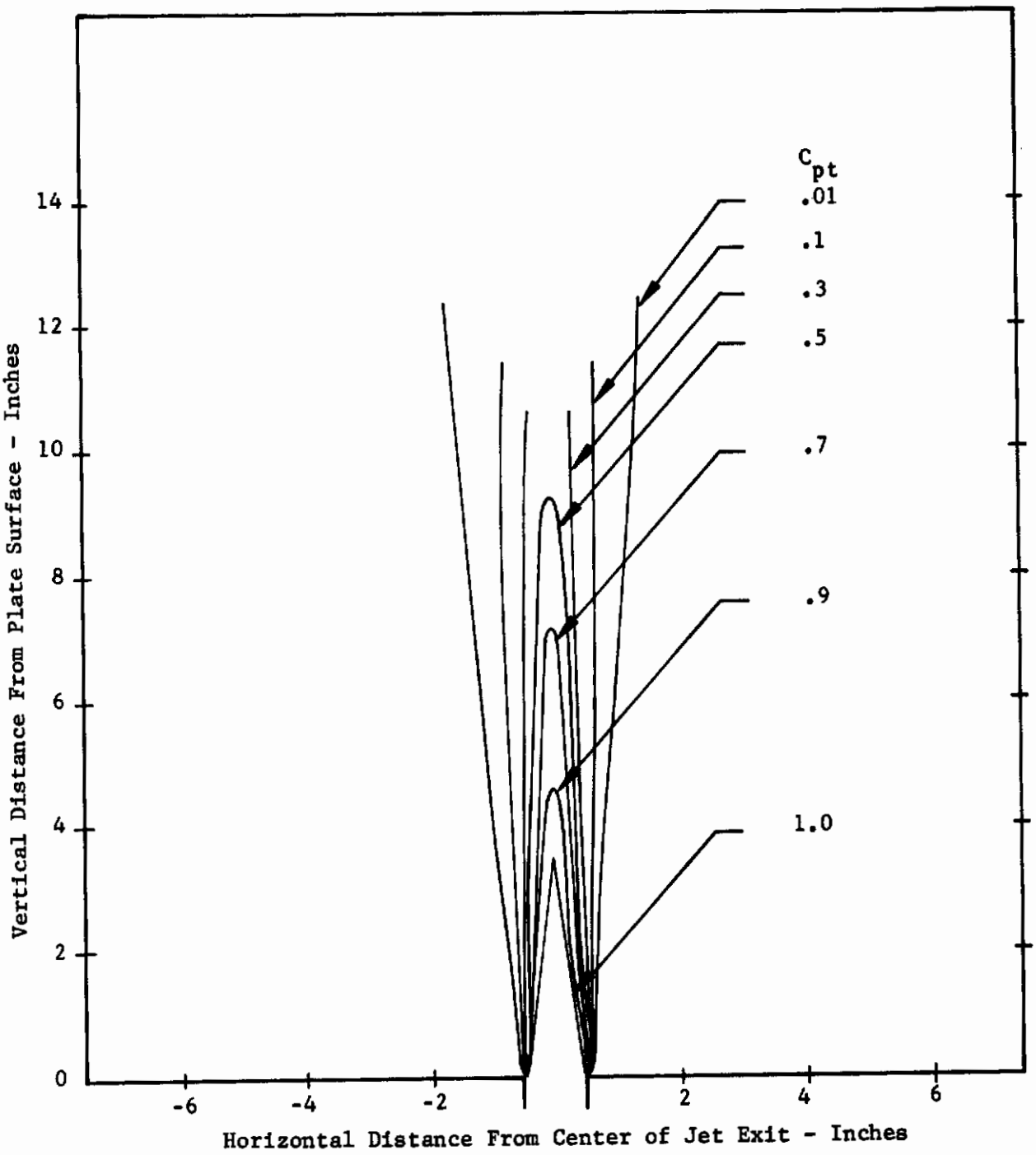

FIGURE 9. CONTOURS OF CONTANT TOTAL PRESSURE COEFFICIENTS FOR A STATIC JET (M = 1 AT EXIT)

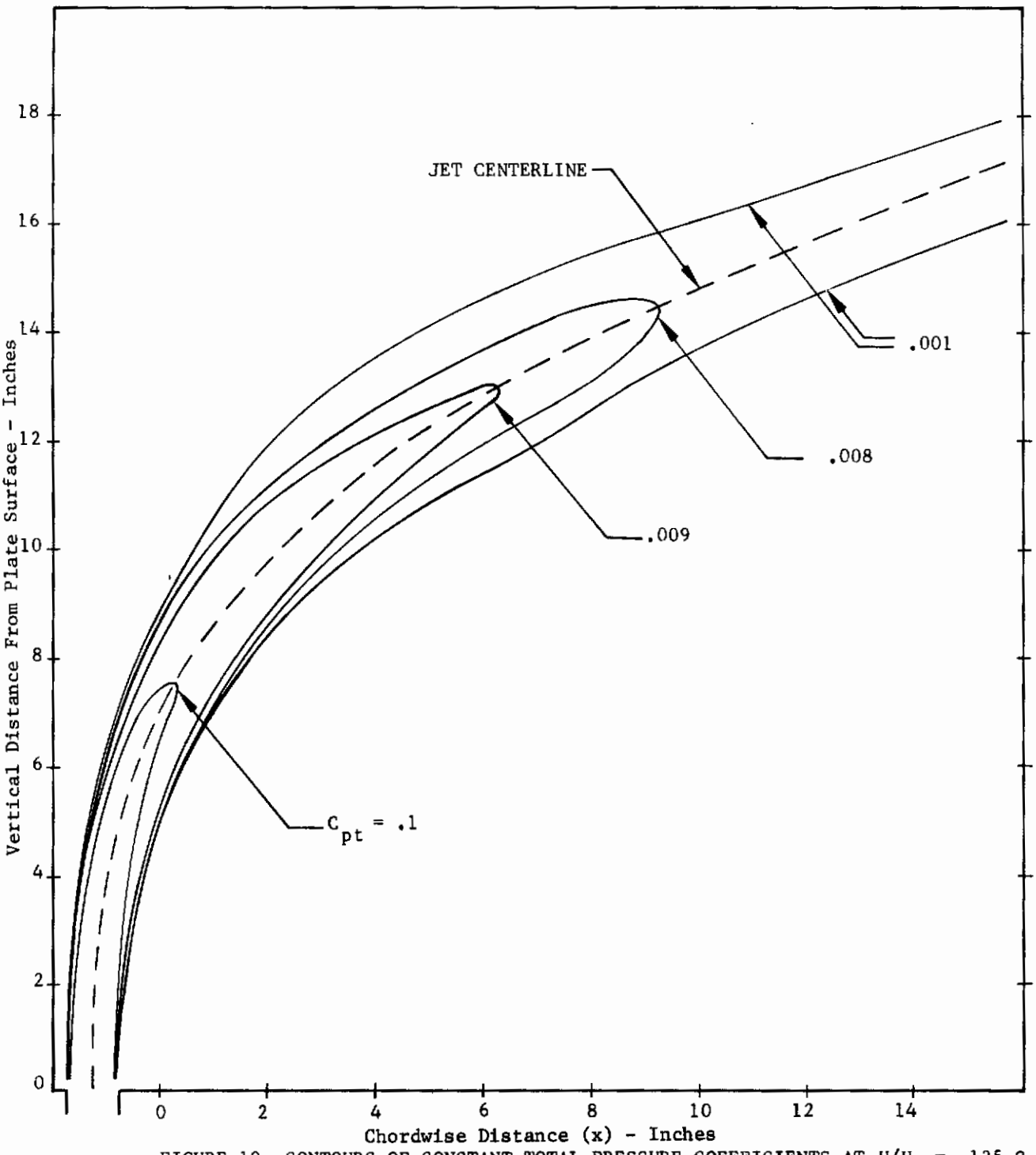

FIGURE 10. CONTOURS OF CONSTANT TOTAL PRESSURE COEFFICIENTS AT U/U_j = .125, β=0°

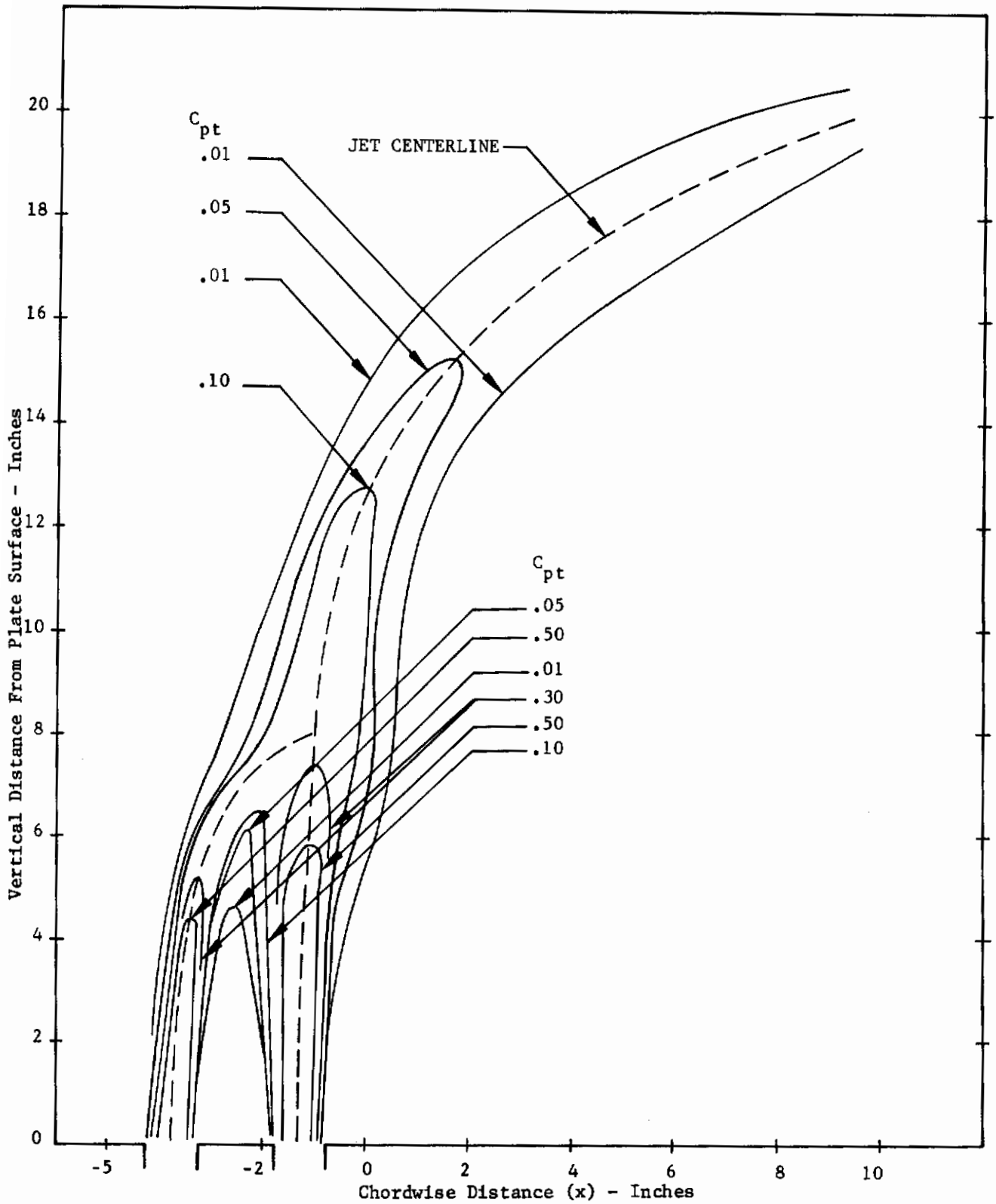

FIGURE 10 (CONTINUED). COUNTOURS OF CONSTANT TOTAL PRESSURE COEFFICIENTS AT U/U_j = .125, β=0° AT A JET SPACING OF 2.5 DIAMETERS

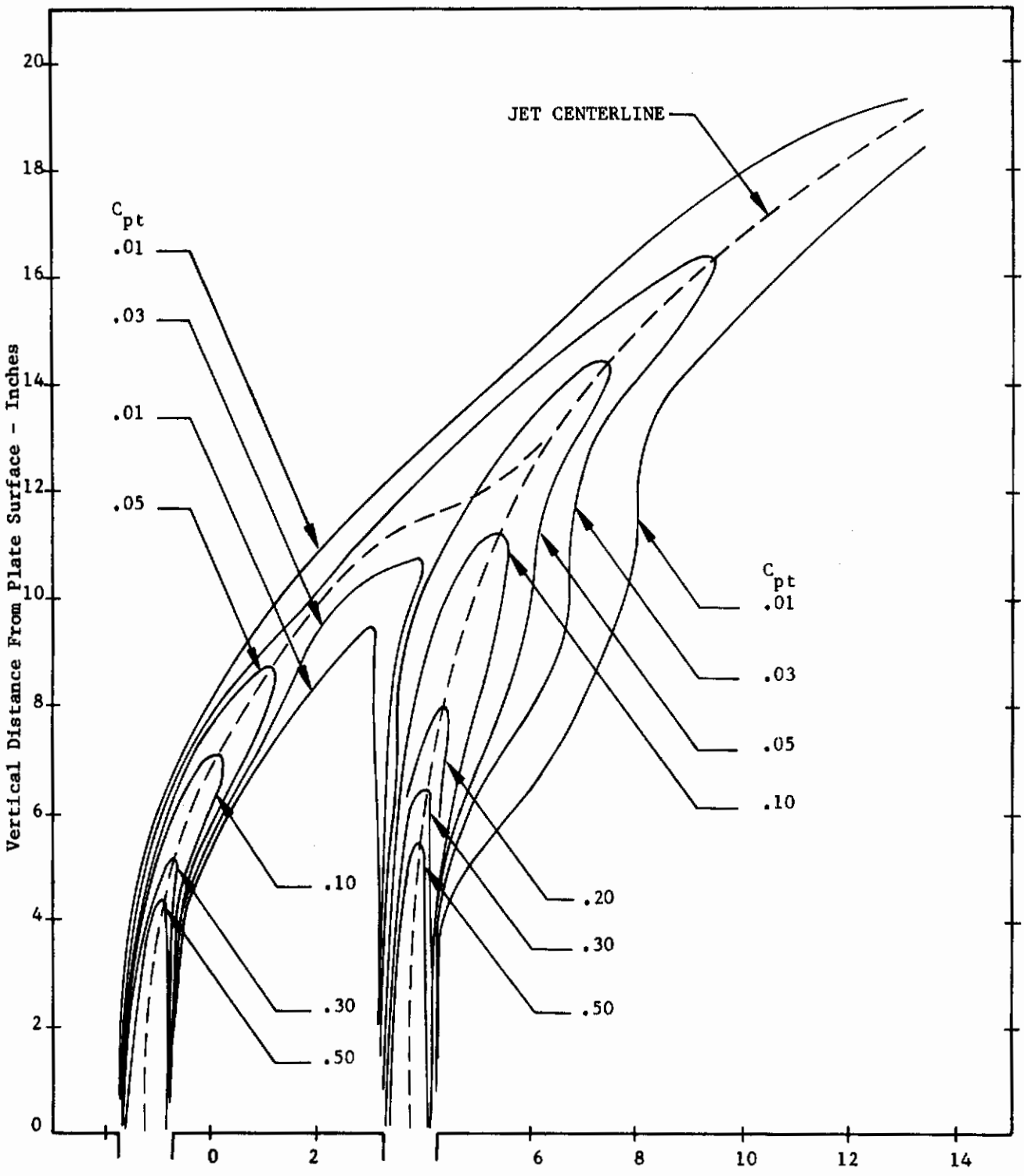

FIGURE 10 (CONTINUED). CONTOURS OF CONSTANT TOTAL PRESSURE COEFFICIENTS AT $U/U_j = .125$, $\beta = 0°$ AT A JET SPACING OF 5 DIAMETERS

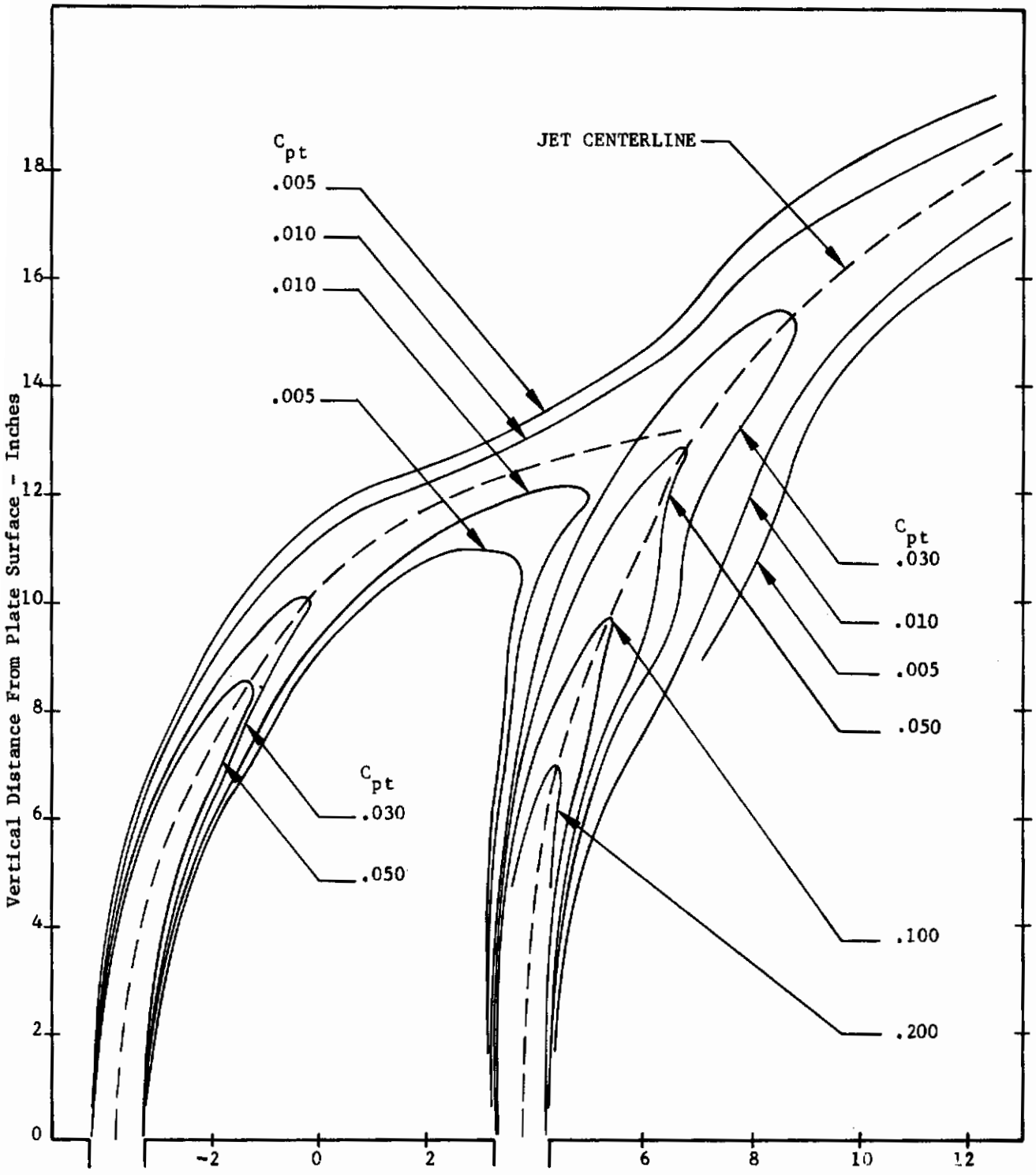

FIGURE 10 (CONCLUDED). CONTOURS OF CONSTANT TOTAL PRESSURE COEFFICIENTS AT $U/U_j = .125$, $\beta = 0°$ AT A JET SPACING OF 7.5 DIAMETERS

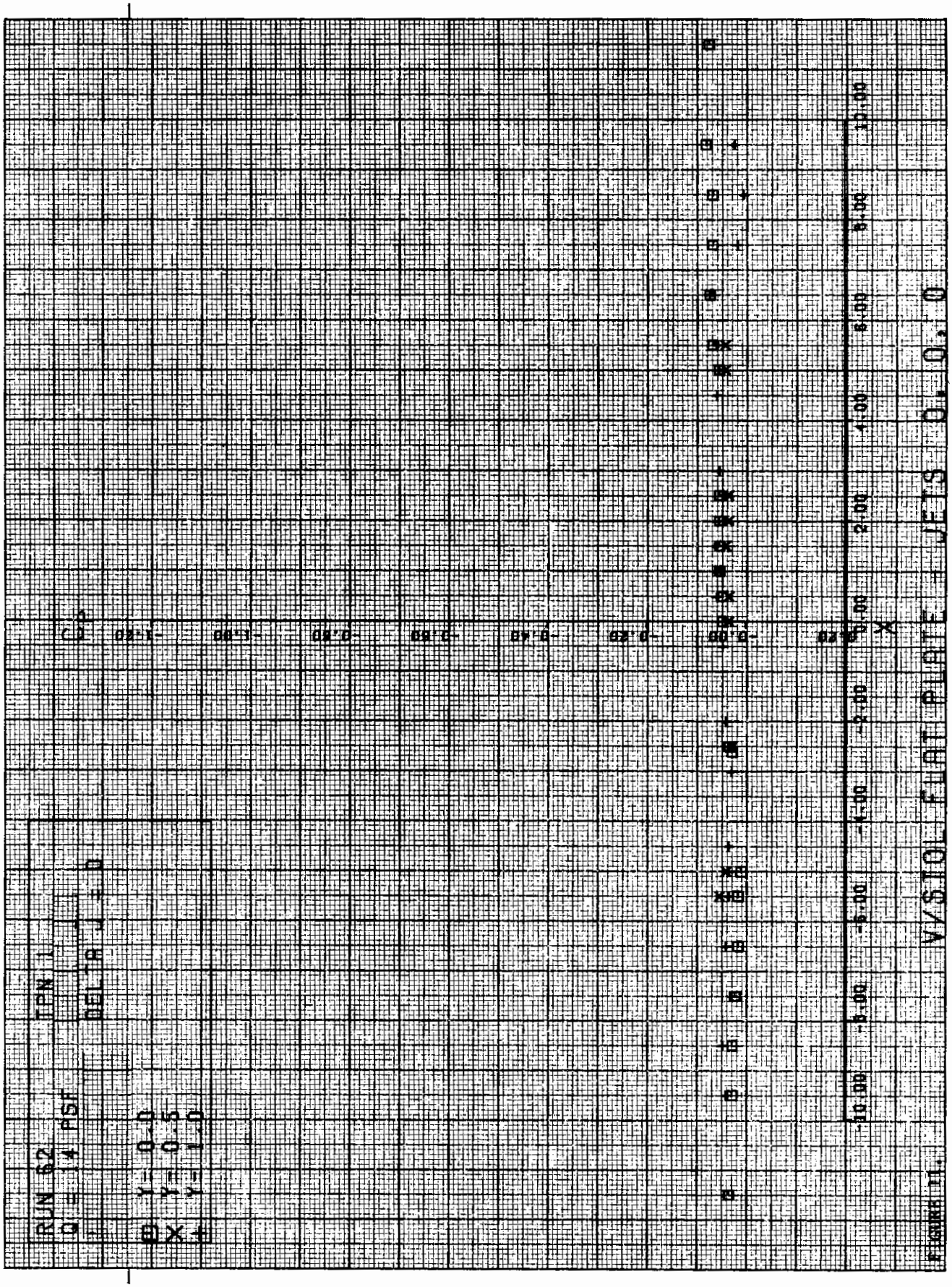

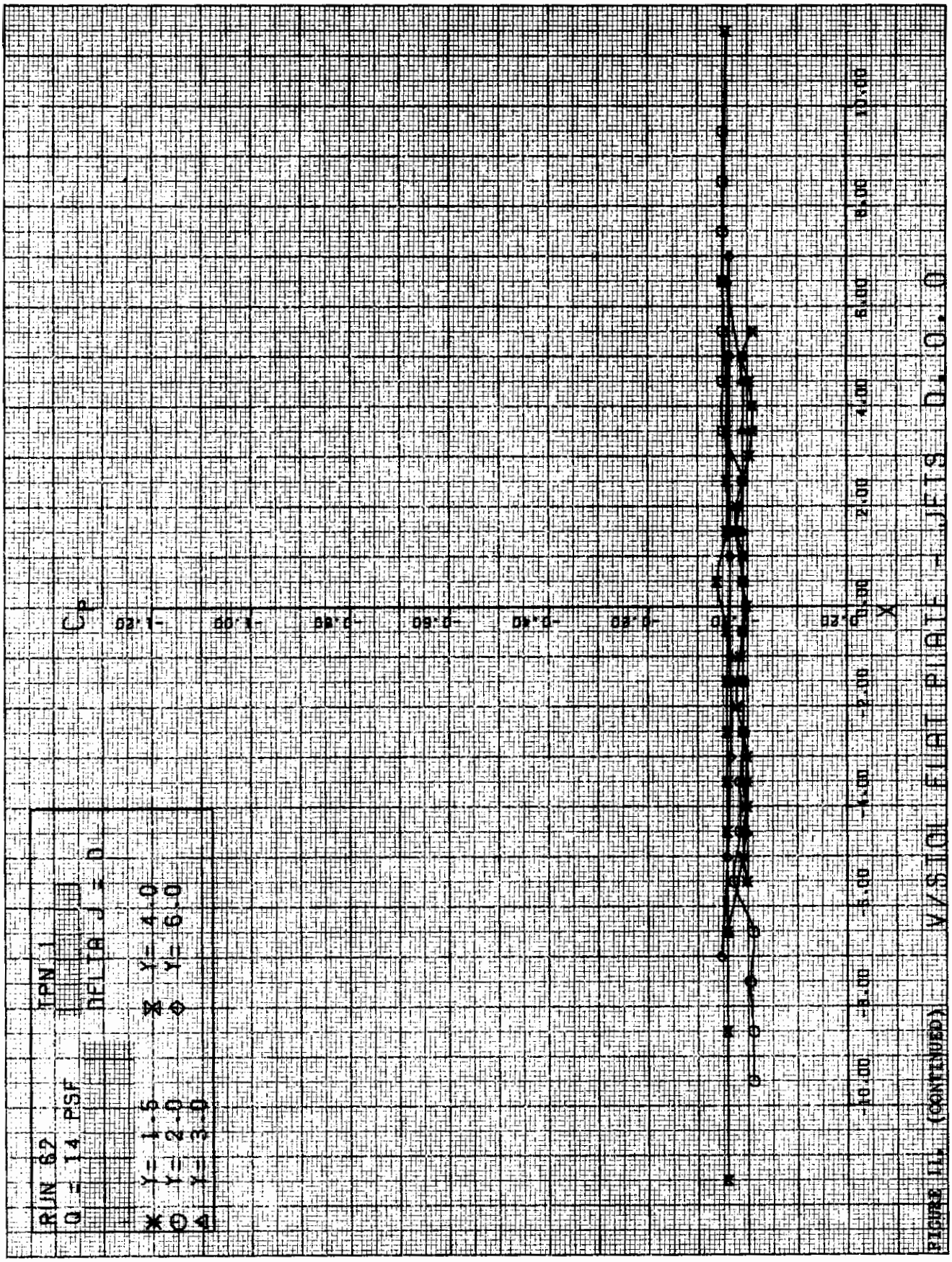

FIGURE 11. (CONTINUED) W/STOL FLAT PLATE - JETS DN, 0.0

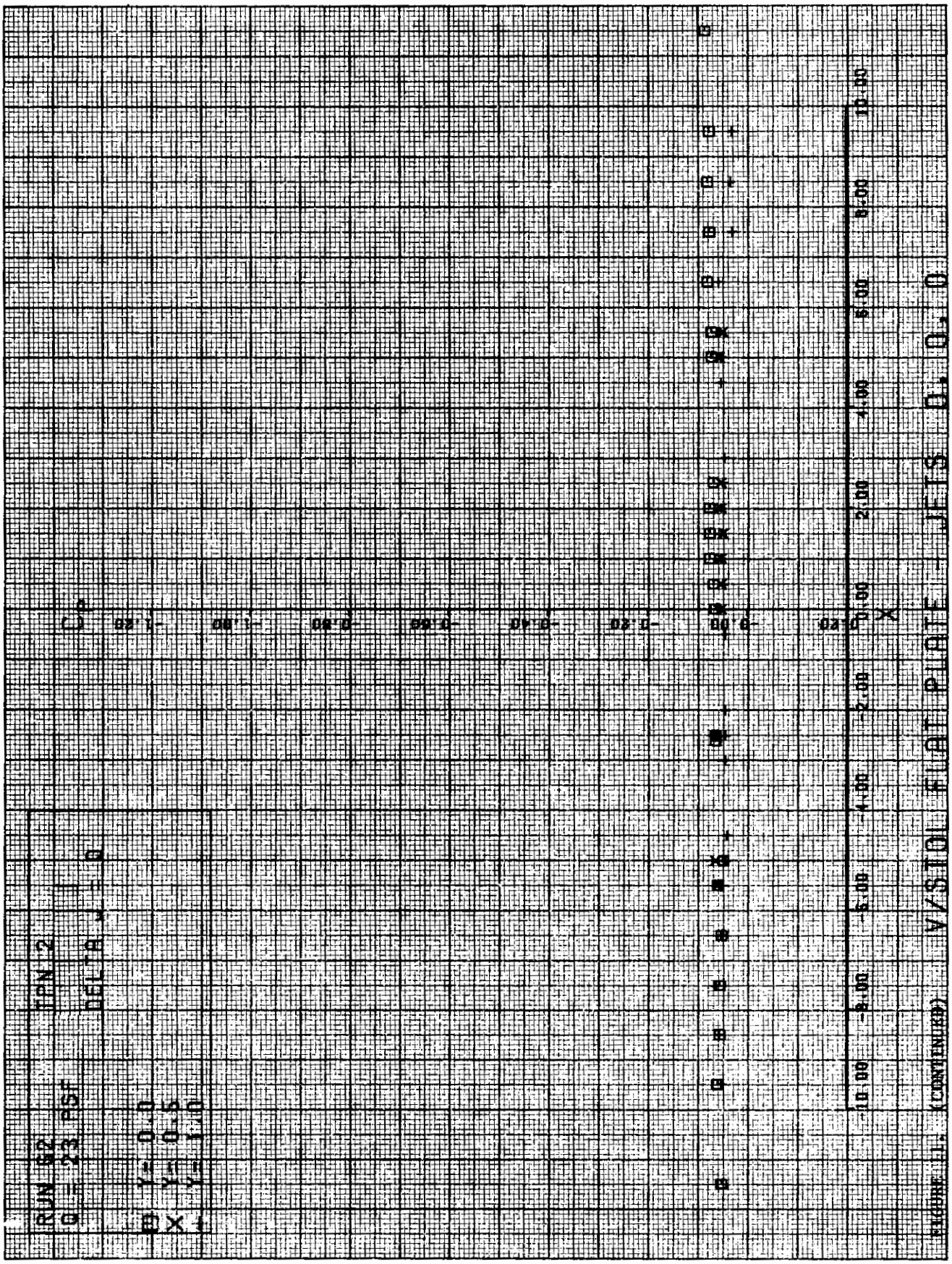

FIGURE 11. (CONTINUED)

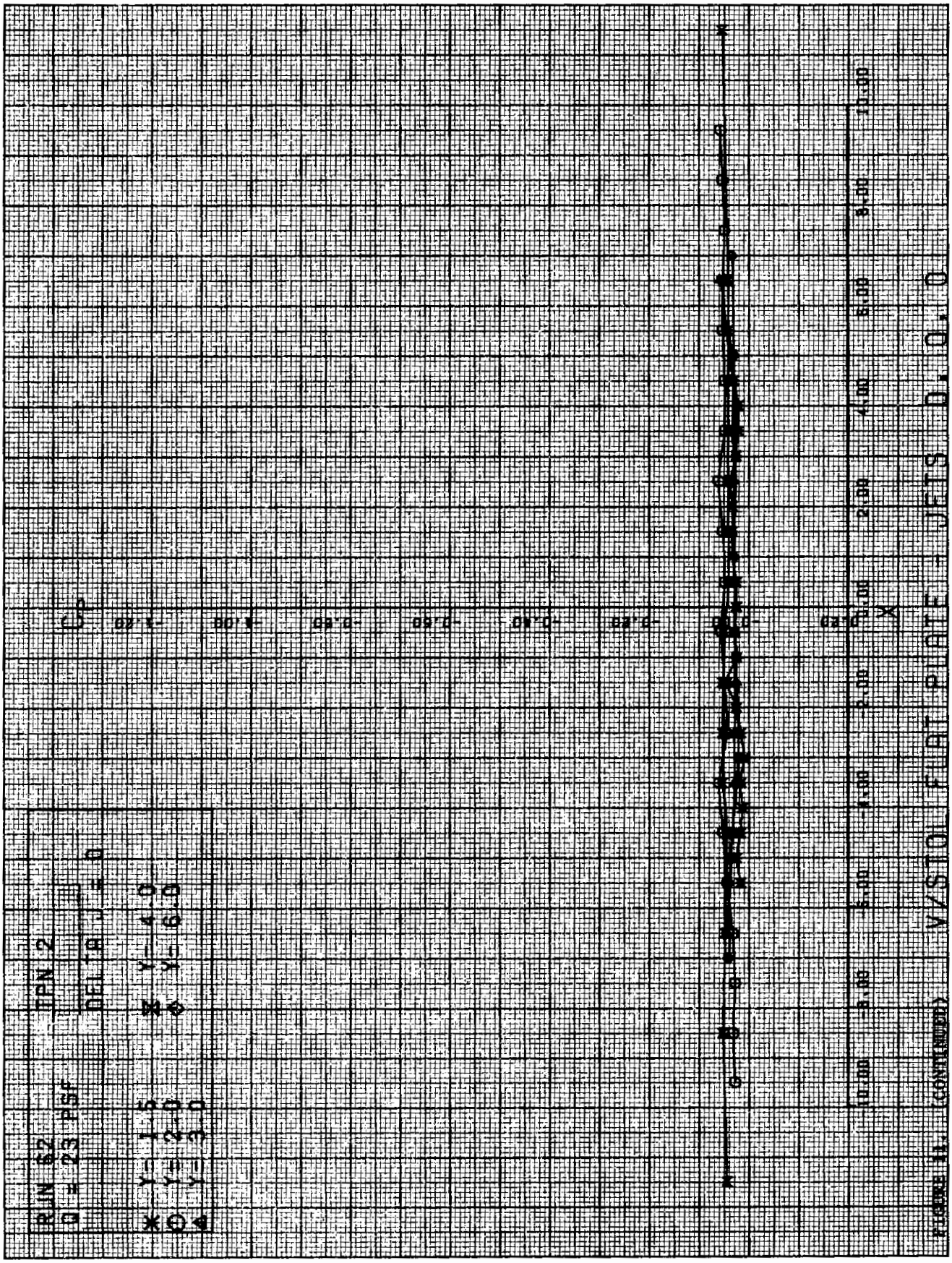

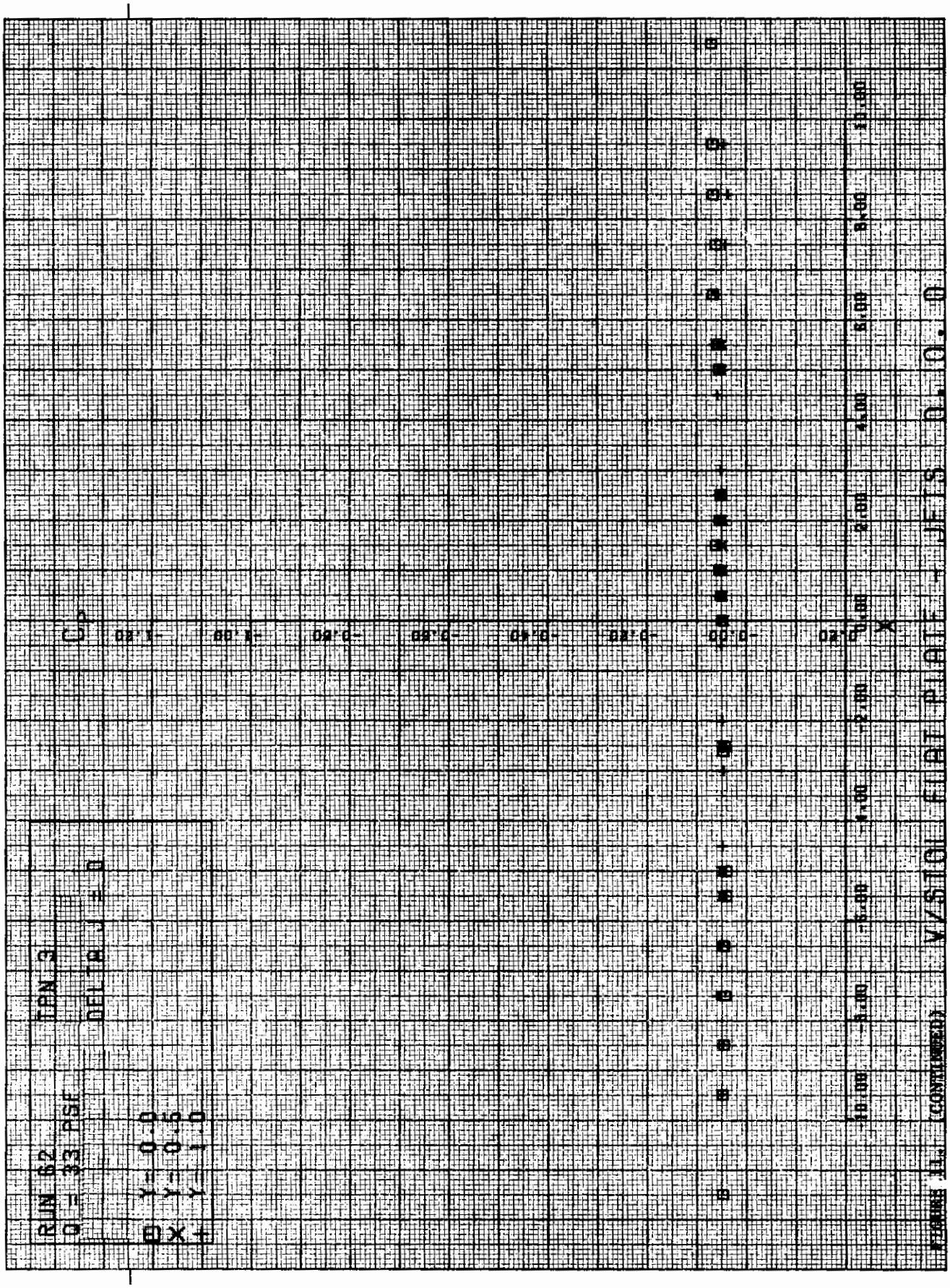

FIGURE 11. (CONTINUED)

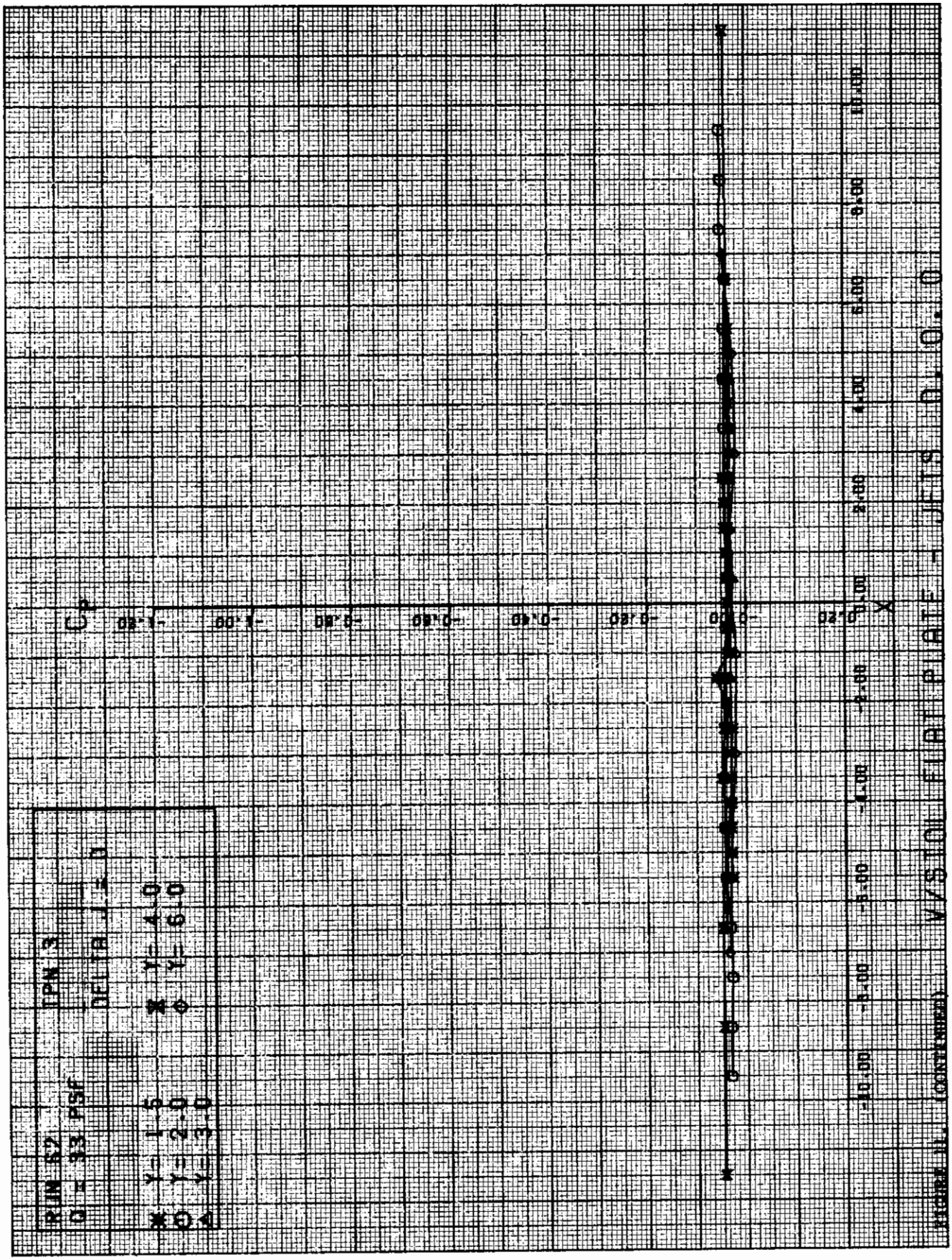

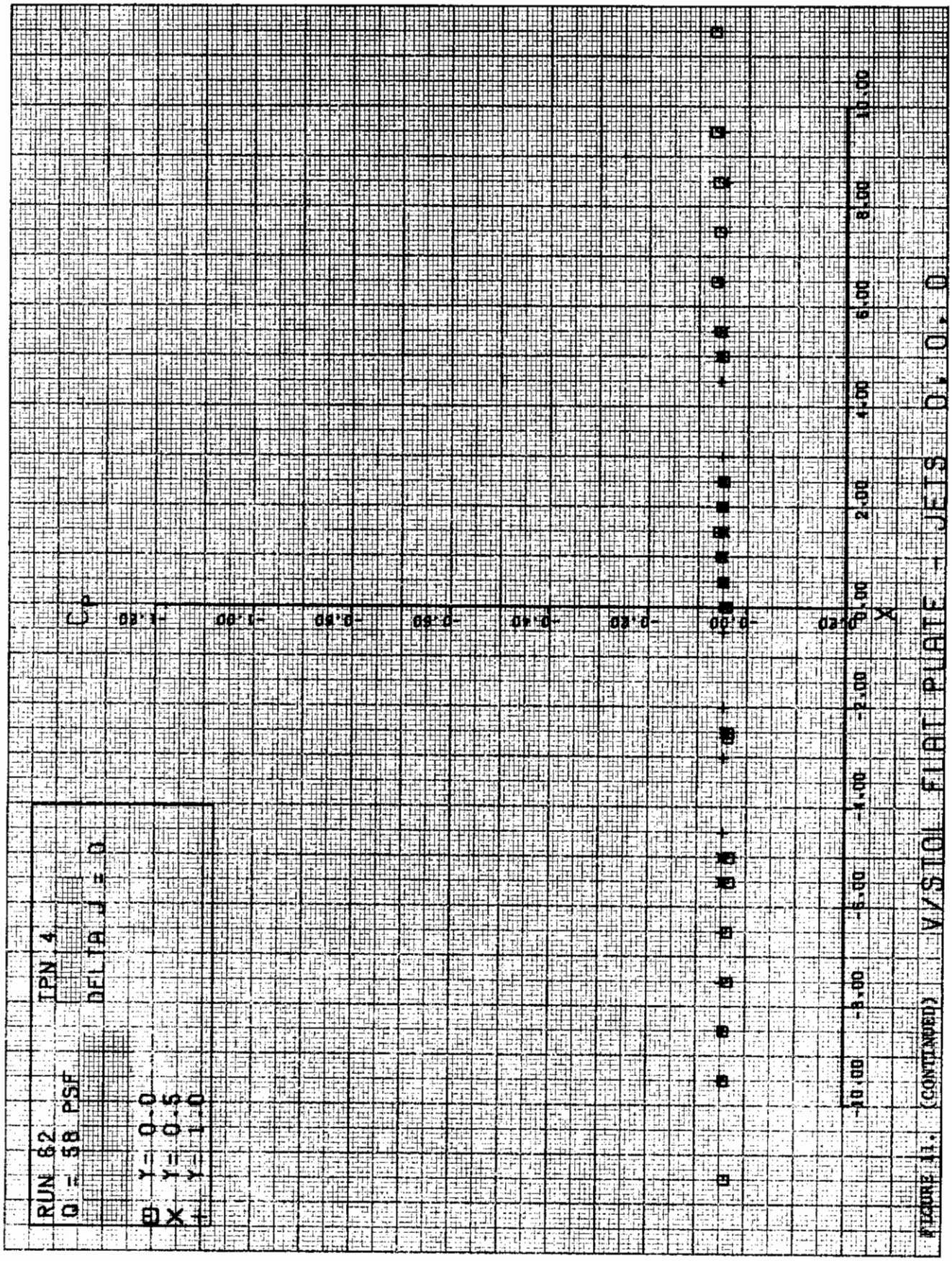

FIGURE 11. (CONTINUED) V/STOL FLAT PLATE + JETS Q, 0, 0

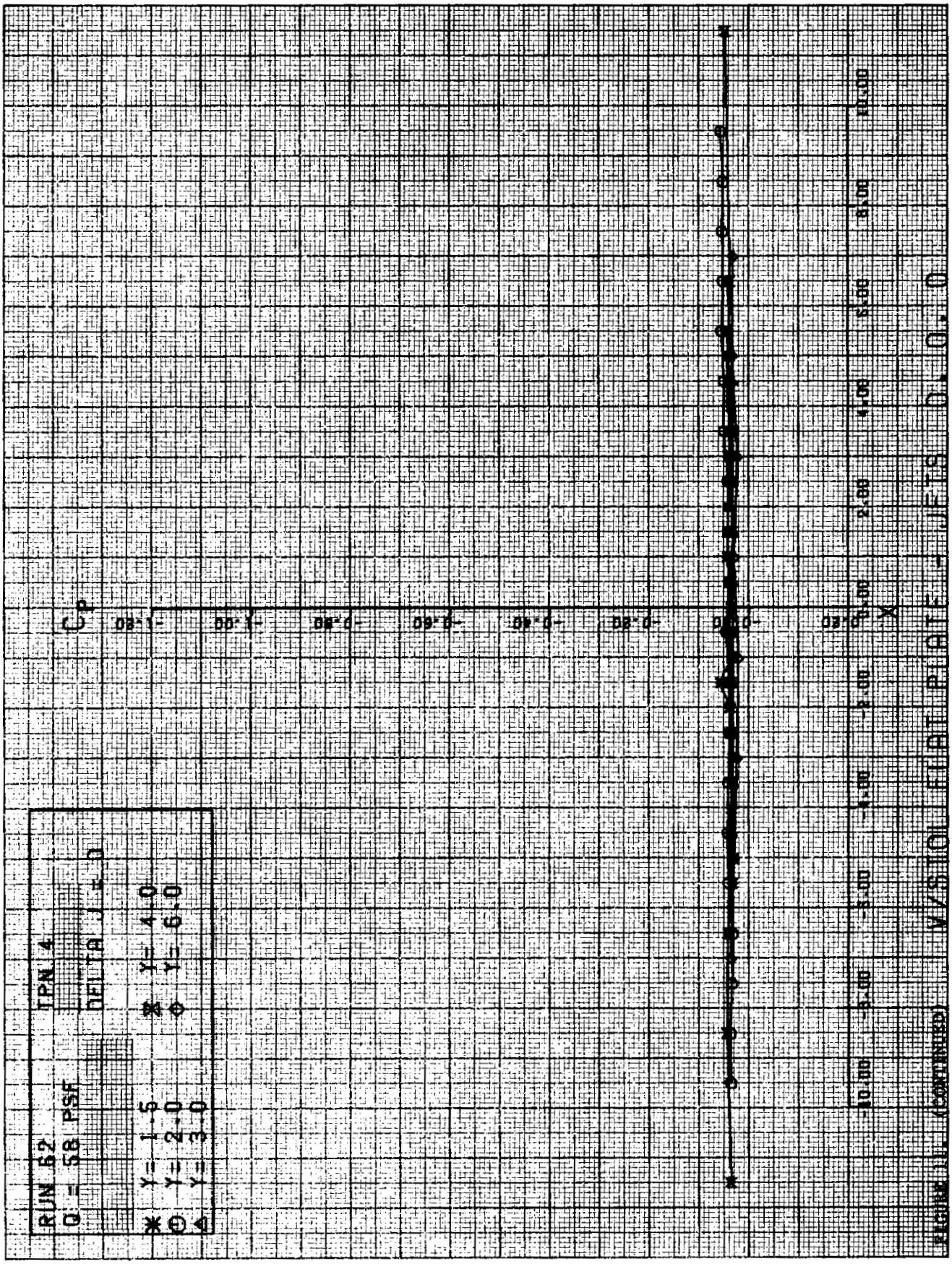

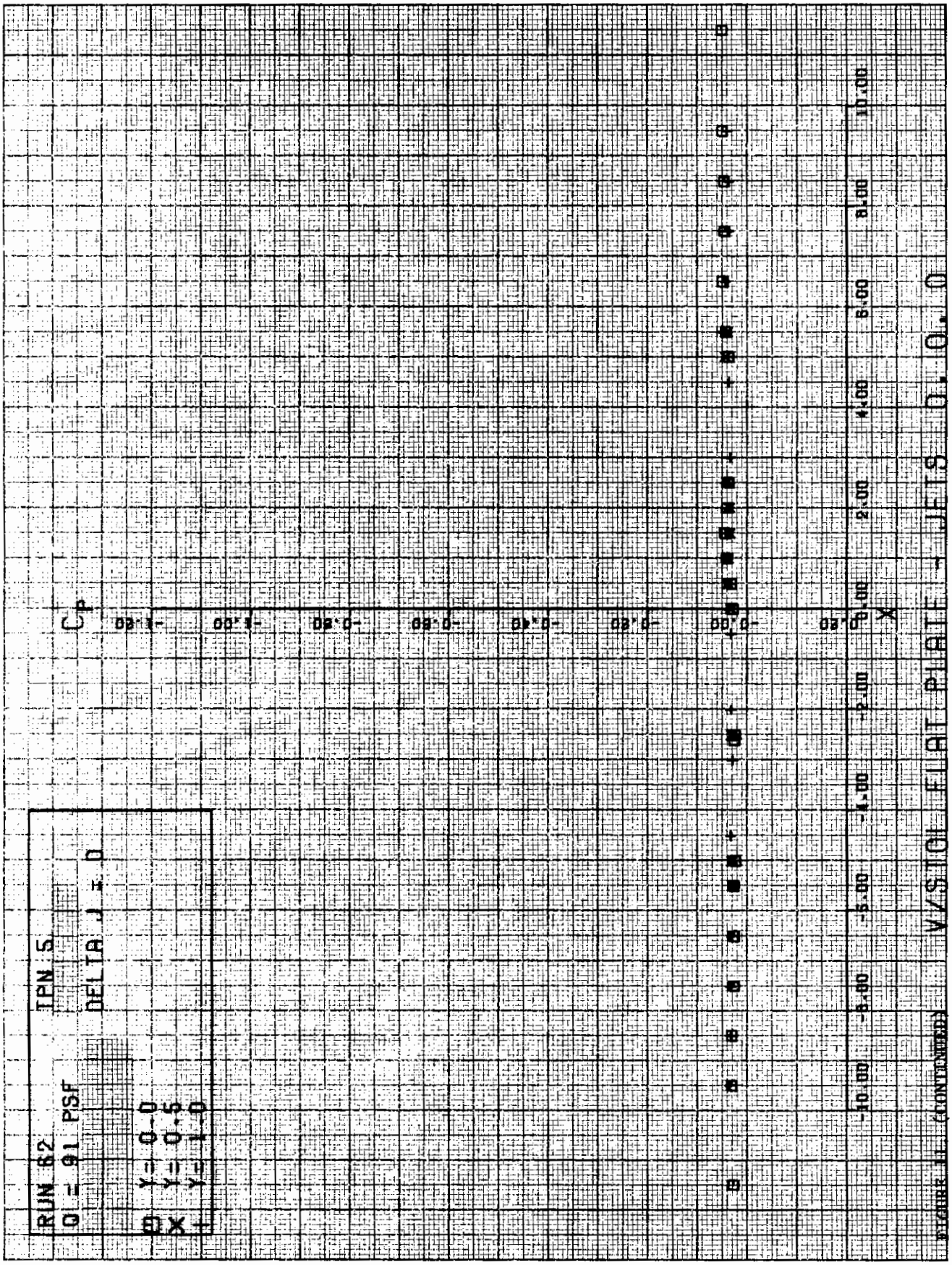

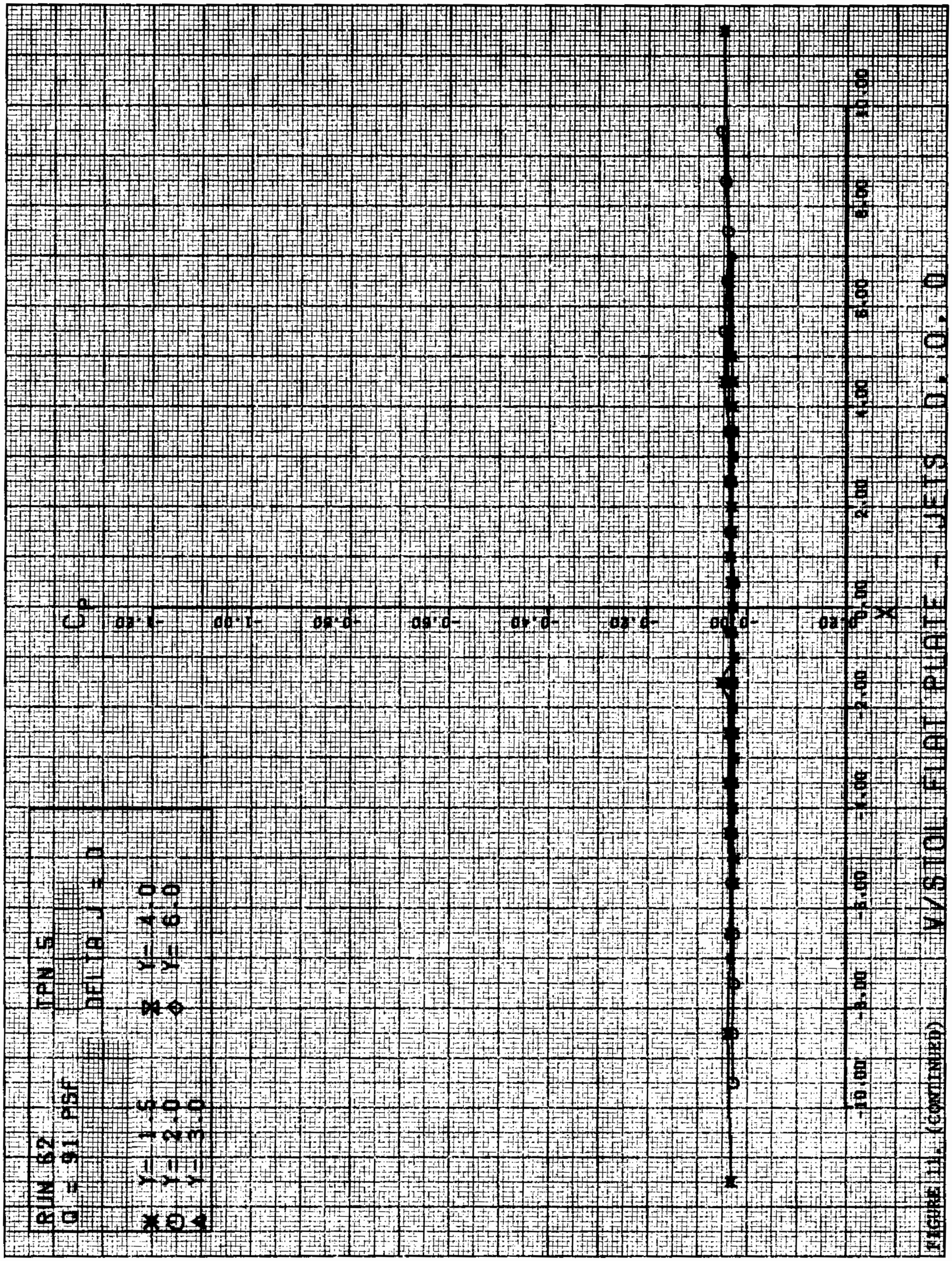

FIGURE 11. (CONTINUED) V/STOL FLAT PLATE - JETS 0, 0, 0

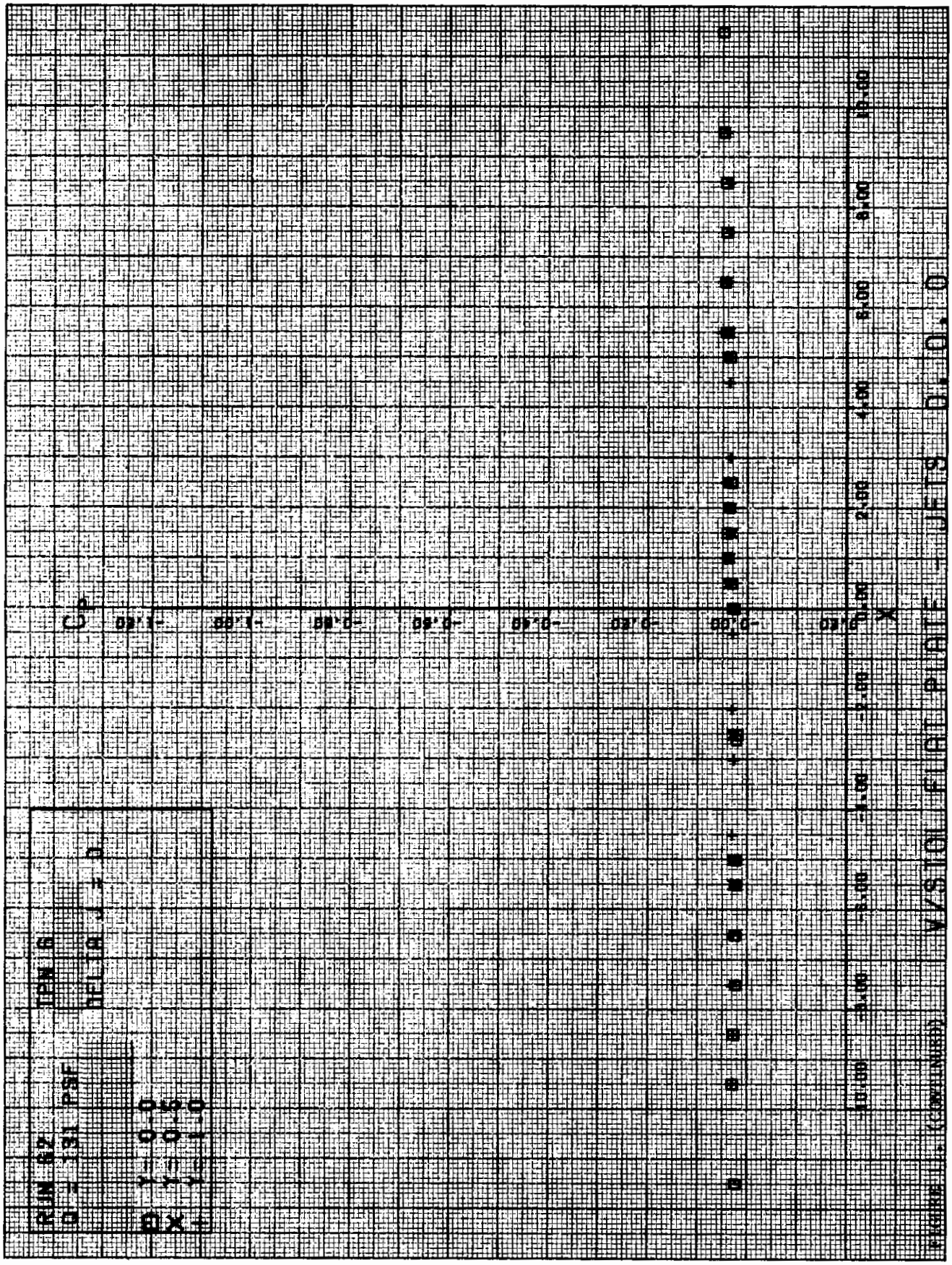

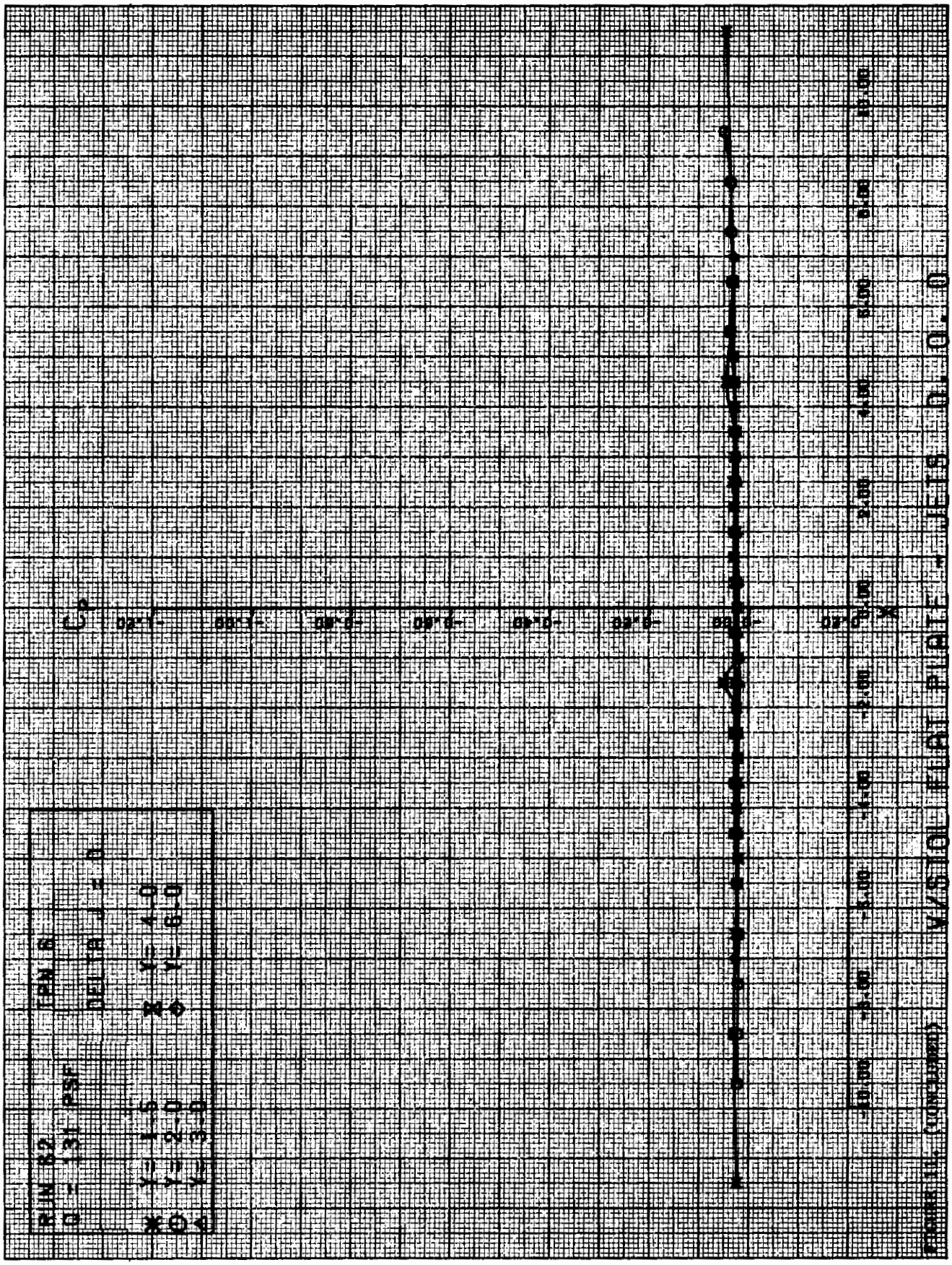

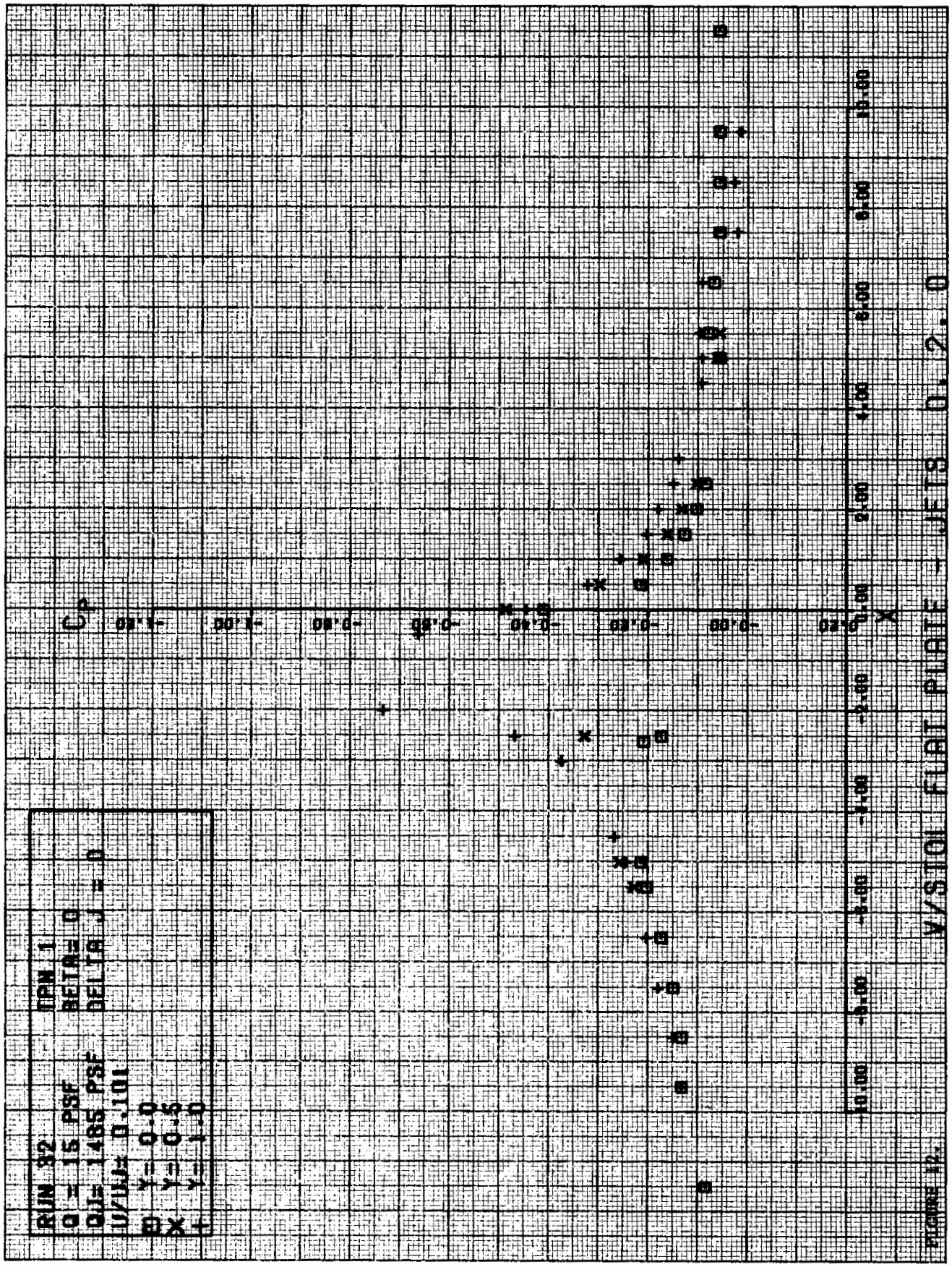

FIGURE 12.

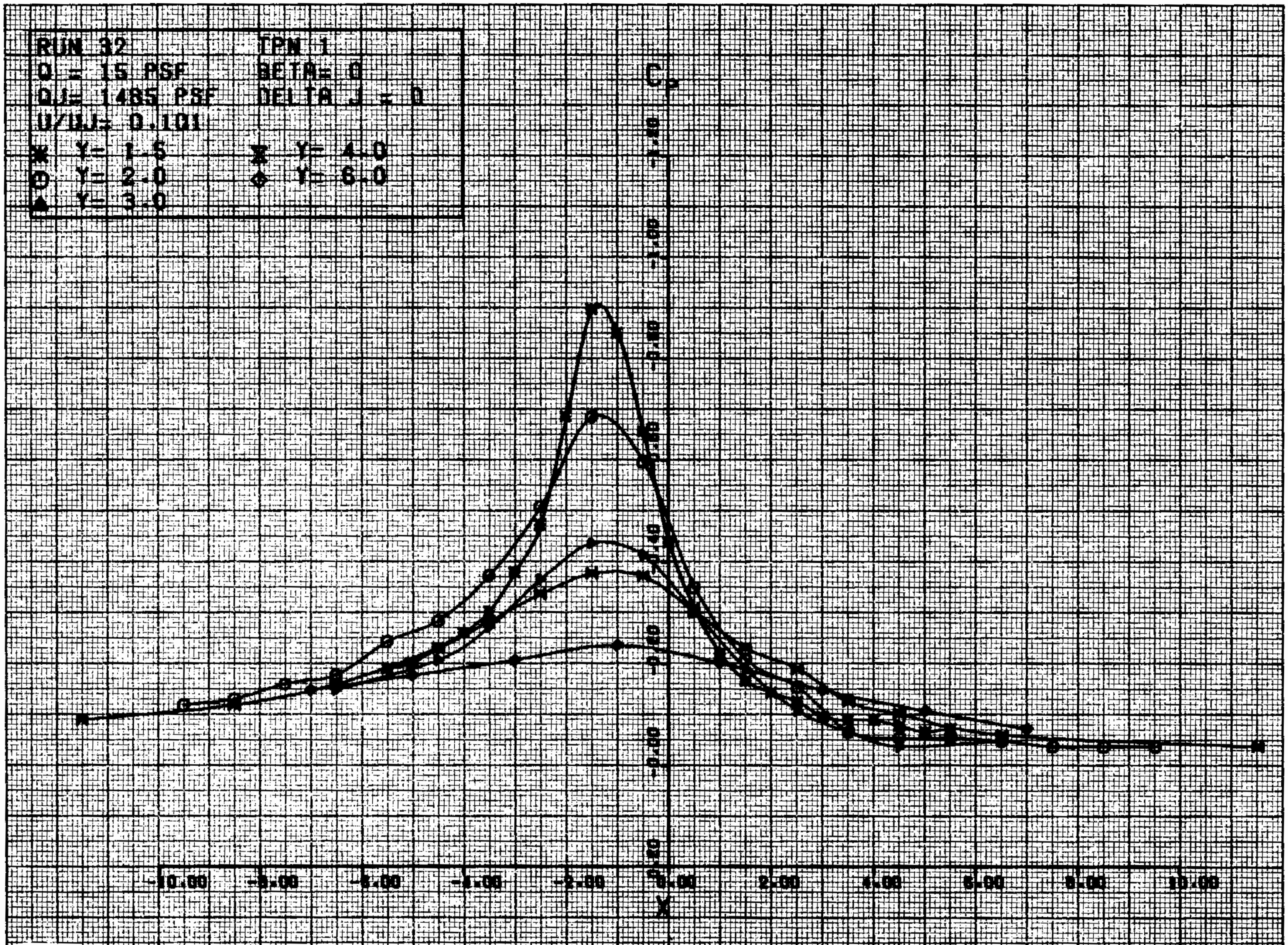

FIGURE 12. (CONTINUED) V/STOL FLAT PLATE - JETS D. 2. 0

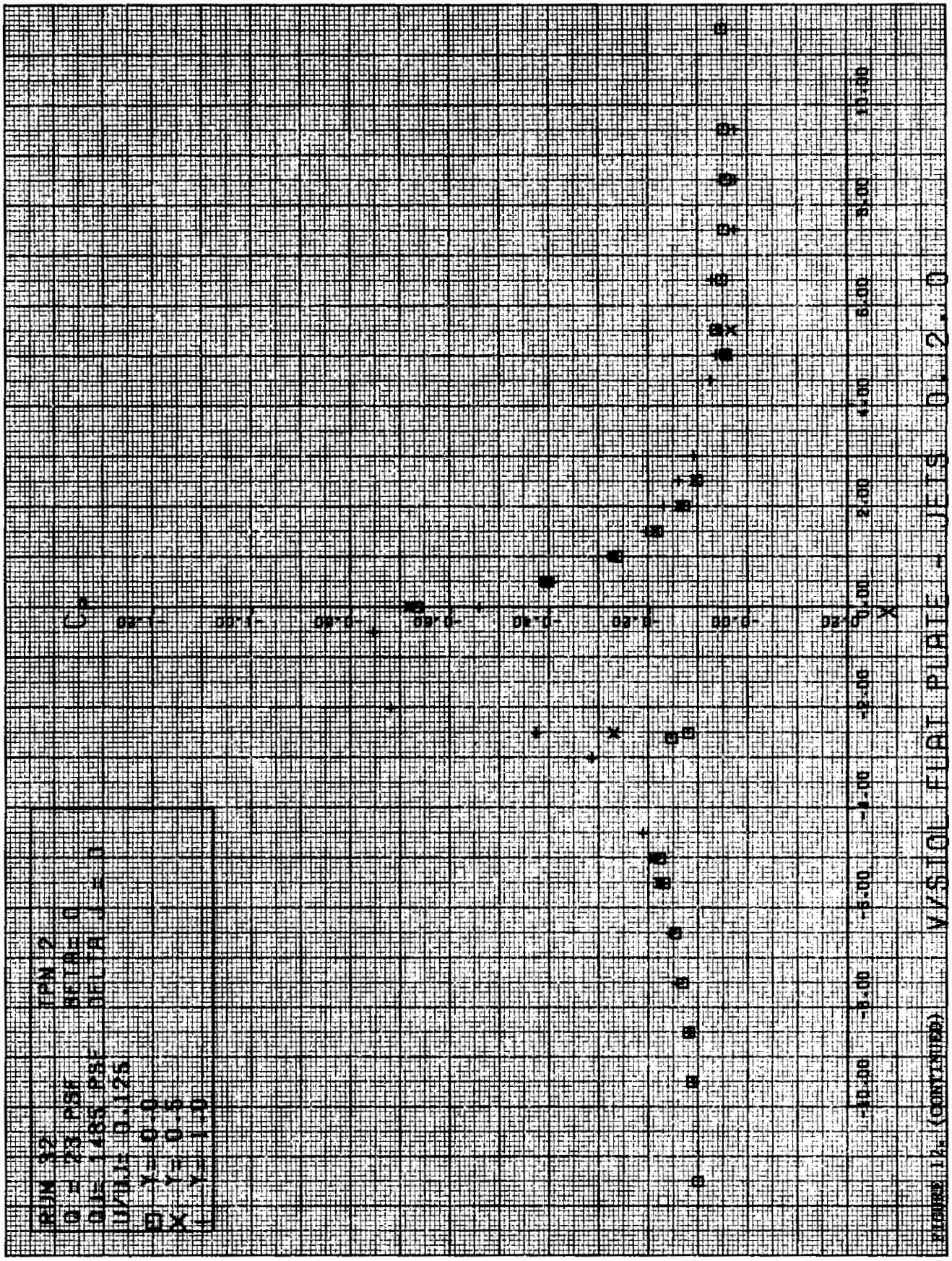

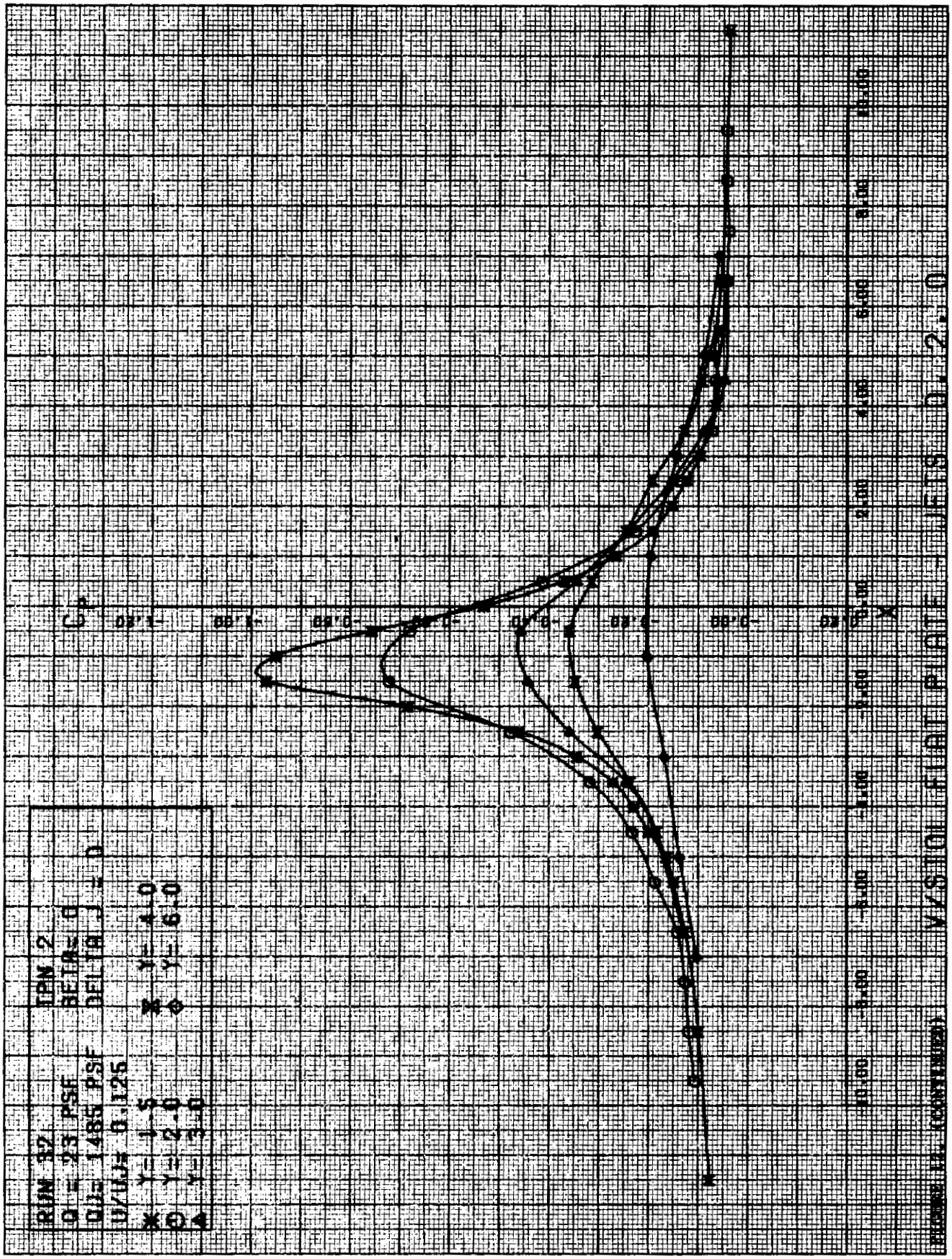

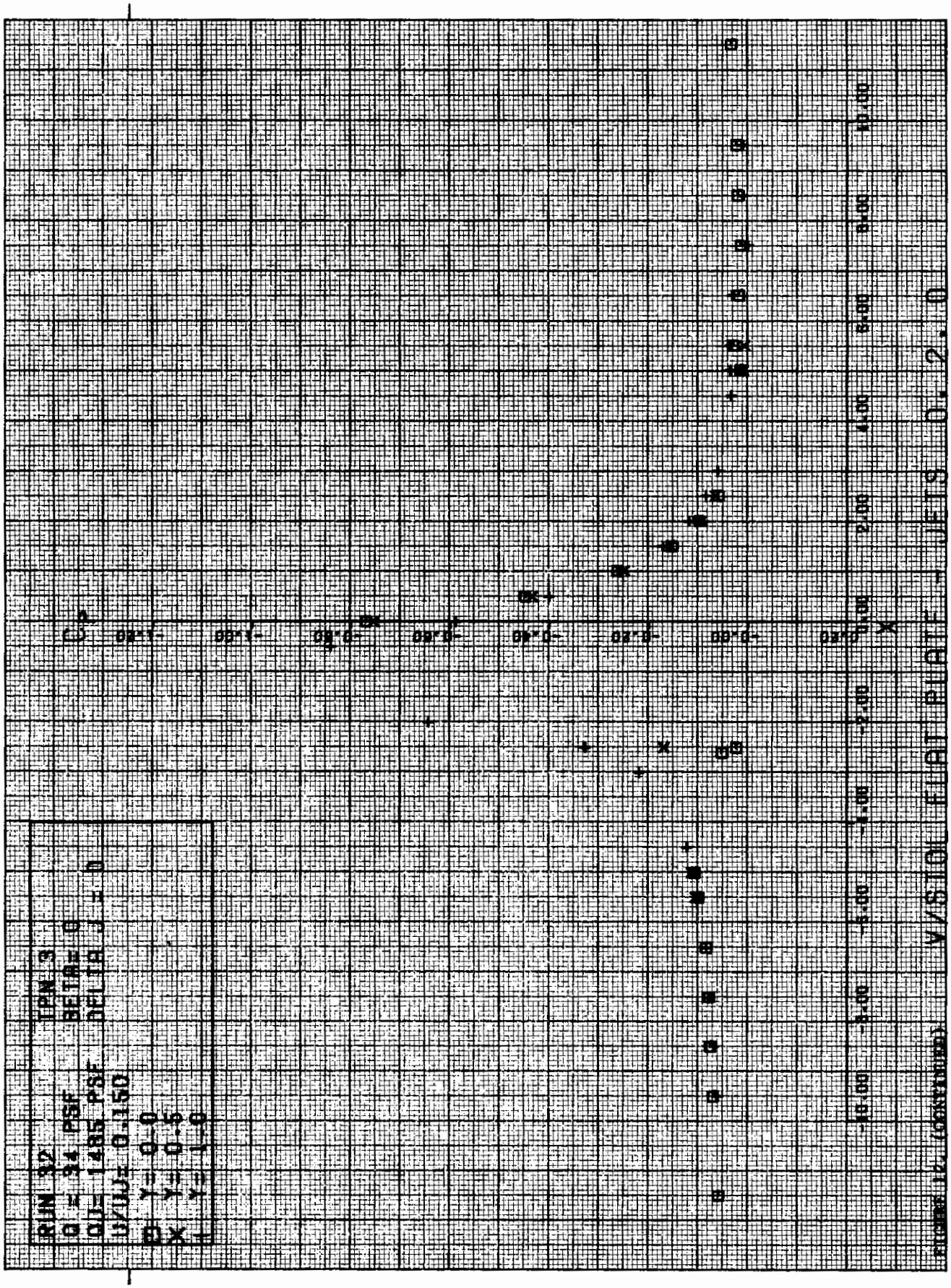

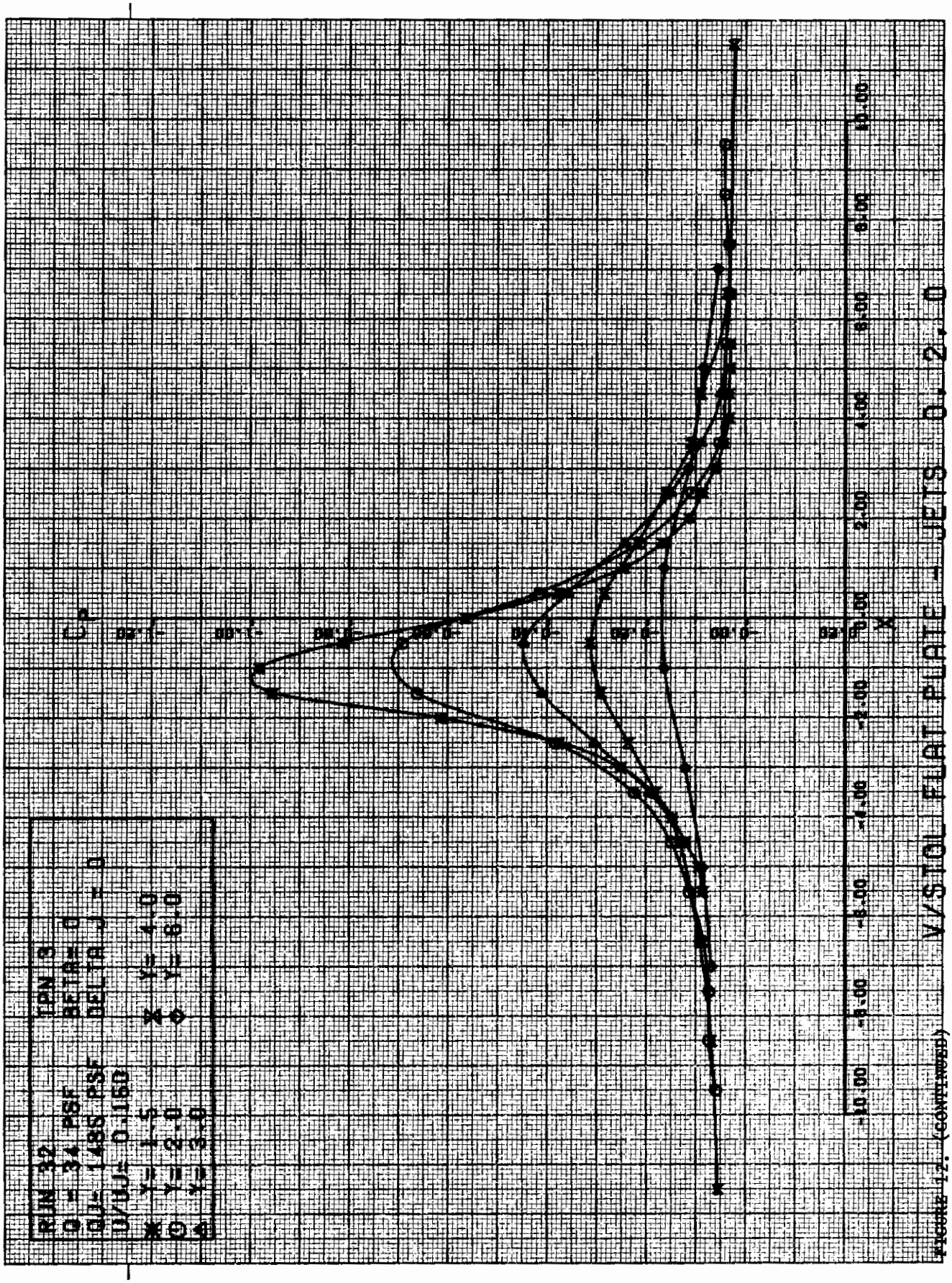

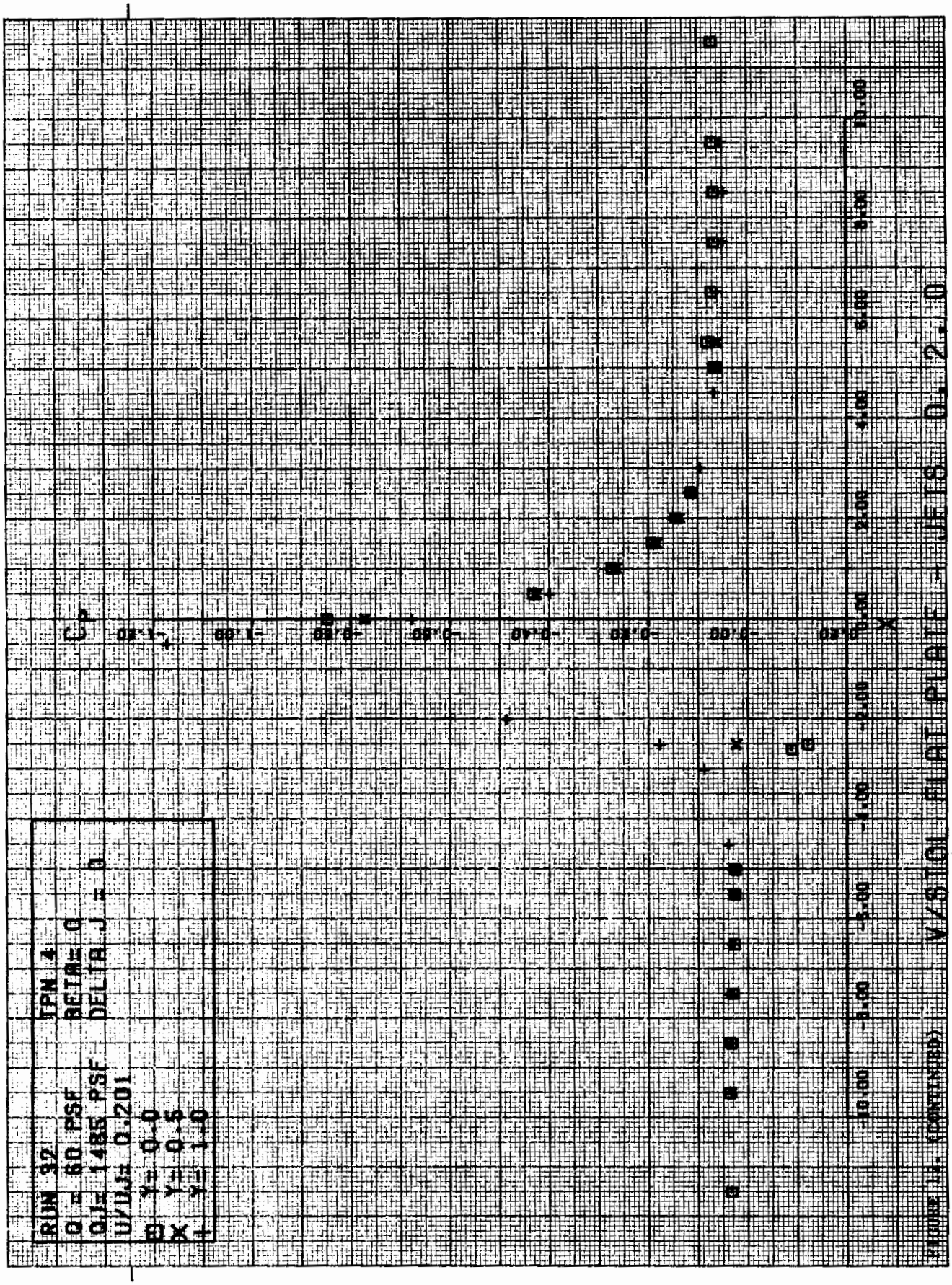

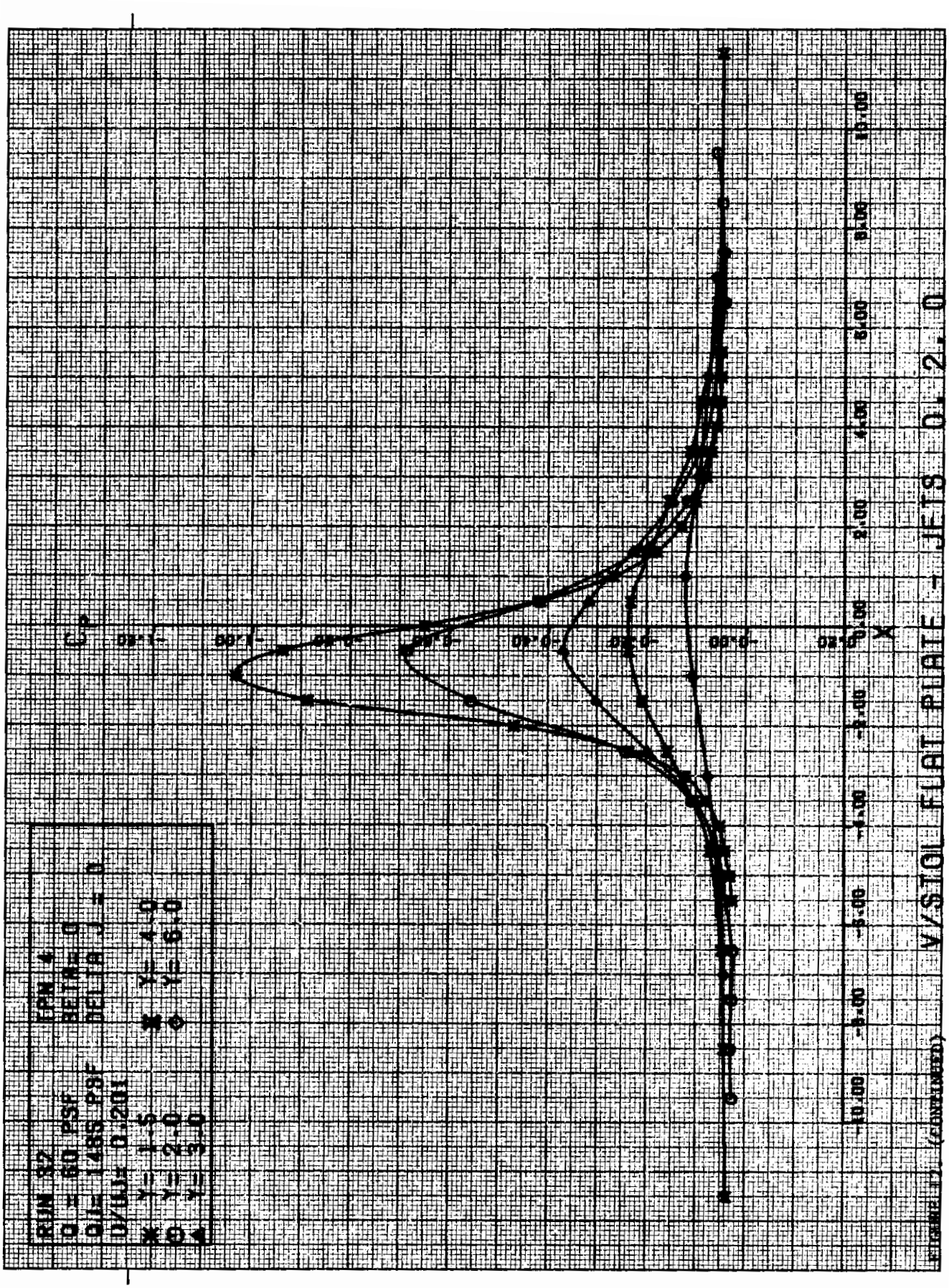

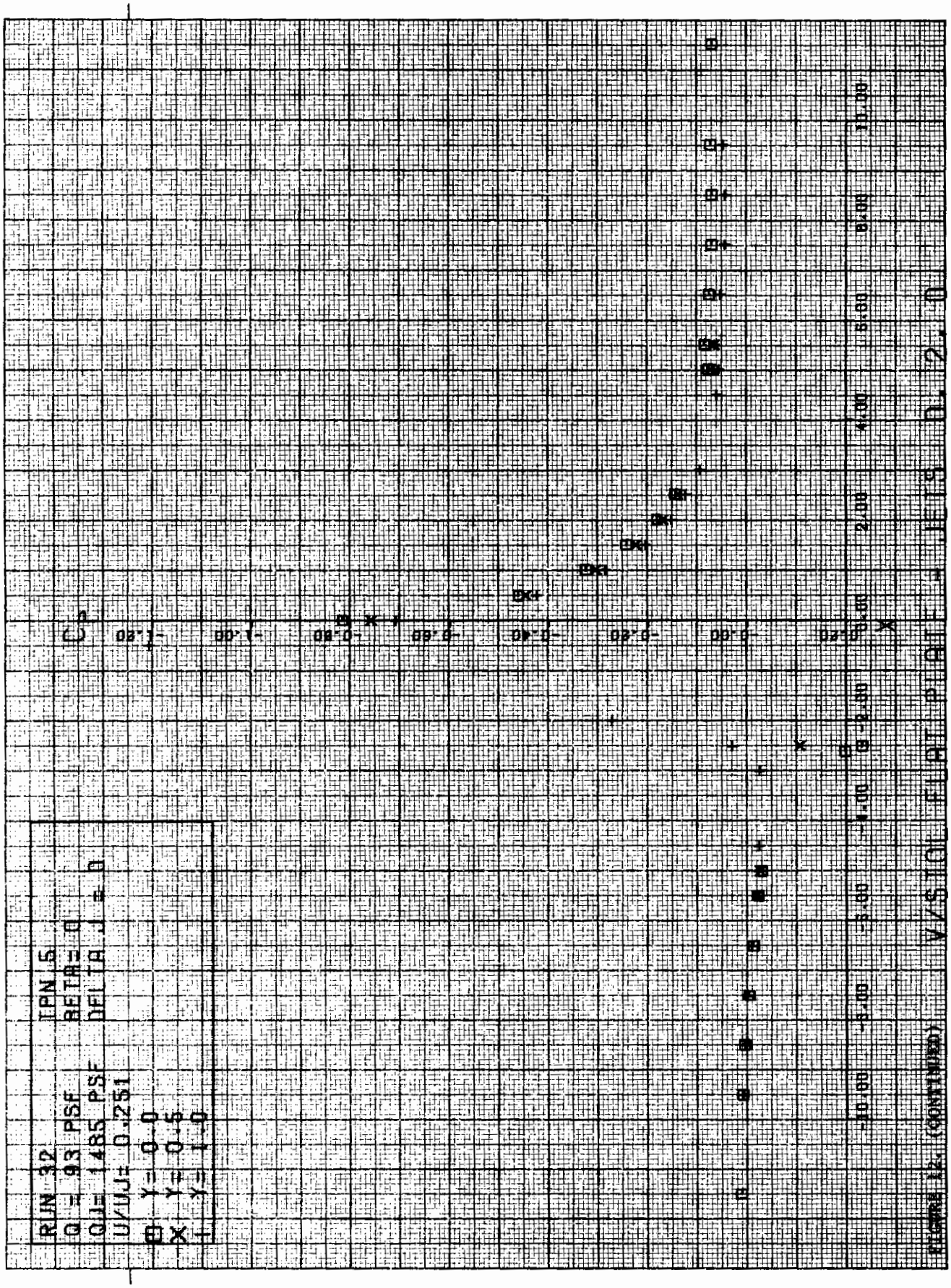

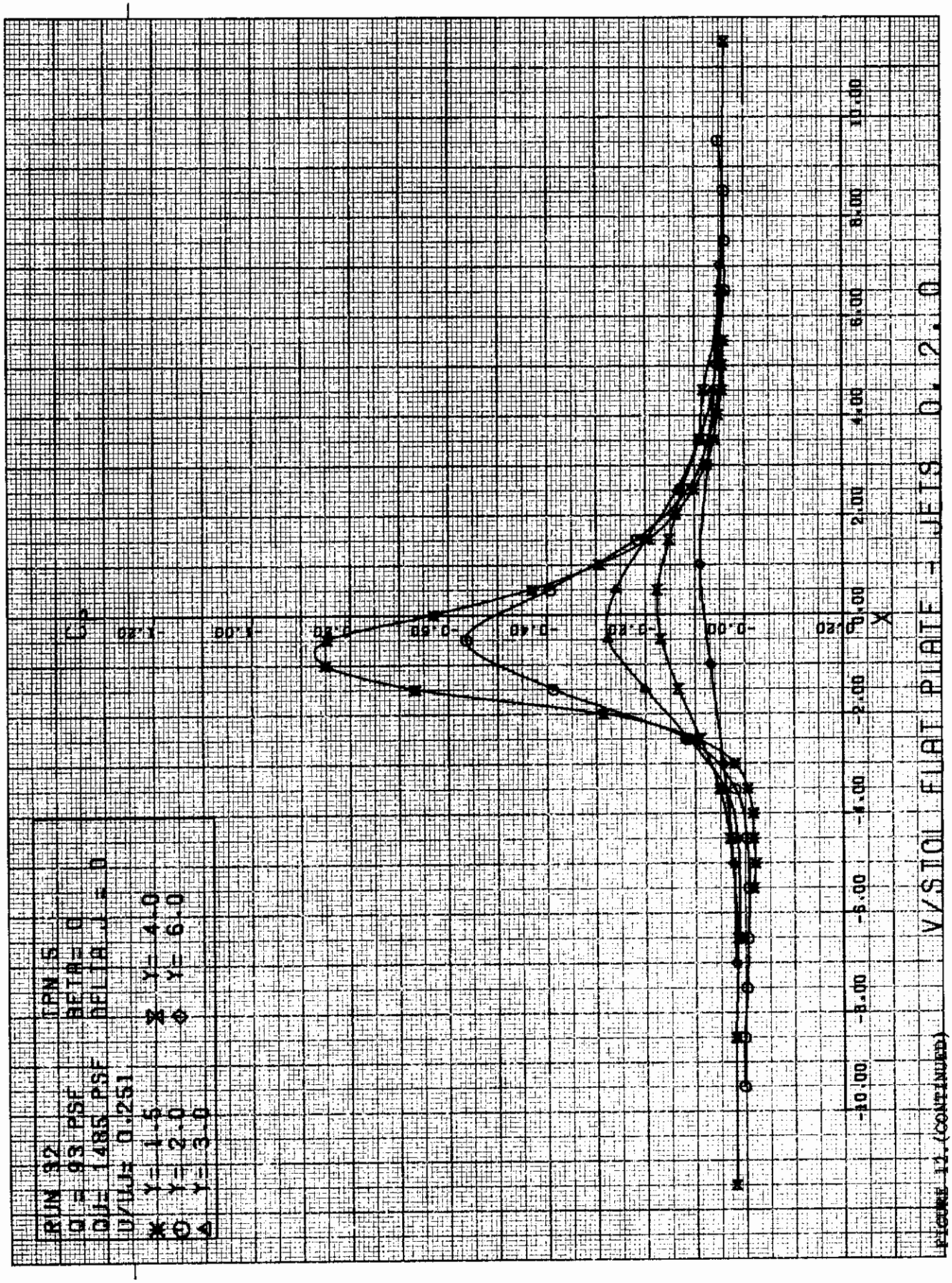

FIGURE 11.(CONTINUED)

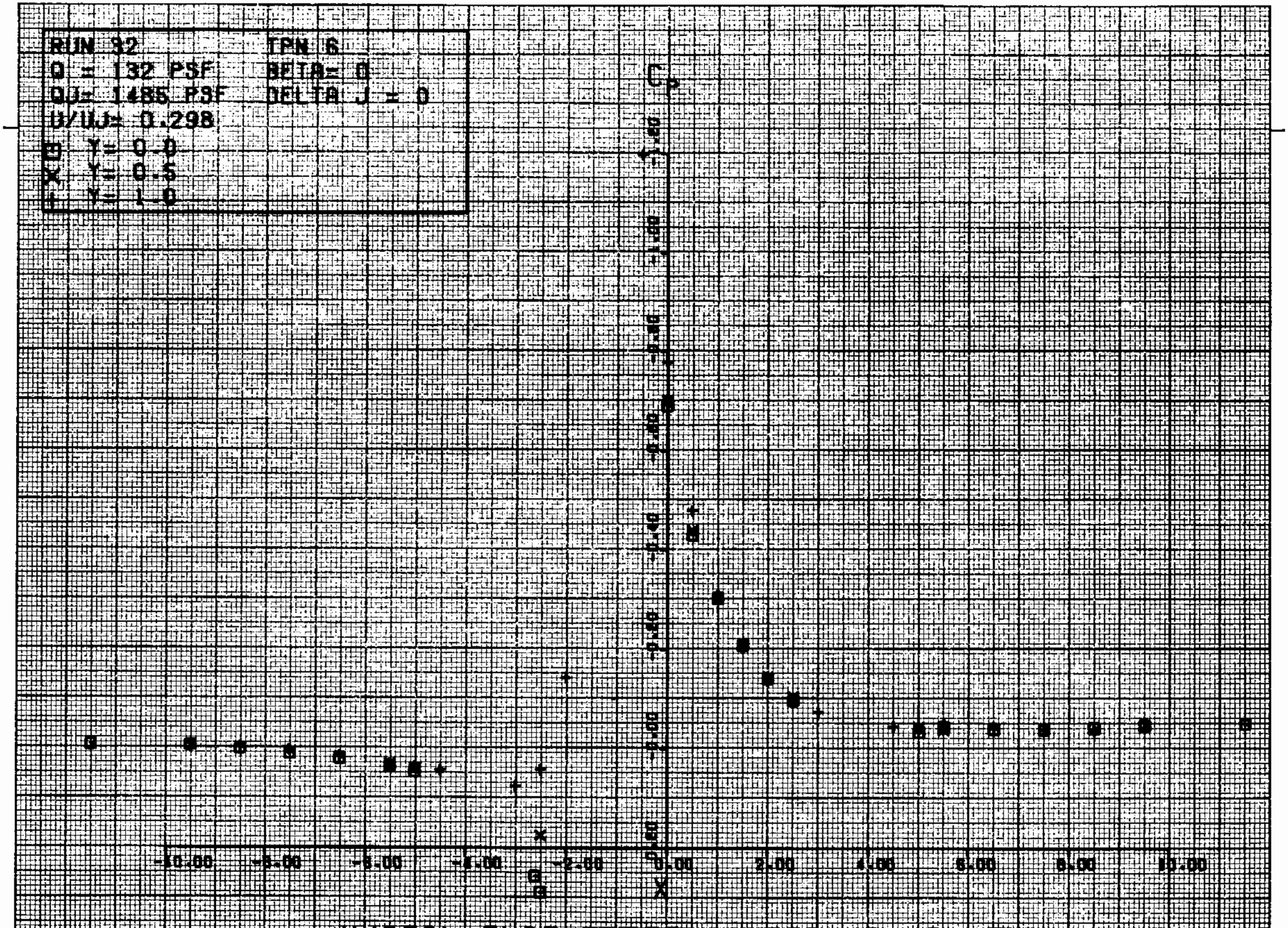

FIGURE 12. (CONTINUED) V/STOL FLAT PLATE - JETS D. 2. 0

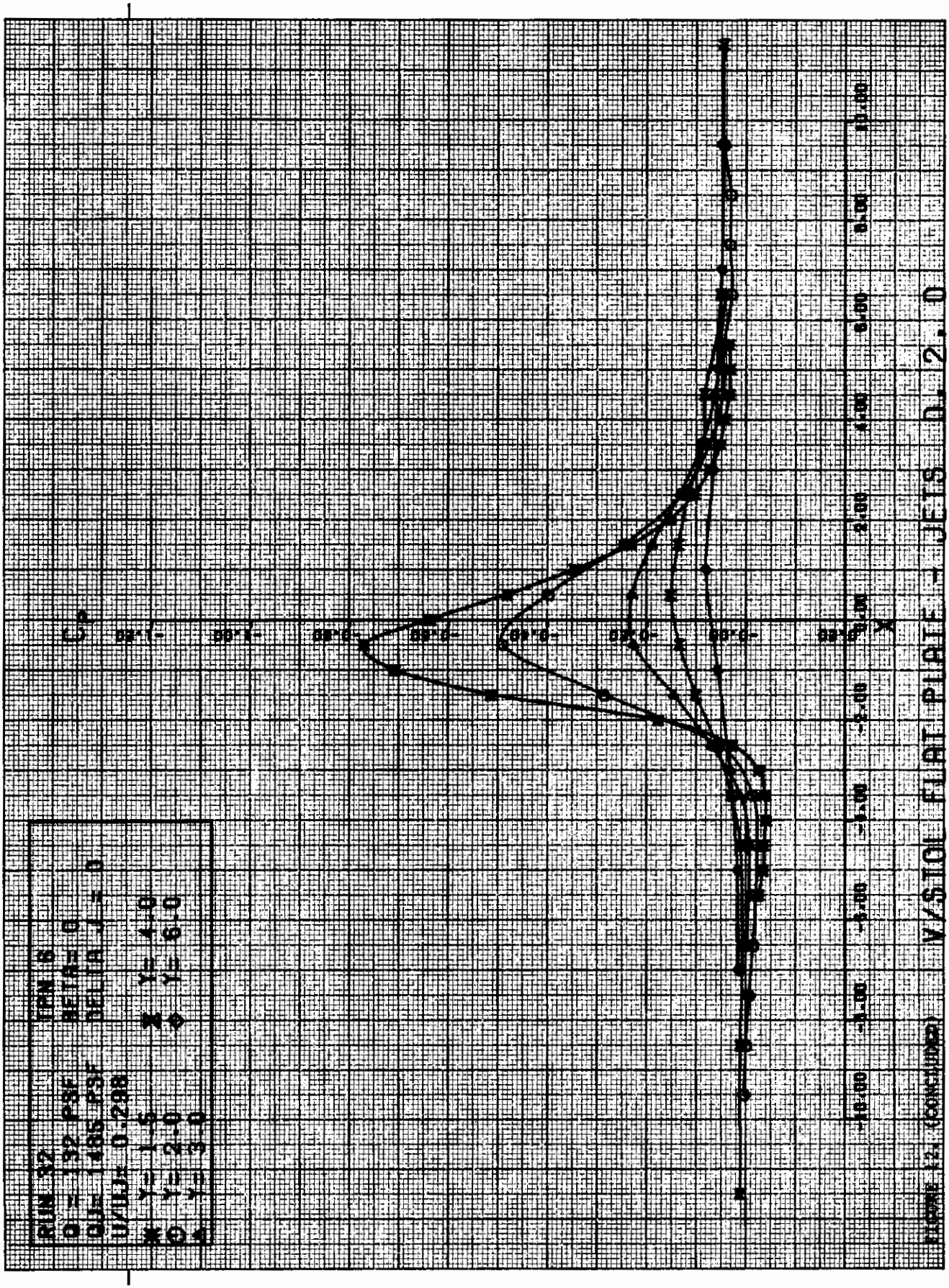

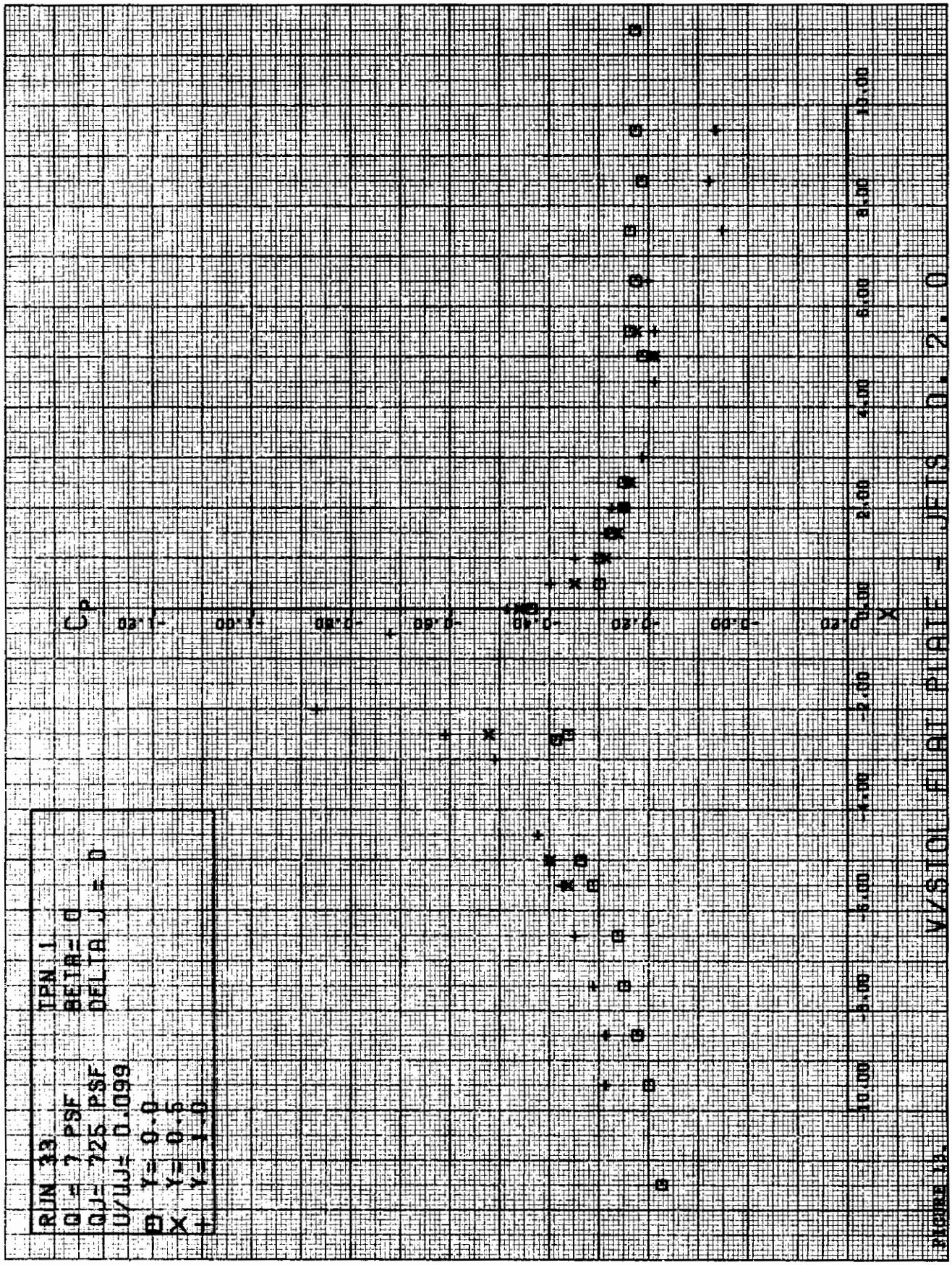

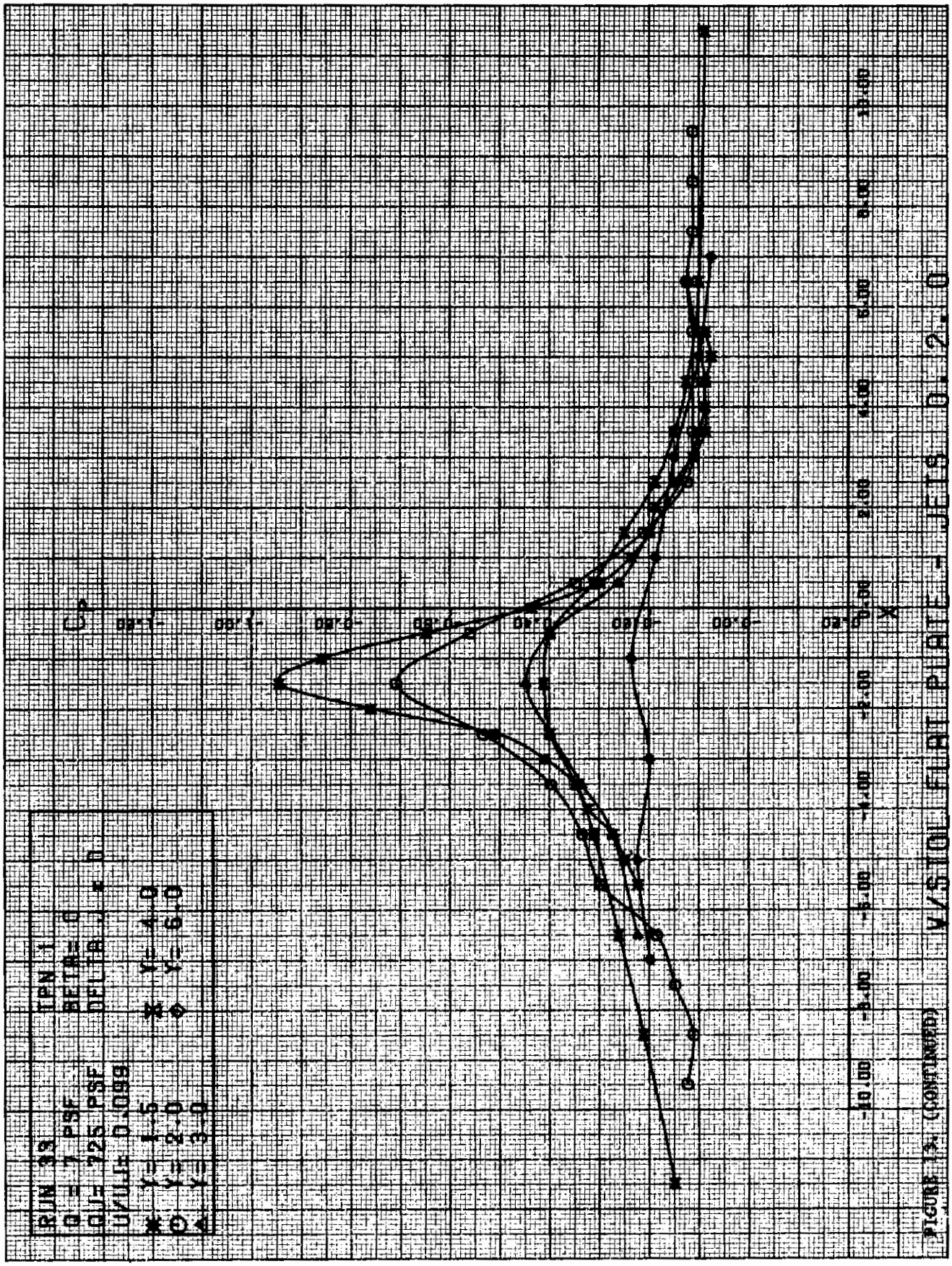

FIGURE 13. (CONTINUED) V/STOL FLAT PLATE - JETS 0. 2. 0

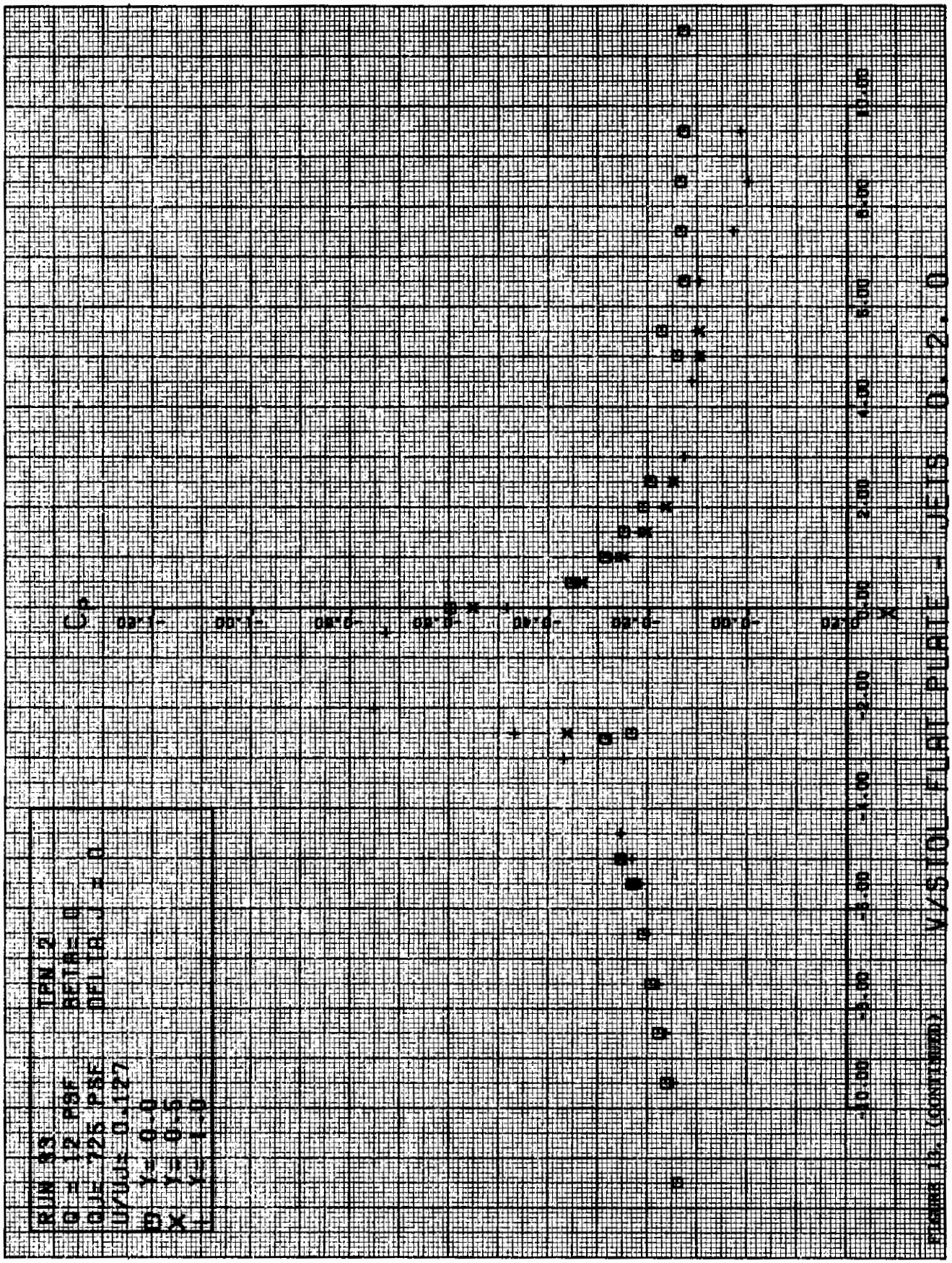

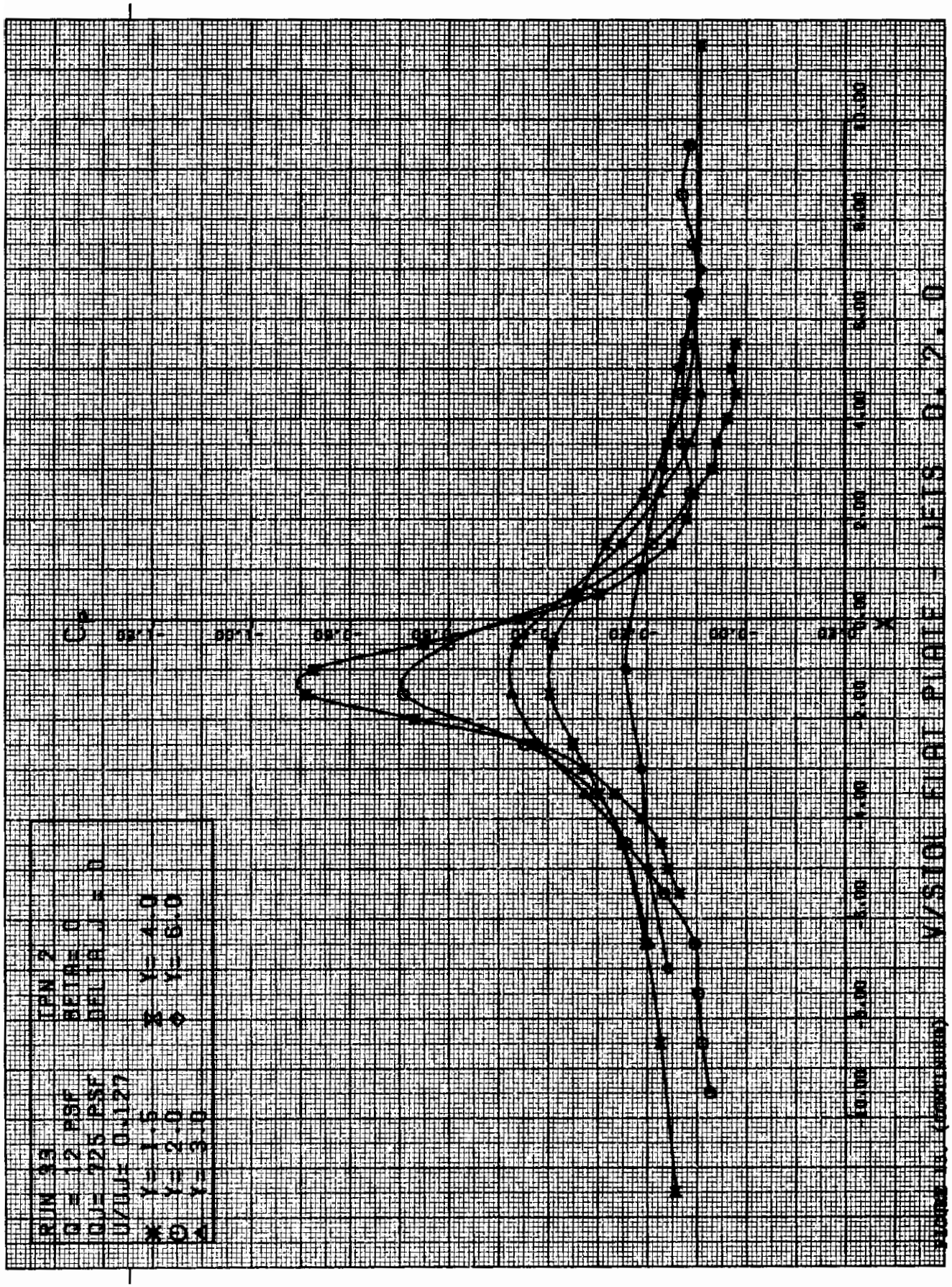

FIGURE 13. (CONTINUED) W/STOL FLAT PLATE + JETS α, 2, 0

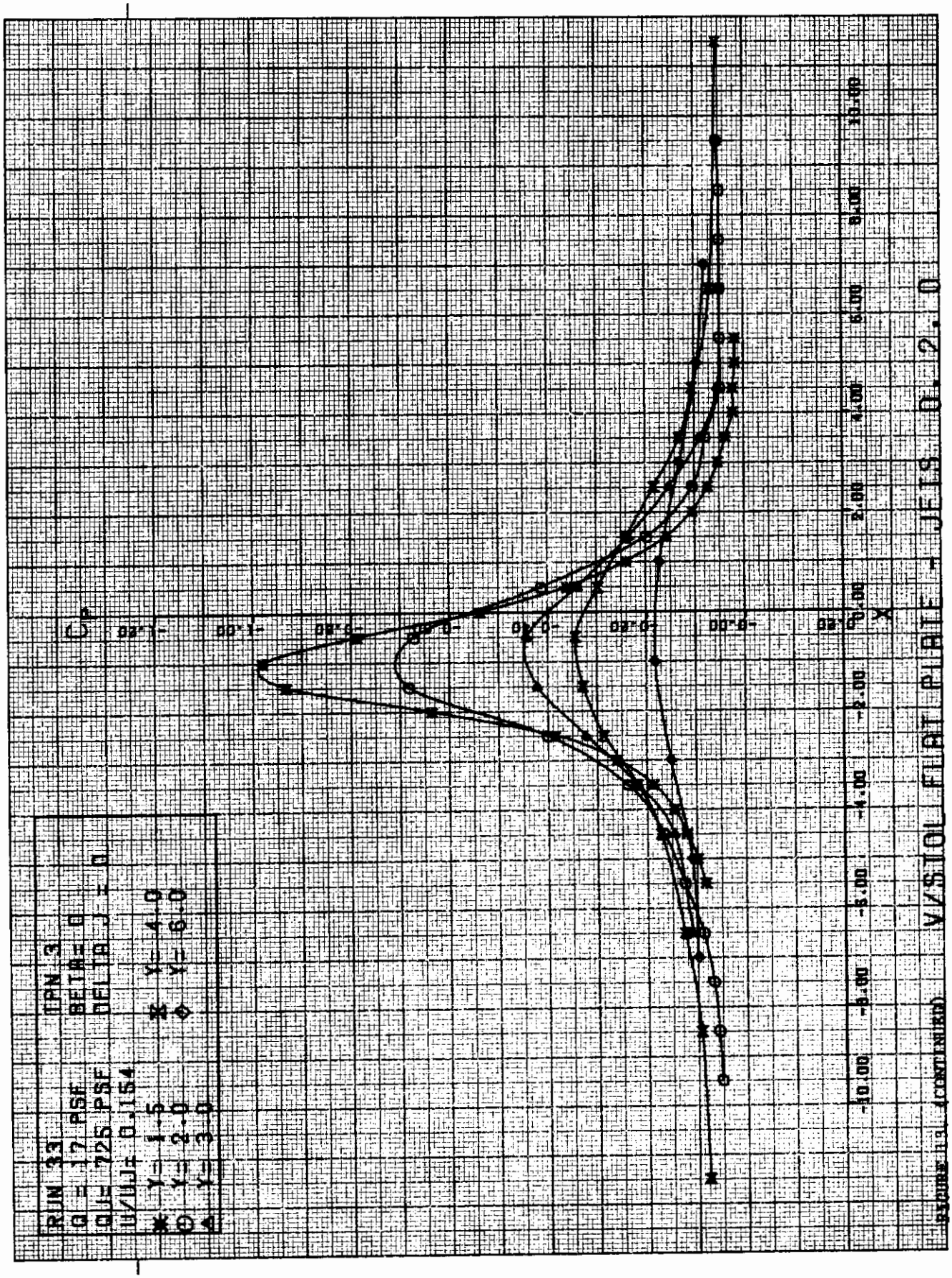

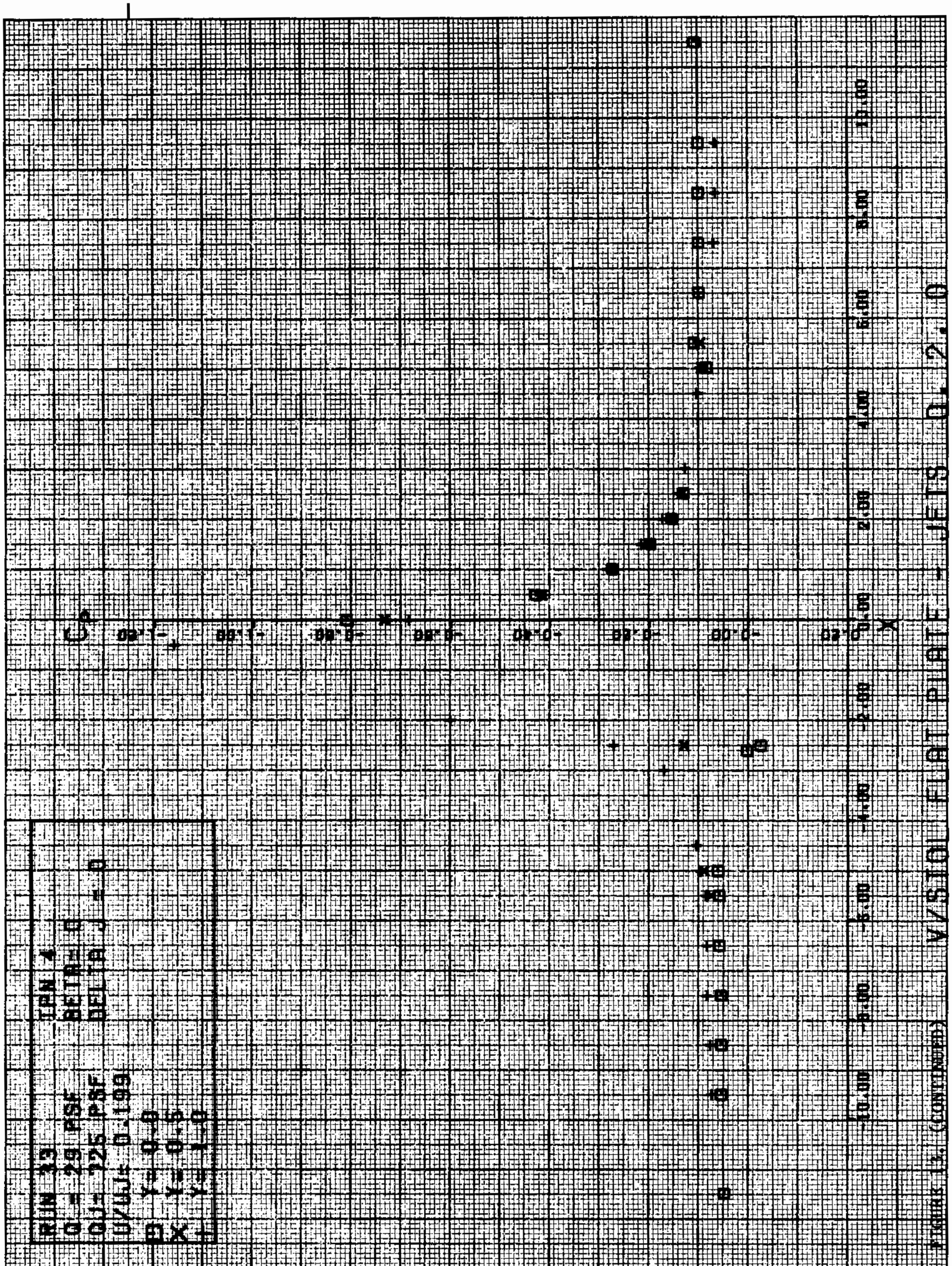

FIGURE 13. (CONTINUED)

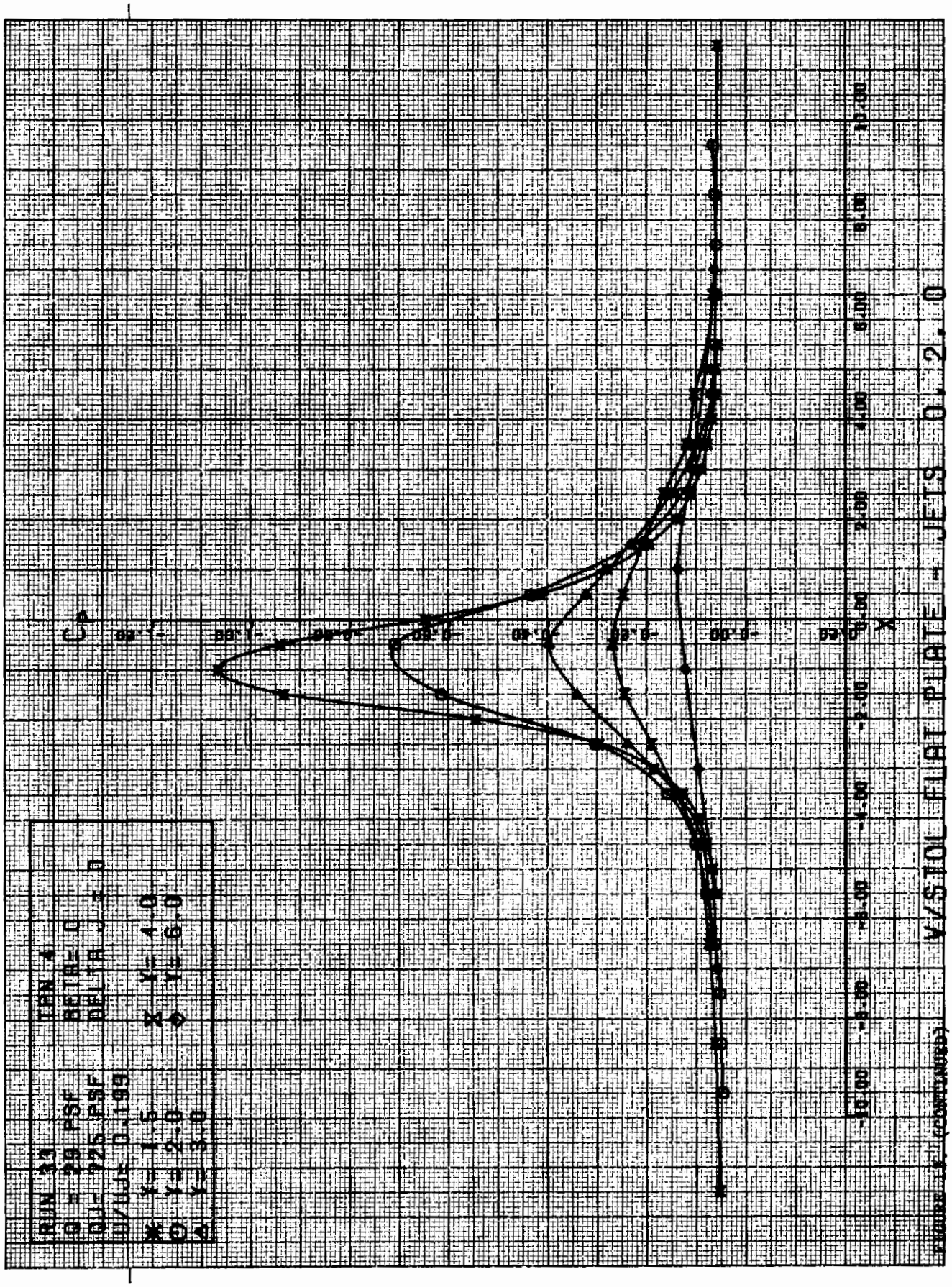

FIGURE 35 (CONTINUED)

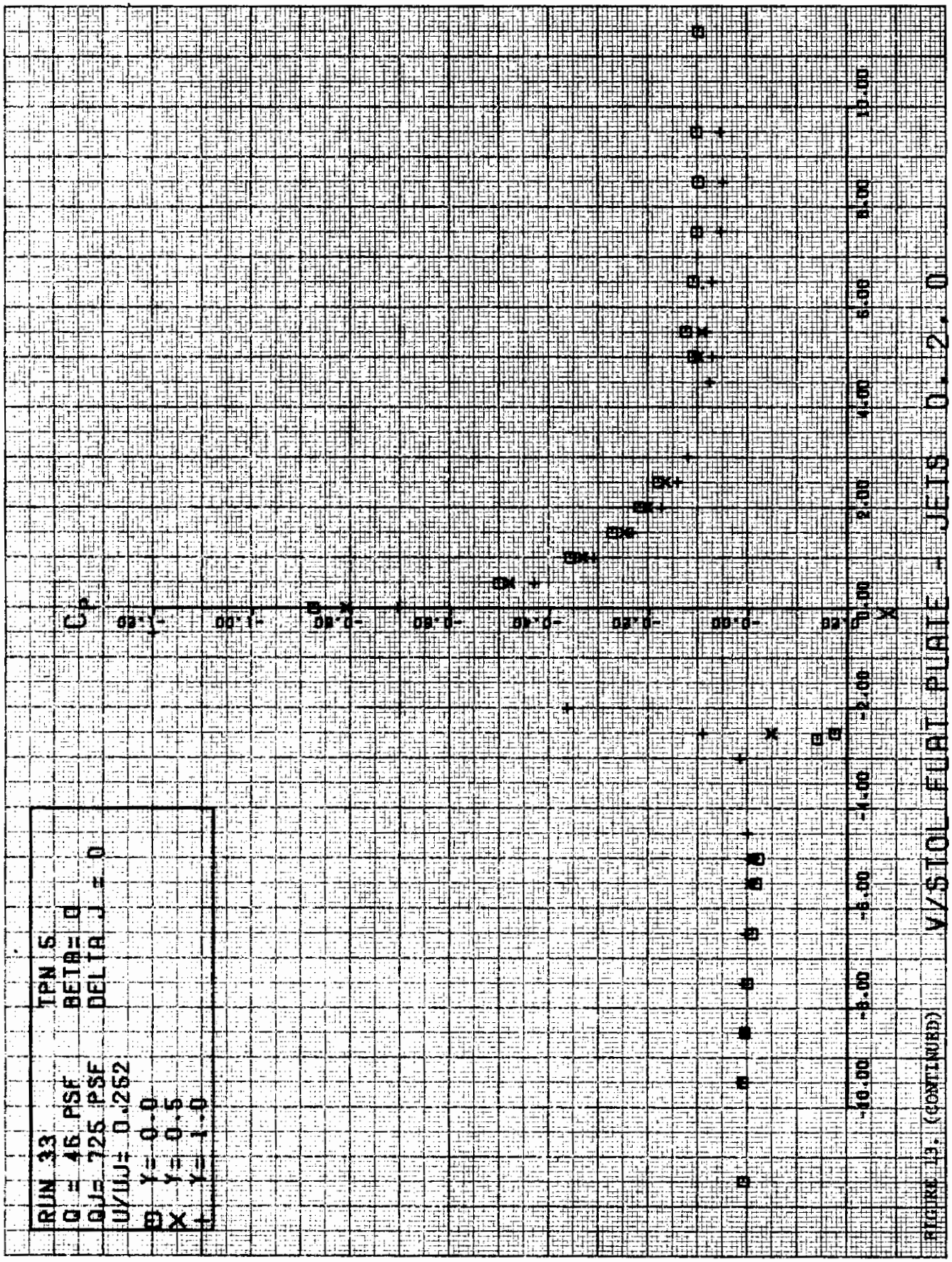

FIGURE 13. (CONTINUED)

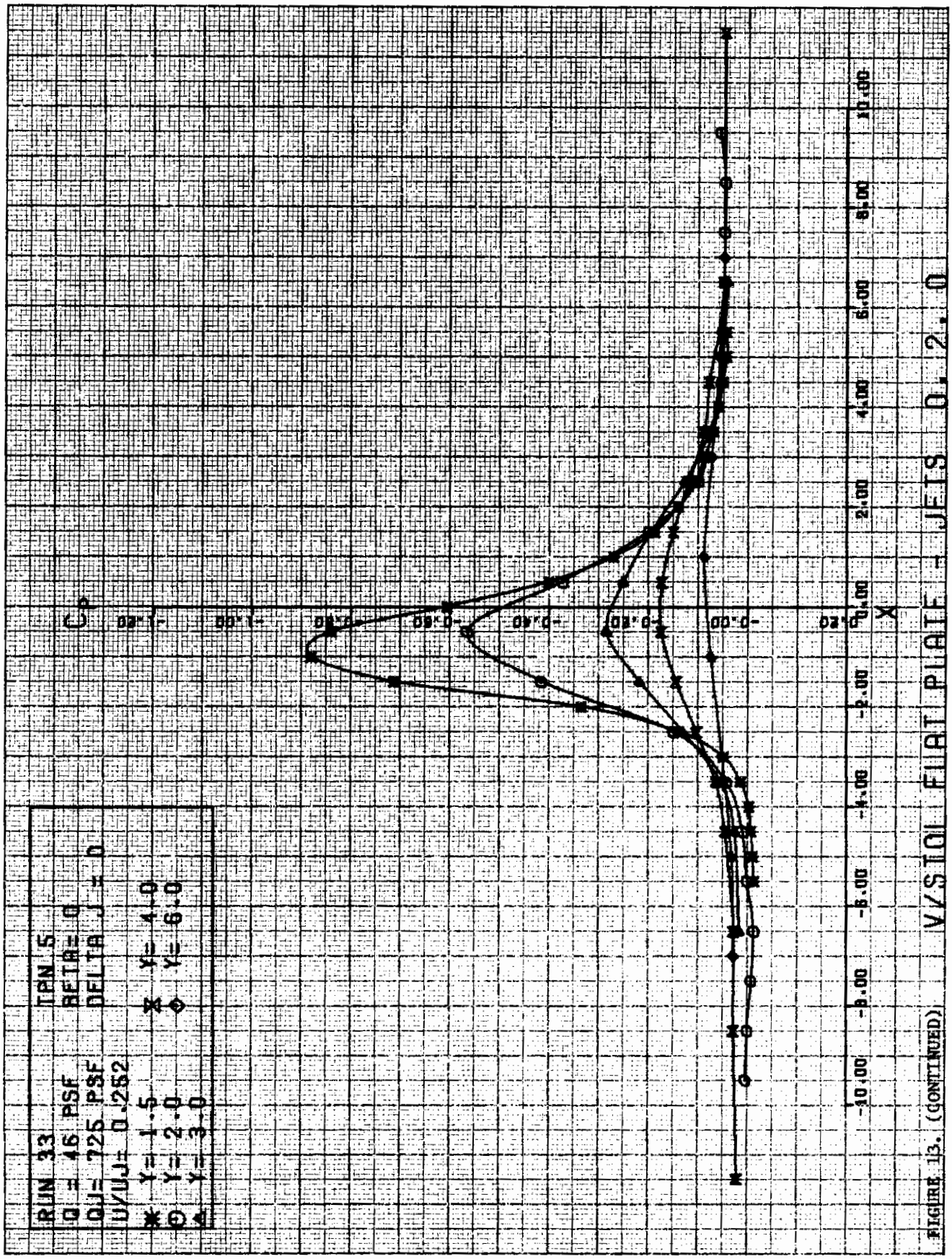

FIGURE 13. (CONTINUED) V/STOL FLAT PLATE - JETS 0, 2, 0

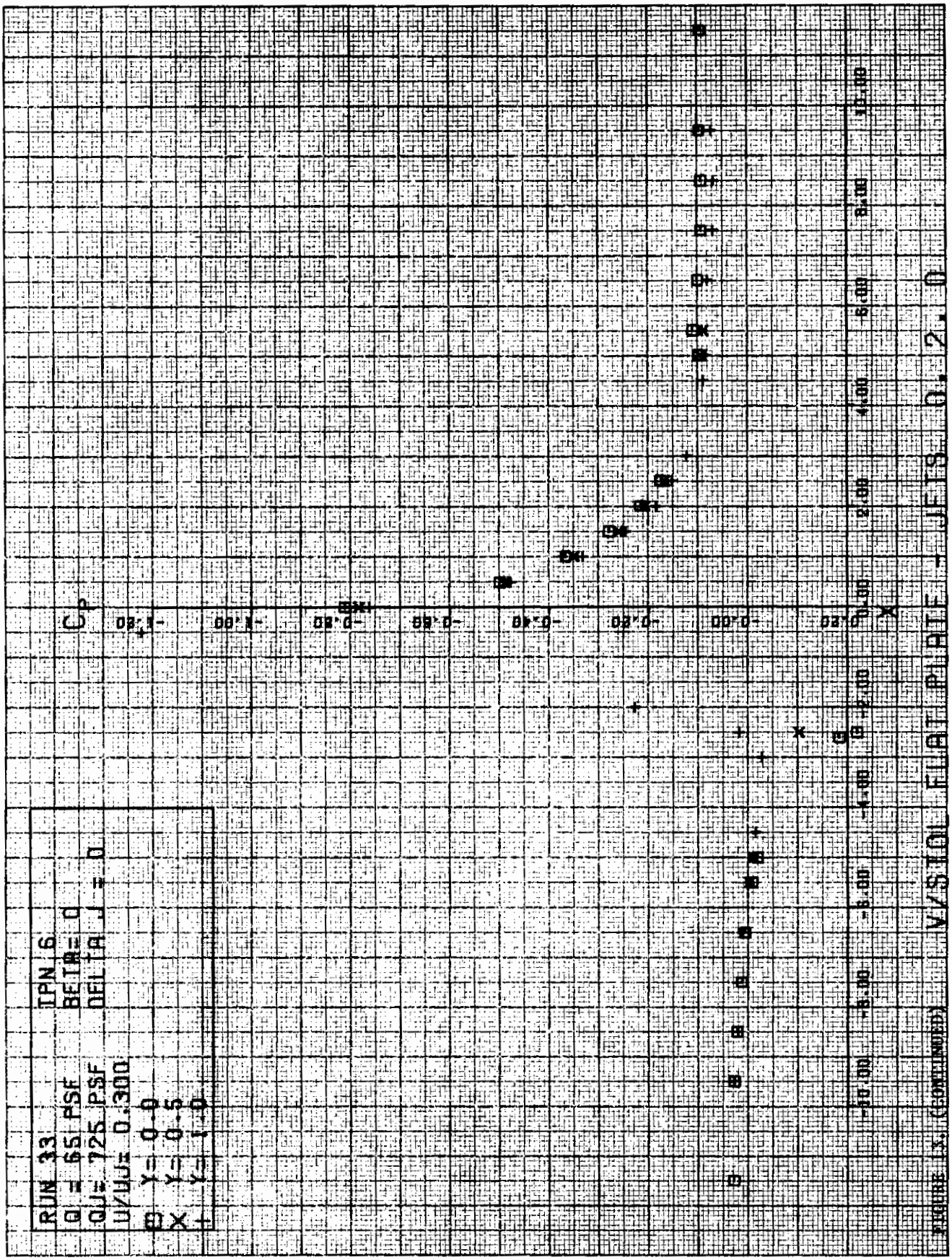

FIGURE 13. (CONCLUDED)

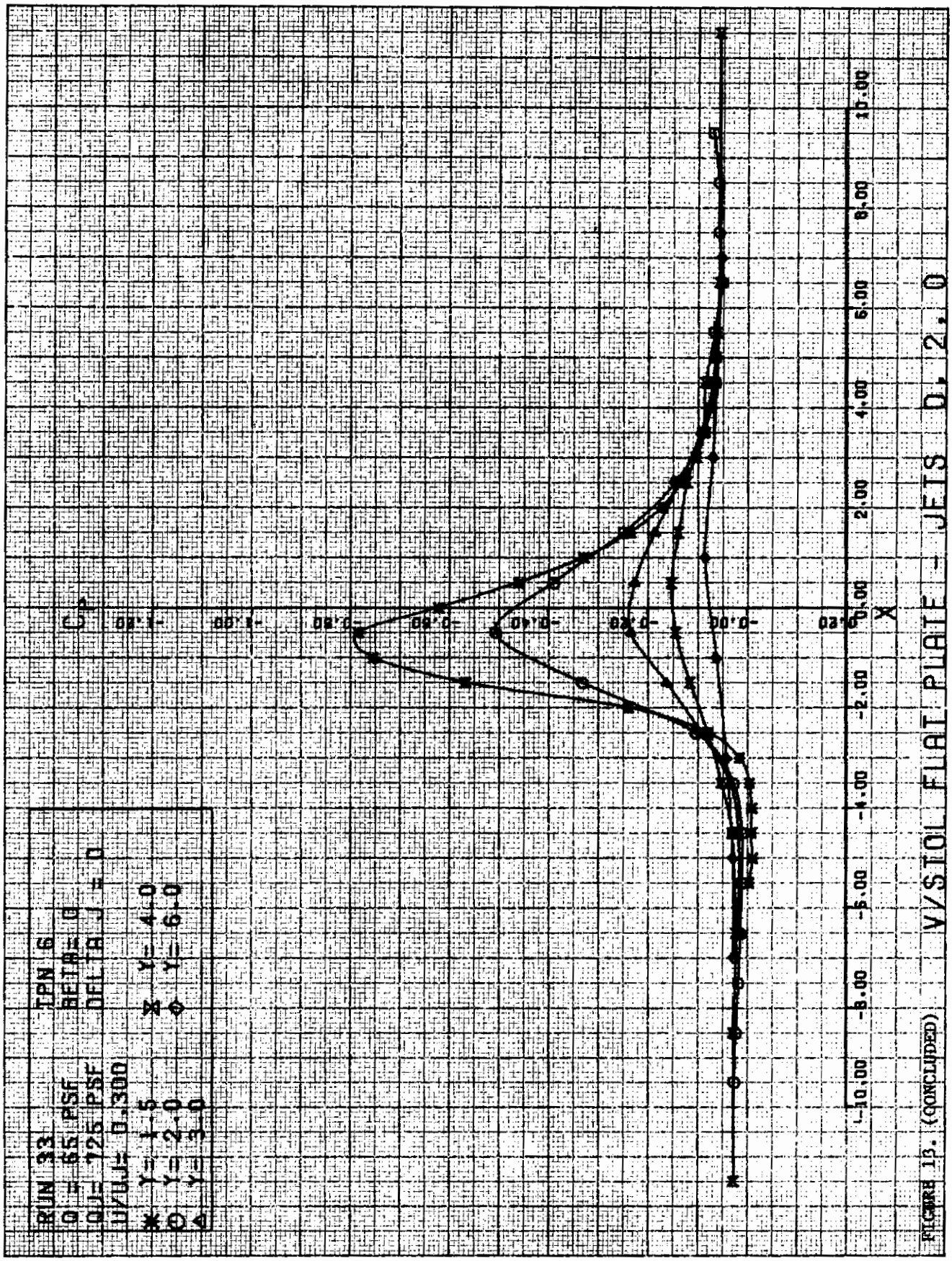

FIGURE 13. (CONCLUDED)

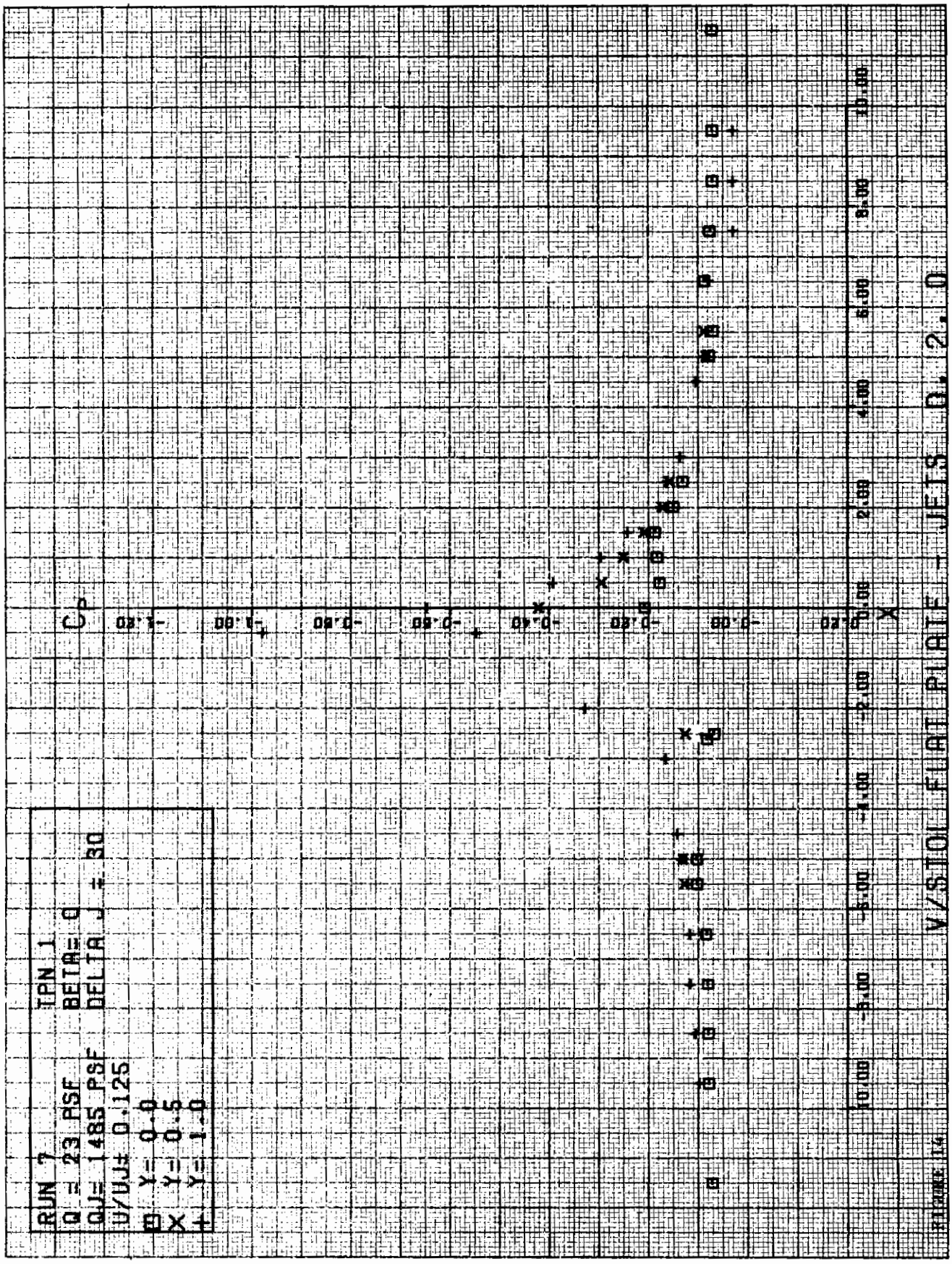

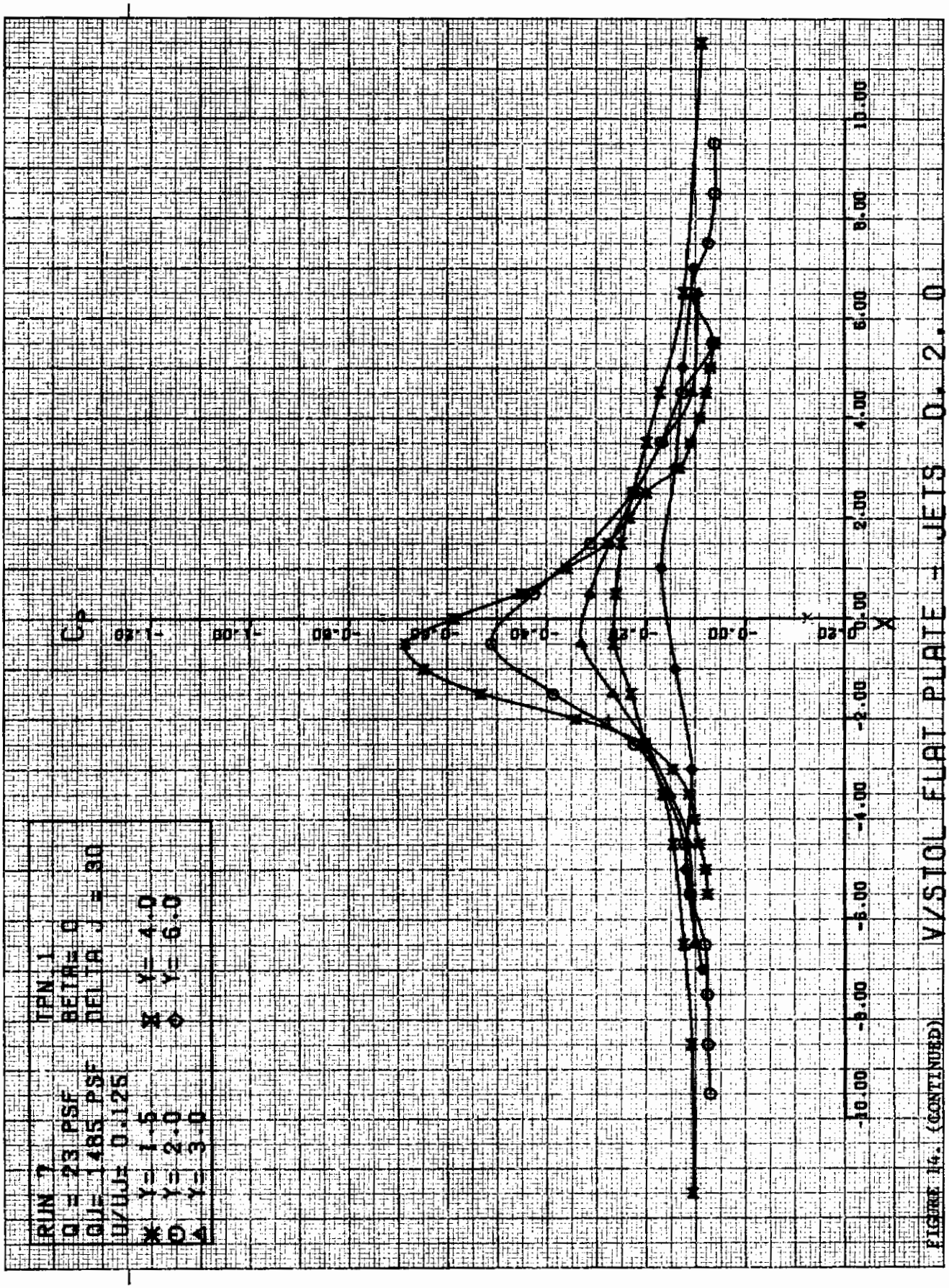

FIGURE 14. (CONTINUED)

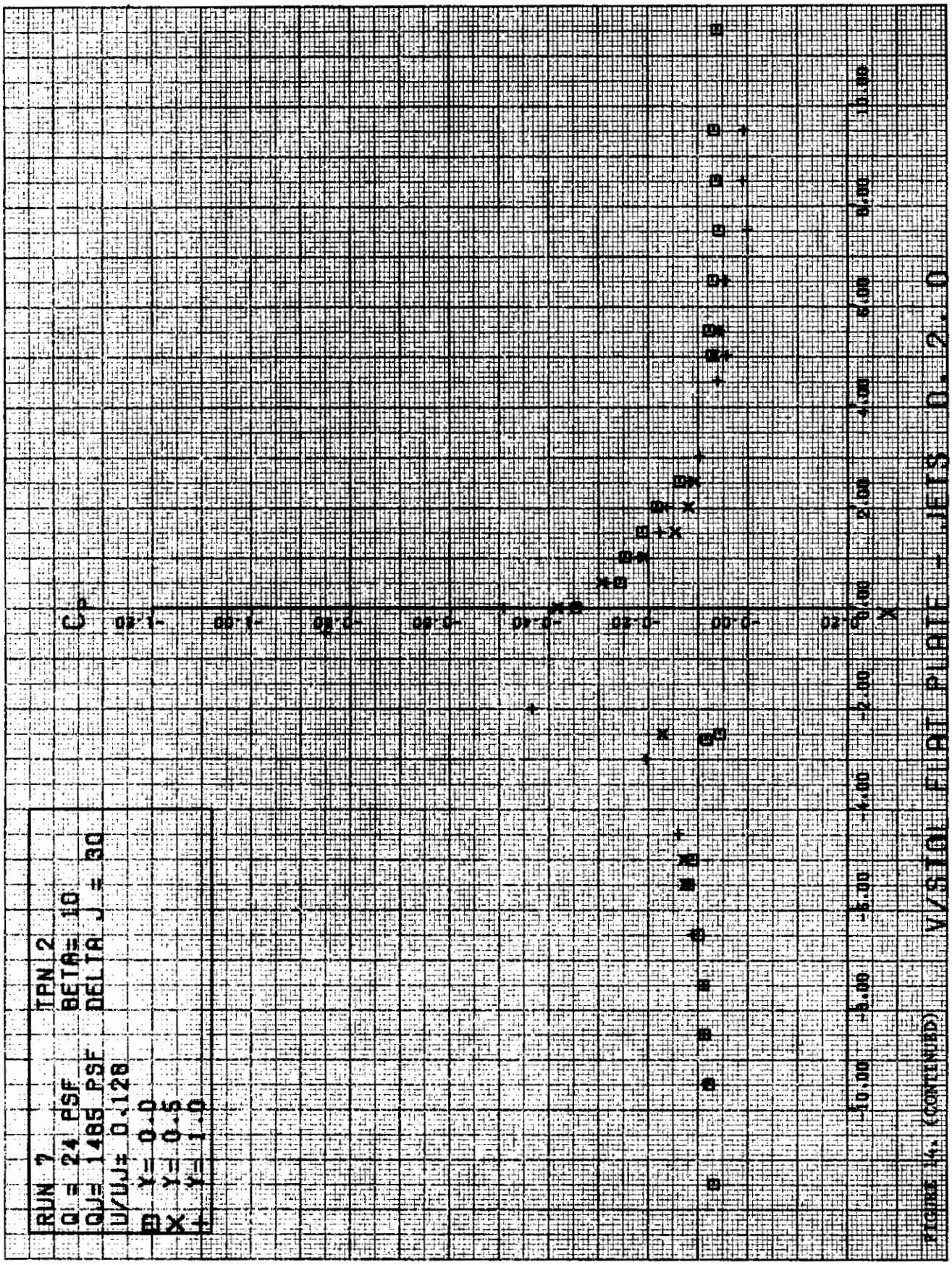

FIGURE 44. (CONTINUED)

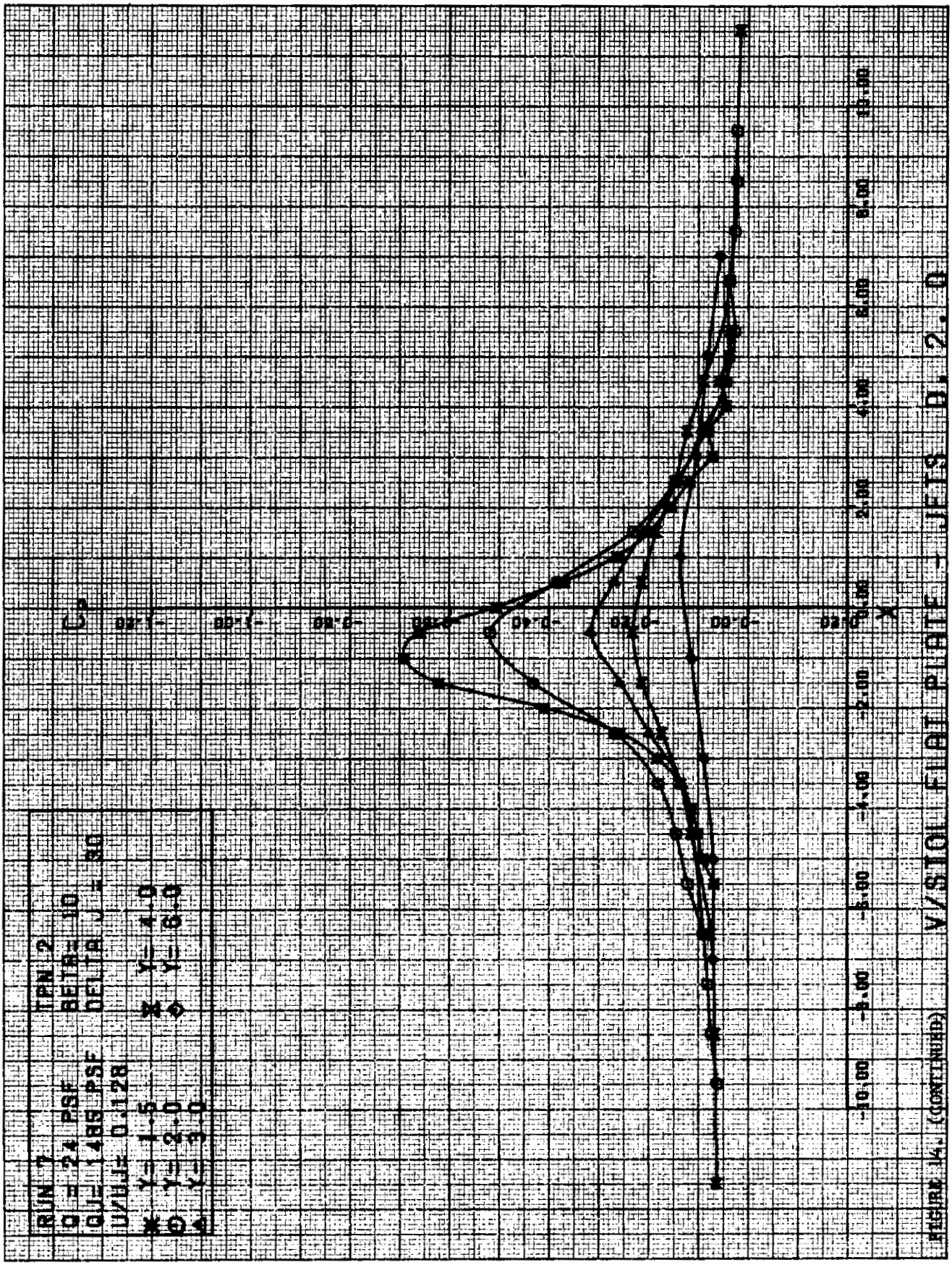

FIGURE 14. (CONTINUED) V/STOL FLAT PLATE - JETS D, 2, D

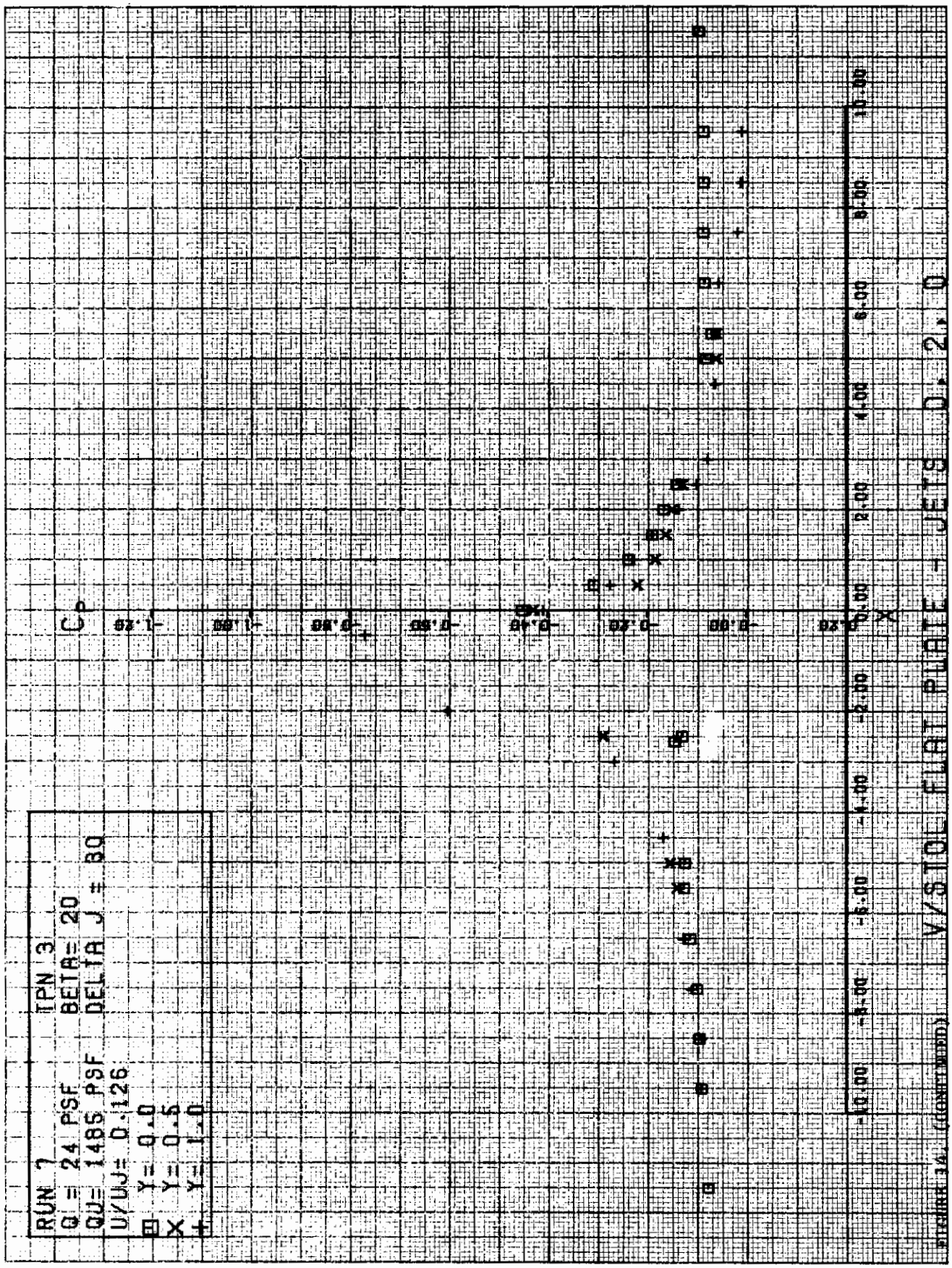

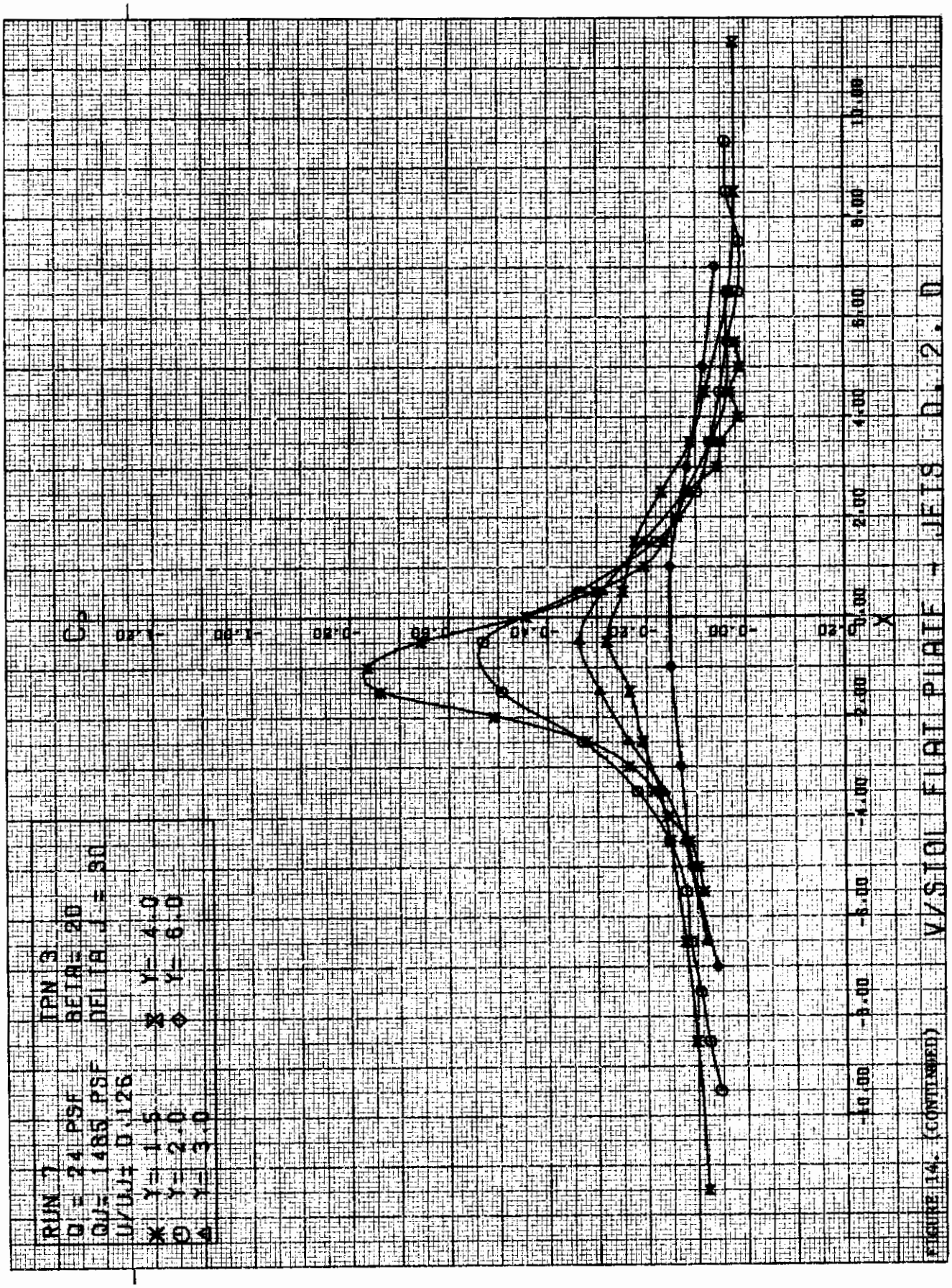

FIGURE 14. (CONTINUED)

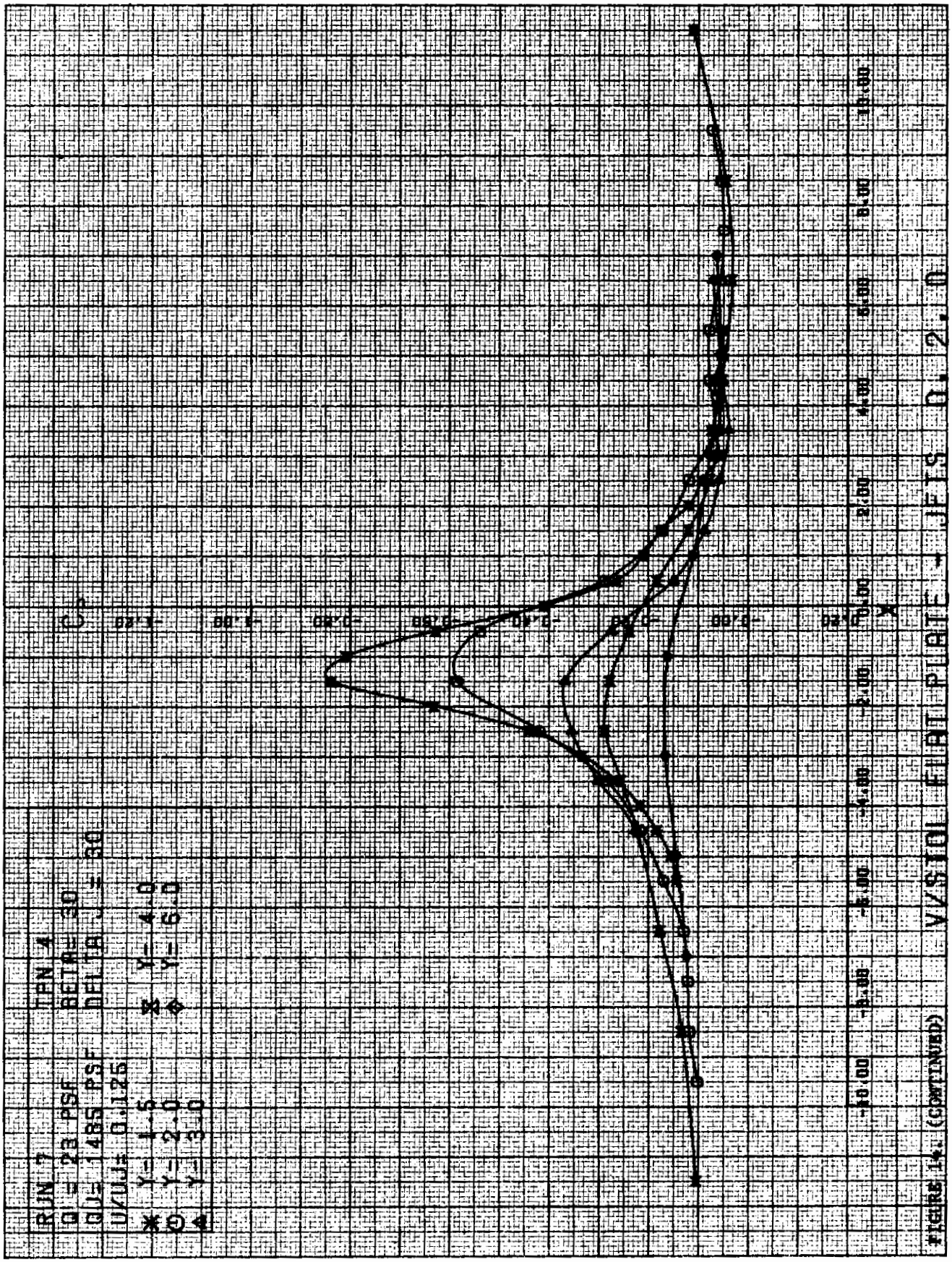

FIGURE 14. (CONTINUED) V/STOL FLAT PLATE + JETS Q, 2, 0

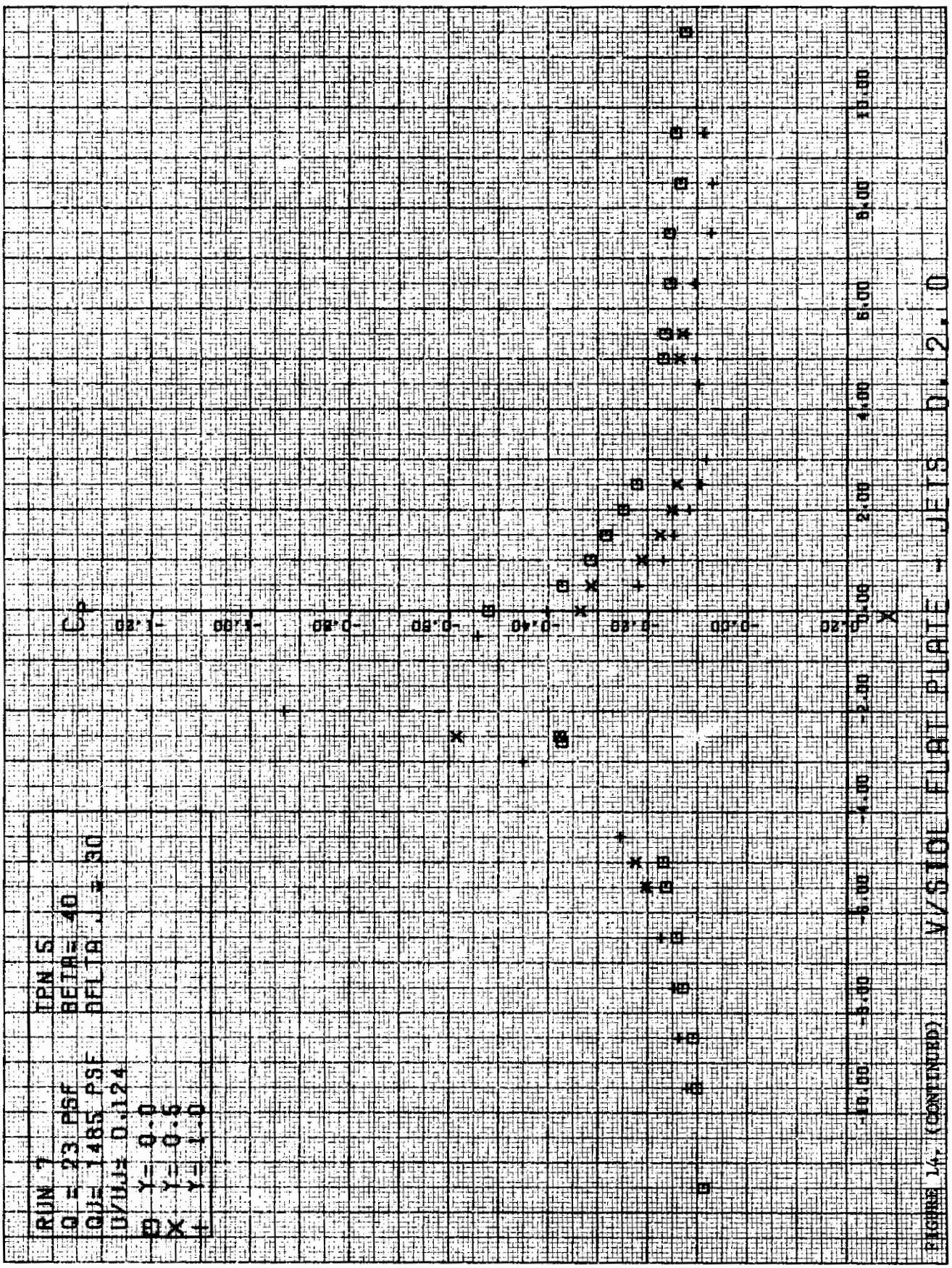

FIGURE 14. (CONTINUED) V/STOL FLAT PLATE + JETS 0. 2. 0

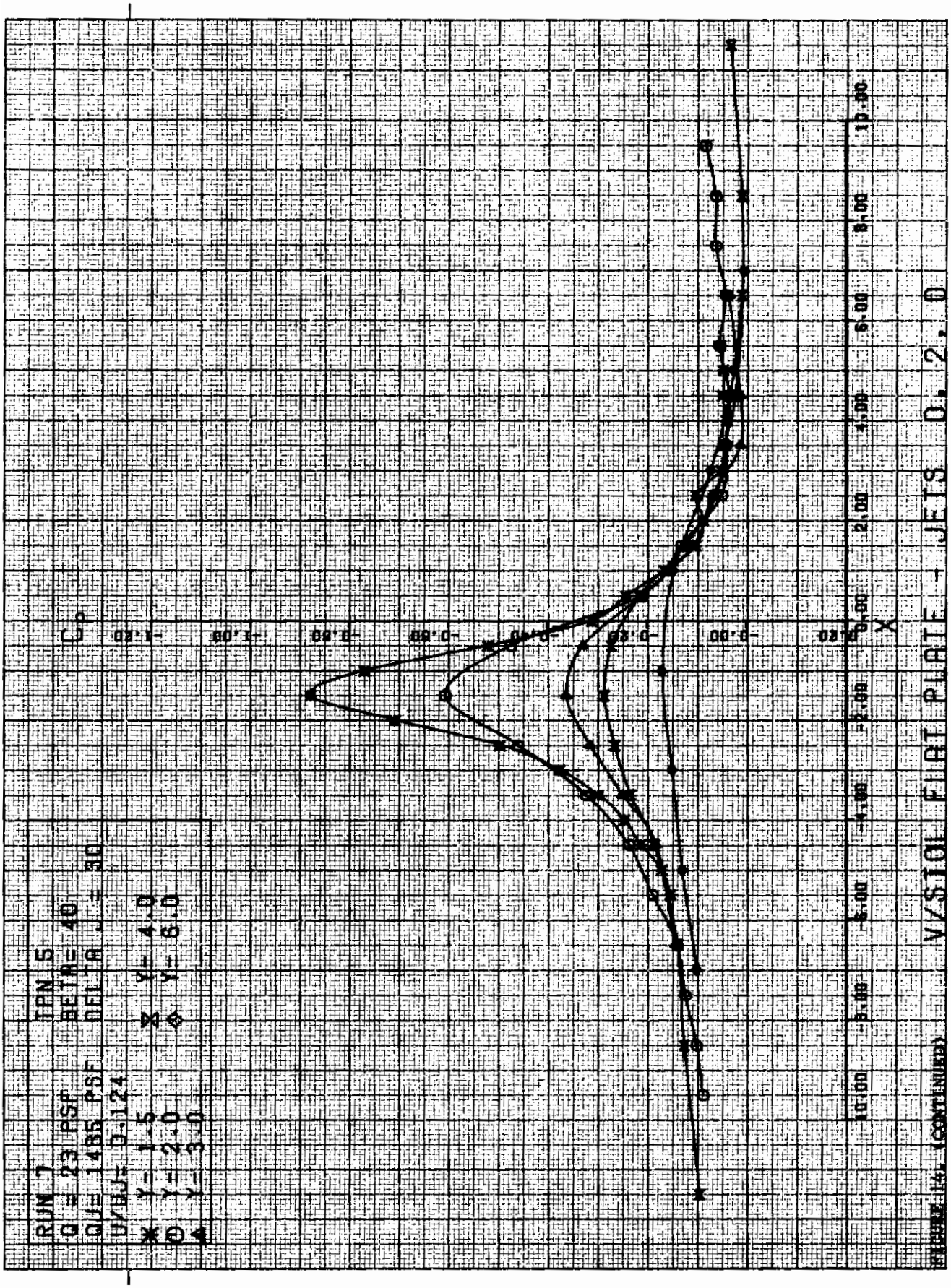

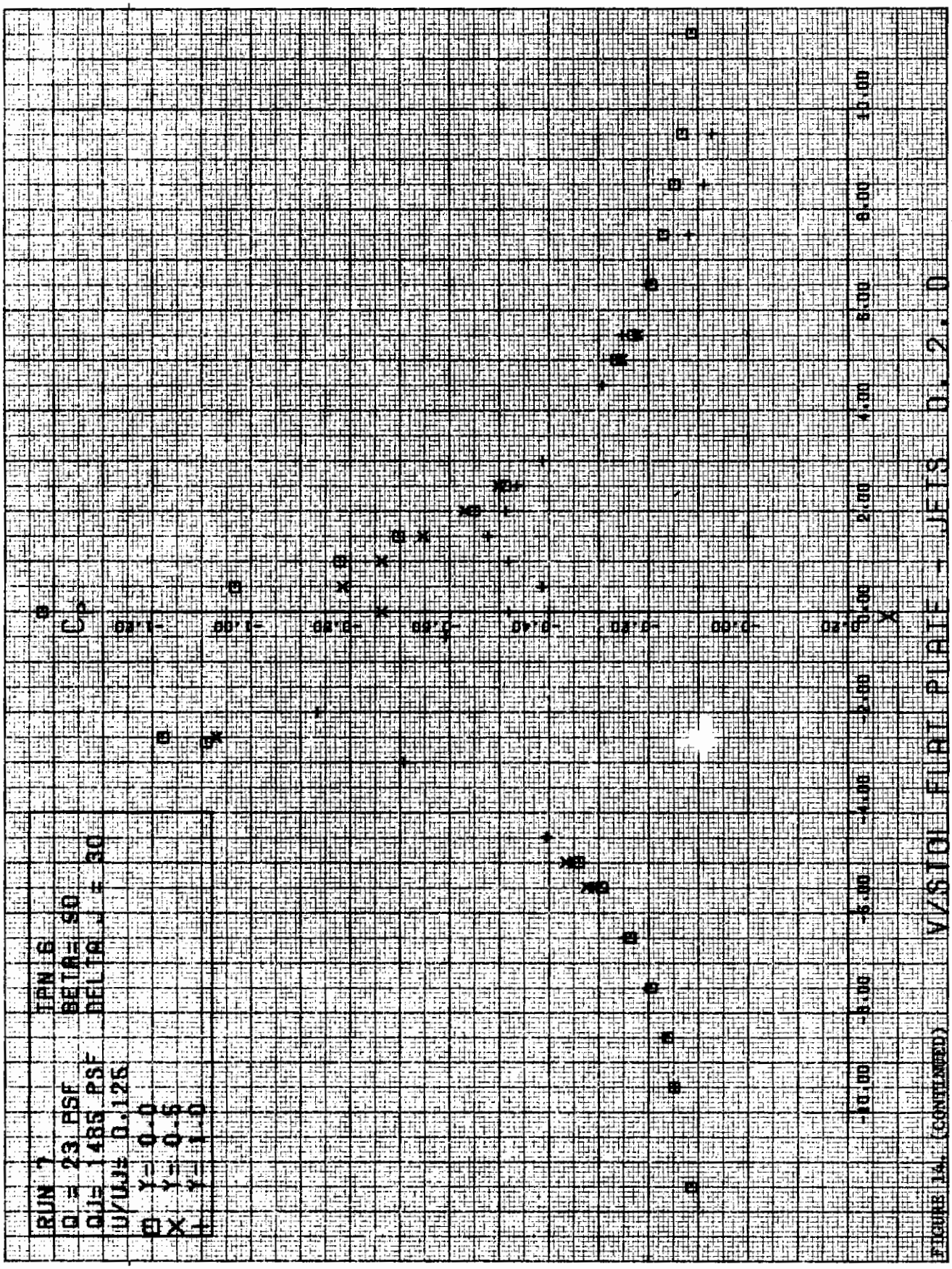

FIGURE 14. (CONTINUED)

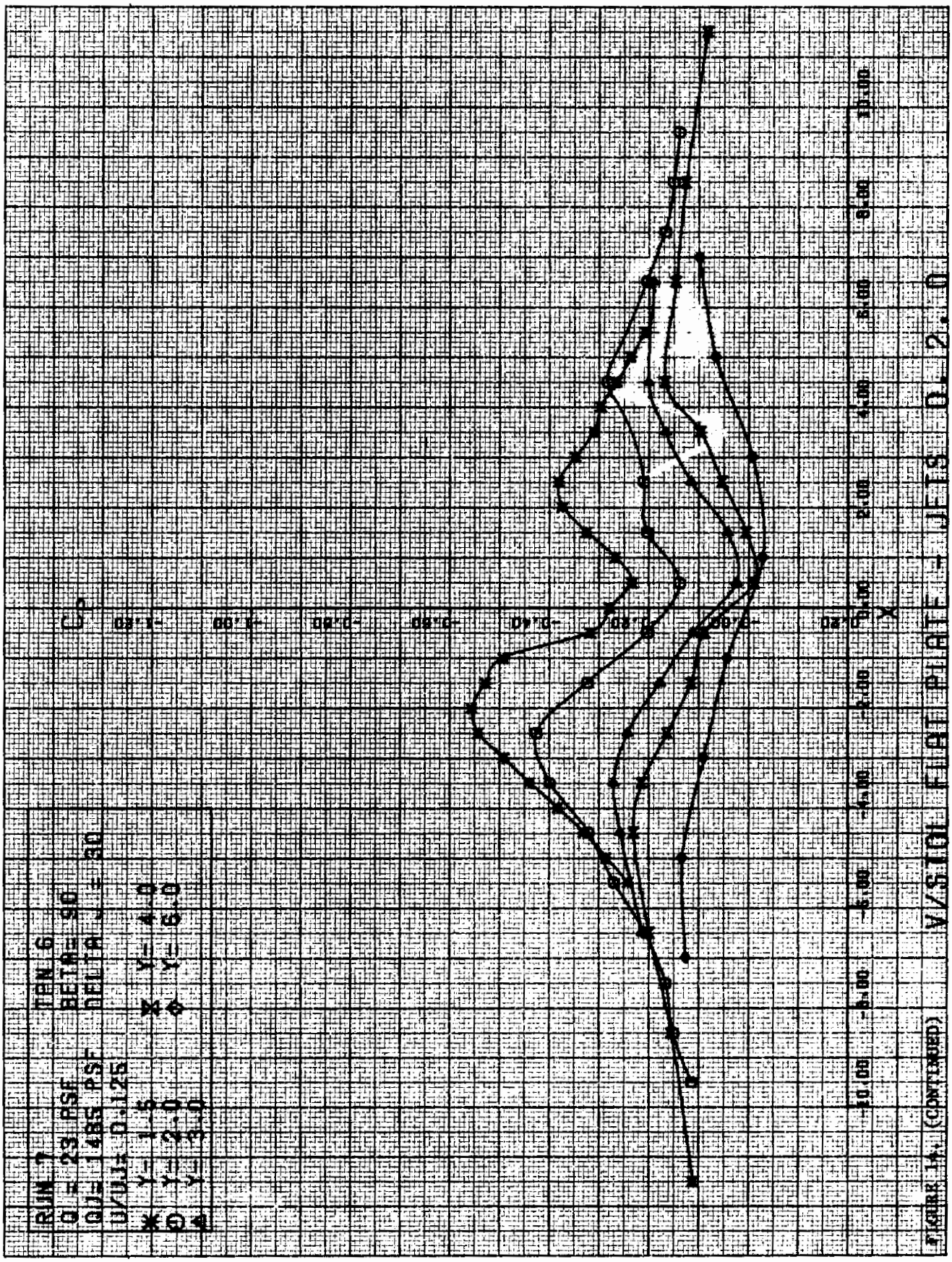

FIGURE 14. (CONTINUED)

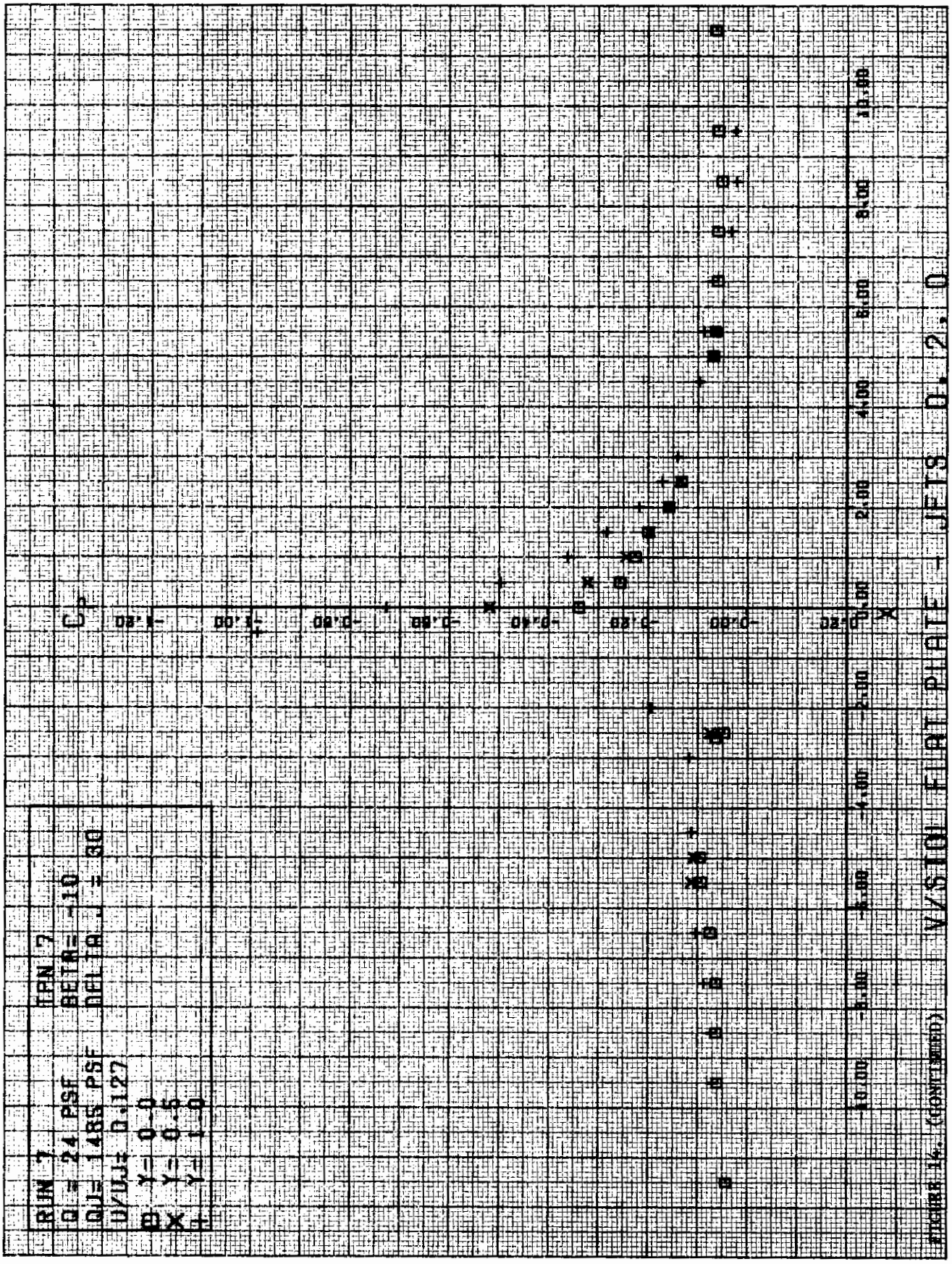

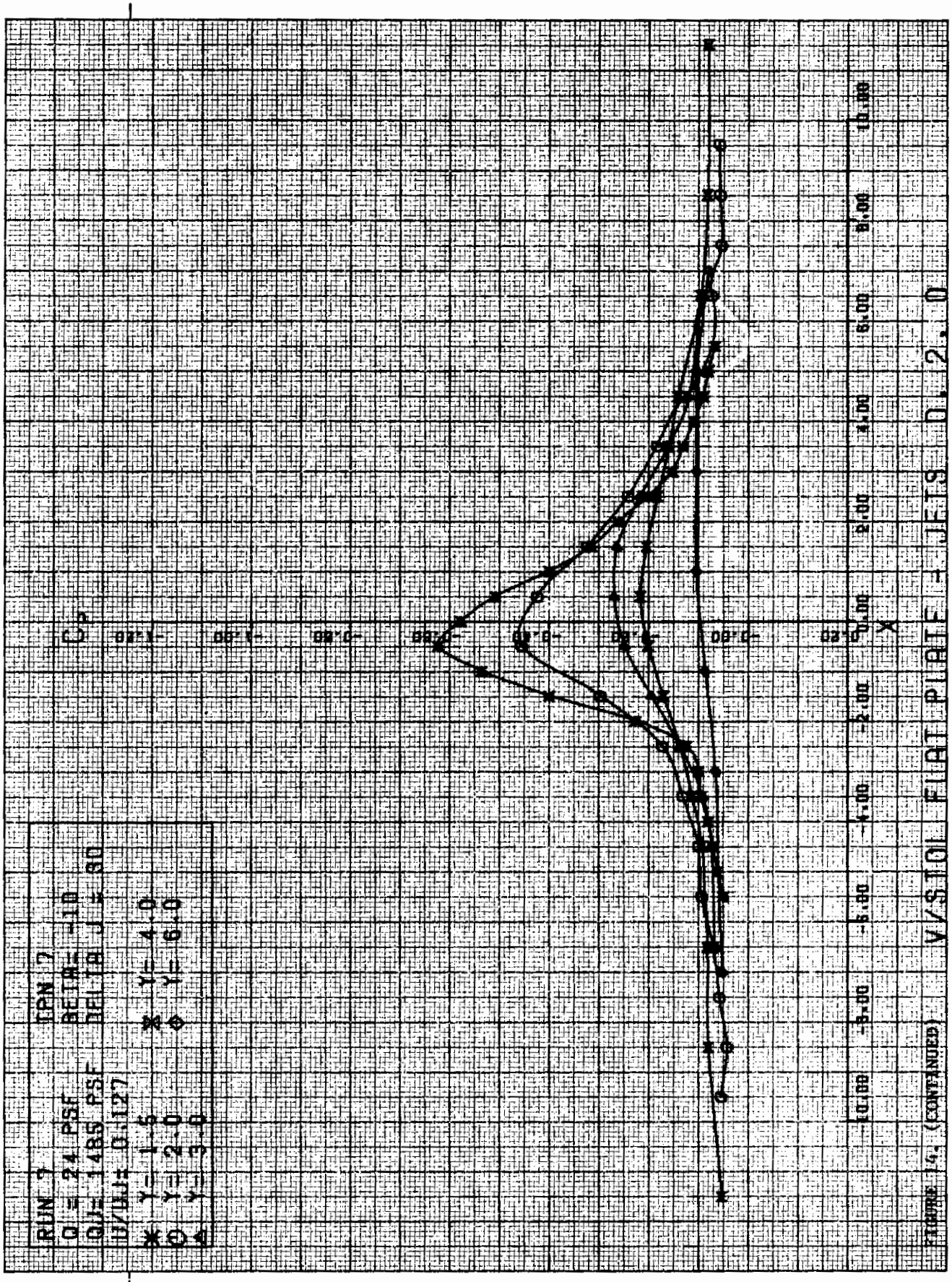

FIGURE 14. (CONTINUED)

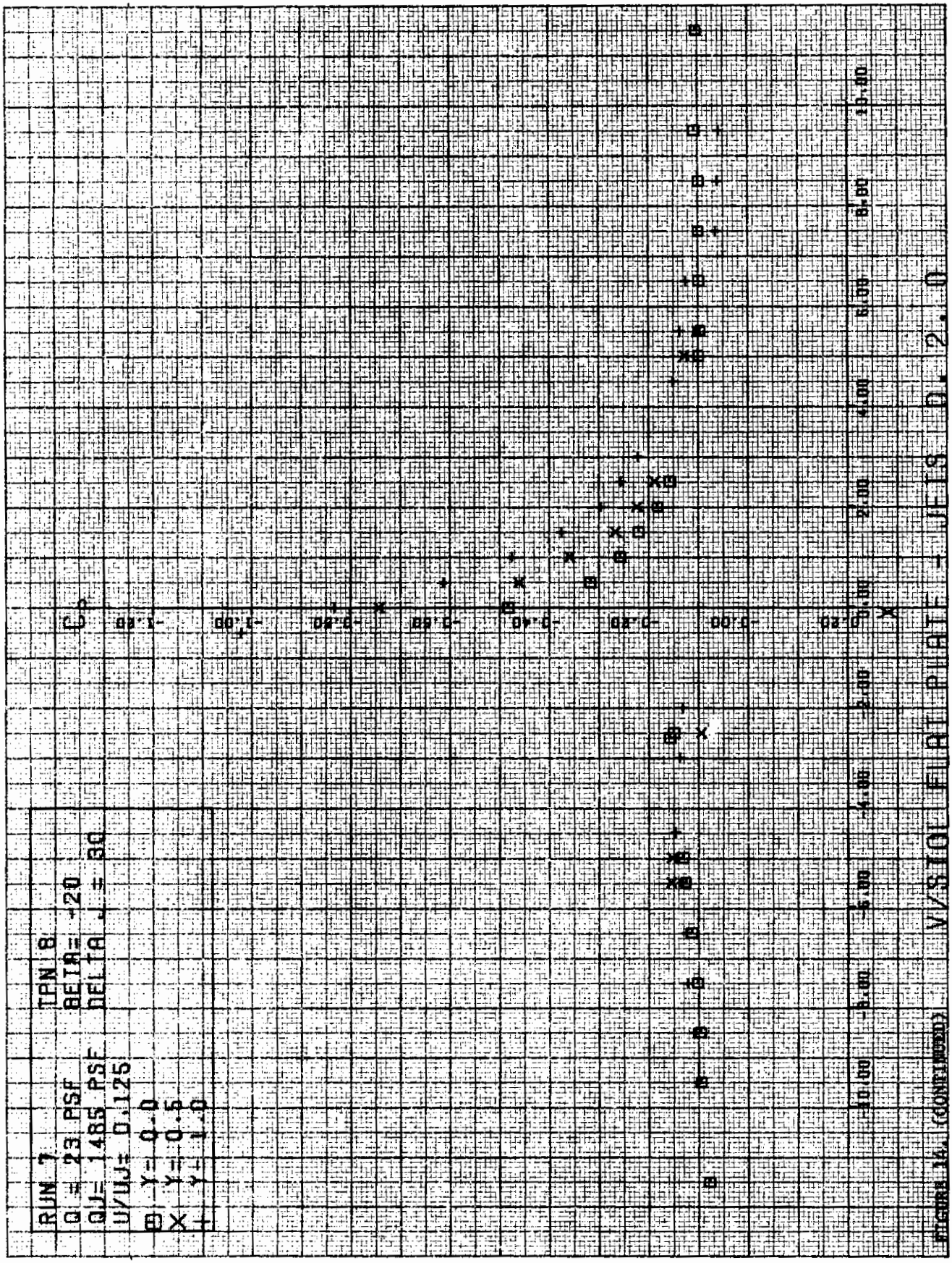

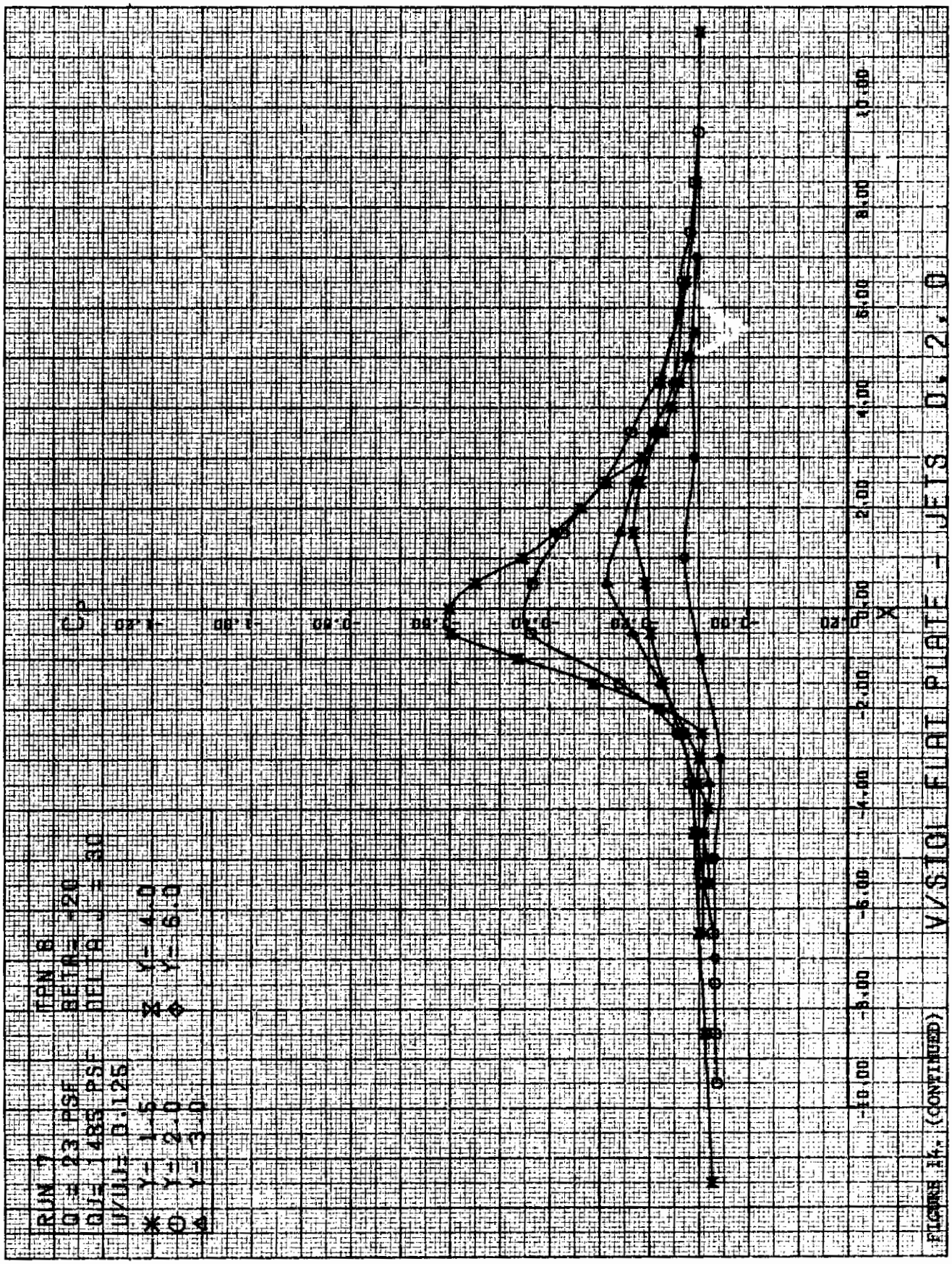

FIGURE 14. (CONTINUED)

FIGURE 14. (CONTINUED)

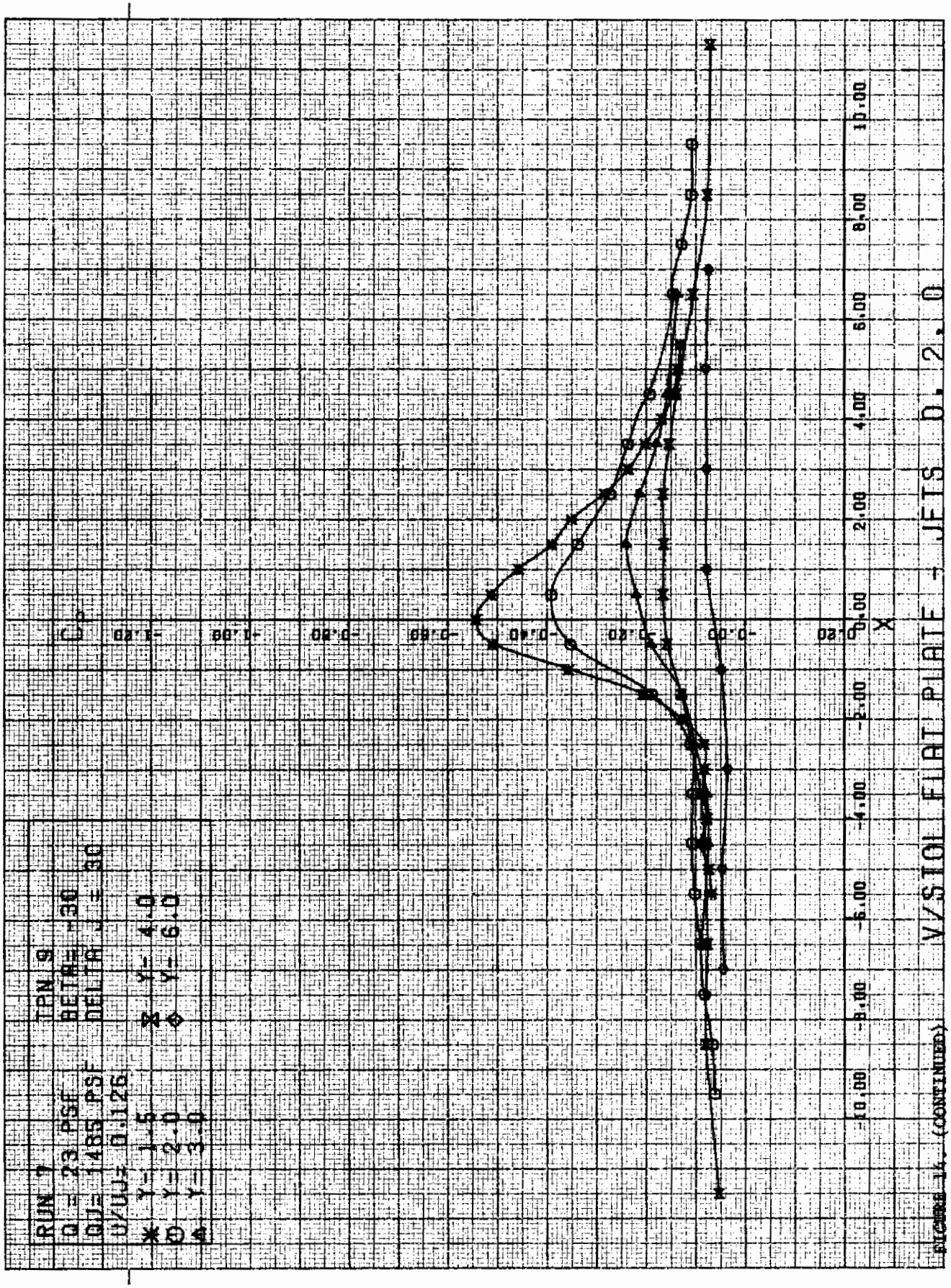

FIGURE 14. (CONTINUED)

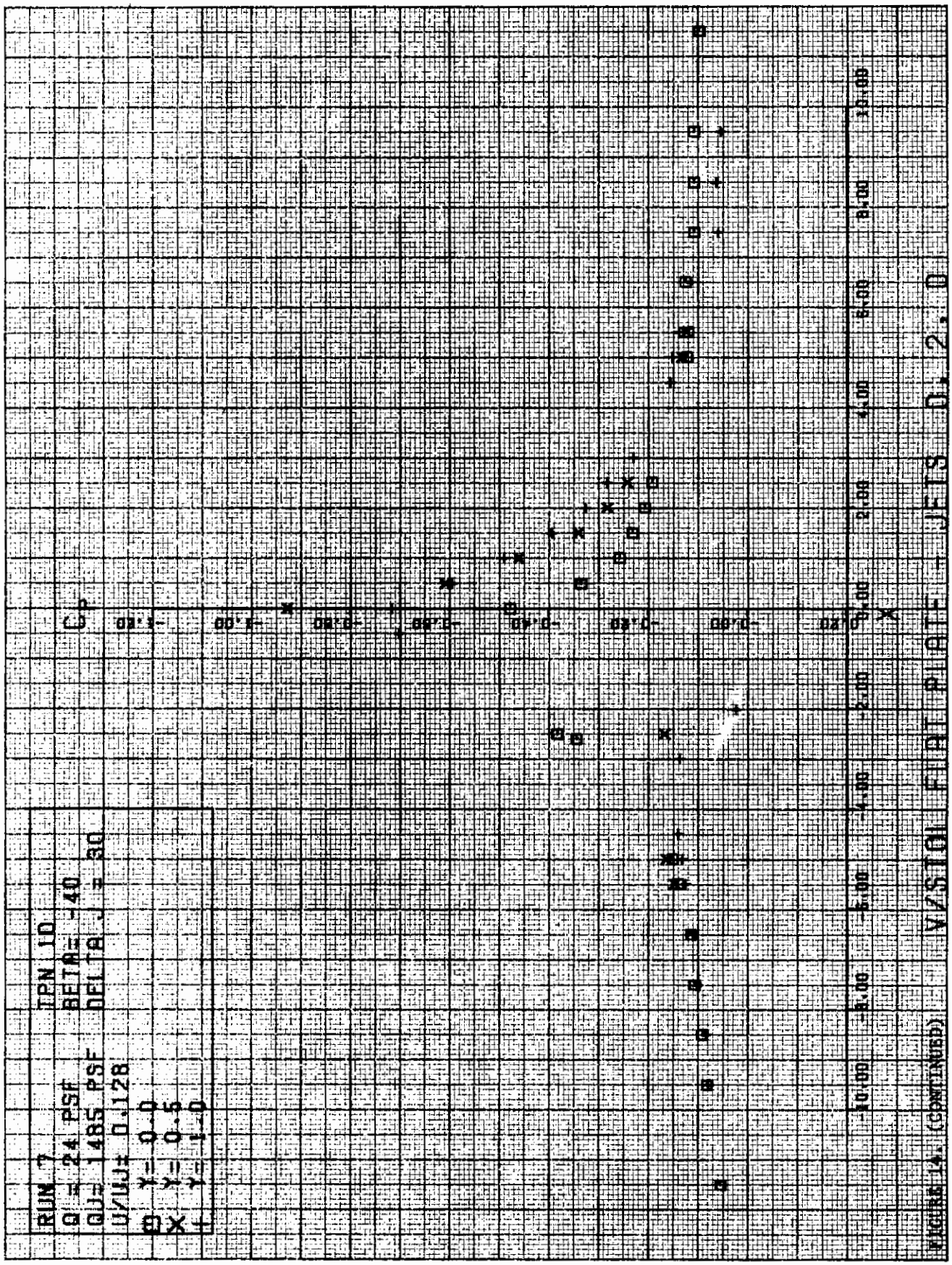

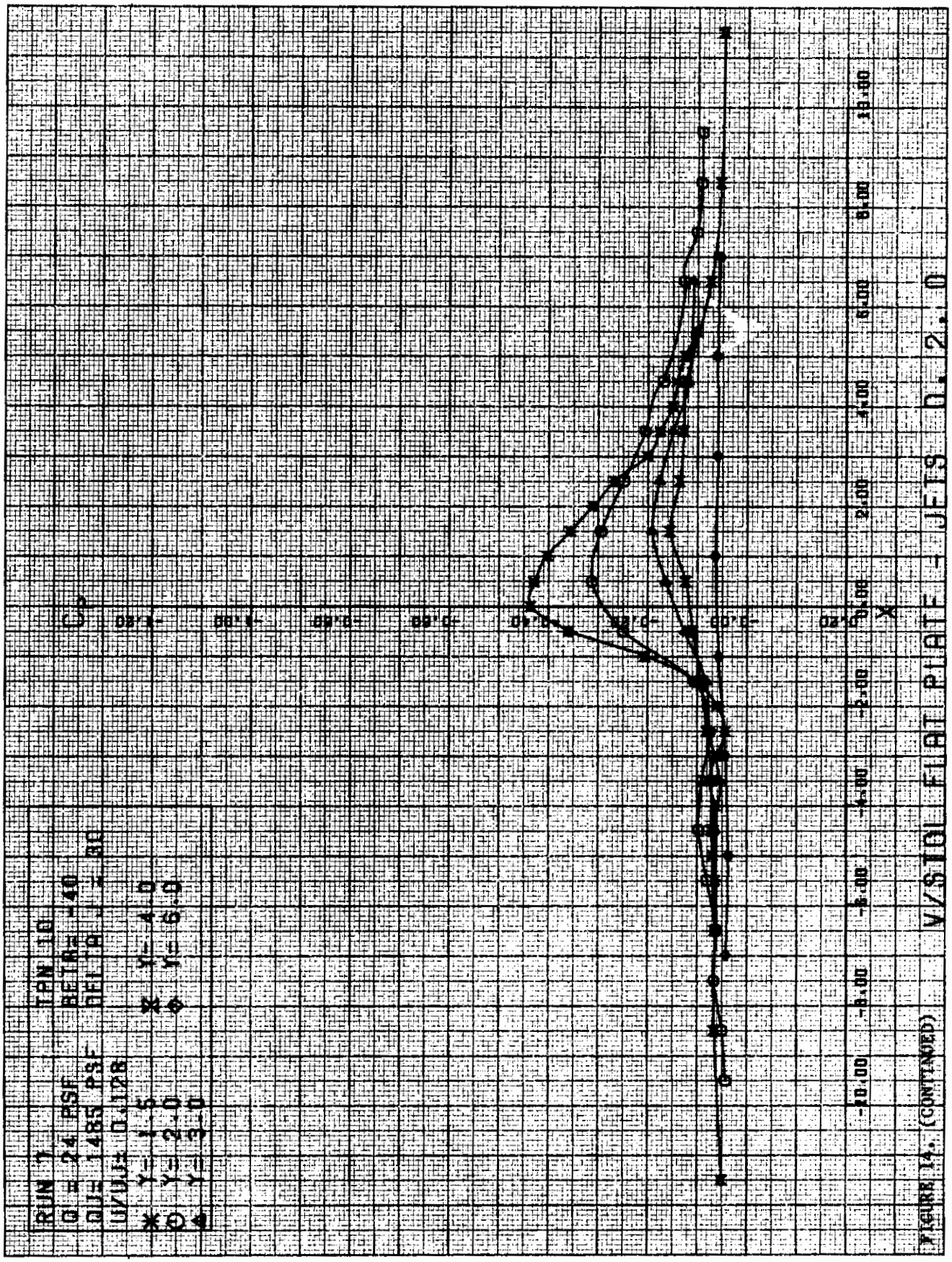

FIGURE 14. (CONTINUED)

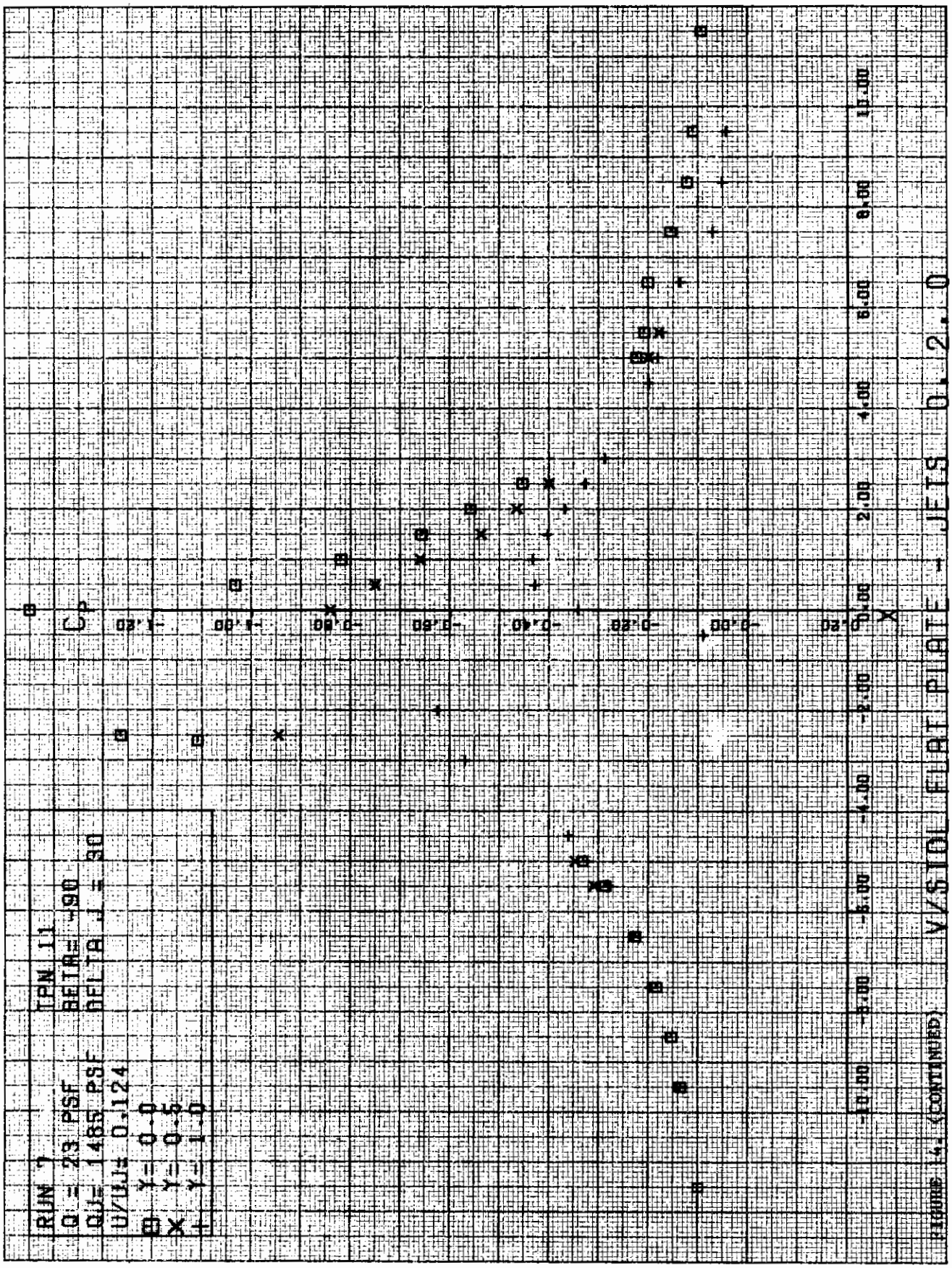

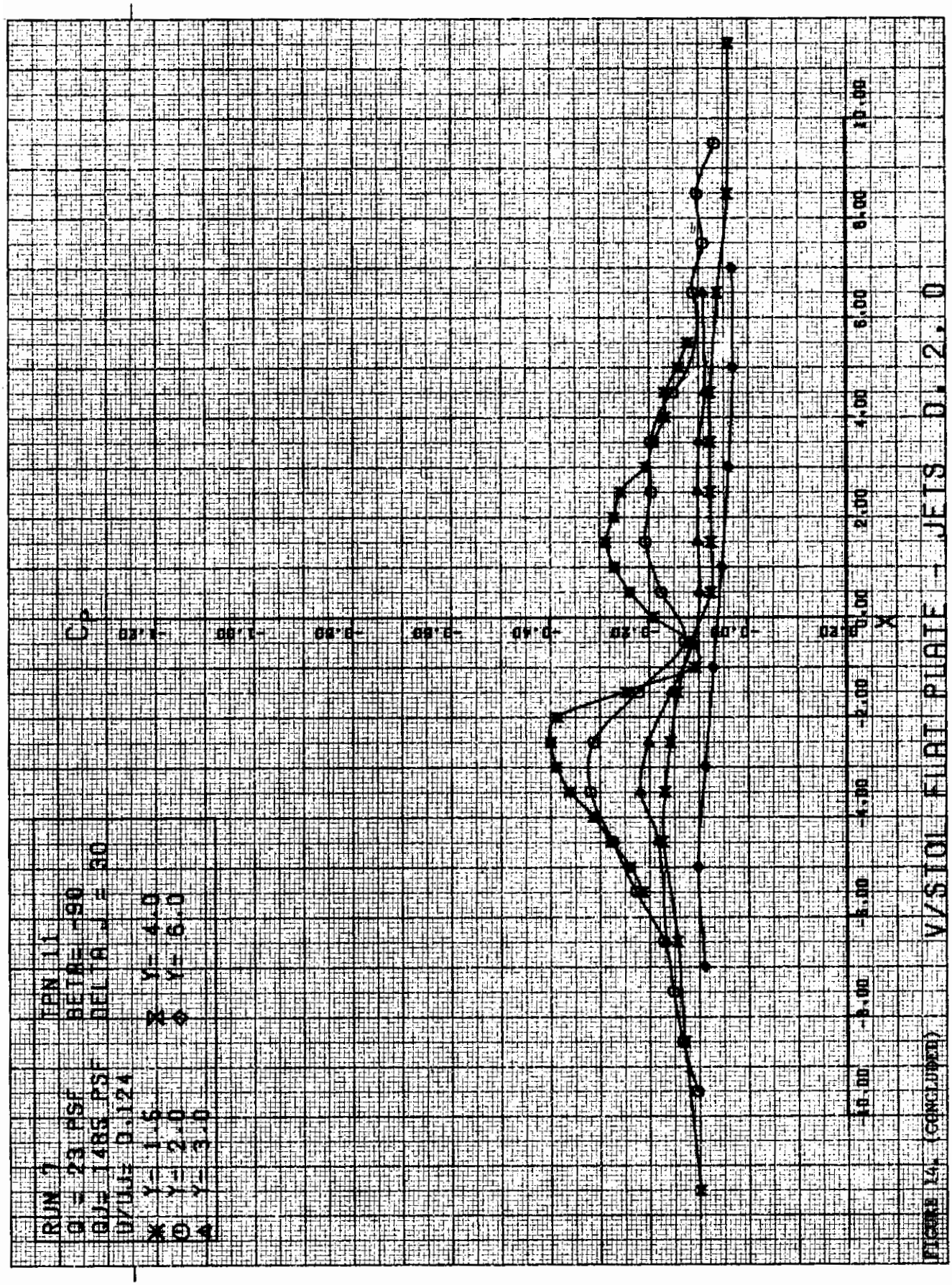

FIGURE 14. (CONCLUDED)

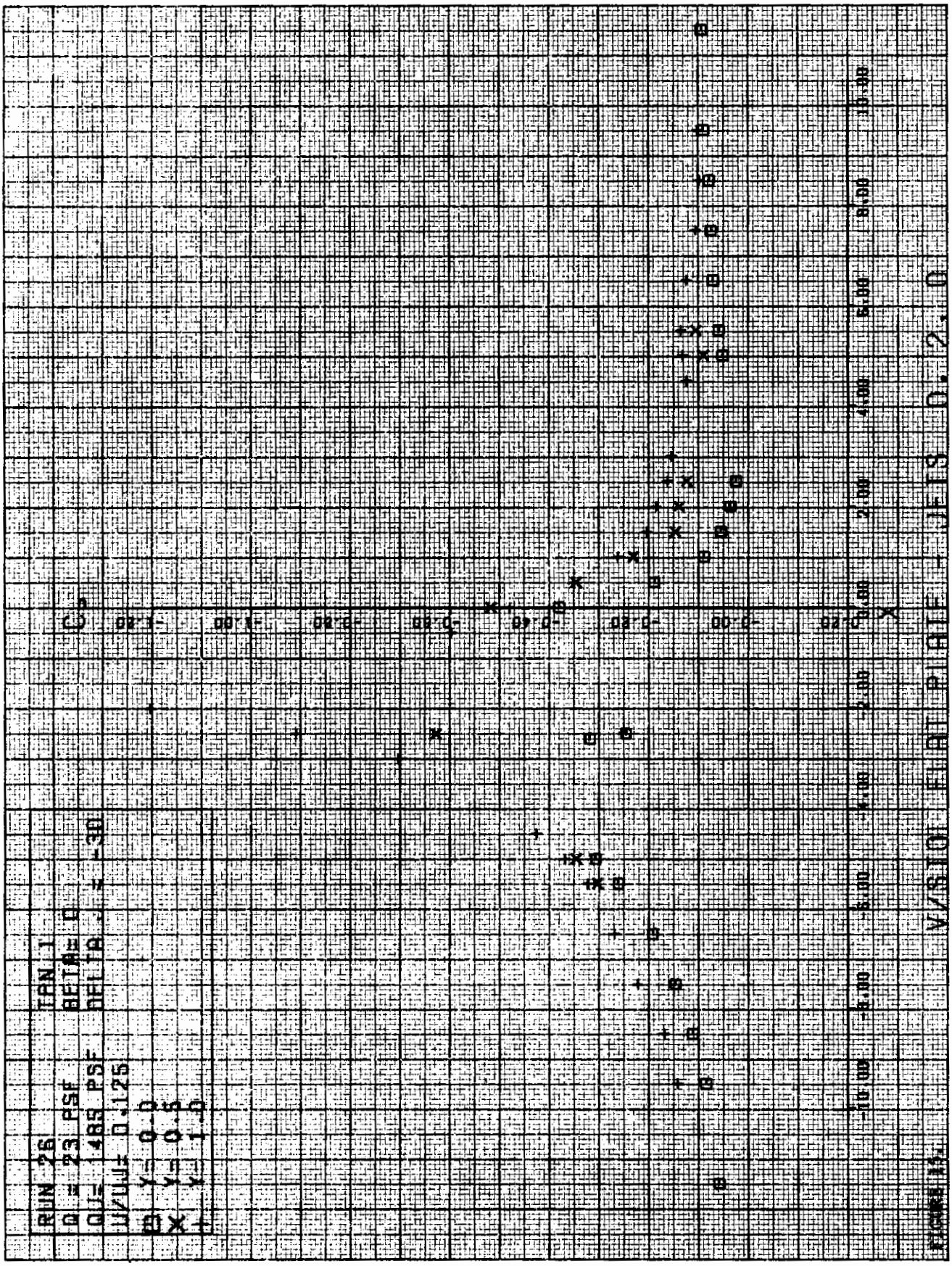

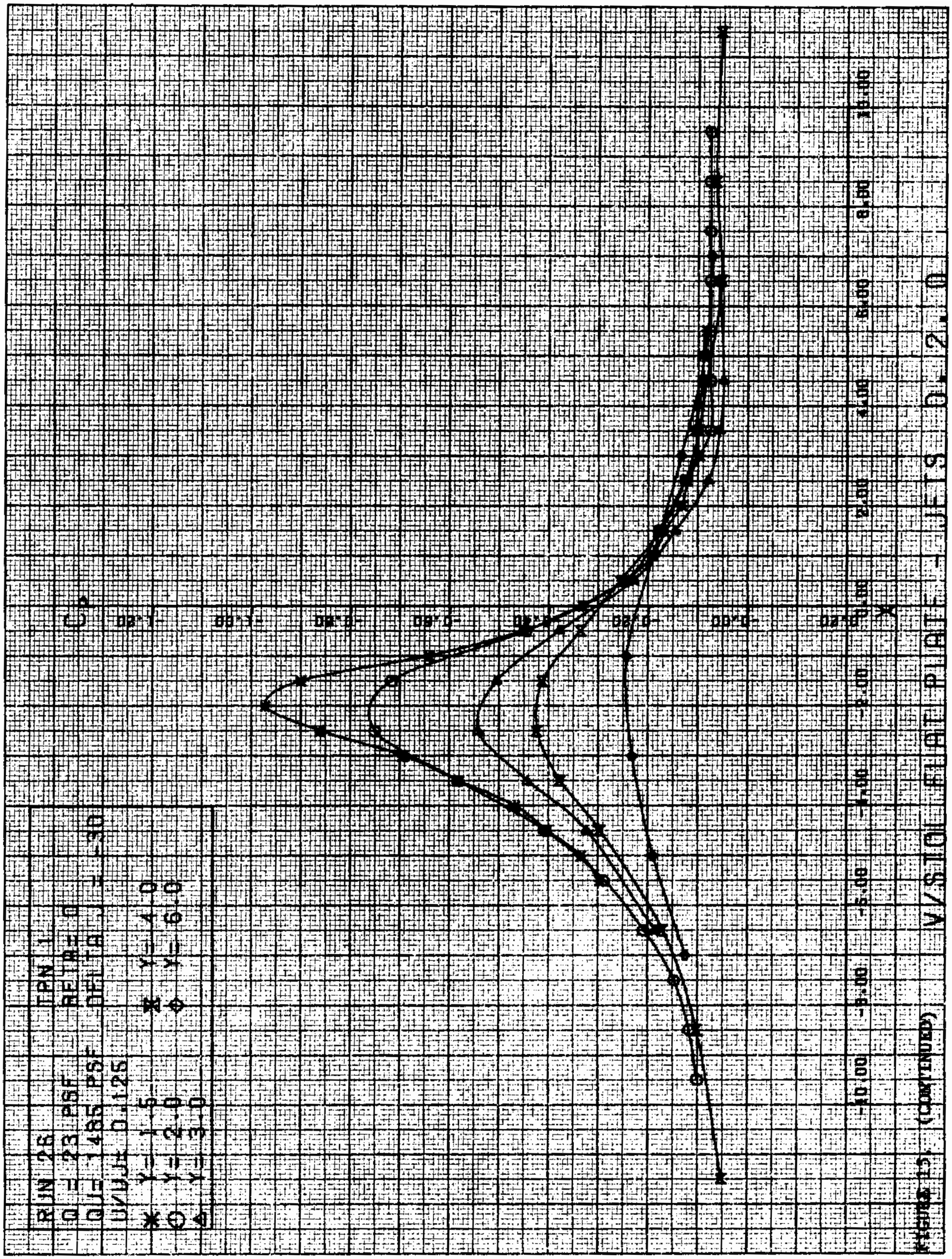

FIGURE 15. (CONTINUED)

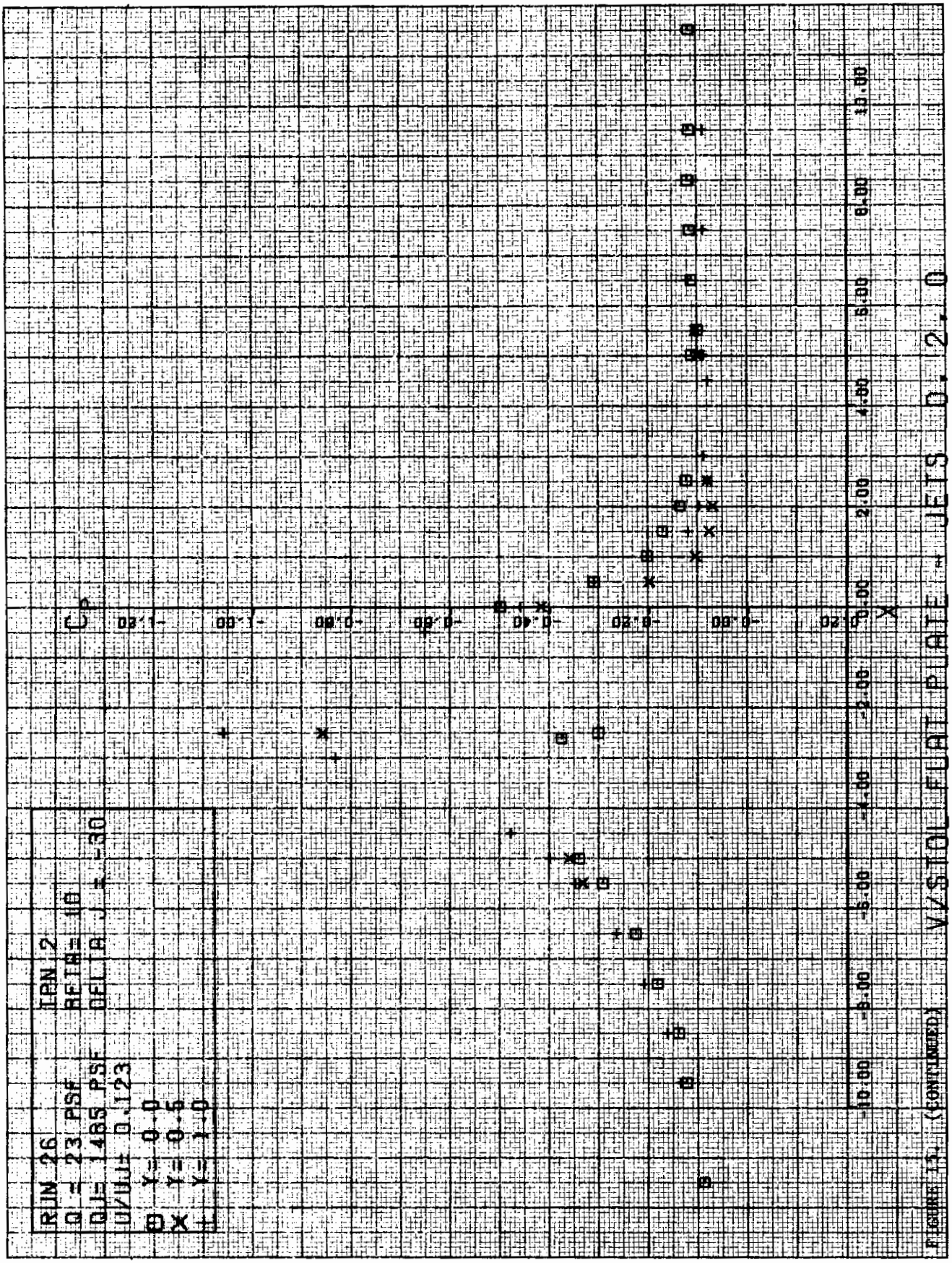

FIGURE 13. (CONTINUED) V/STOL FLAT PLATE + JETS 0.2, 0

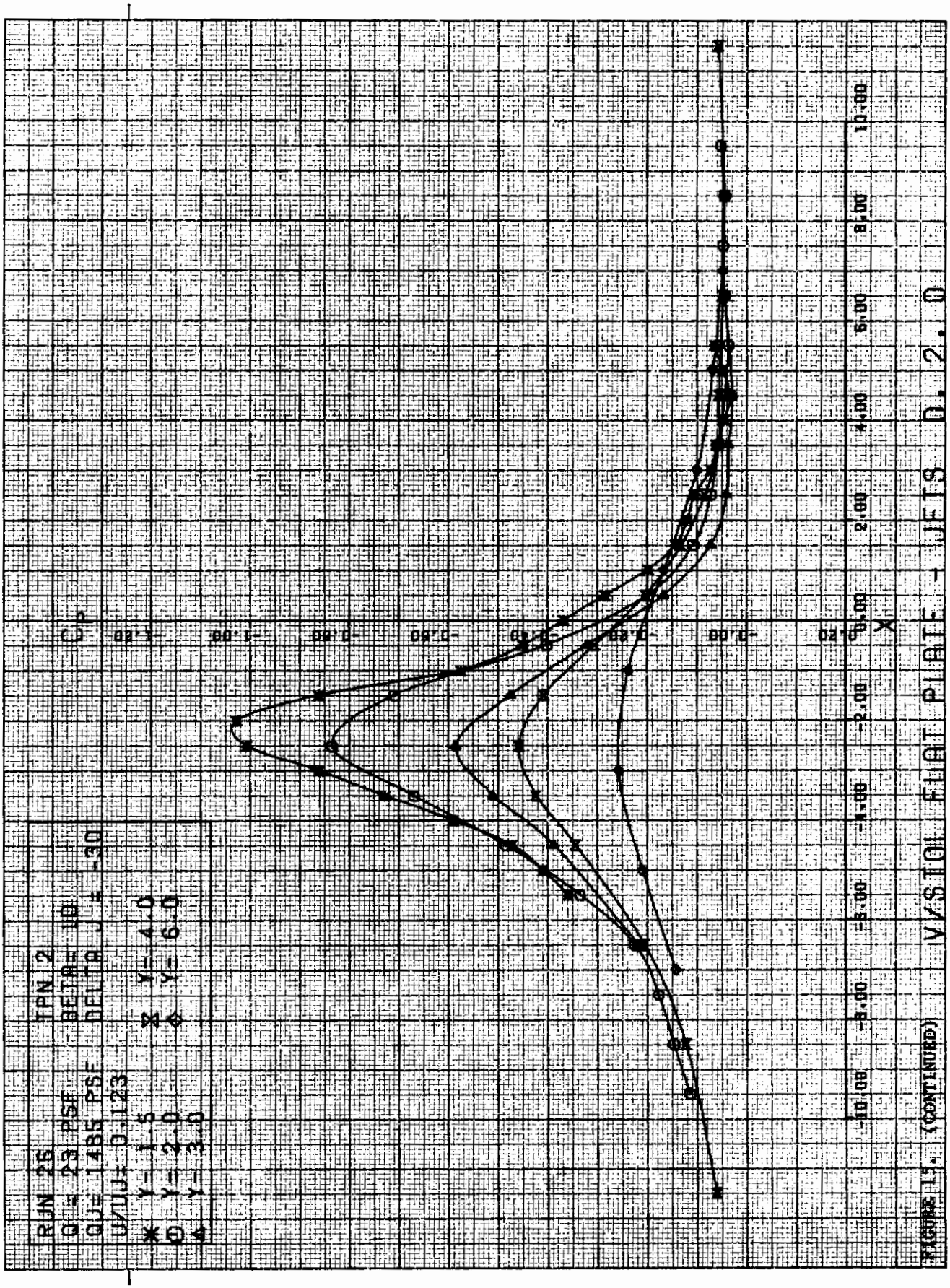

FIGURE 15. (CONTINUED)

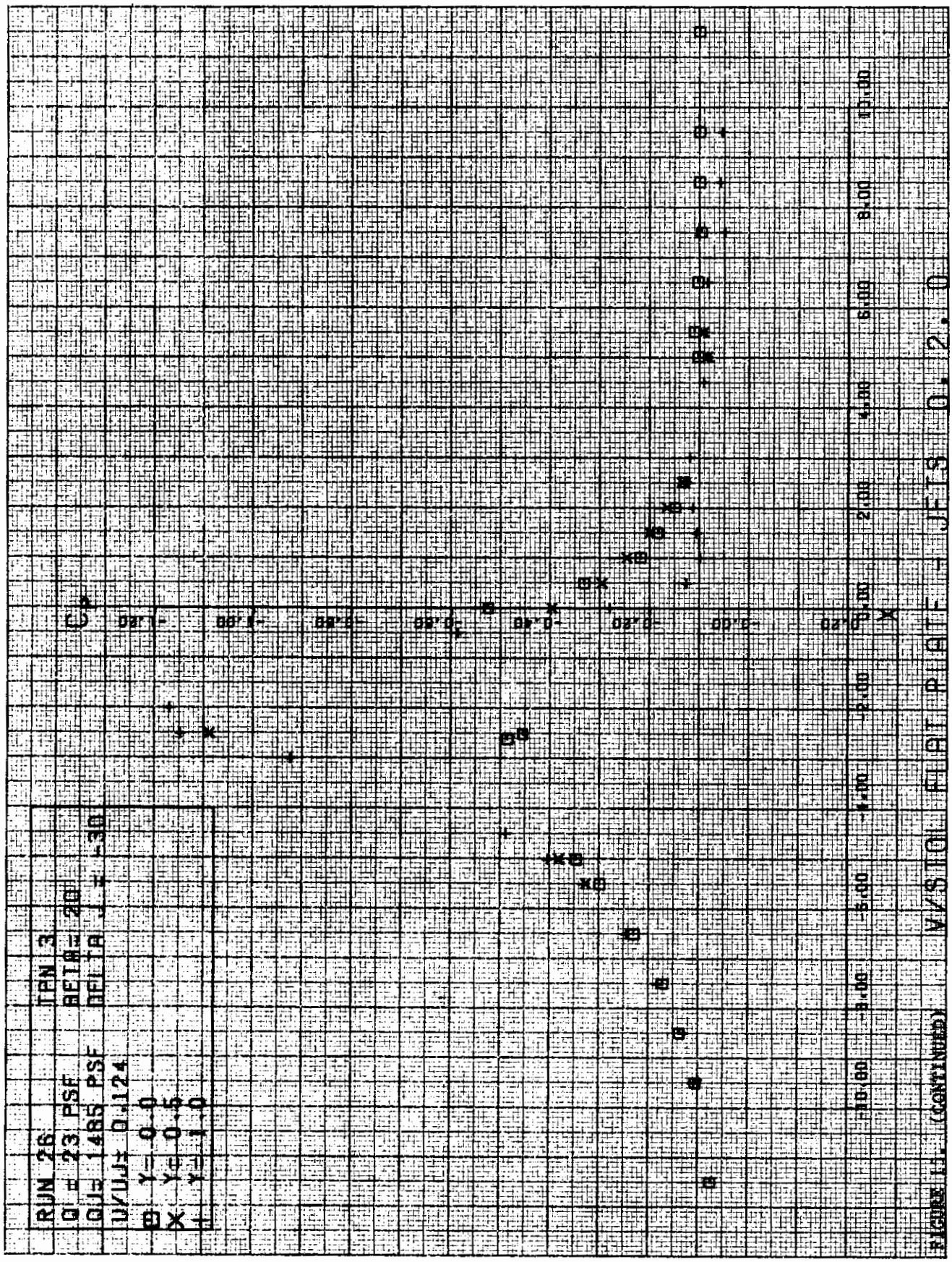

FIGURE 11. (CONTINUED)

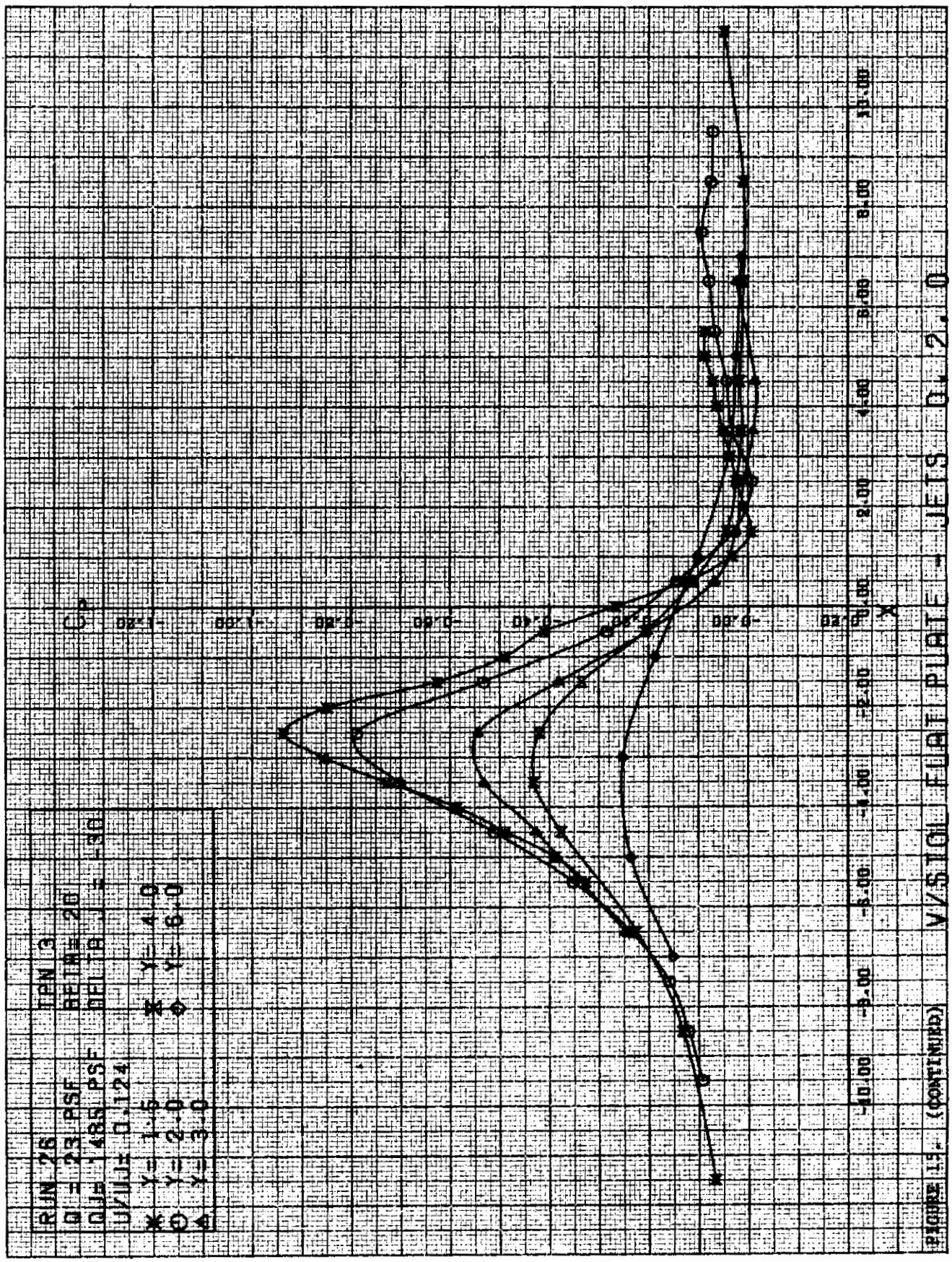

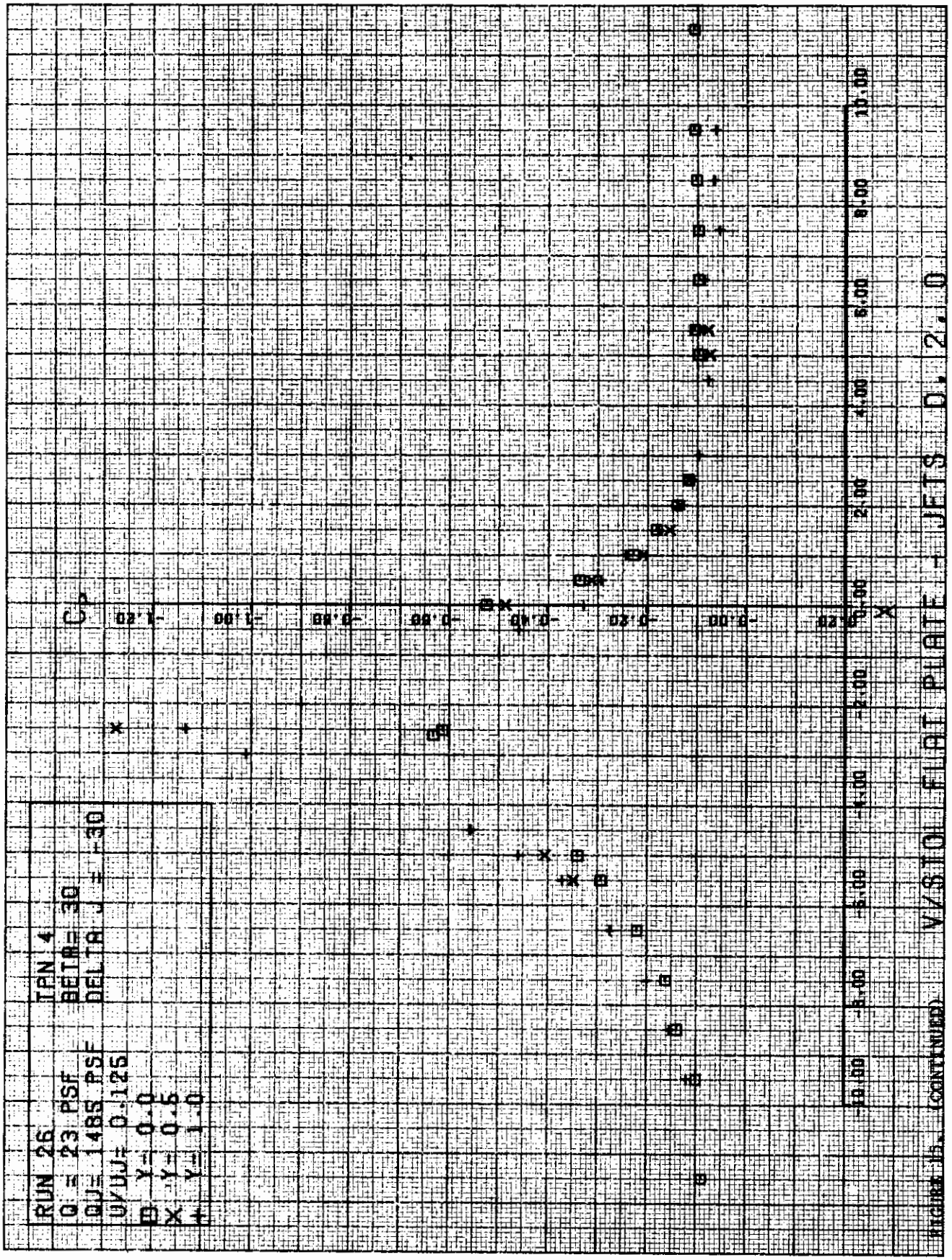

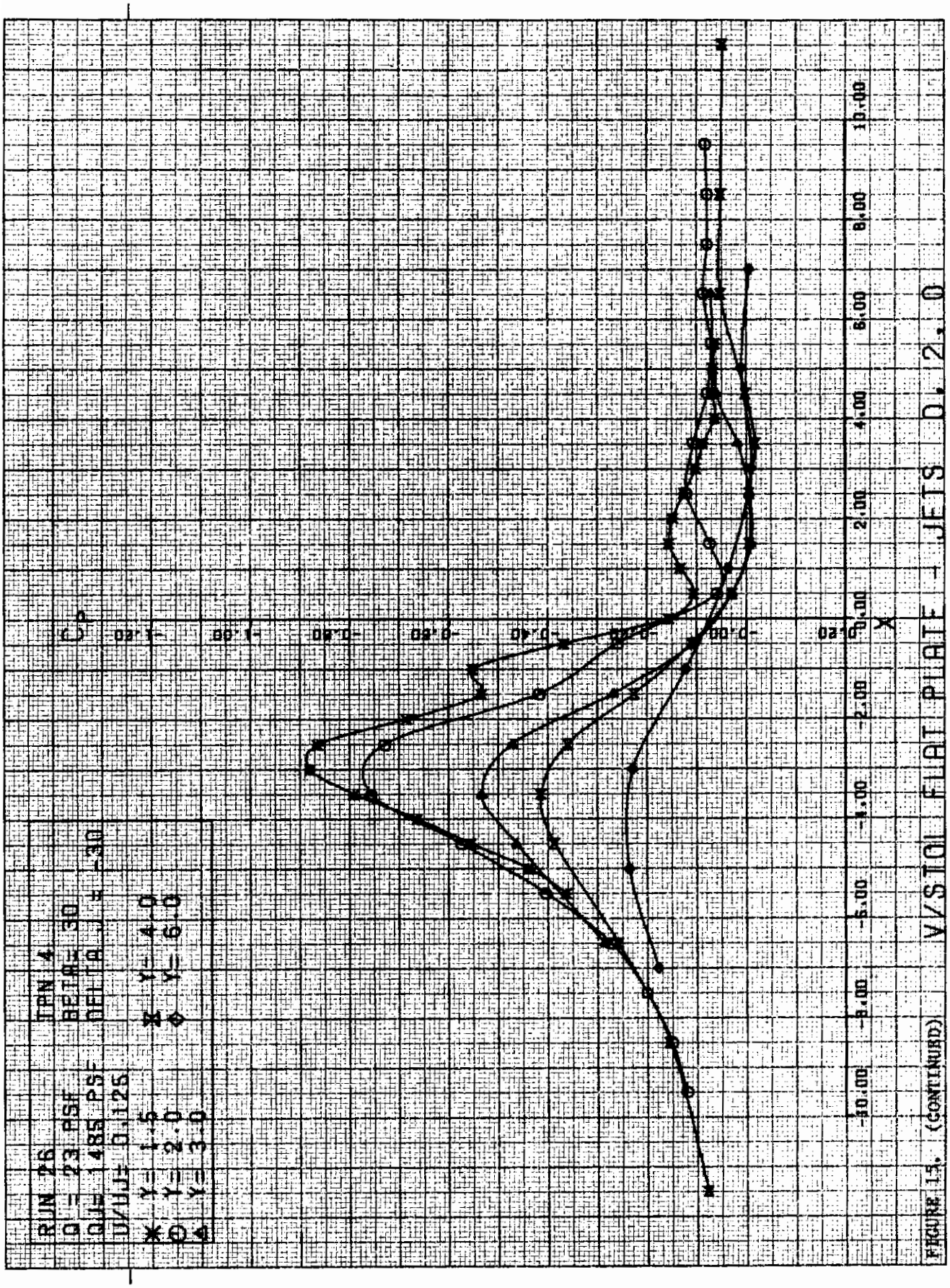

FIGURE 15. (CONTINUED)

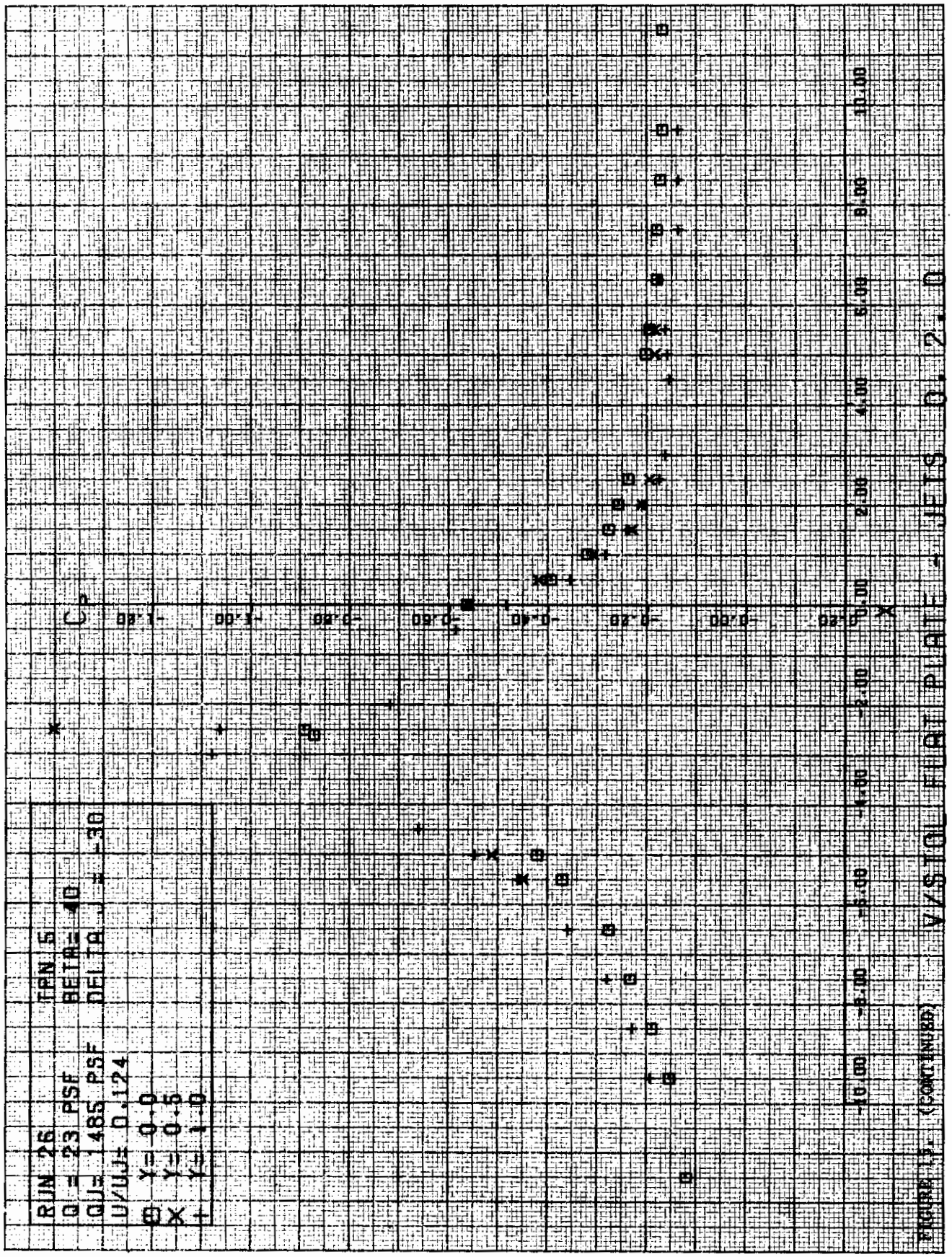

FIGURE 13. (CONTINUED)

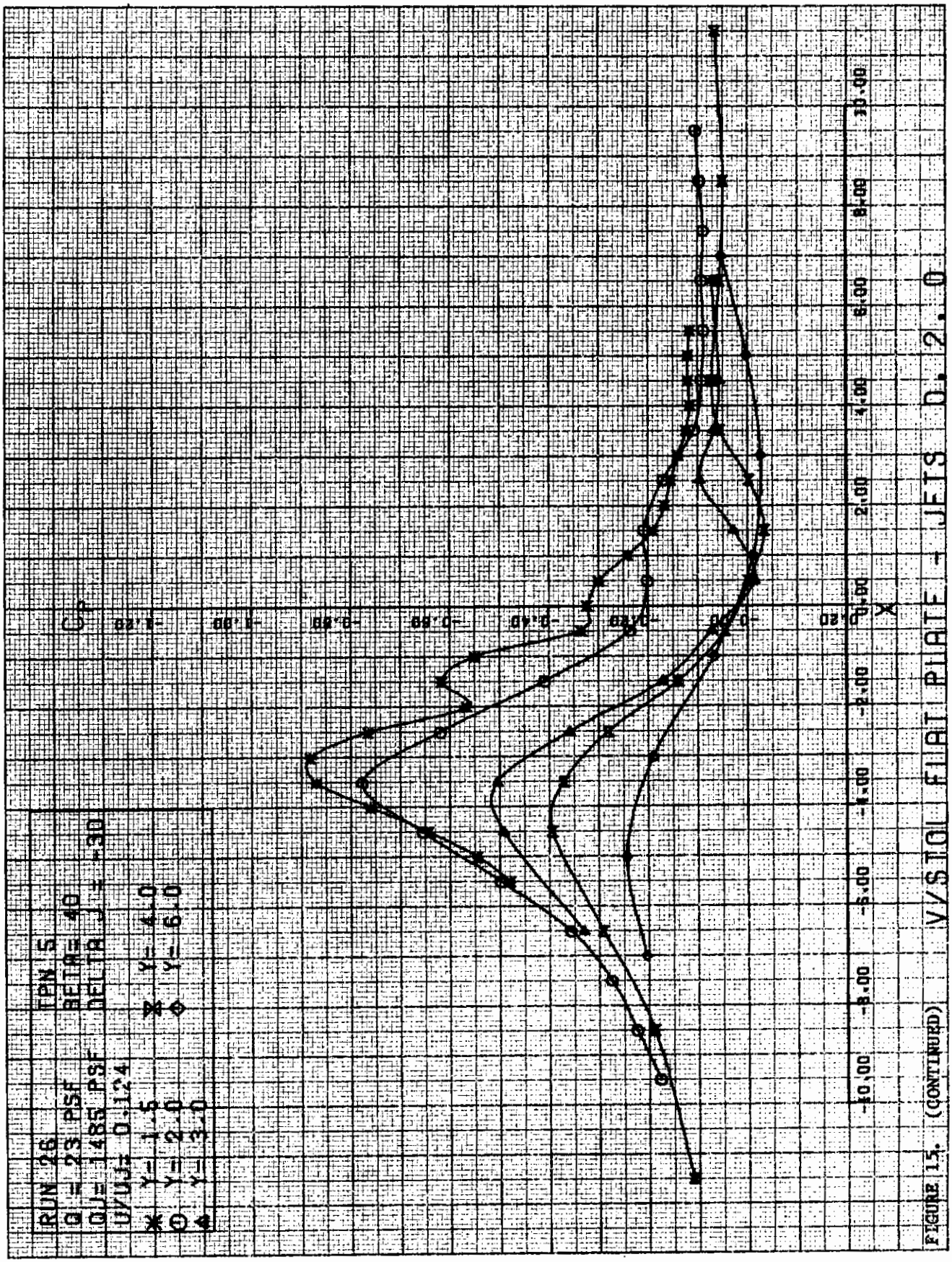

FIGURE 15. (CONTINUED)

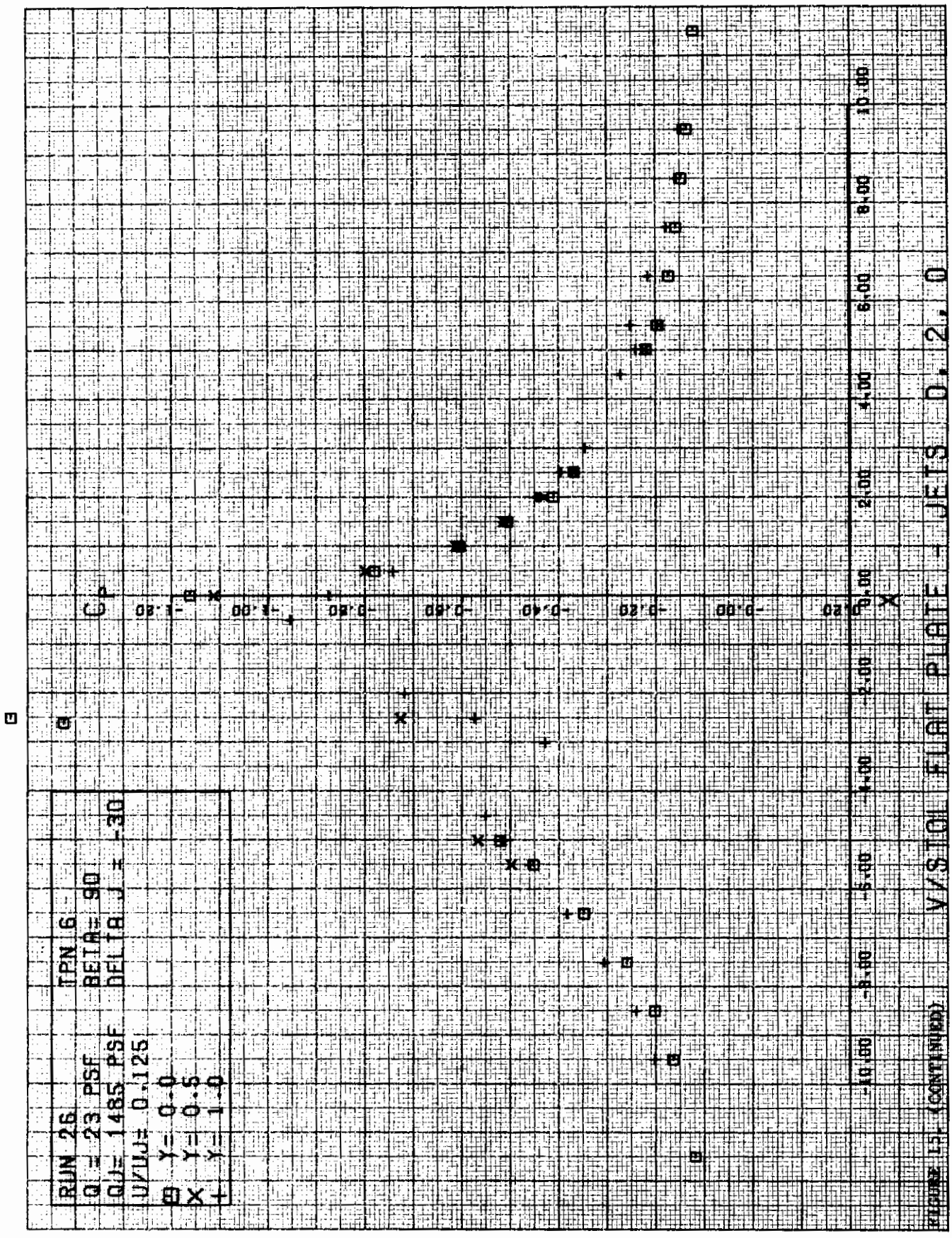

FIGURE 53. (CONTINUED)

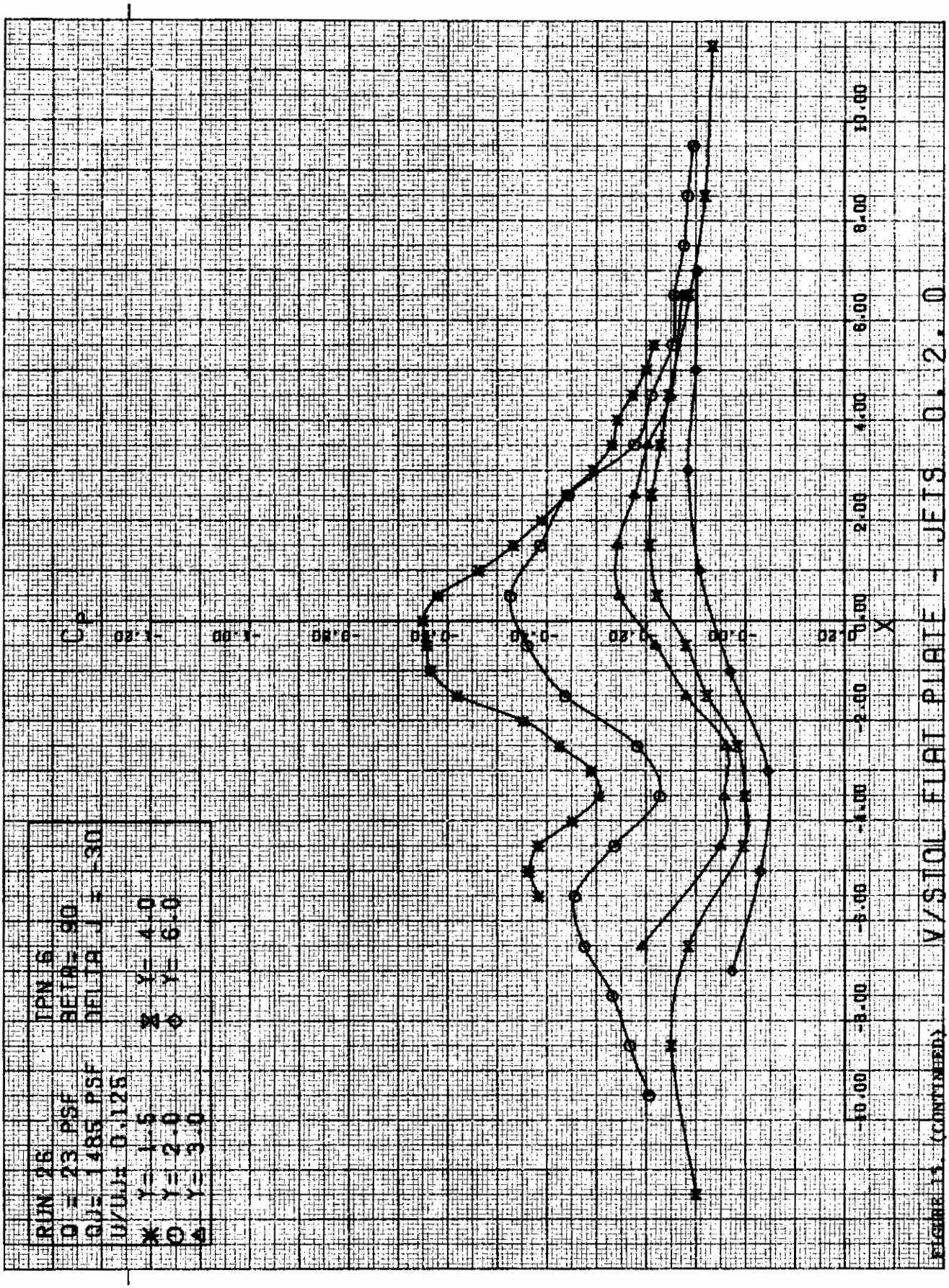

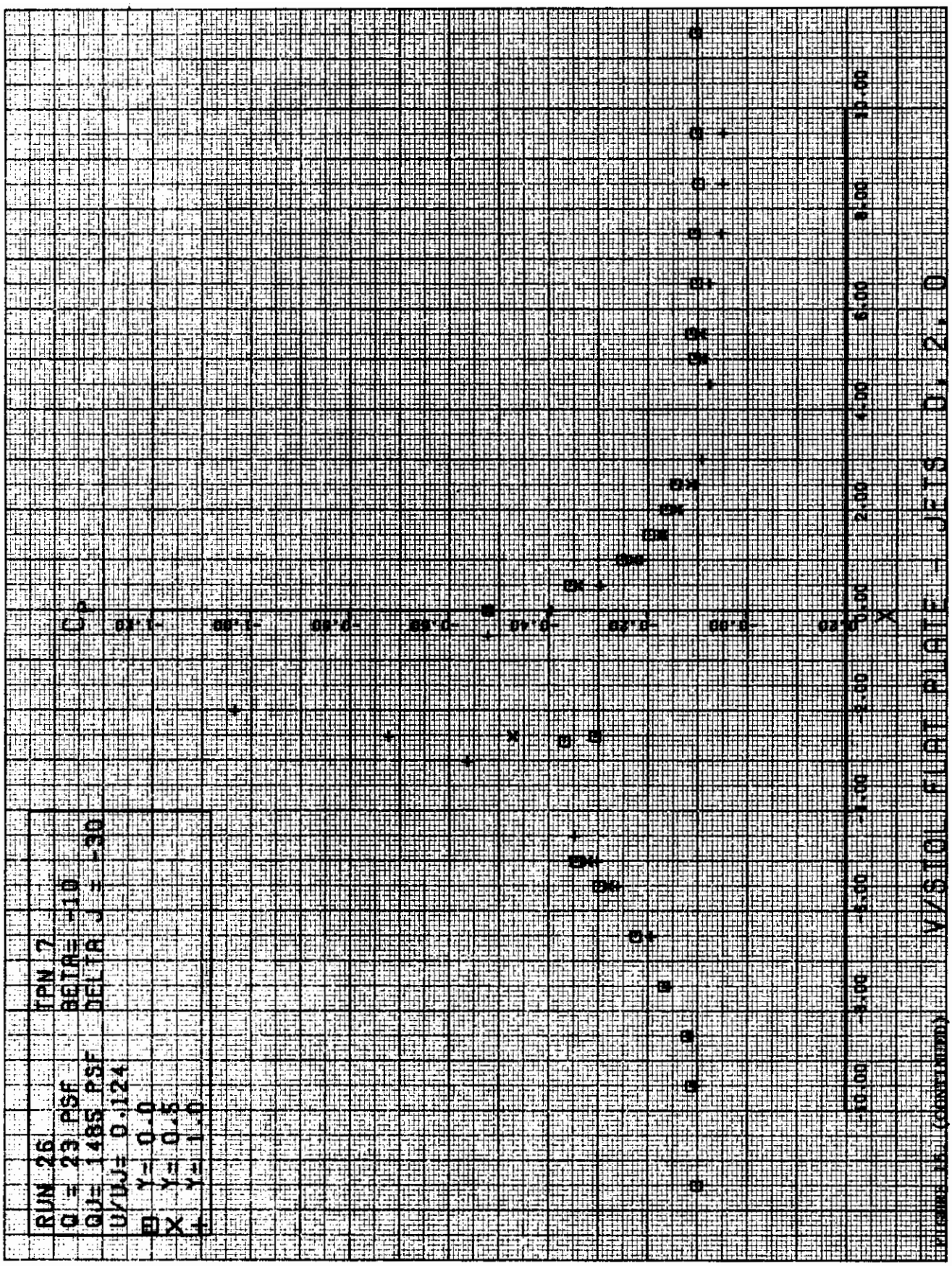

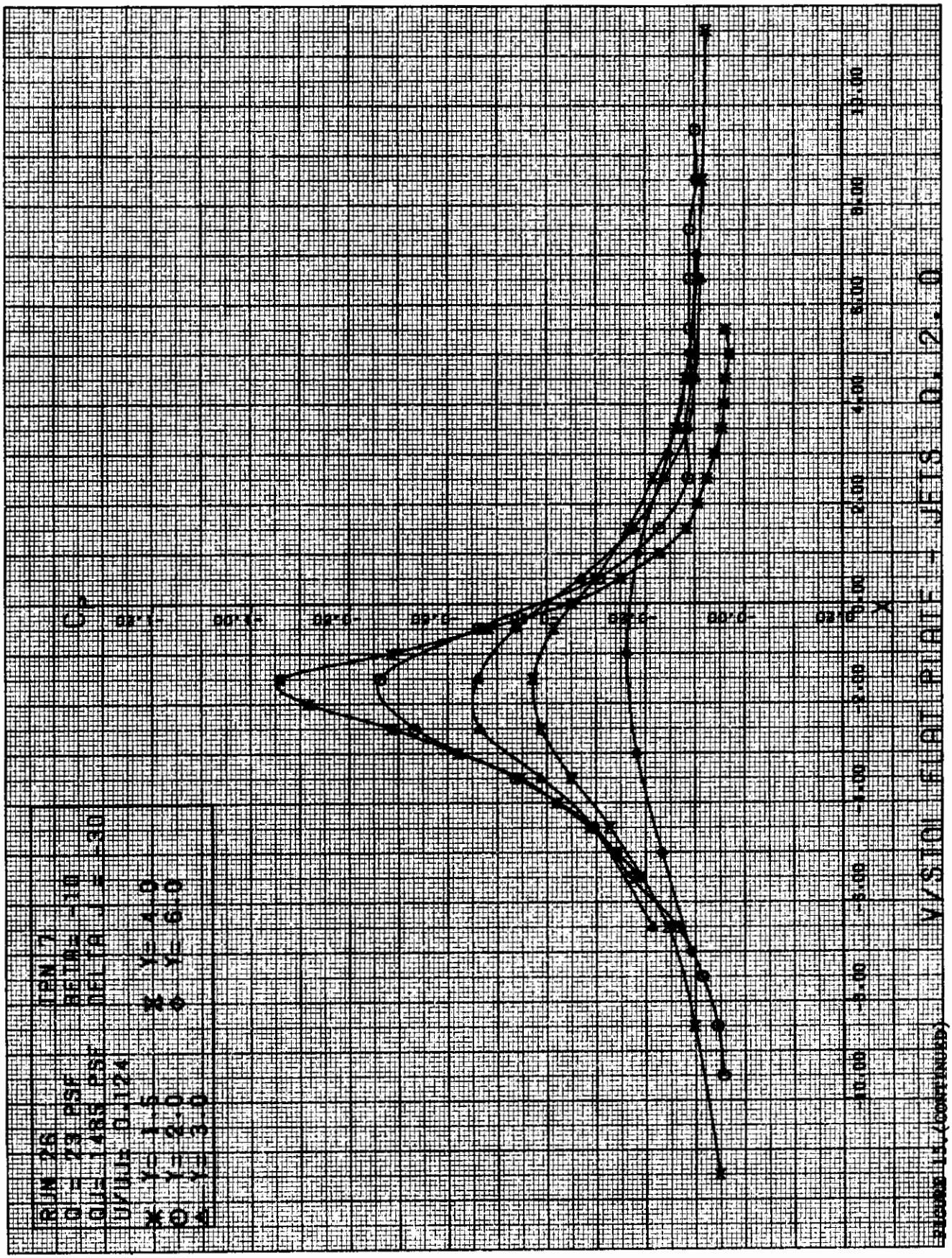

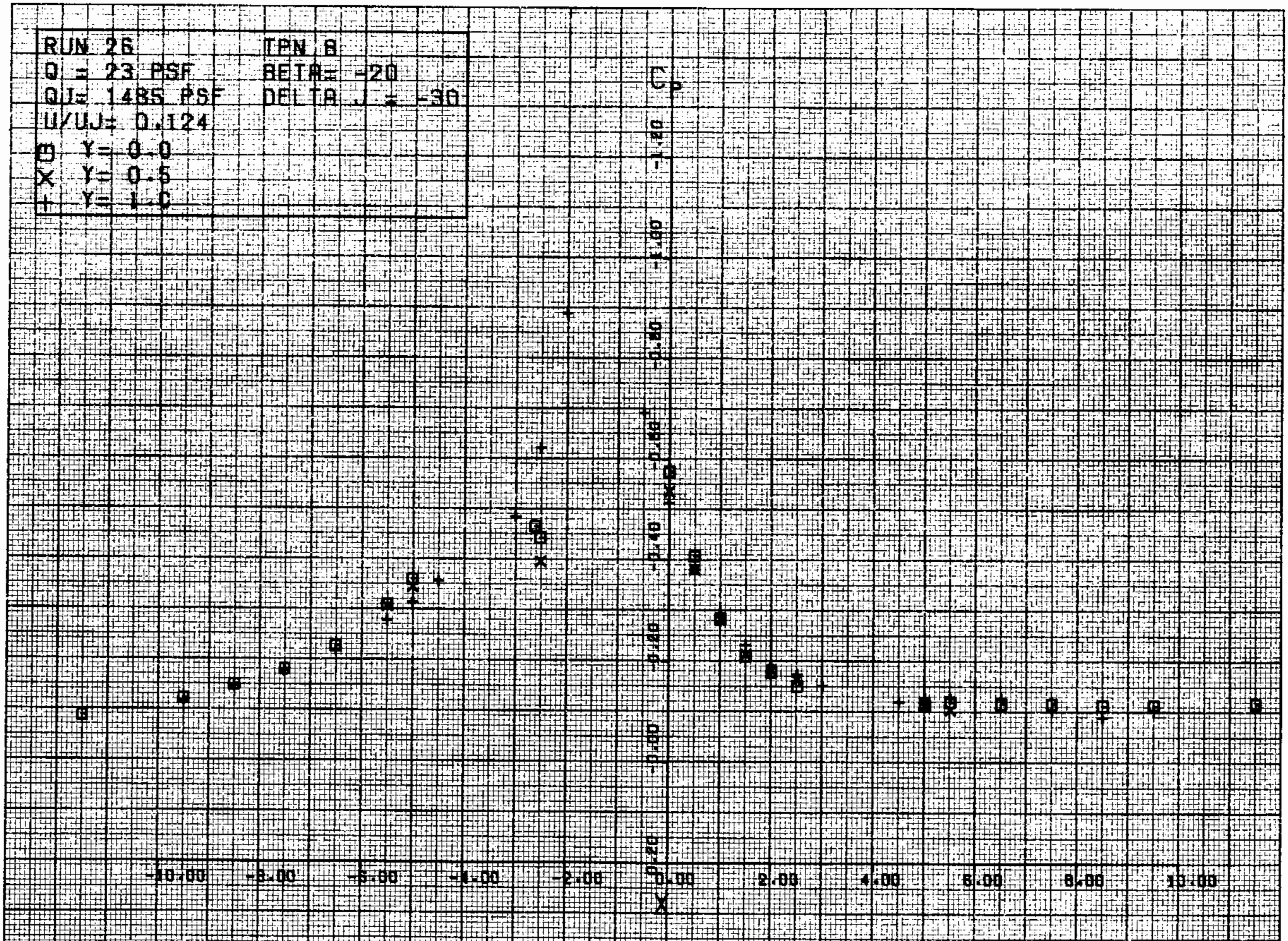

FIGURE 15. (CONTINUED) V/STOL FLAT PLATE + JETS D. 2. D

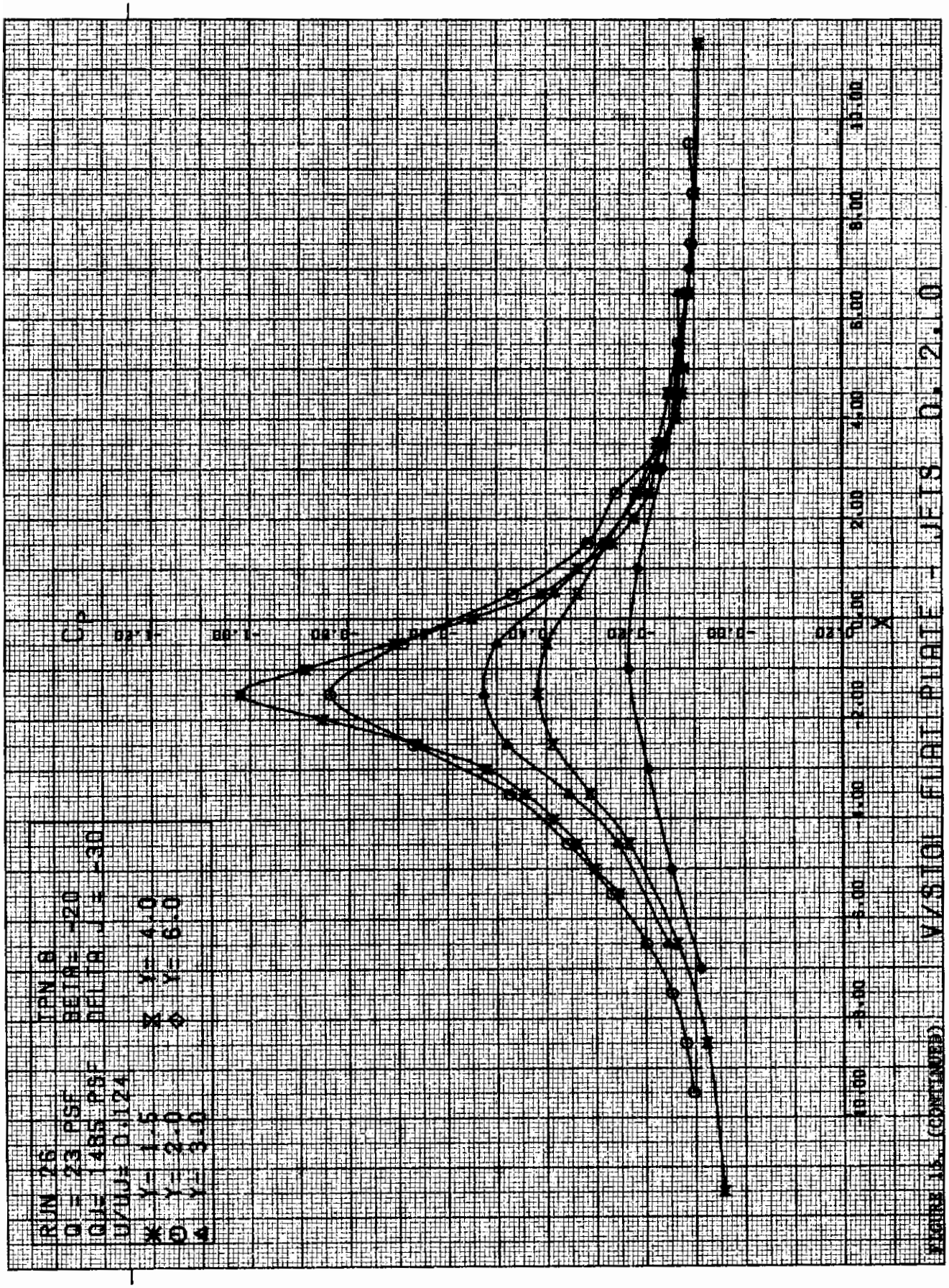

FIGURE 15. (CONTINUED)

V/STOL FLAT PLATE - JETS 0, 2, 0

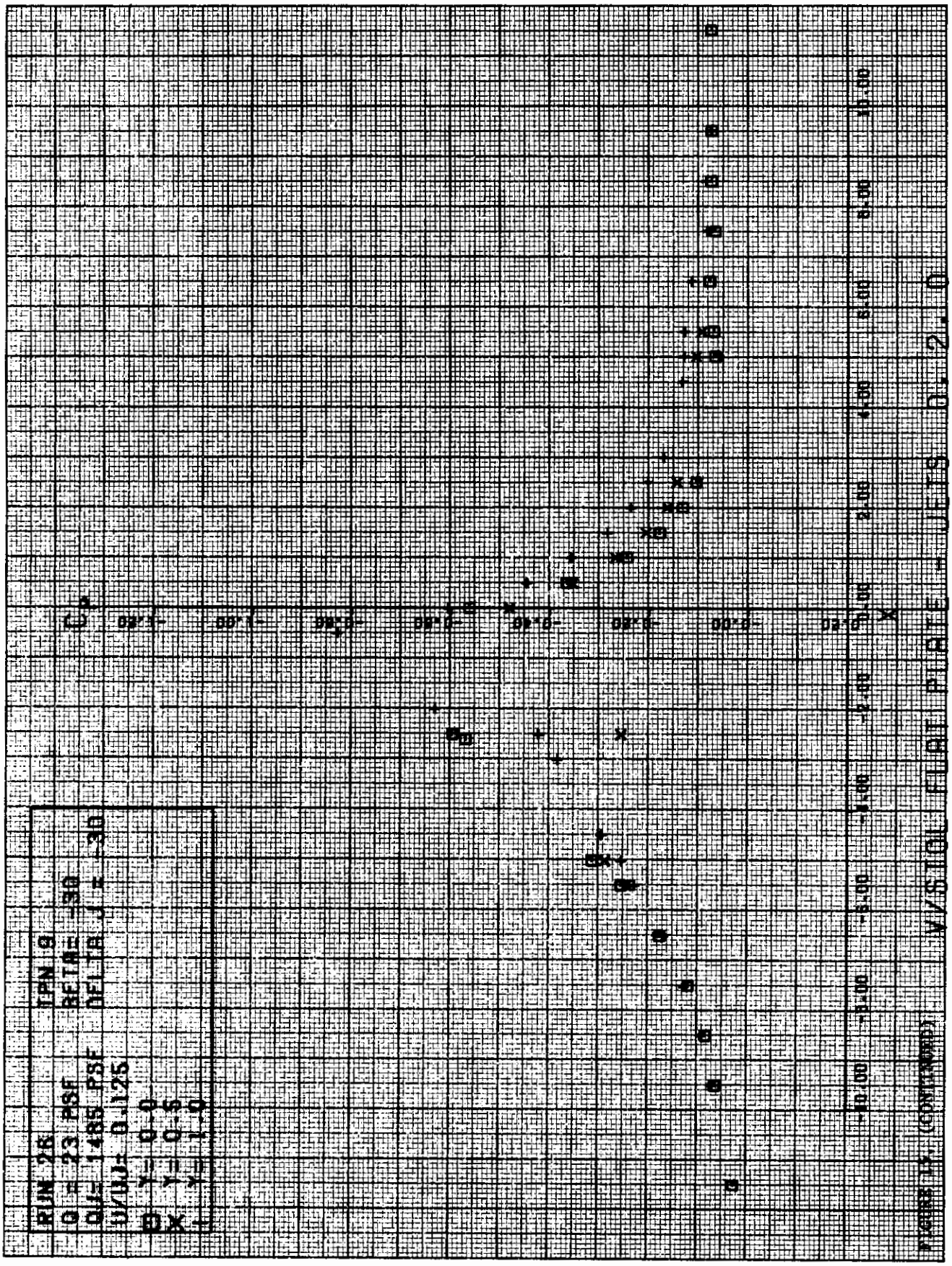

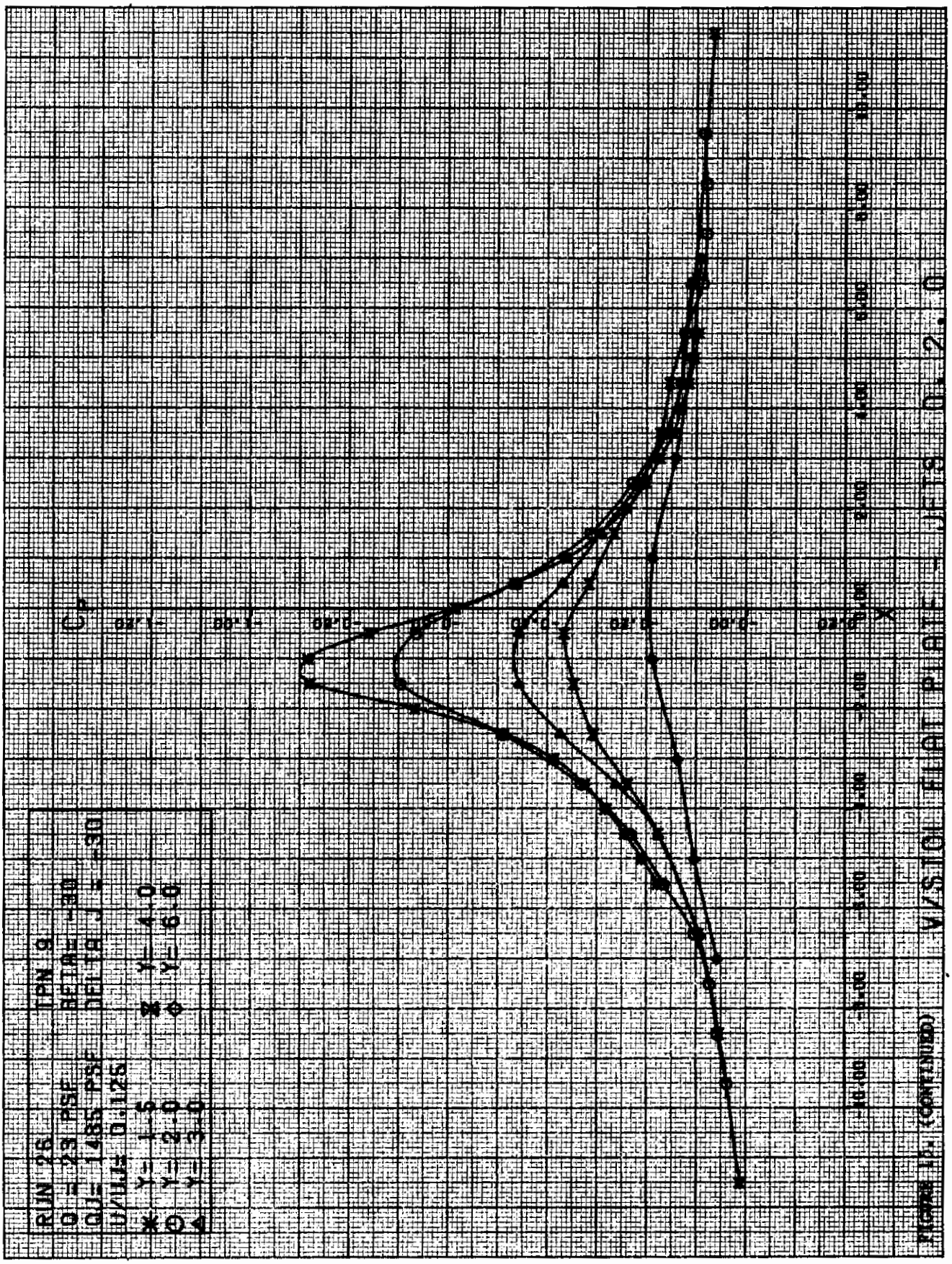

FIGURE 17. (CONTINUED)

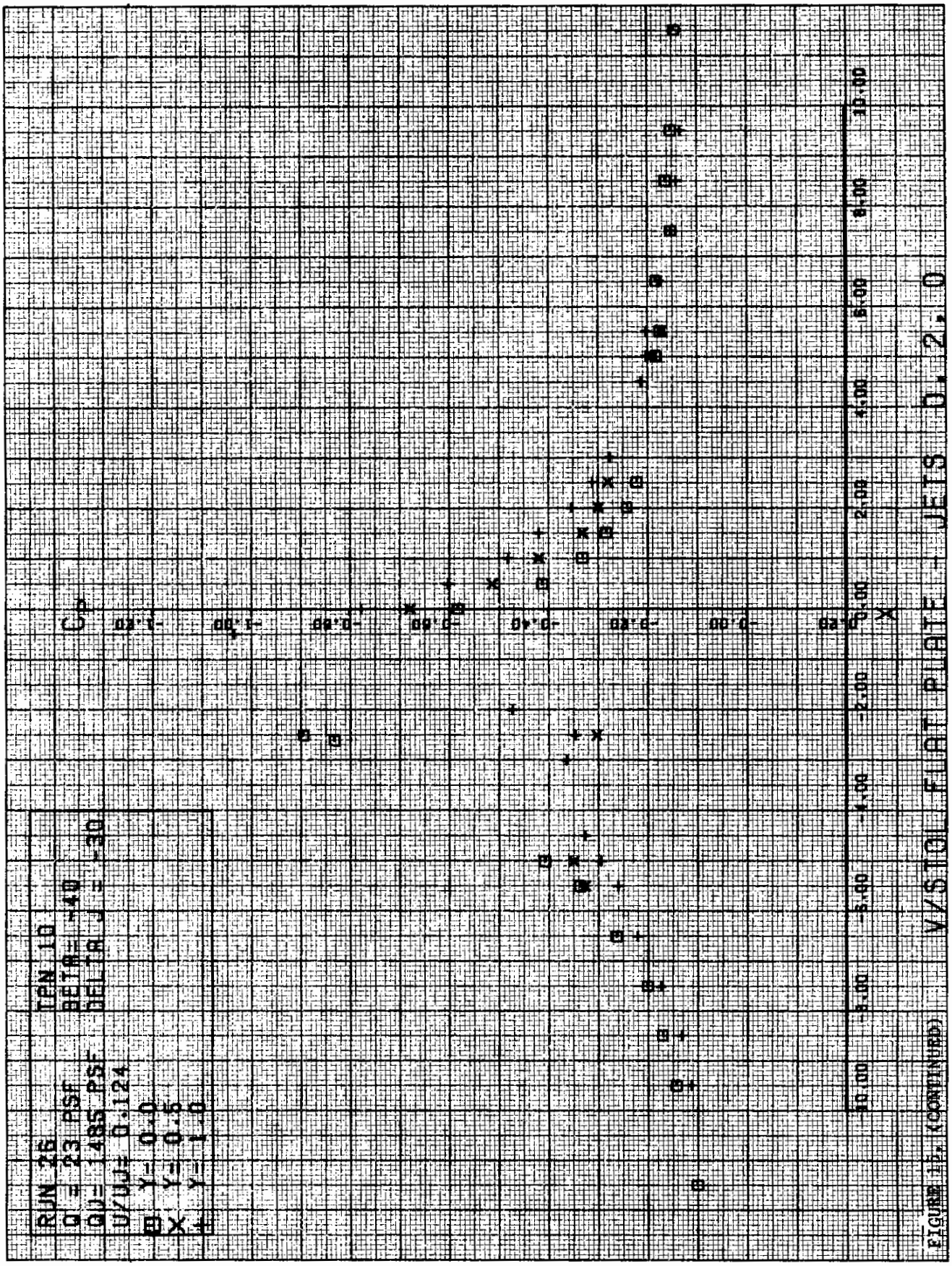

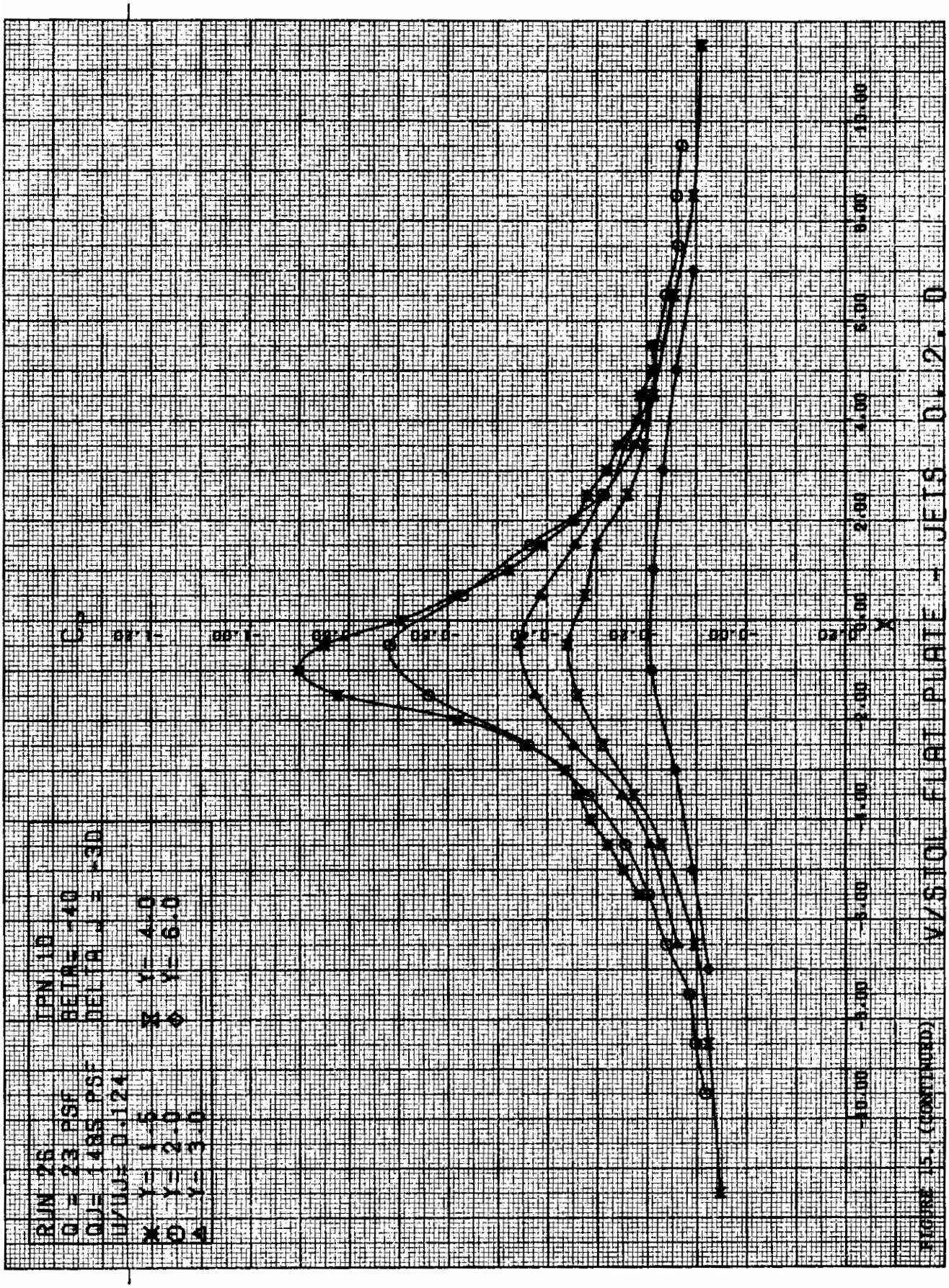

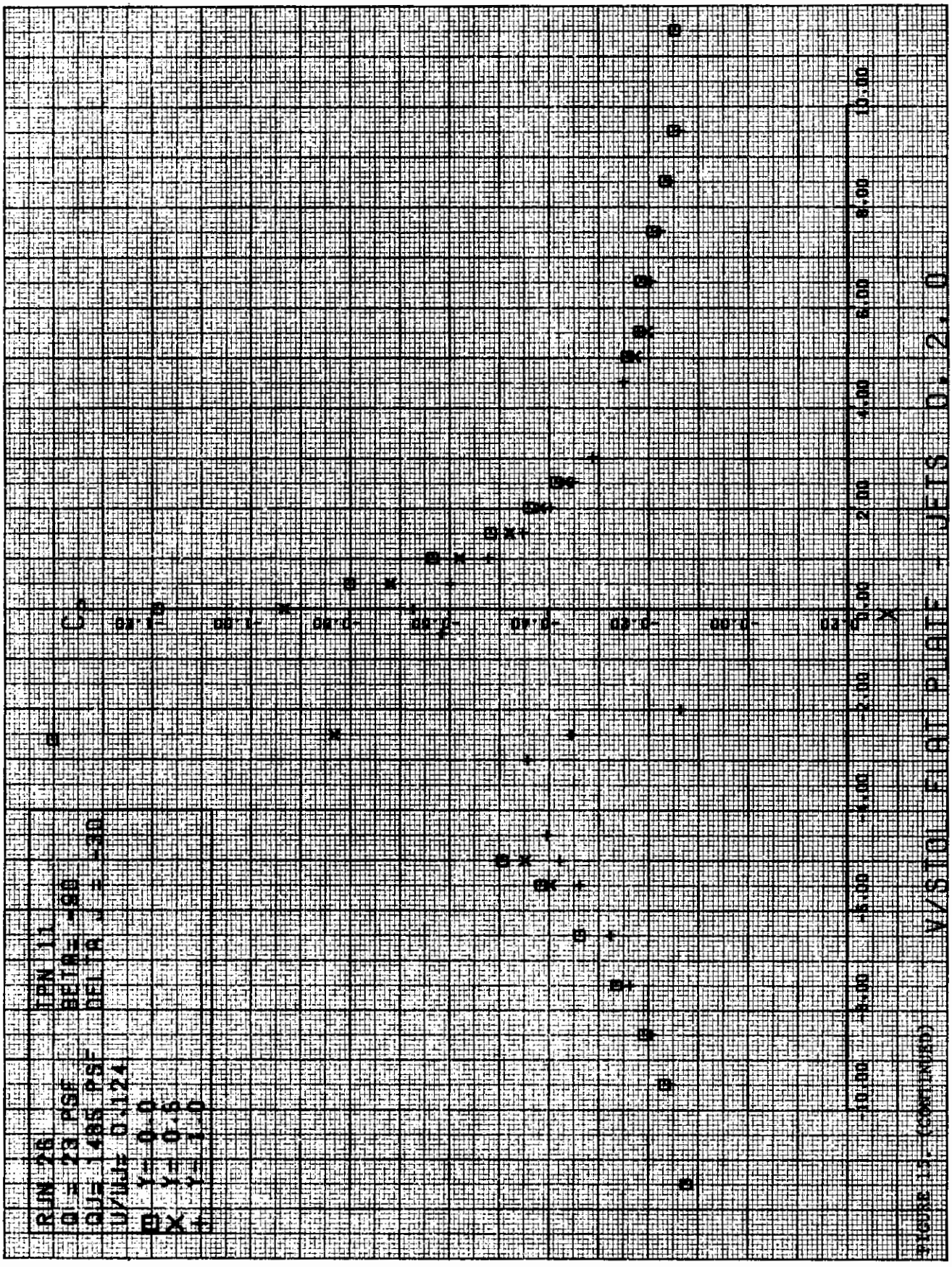

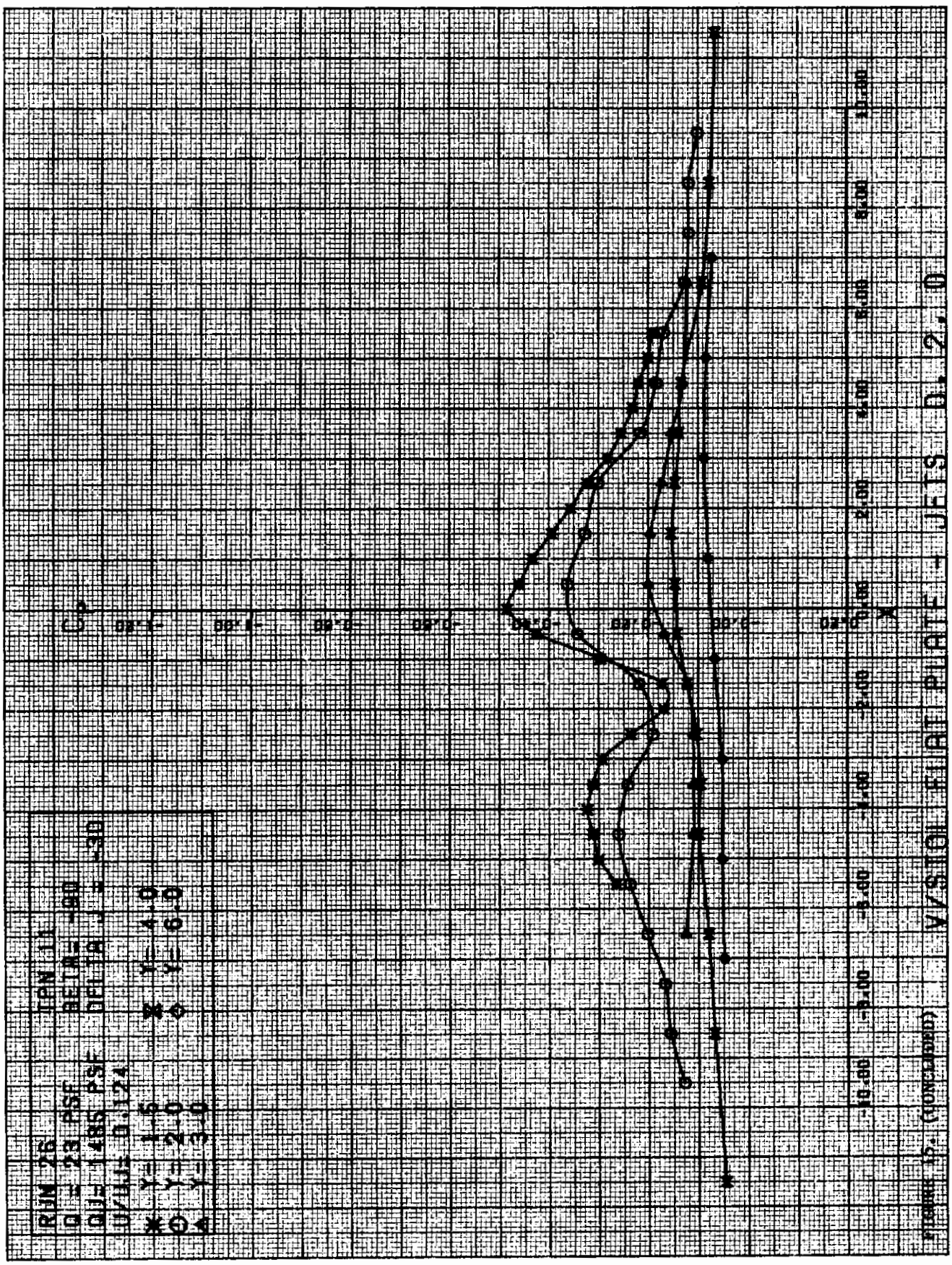

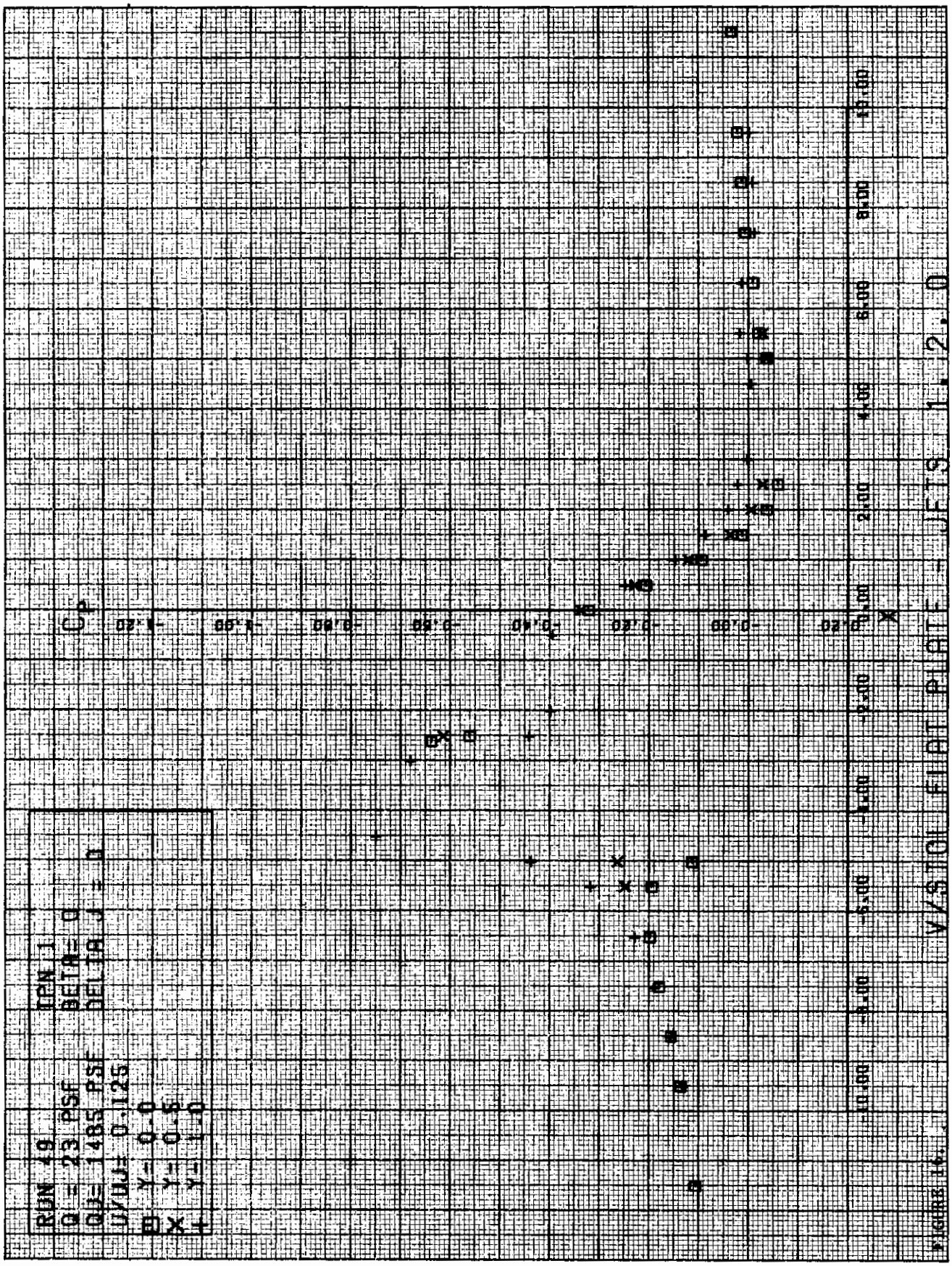

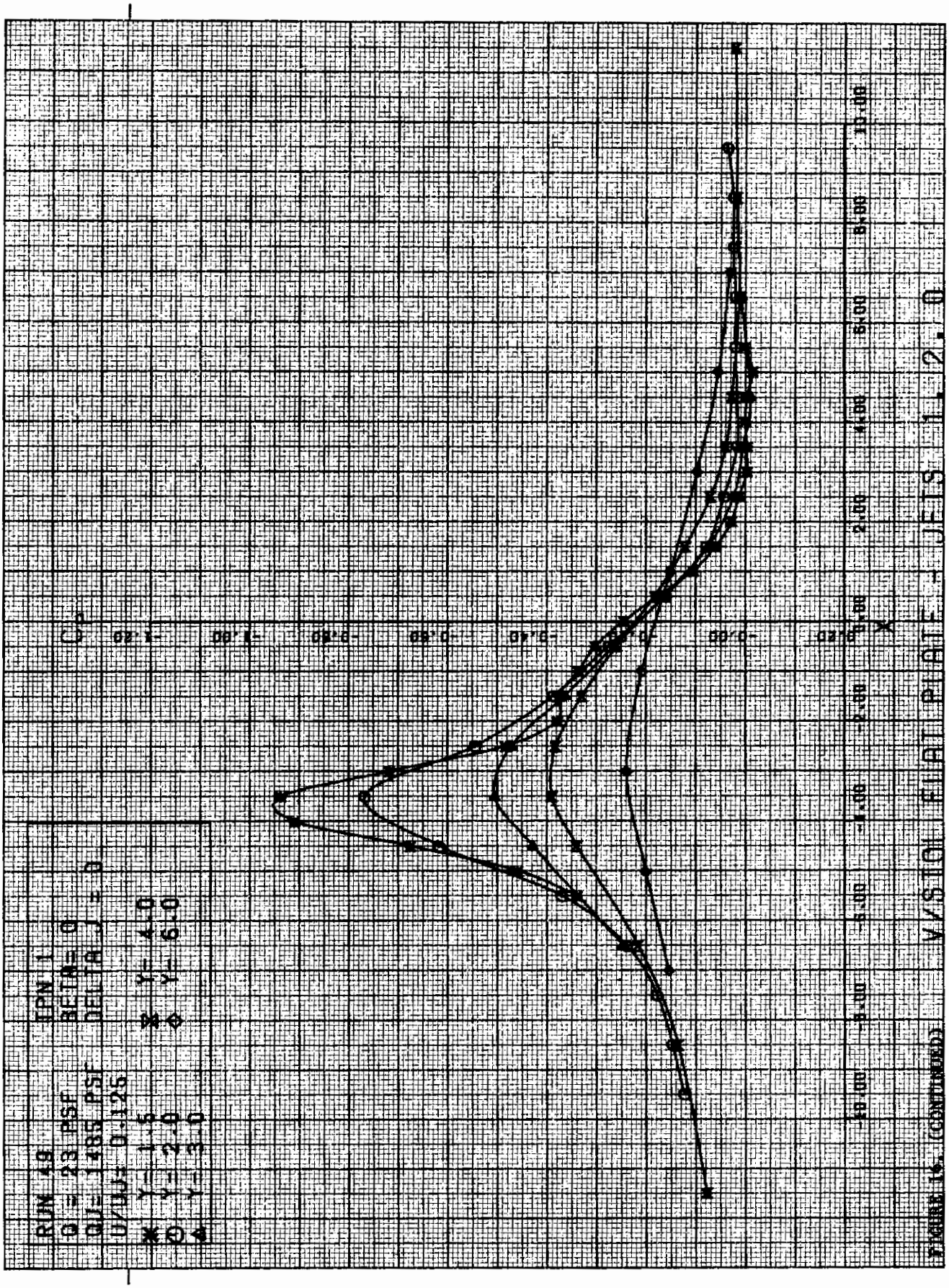

FIGURE 16. (CONTINUED)

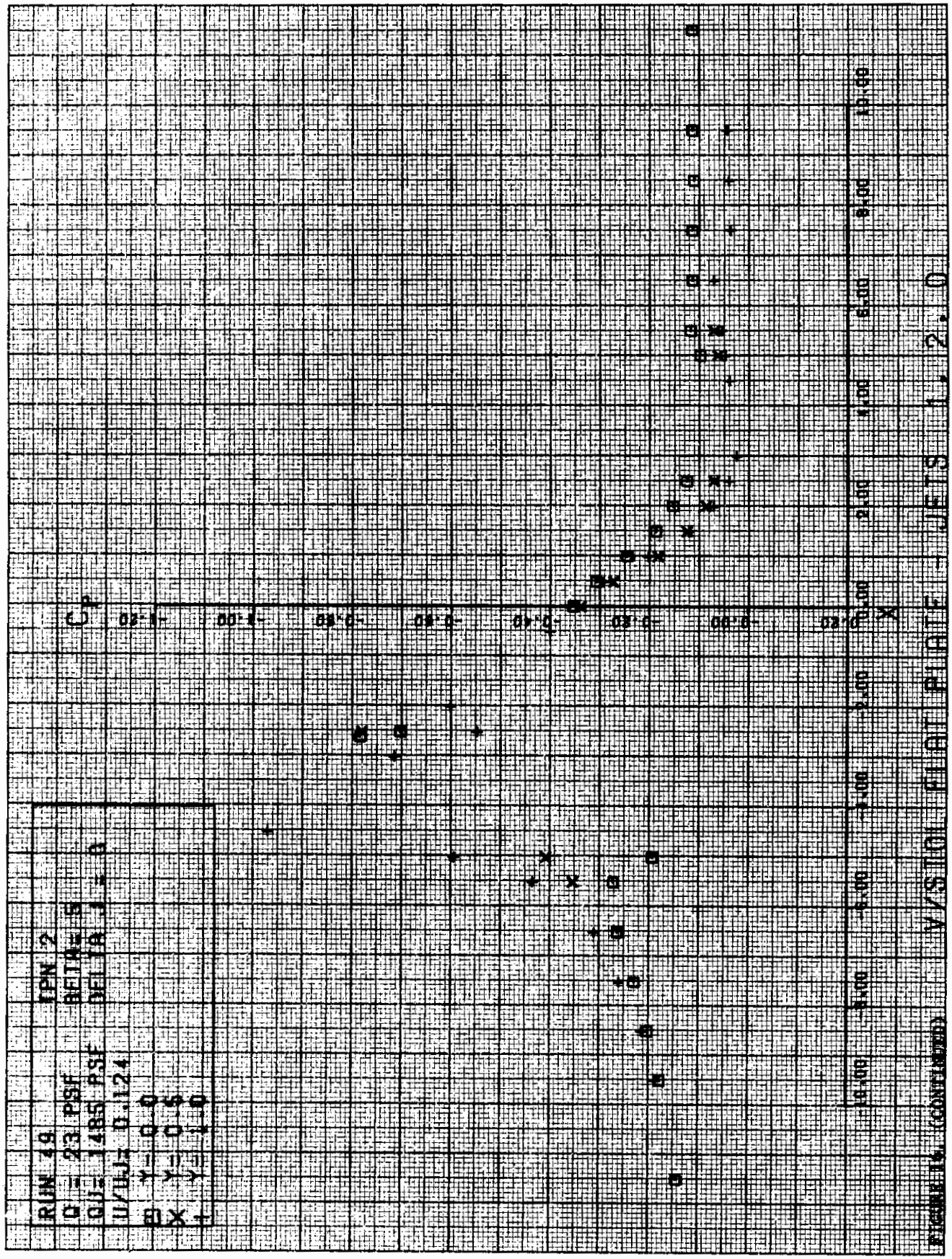

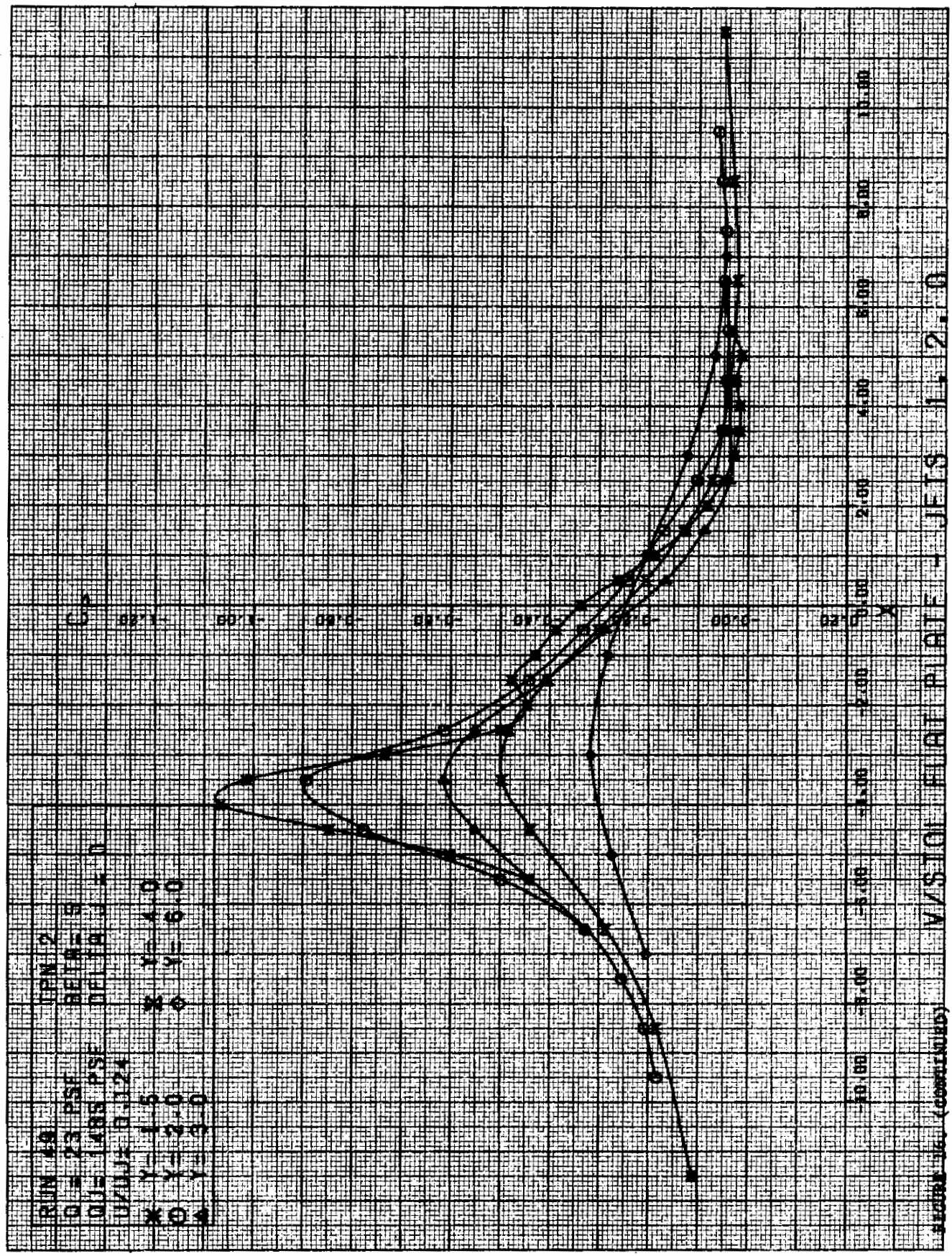

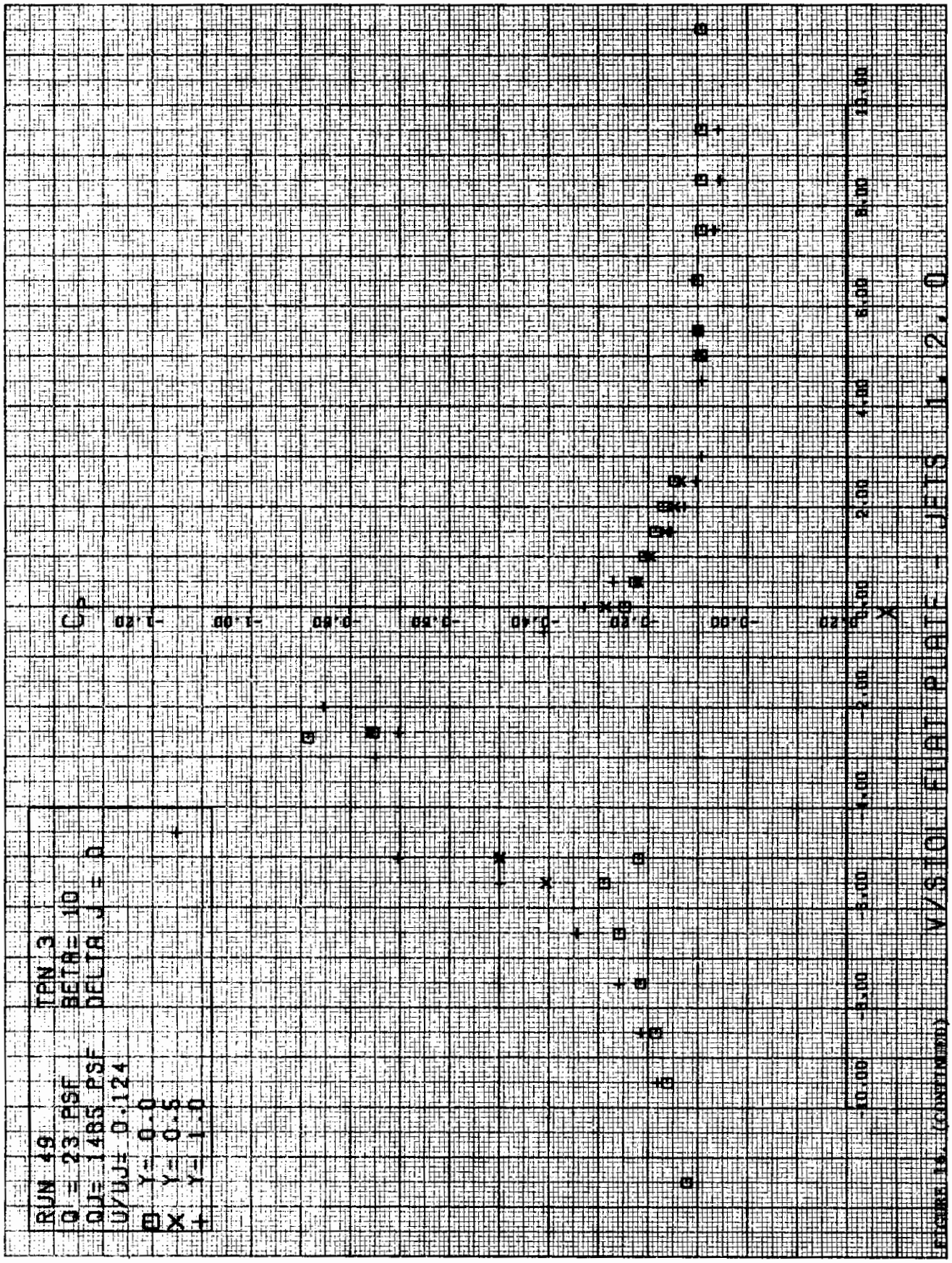

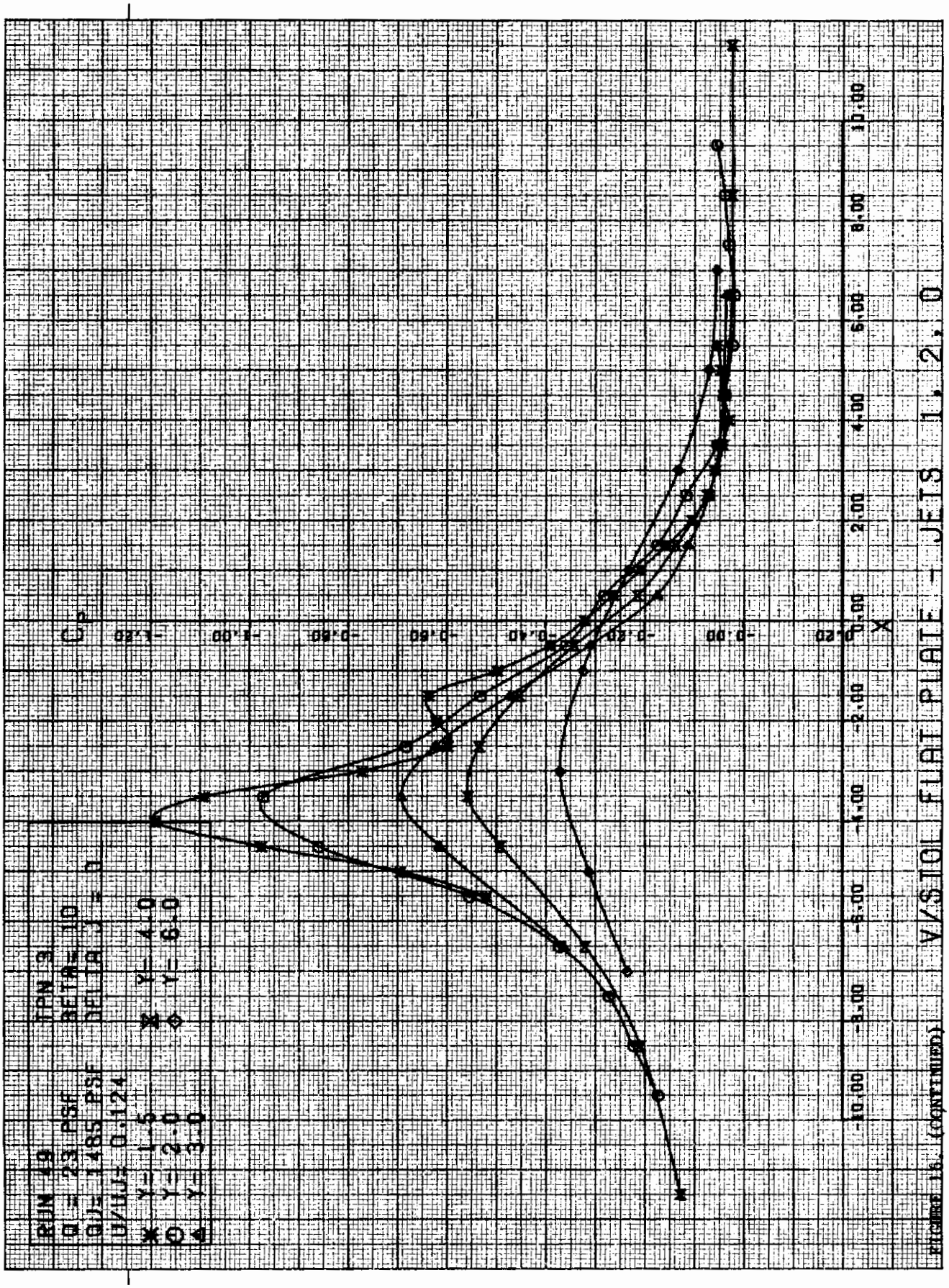

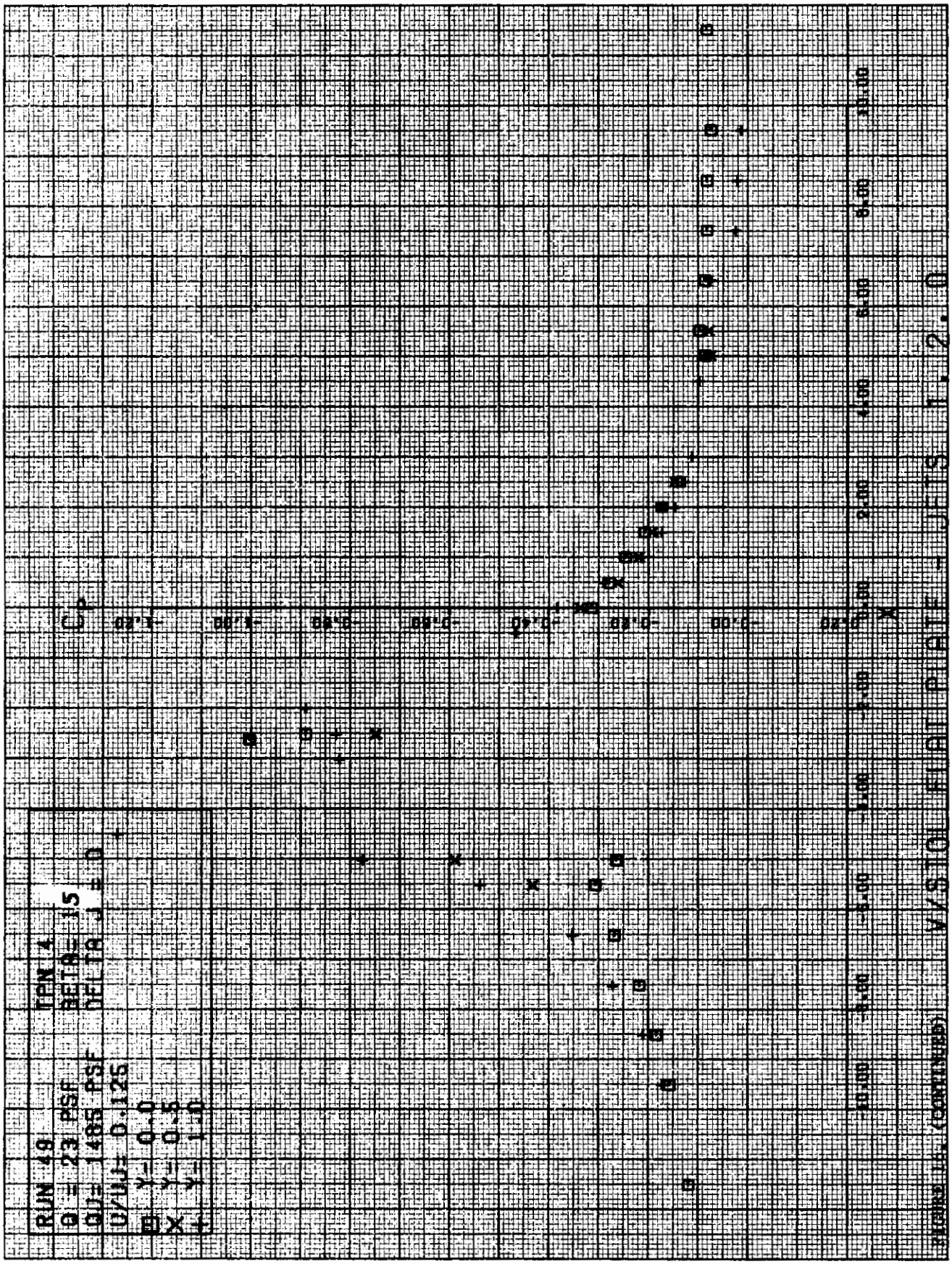

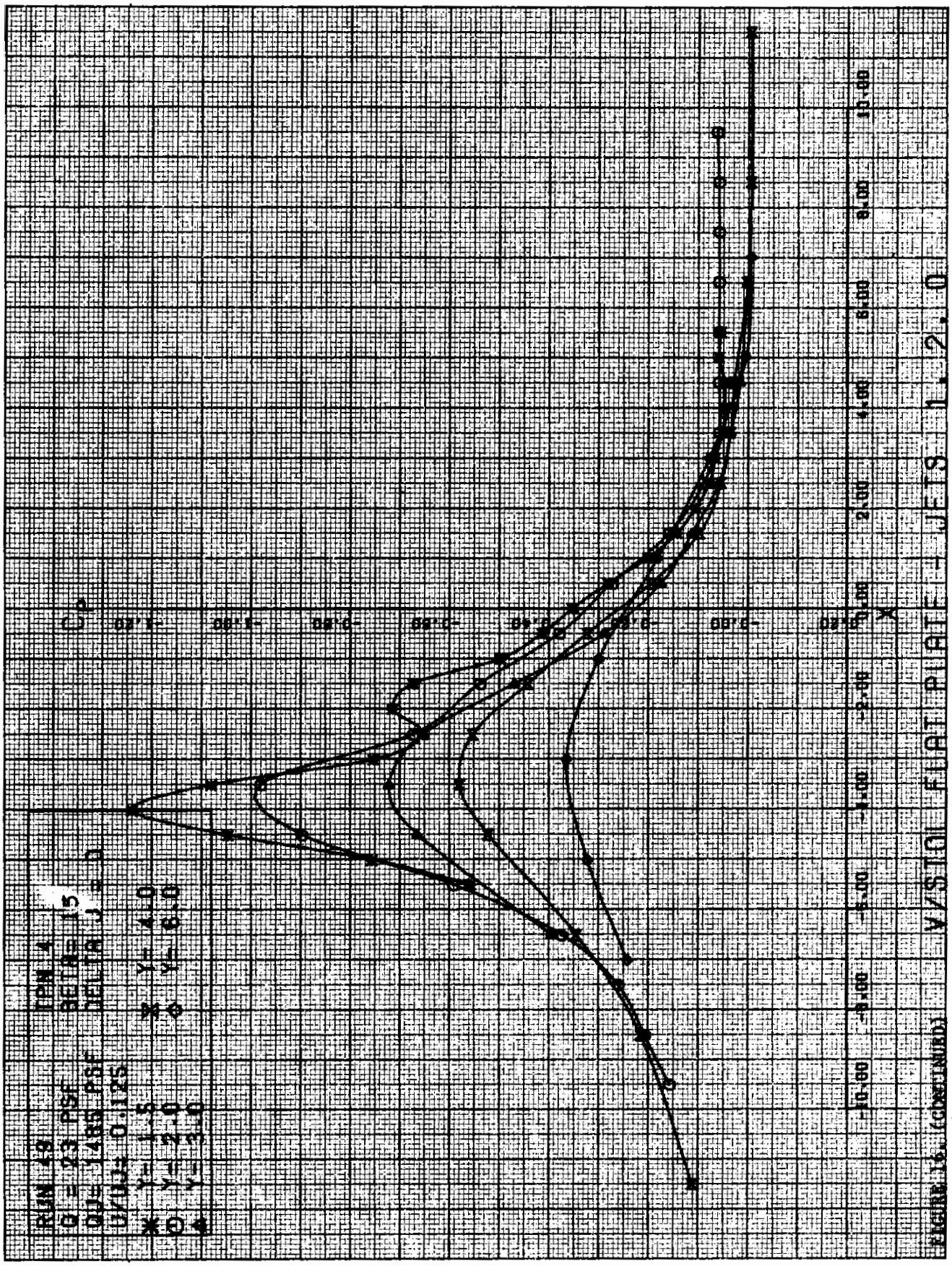

FIGURE 16. (CONCLUDED) V/STOL FLAT PLATE JETS h.2.0

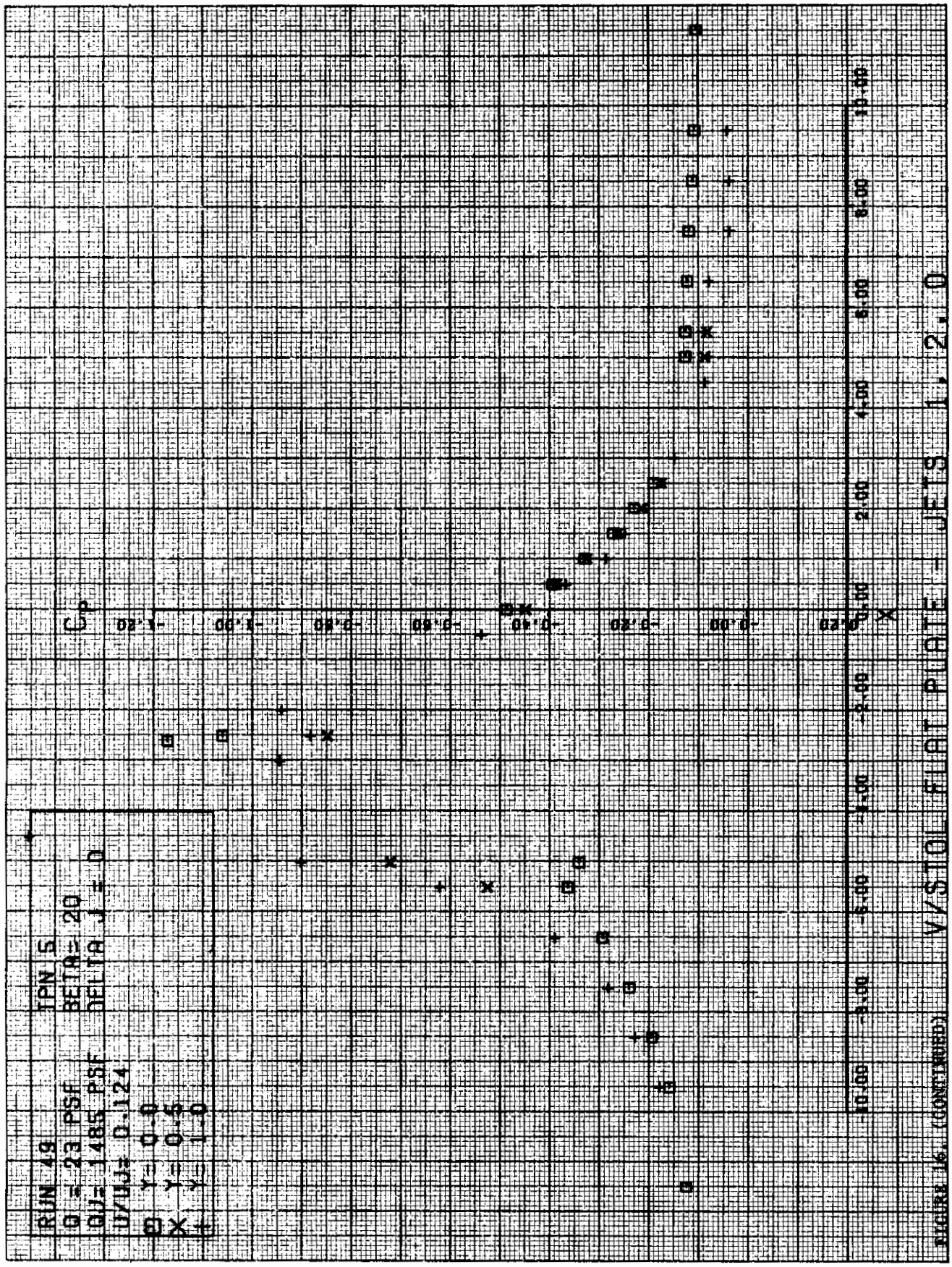

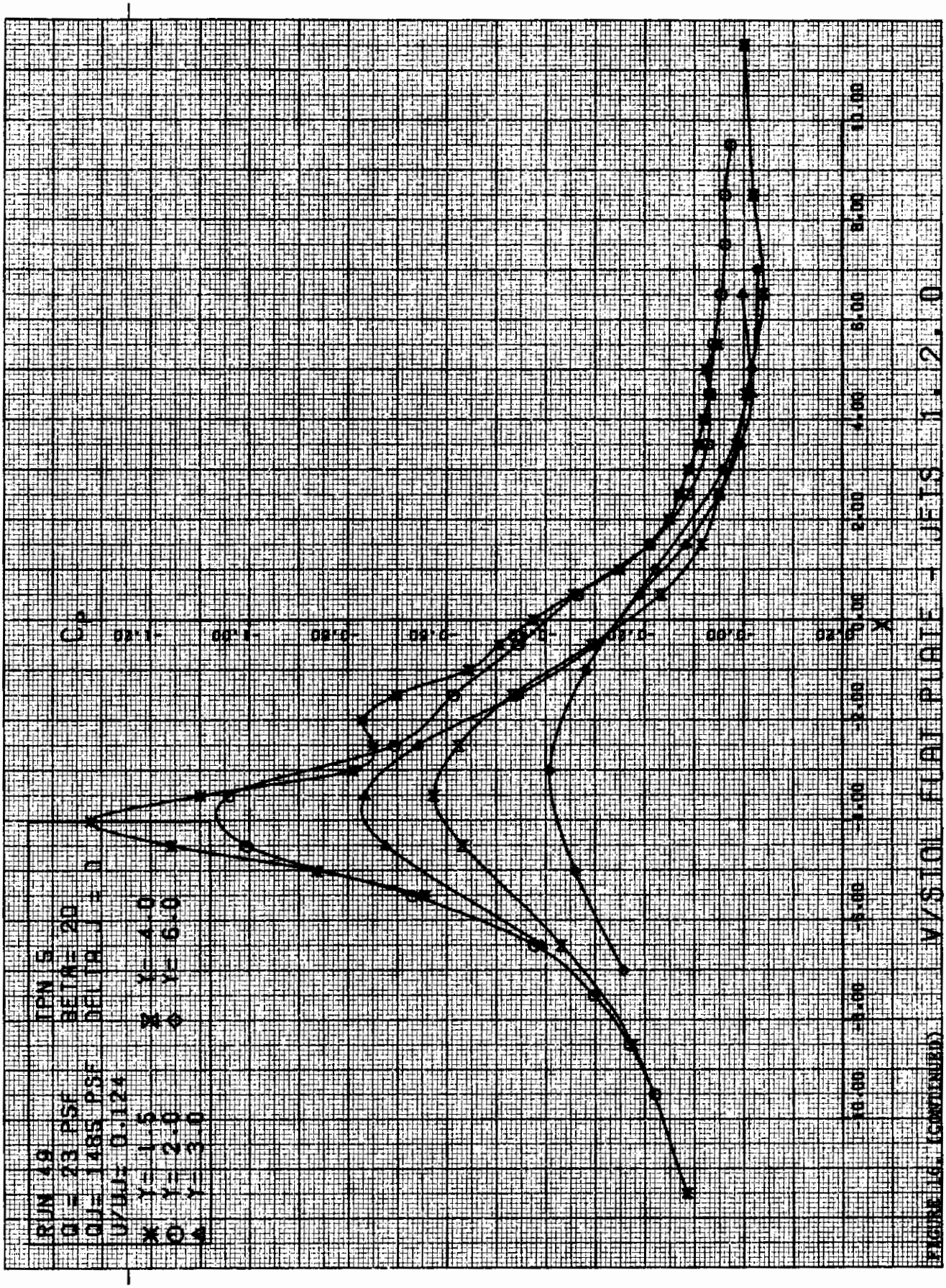

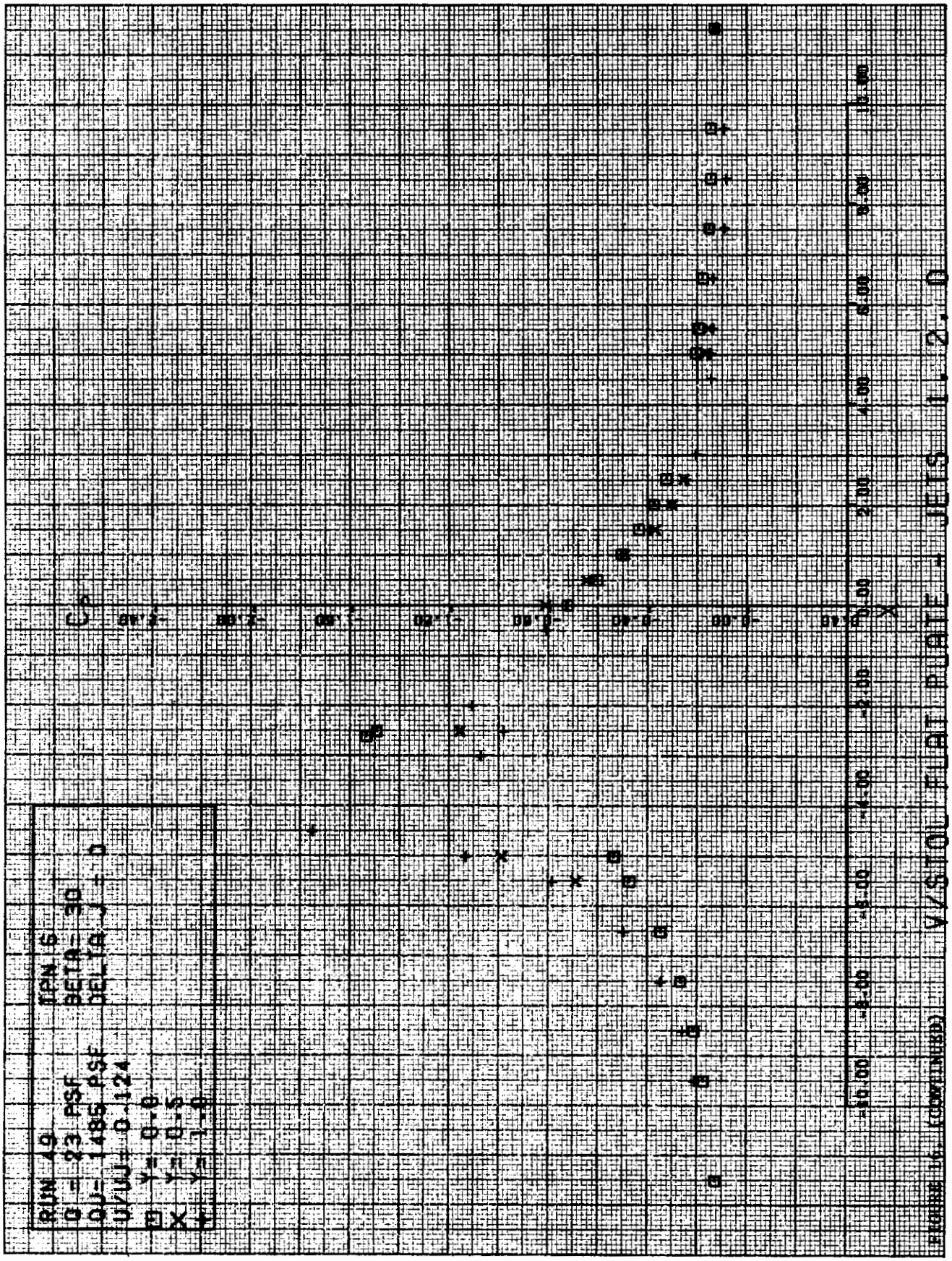

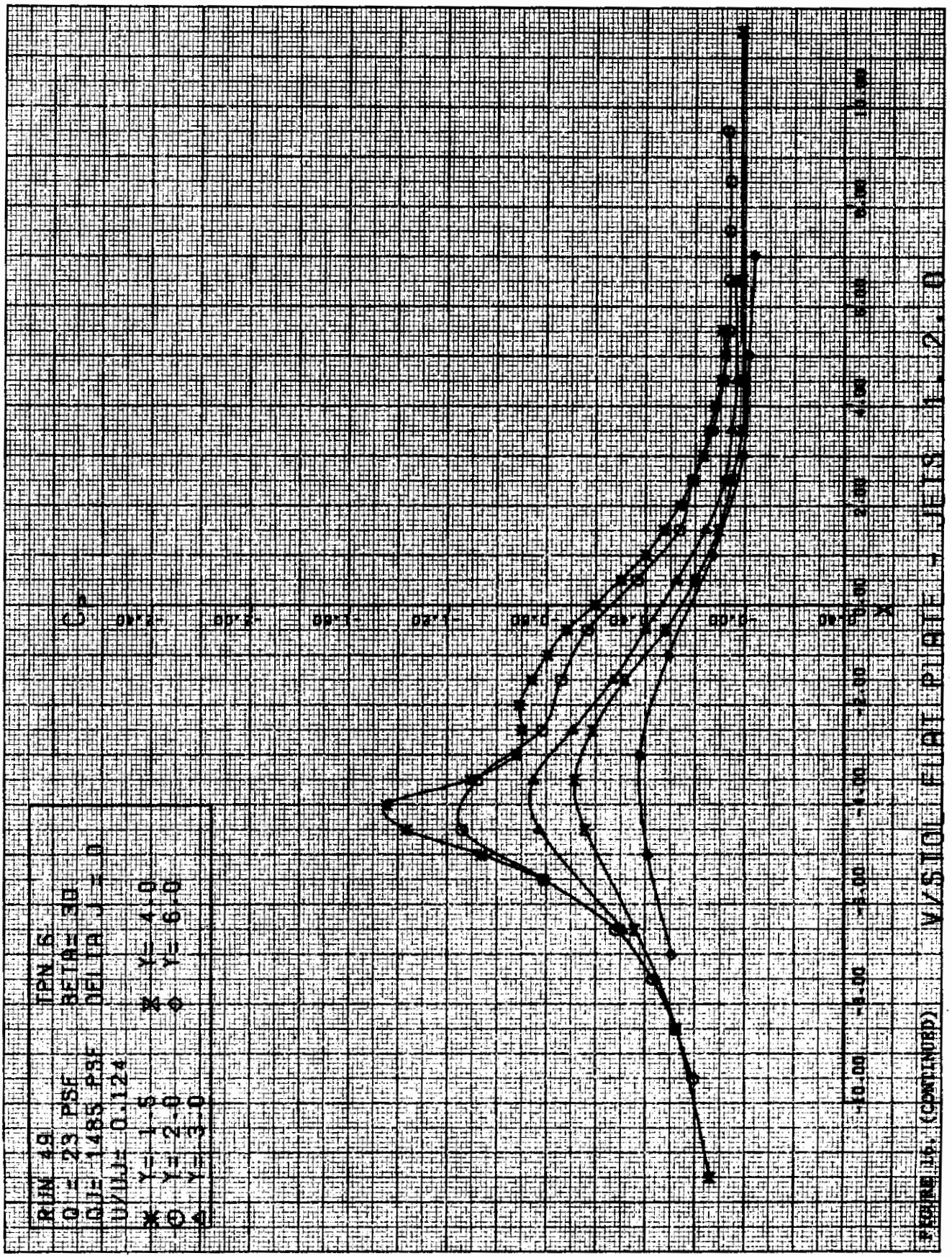

FIGURE 16. (CONTINUED) V/5 TOL FLAT PLATE - JETS 1, 2, 0

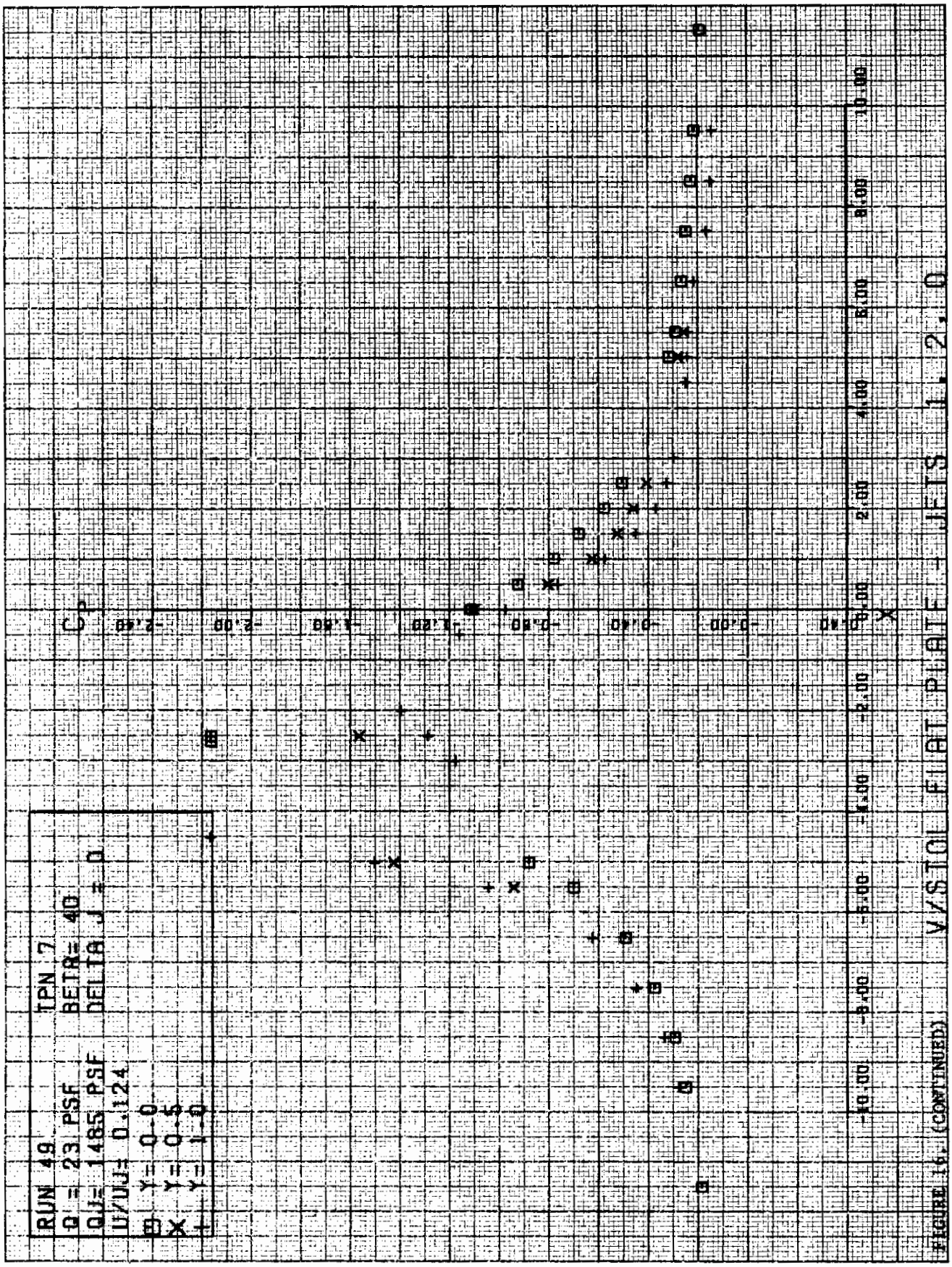

FIGURE 16. (CONTINUED)

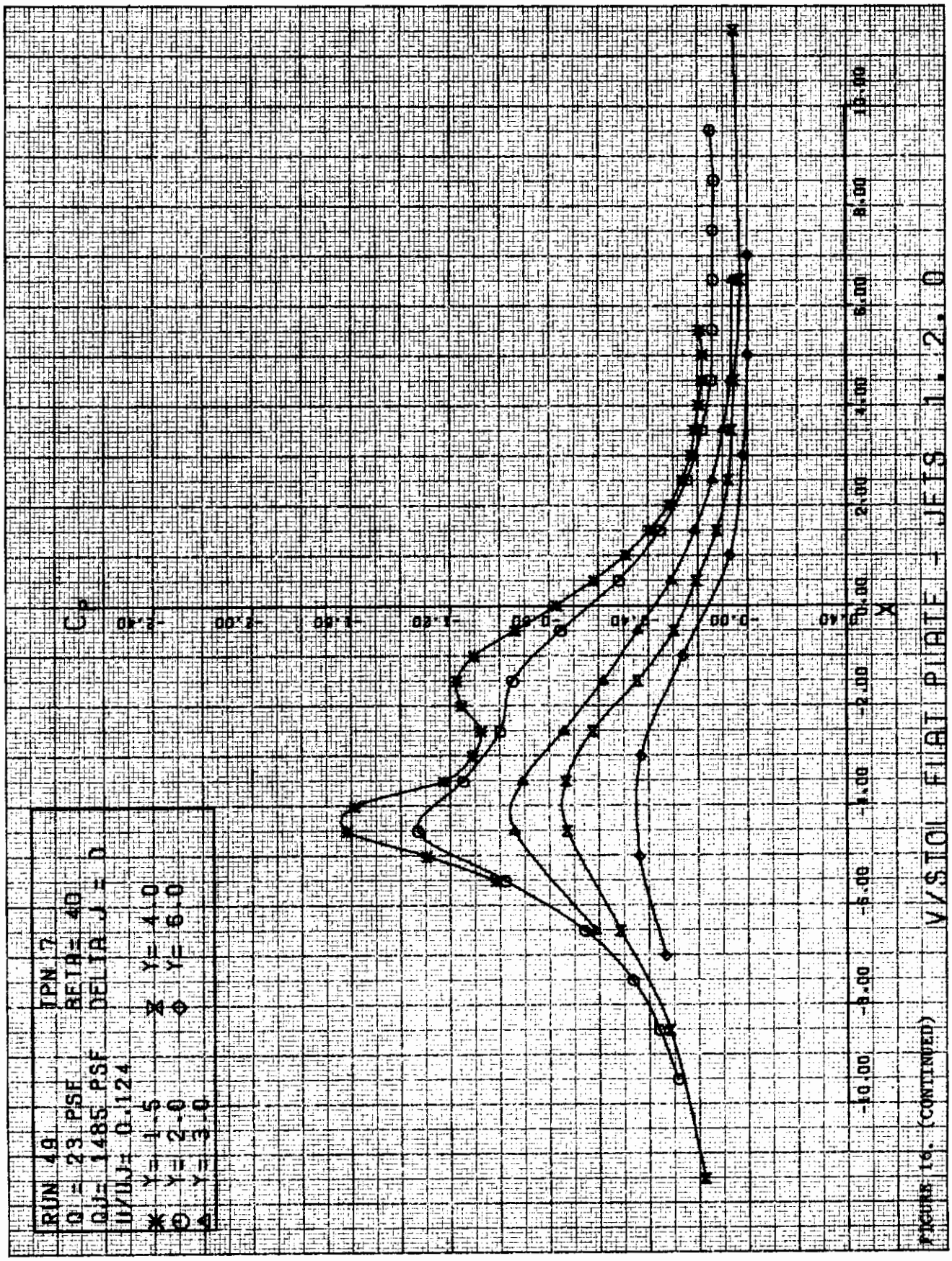

FIGURE 16. (CONTINUED)

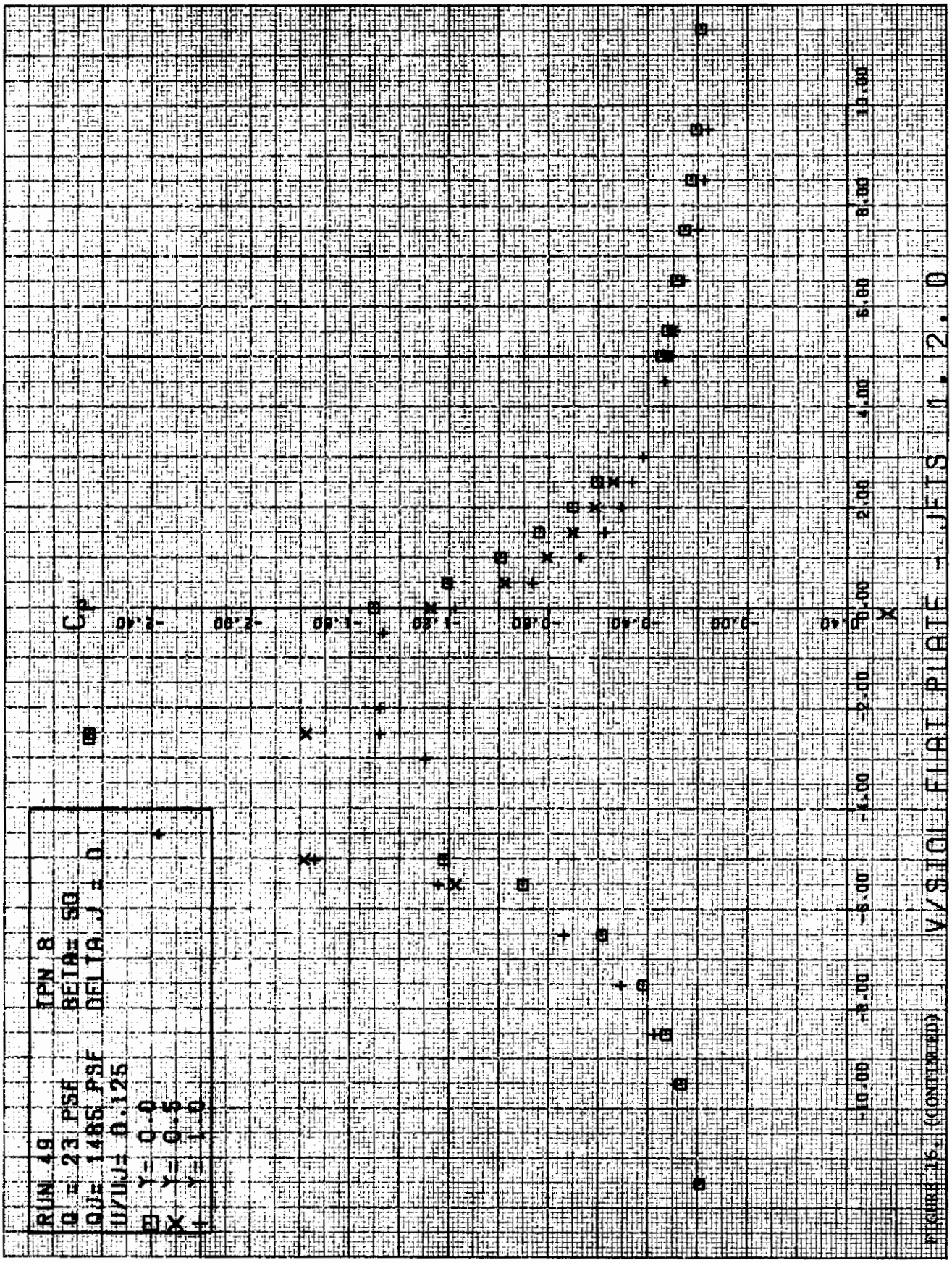

FIGURE 16. (CONTINUED)

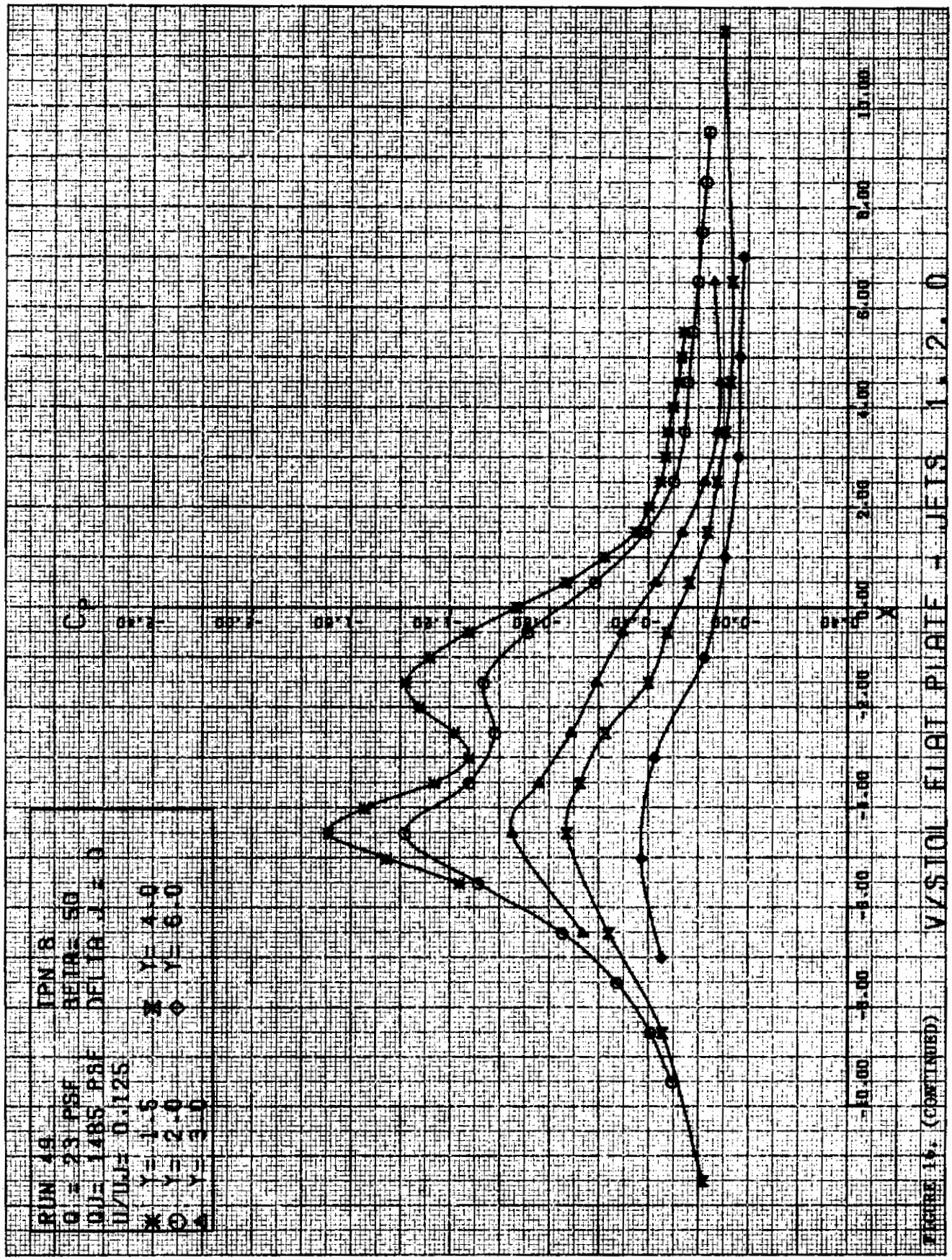

FIGURE 16. (CONTINUED)

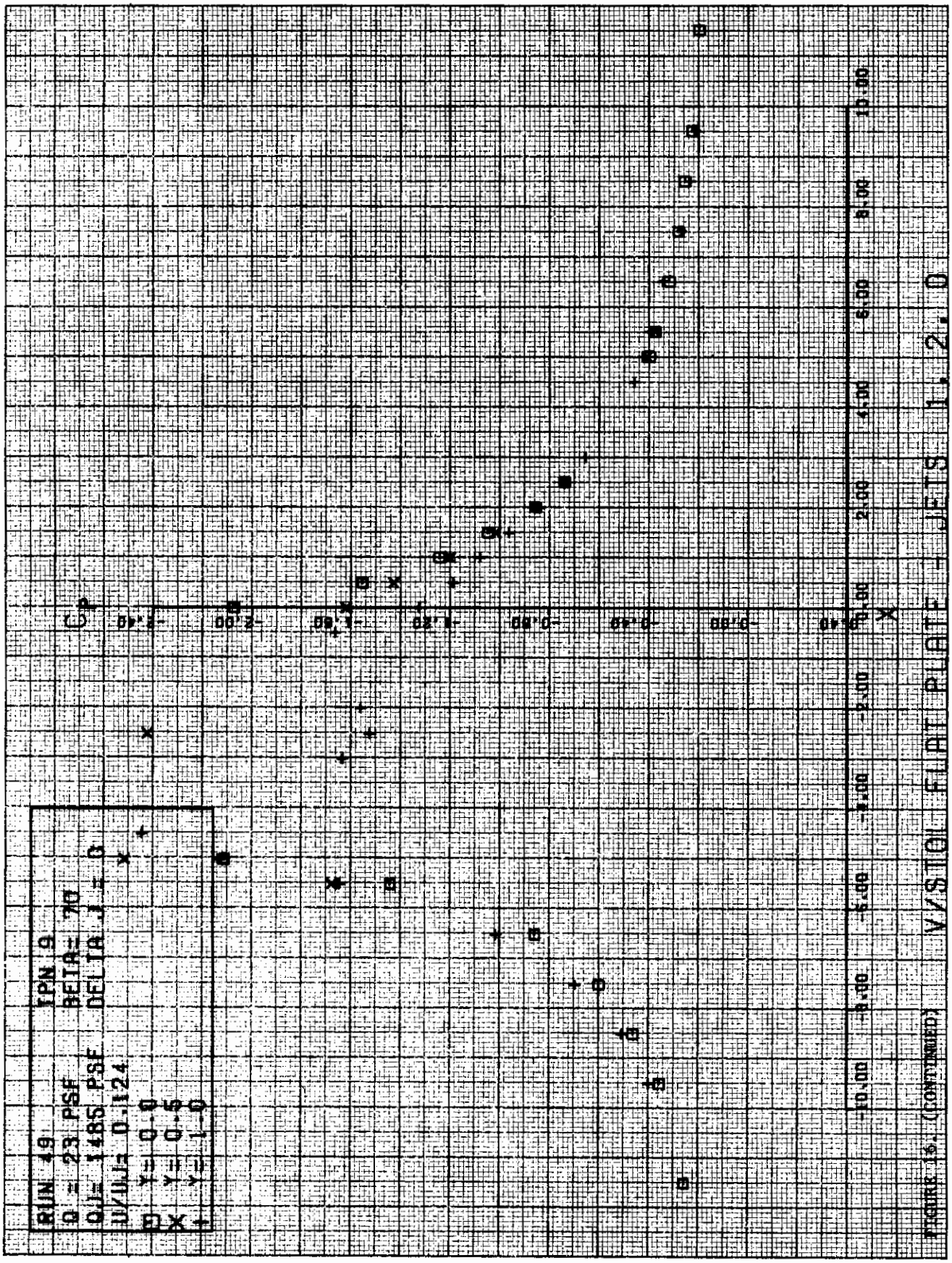

FIGURE 16. (CONTINUED) V/STOL FLAT PLATE - JETS 1, 2, 0

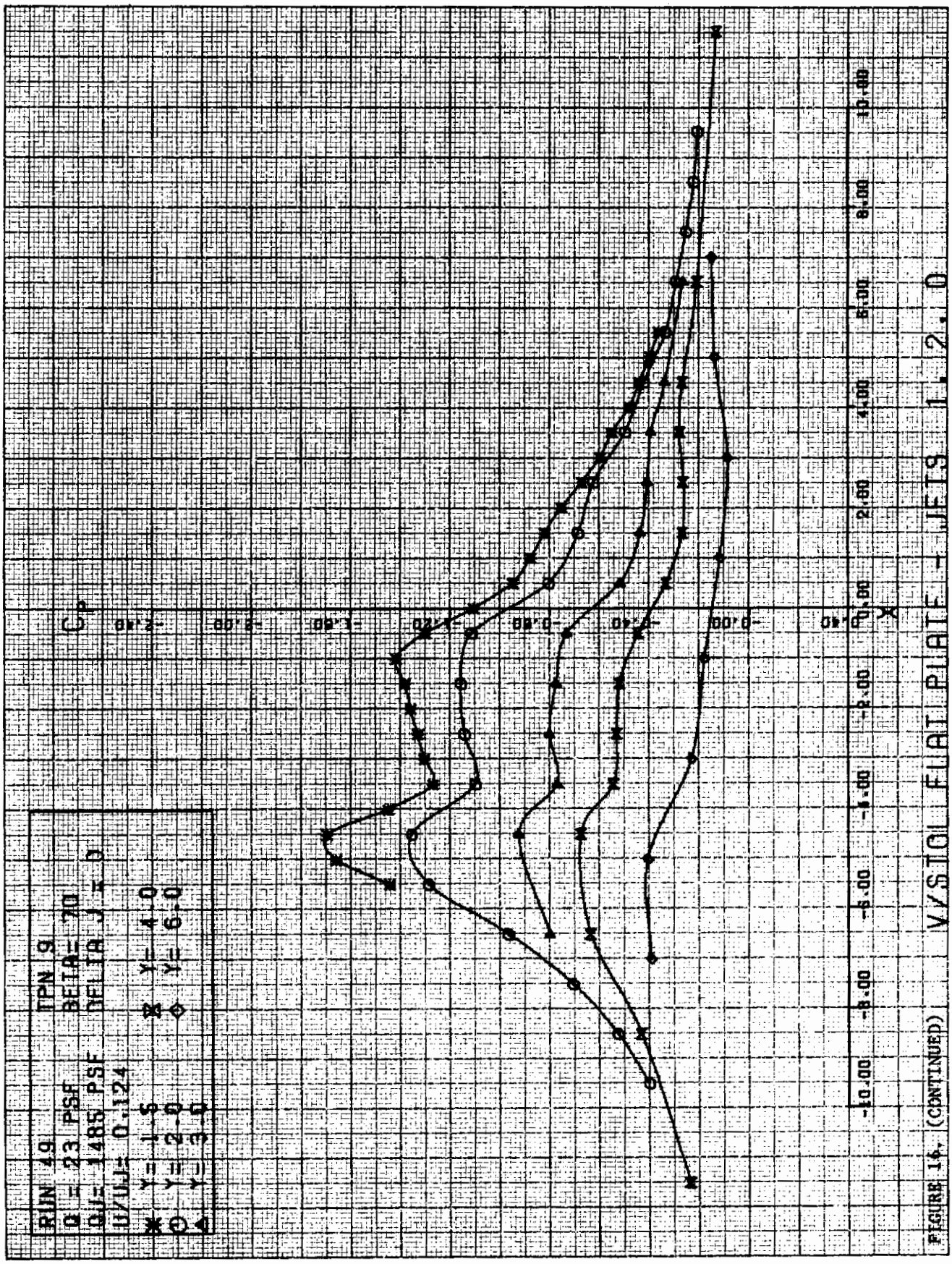

FIGURE 16. (CONTINUED)

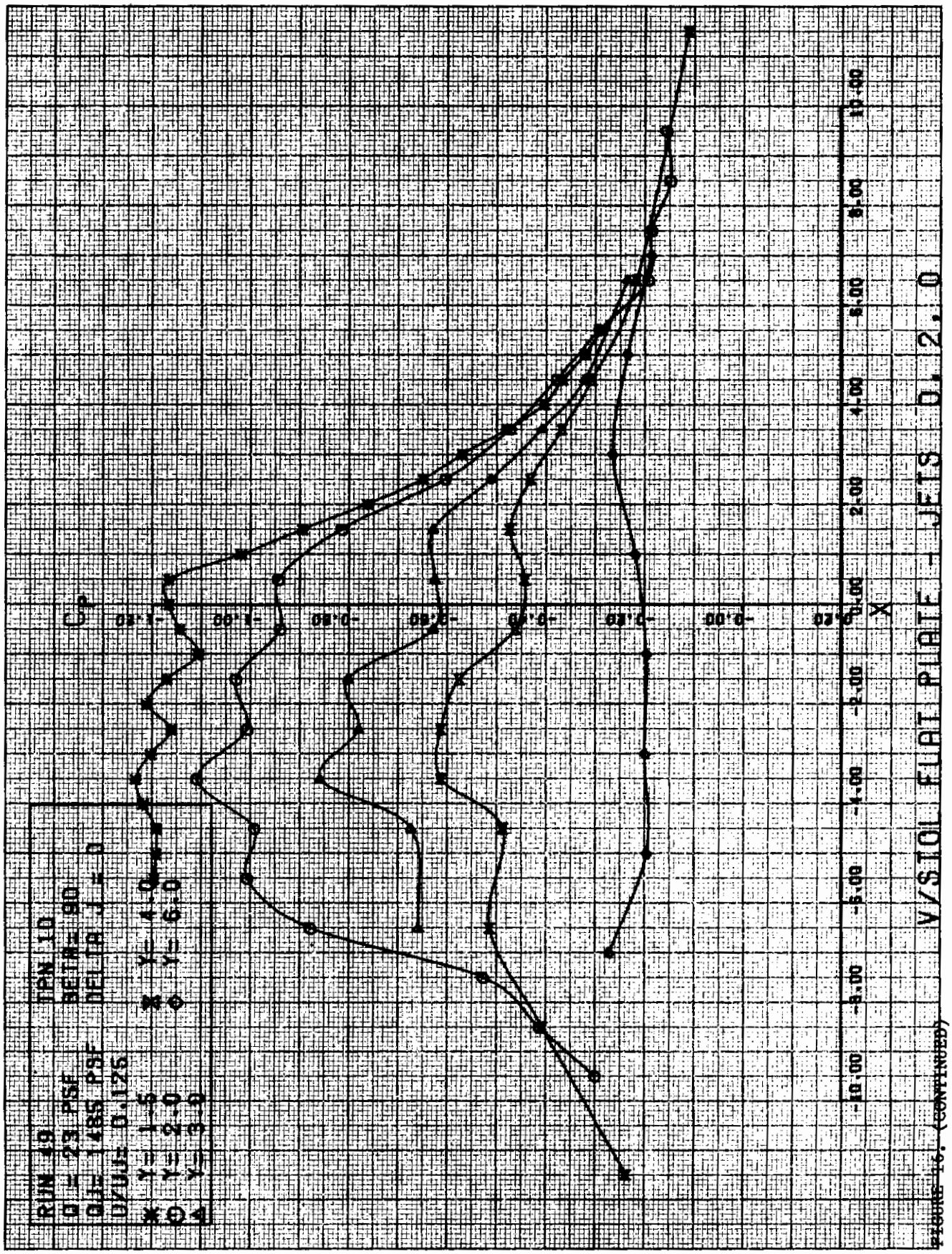

FIGURE 16. (CONTINUED)

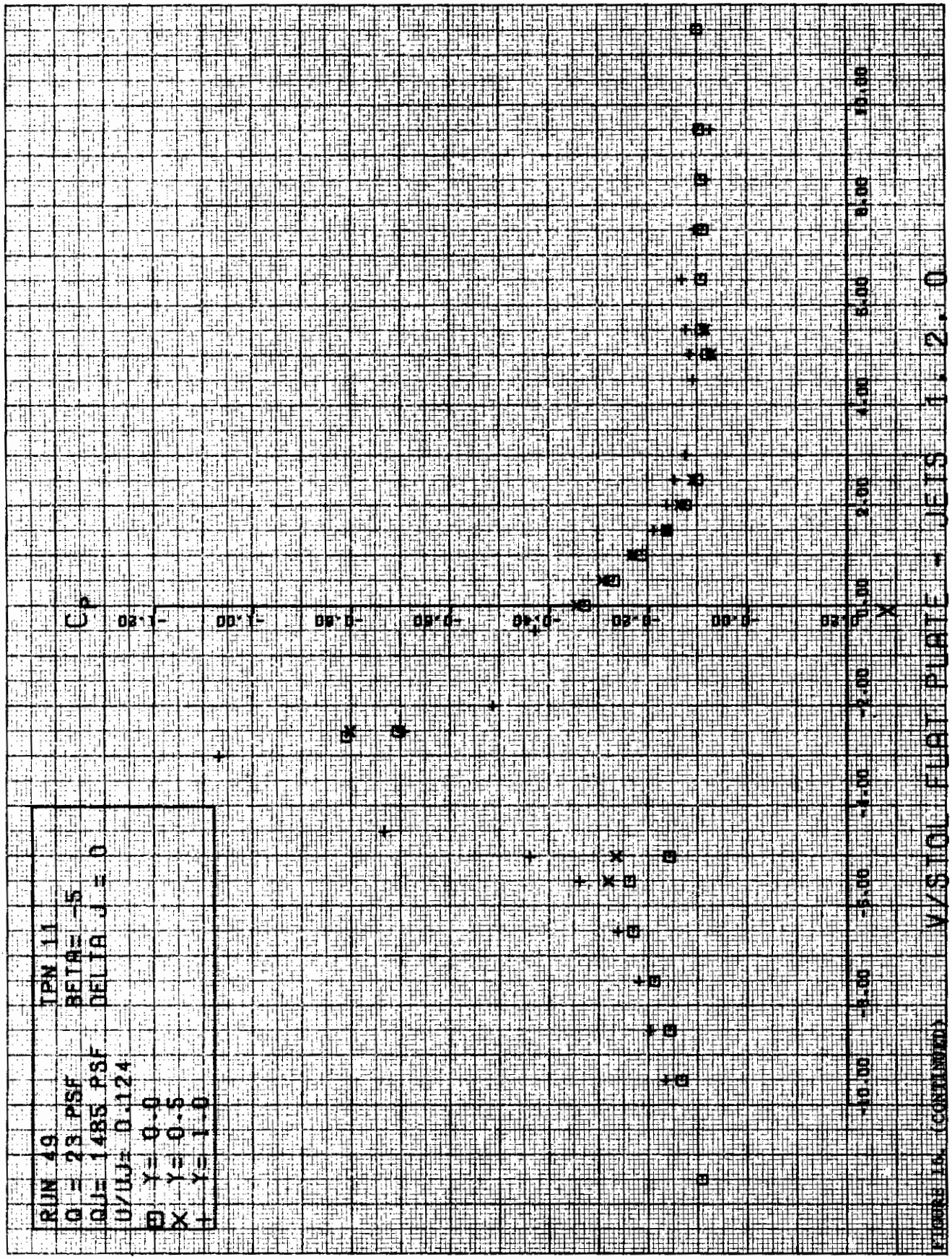

FIGURE 16. (CONTINUED)

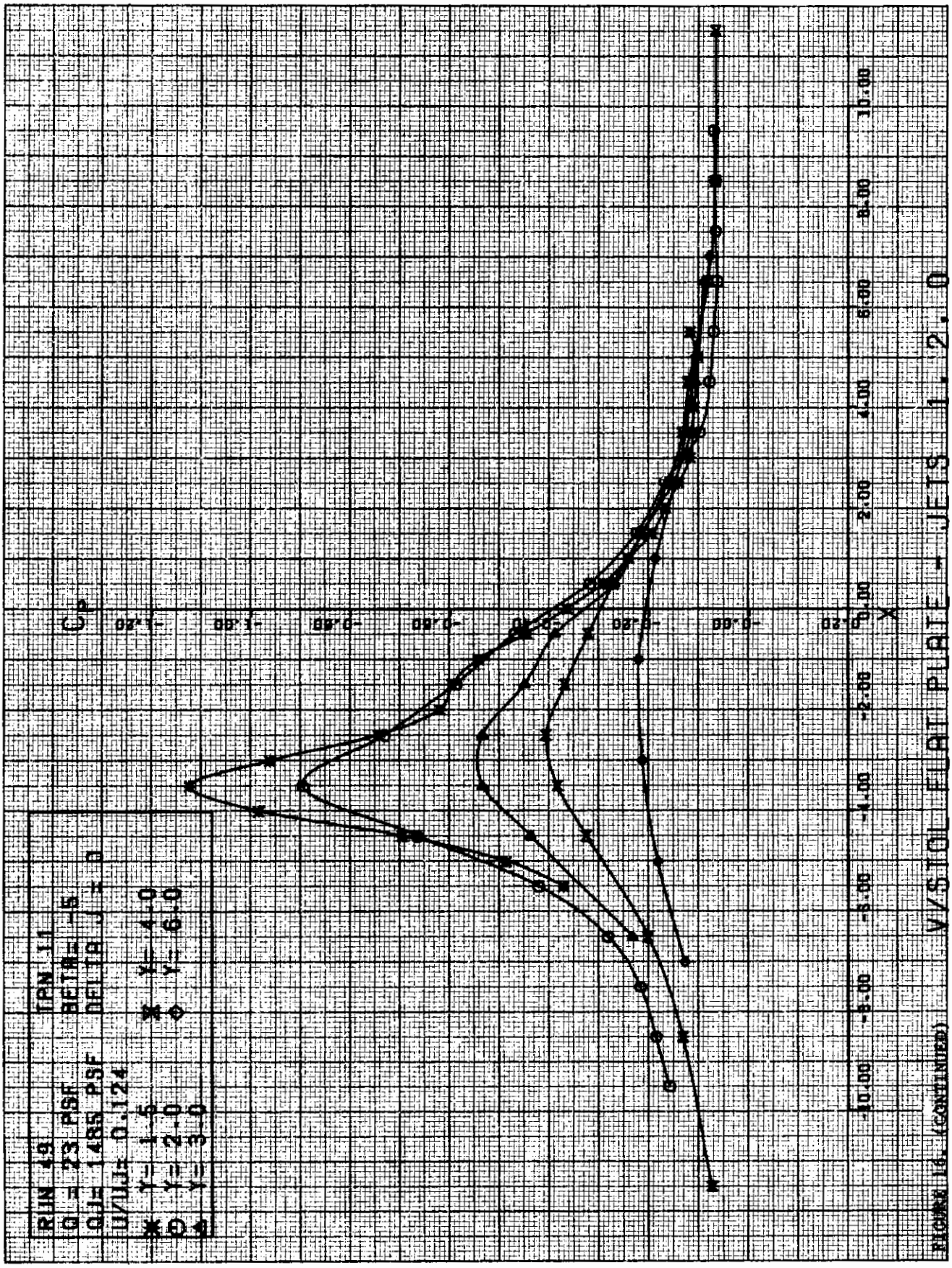

FIGURE 16. (CONTINUED)

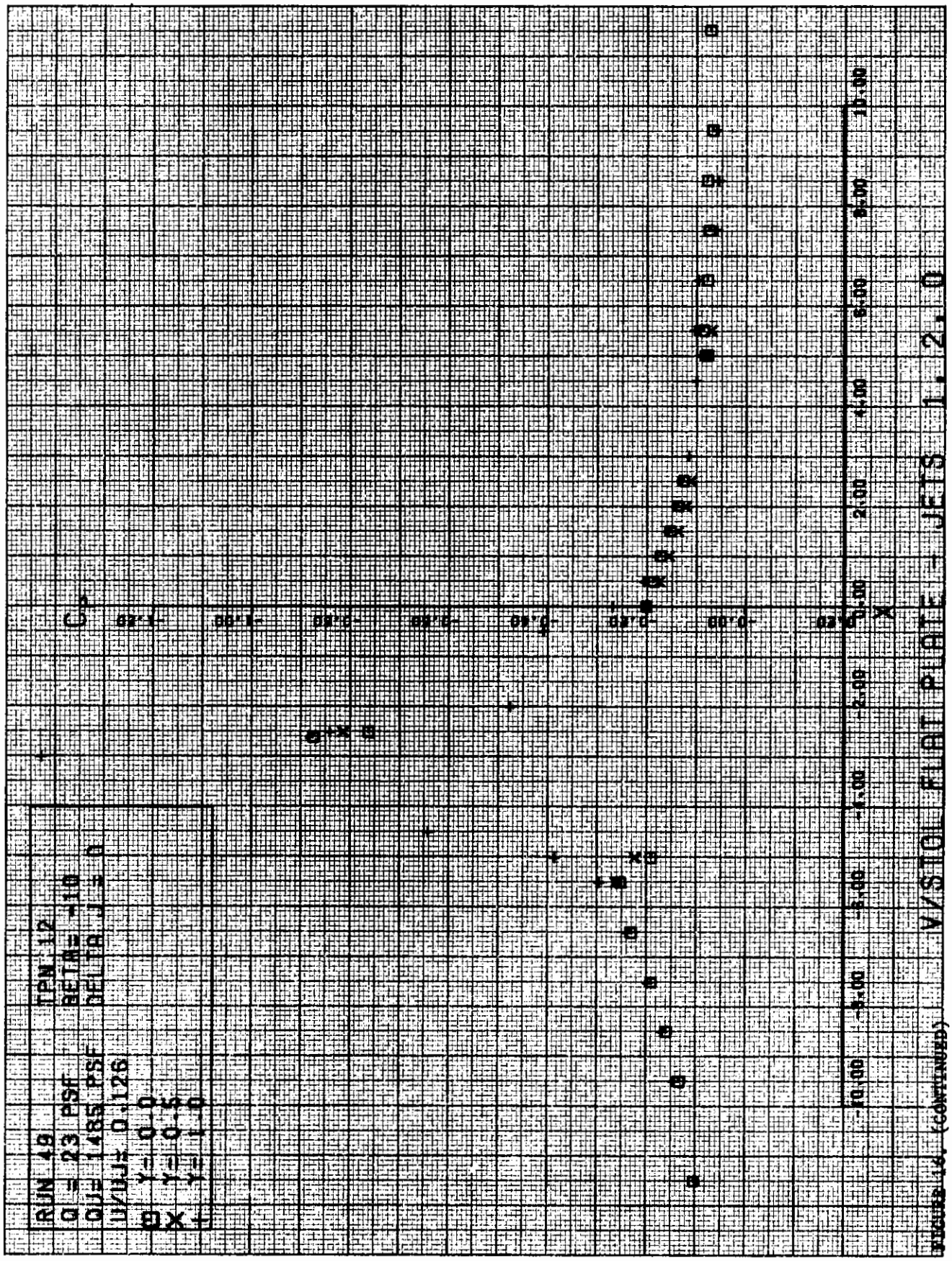

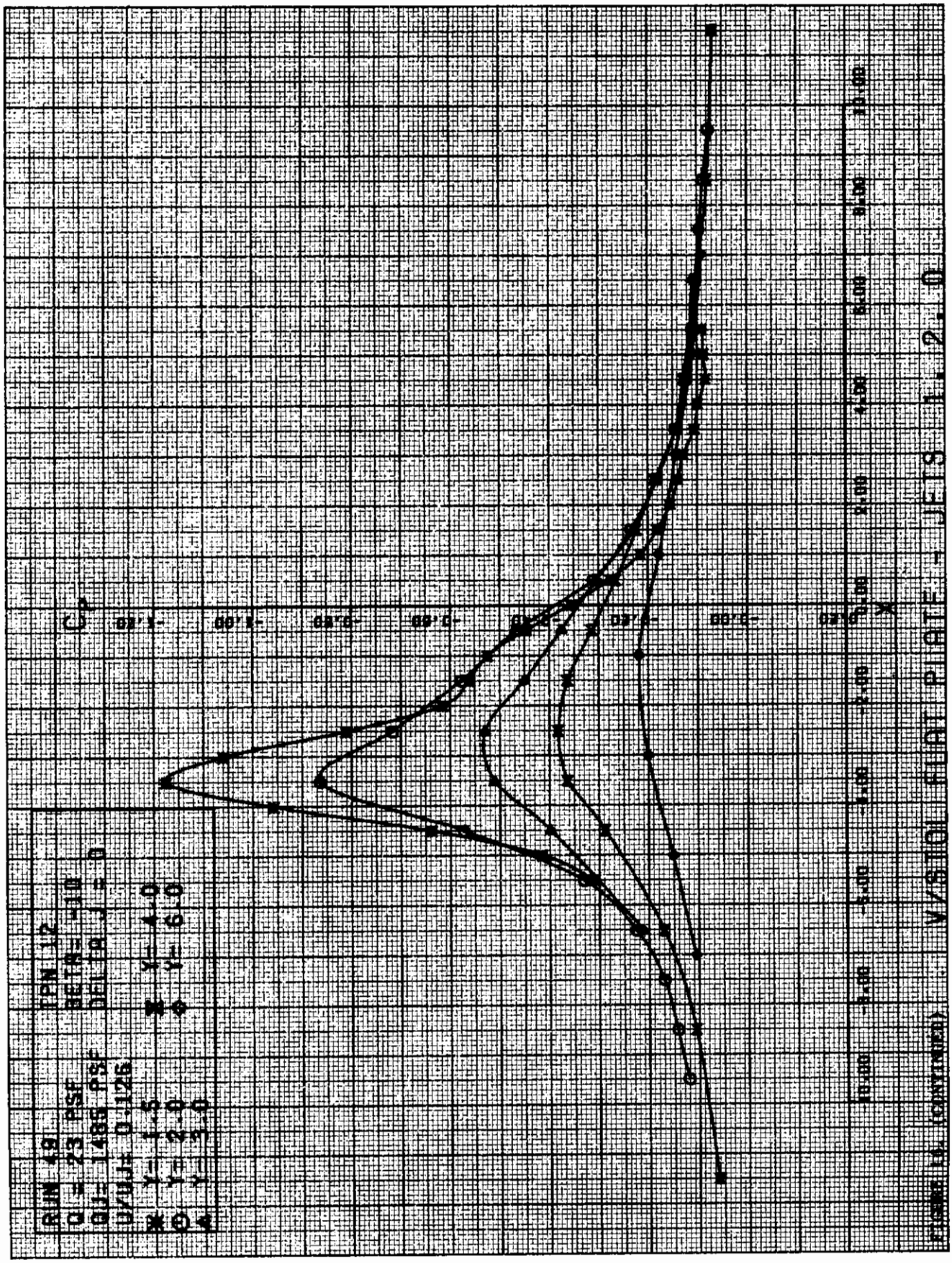

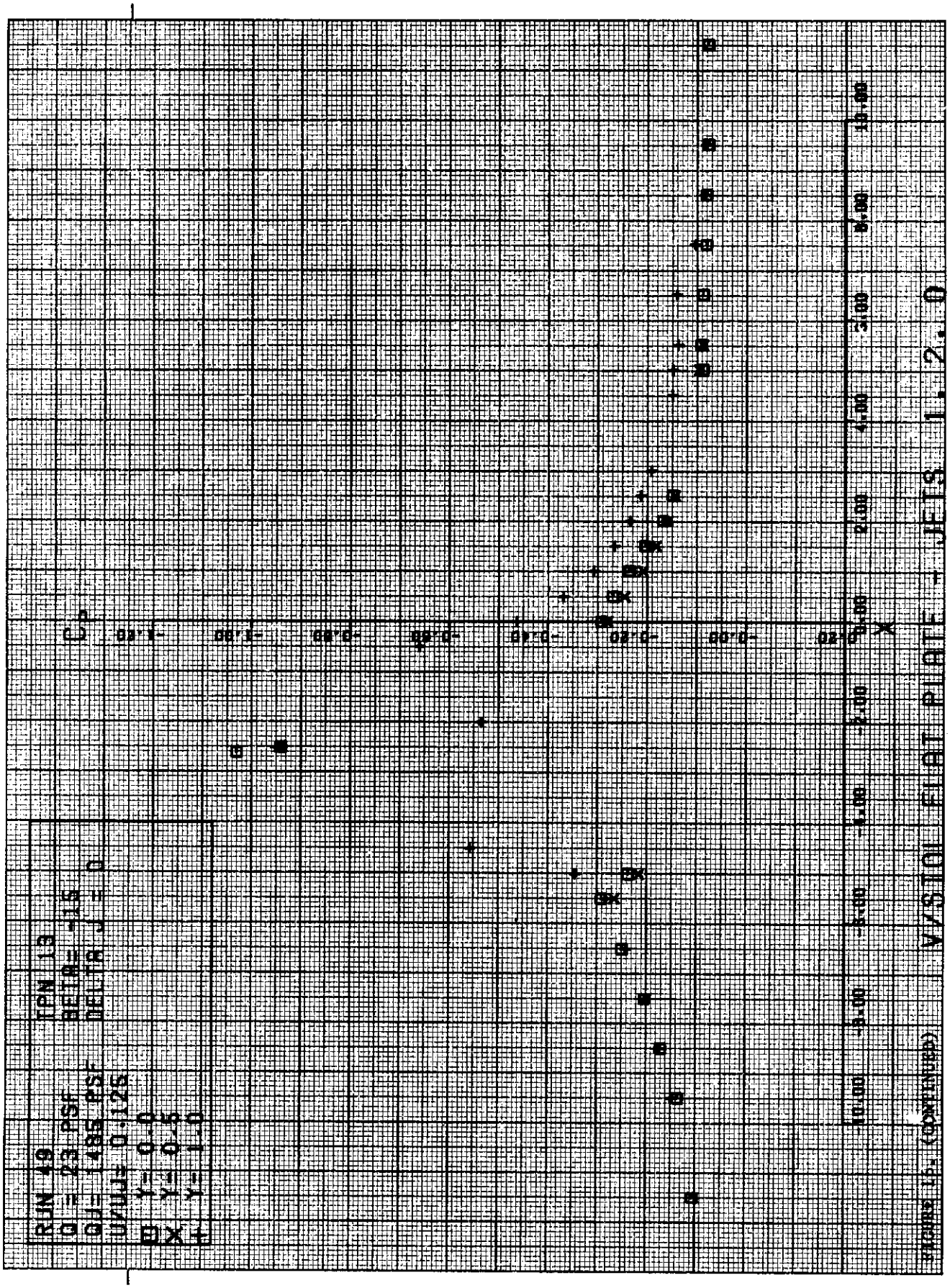

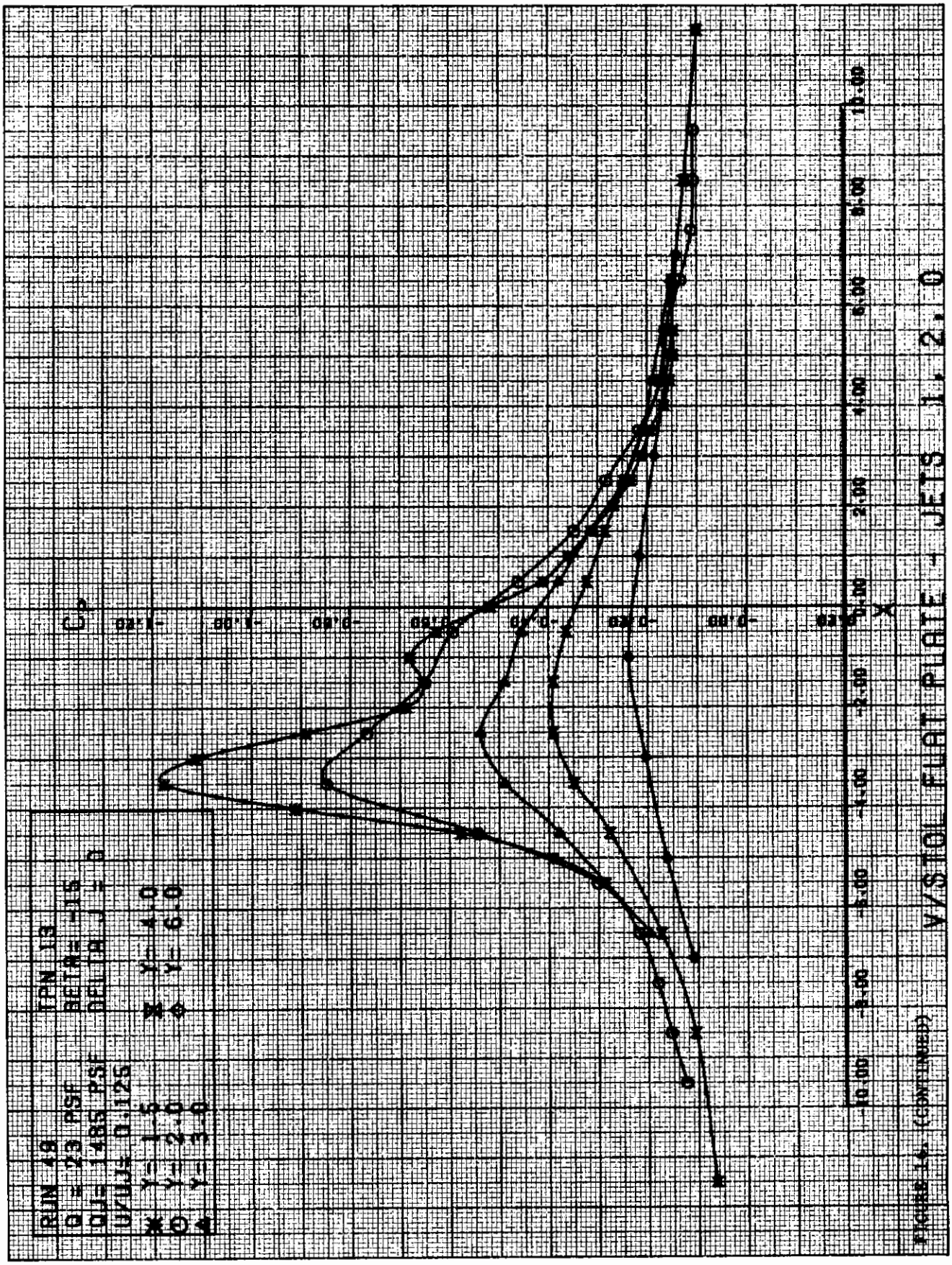

FIGURE 14. (CONTINUED)

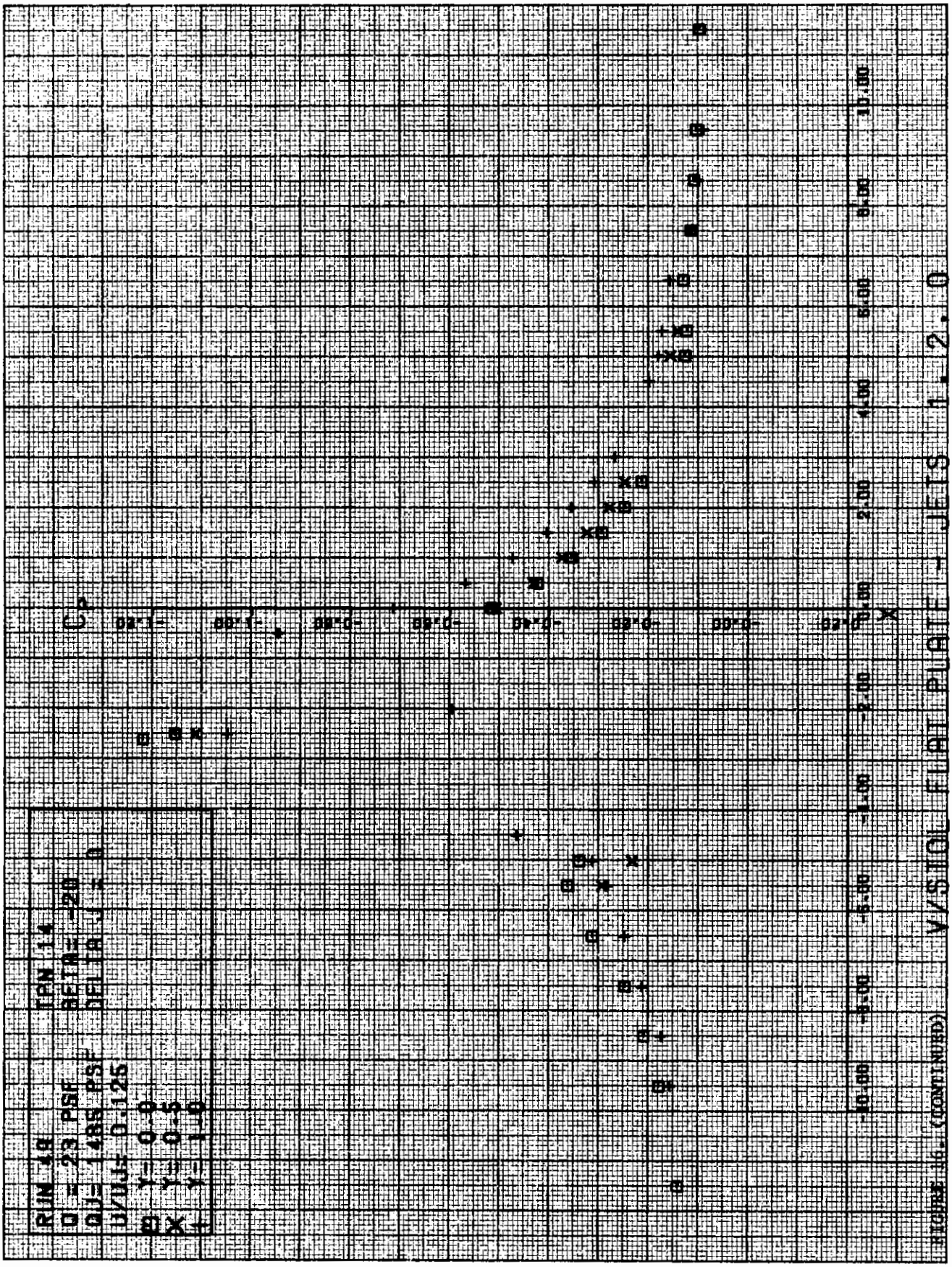

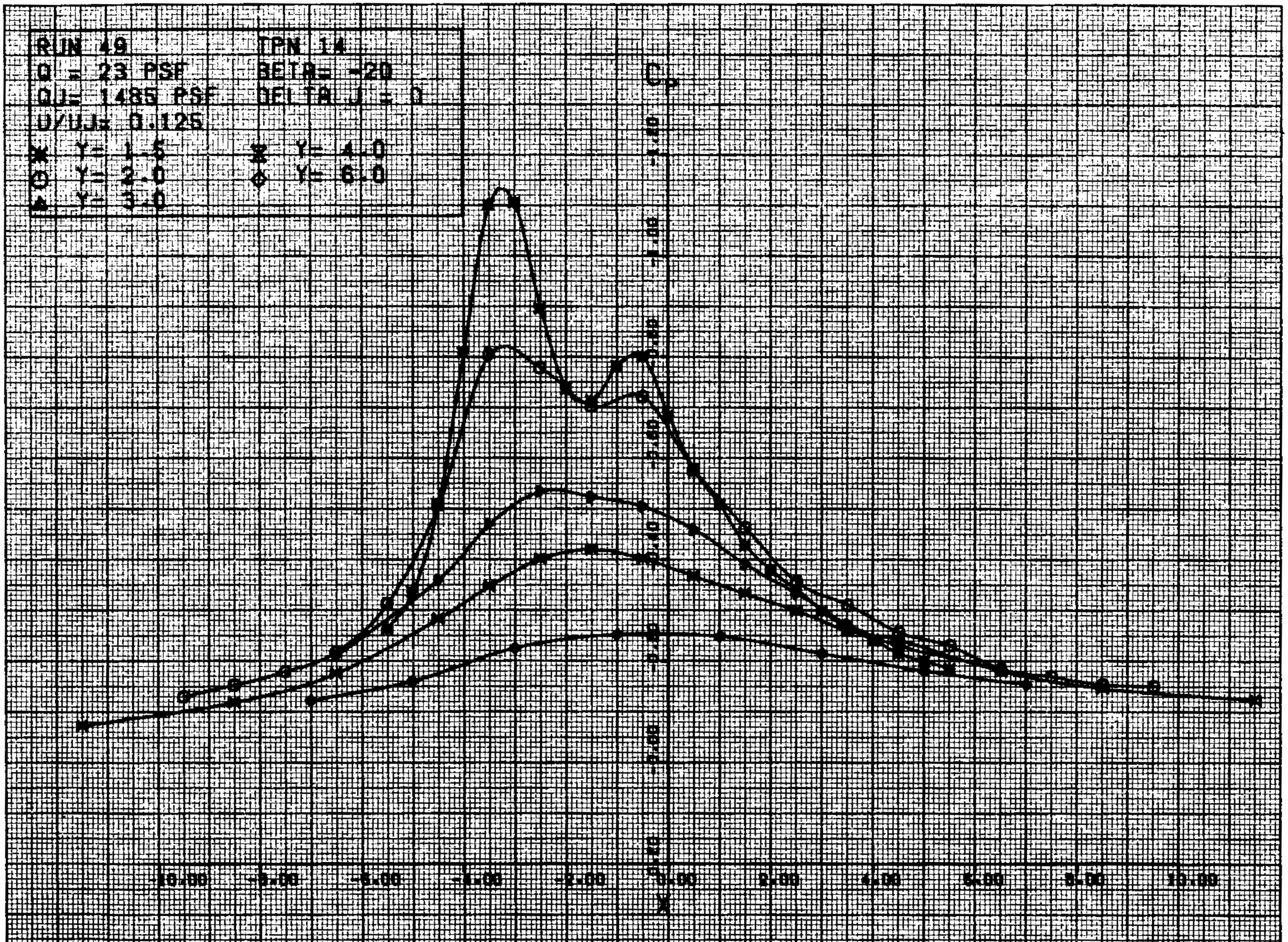

FIGURE 16. (CONTINUED) V/STOL FLAT PLATE - JETS 1, 2, 0

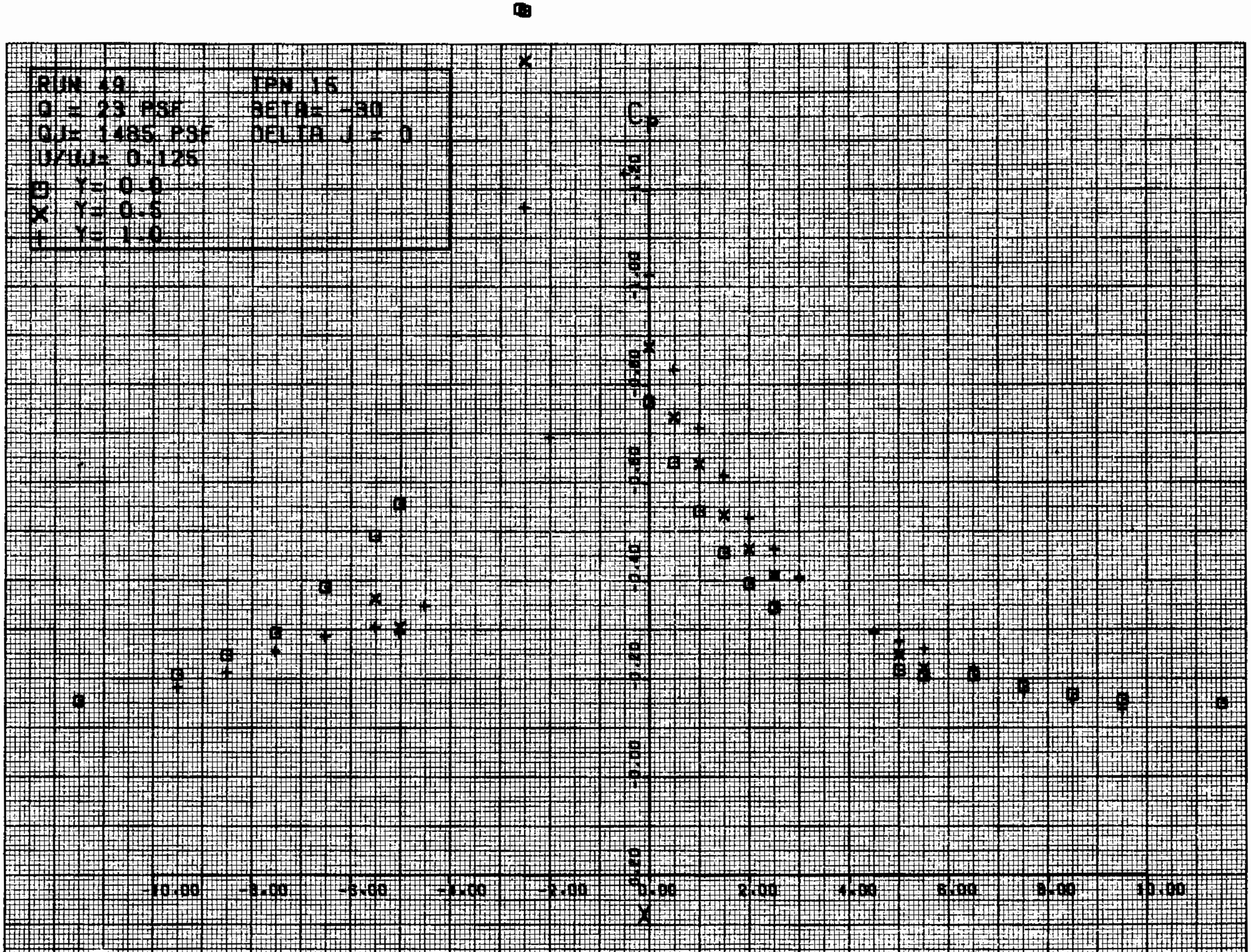

FIGURE 16. (CONTINUED) V/STOL FLAT PLATE - JETS 1, 2, 0

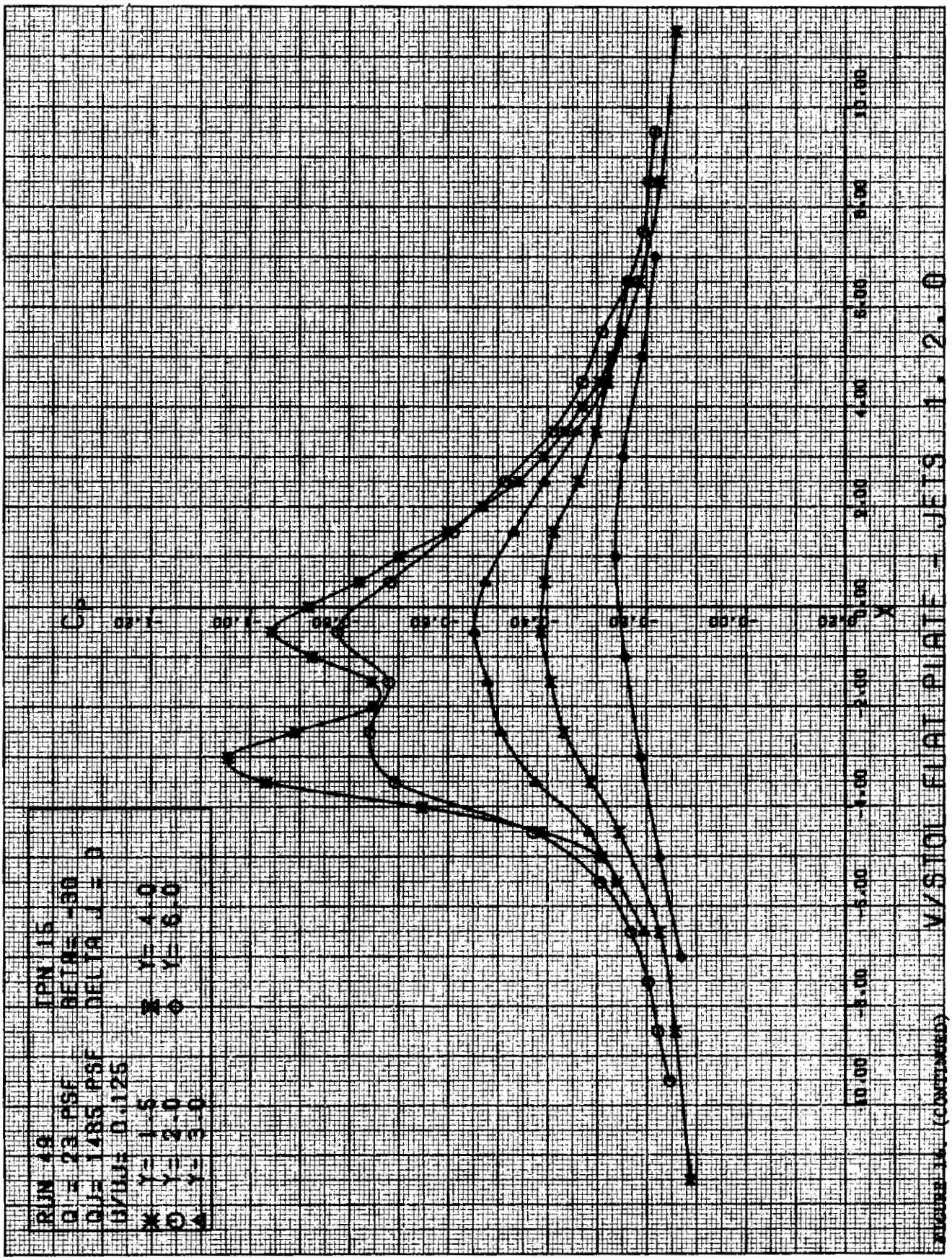

FIGURE 36. (CONTINUED)

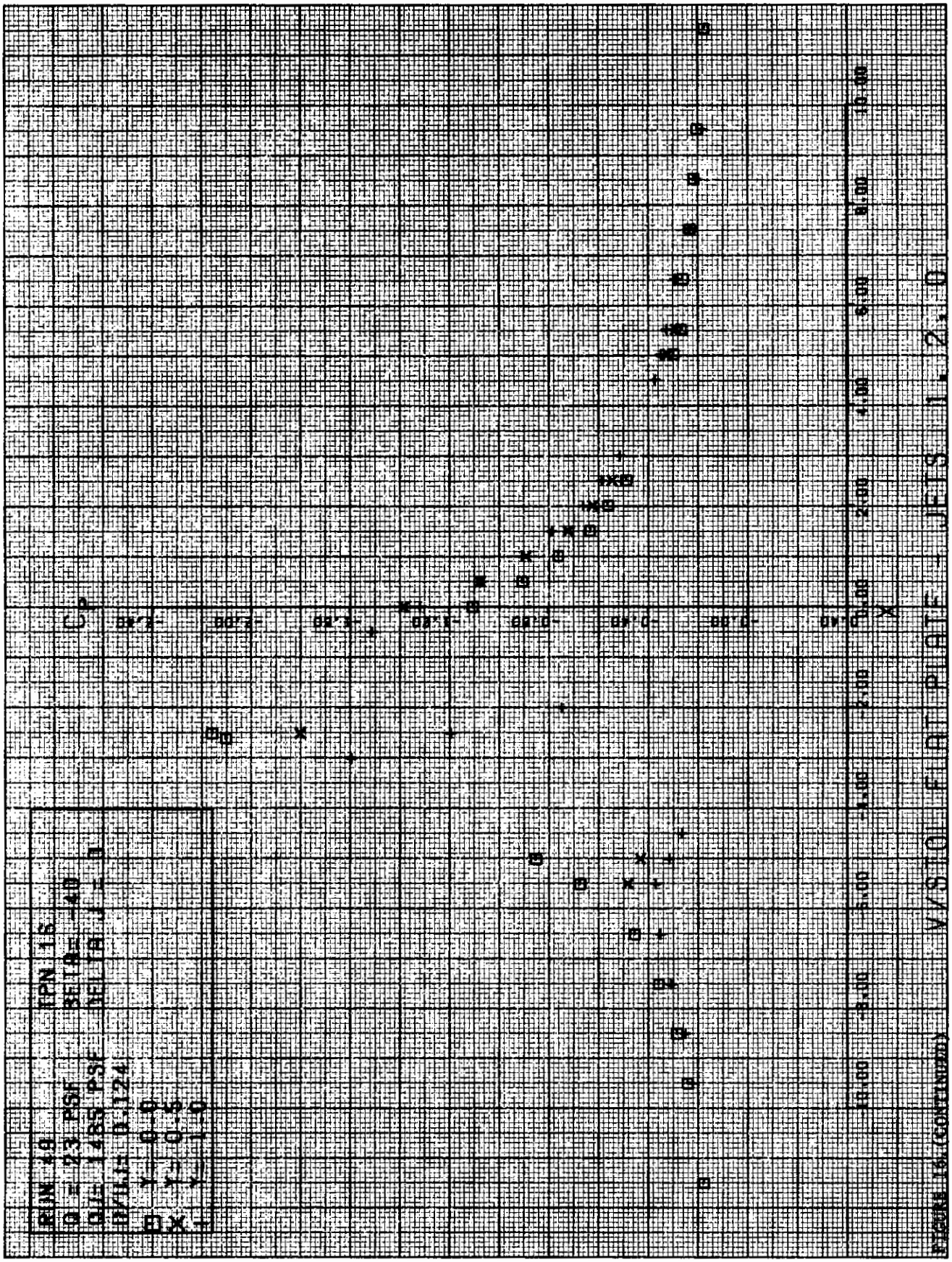

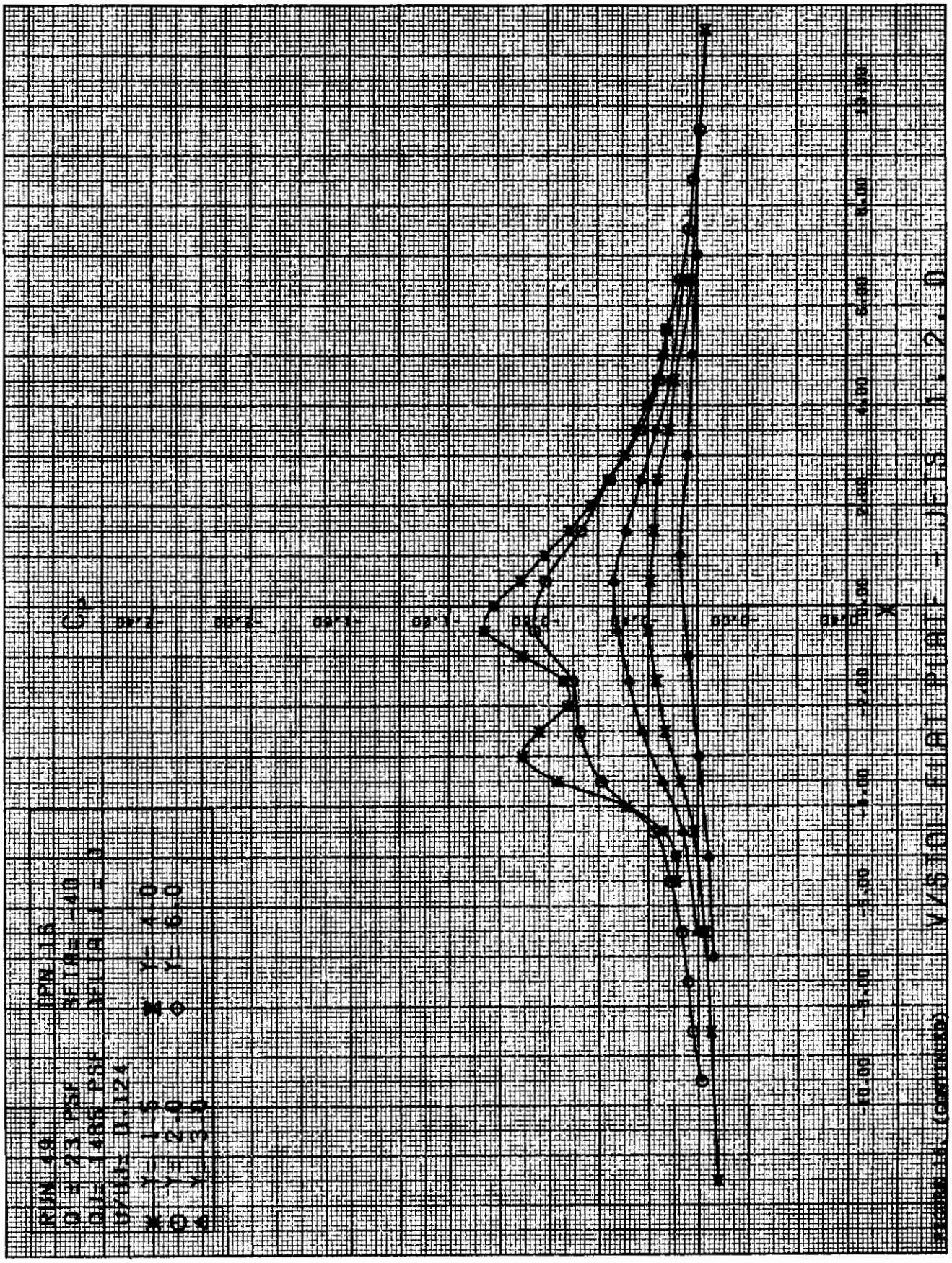

141

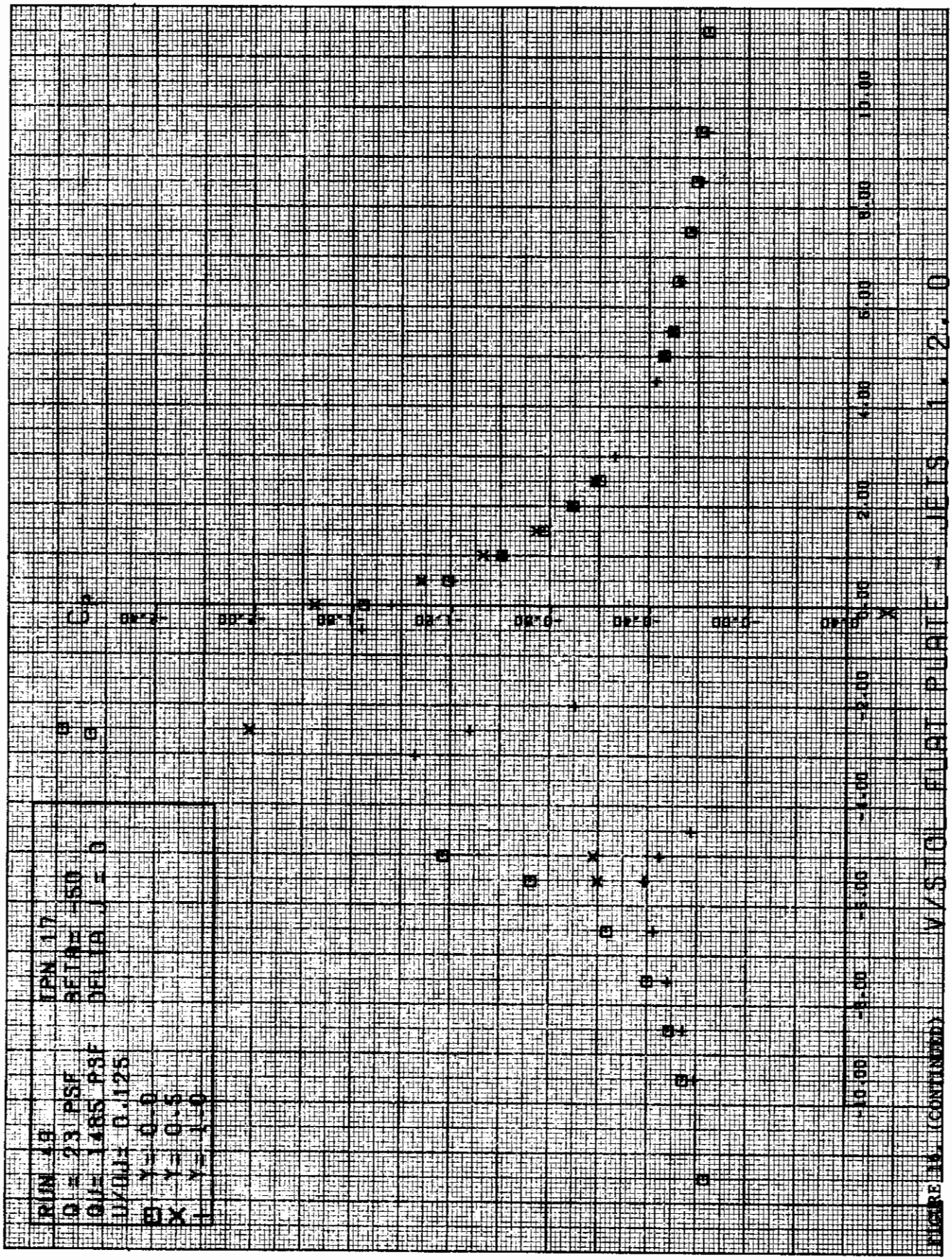

FIGURE 14. (CONTINUED)

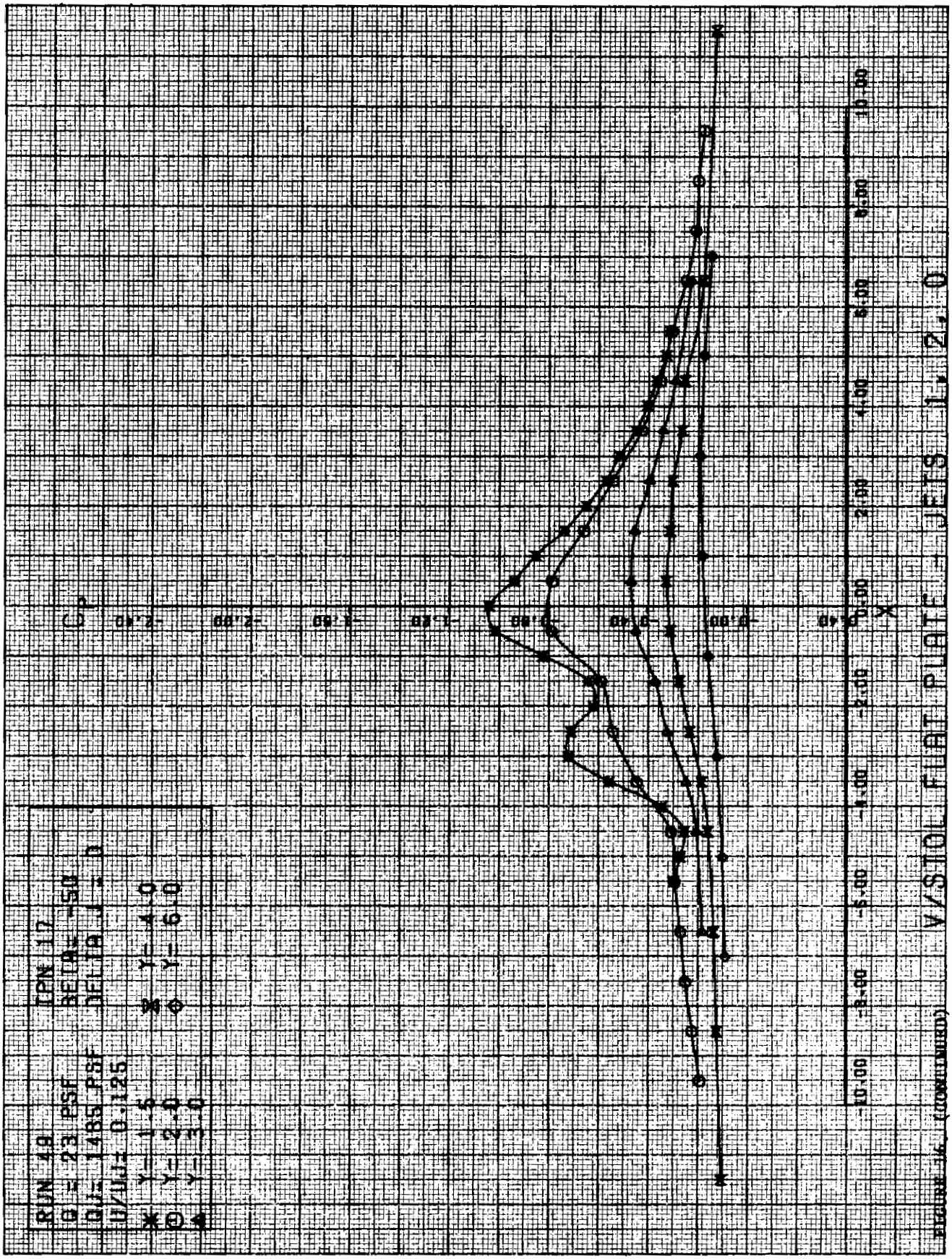

FIGURE 36. (CONCLUDED)

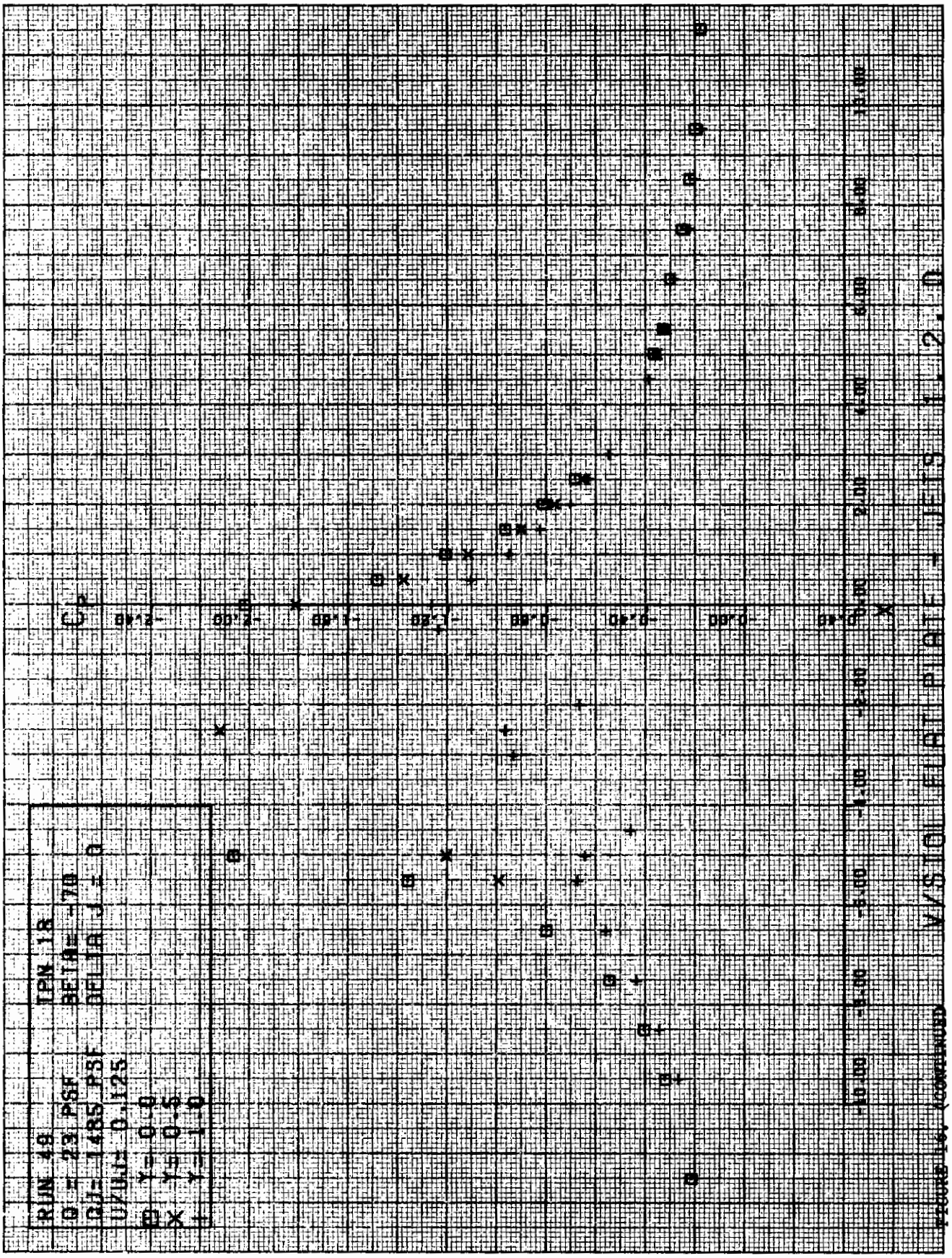

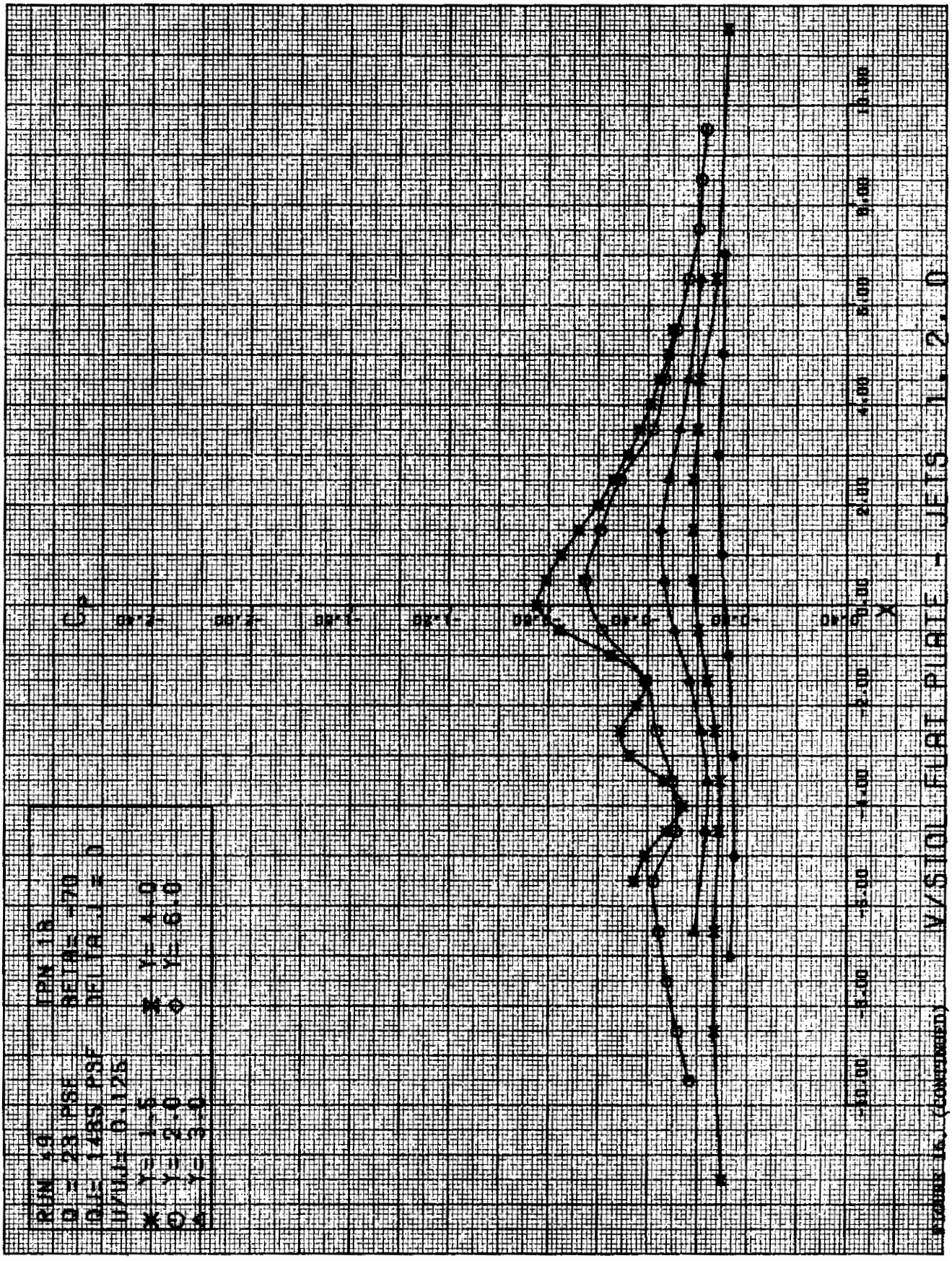

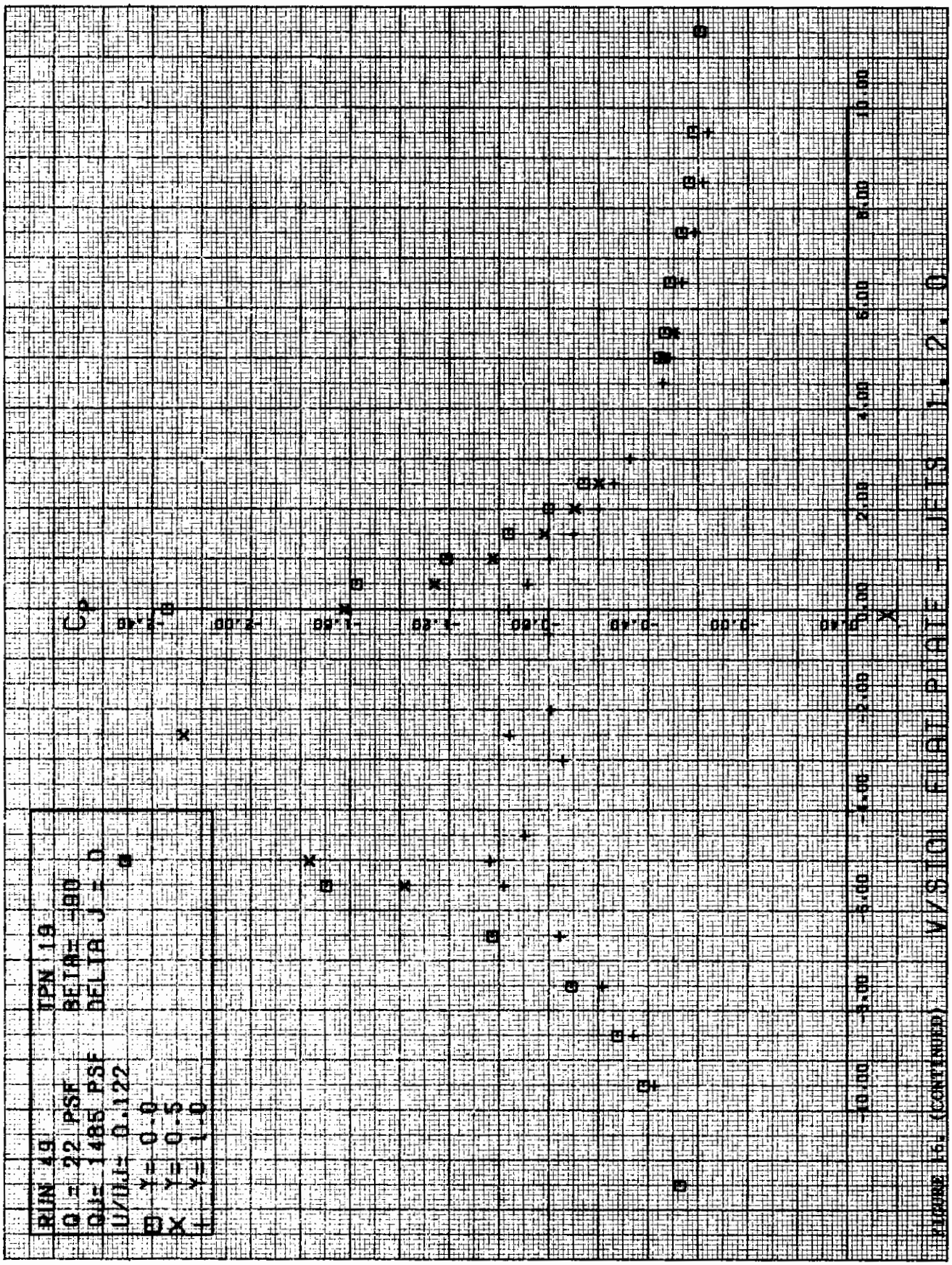

FIGURE 16. (CONTINUED) W/S 101 FLAT PLATE - JET 9

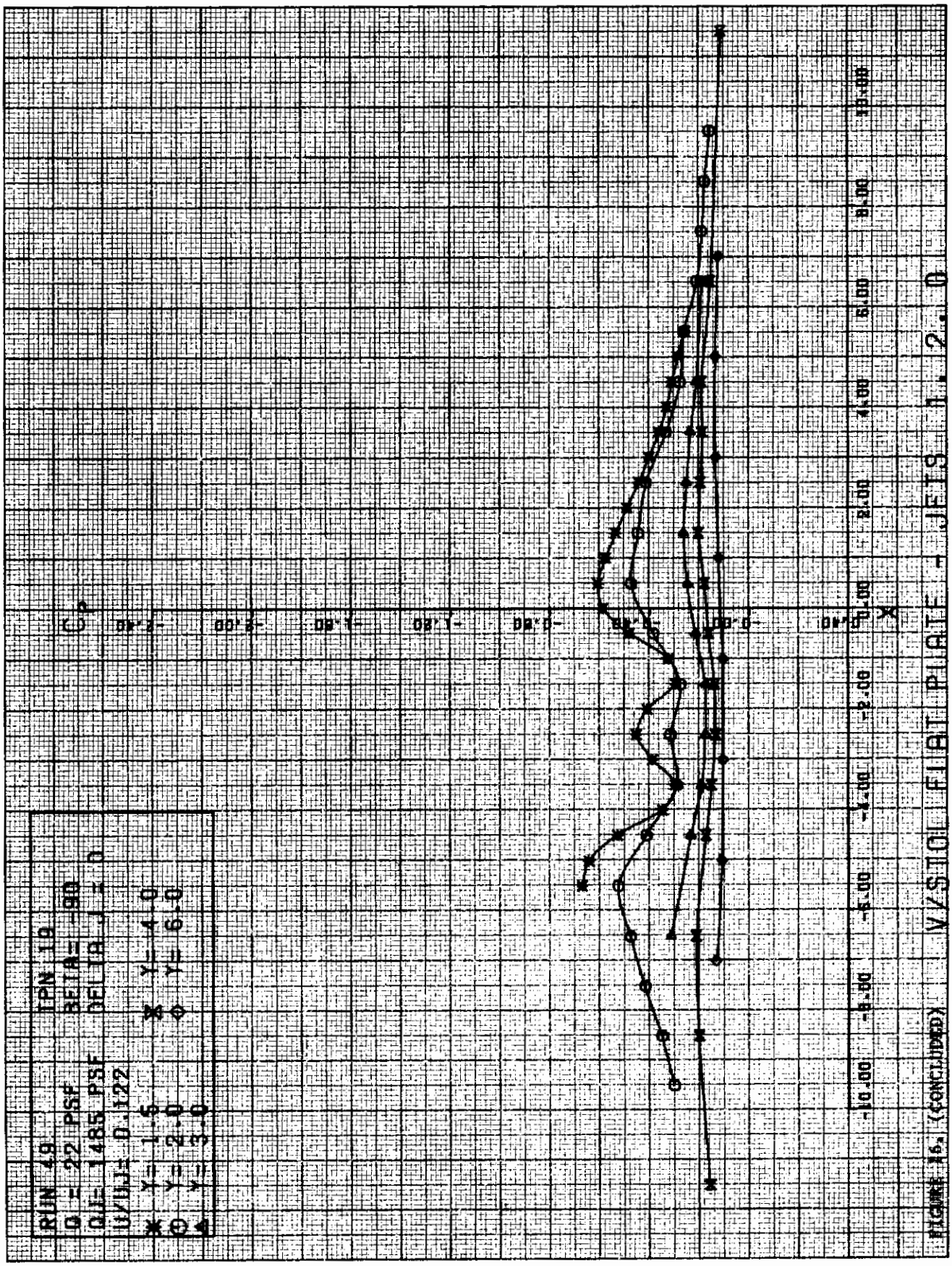

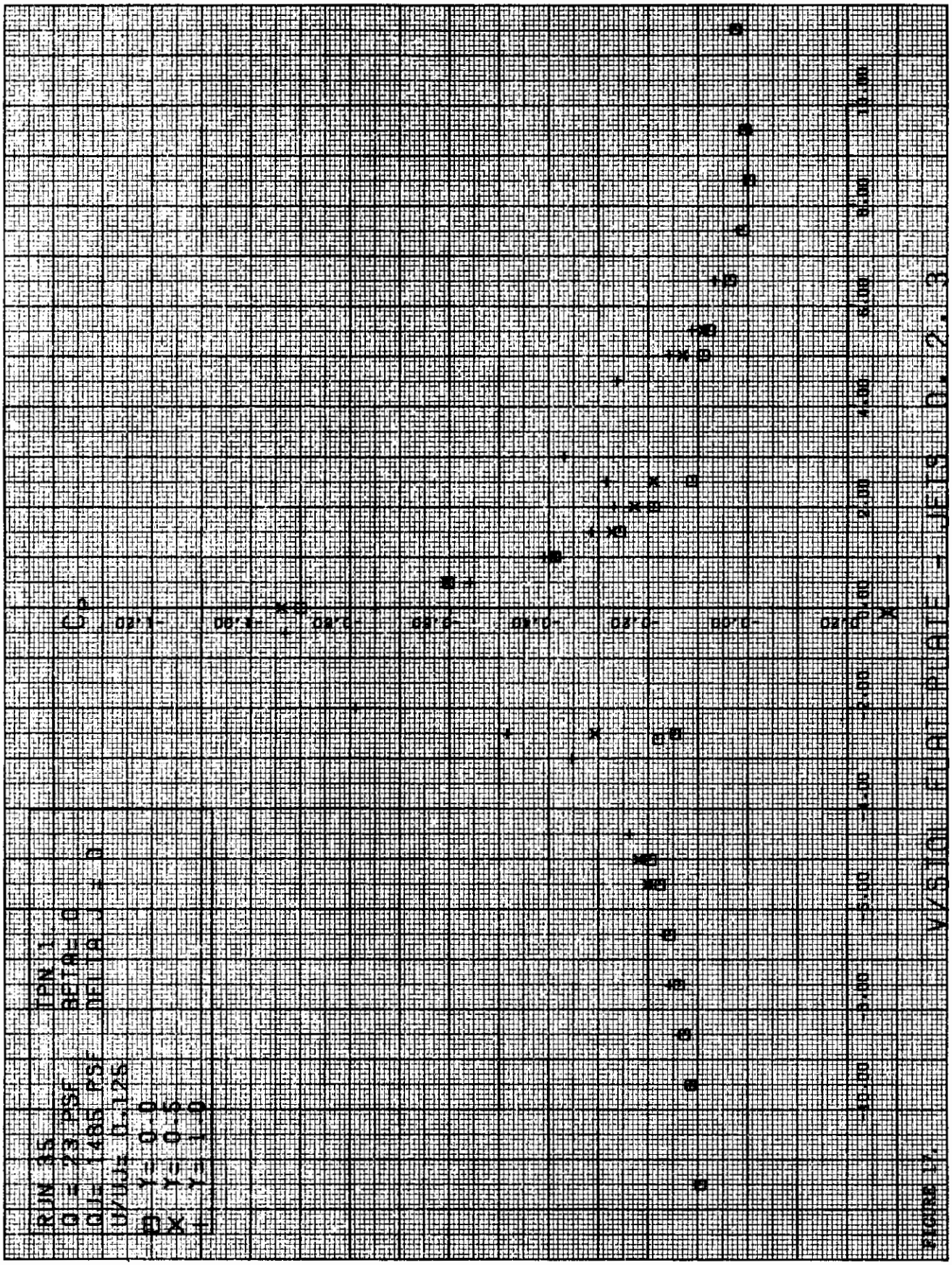

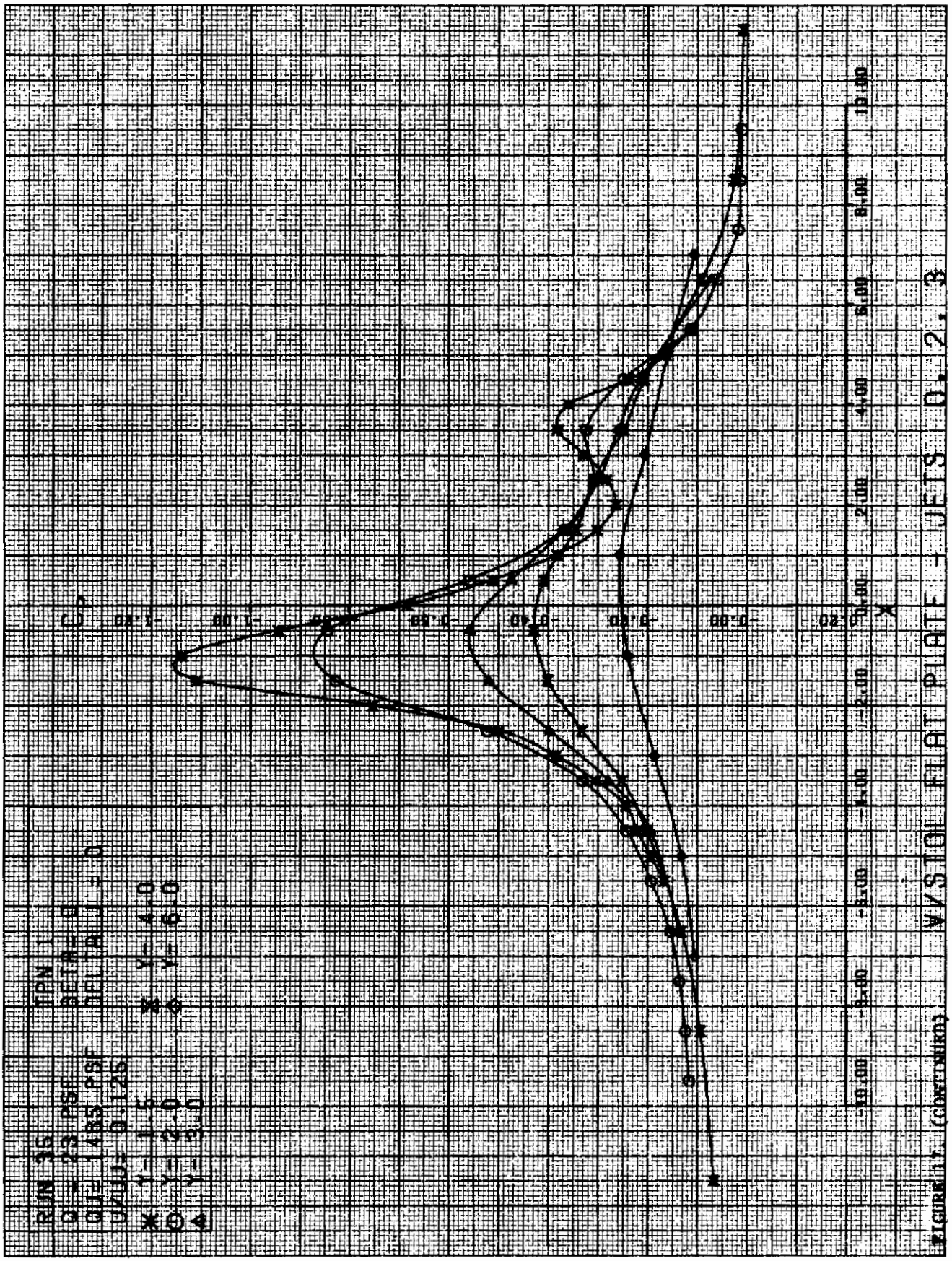

FIGURE 11. (CONCLUDED) V/STOL FLAT PLATE - JETS 0, 2, 3

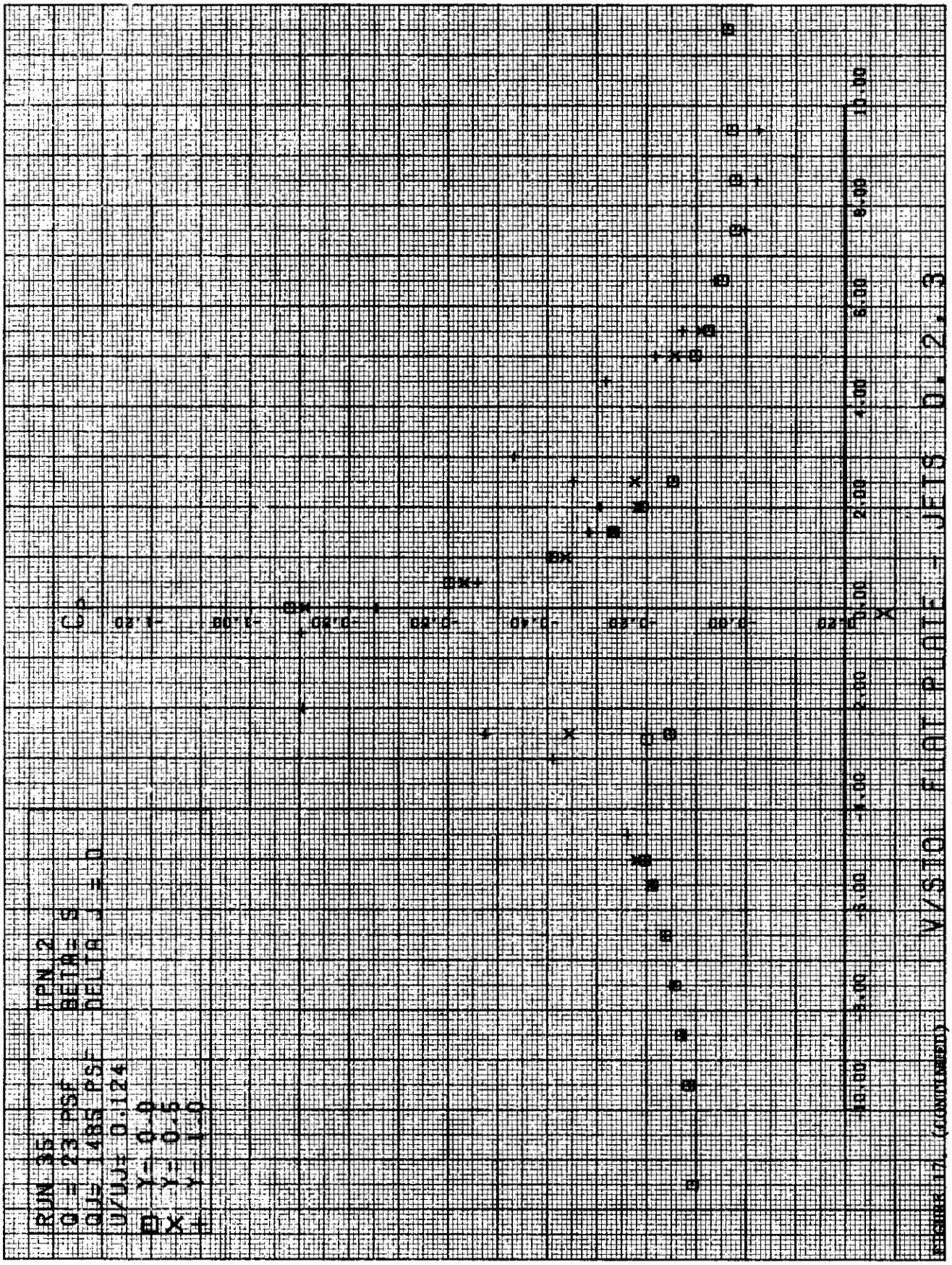

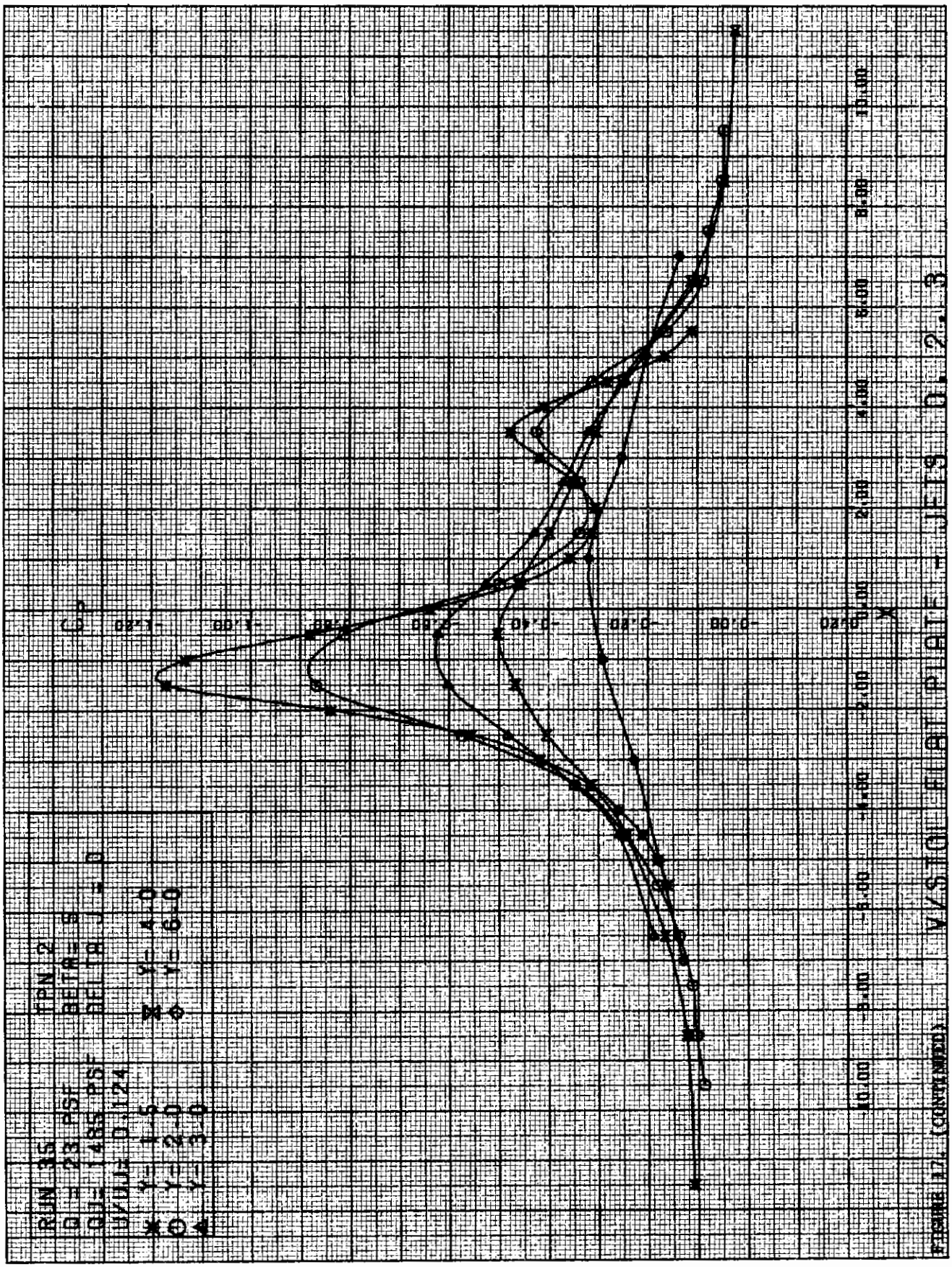

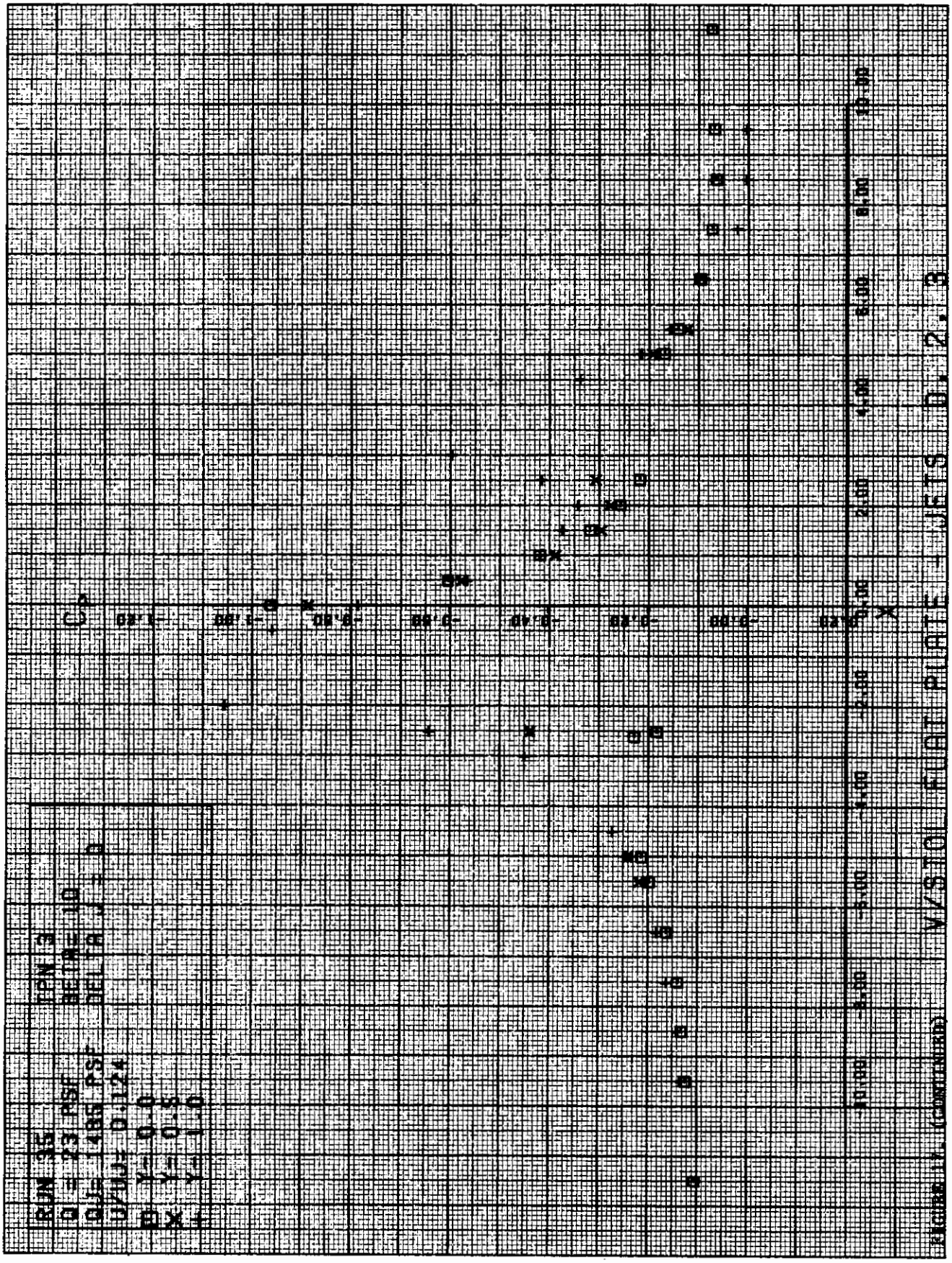

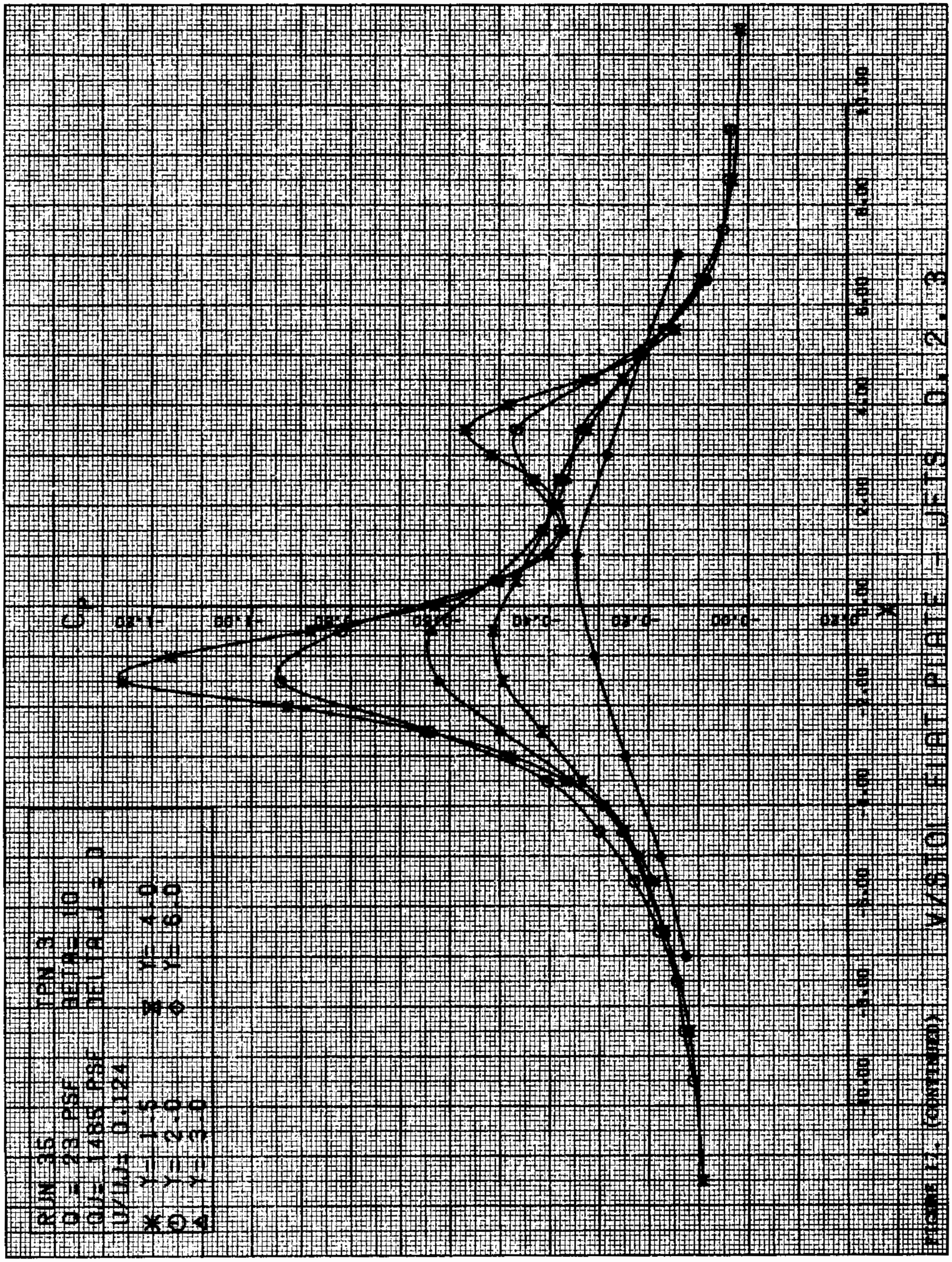

FIGURE 17. (CONTINUED) V/STOL FLAT PLATE - JETS 0, 2, 3

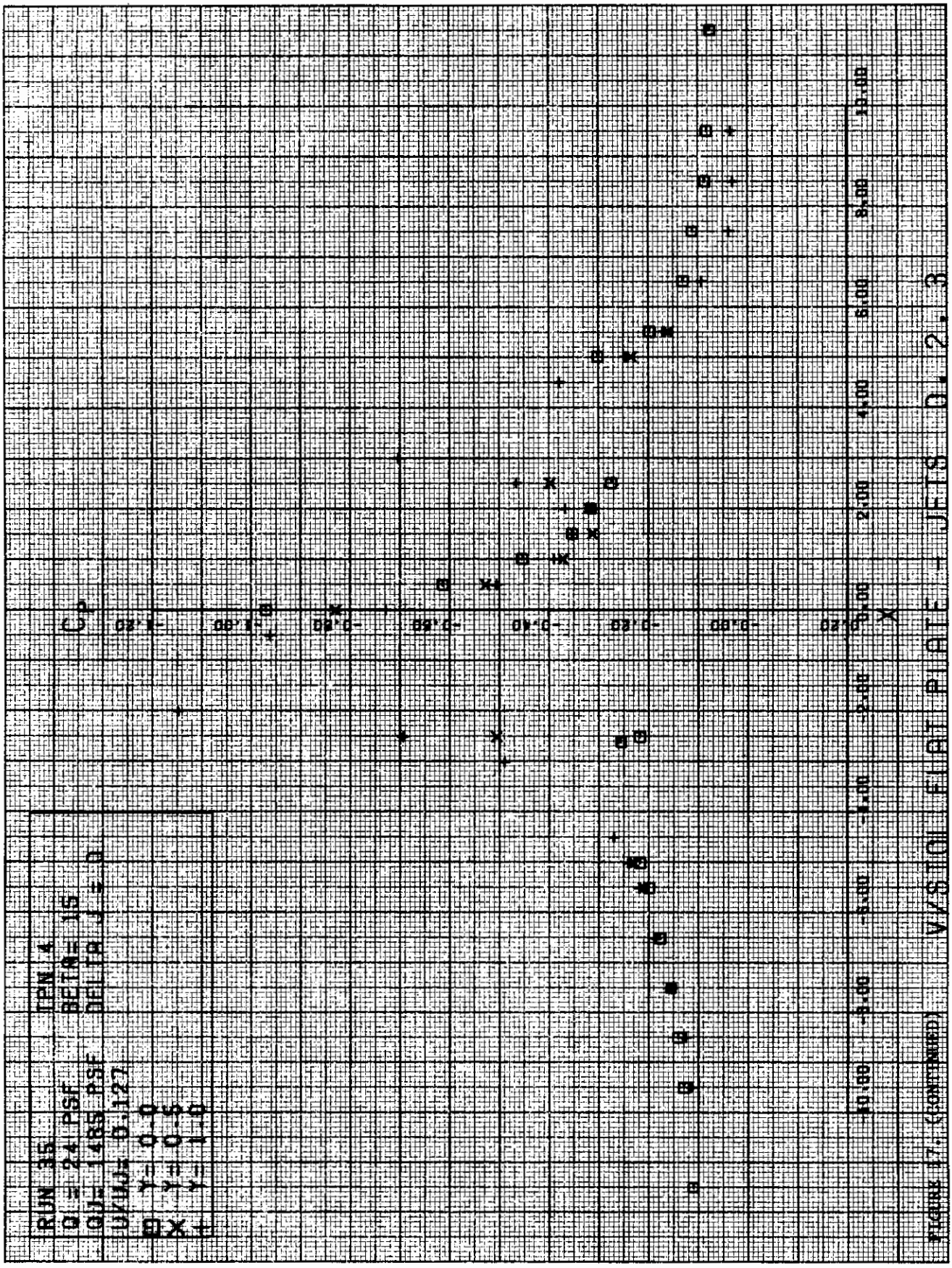

FIGURE 17. (CONTINUED)

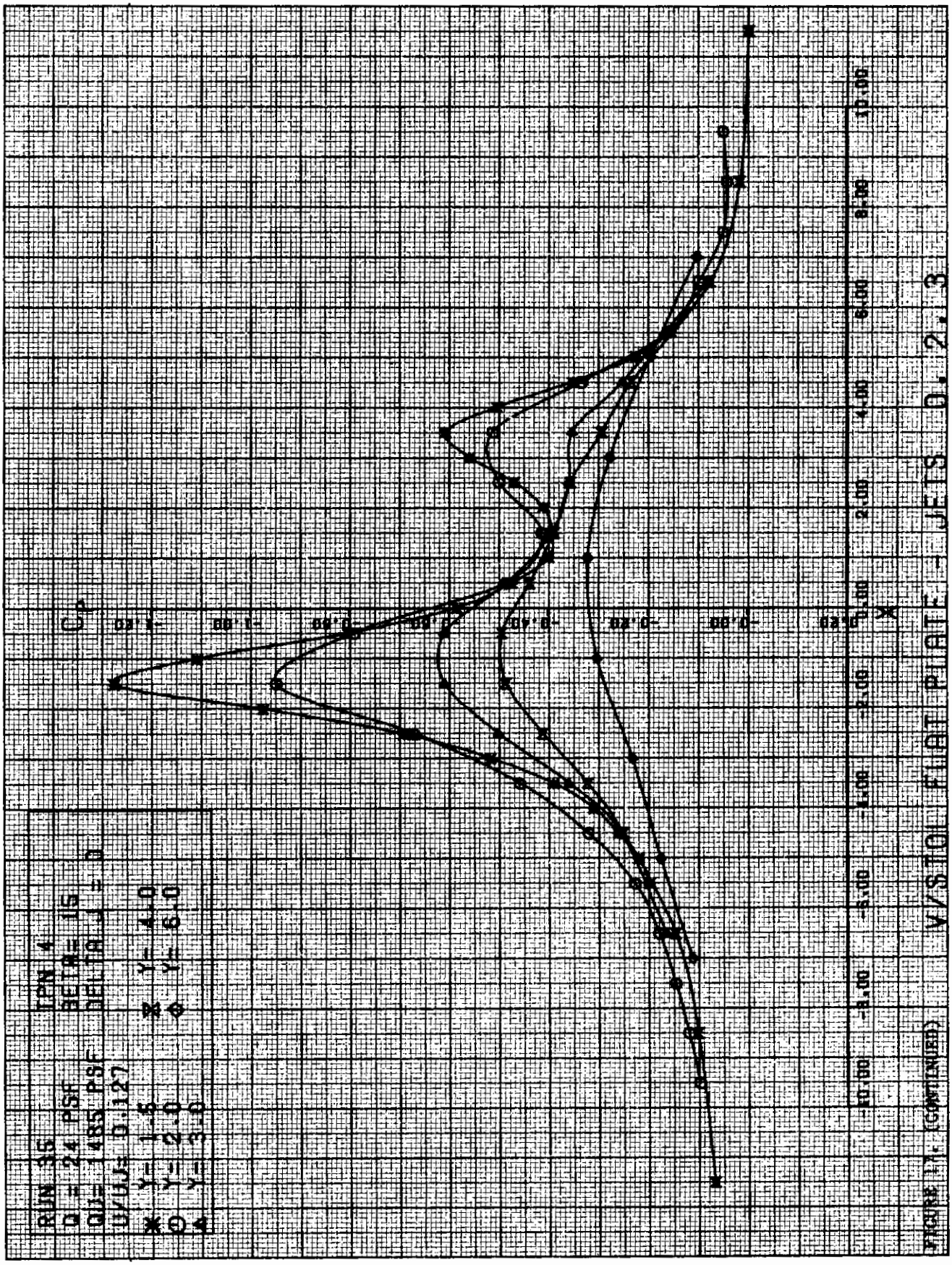

FIGURE 17. (CONTINUED) V/STOL FLAT PLATE - JETS 0, 2, 3

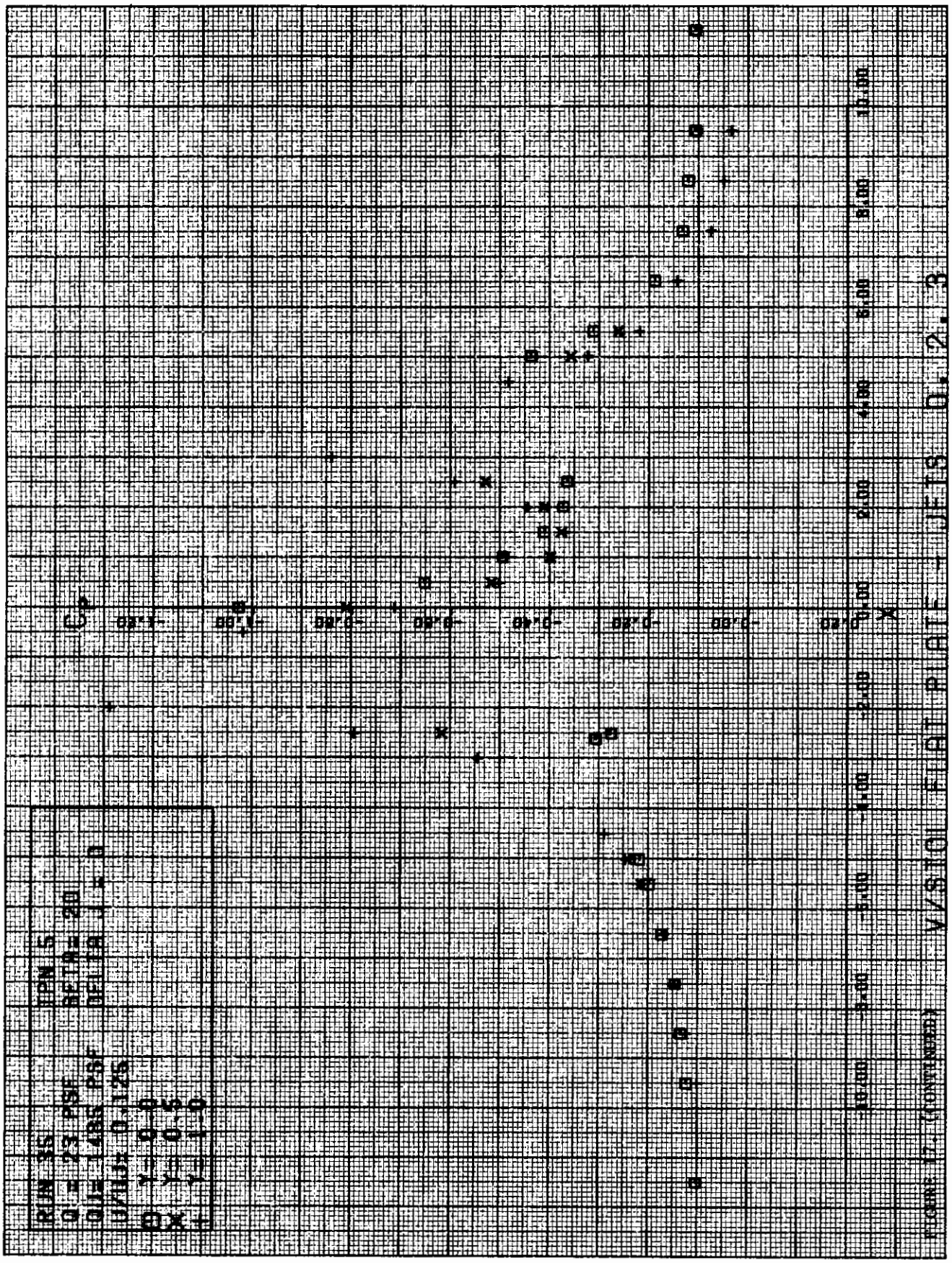

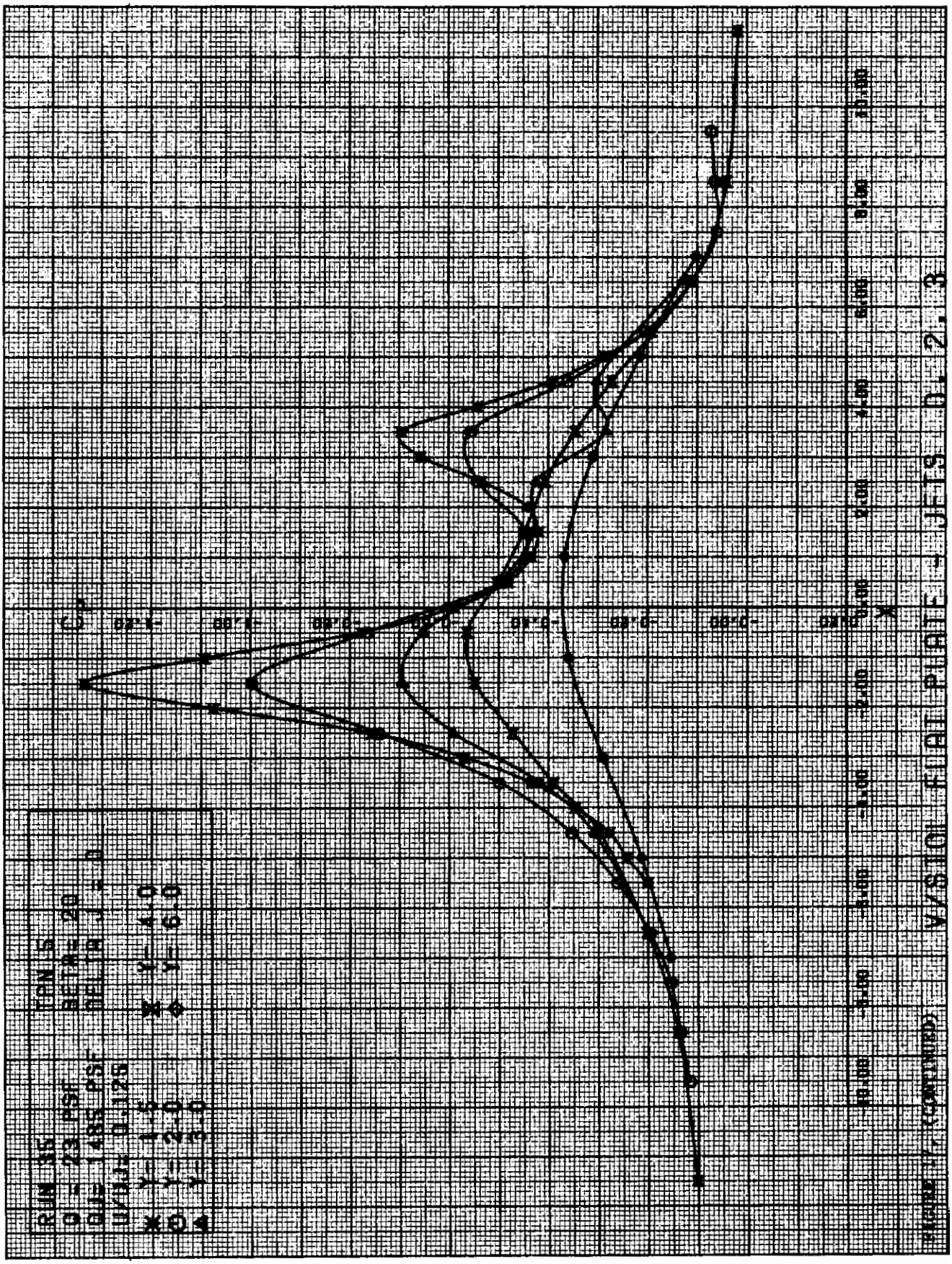

FIGURE 77. (CONTINUED) V/STOL FLAT PLATE JET 3 0.2

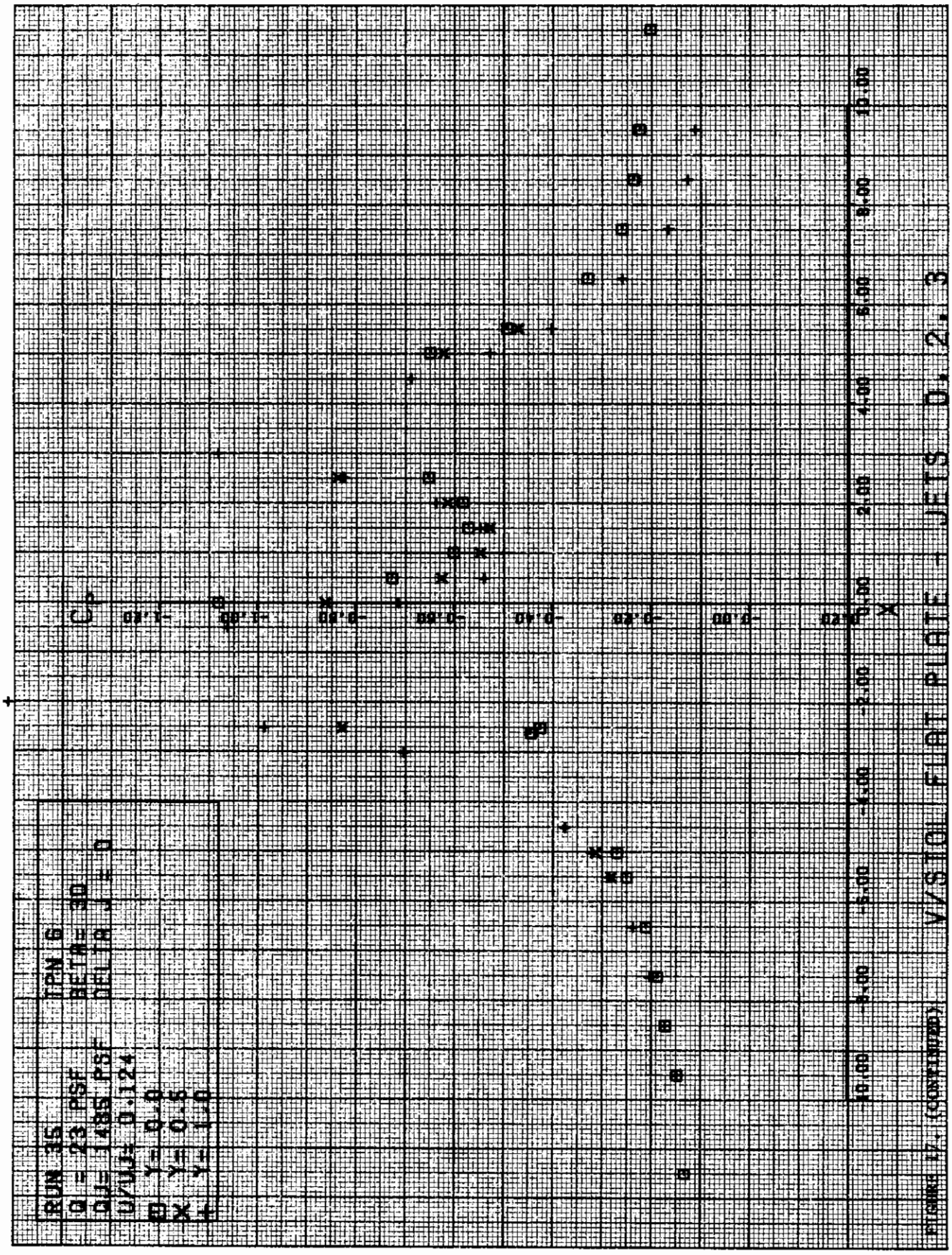

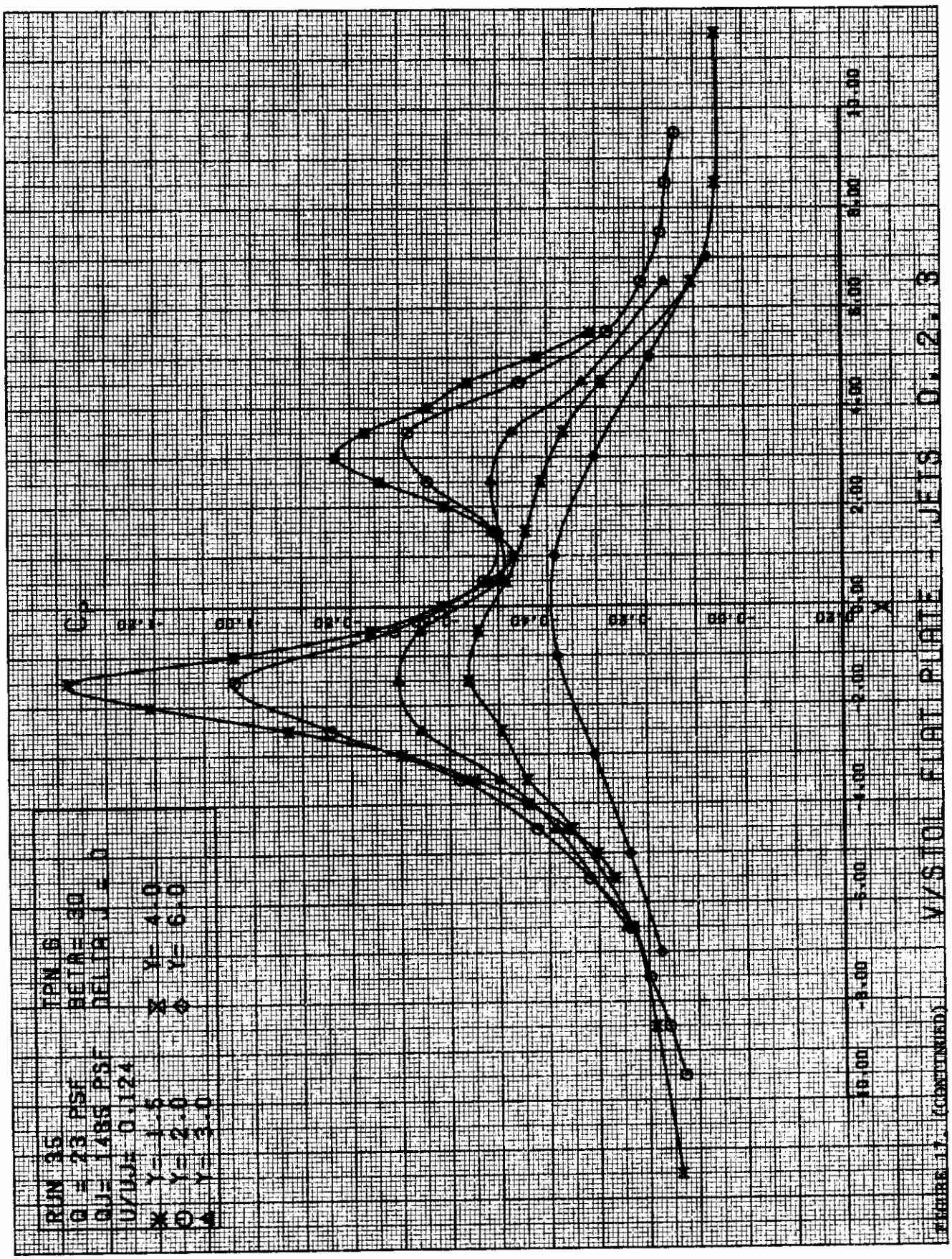

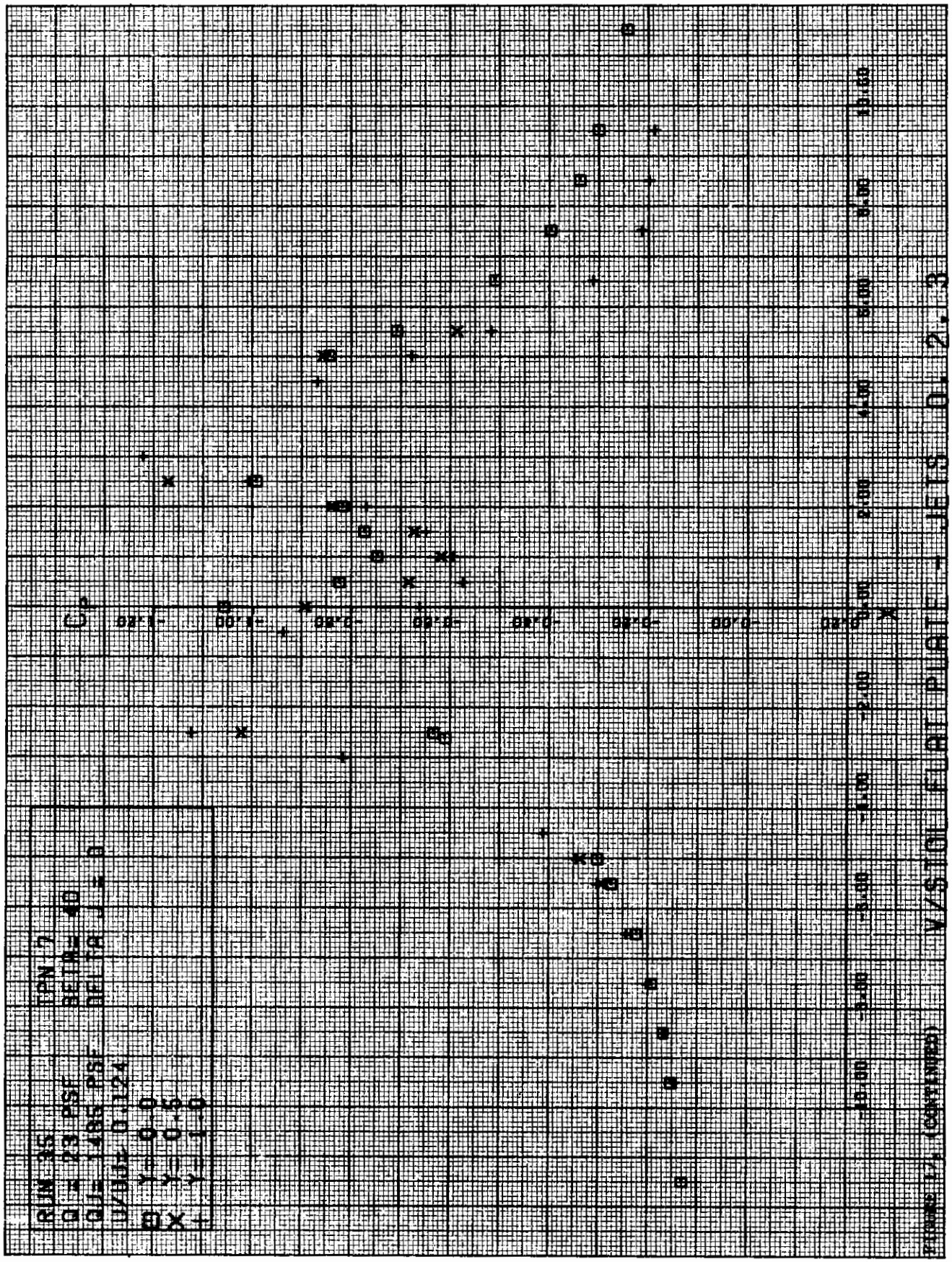

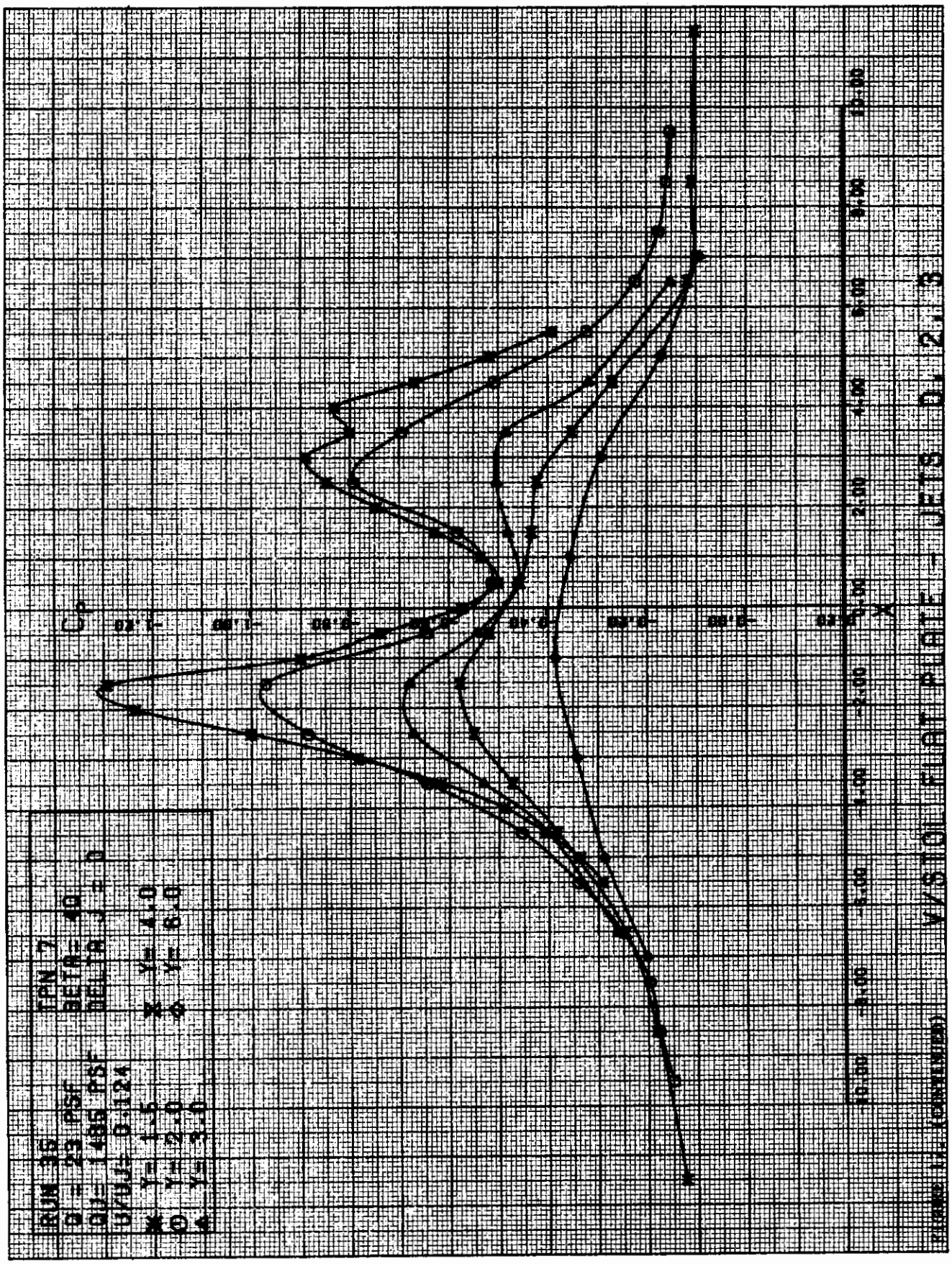

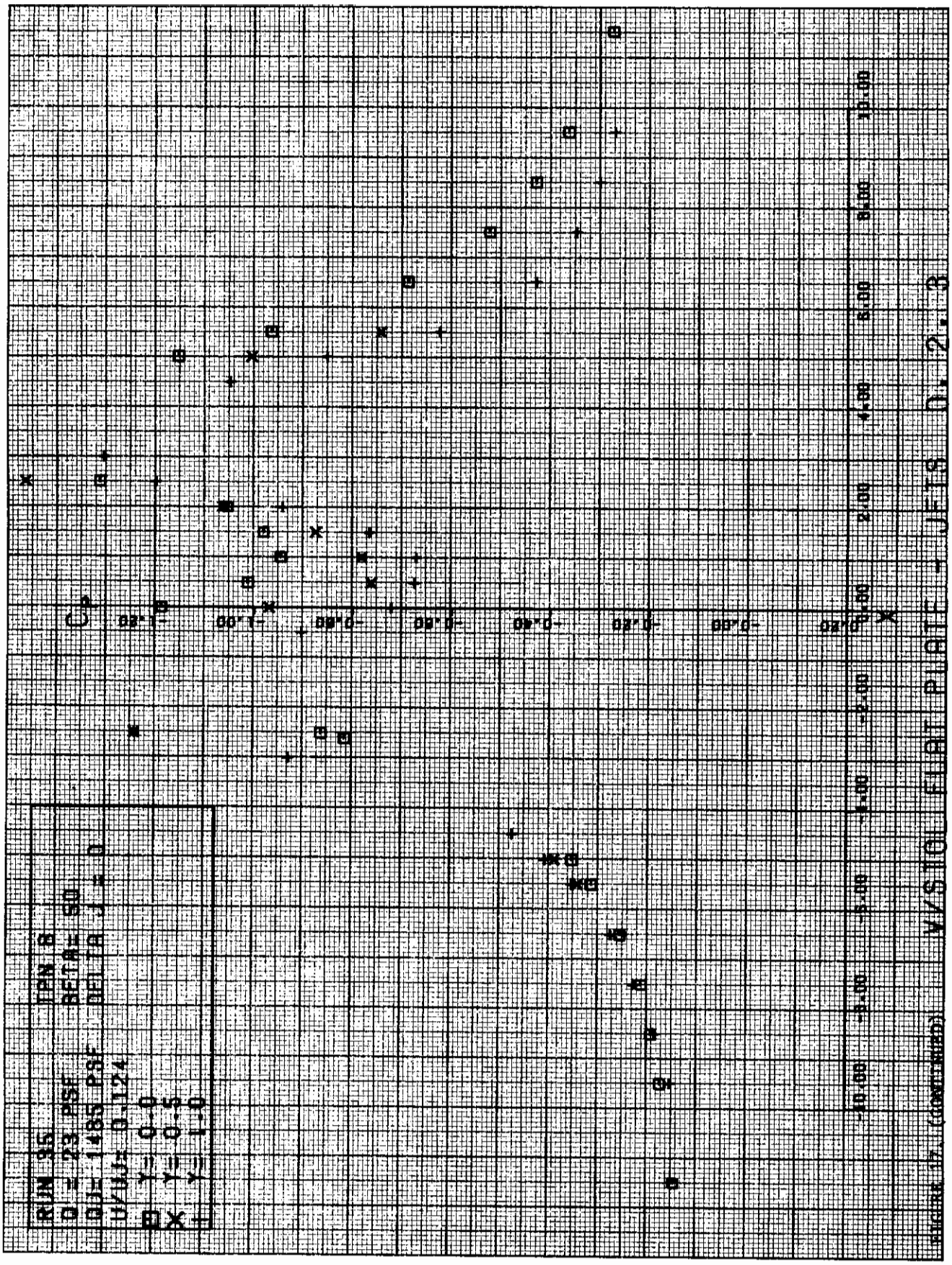

FIGURE 17. (CONTINUED)

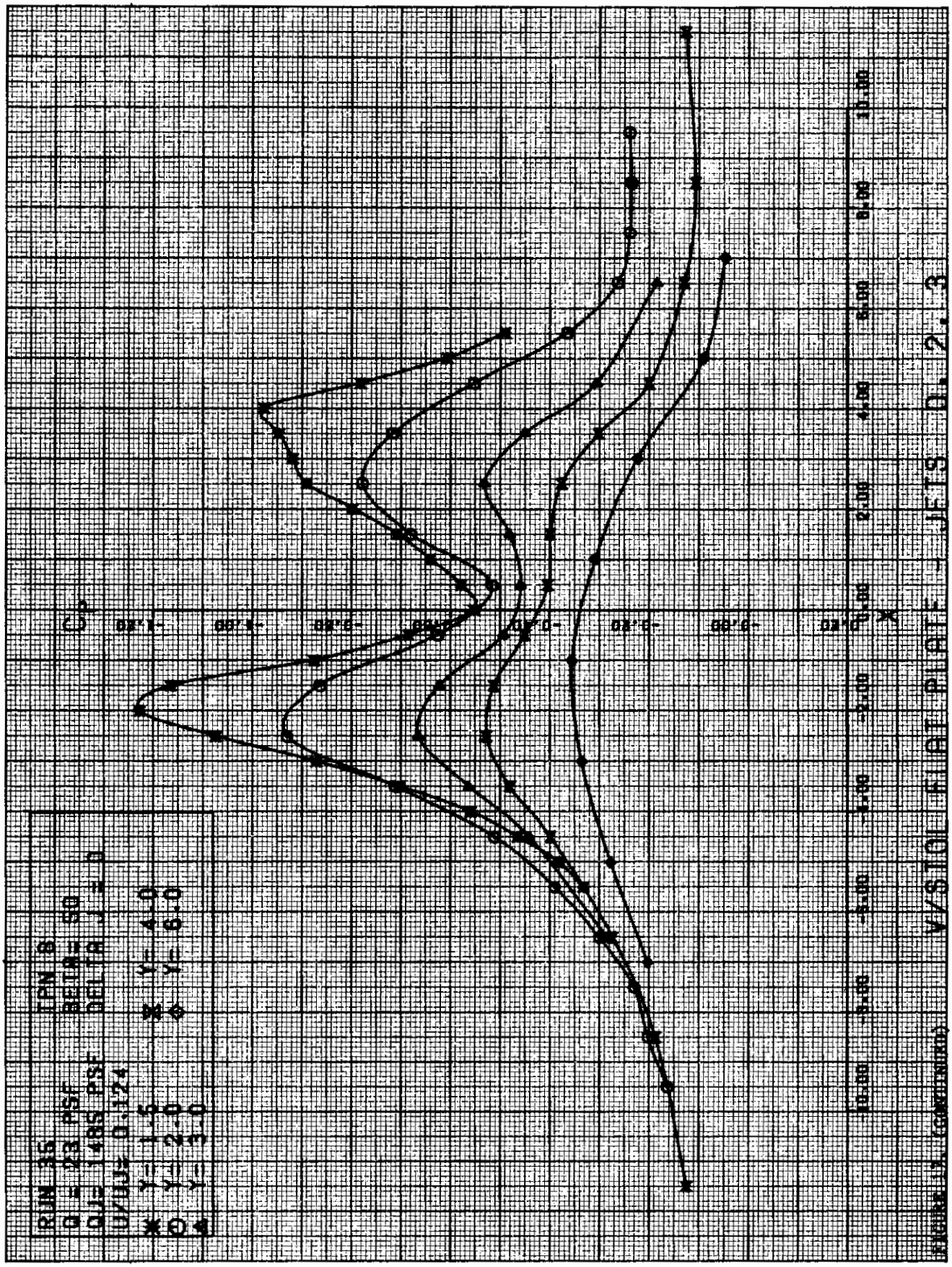

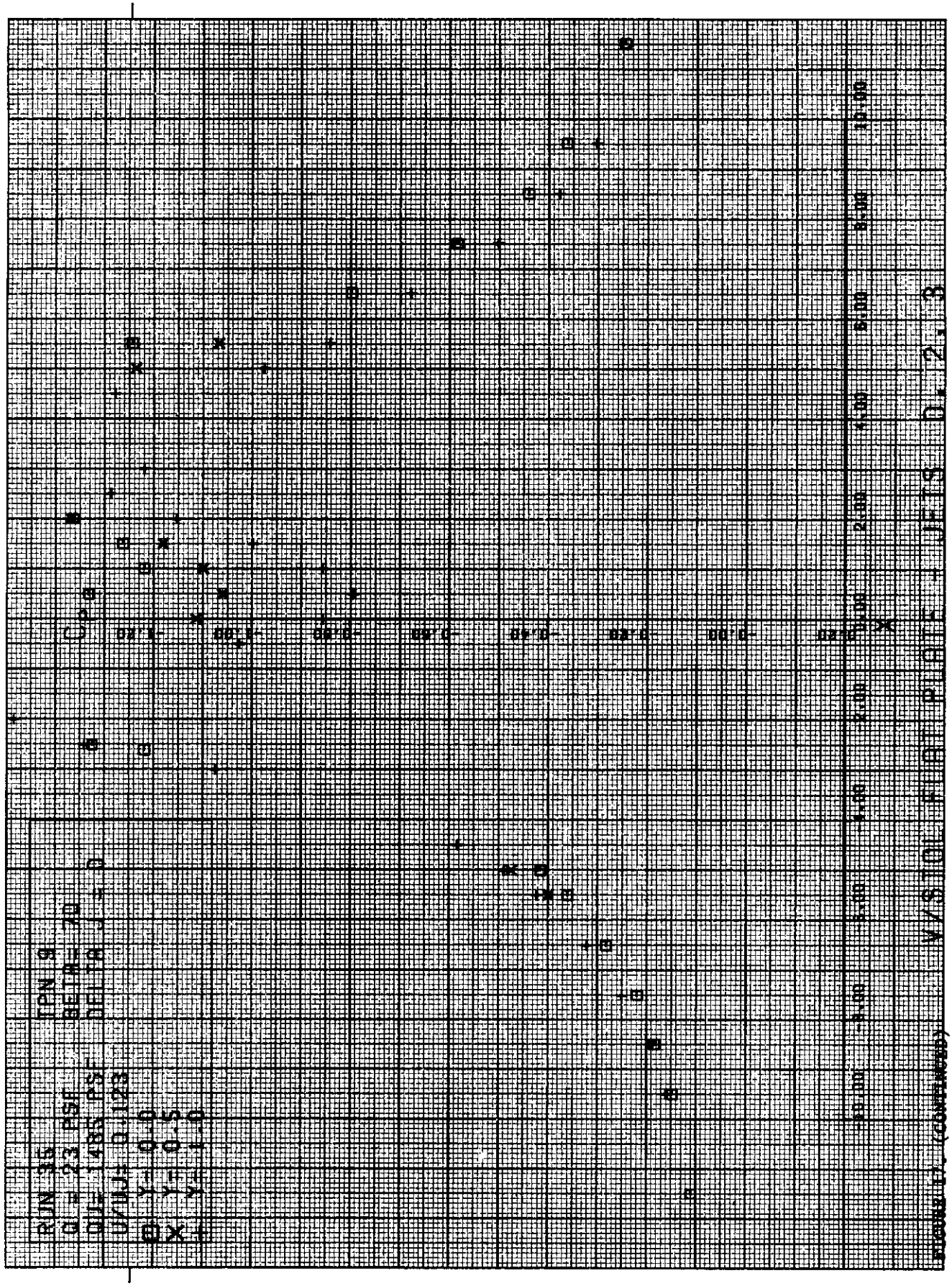

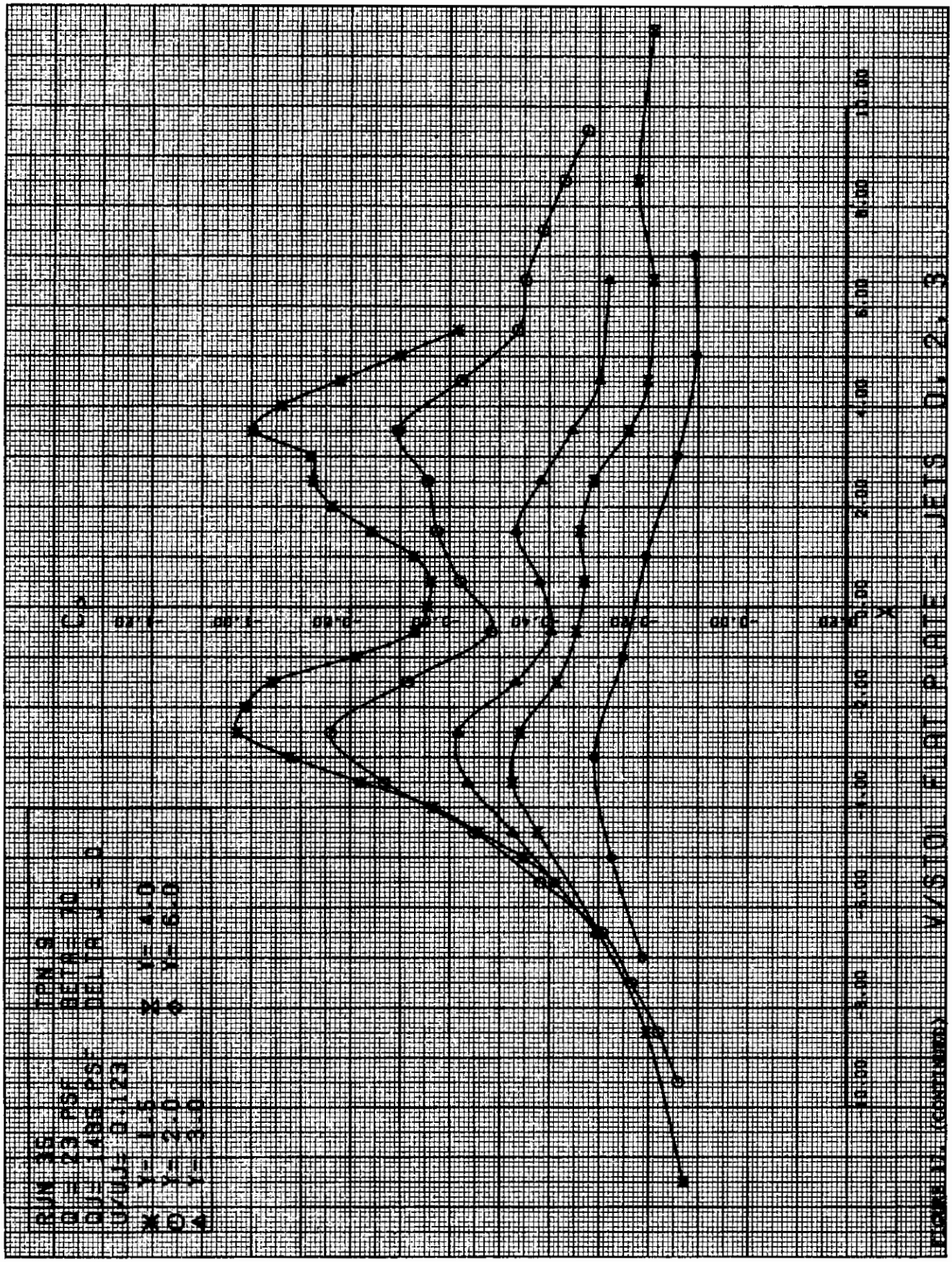

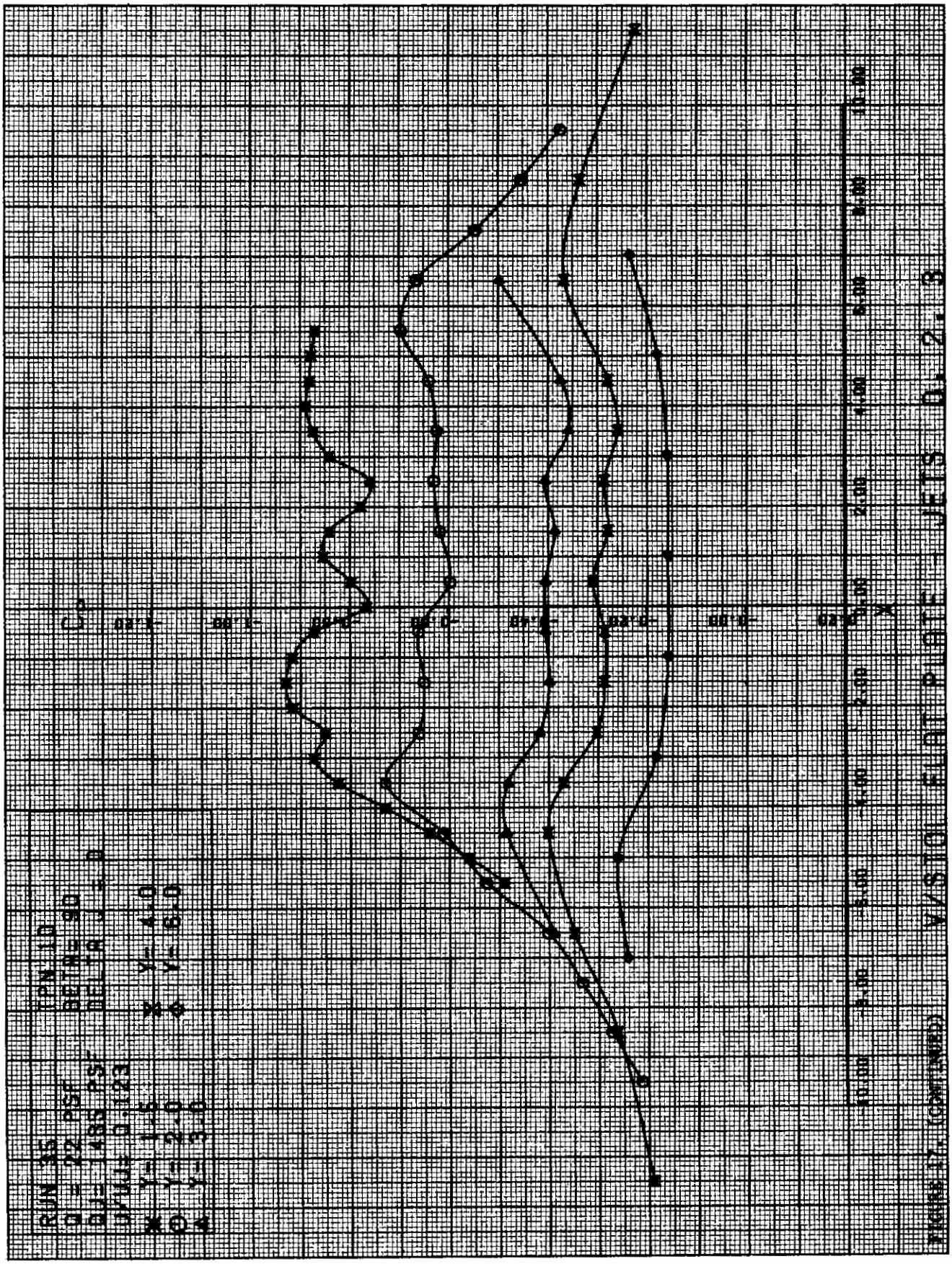

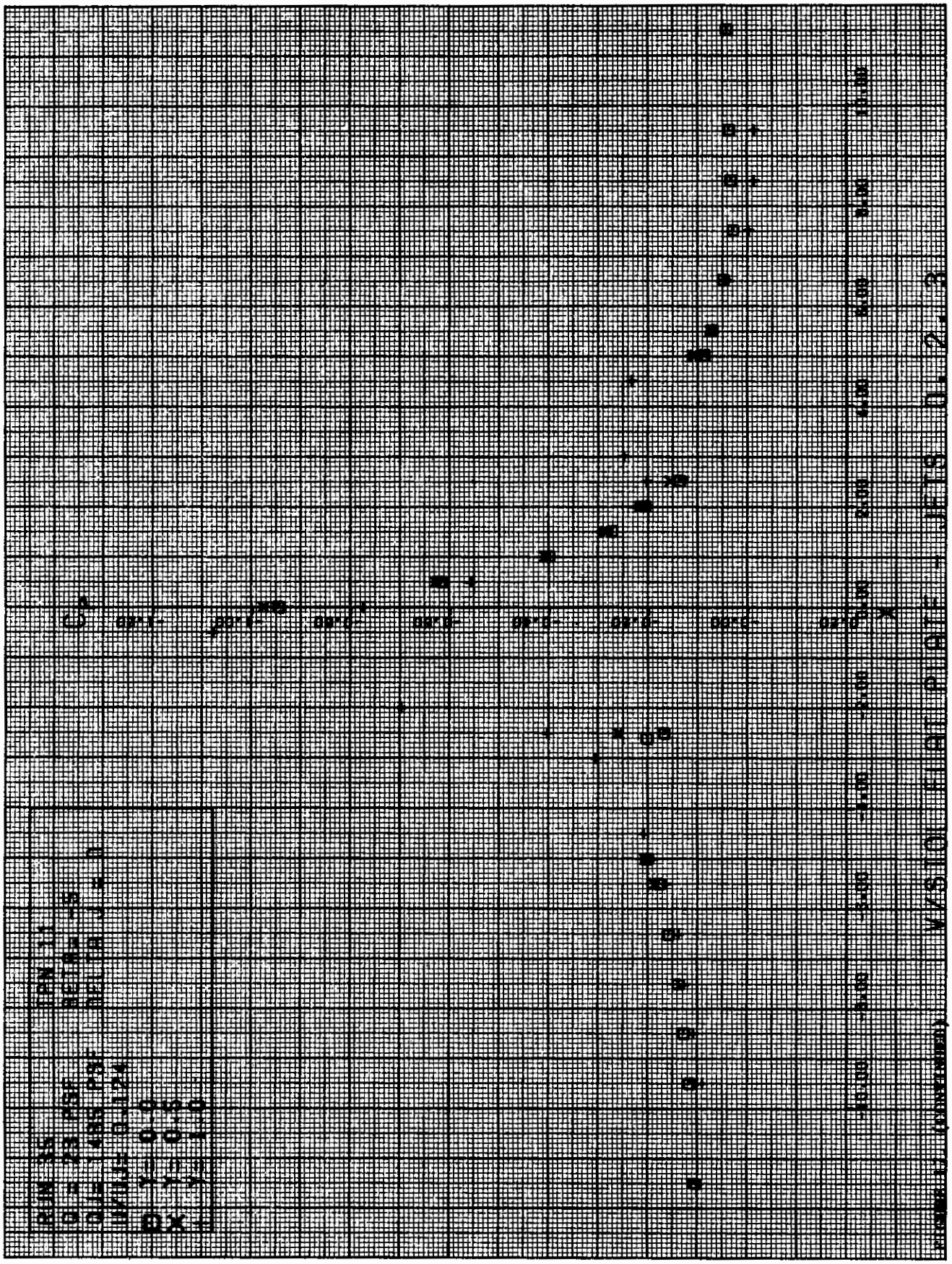

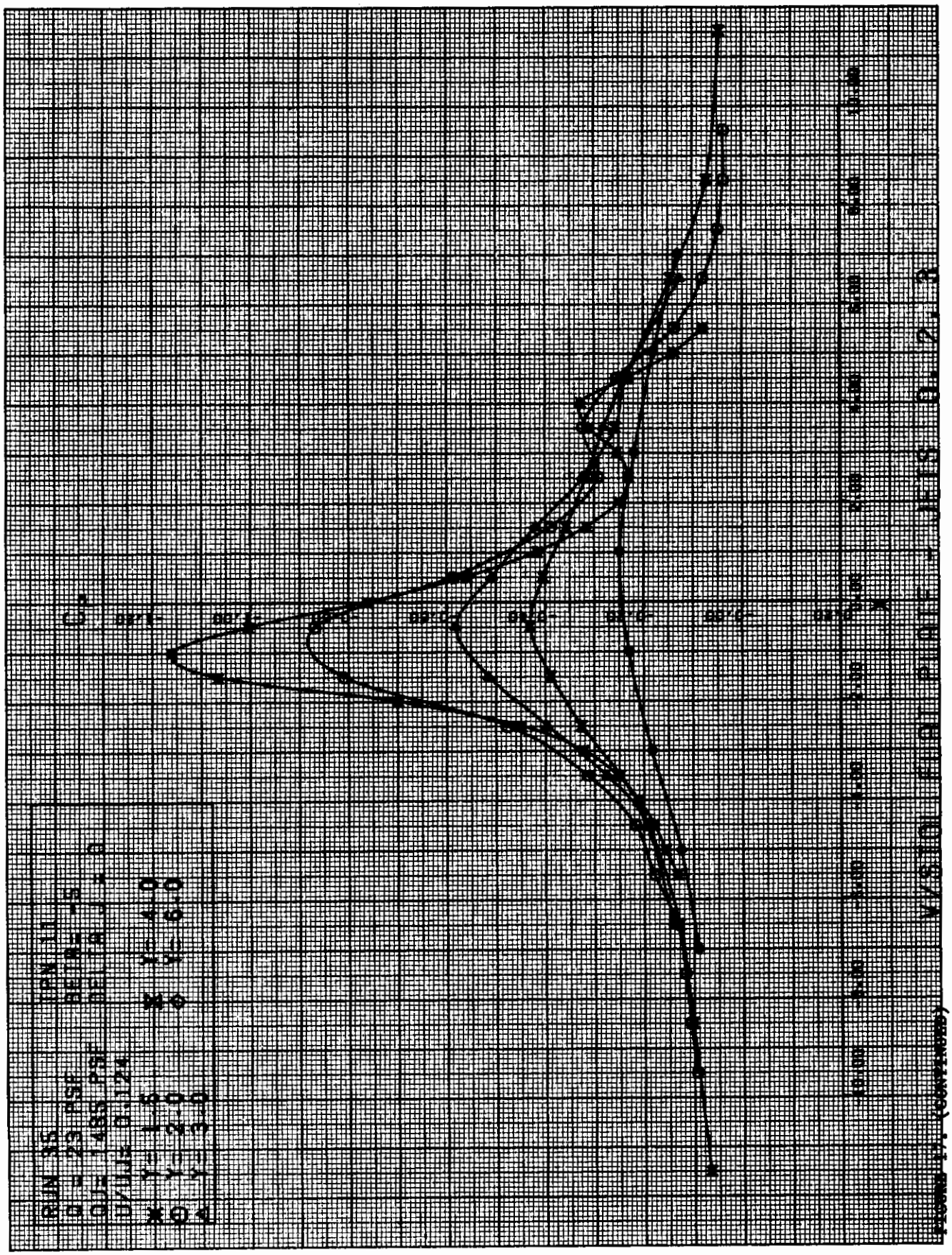

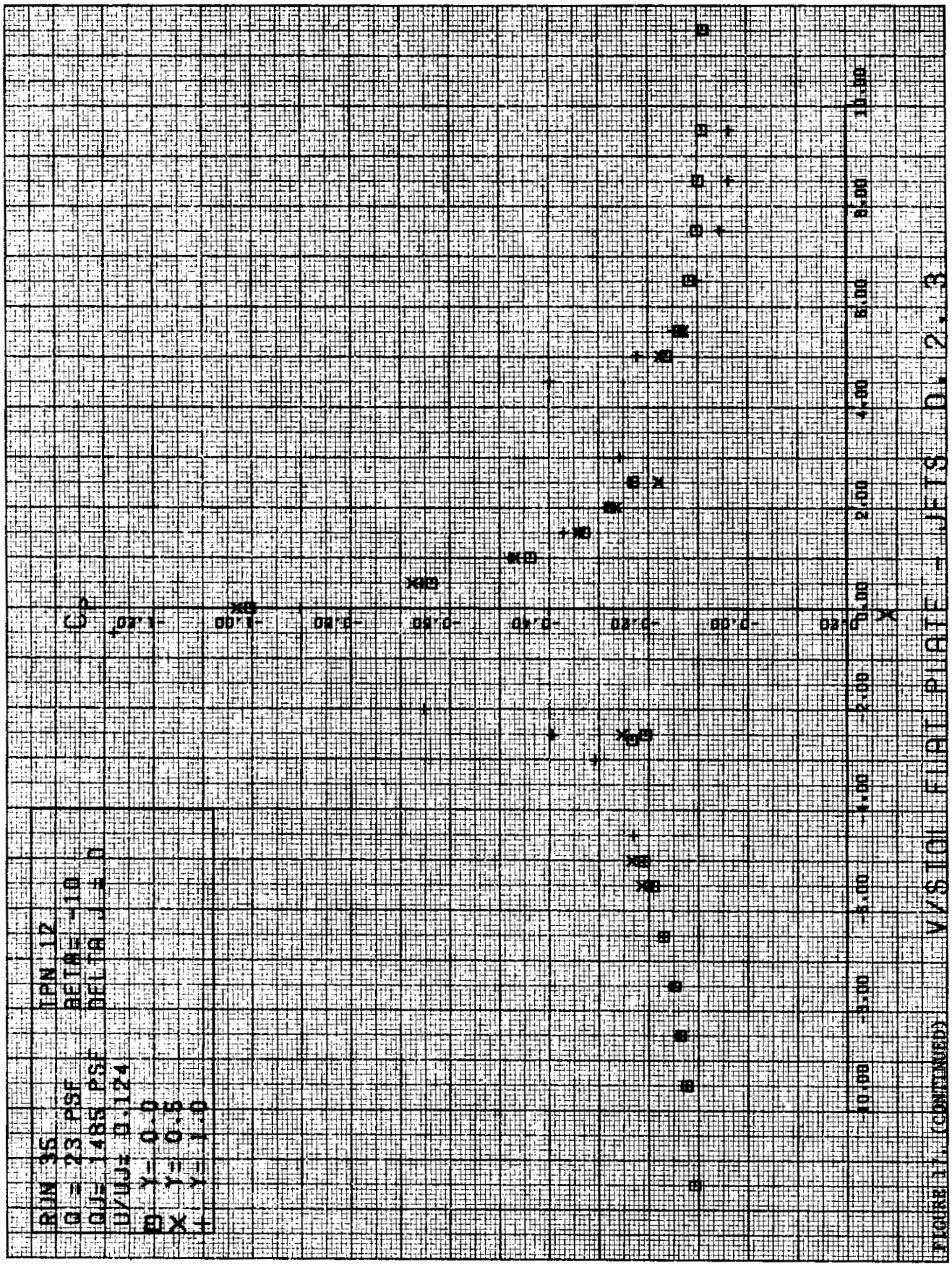

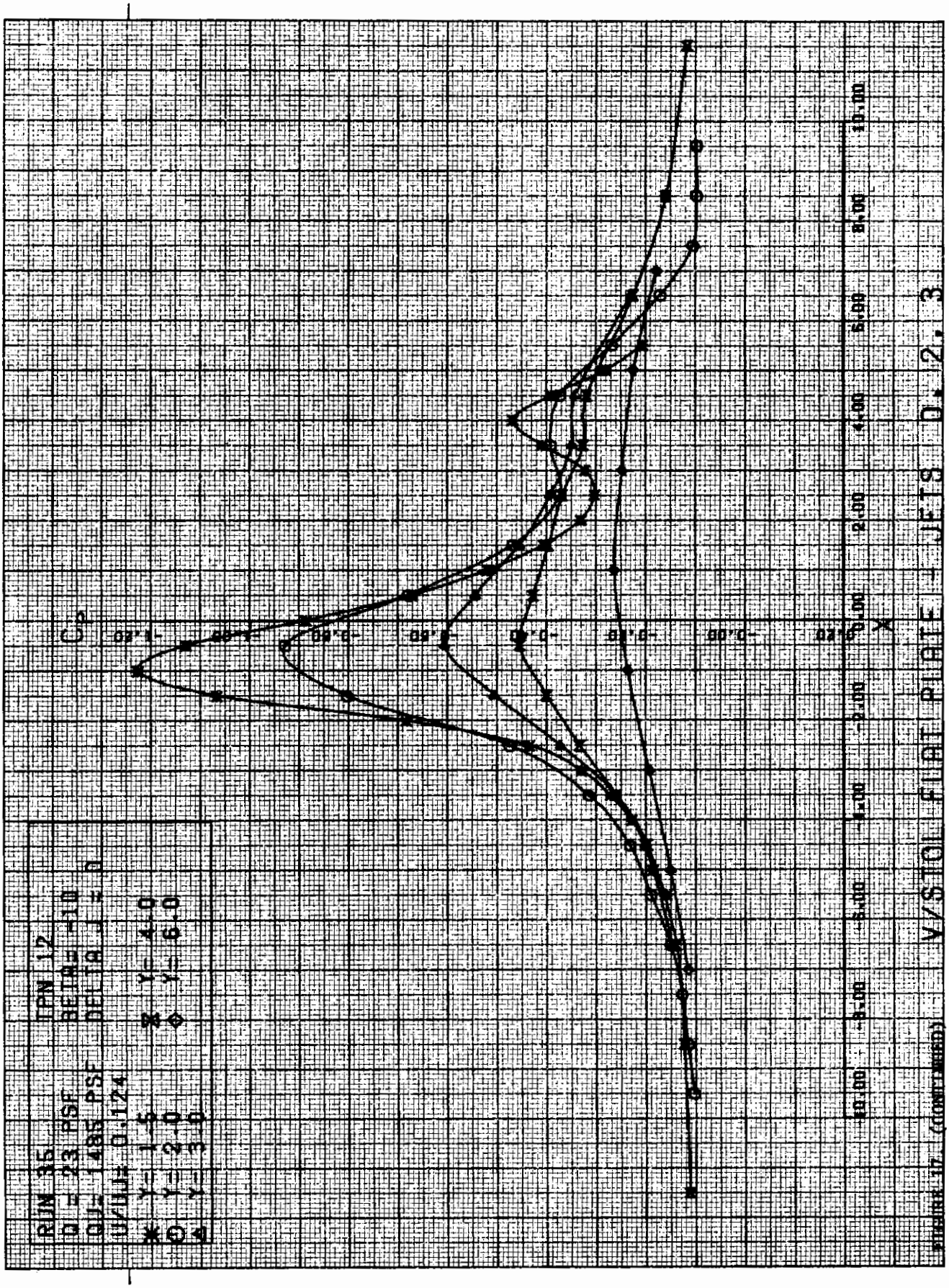

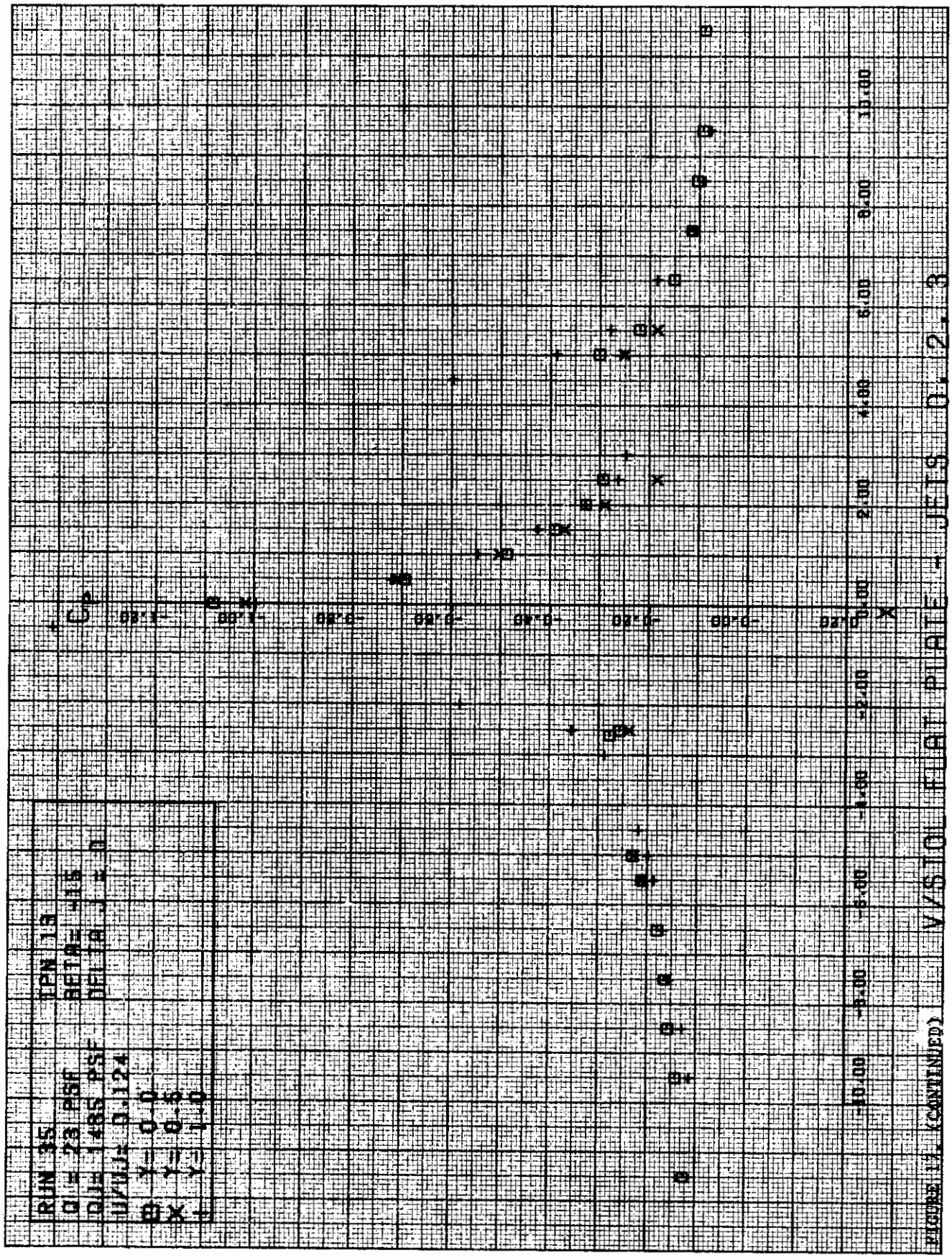

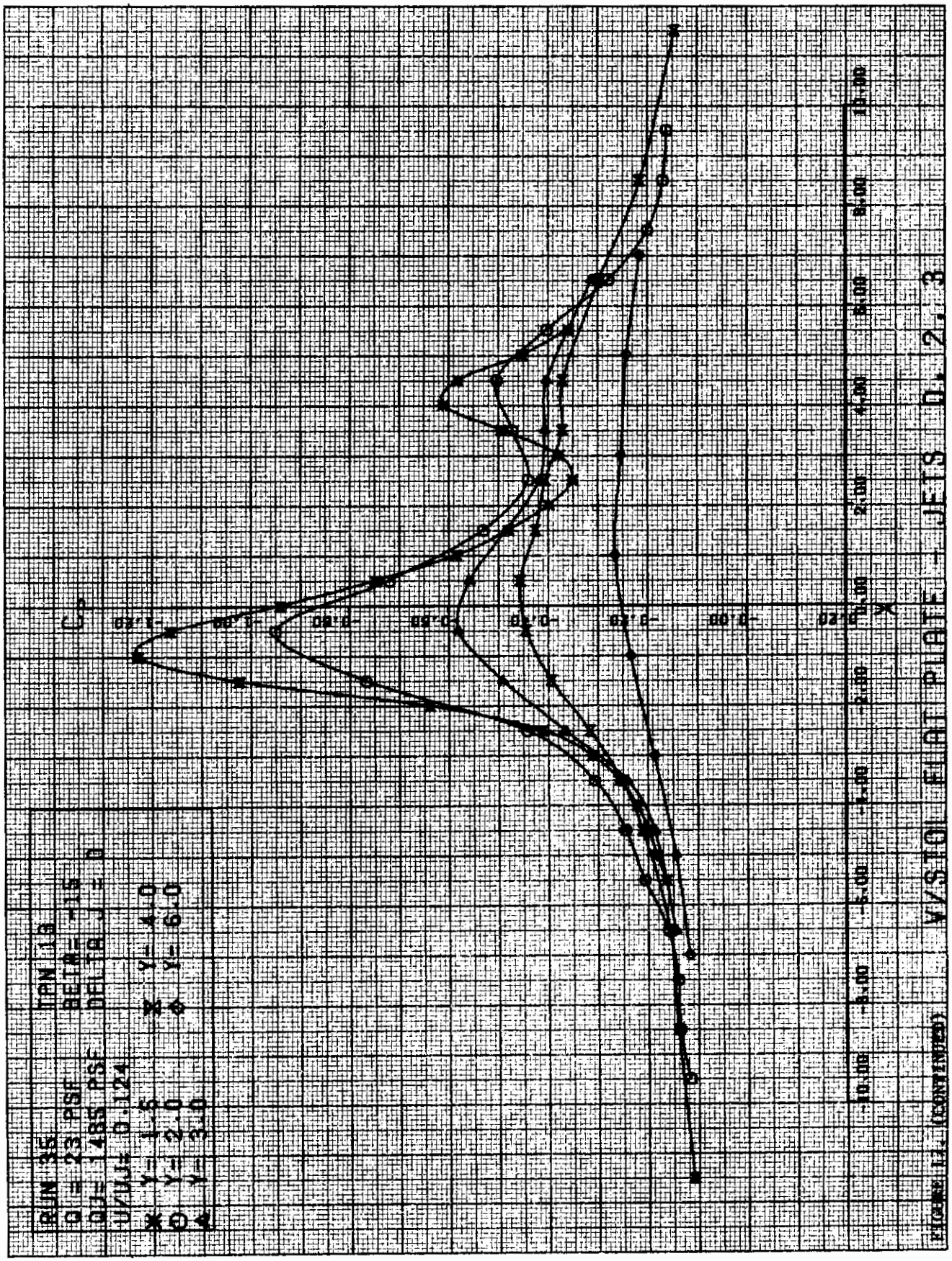

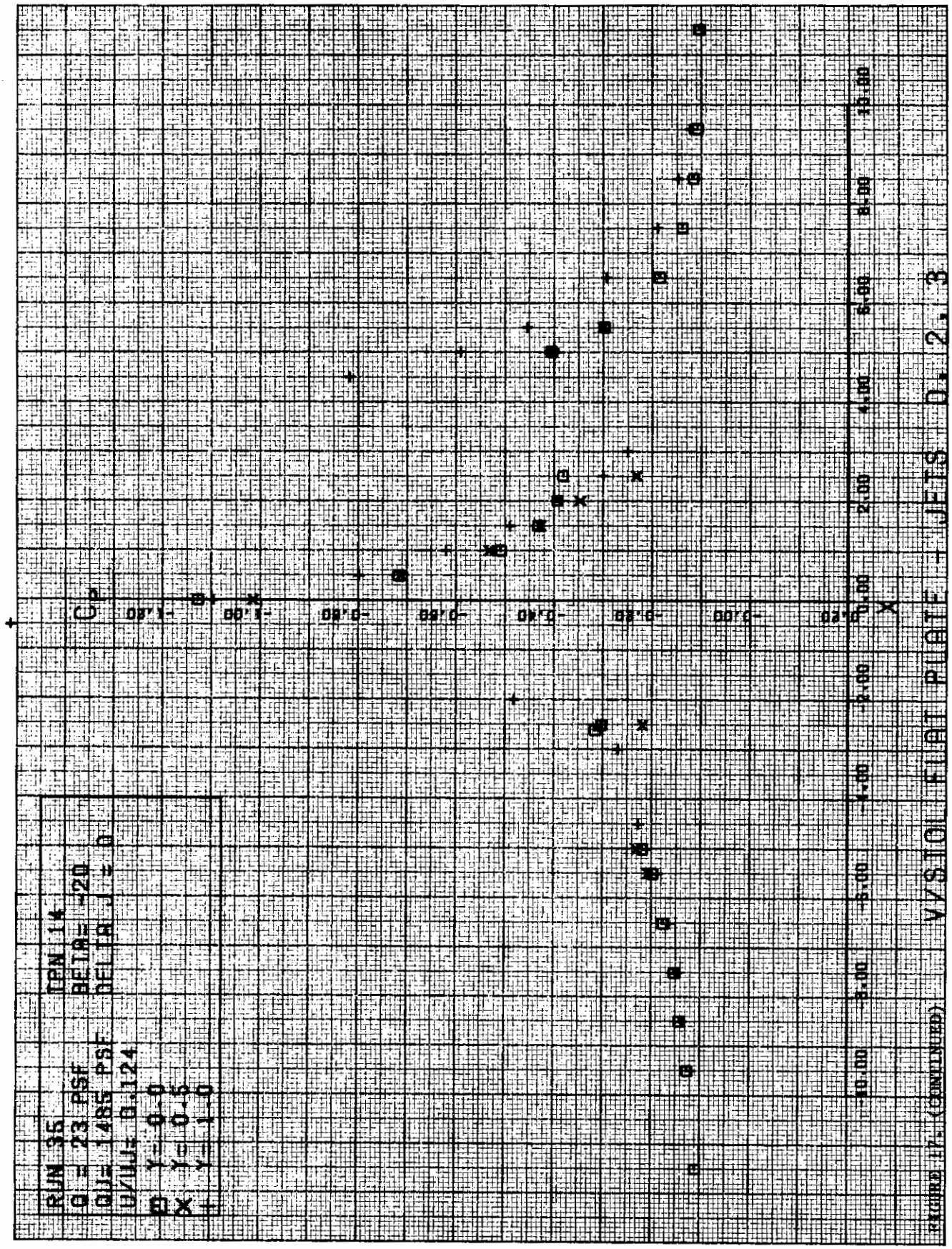

FIGURE 17. (CONTINUED)

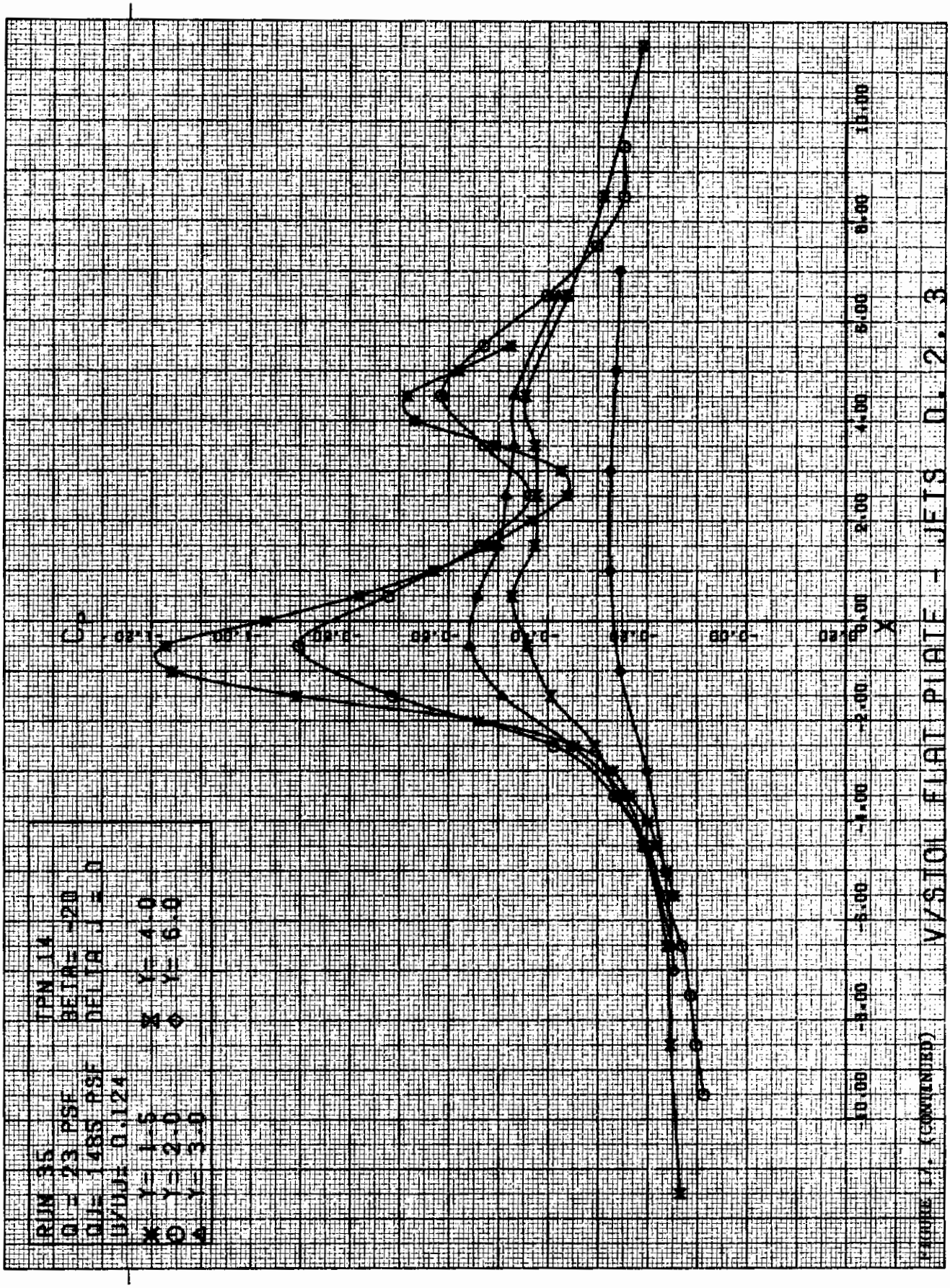

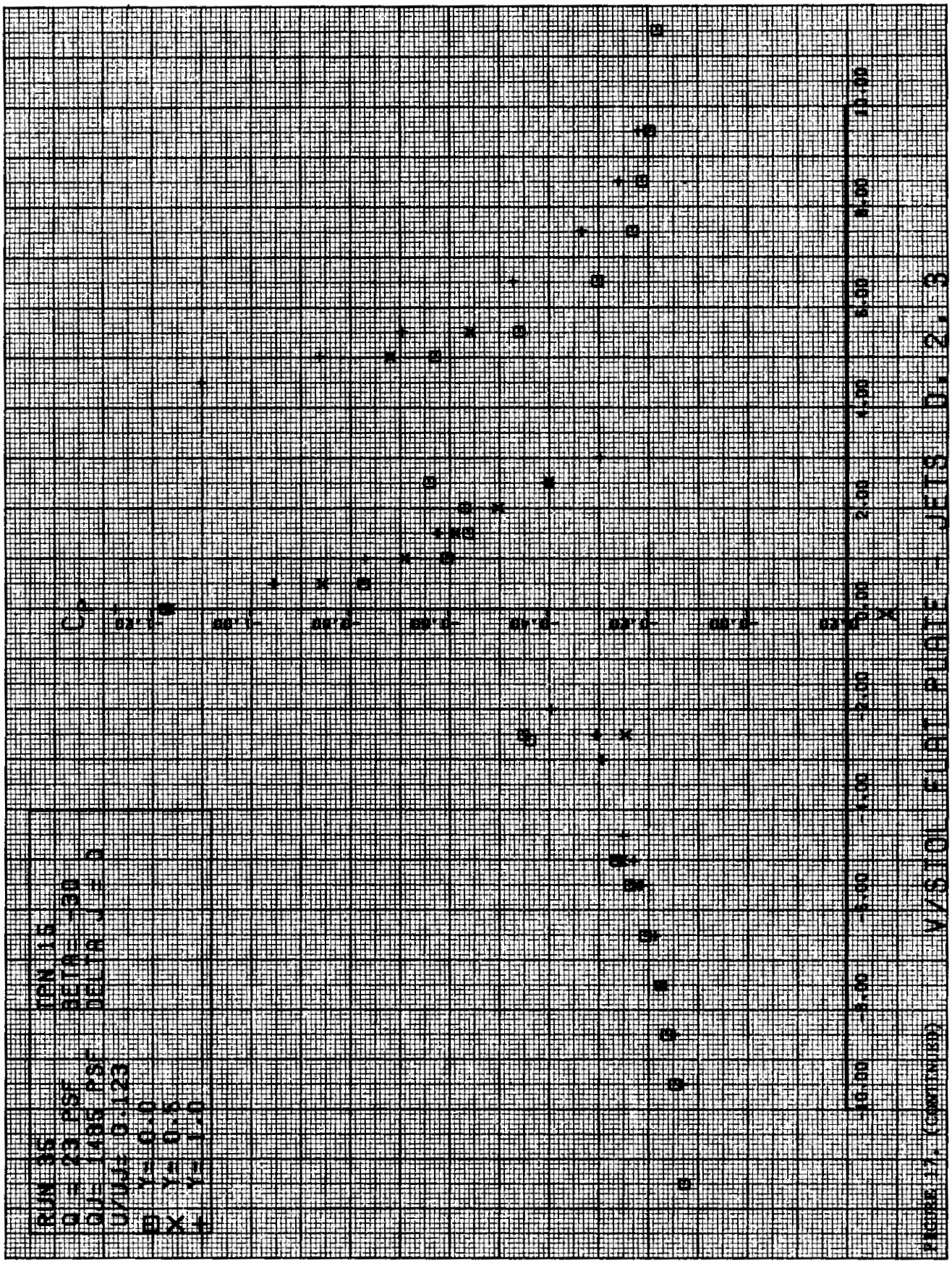

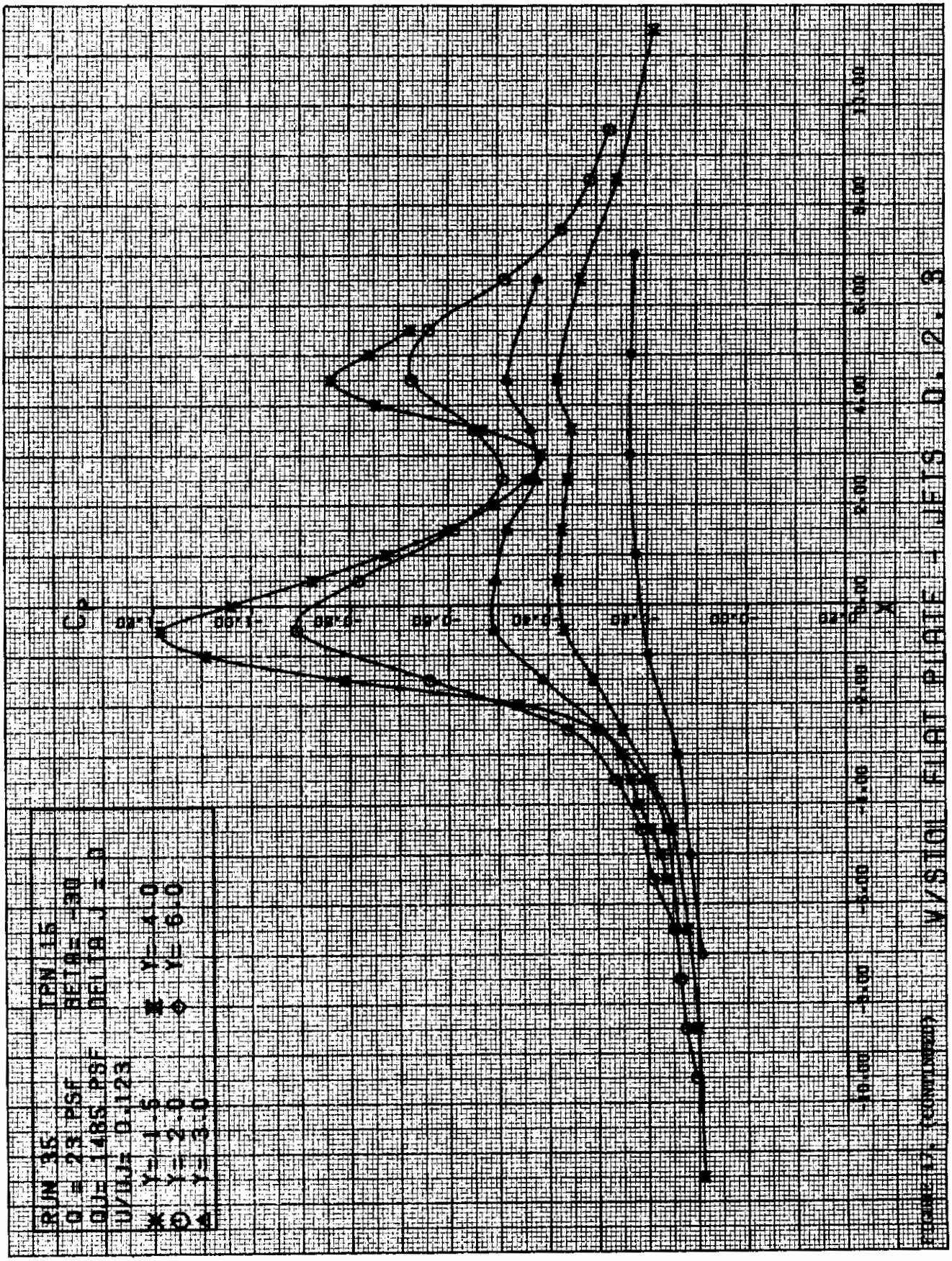

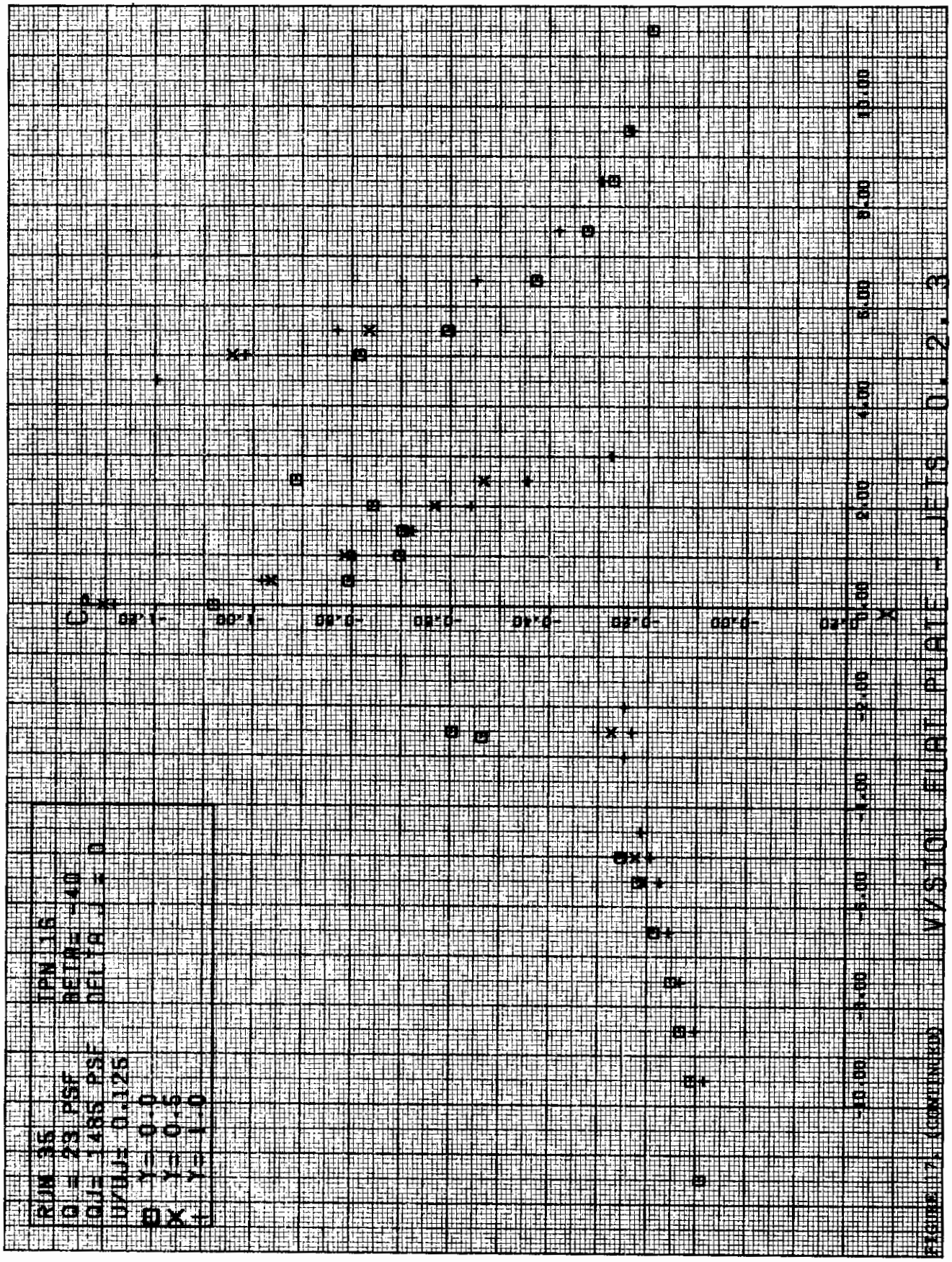

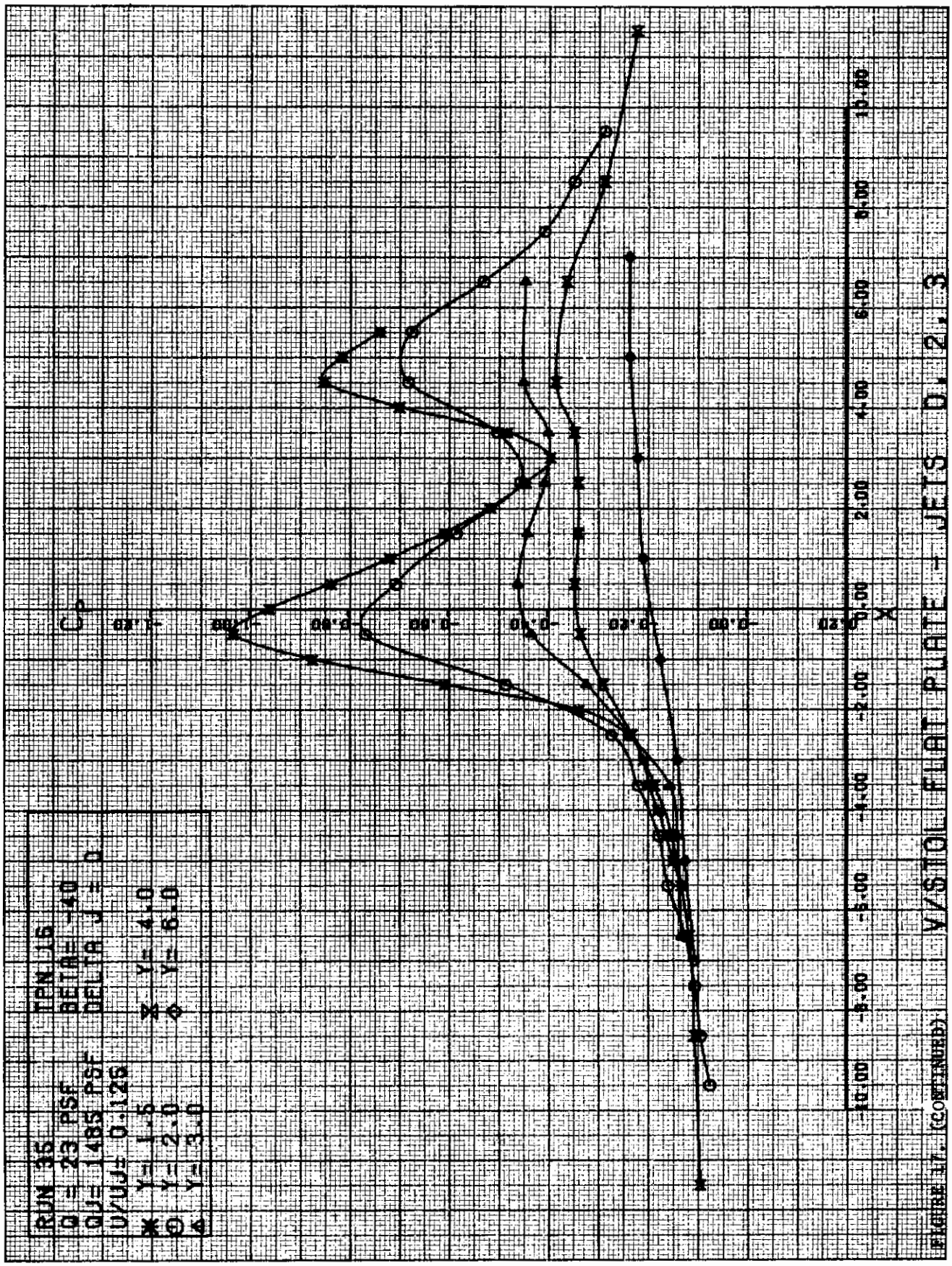

FIGURE 17. (CONTINUED)

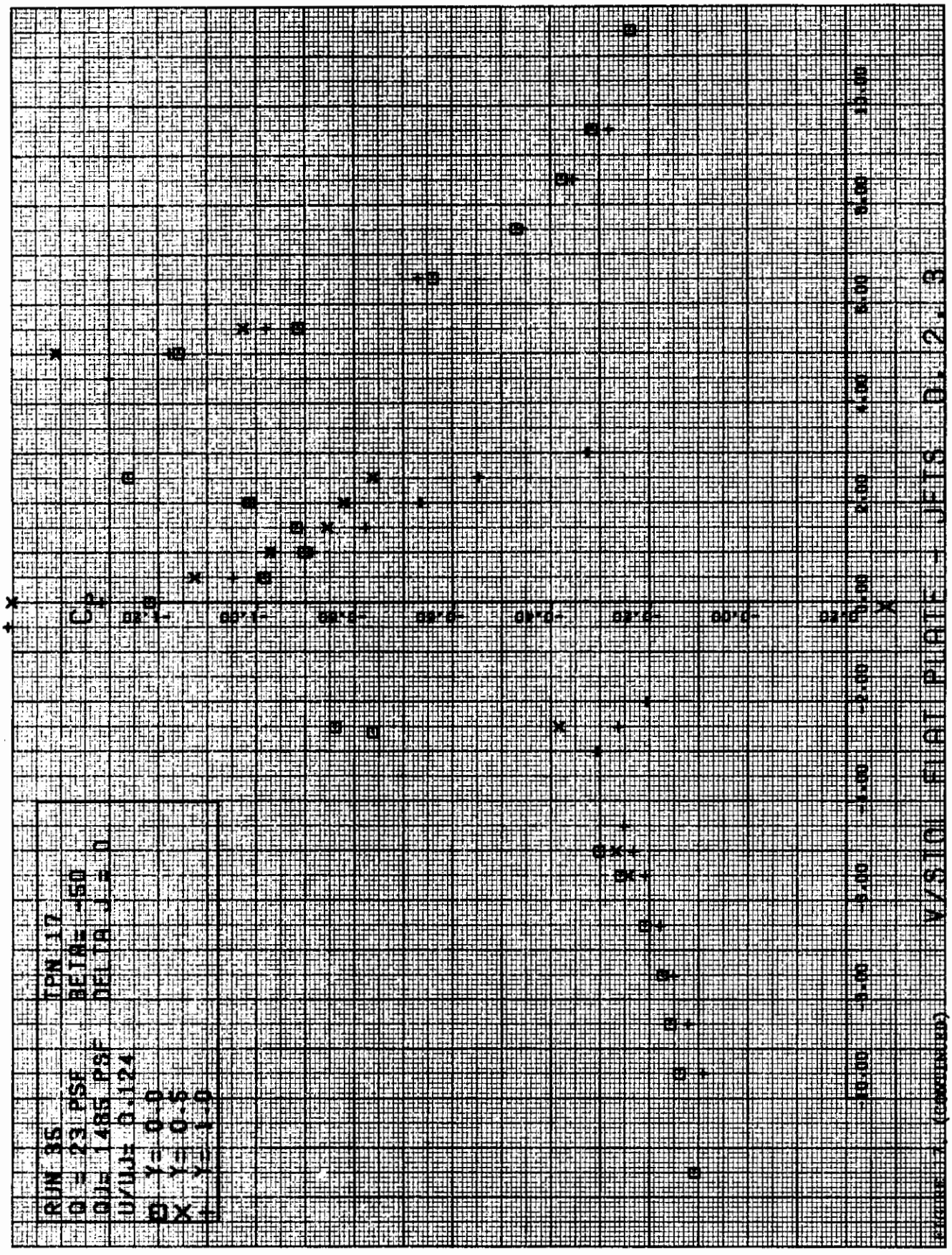

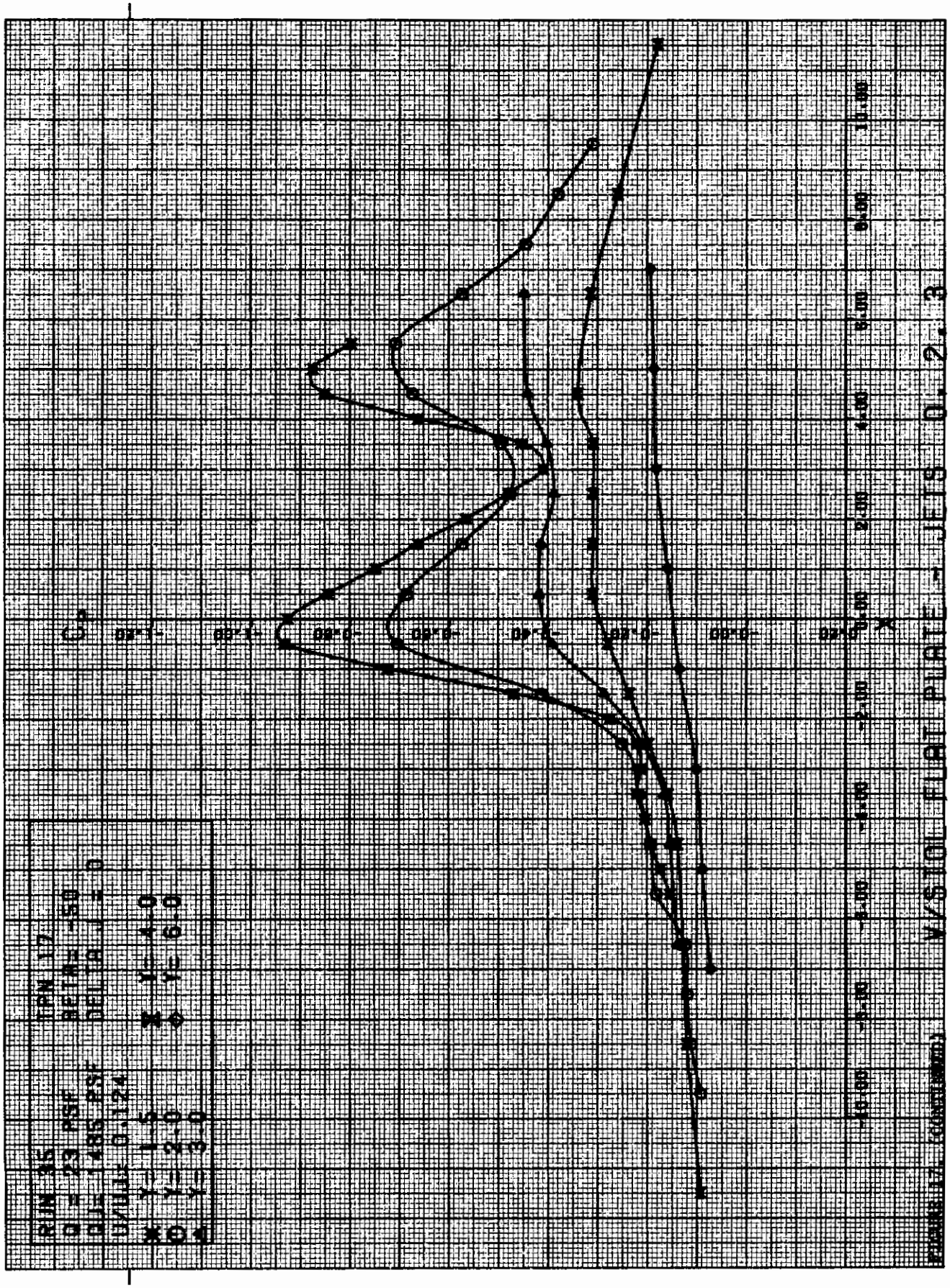

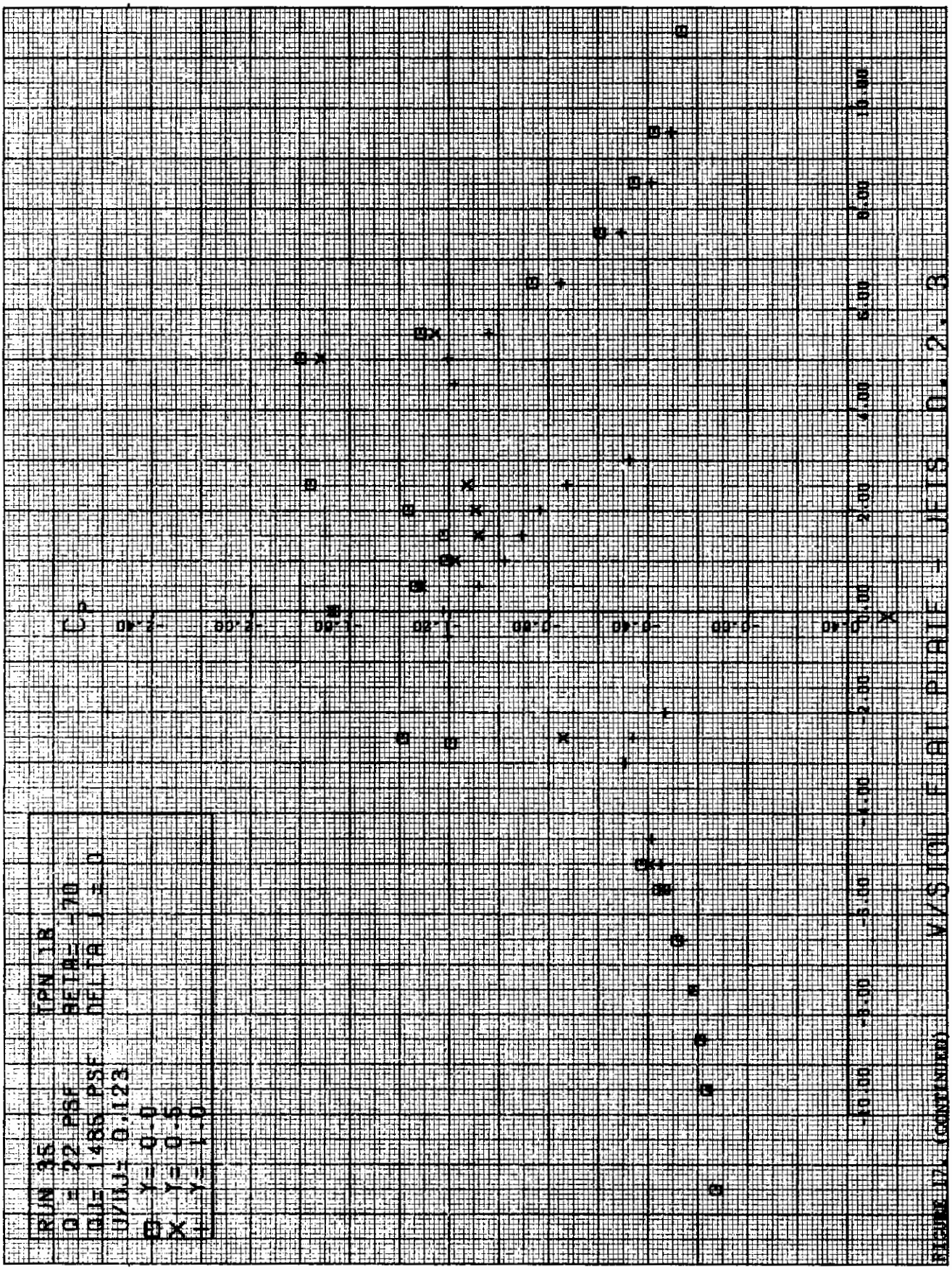

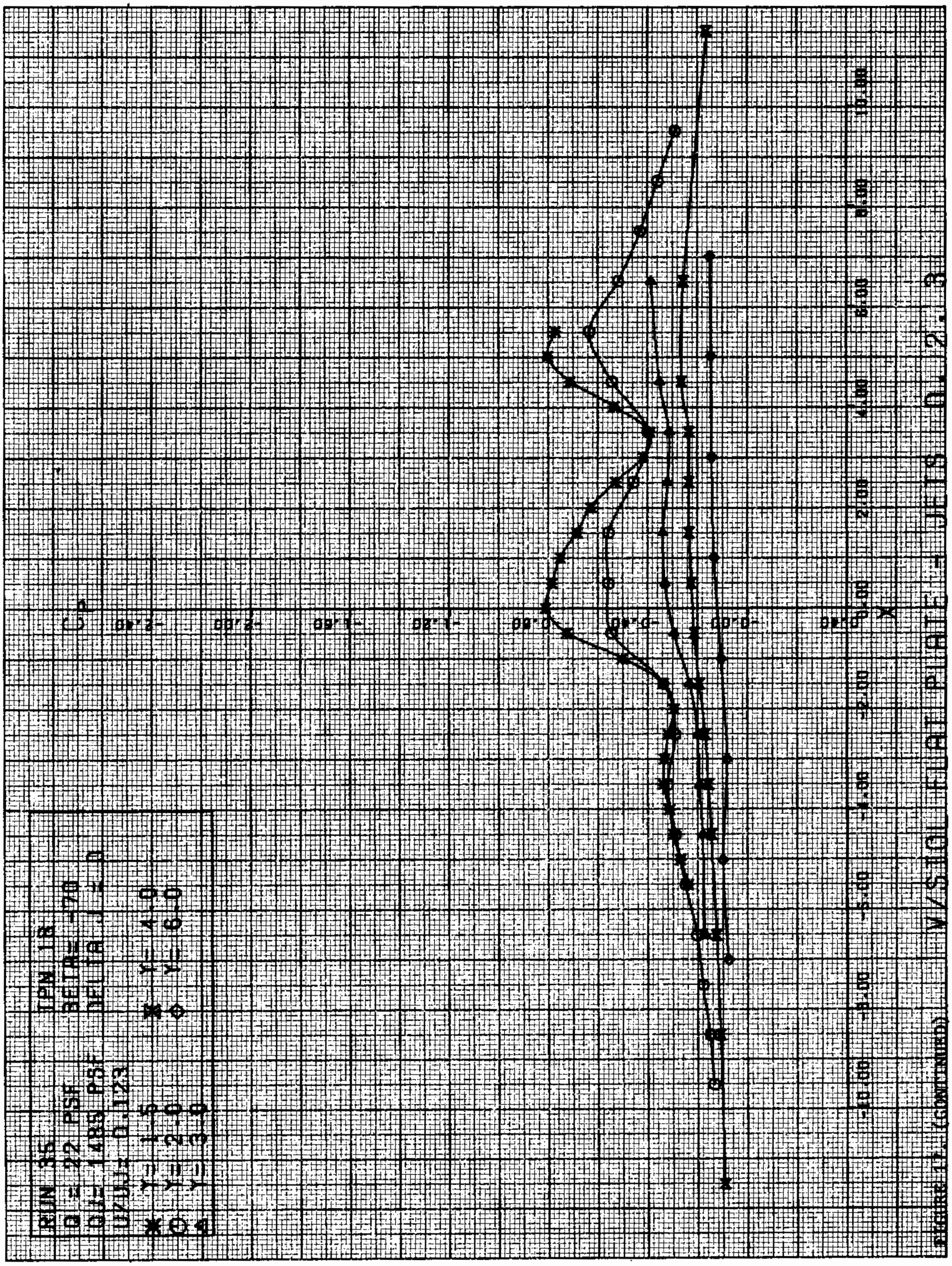

FIGURE 17. (CONTINUED) V/STOL FLAT PLATE - JETS 0, 2, 3

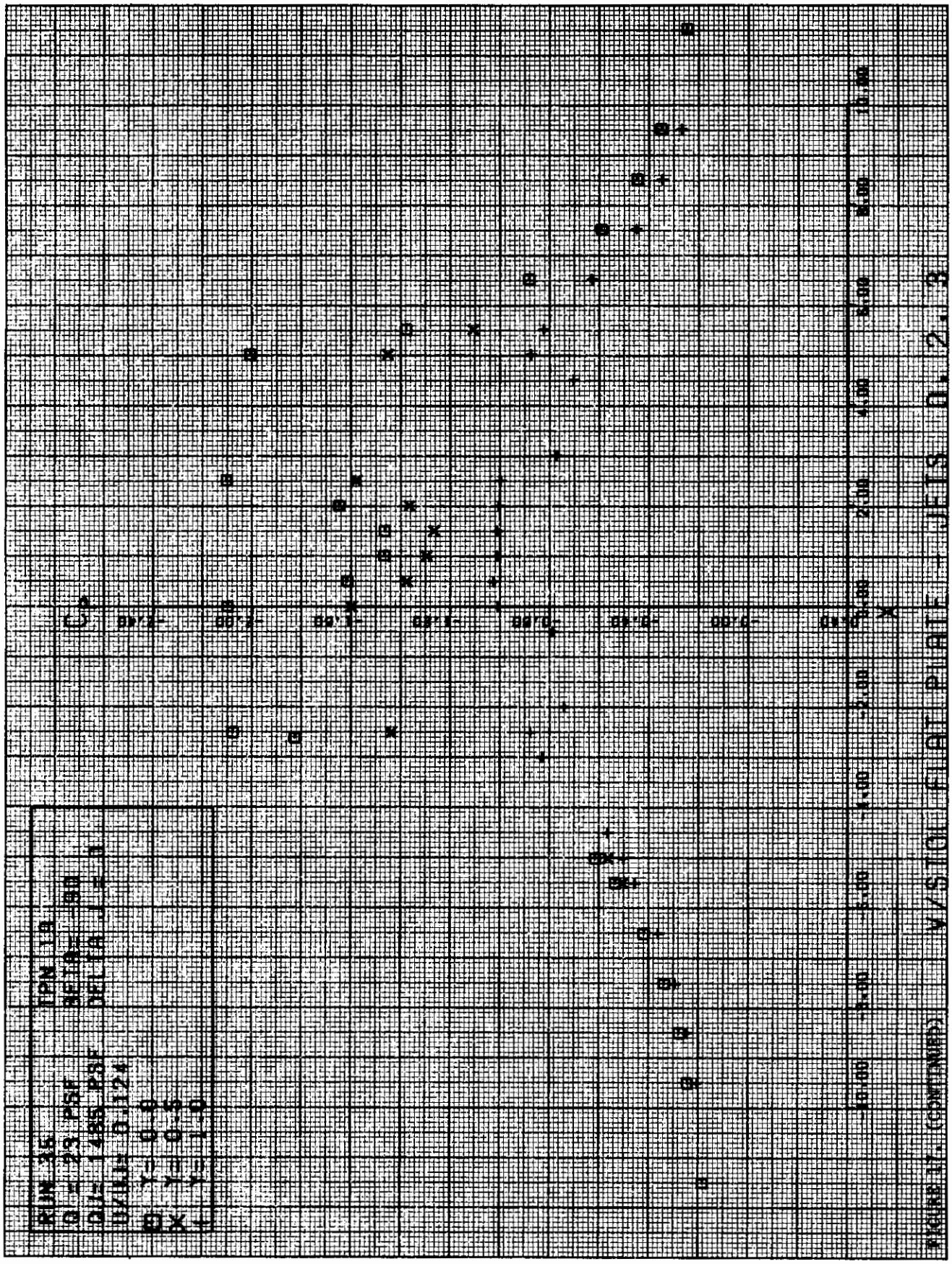

FIGURE 37. (CONTINUED)

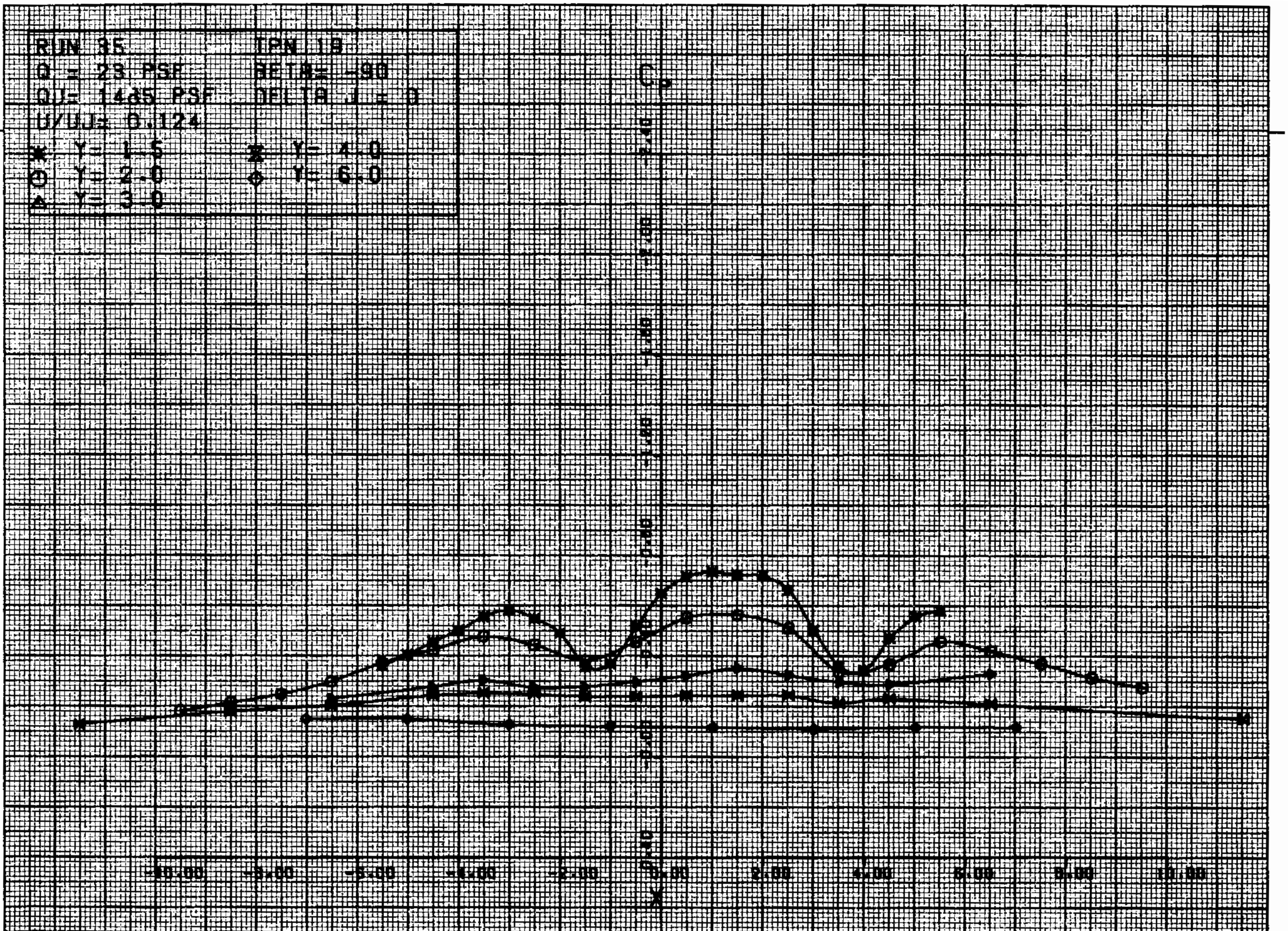

FIGURE 17. (CONCLUDED) V/STOL FLAT PLATE - JETS D. 2. 3

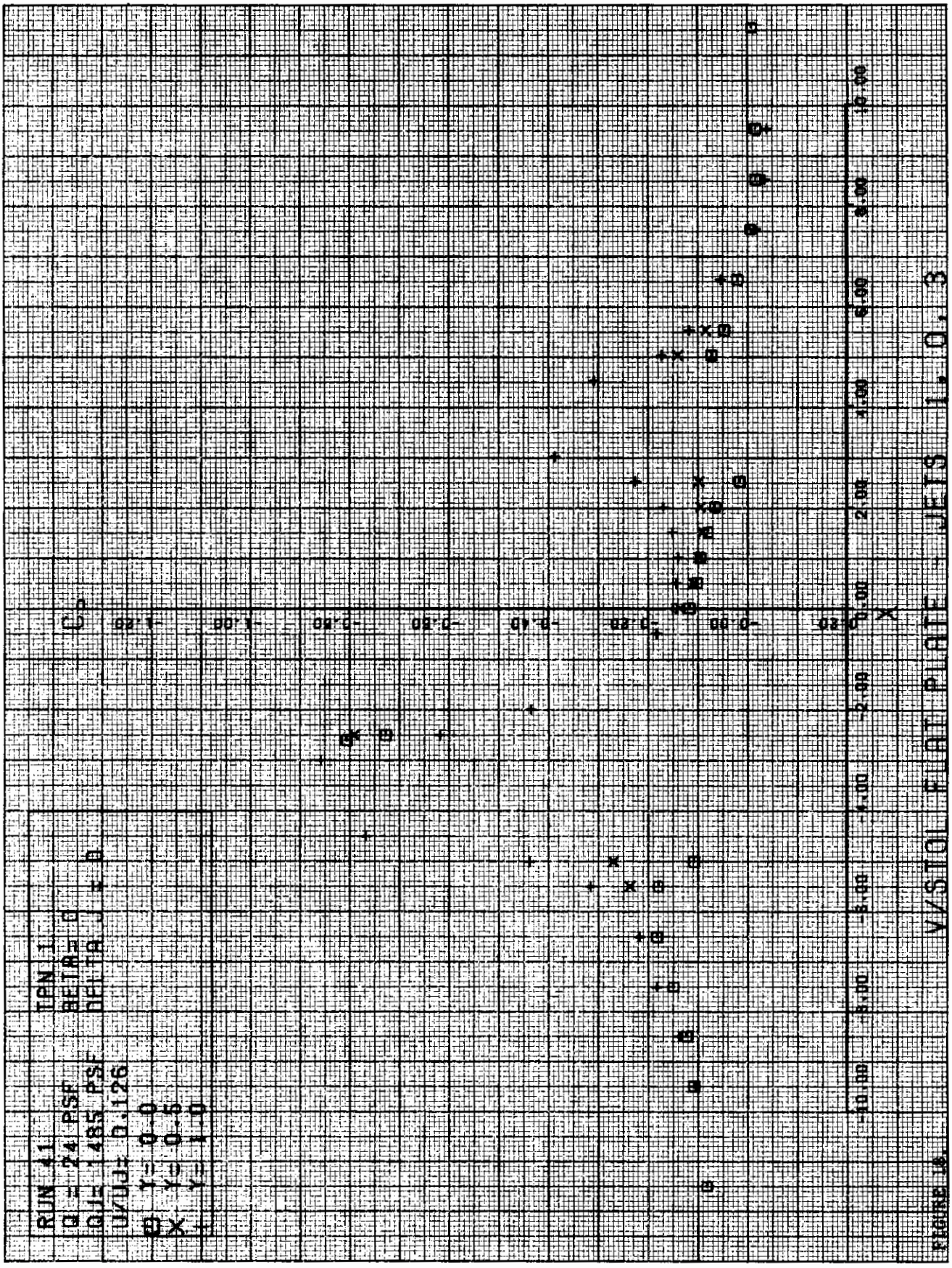

FIGURE 36.

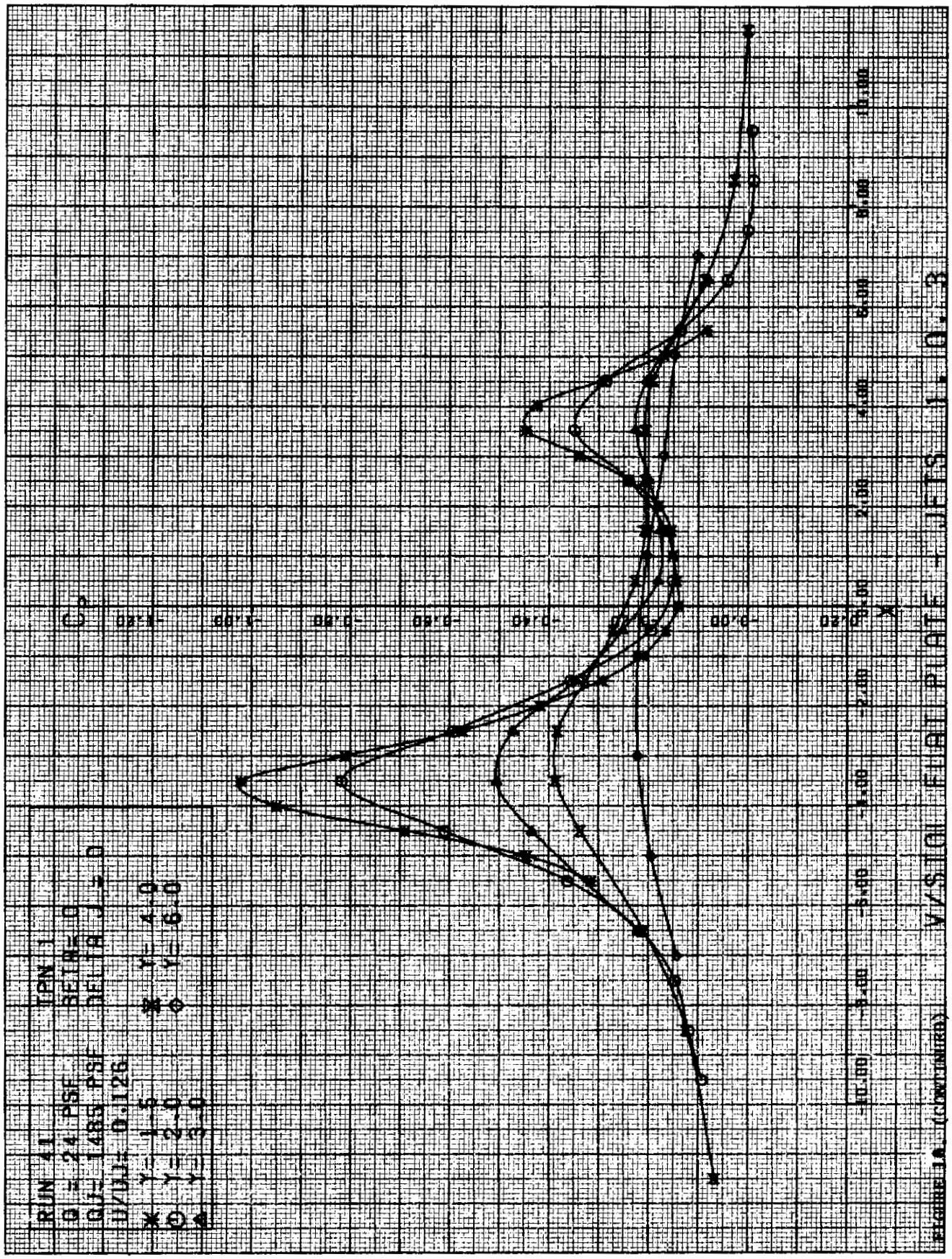

FIGURE 14. (CONCLUDED)

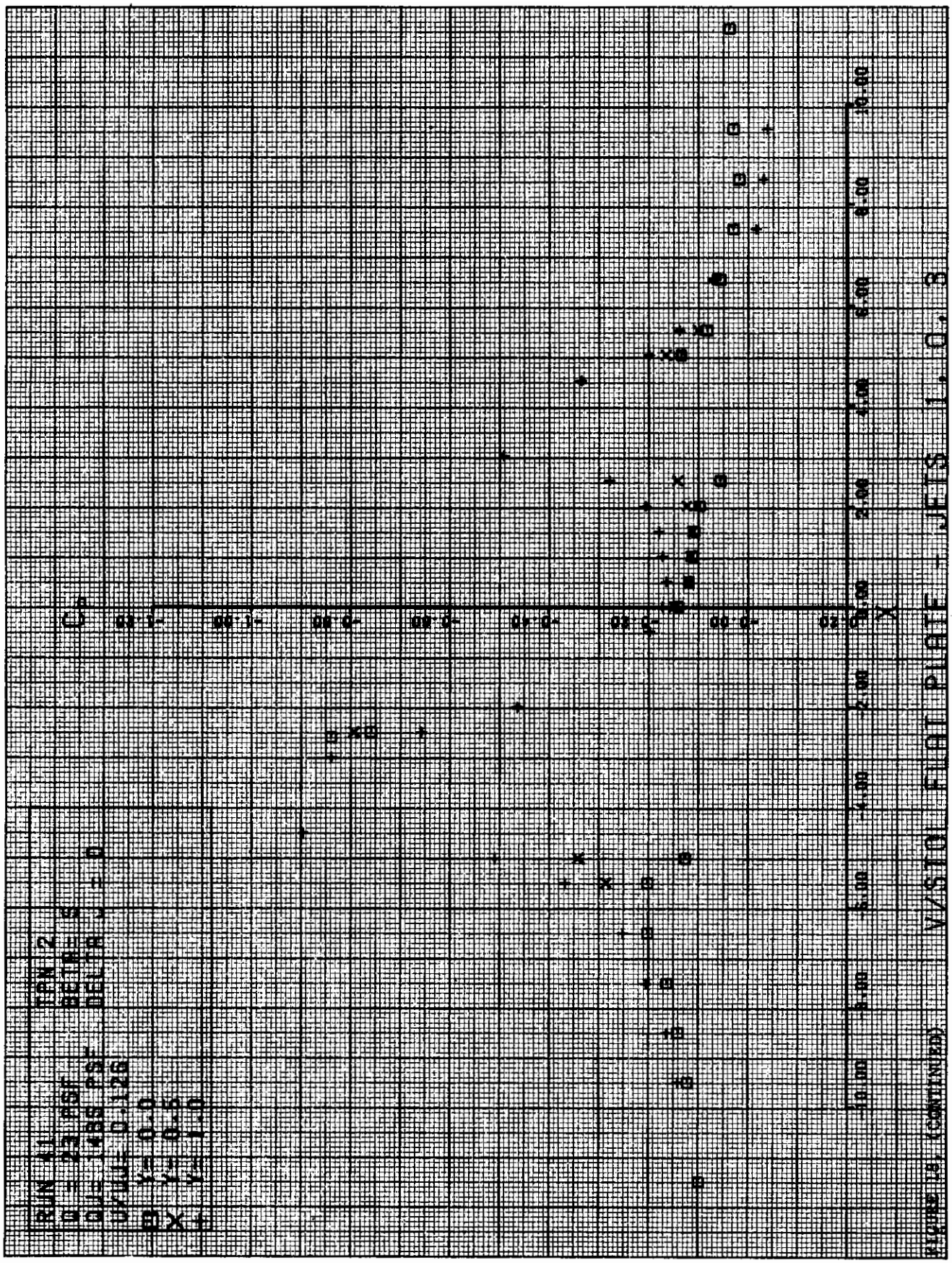

FIGURE 18. (CONTINUED)

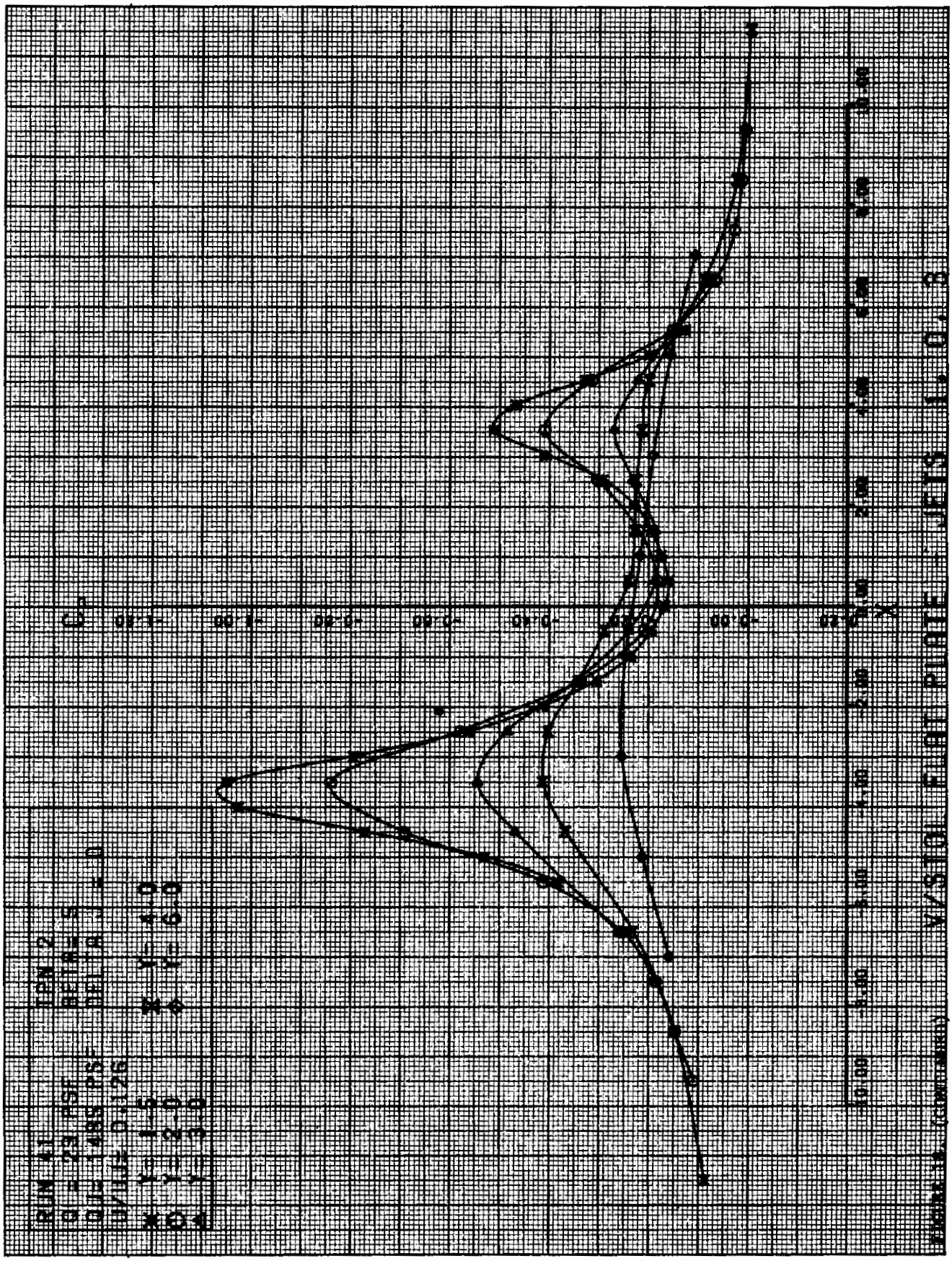

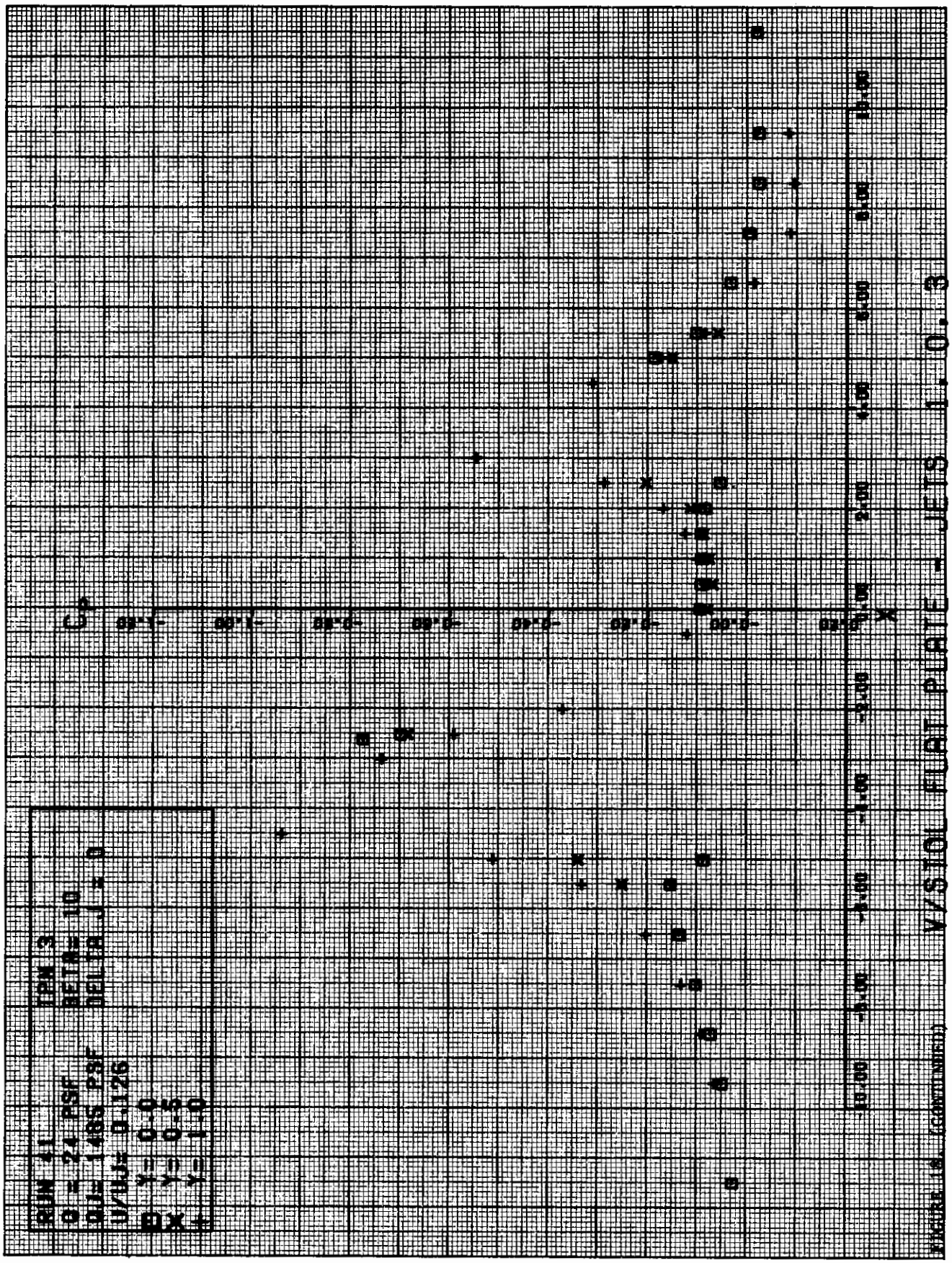

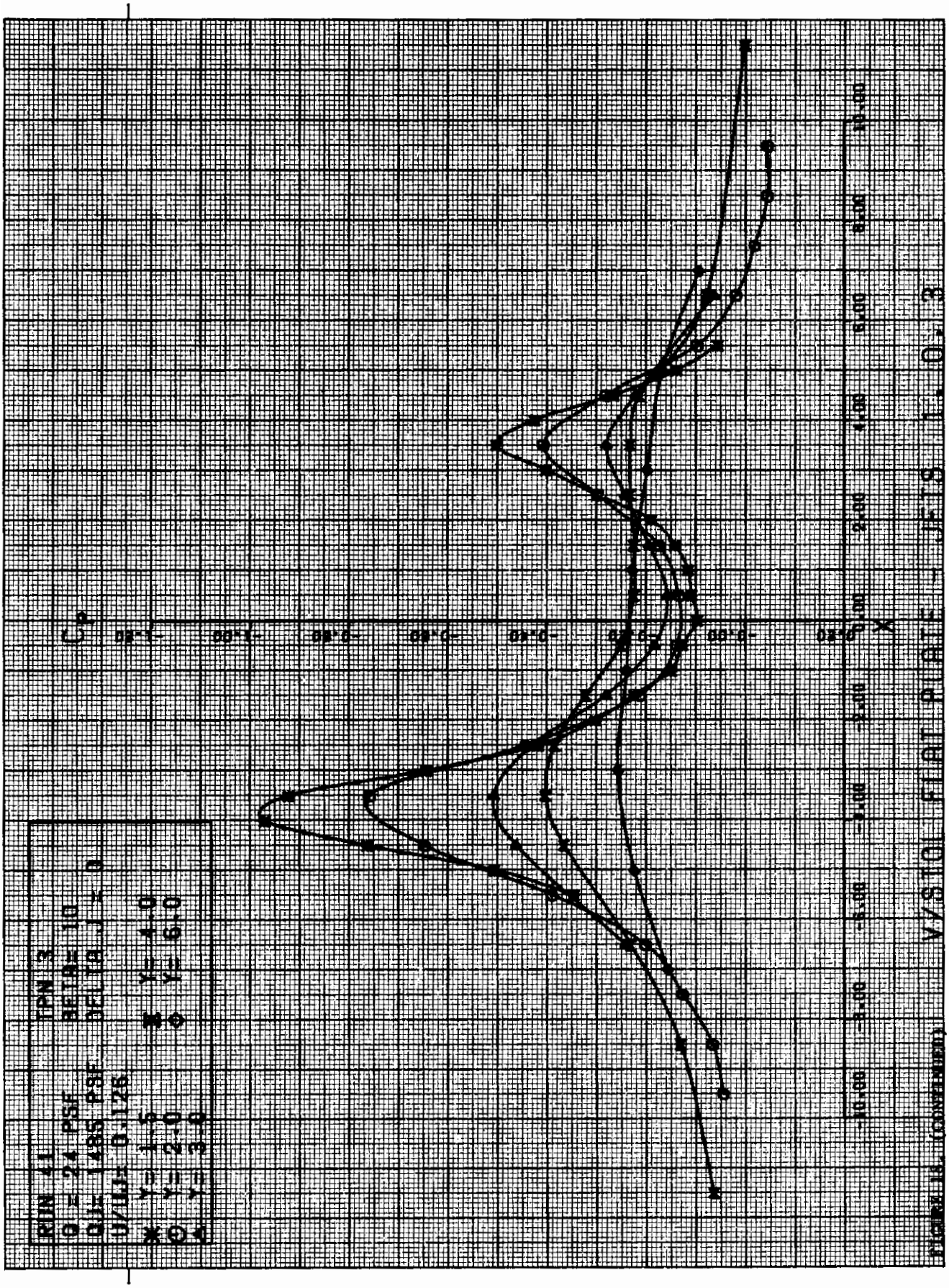

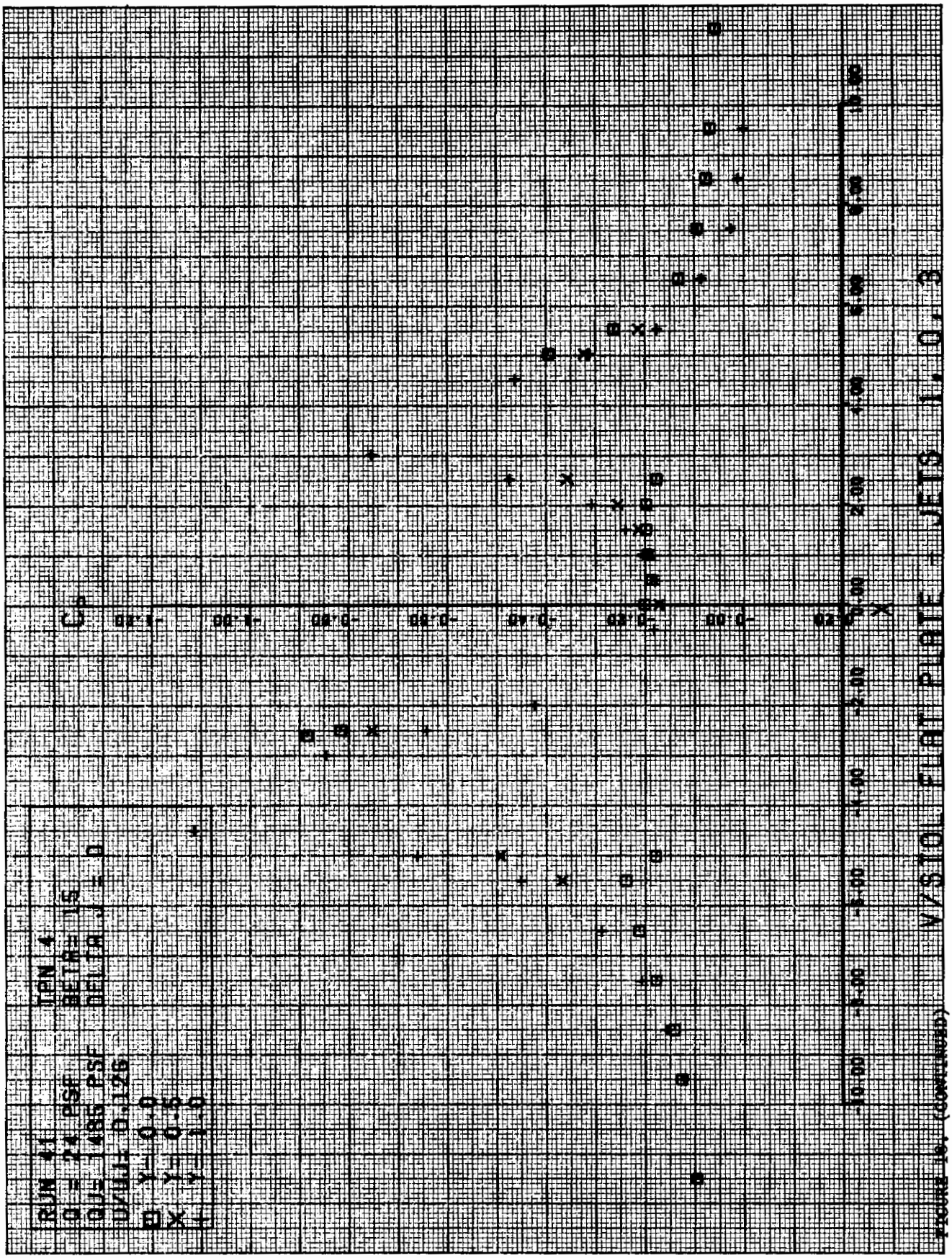

FIGURE 10. (CONCLUDED)

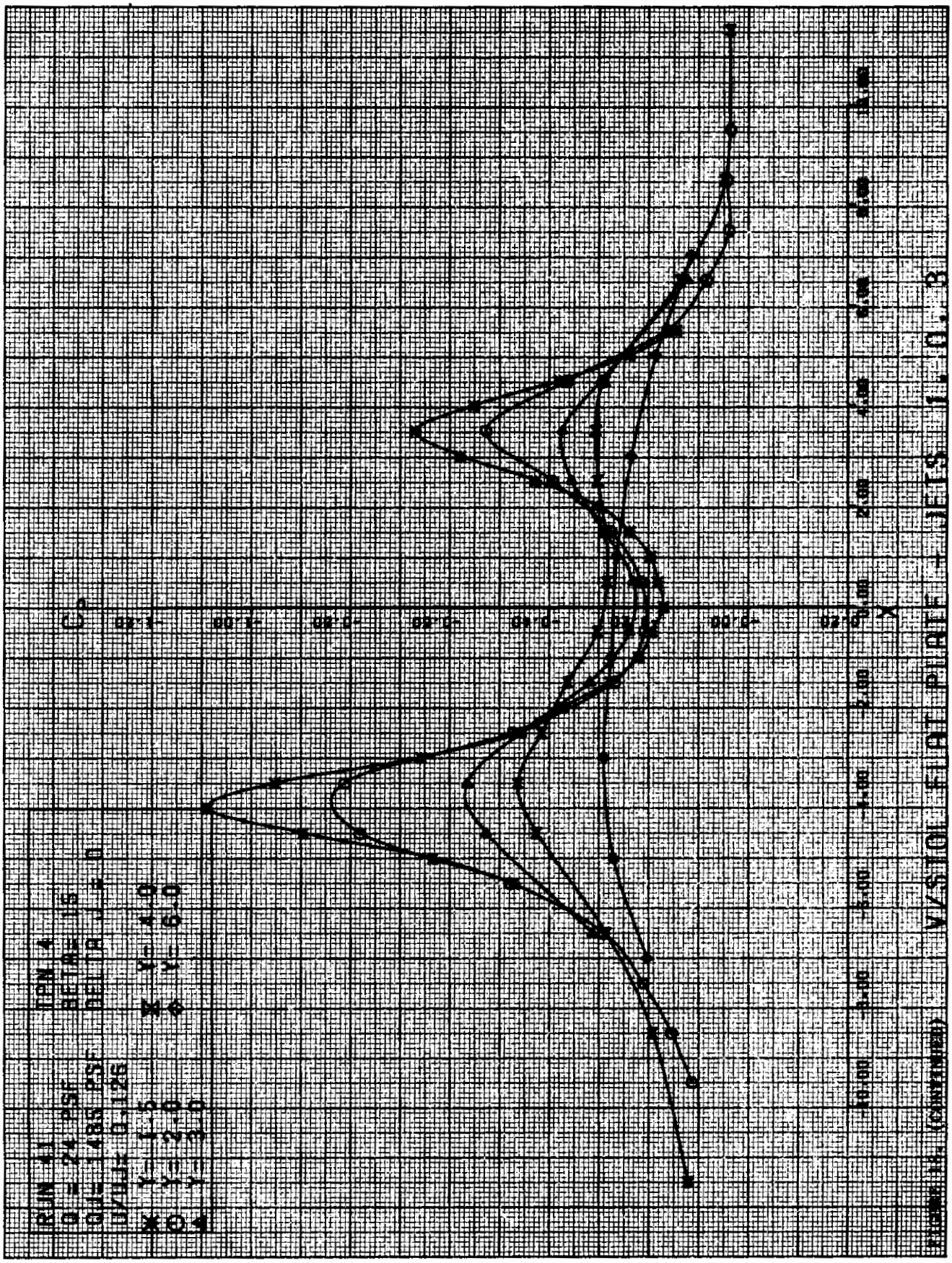

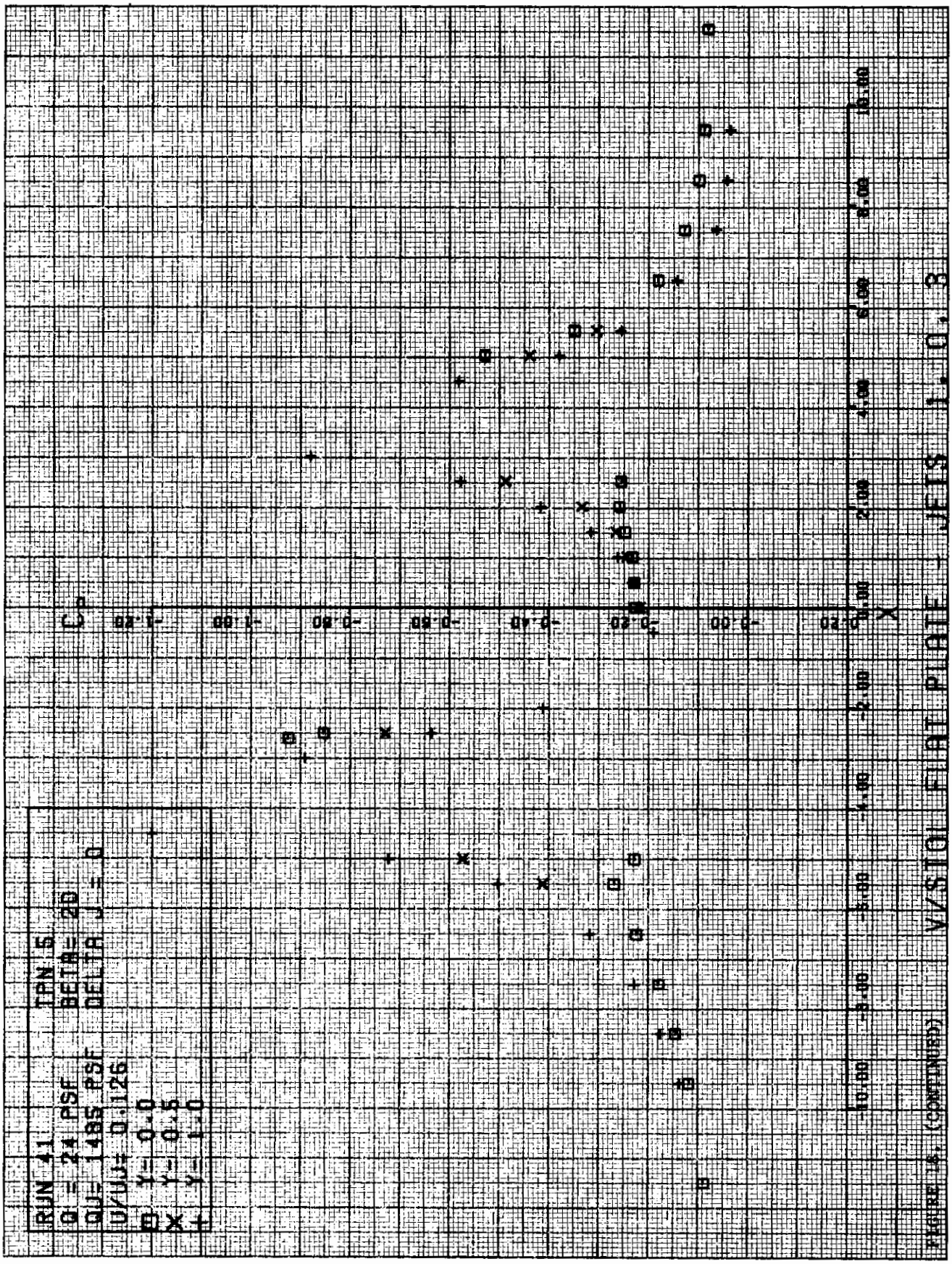

FIGURE 16. (CONTINUED)

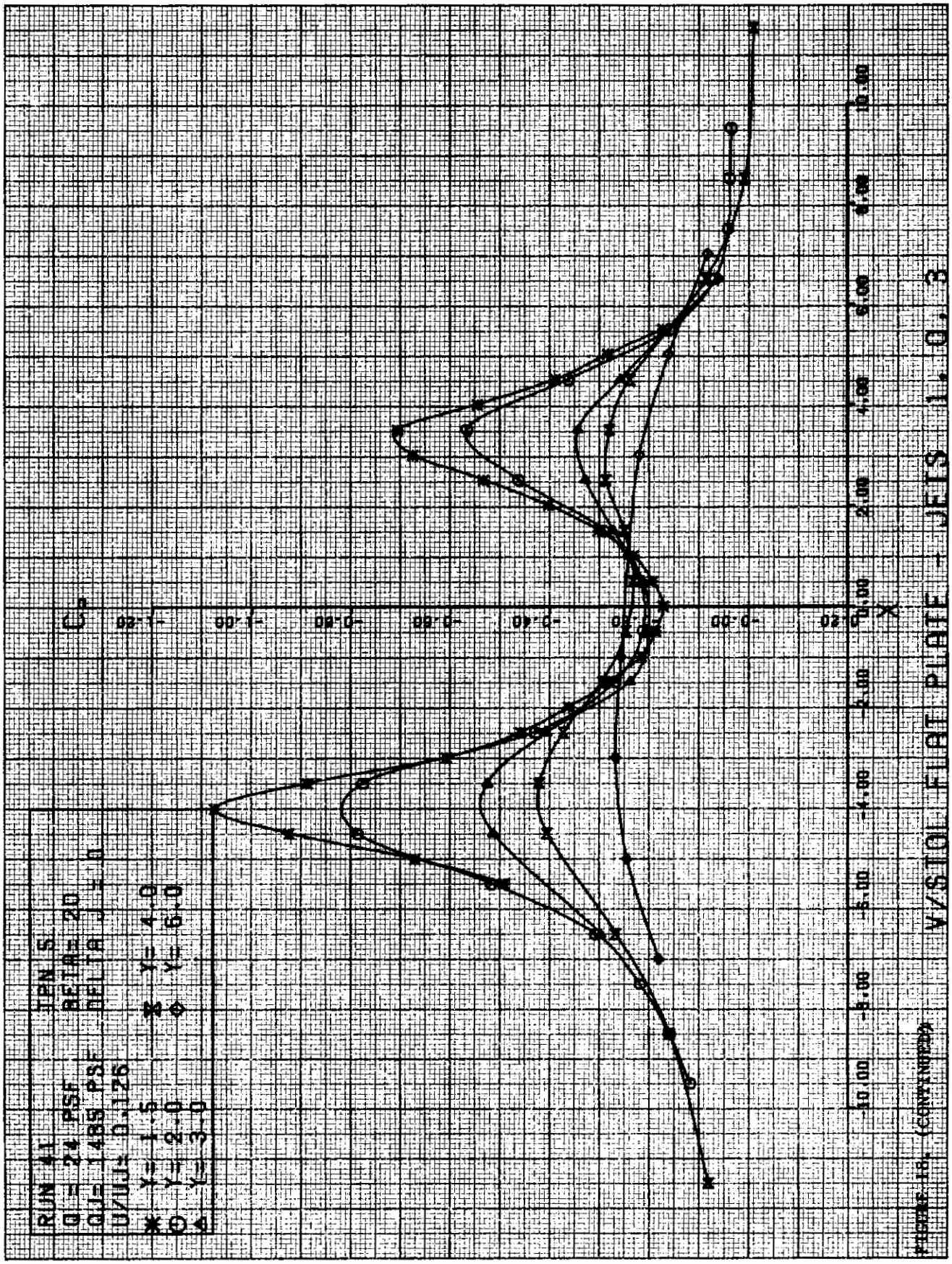

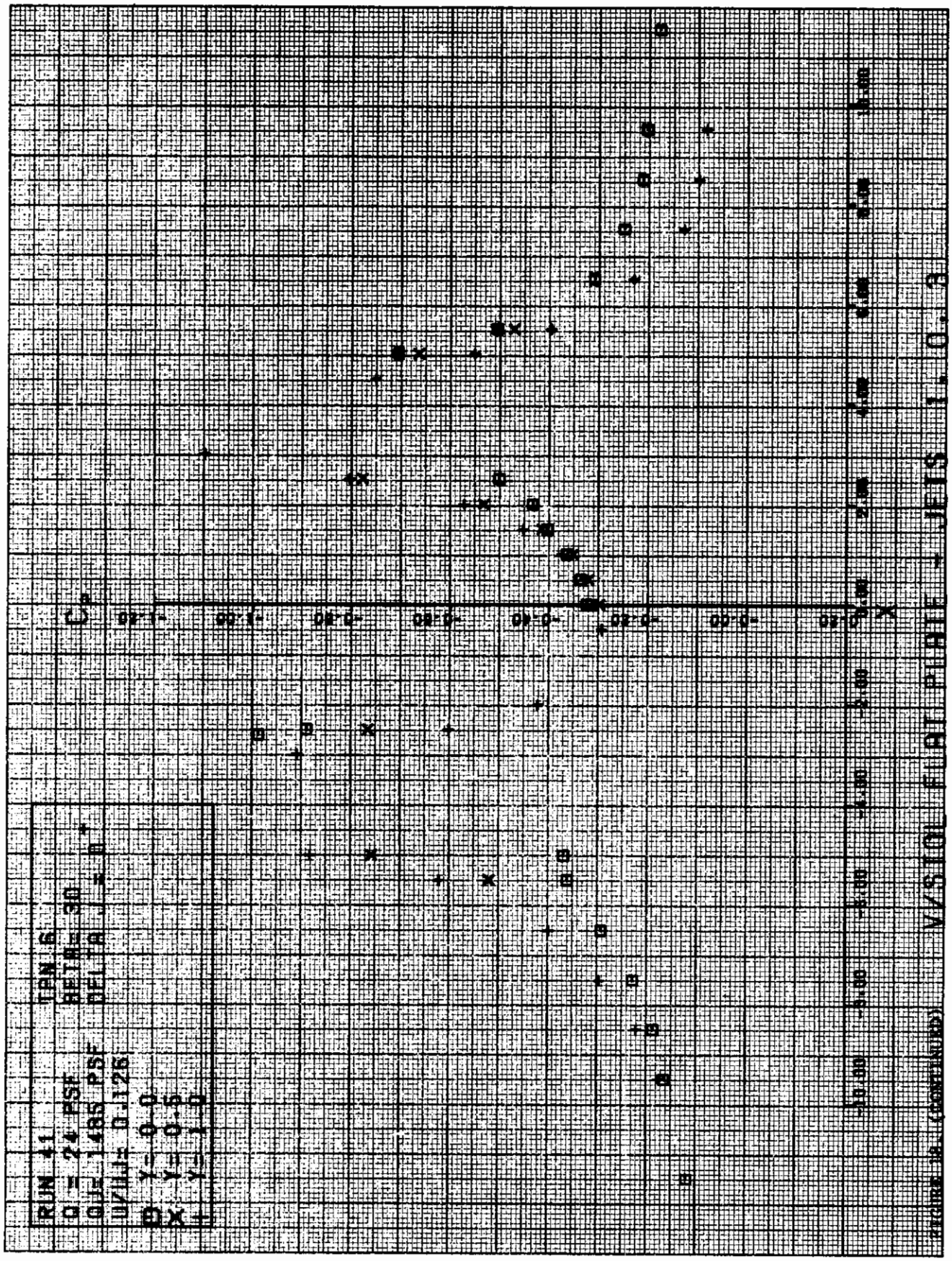

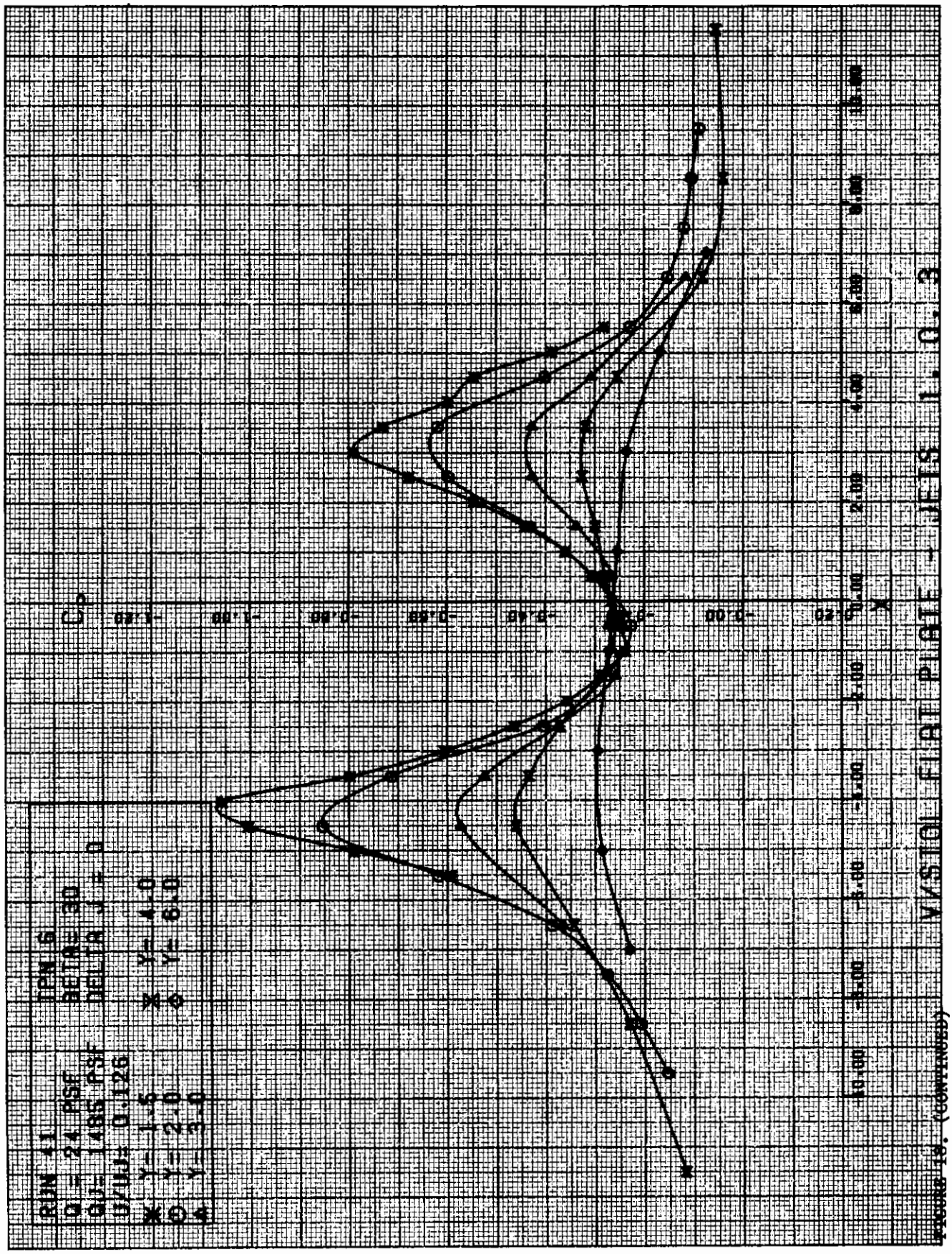

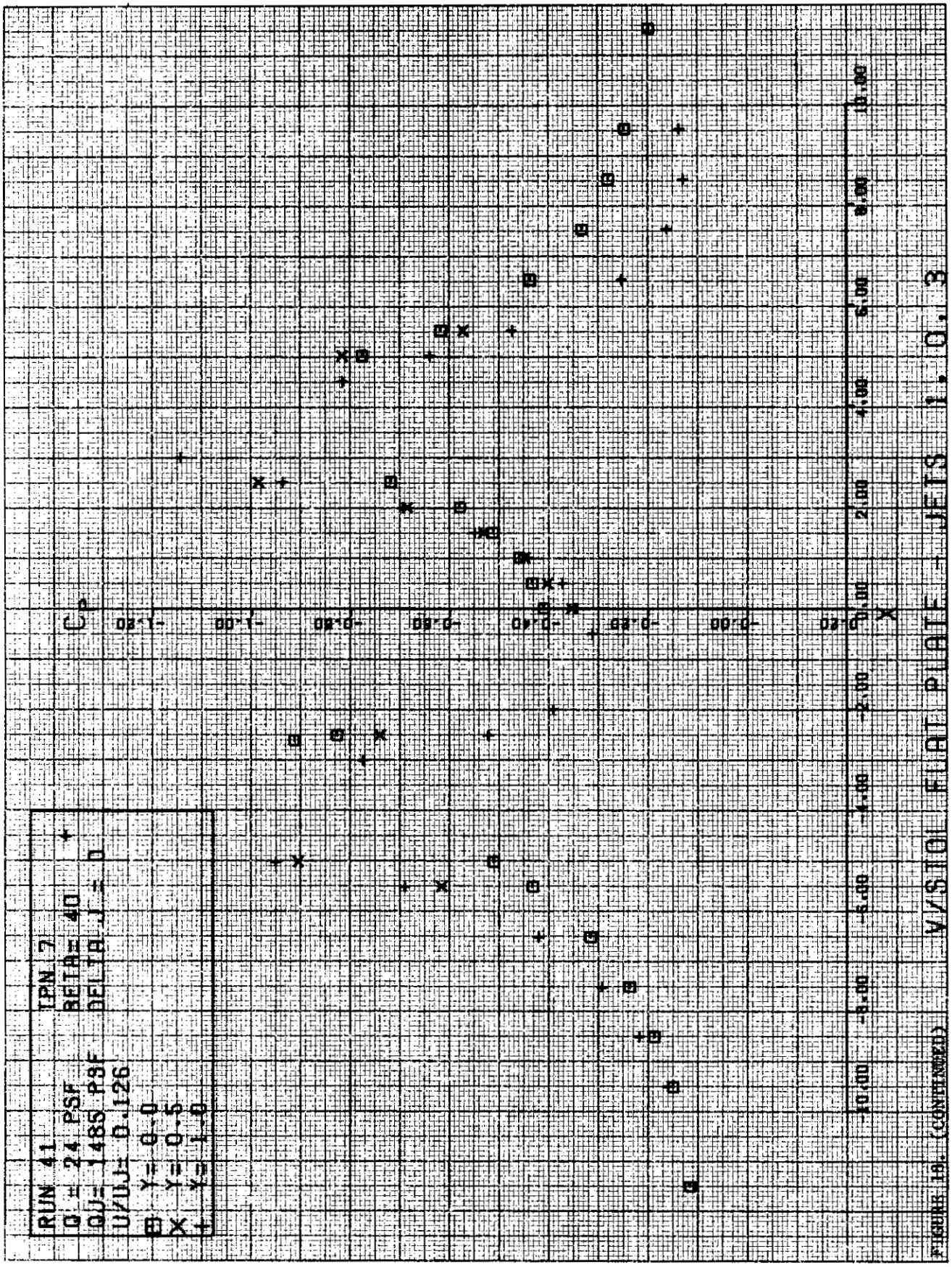

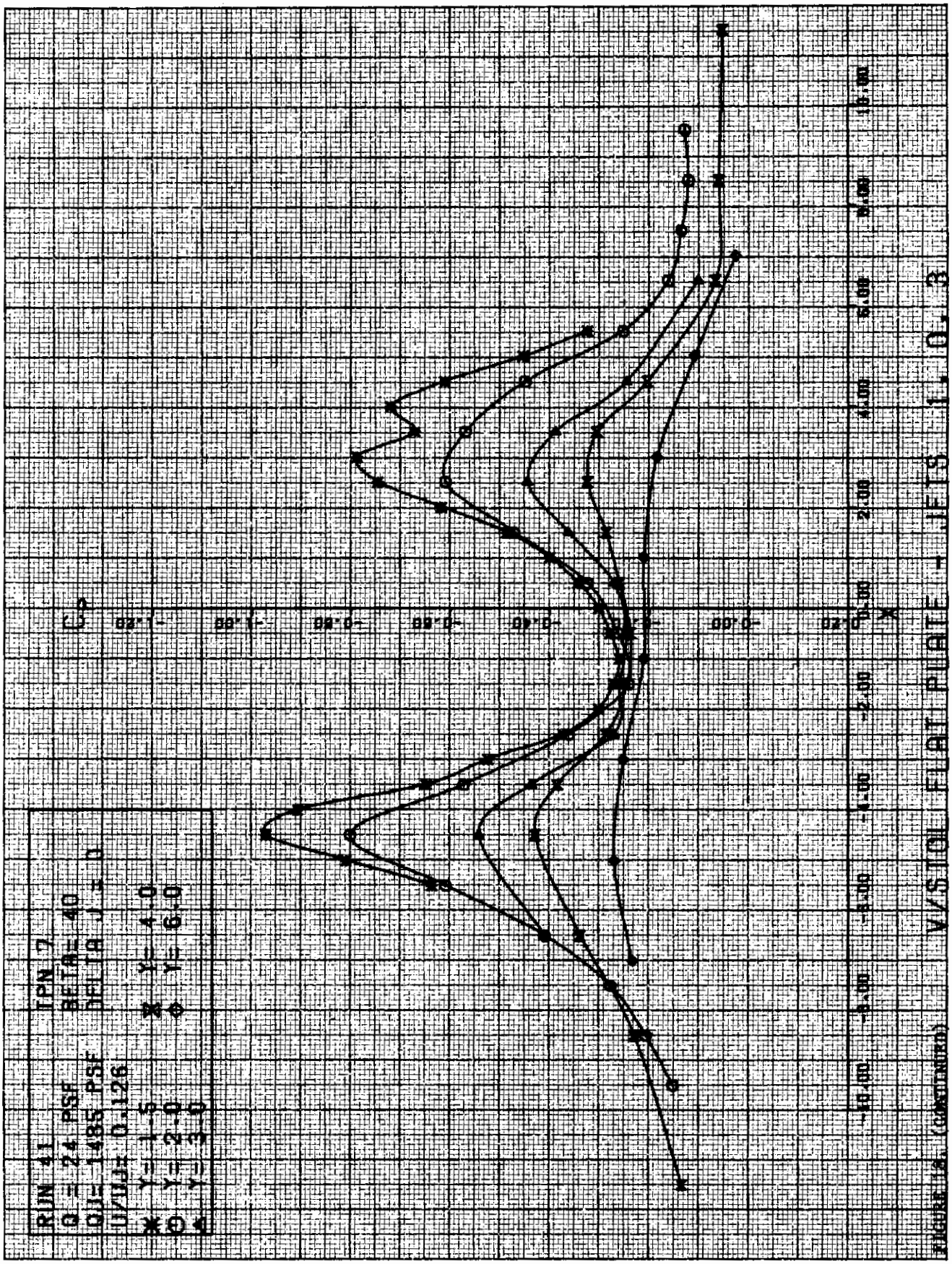

FIGURE 14. (CONTINUED)

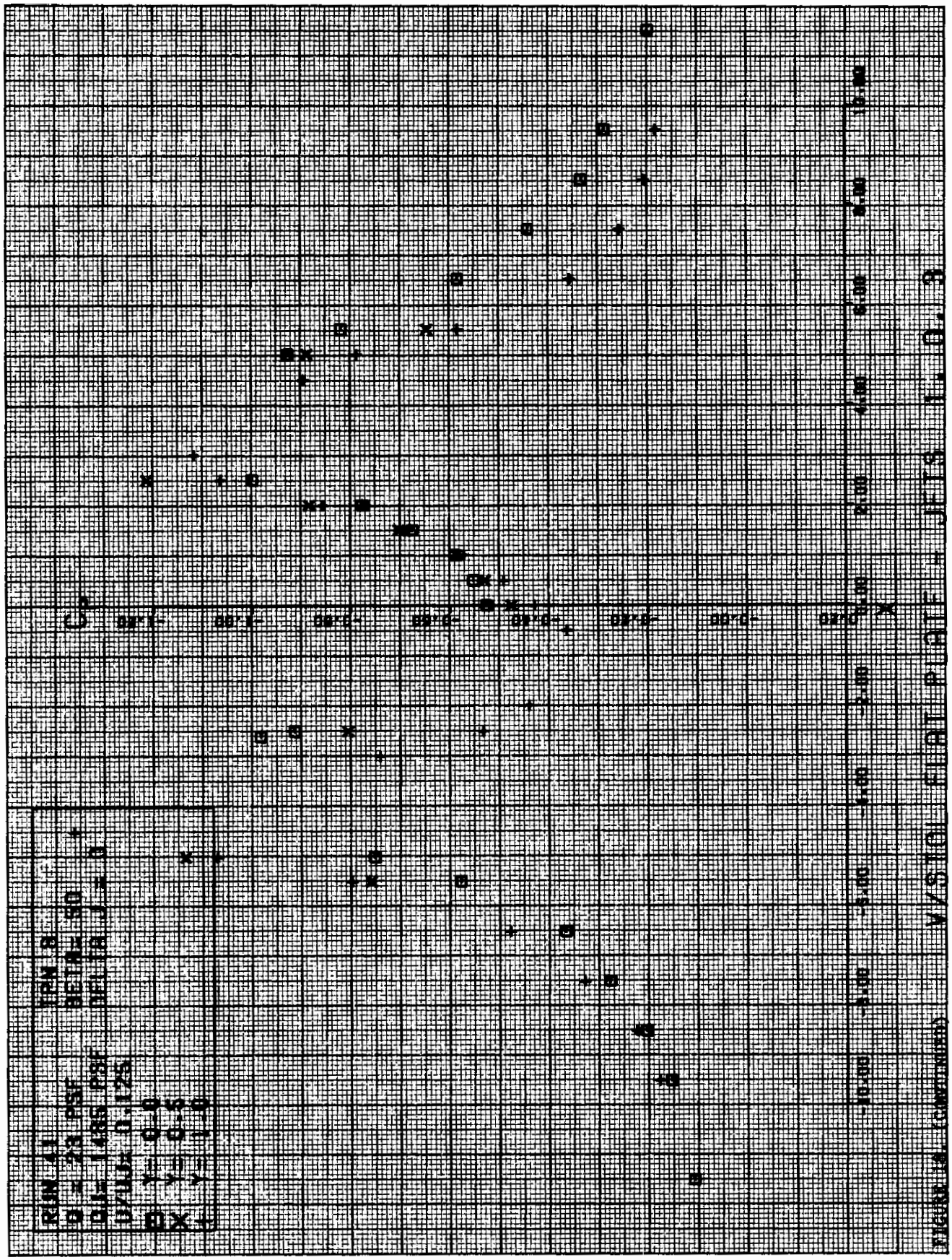

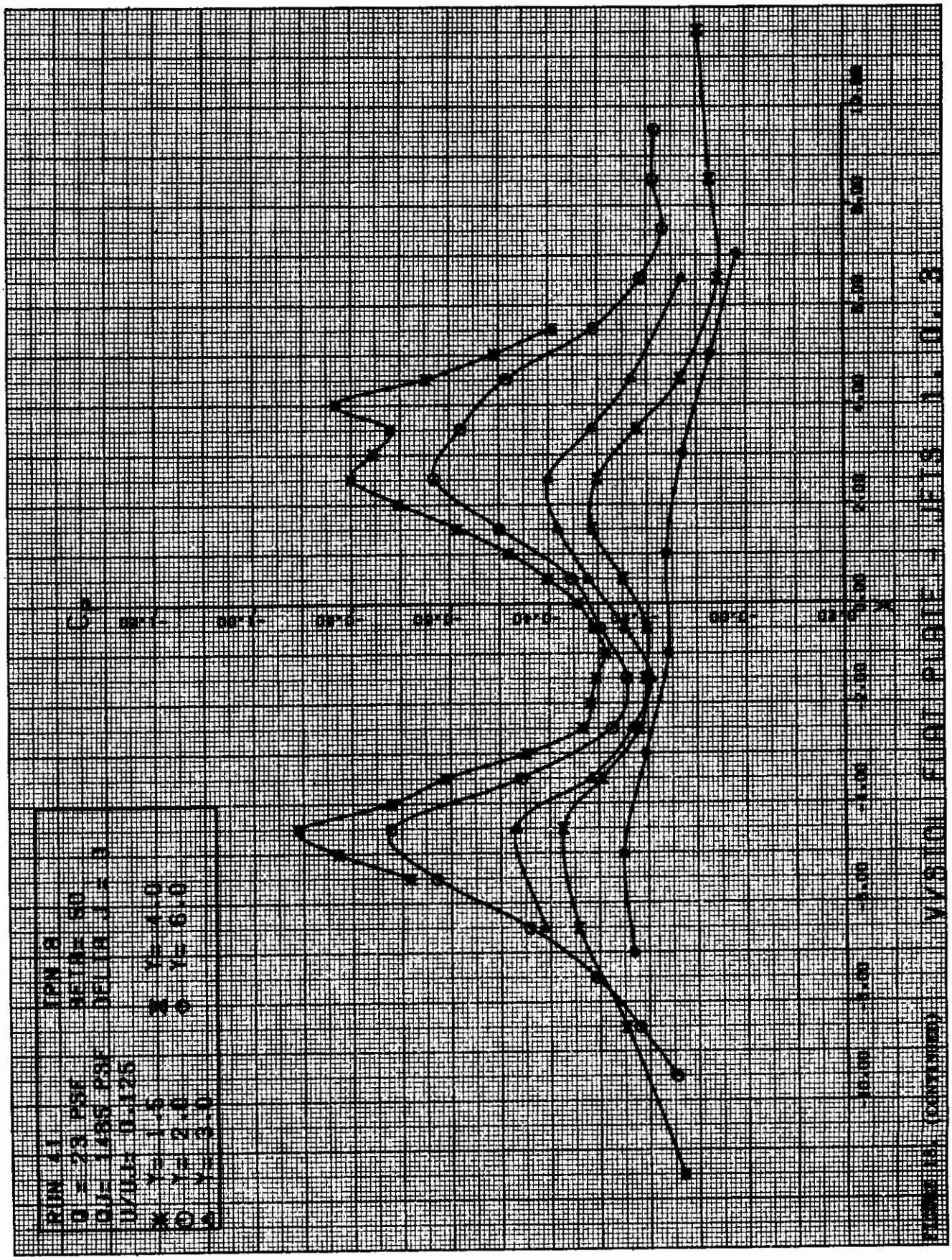

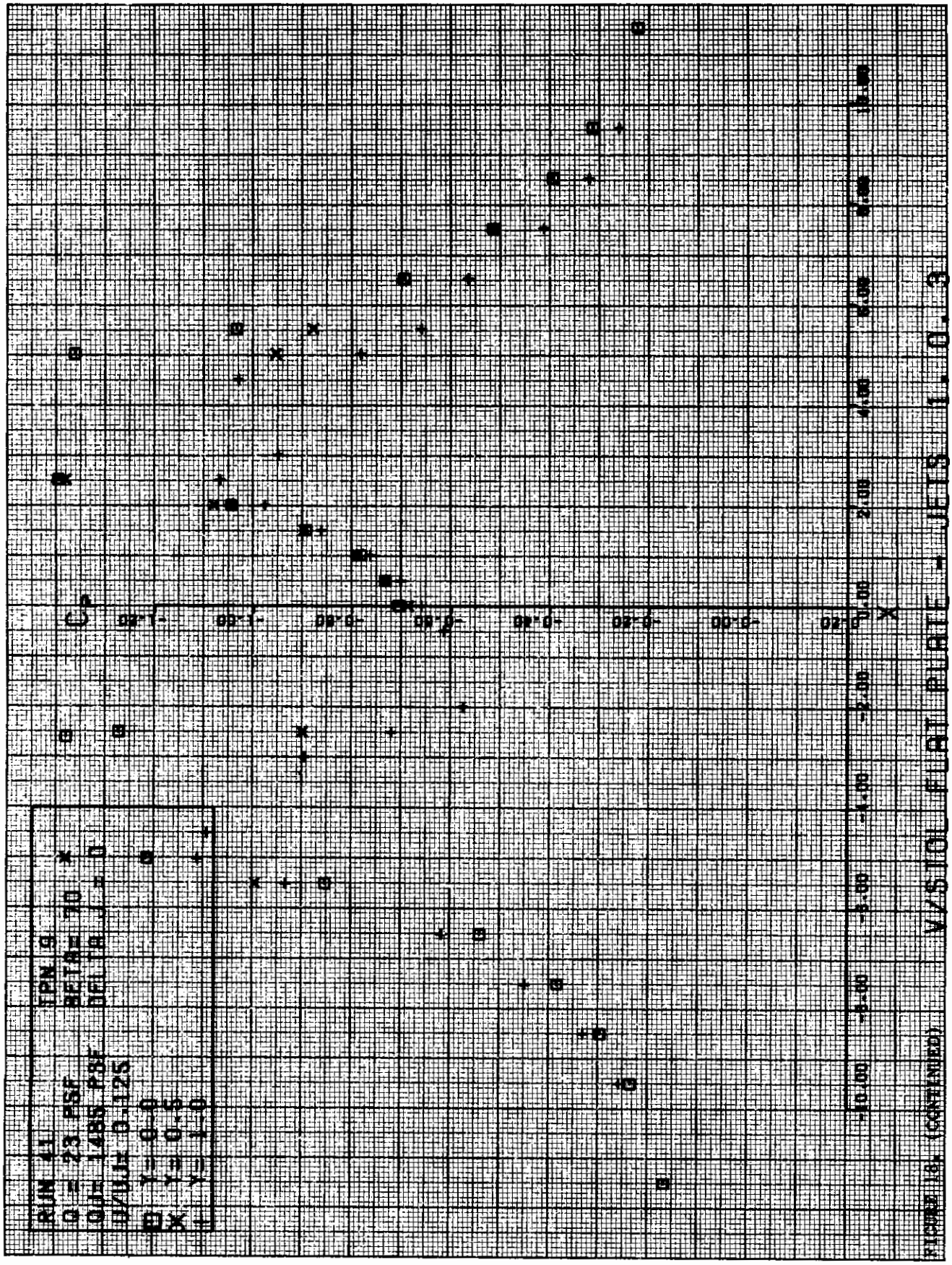

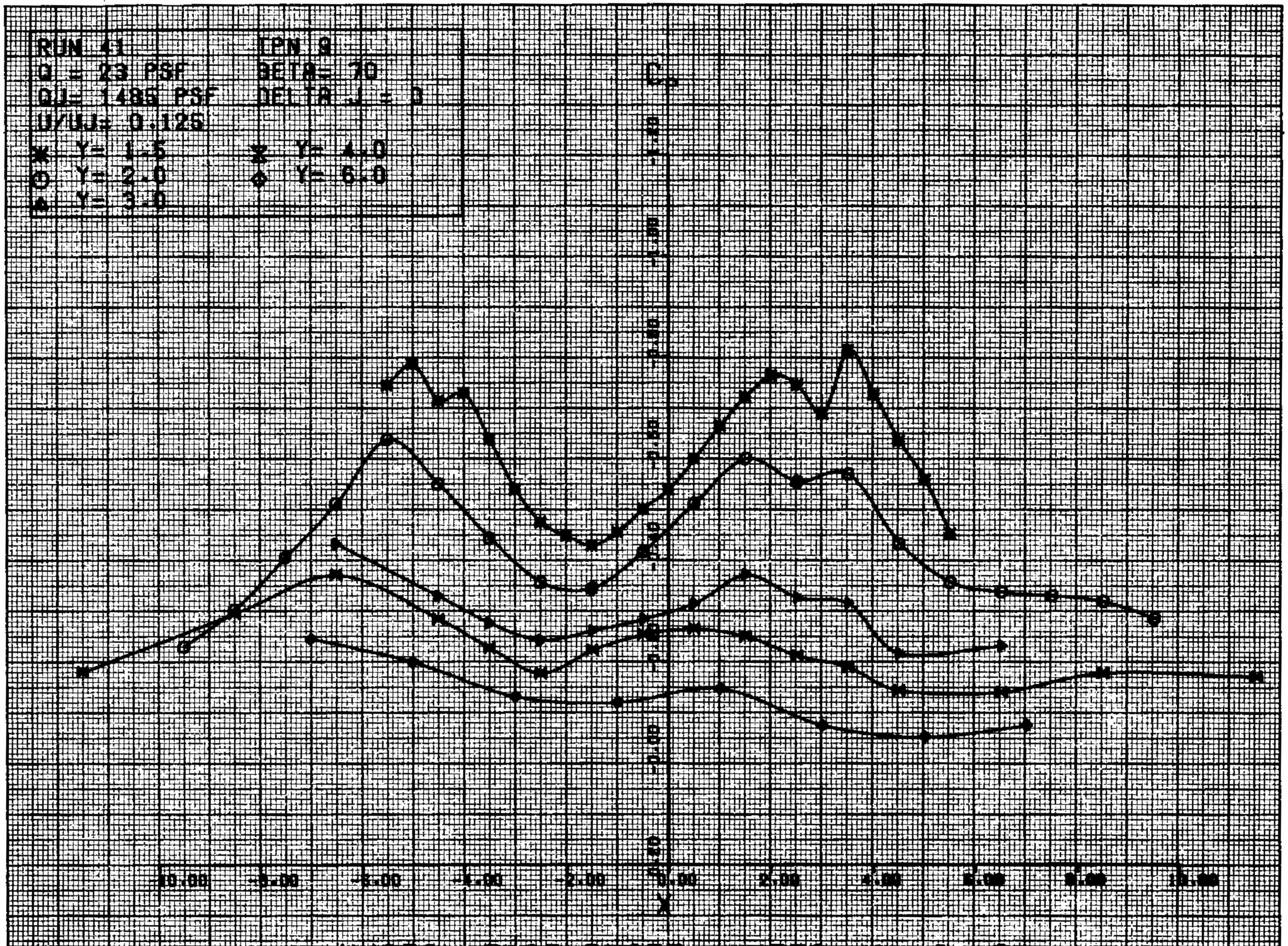

FIGURE 15. (CONTINUED) V/STOL FLAT PLATE - JETS 1, 0, 3

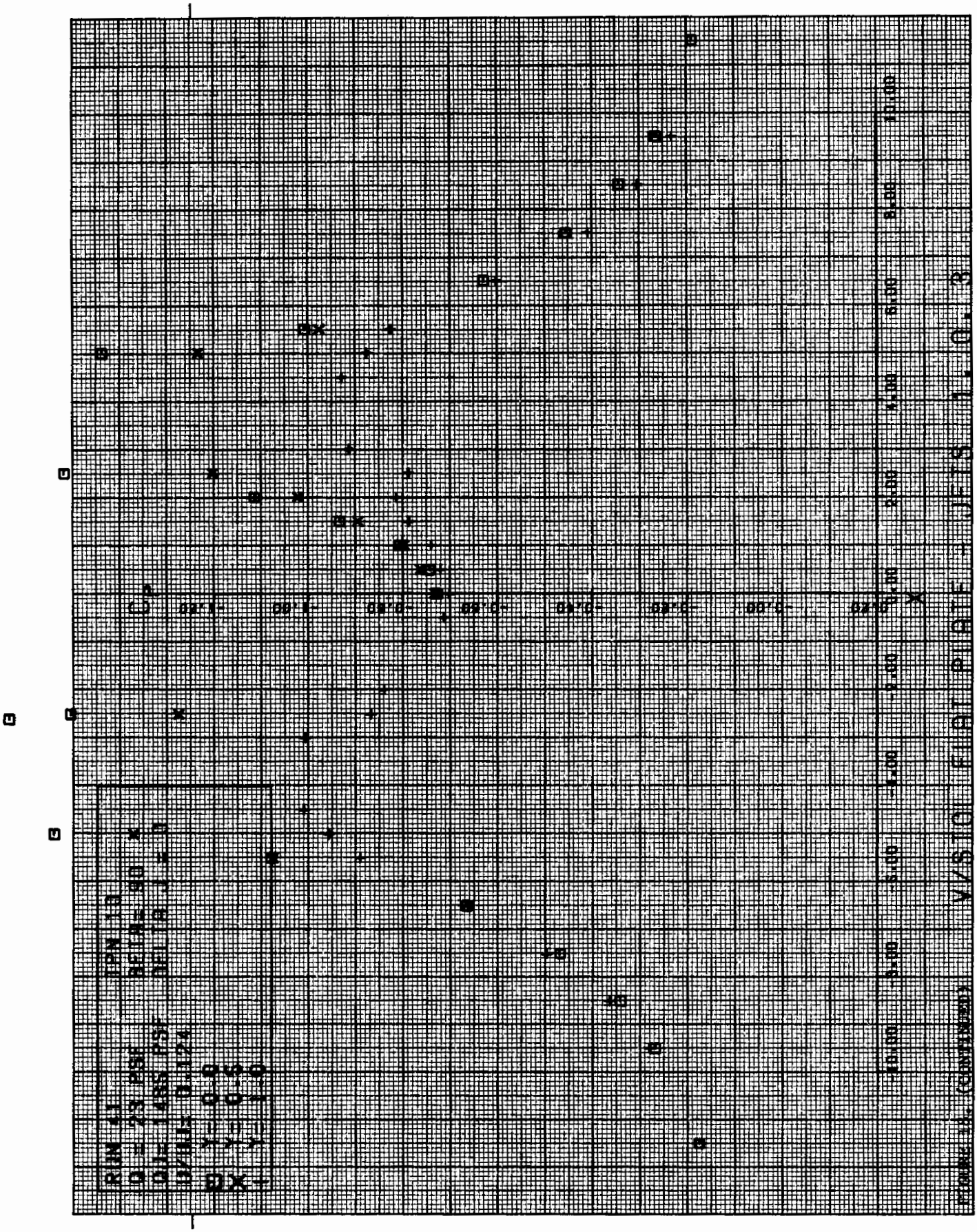

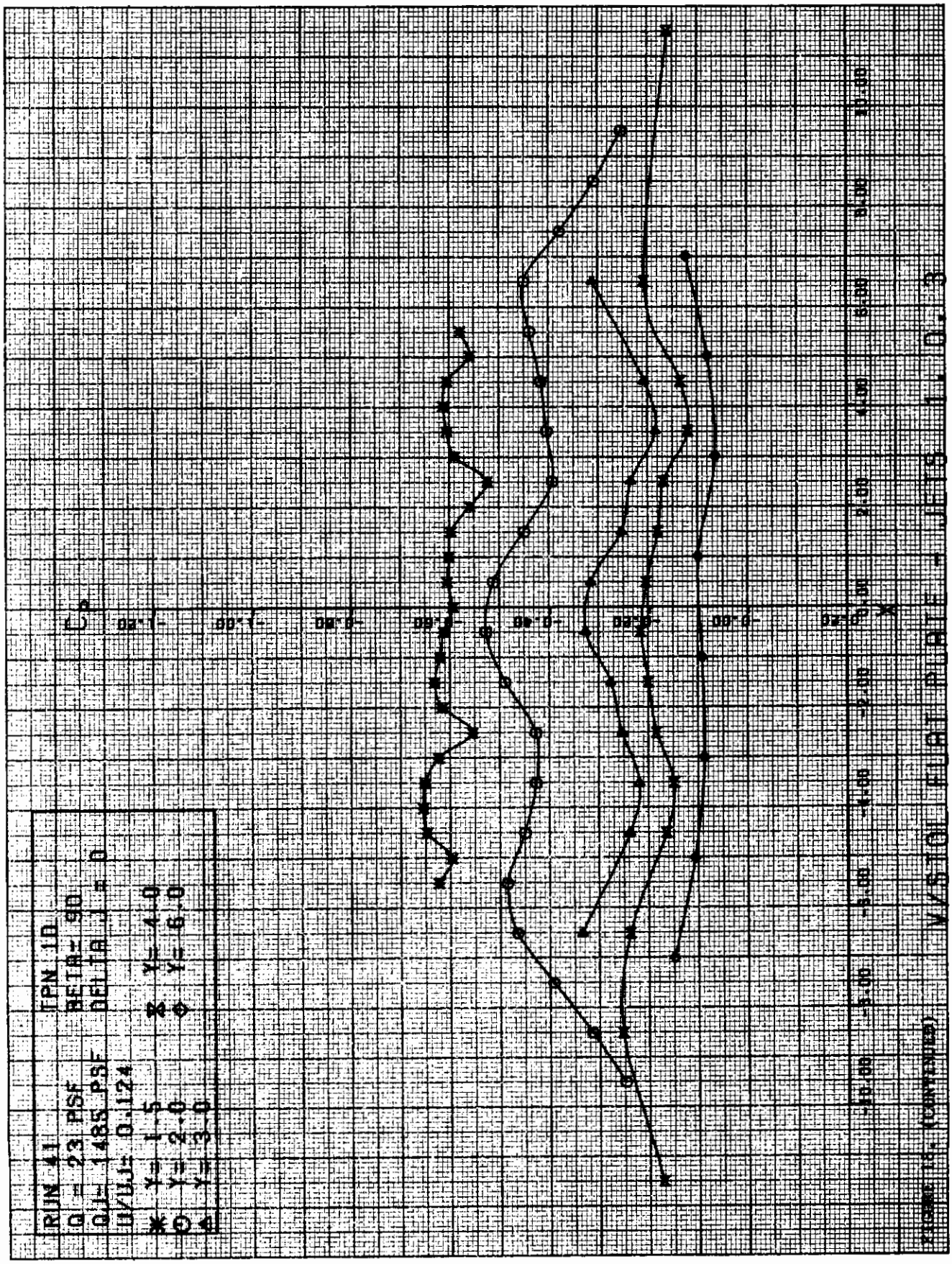

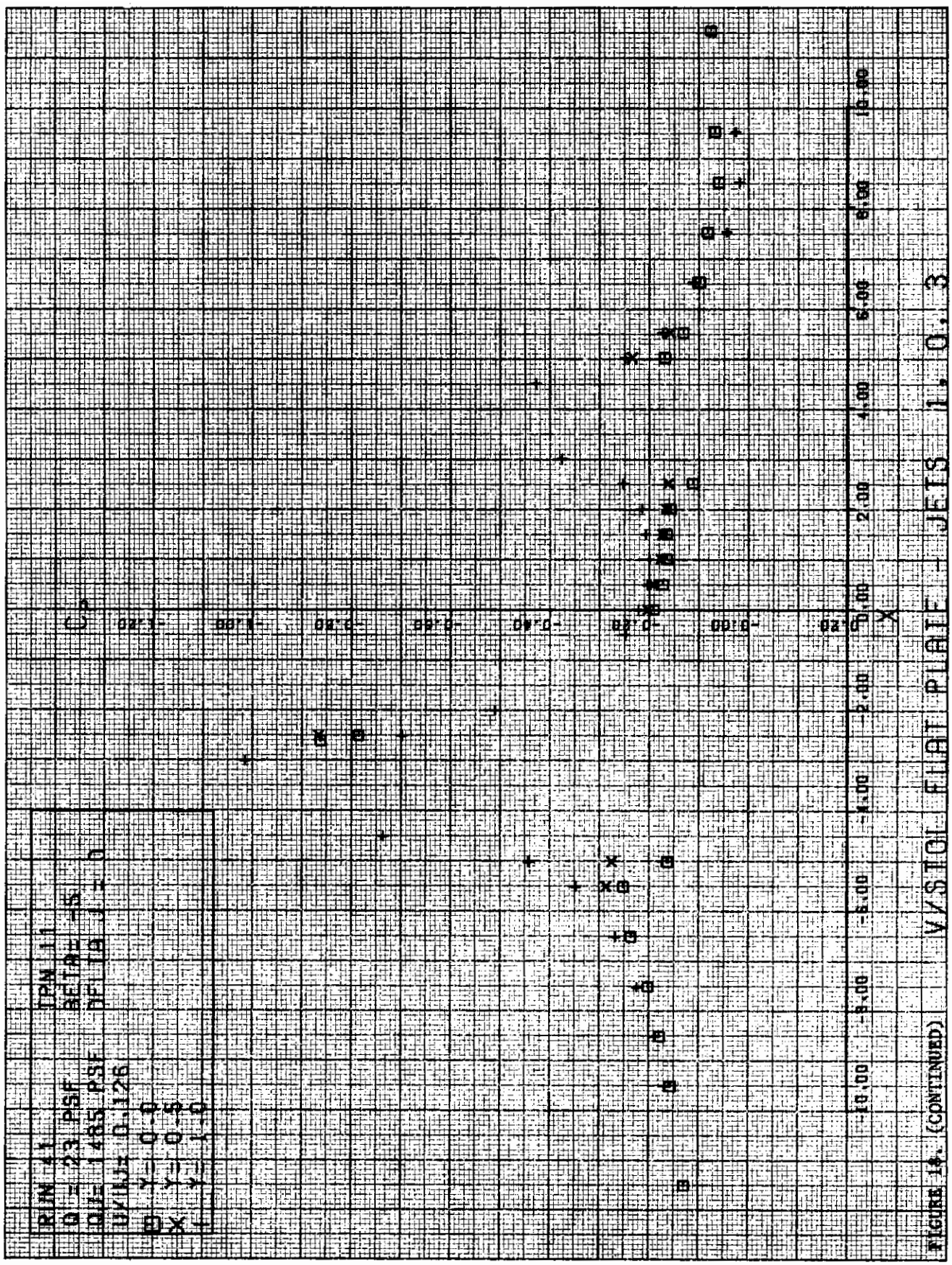

FIGURE 19. (CONTINUED)

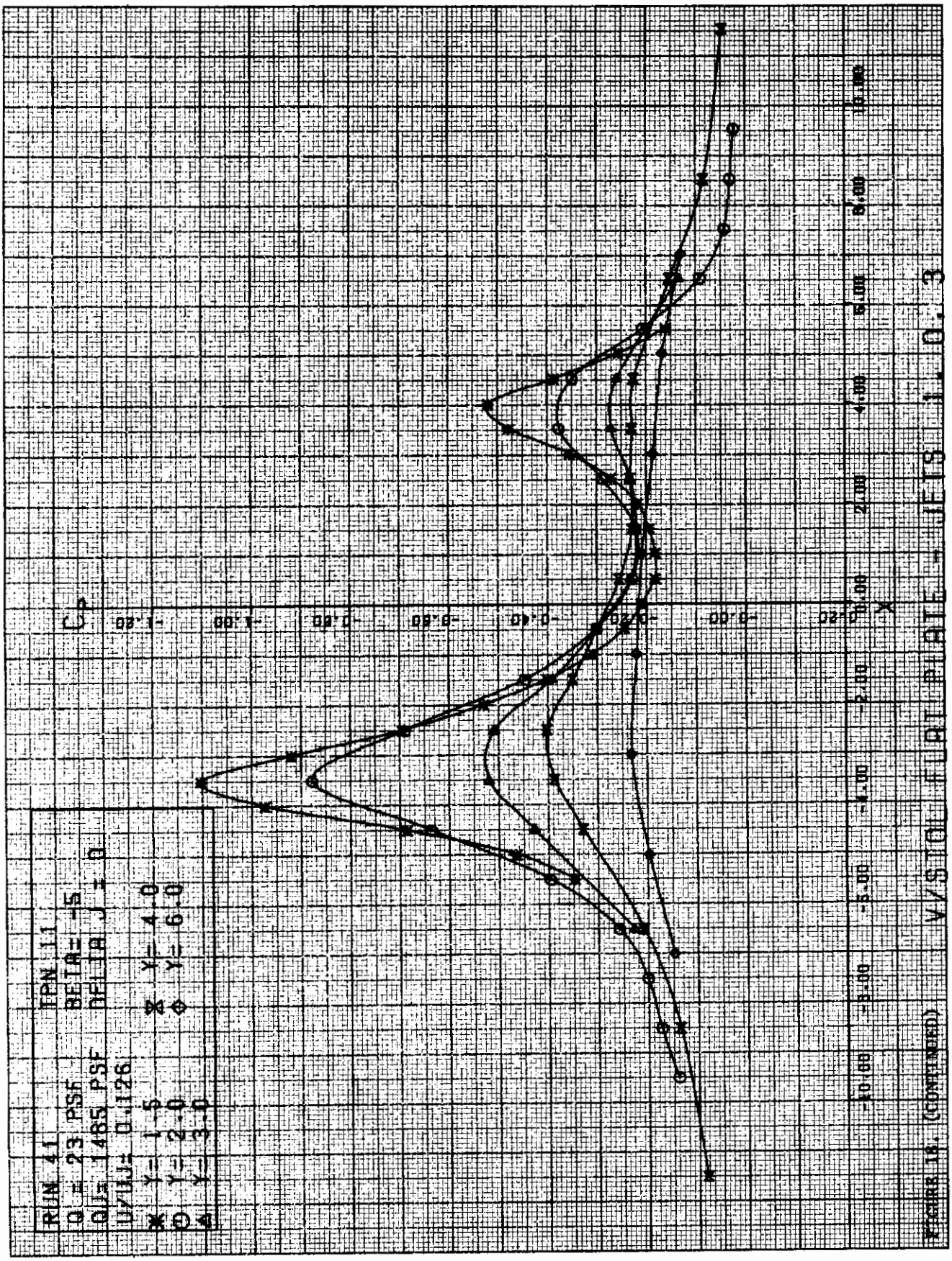

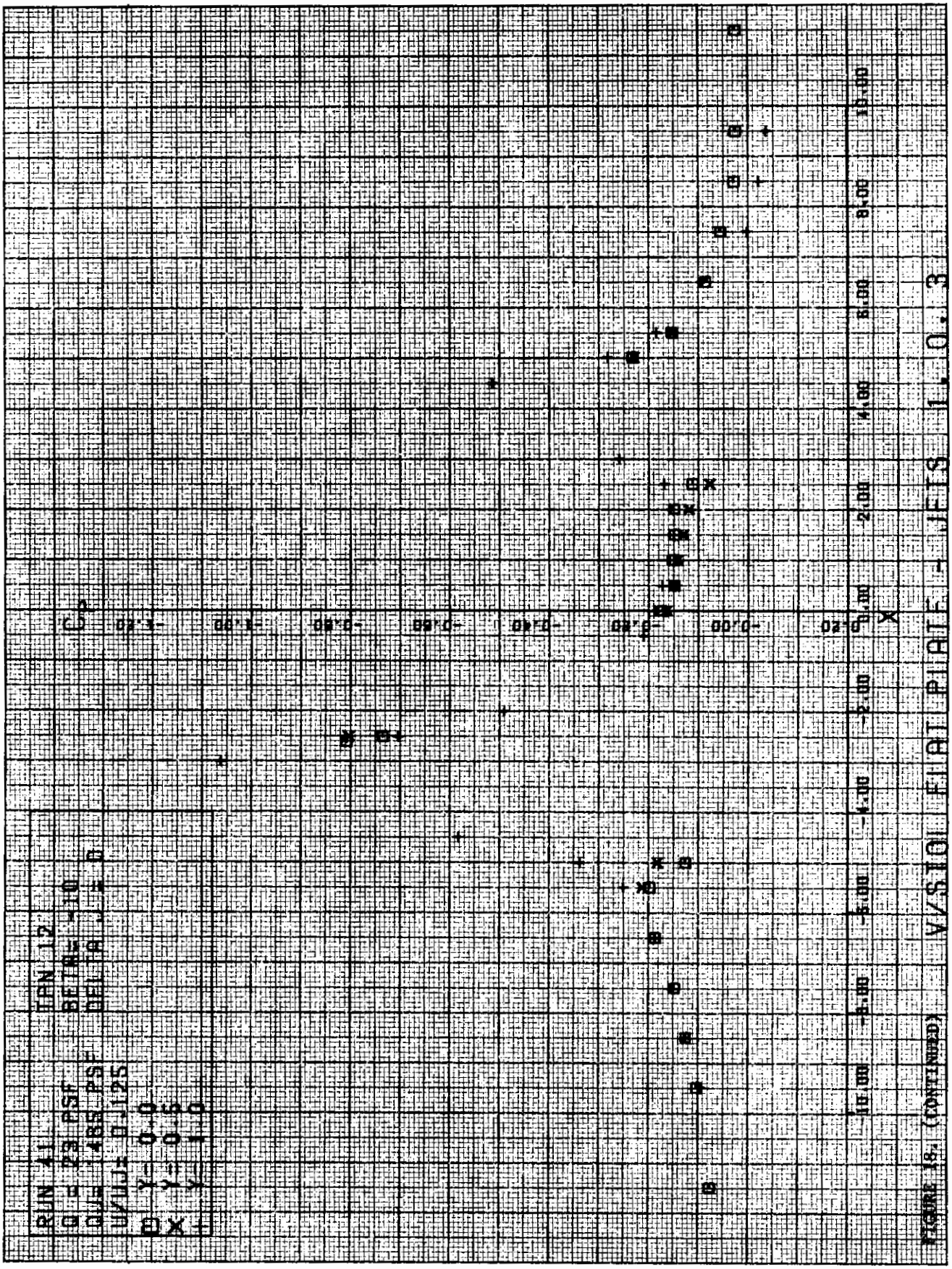

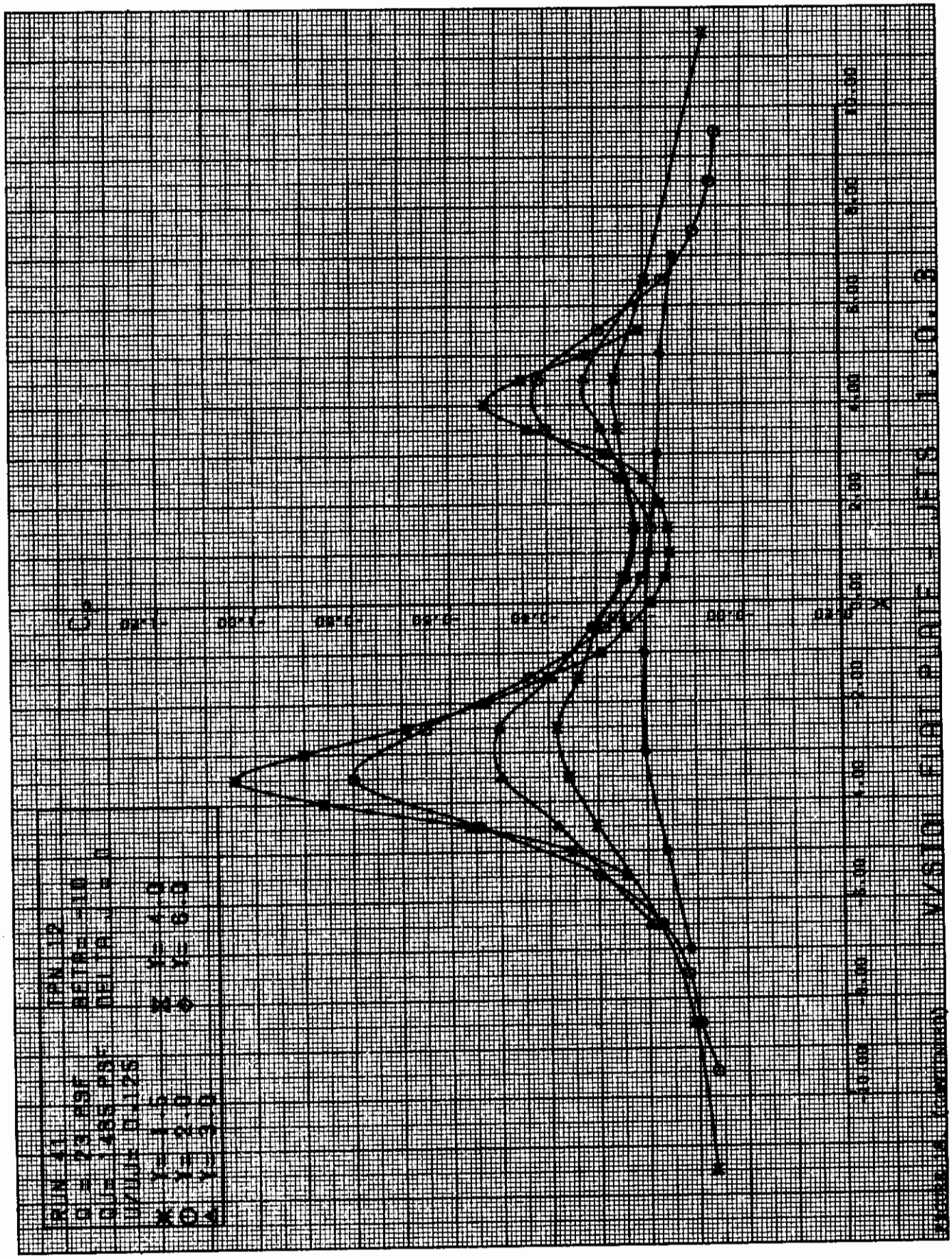

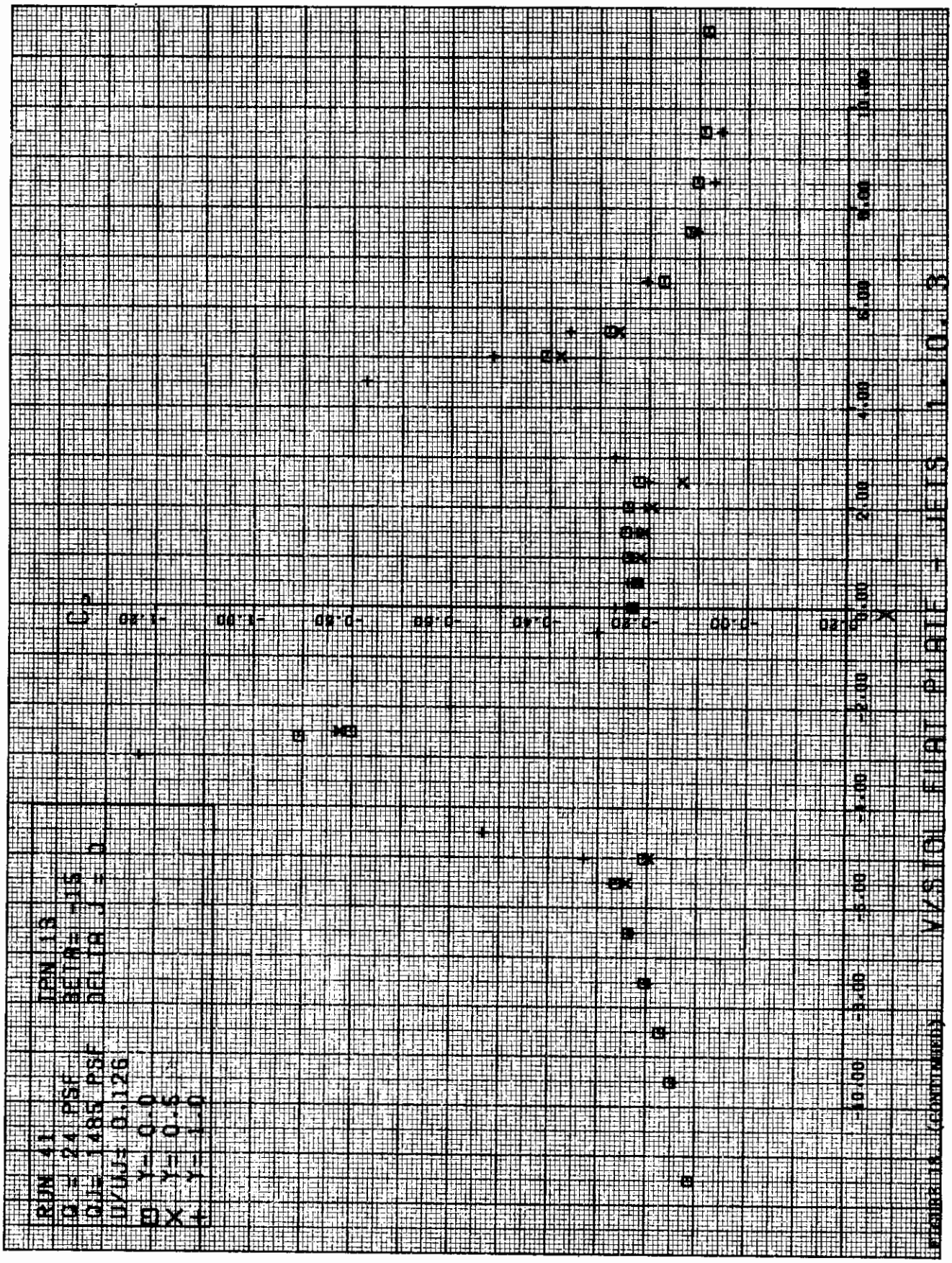

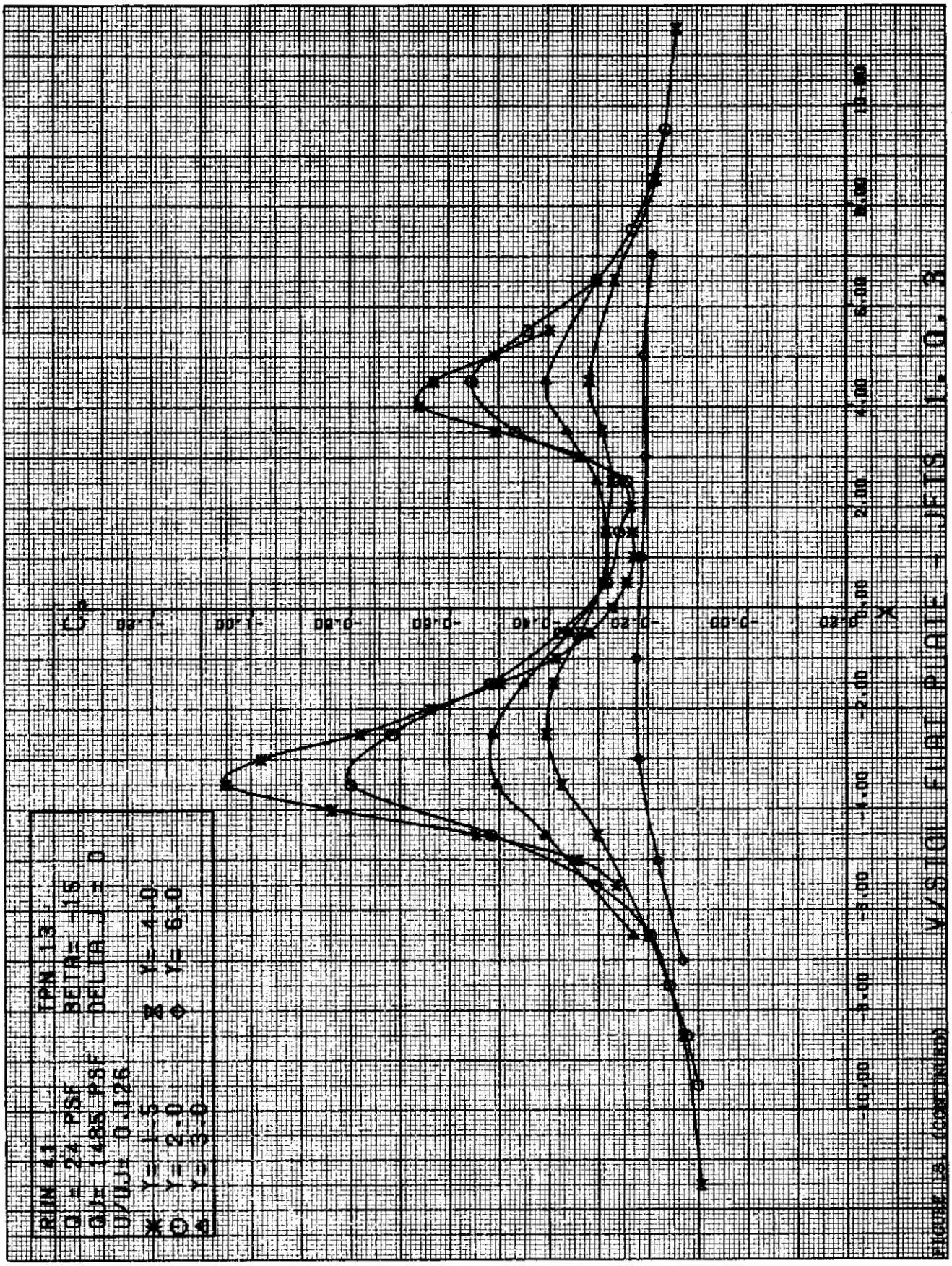

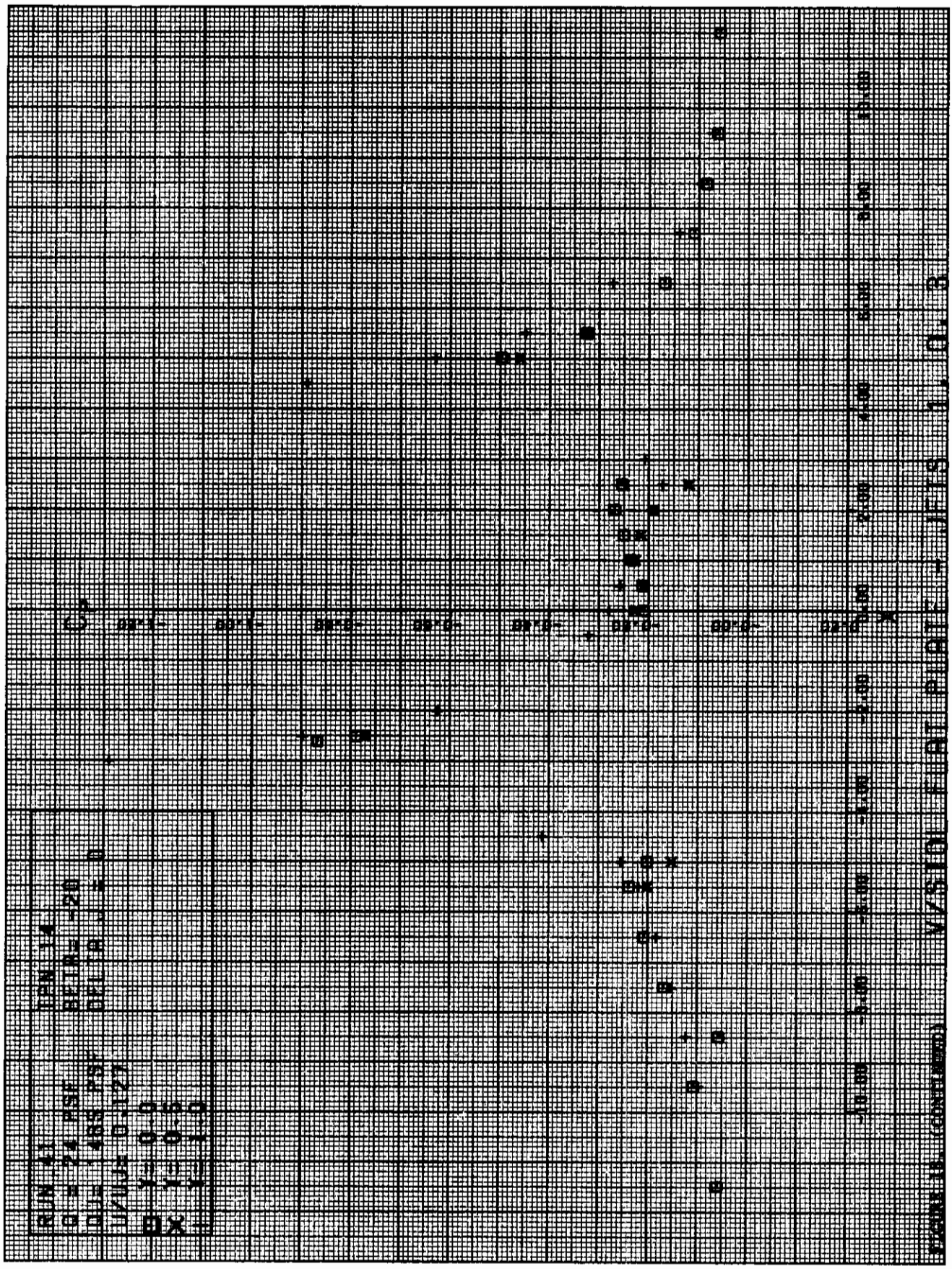

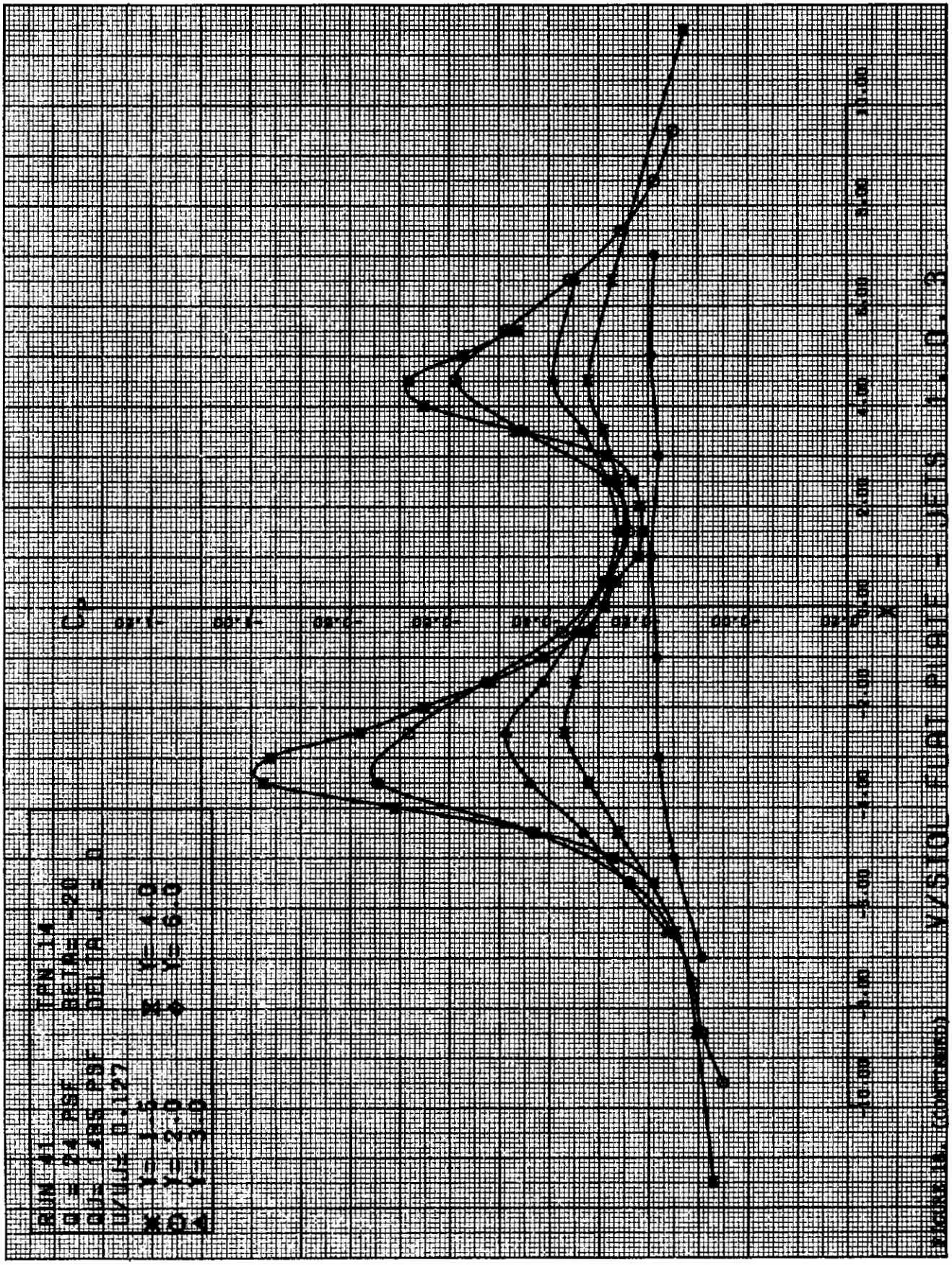

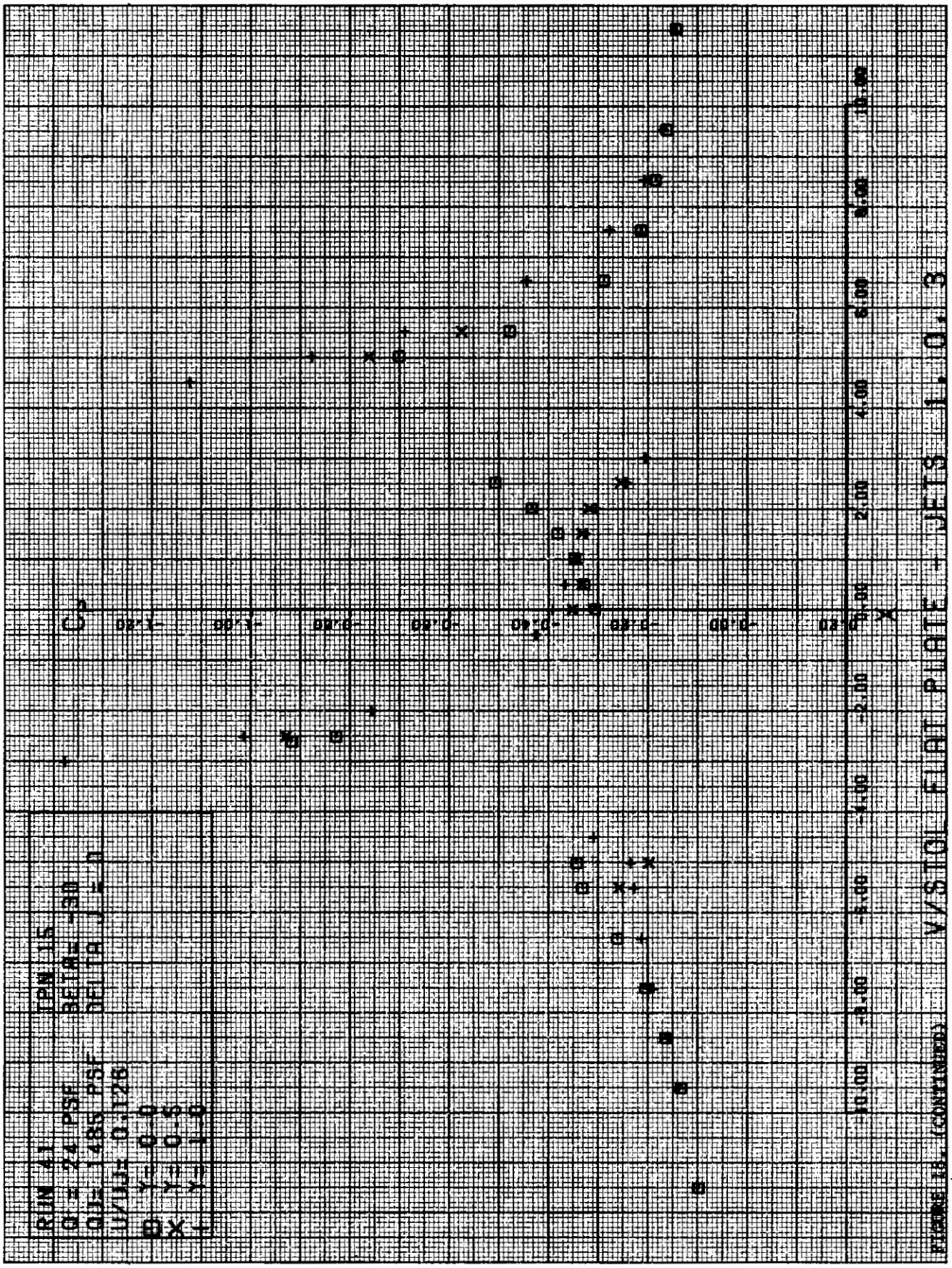

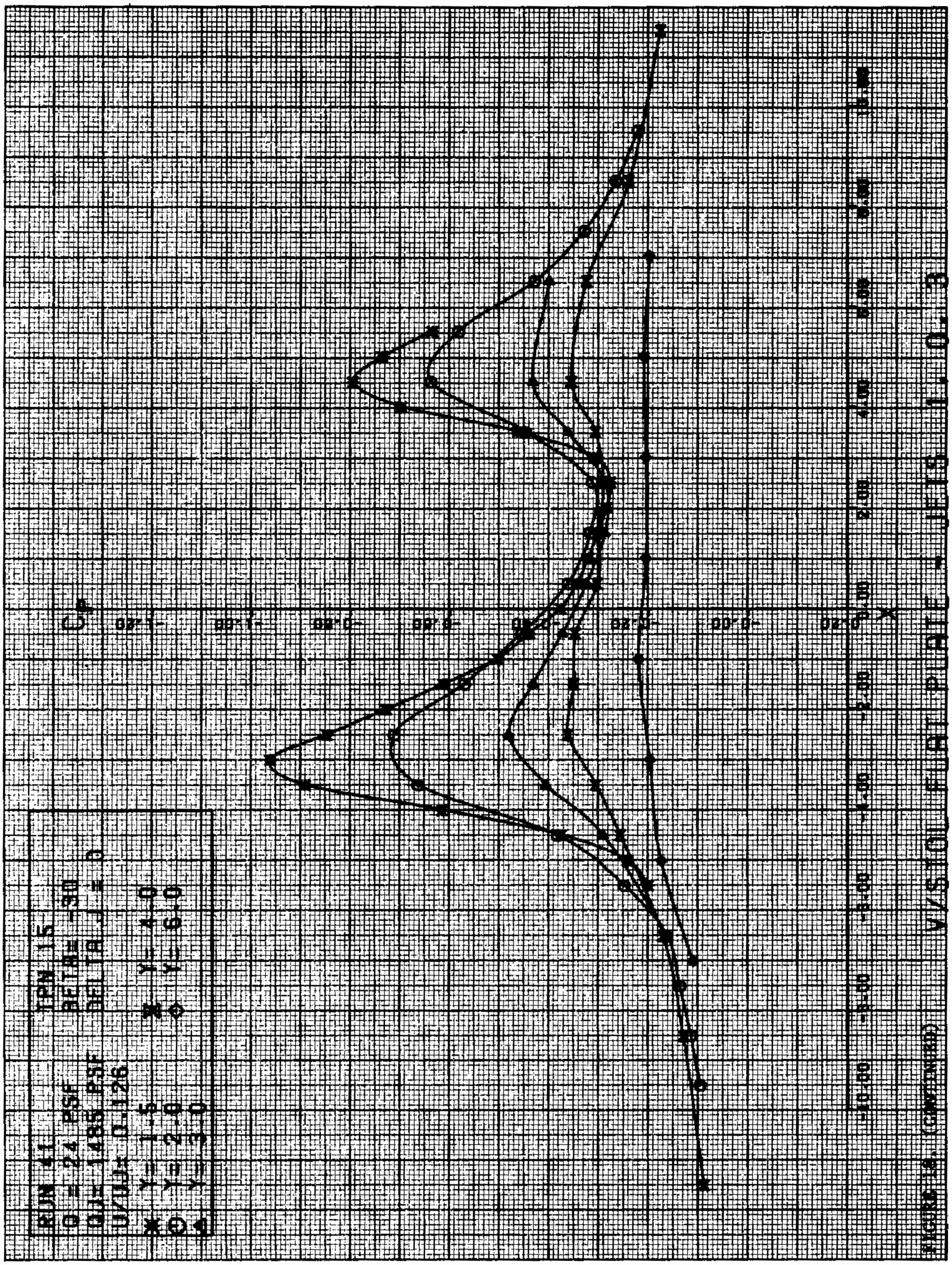

FIGURE 18. (CONTINUED) V/STOL FLAT PLATE - JETS 1, 0, 3

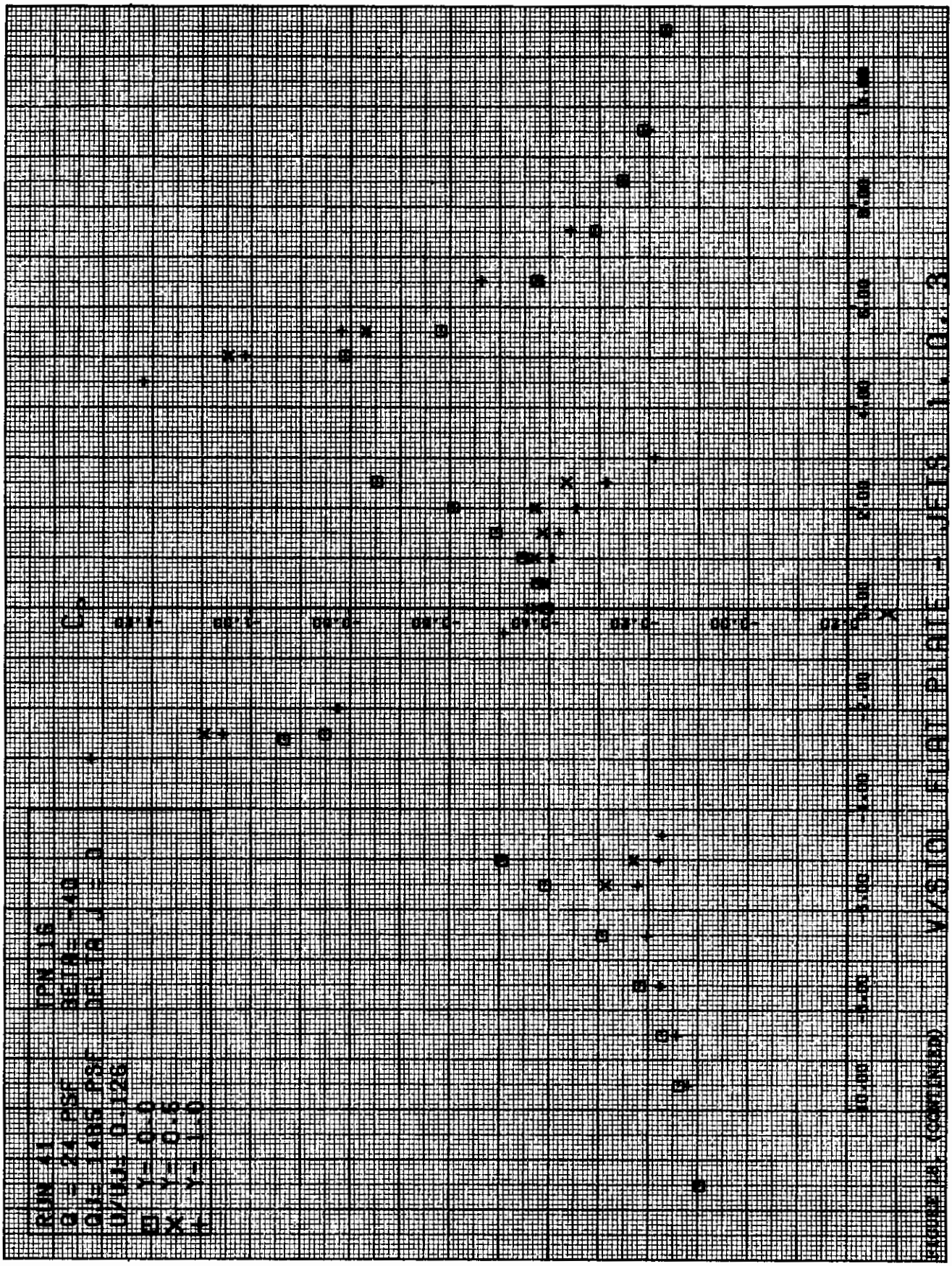

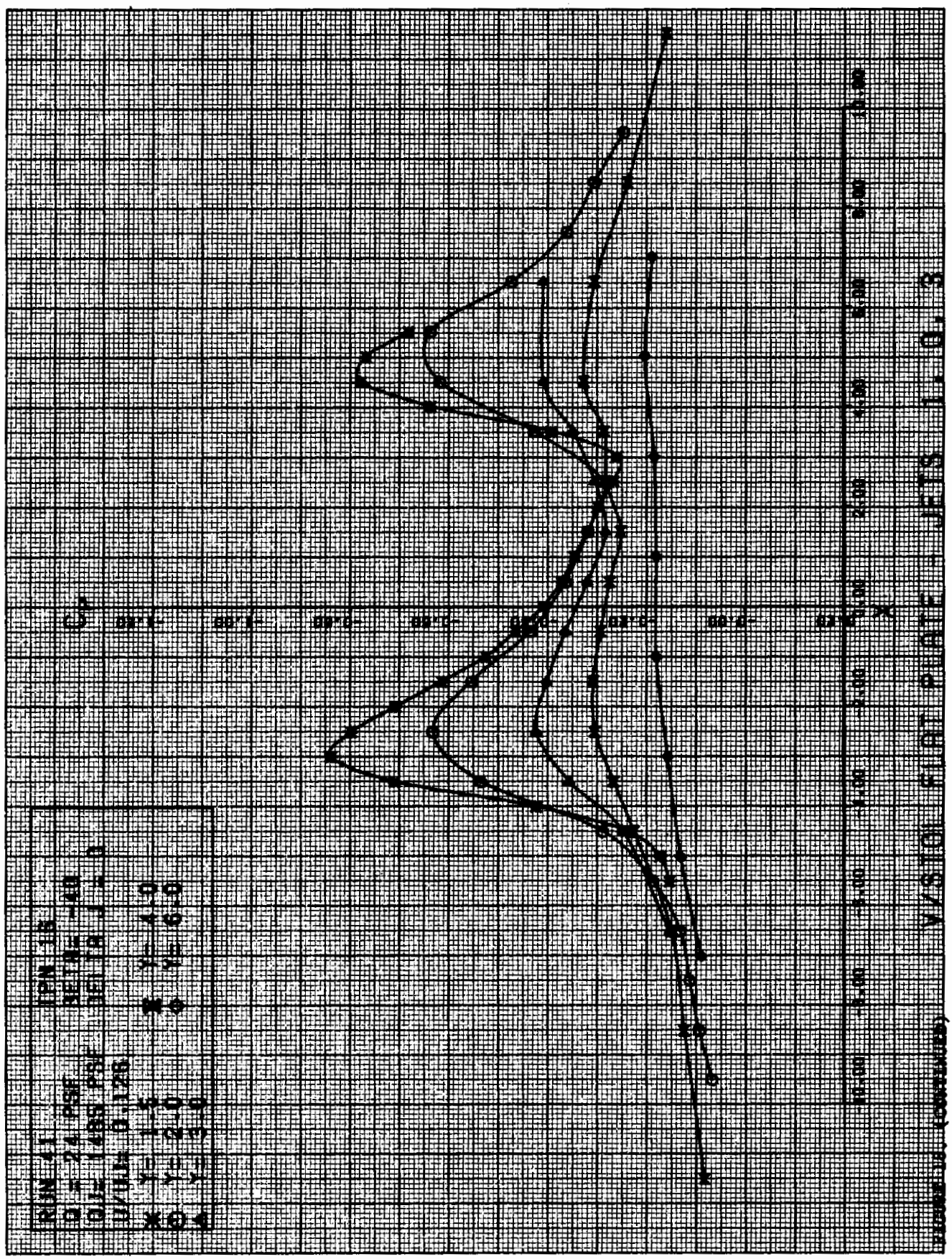

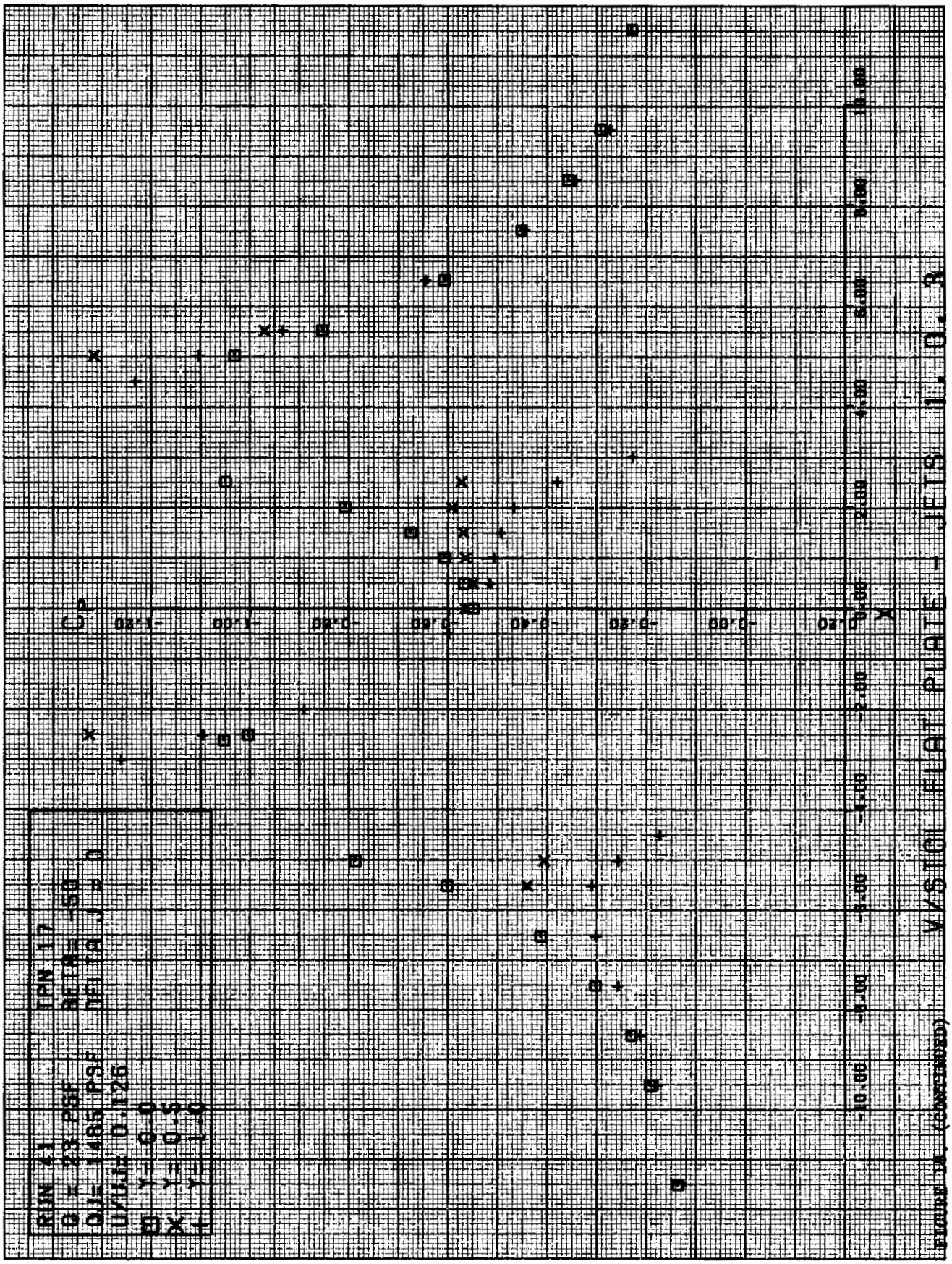

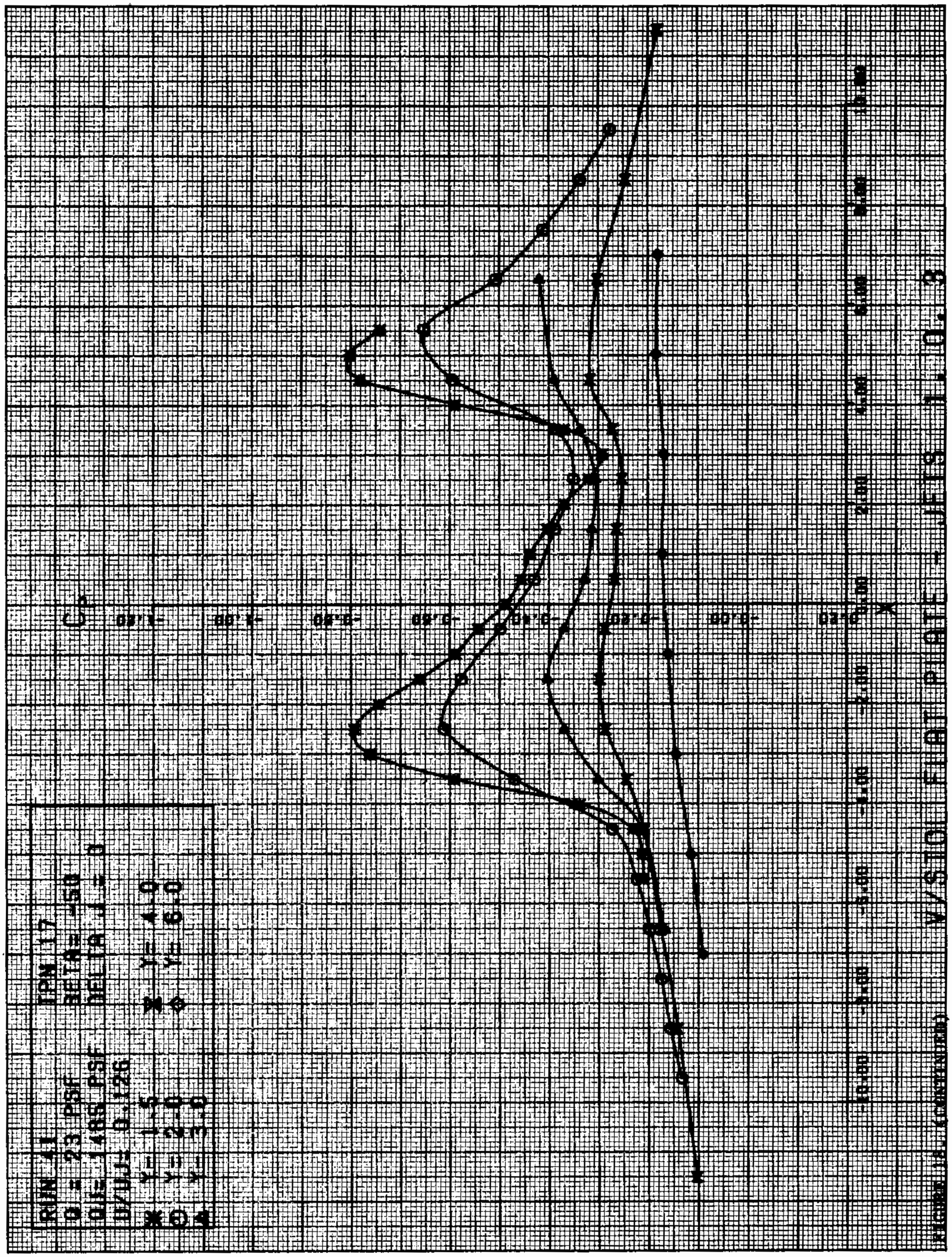

FIGURE 14. (CONTINUED)

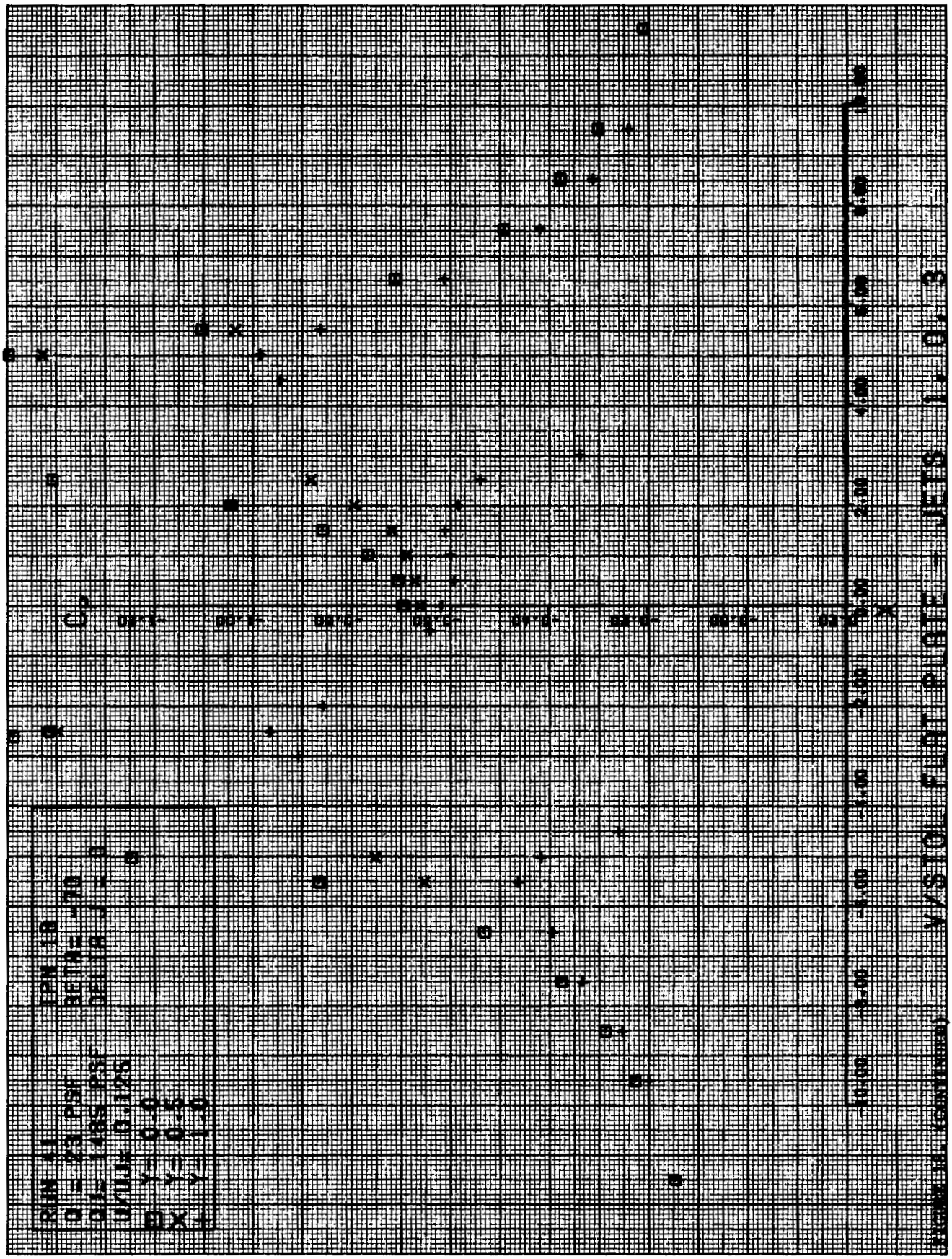

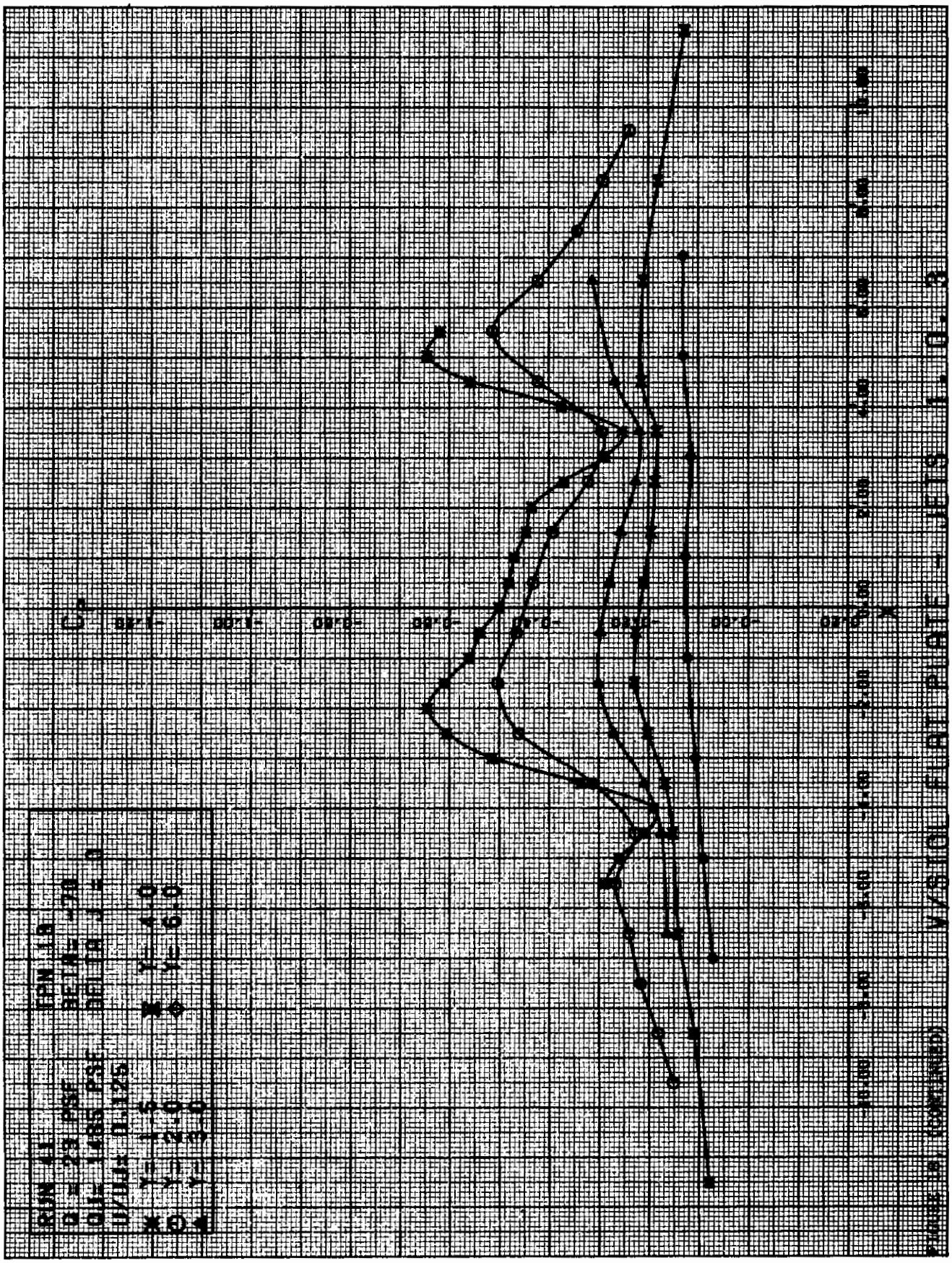

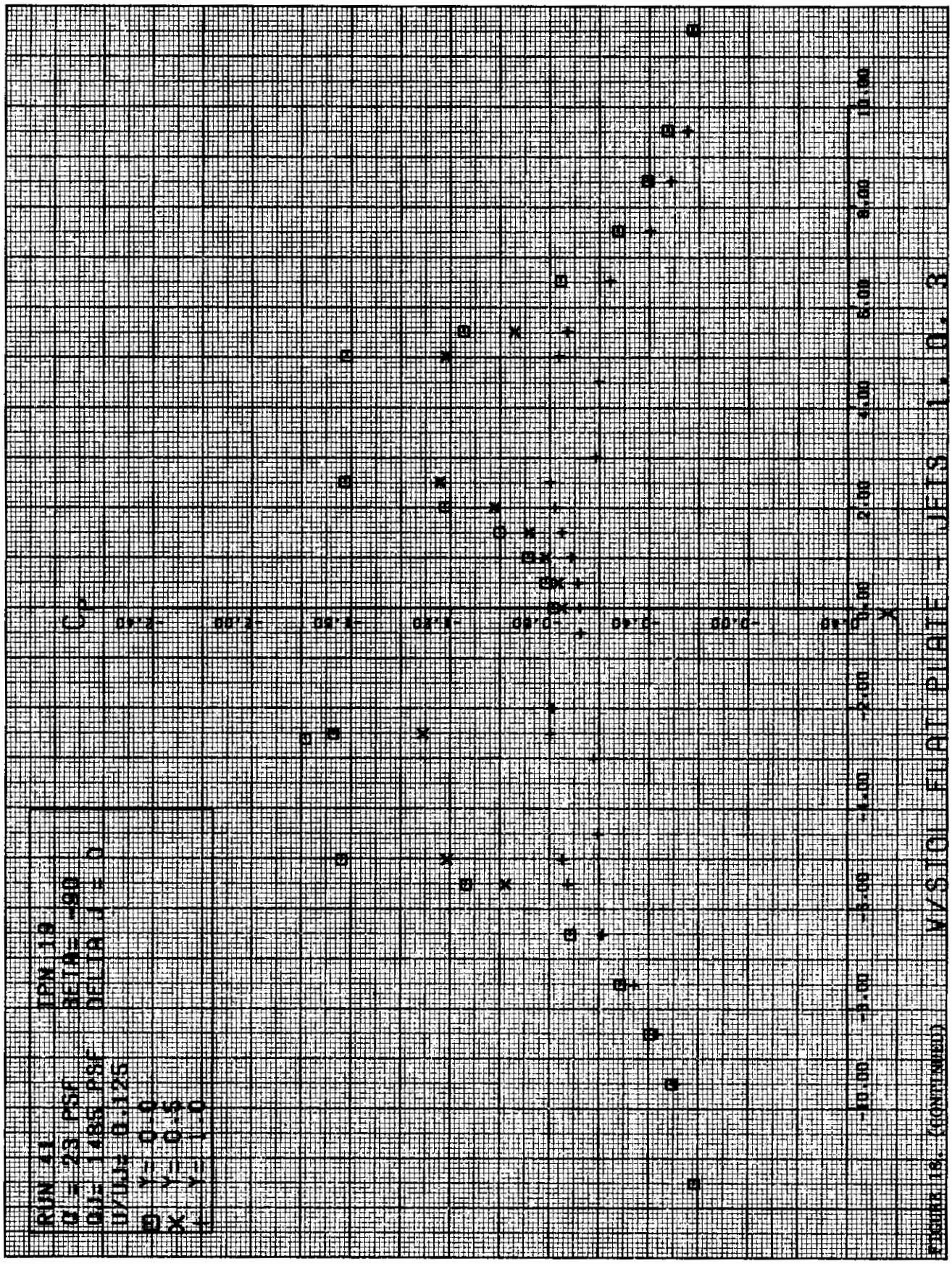

FIGURE 18. (CONTINUED)

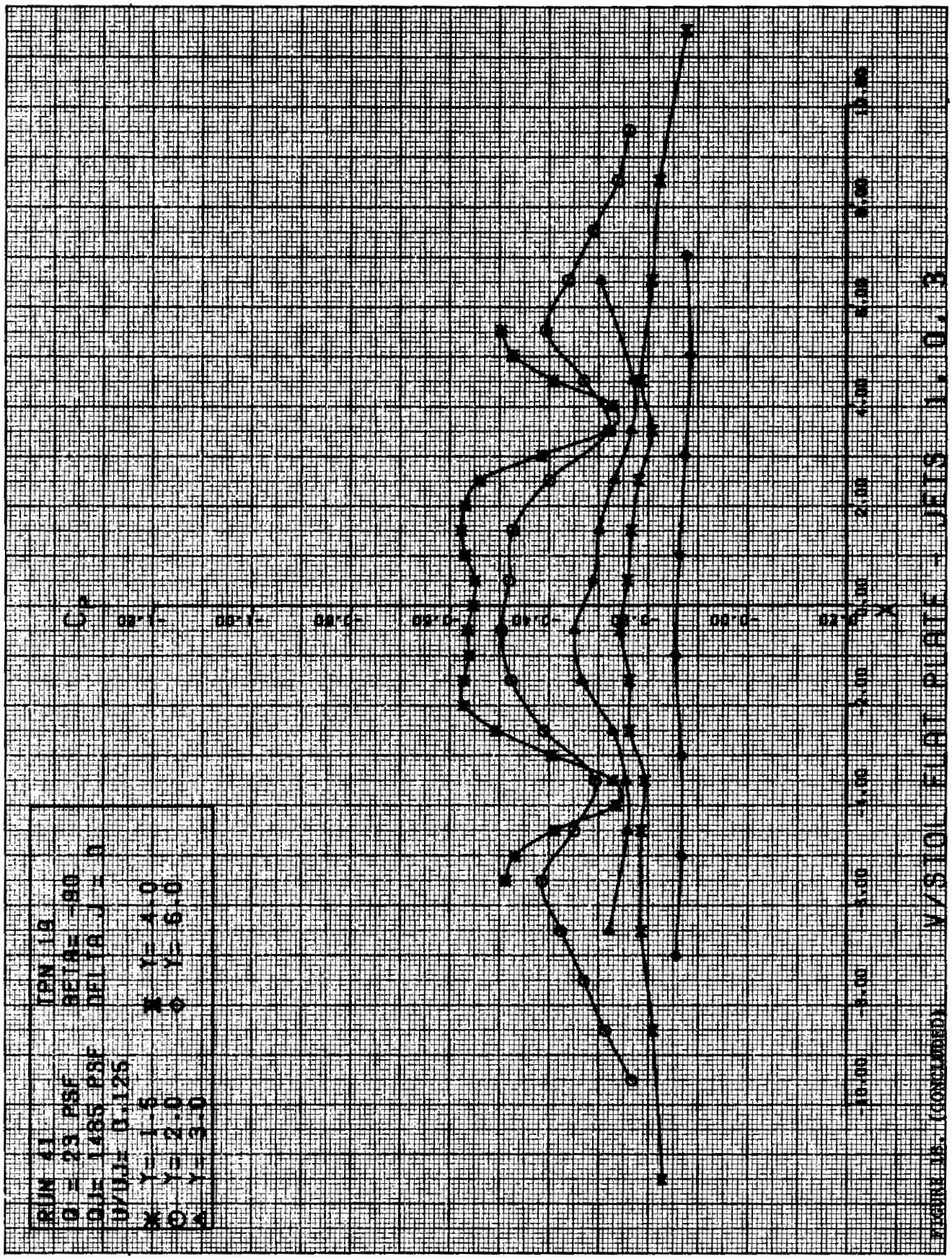

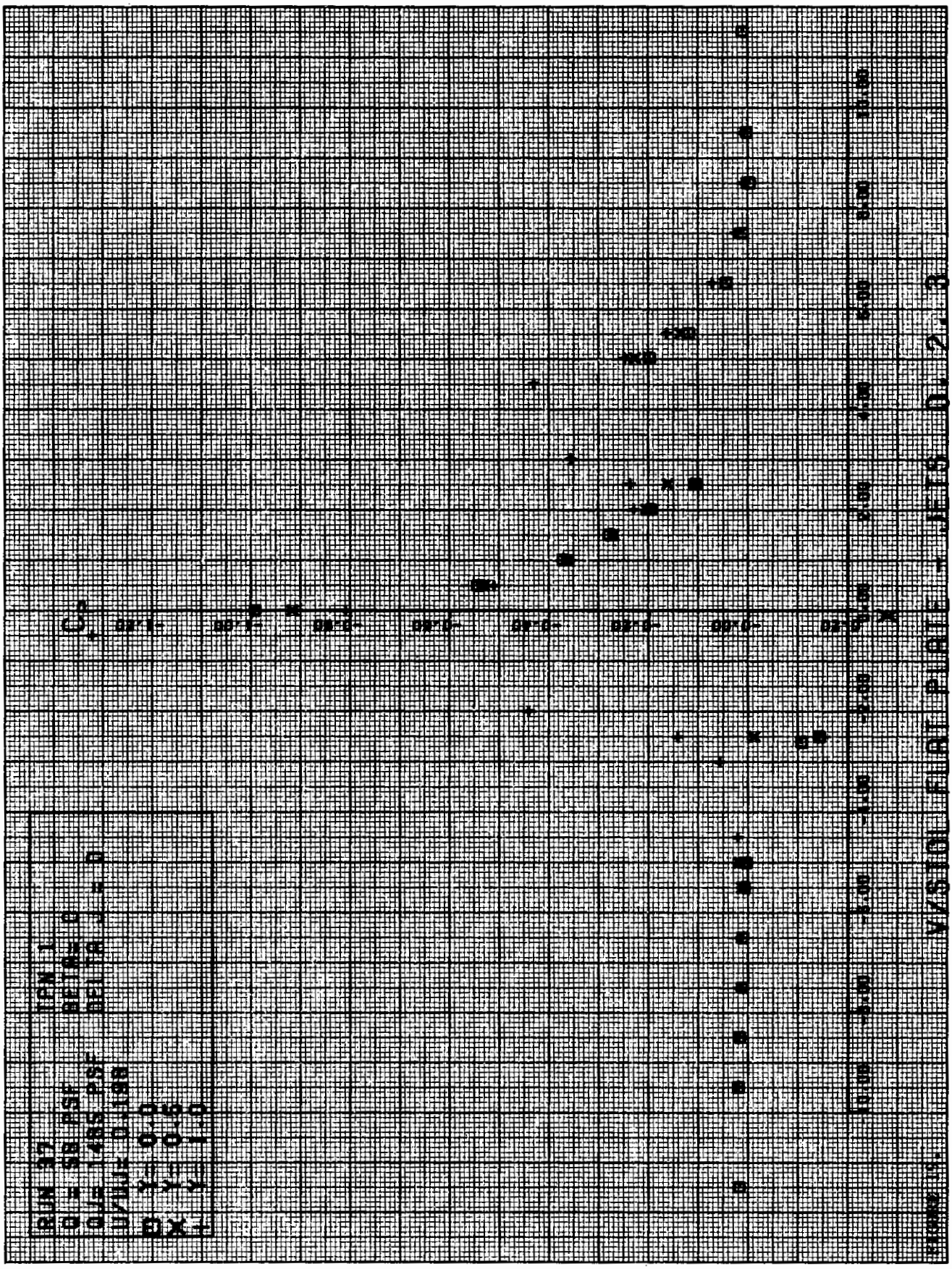

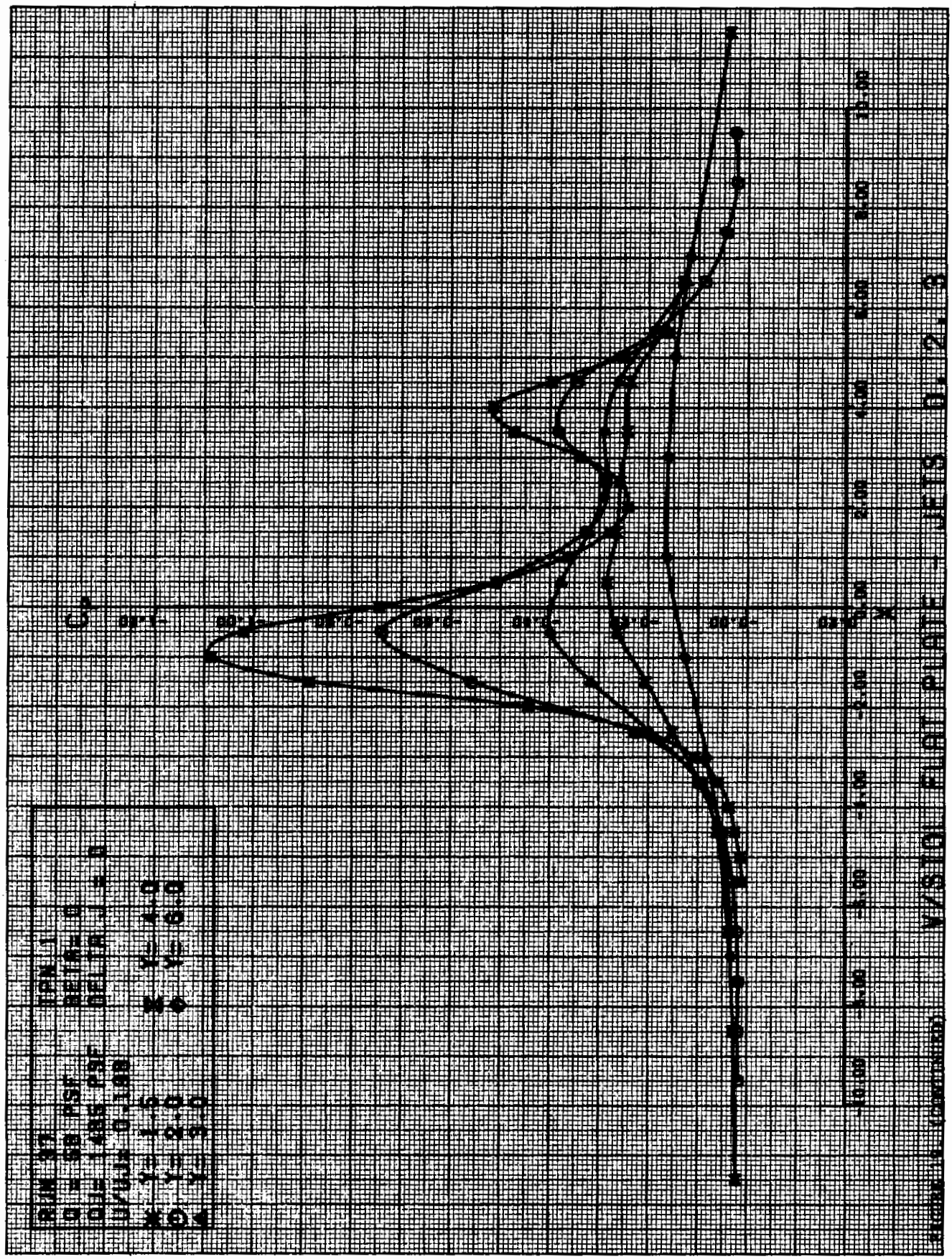

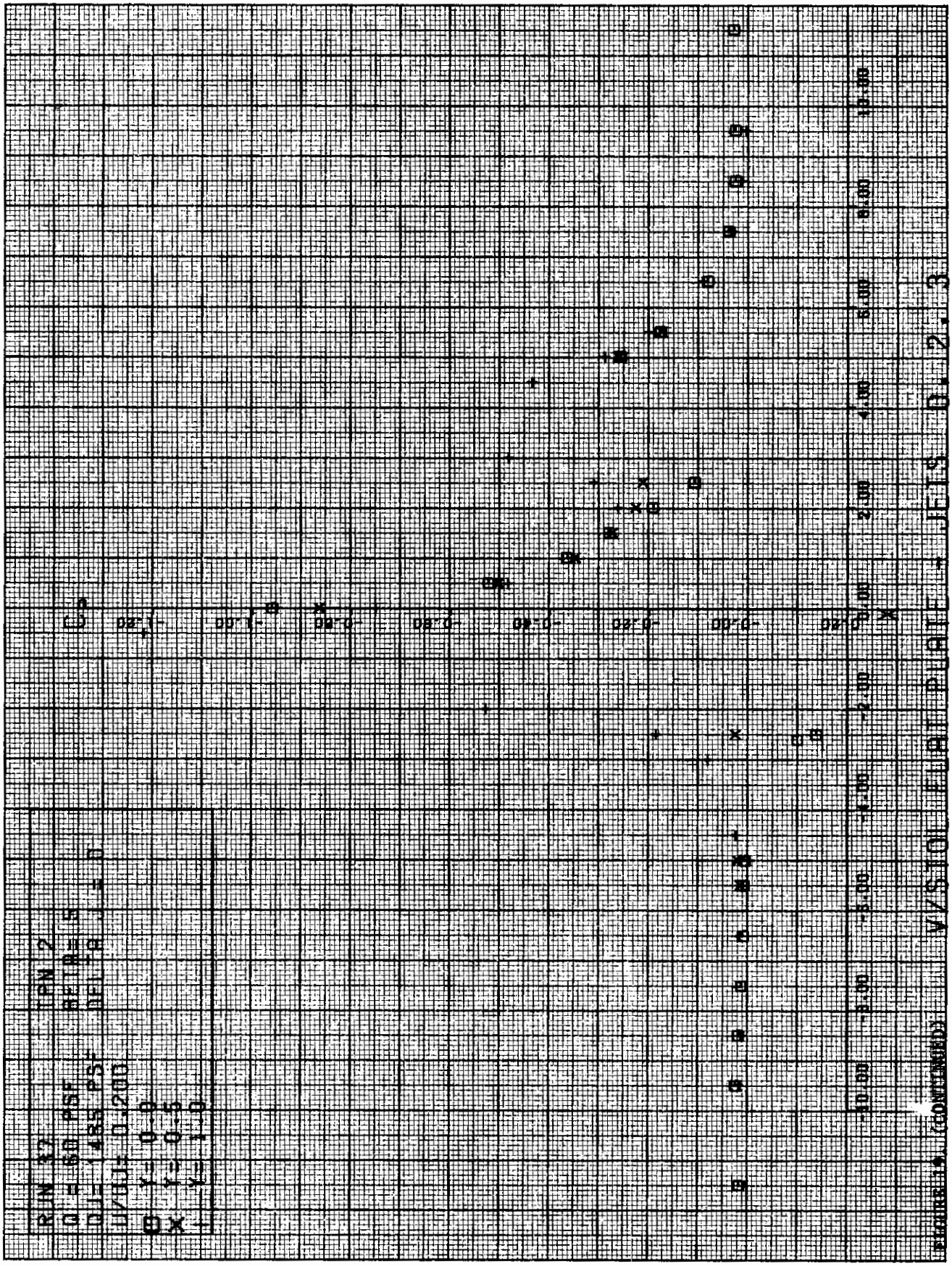

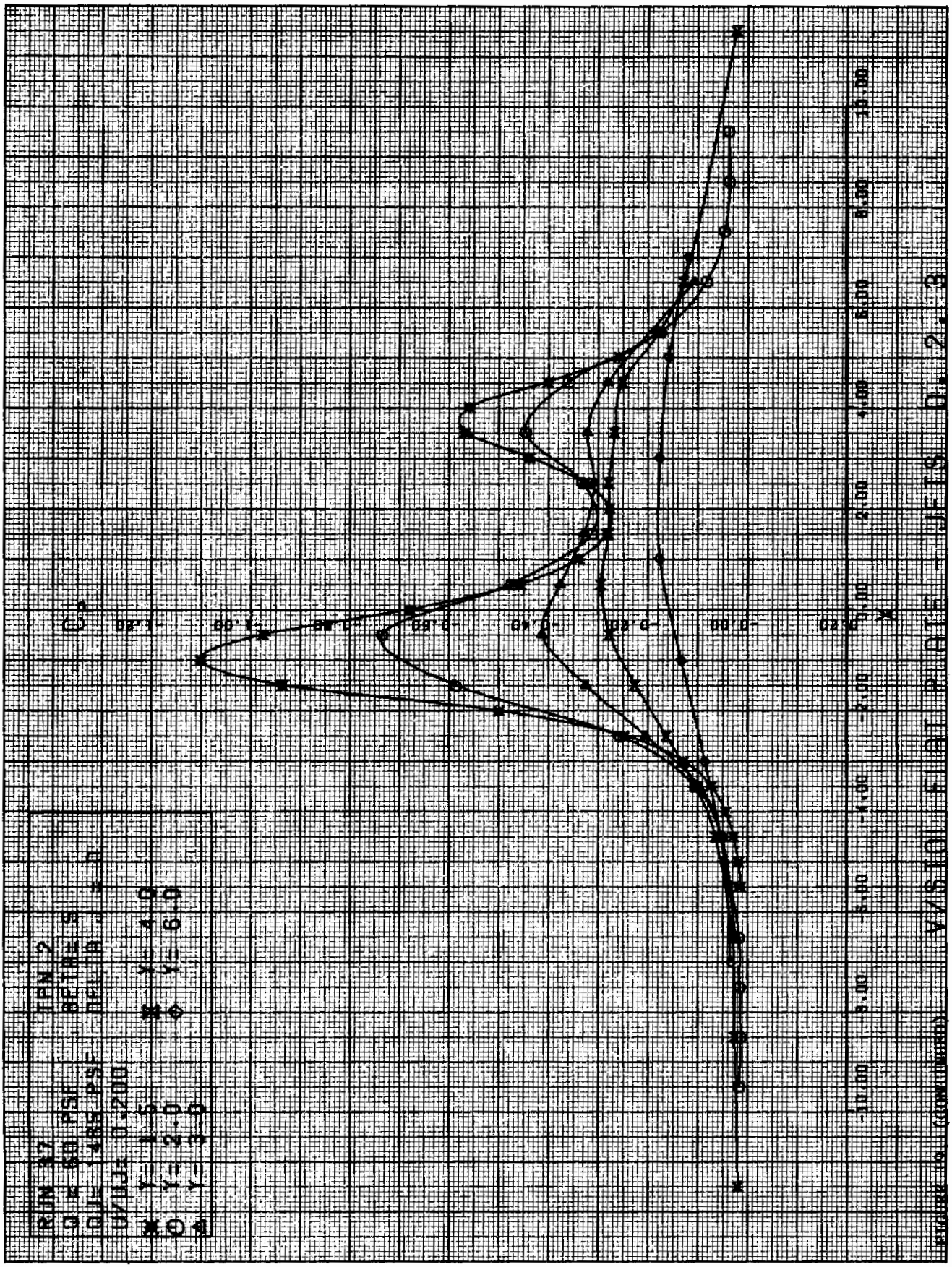

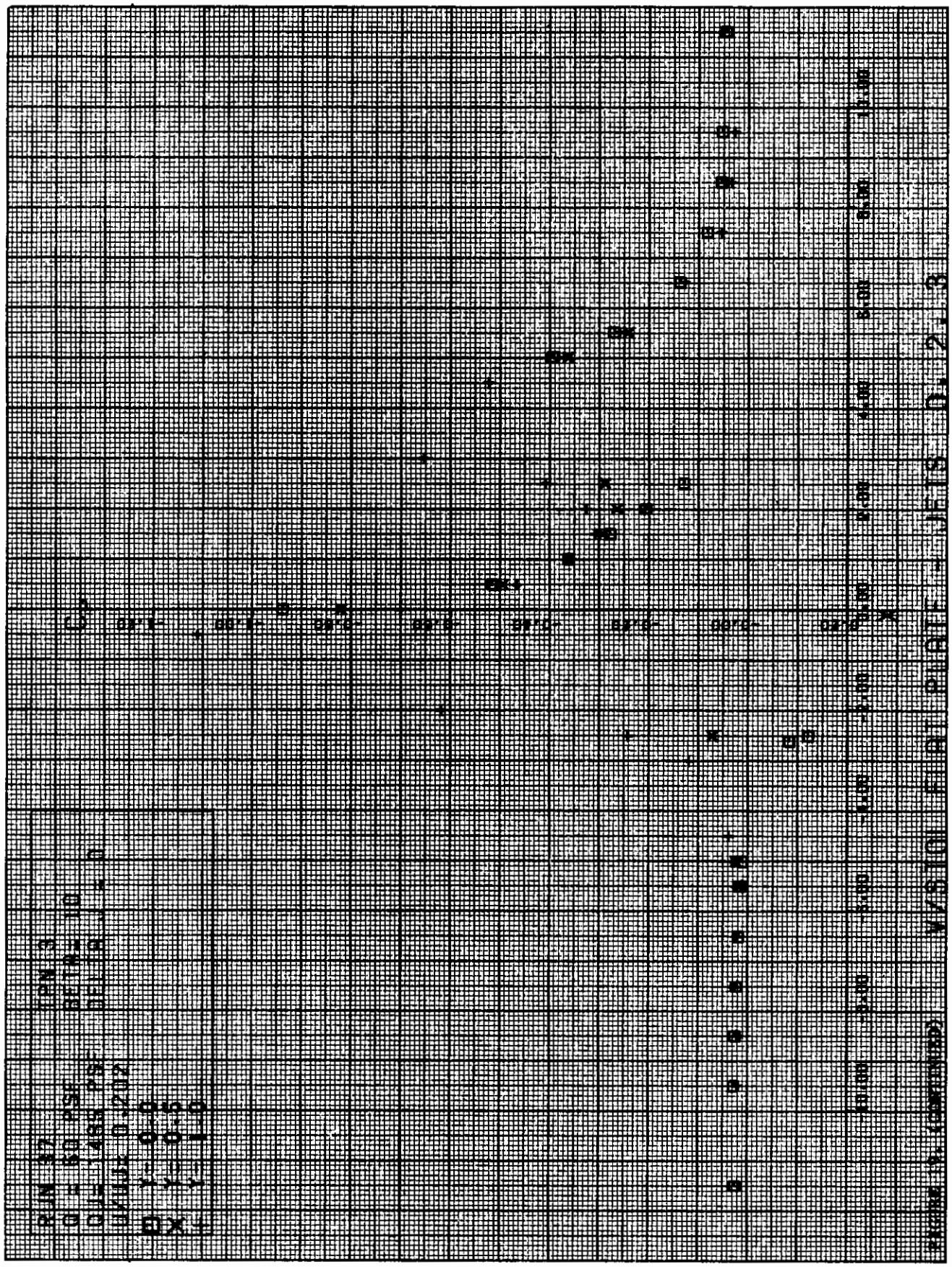

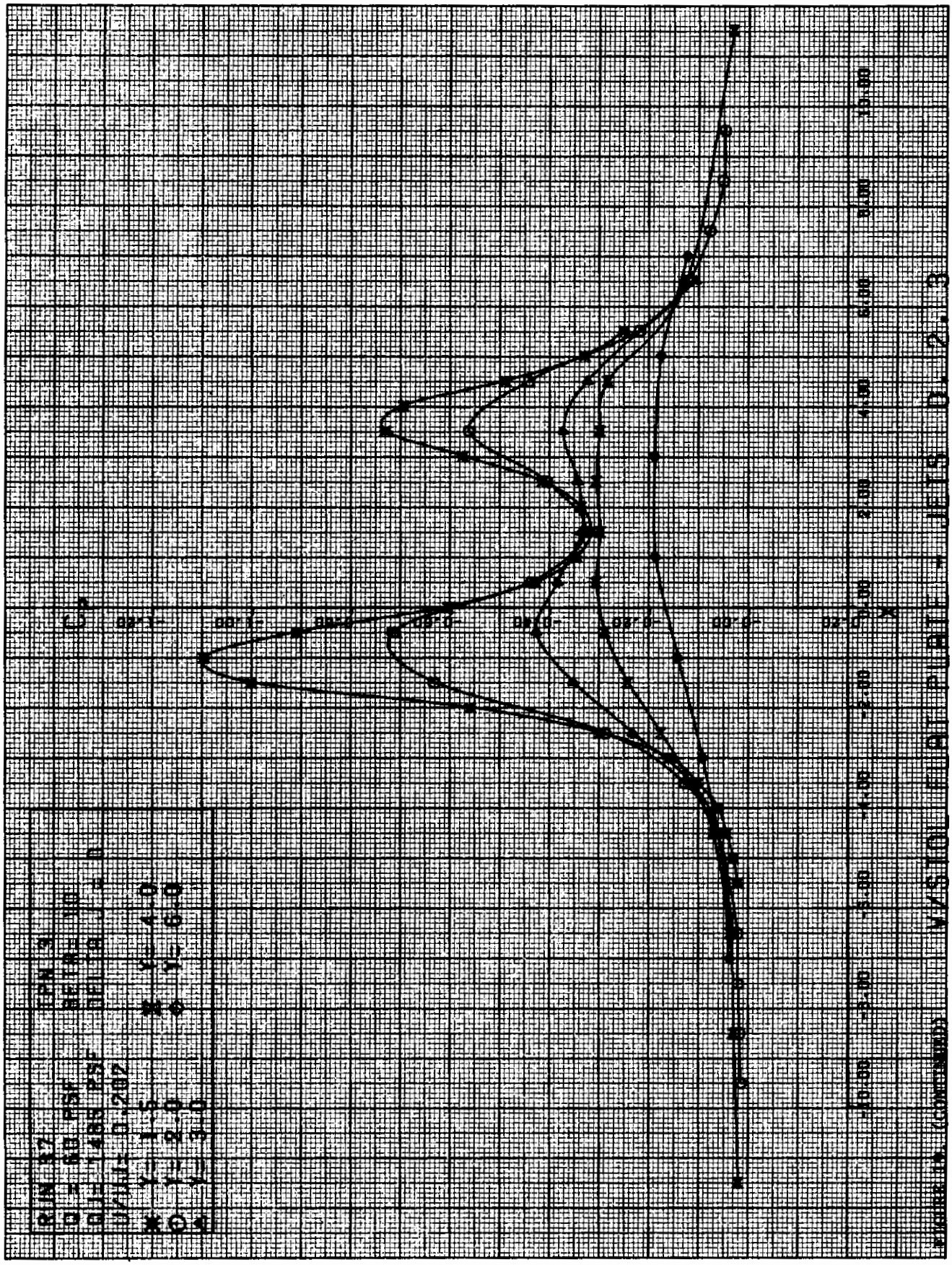

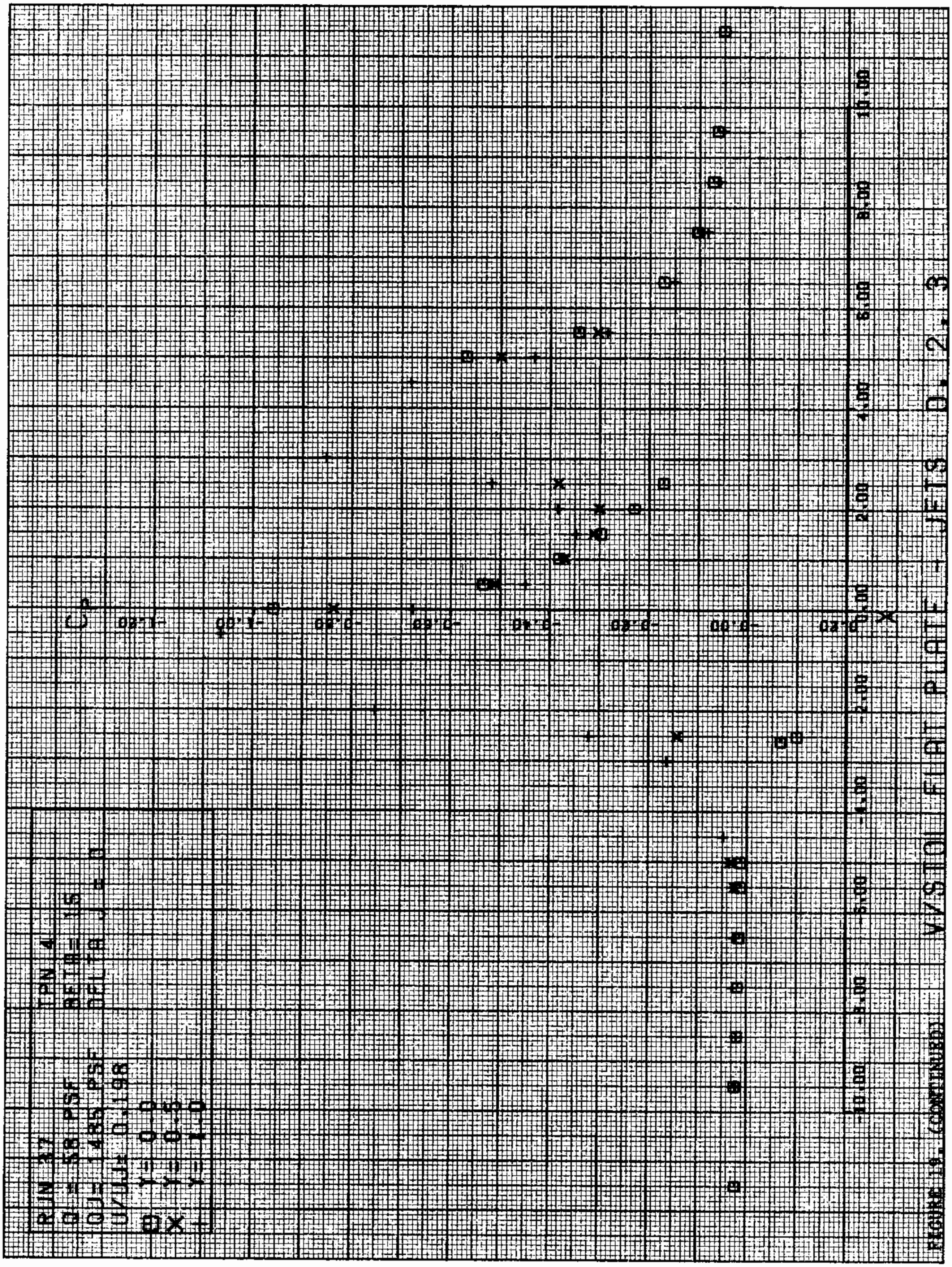

FIGURE 19. (CONTINUED) V/STOL FLAT PLATE - JETS D. 2, 3

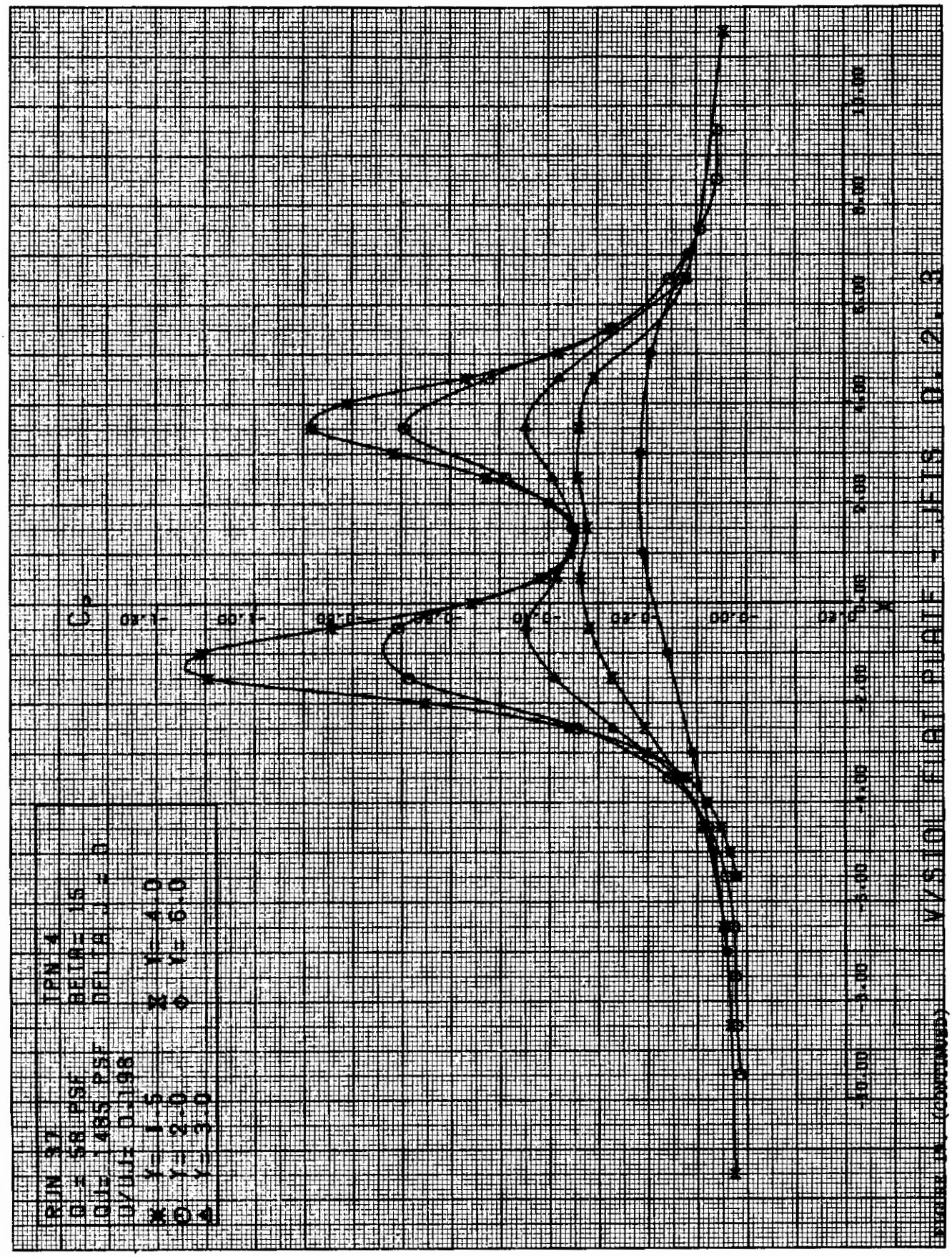

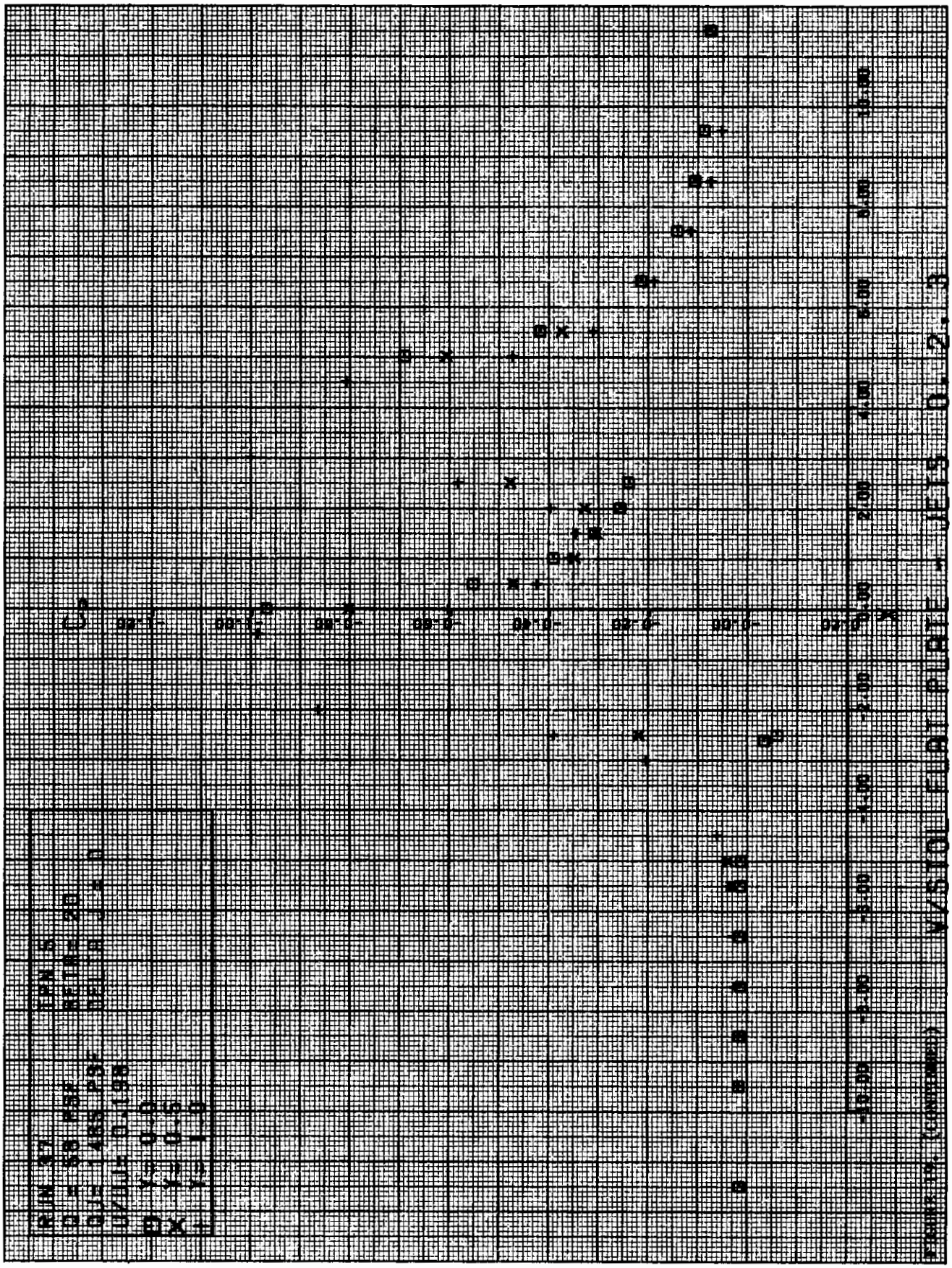

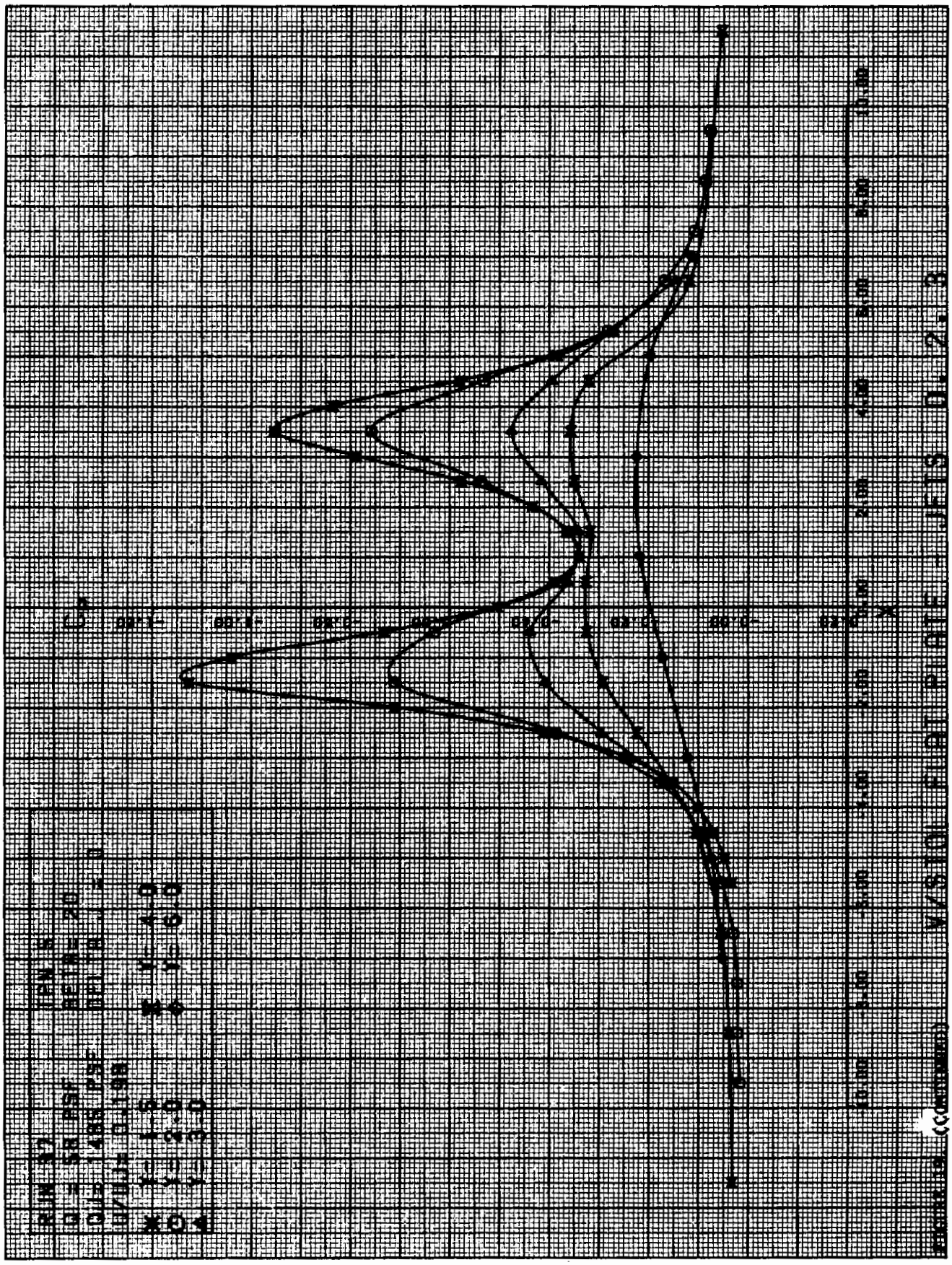

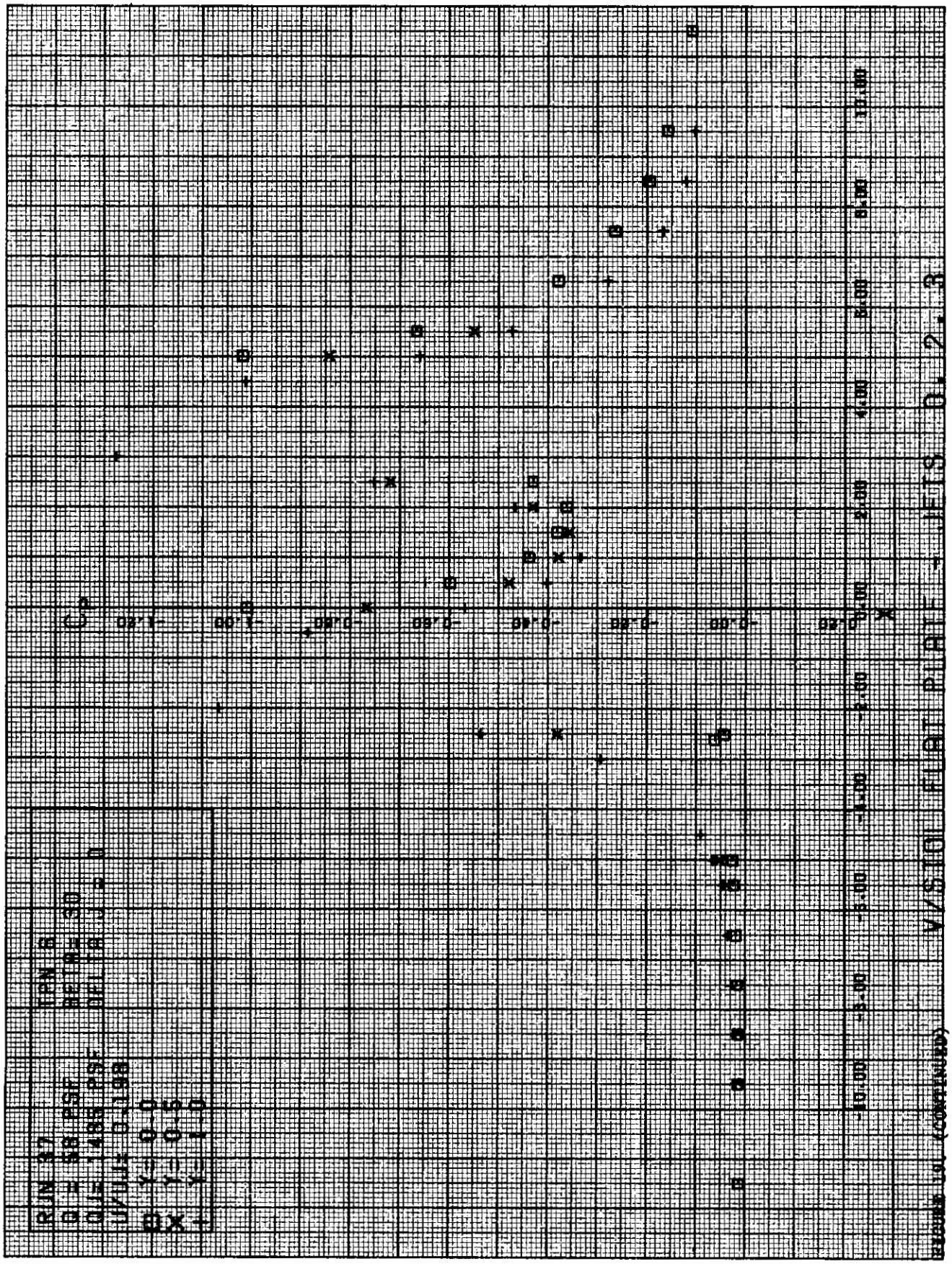

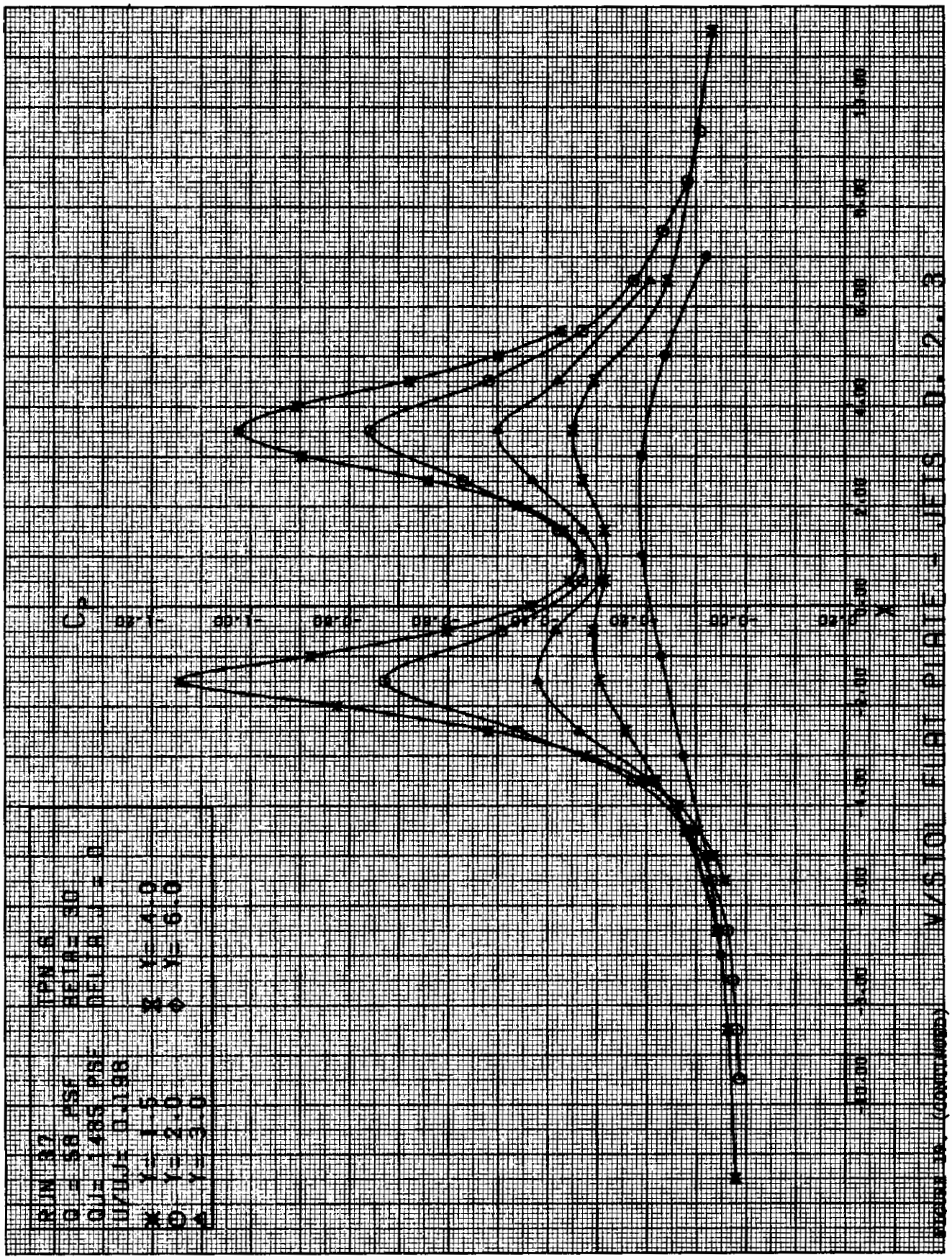

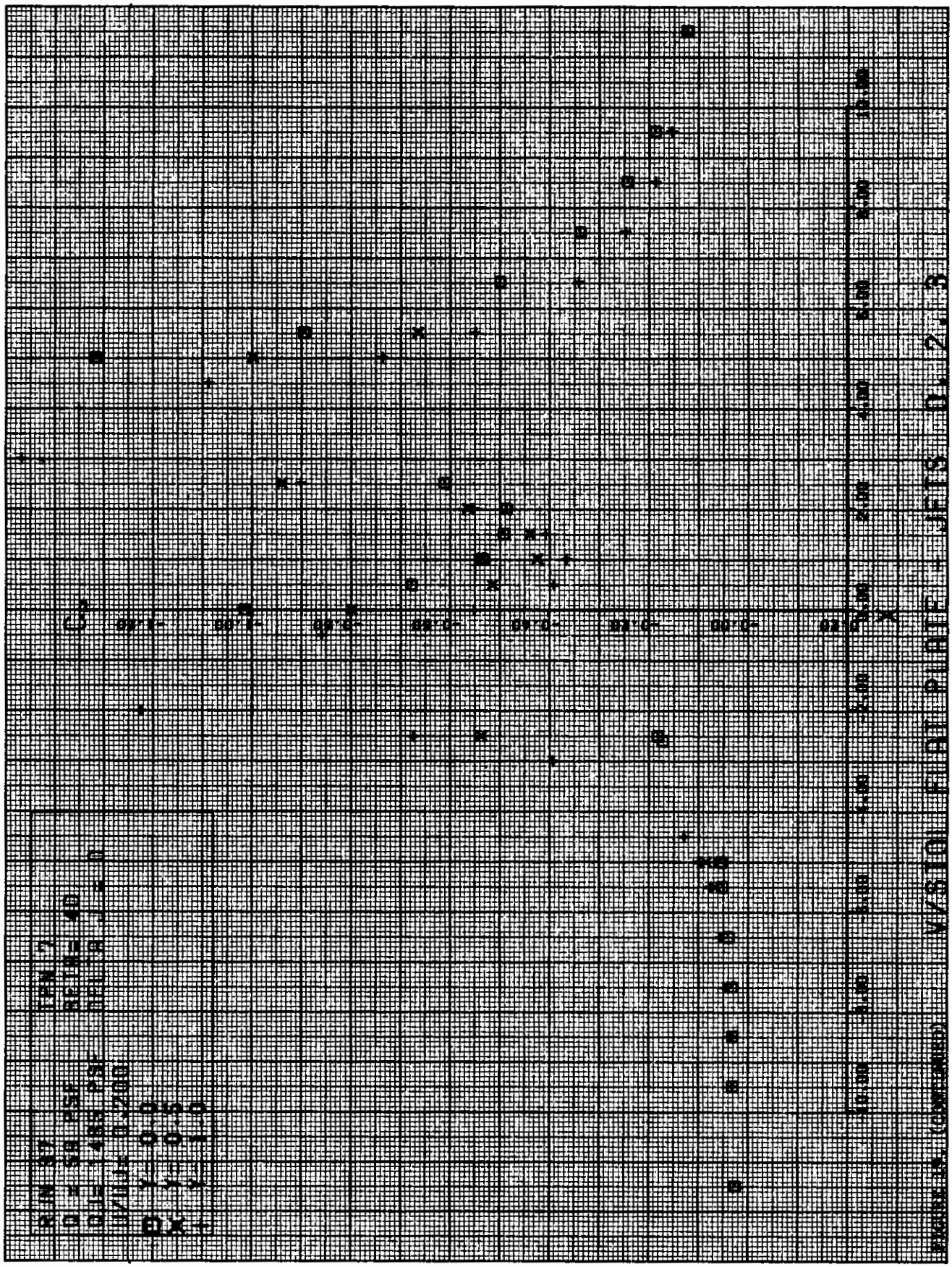

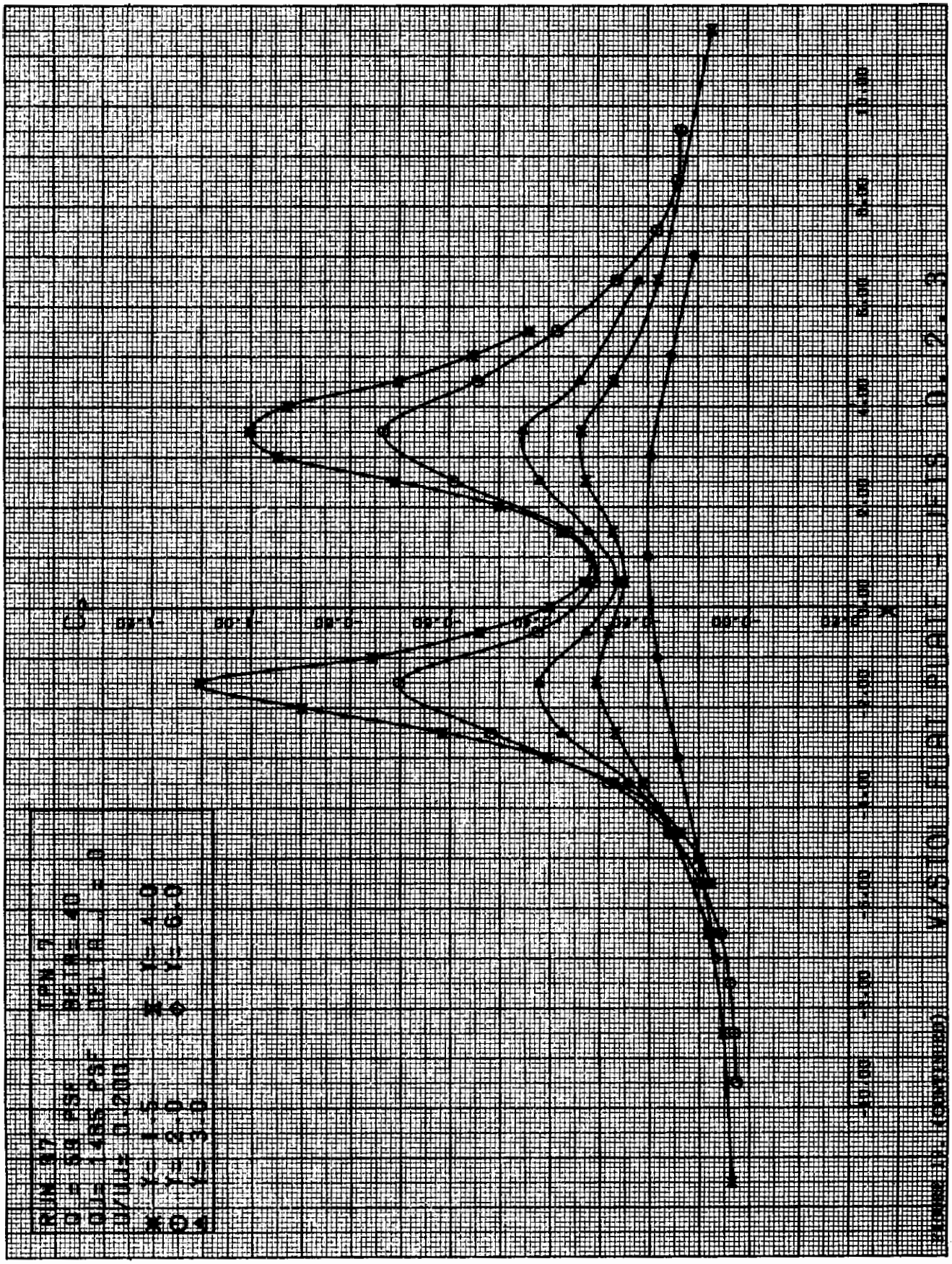

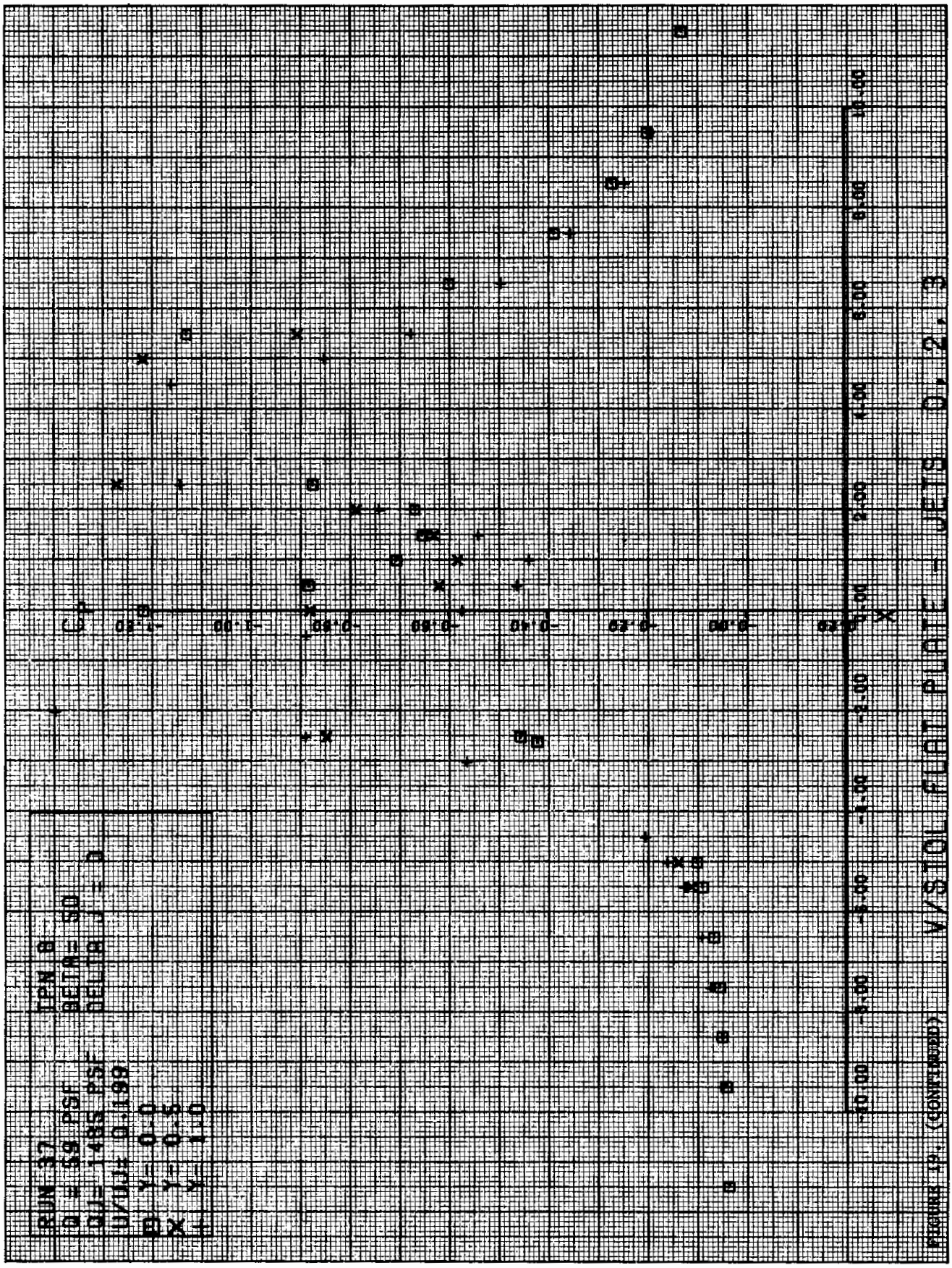

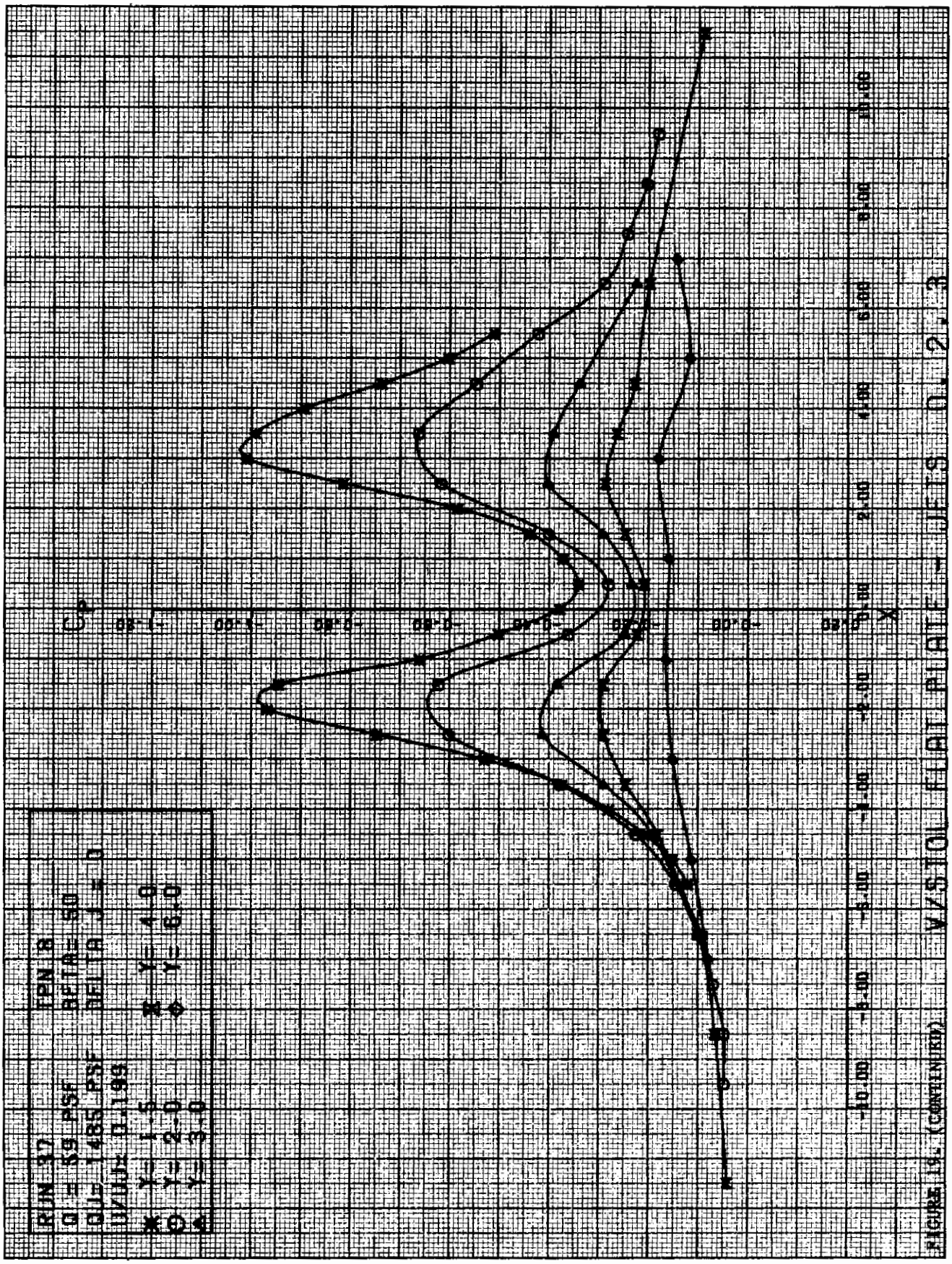

FIGURE 19. (CONTINUED)

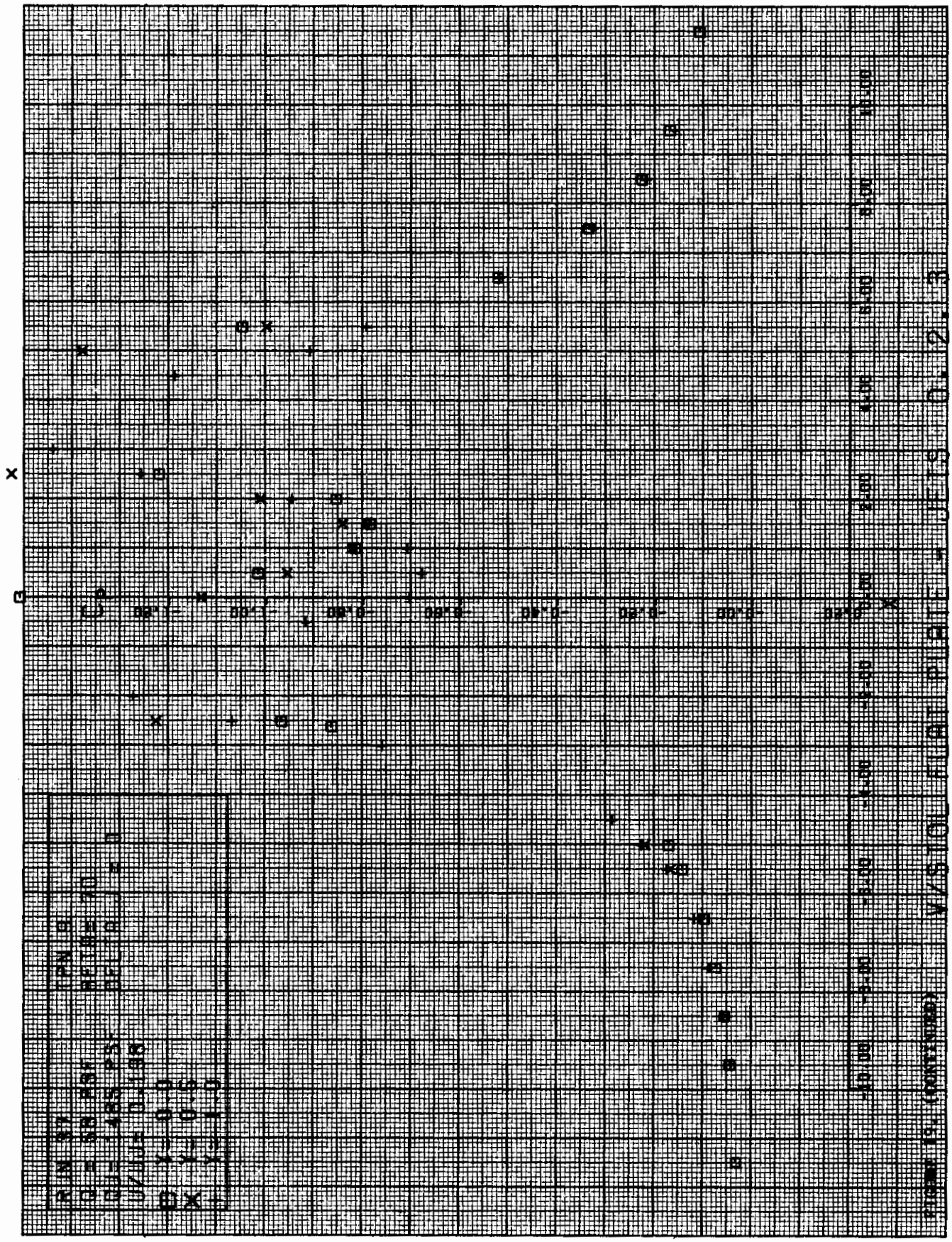

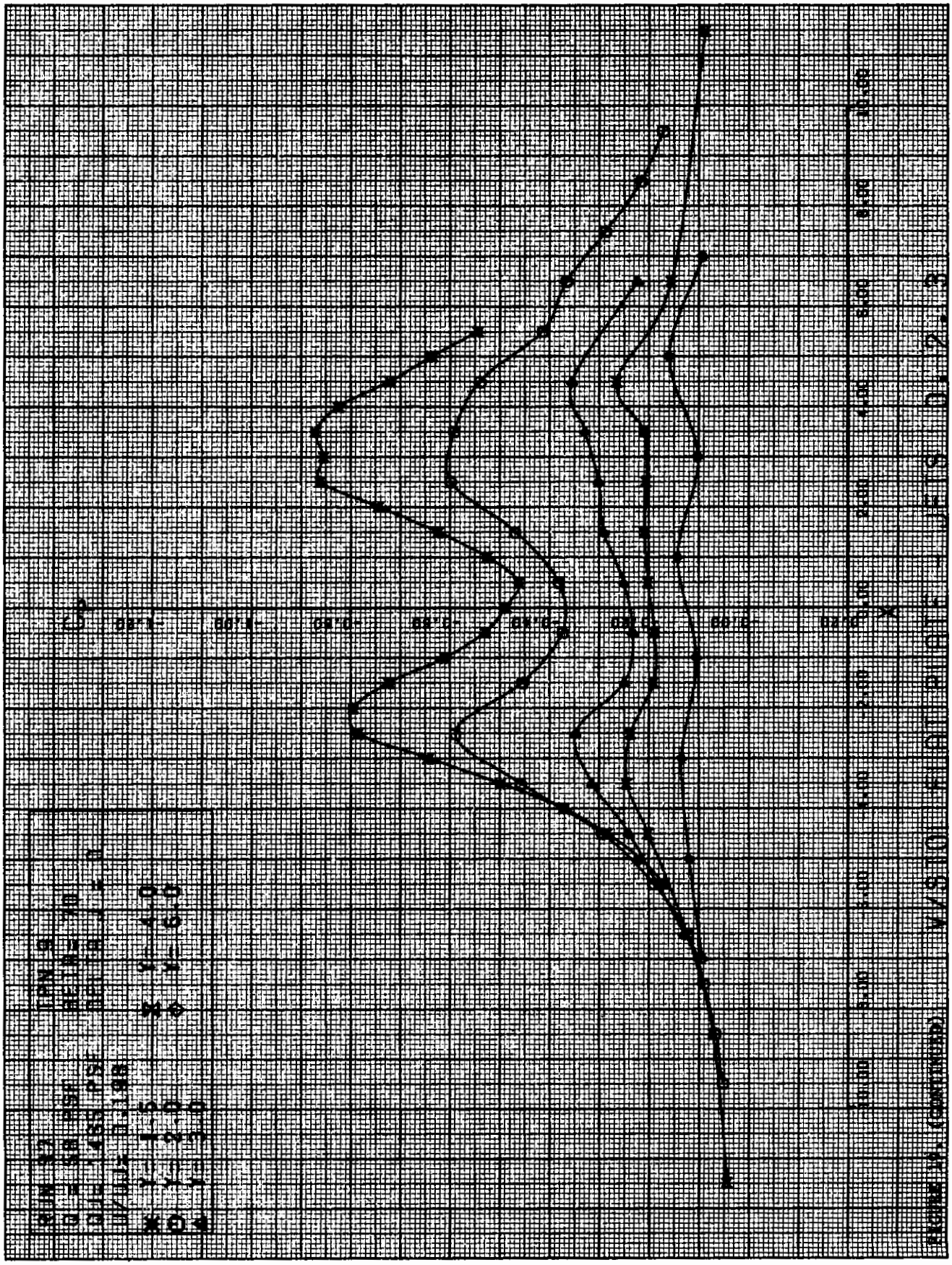

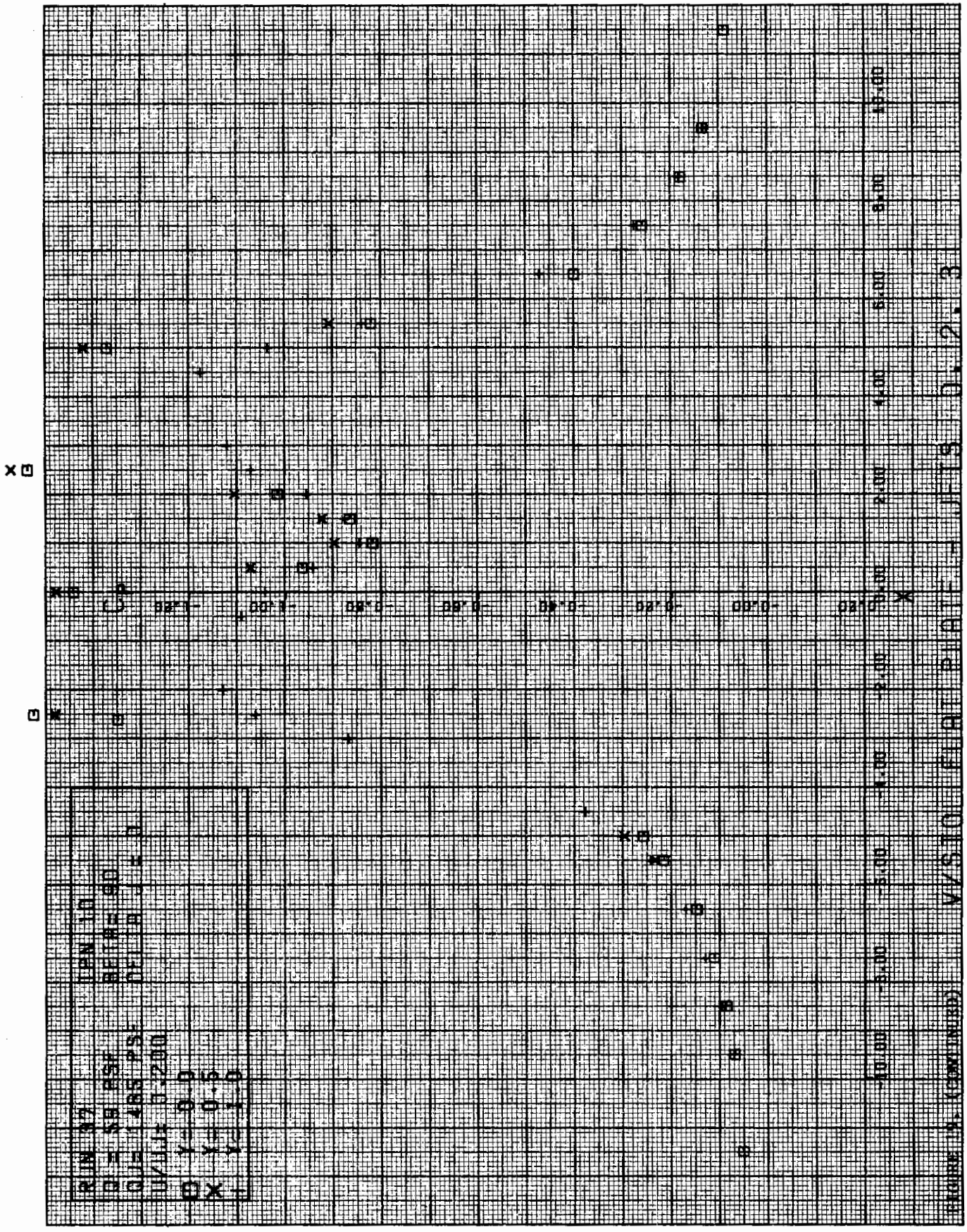

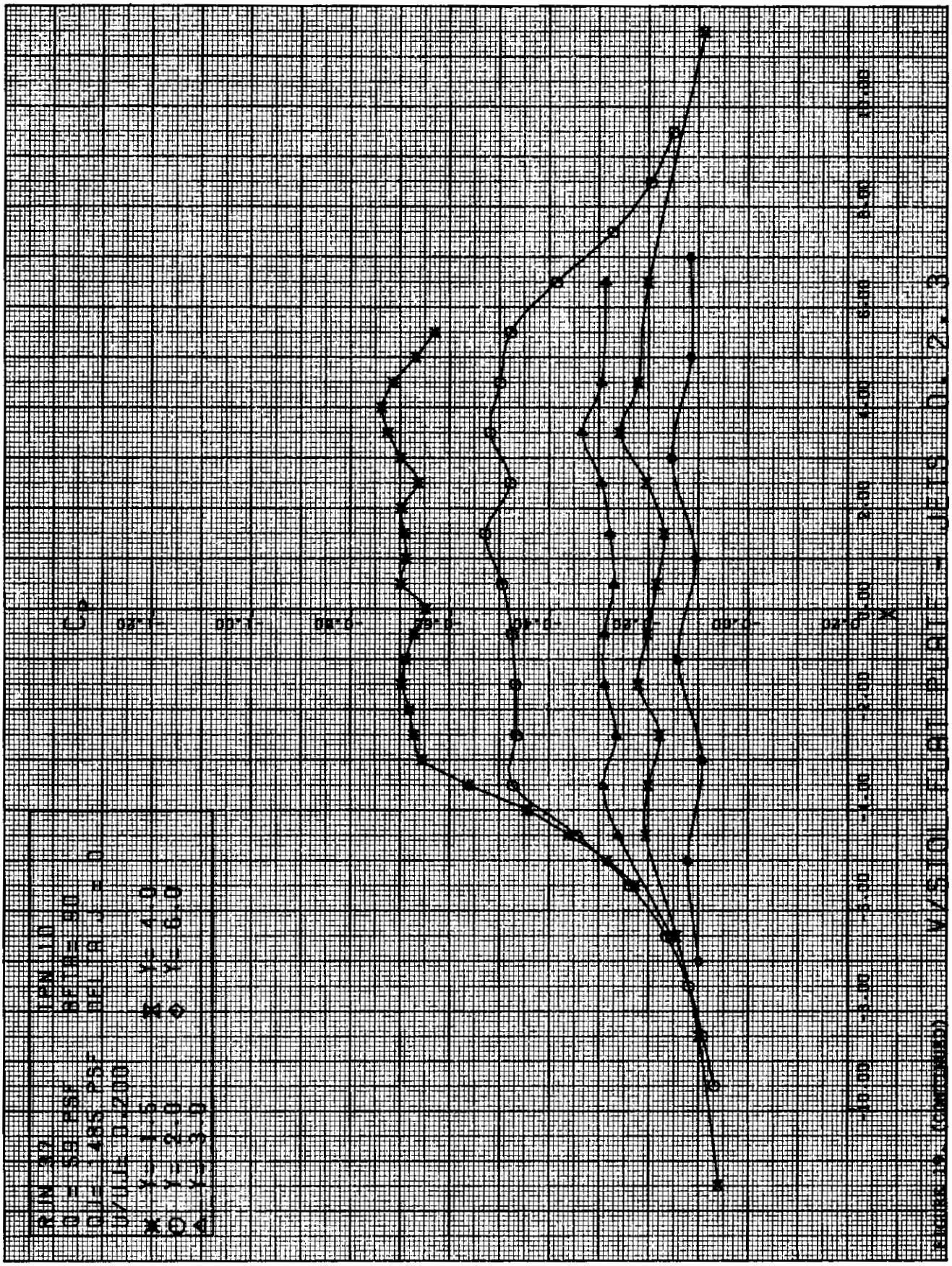

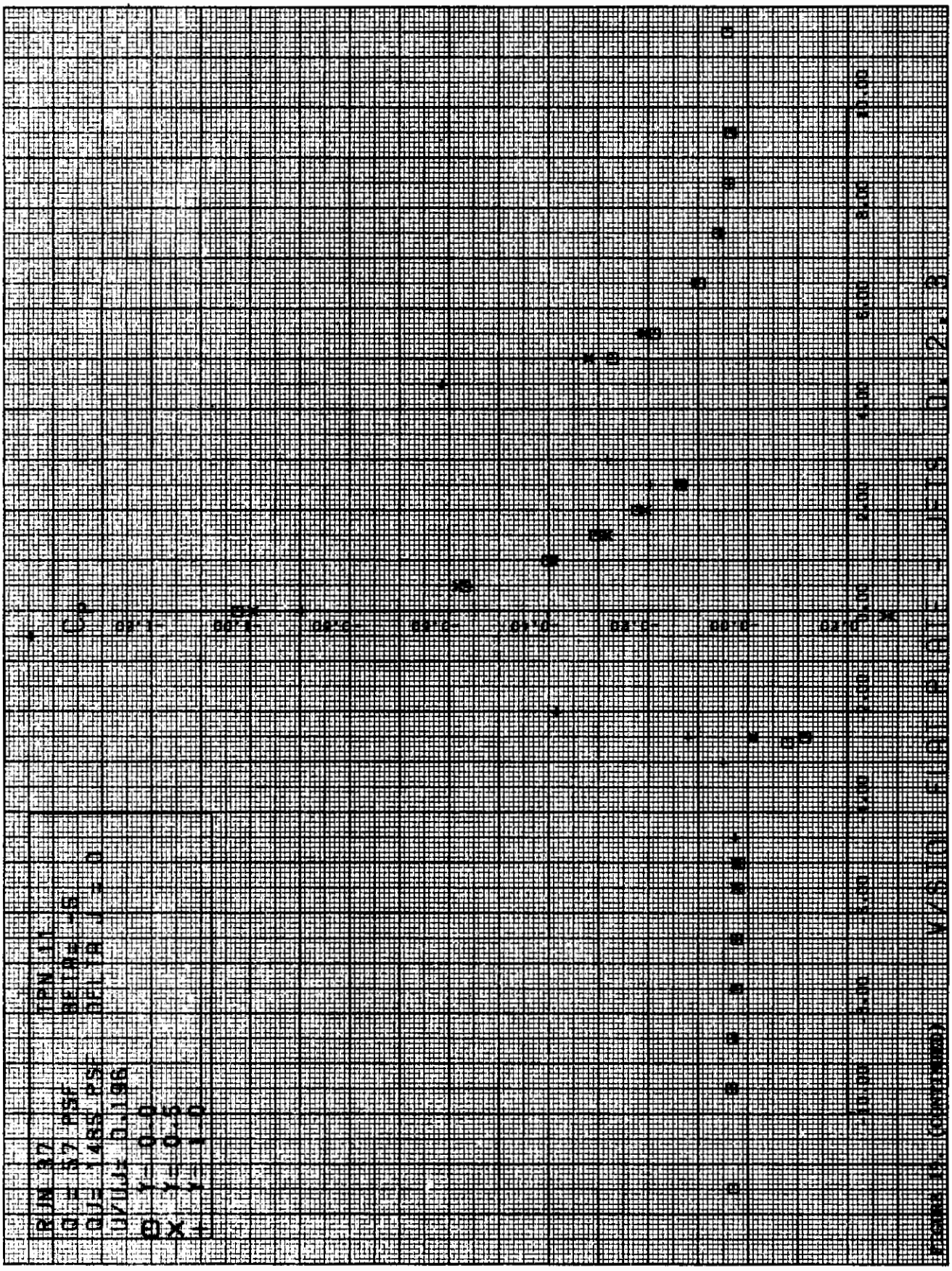

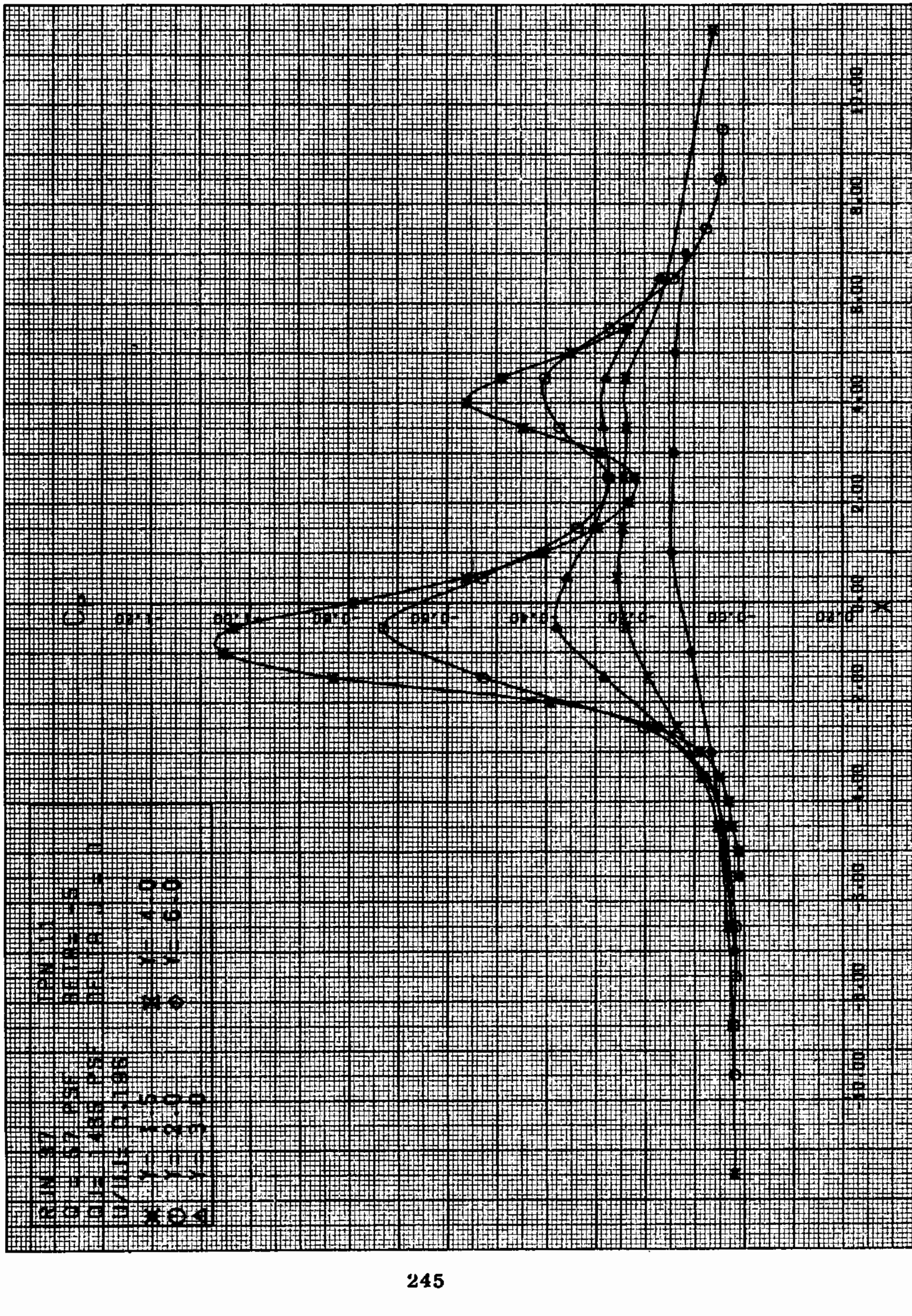

FIGURE 19. (CONTINUED) V/STOL FLAT PLATE - JETS D.2.3

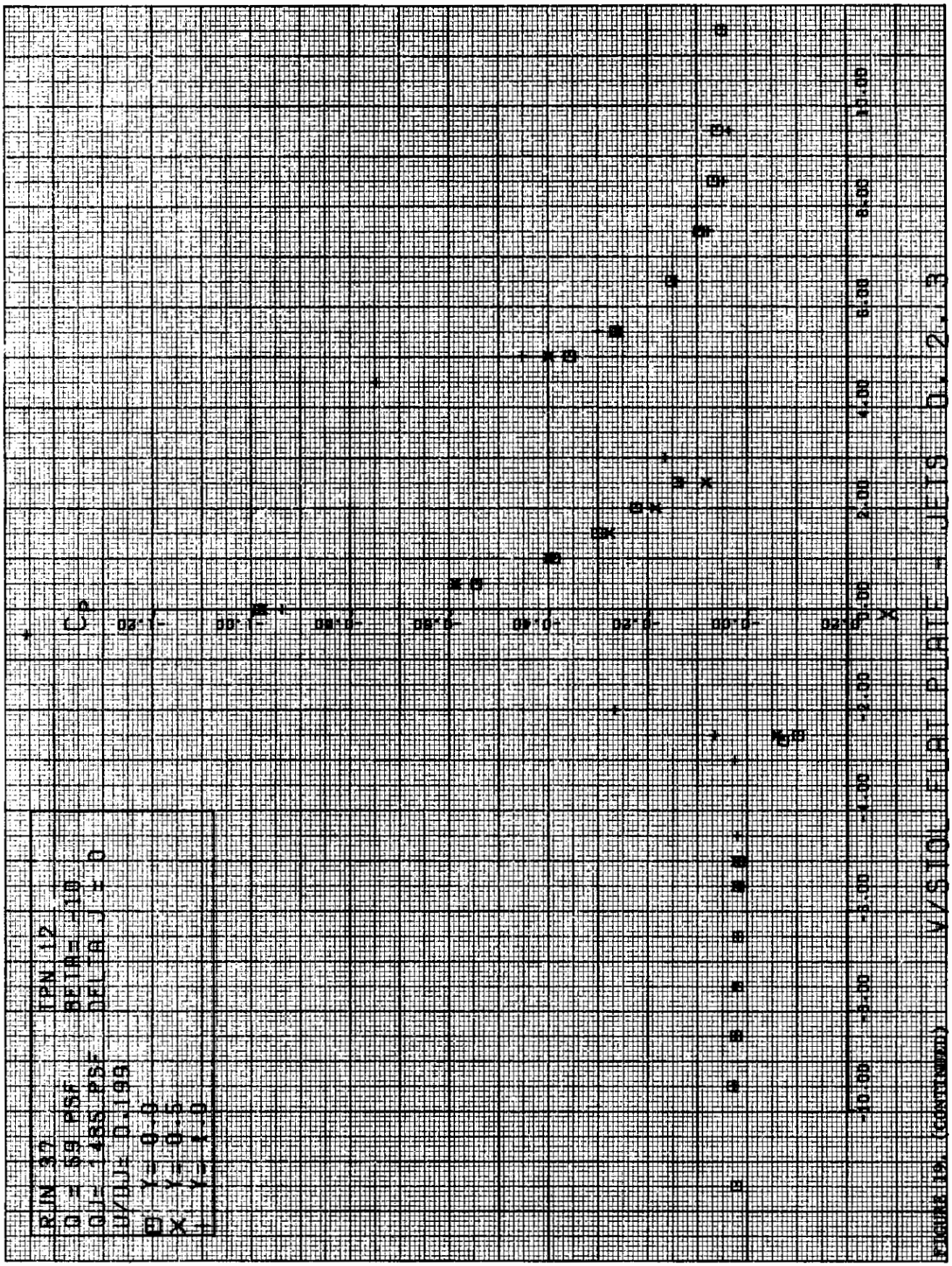

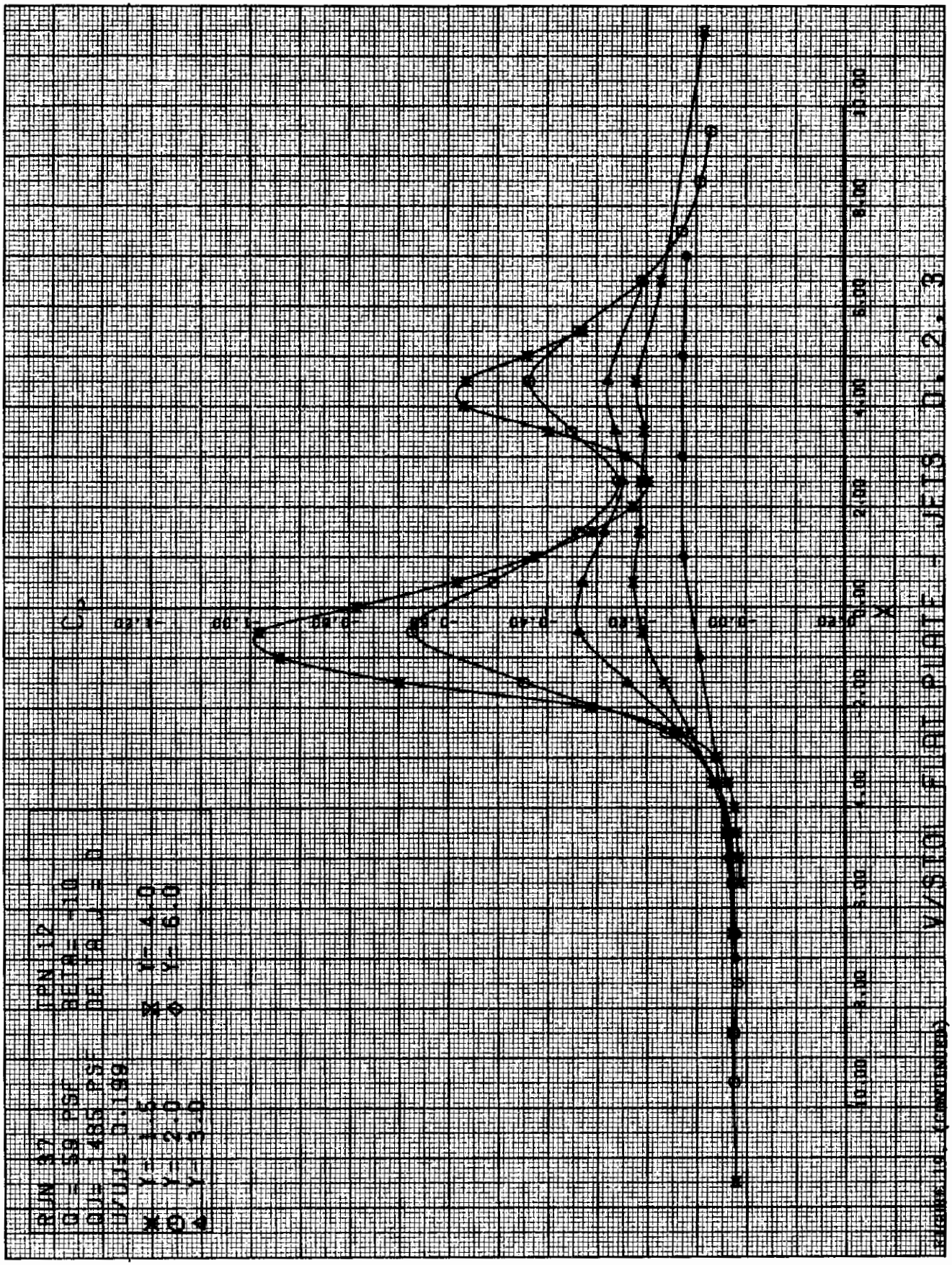

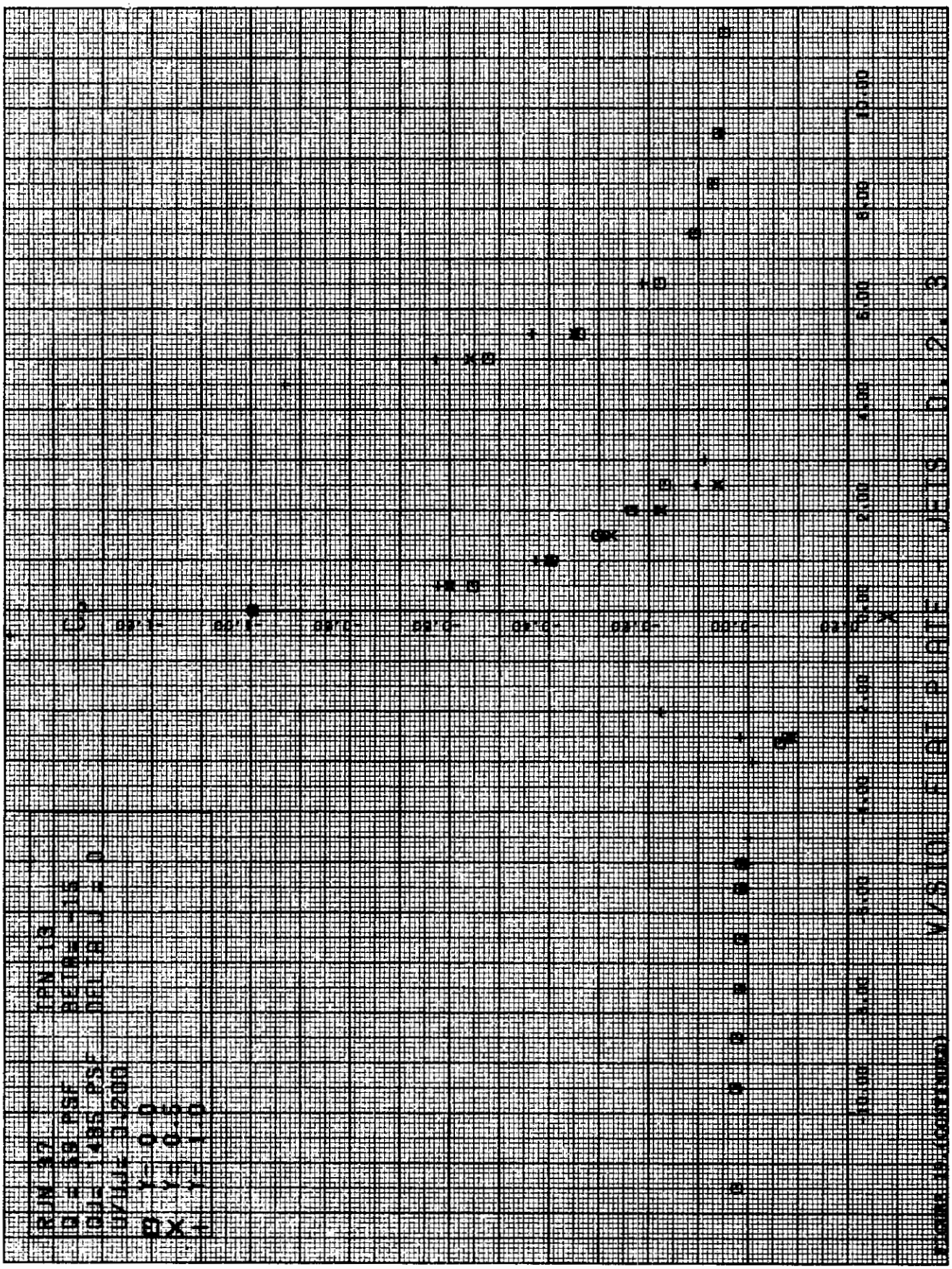

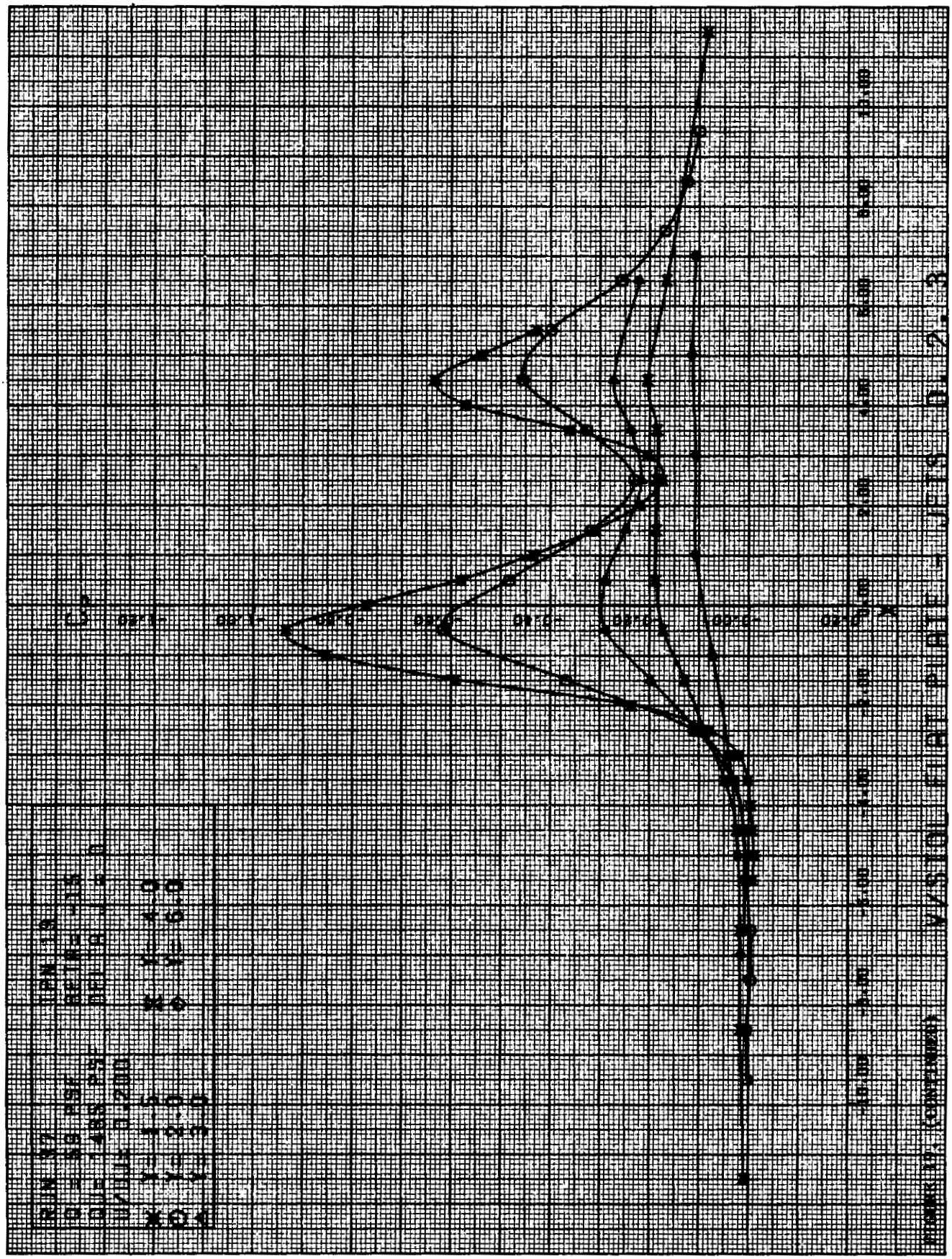

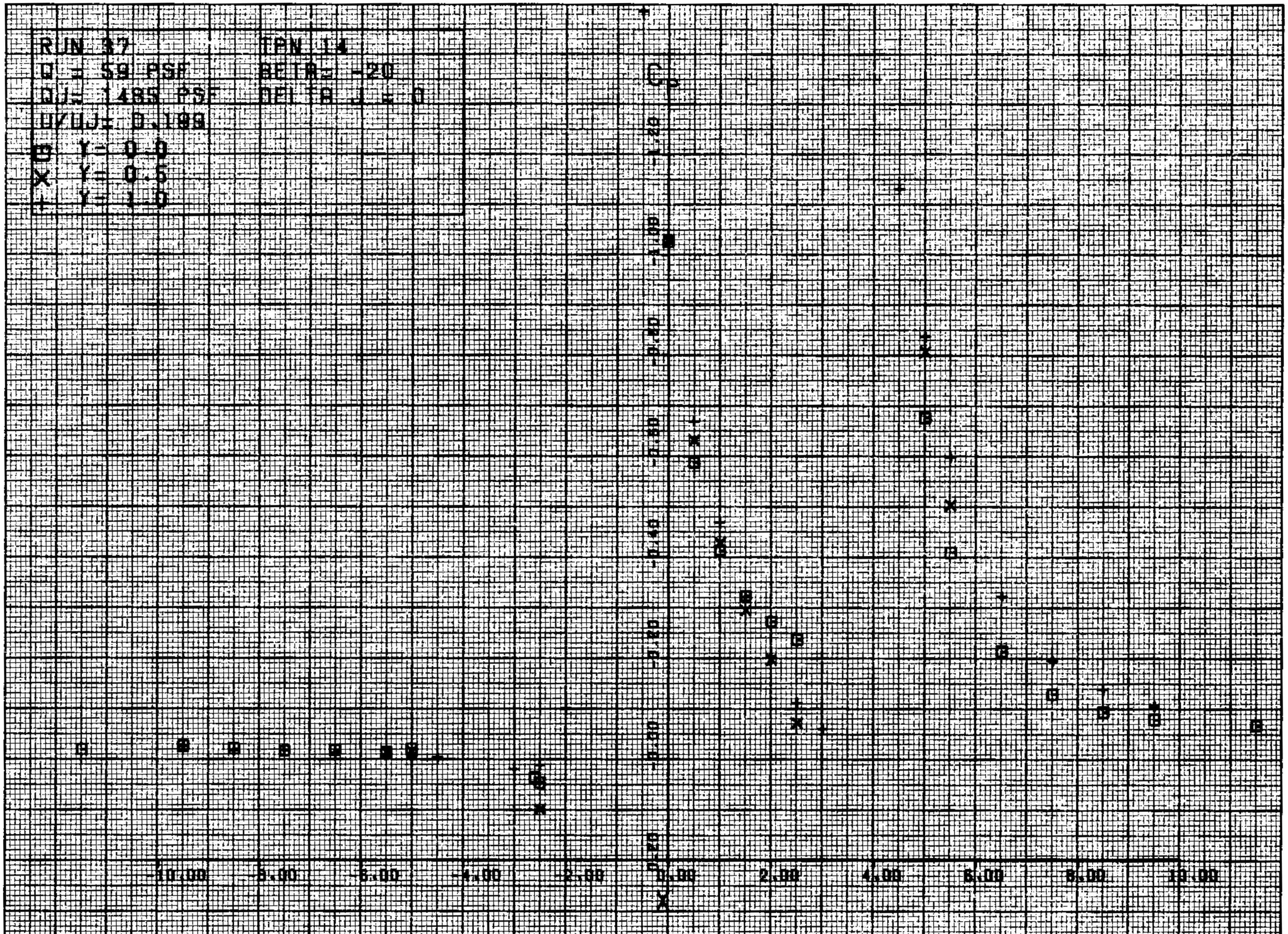

FIGURE 19.(CONTINUED) V/STOL FLAT PLATE - JETS D: 2, 3

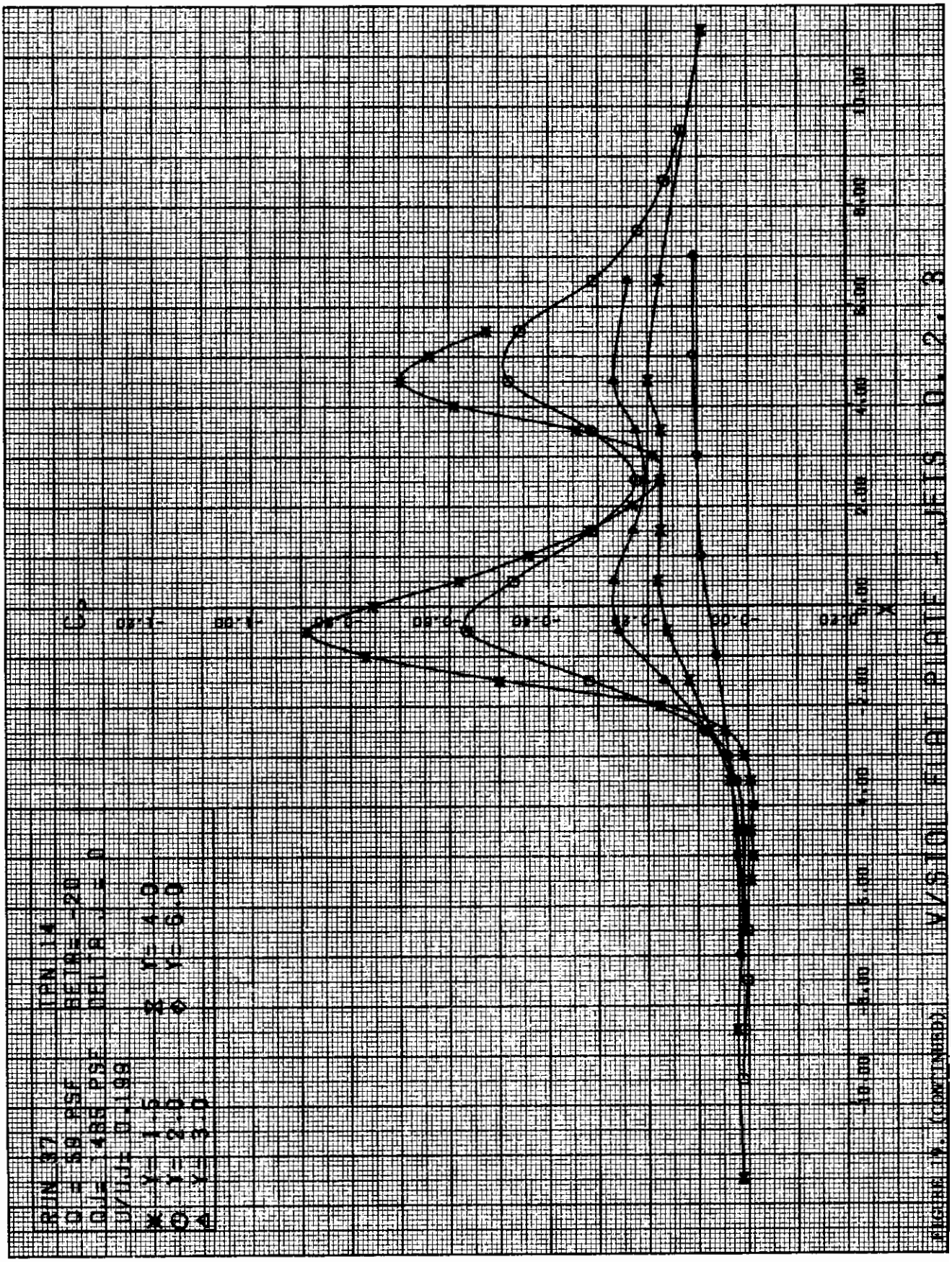

Figure 14. (Continued)

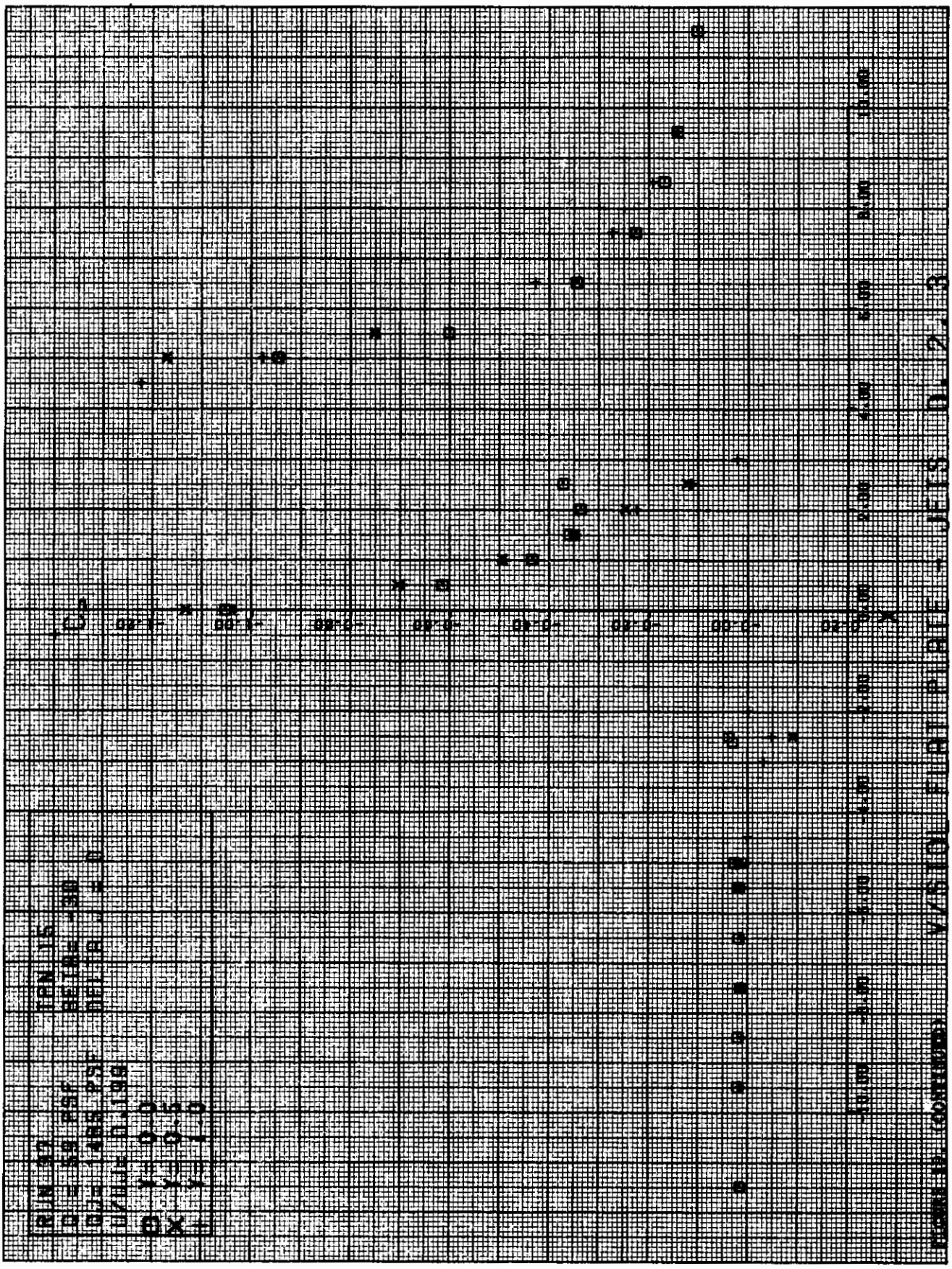

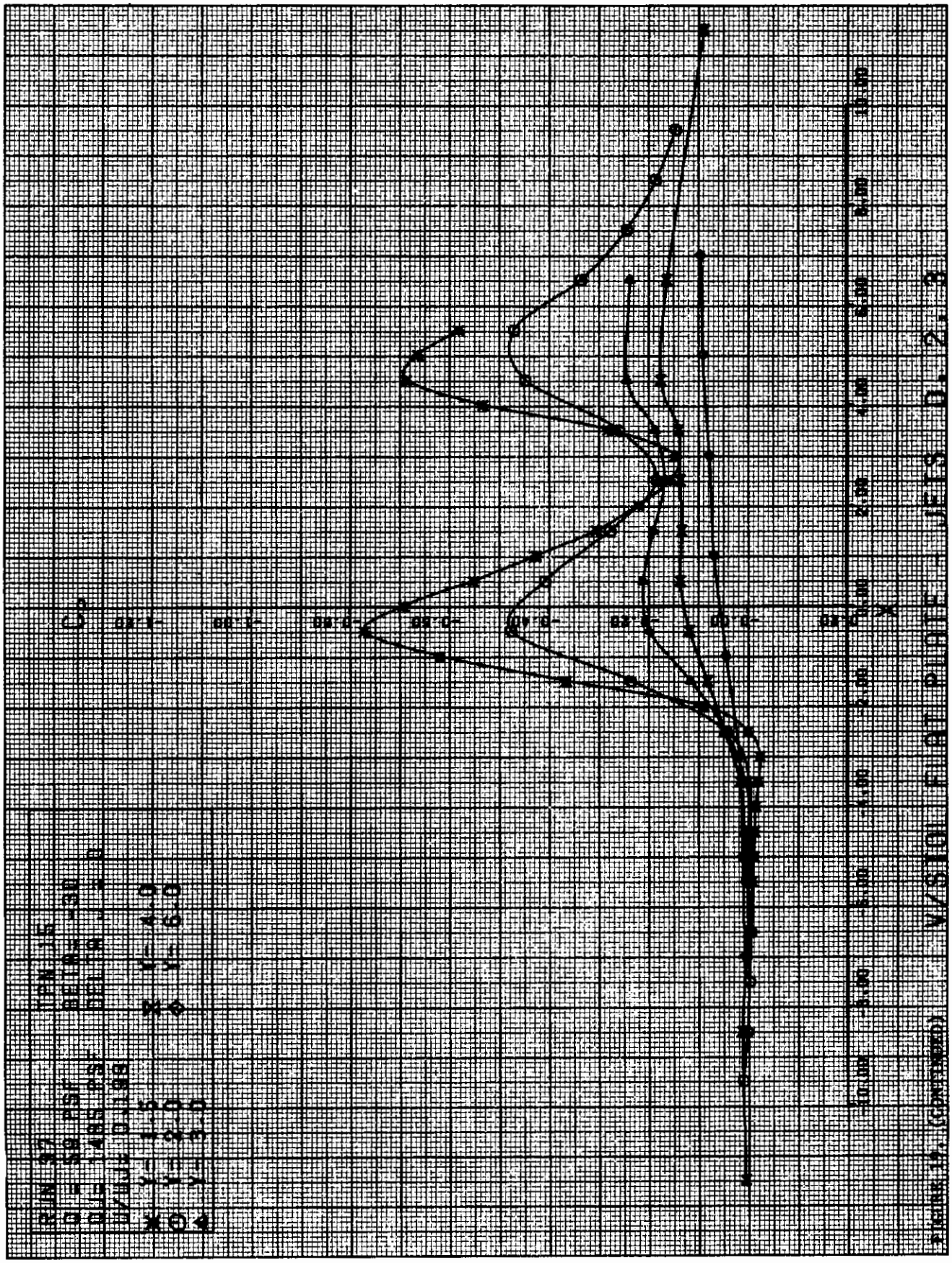

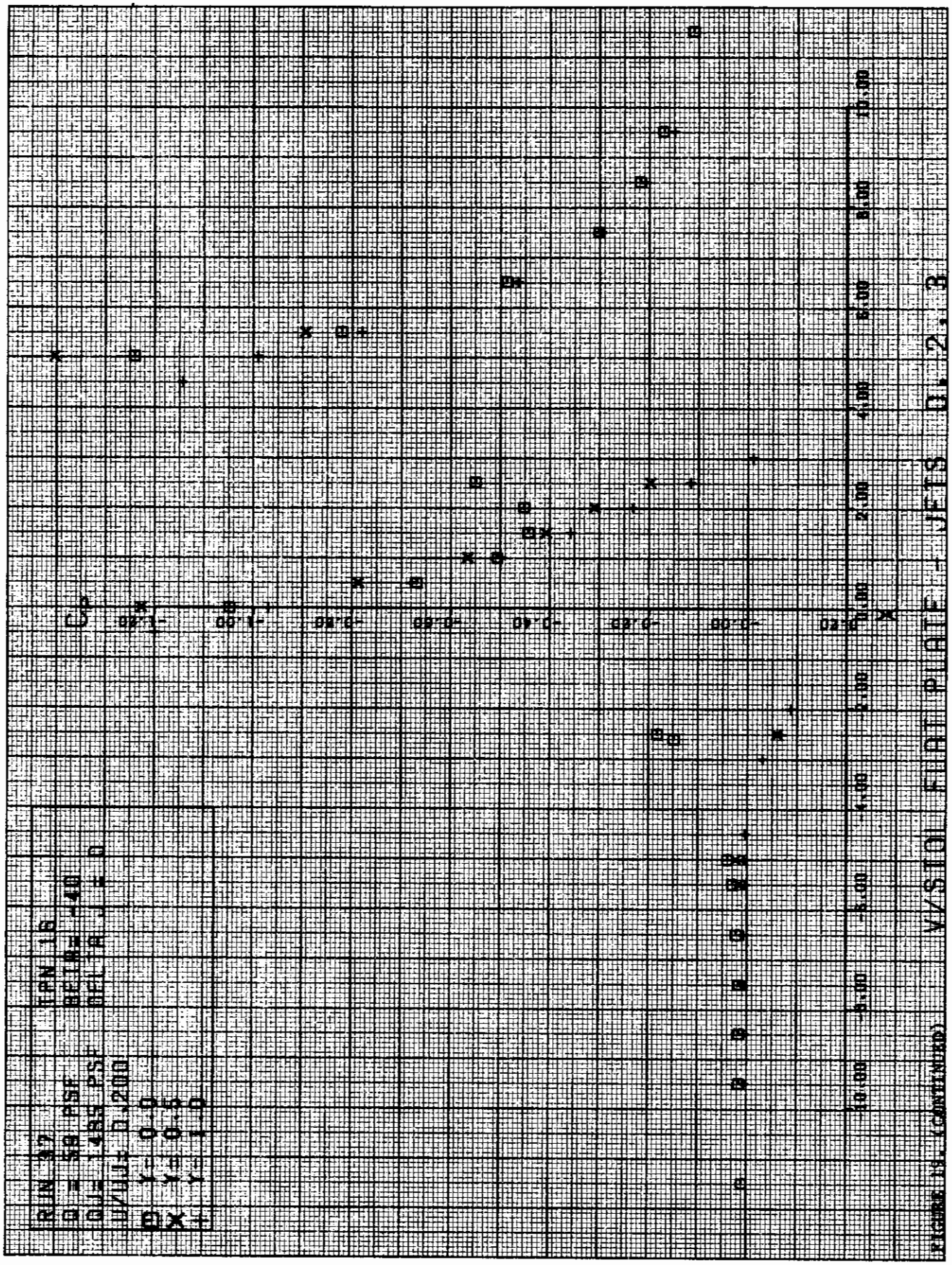

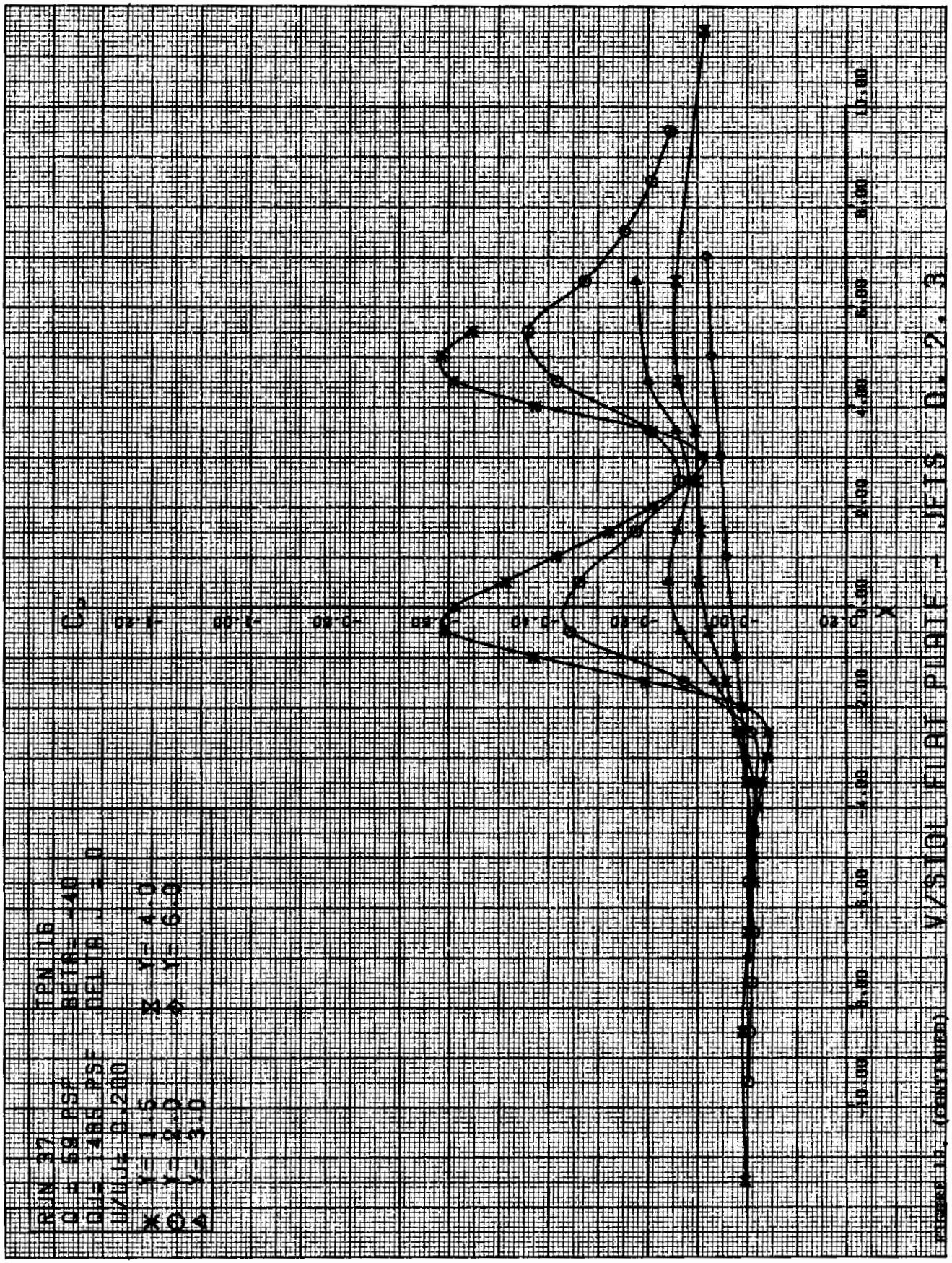

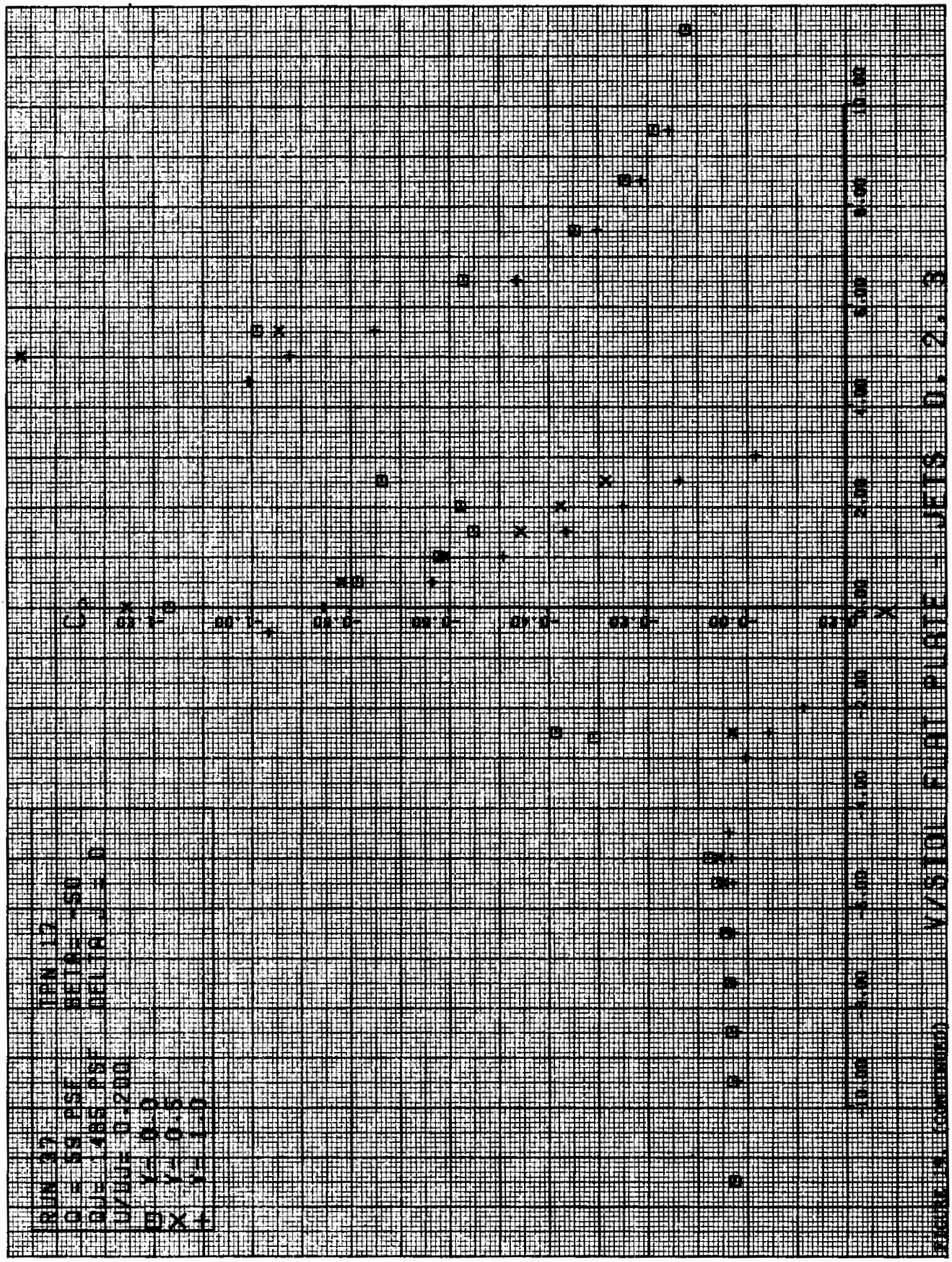

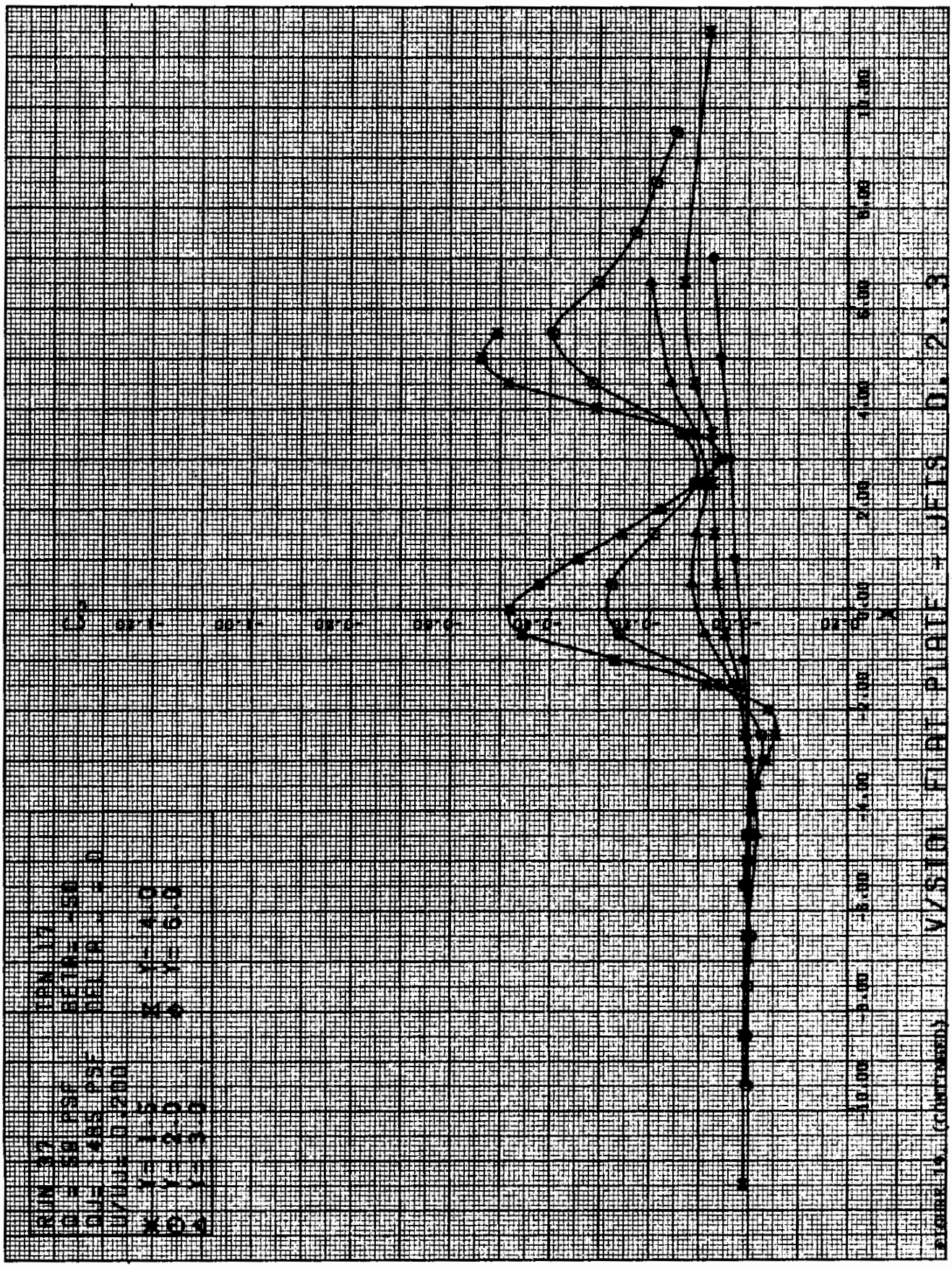

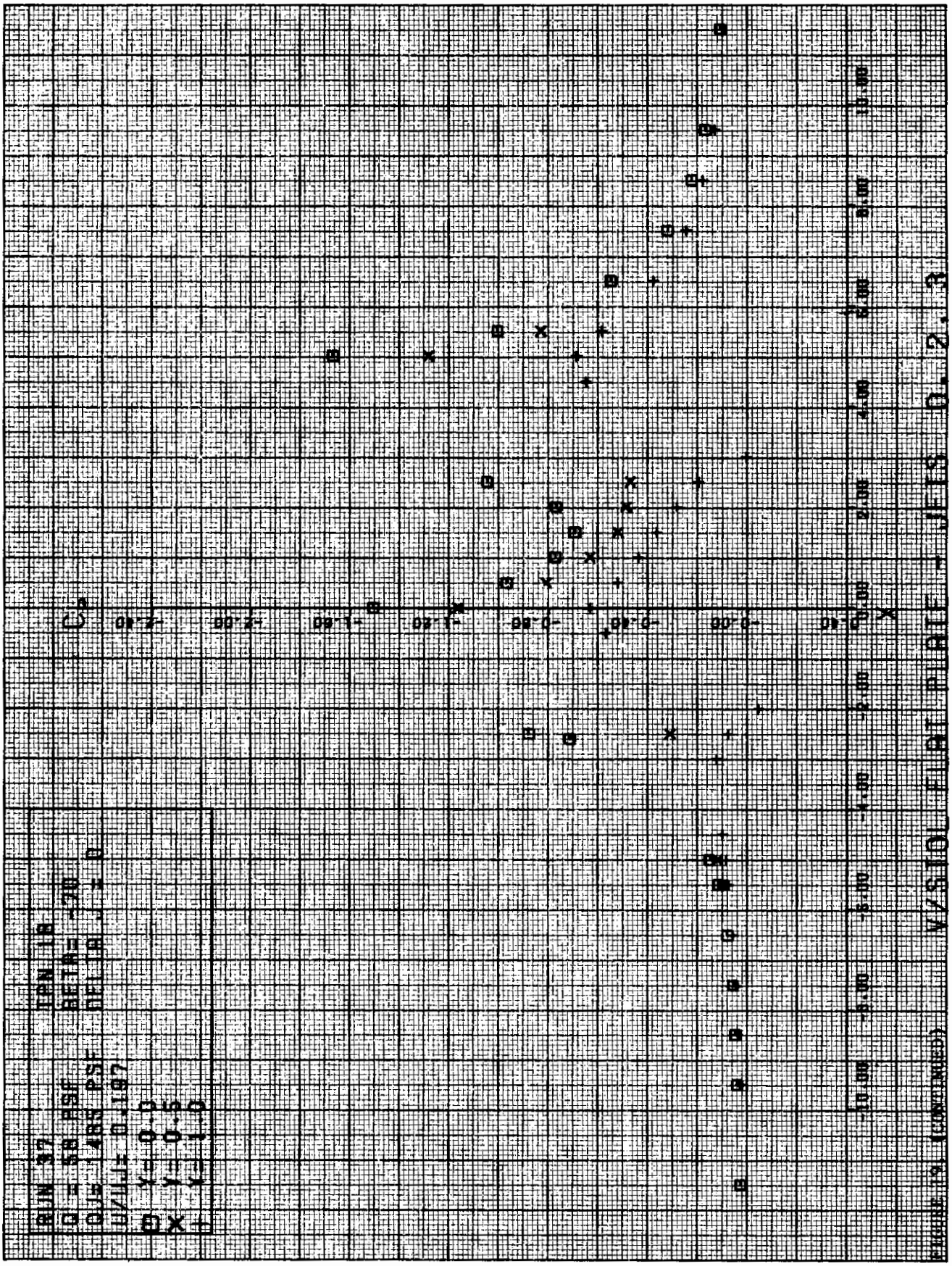

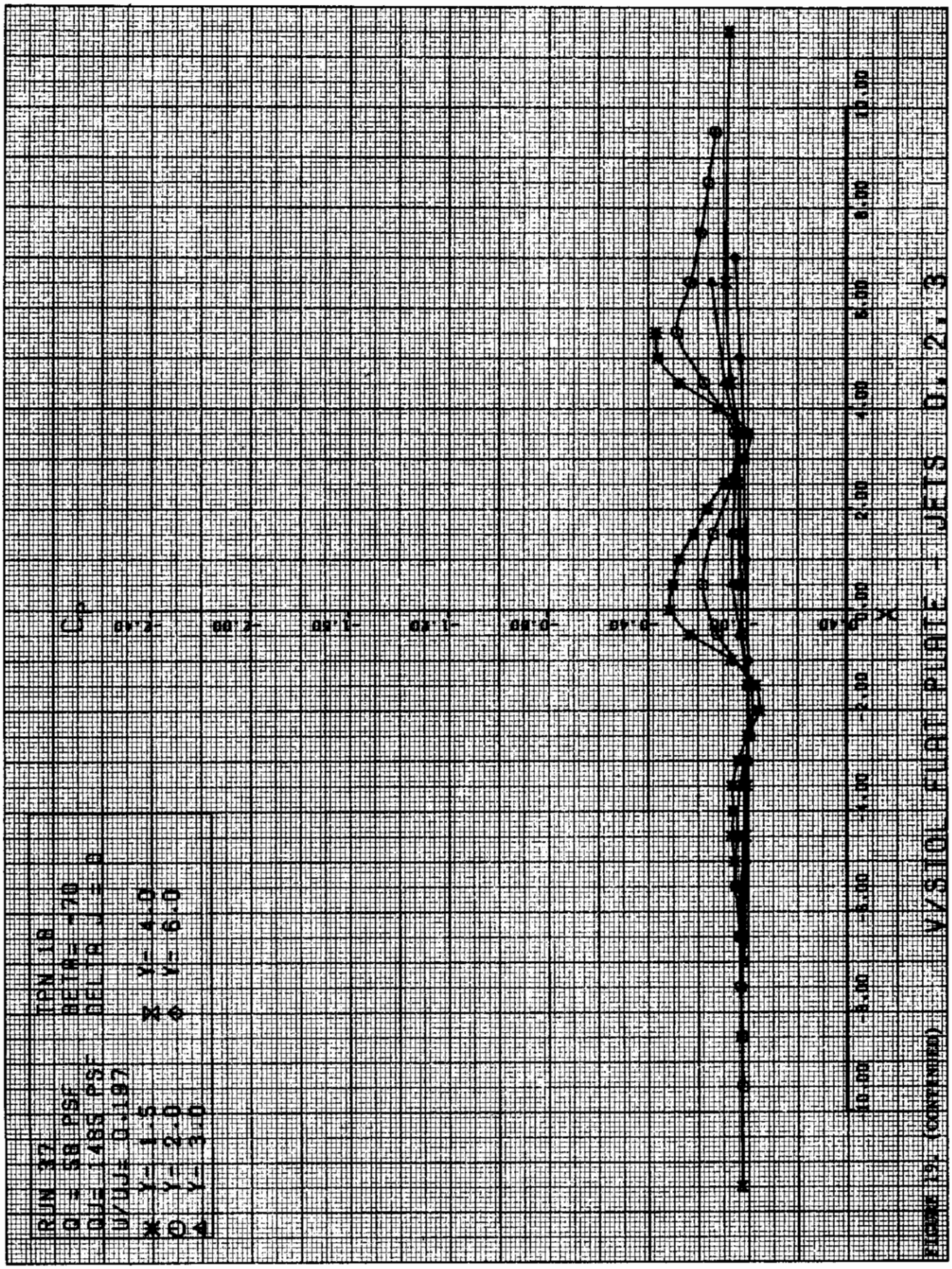

FIGURE 12. (CONTINUED)

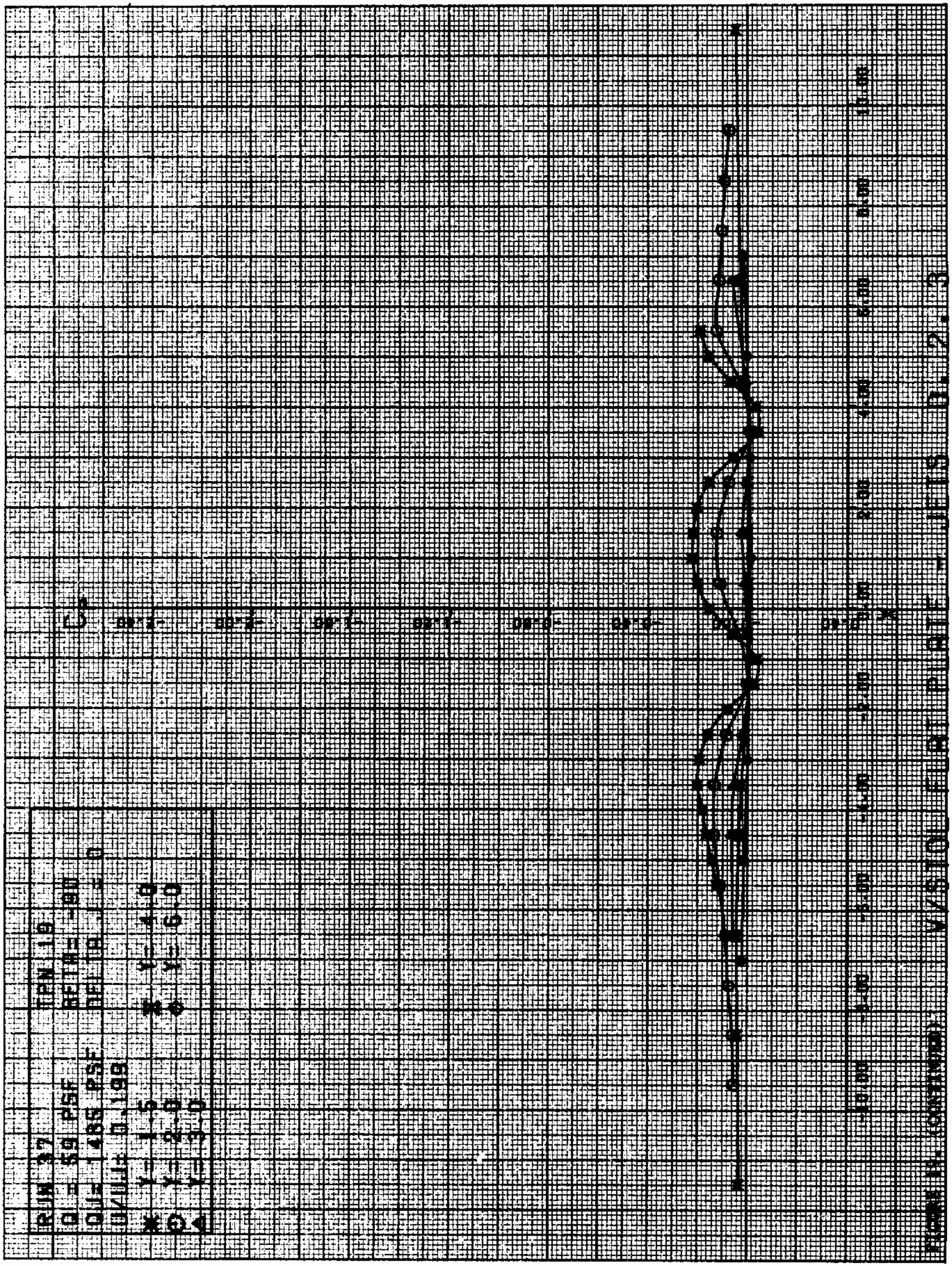

FIGURE 14. (CONTINUED)

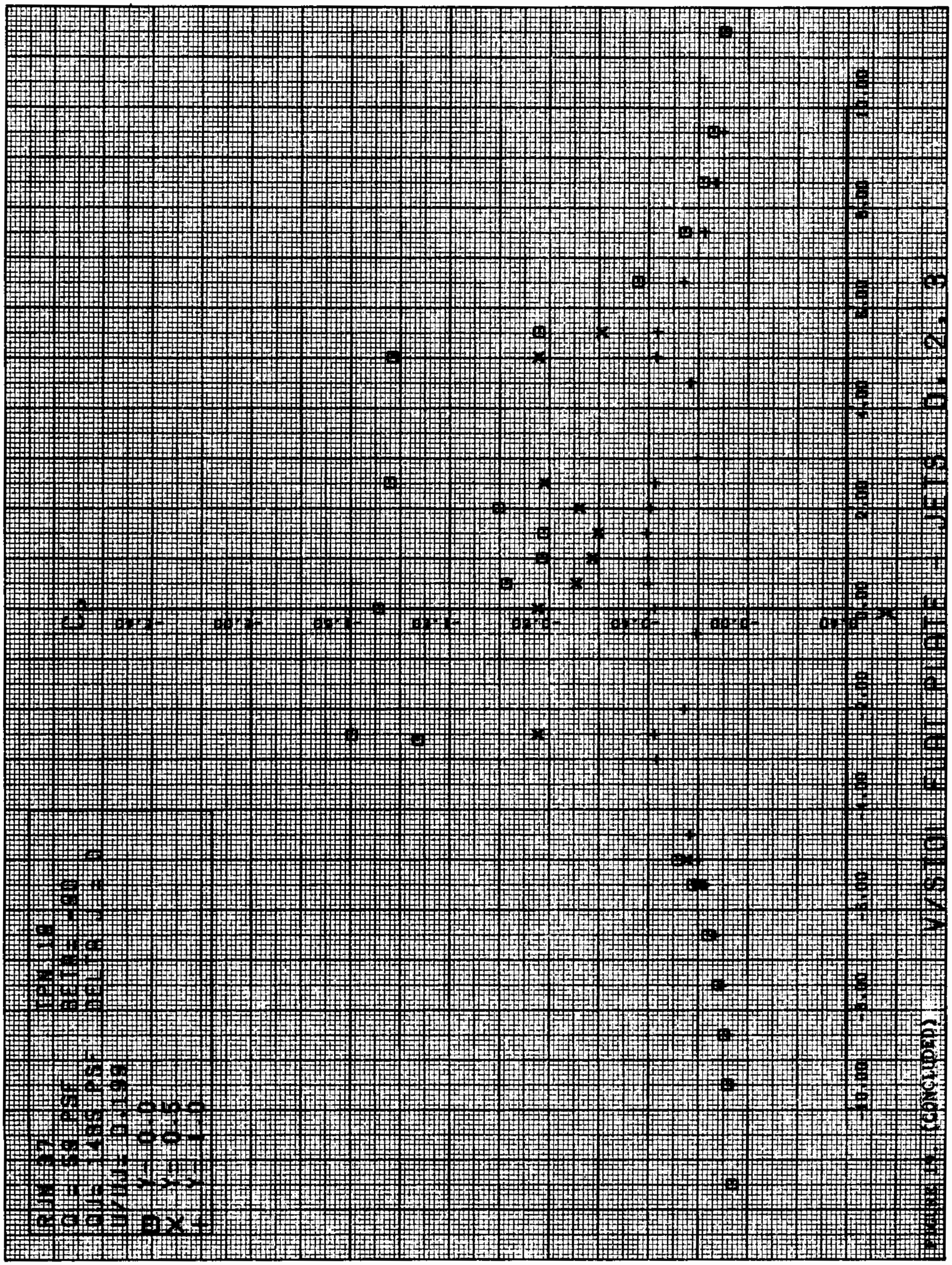

FIGURE 14. (CONCLUDED) V/STOL FLAT PLATE - JETS 0, 2, 3

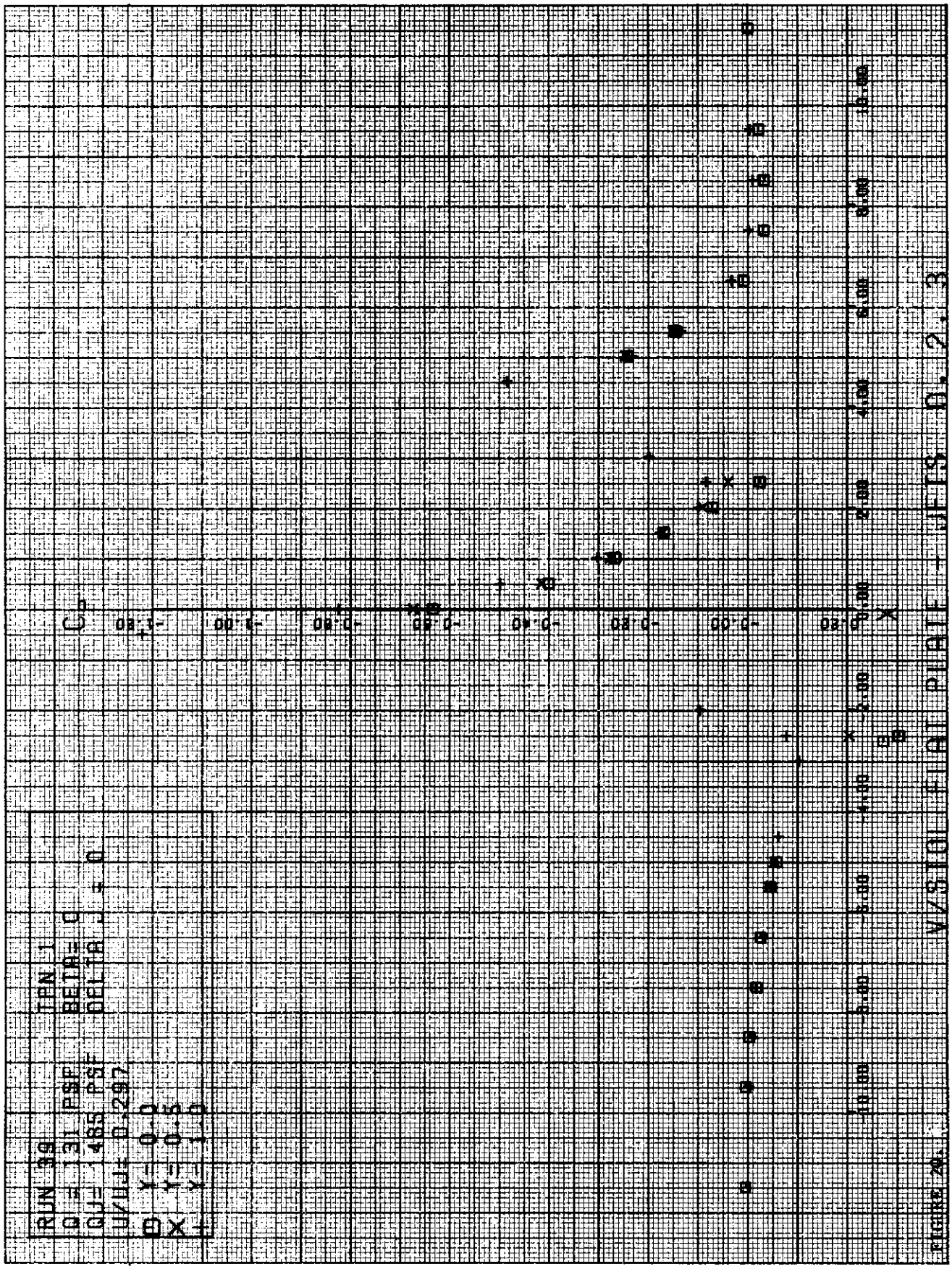

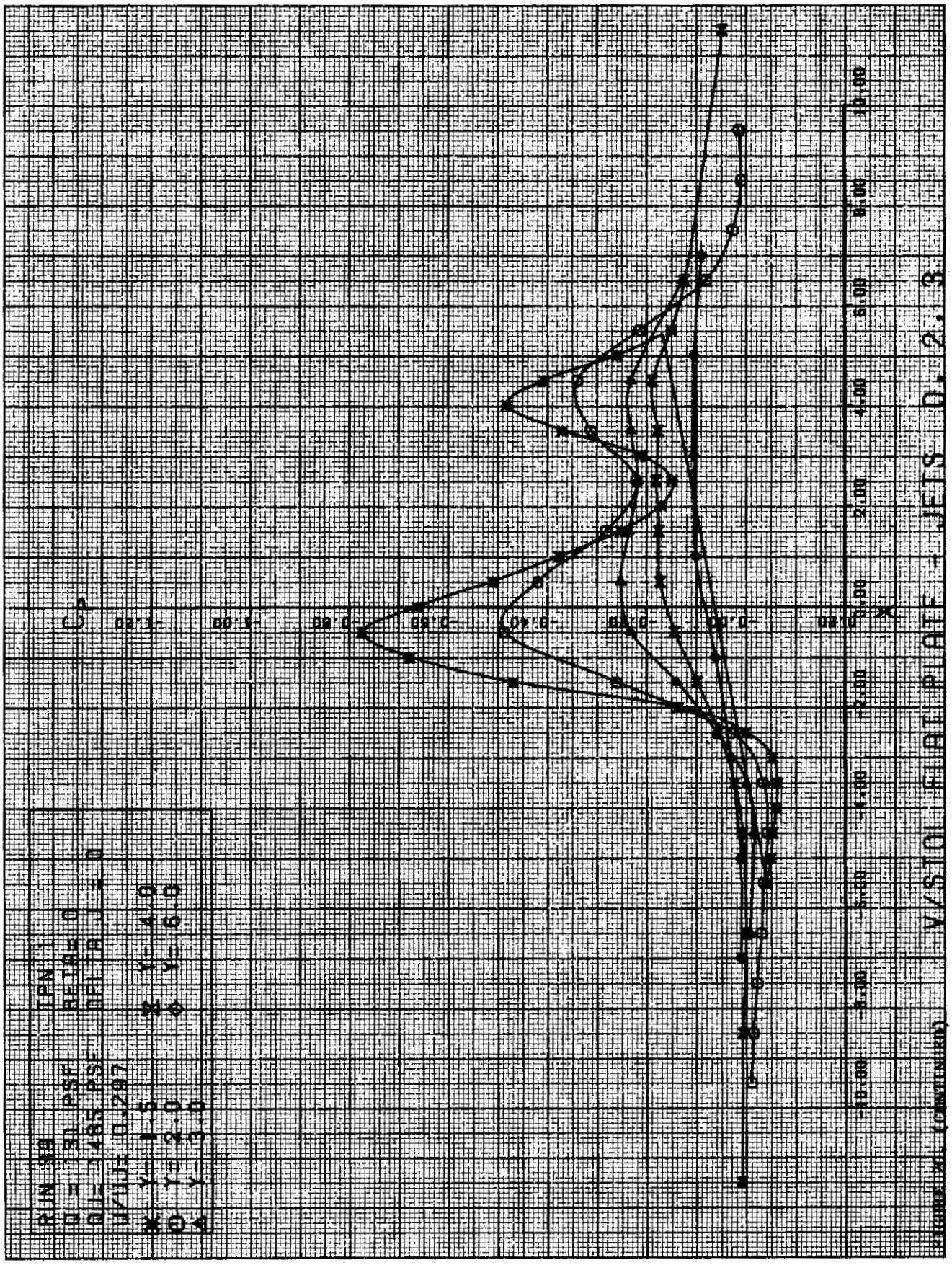

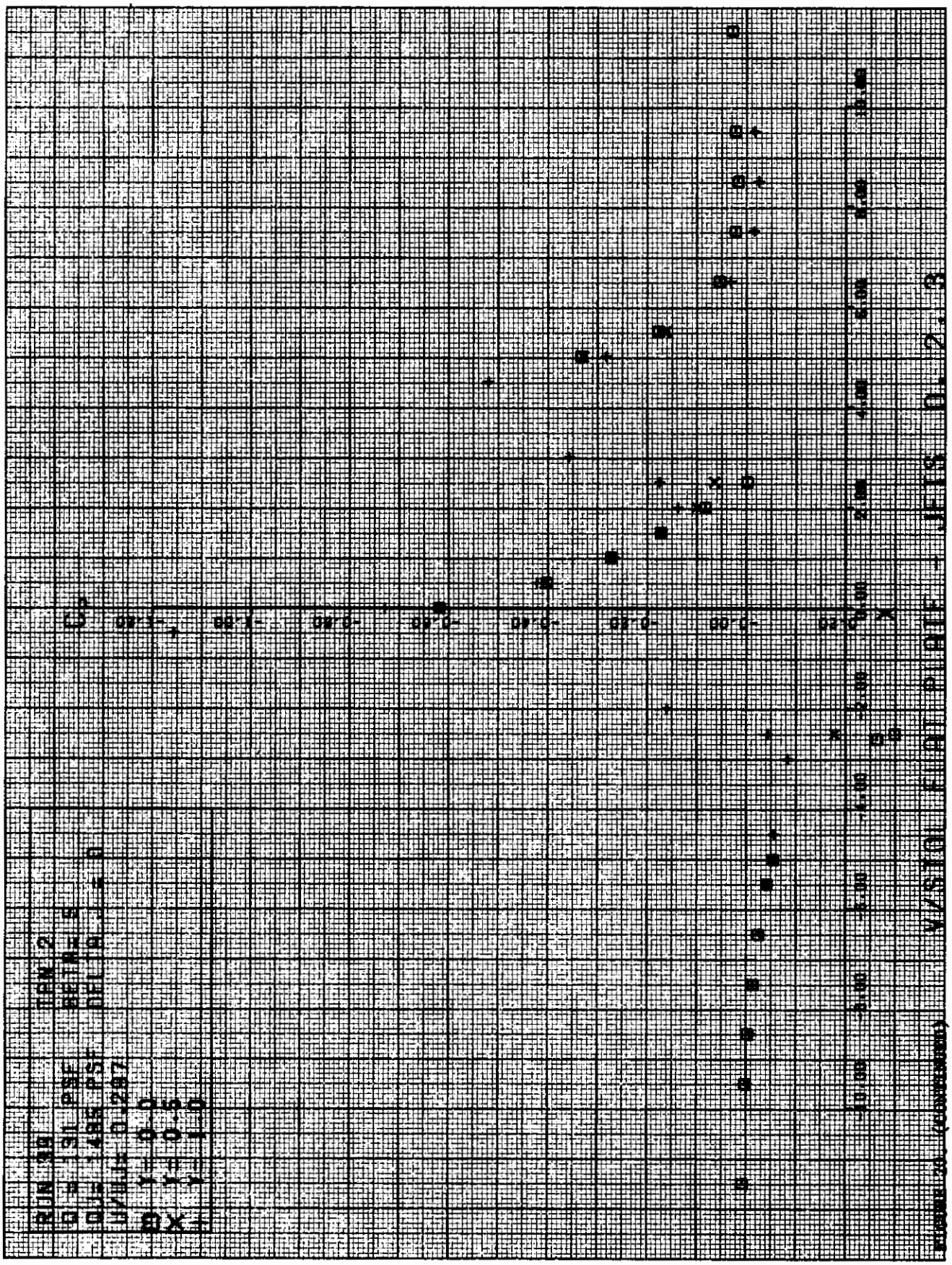

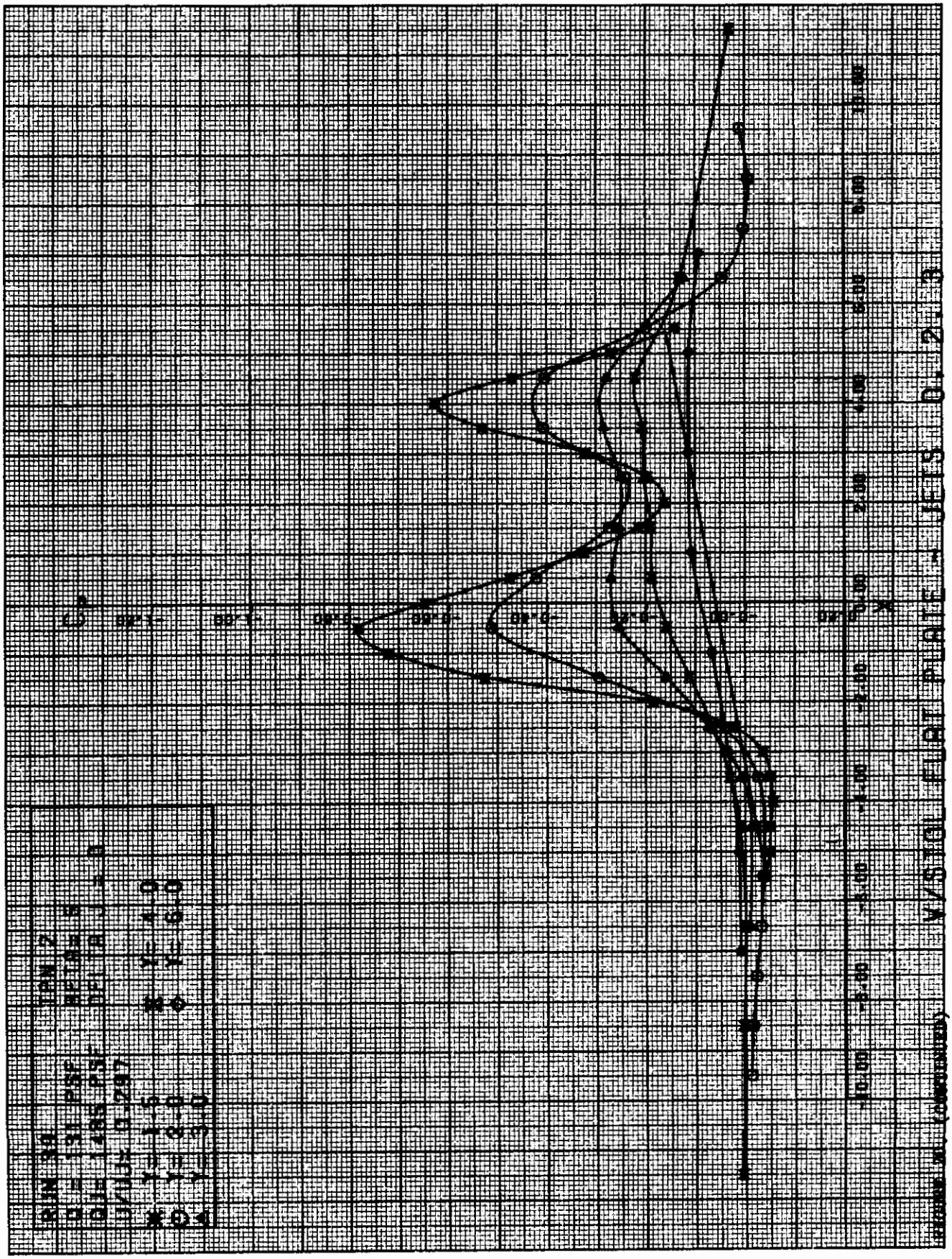

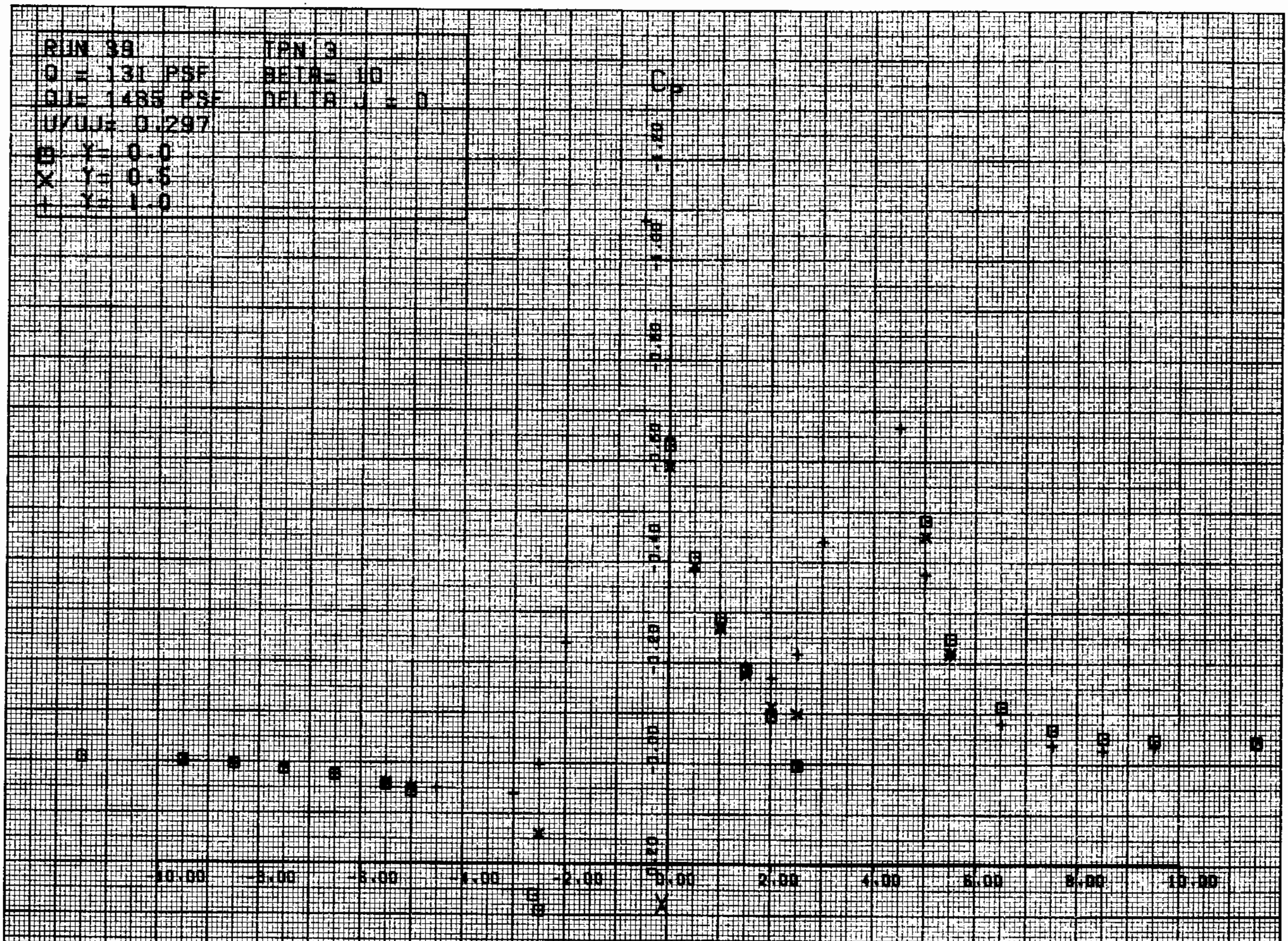

FIGURE 20. (CONTINUED) V/STOL FLAT PLATE - JETS 0, 2, 3

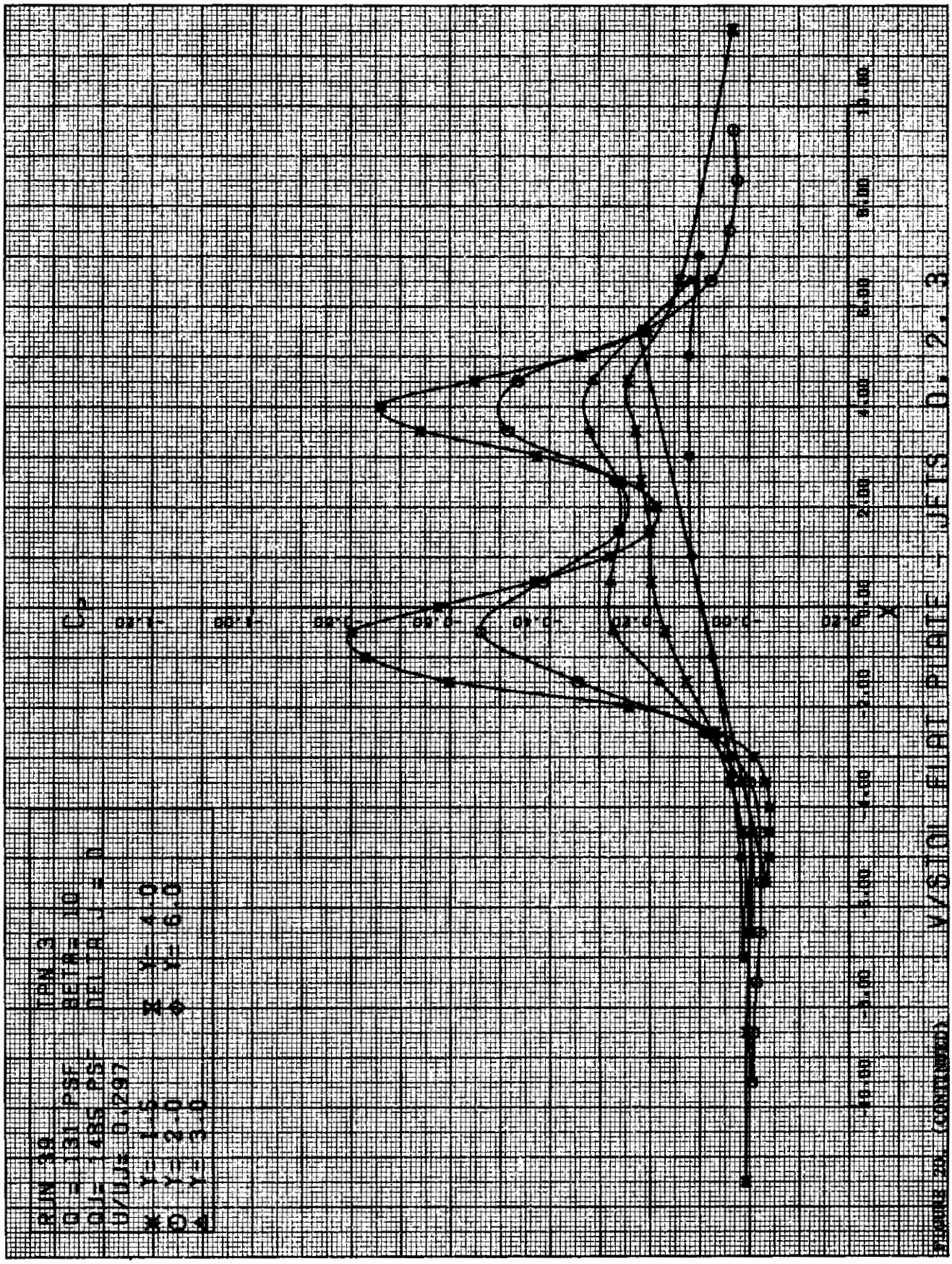

FIGURE 29. (CONTINUED)

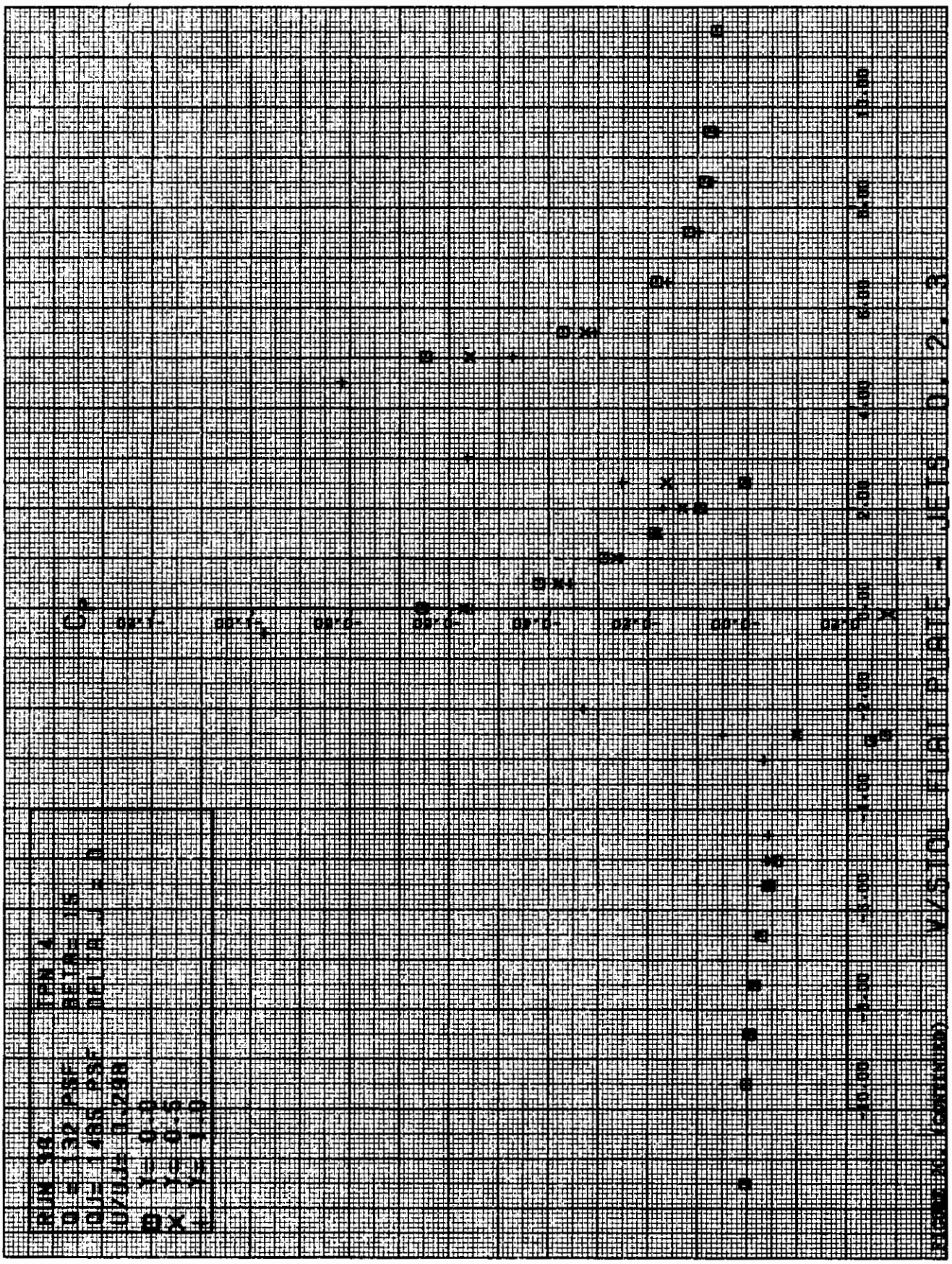

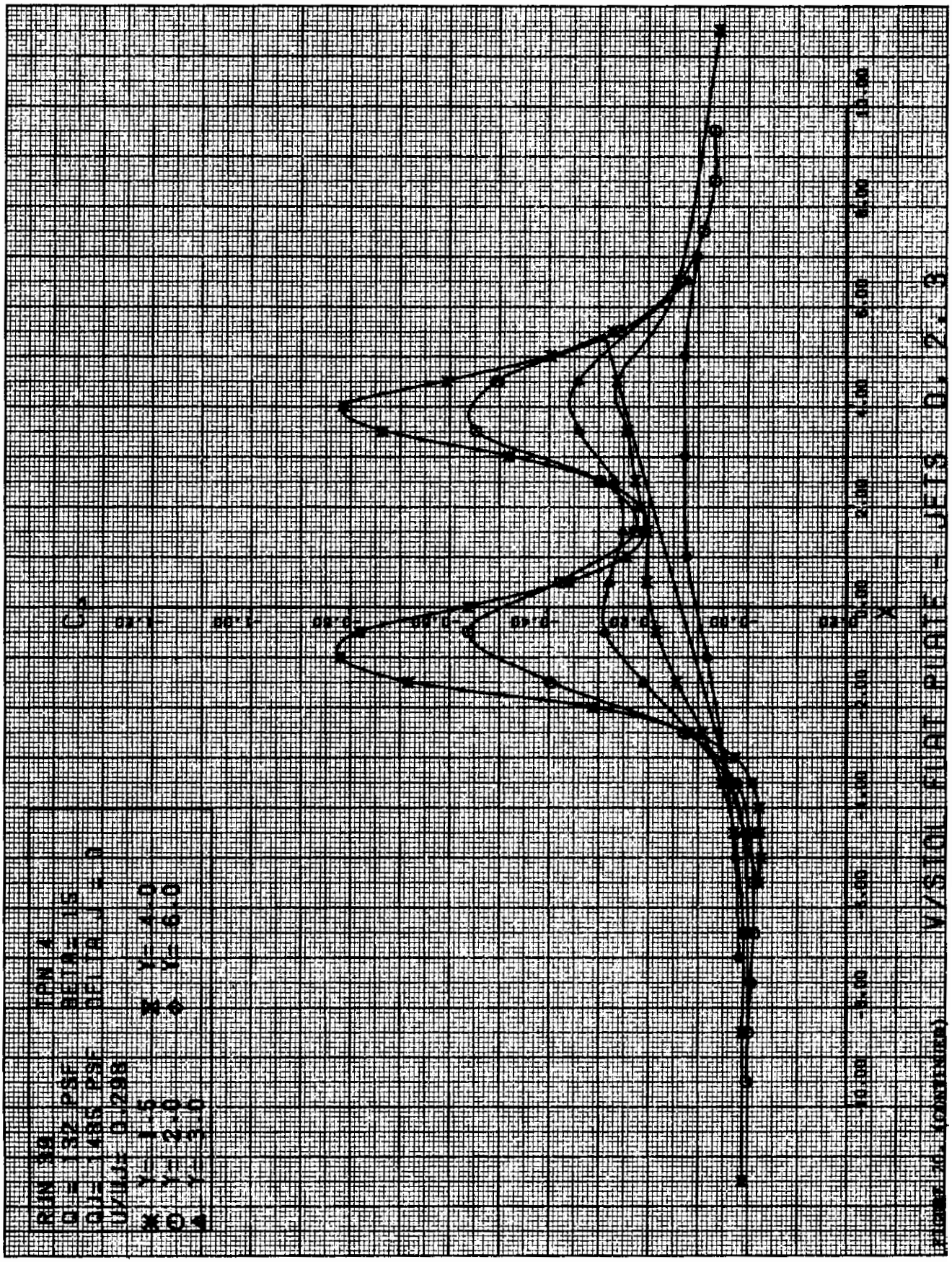

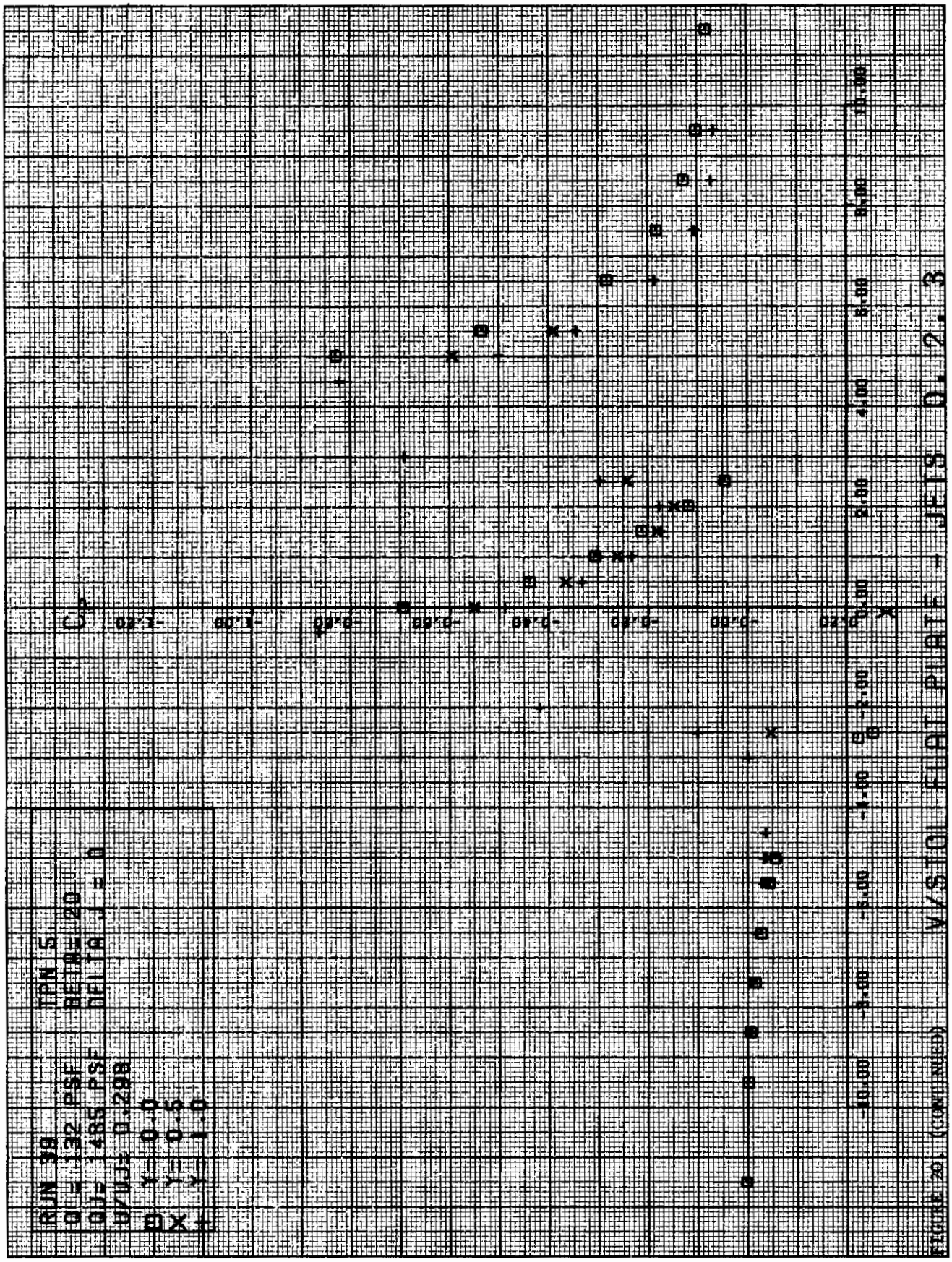

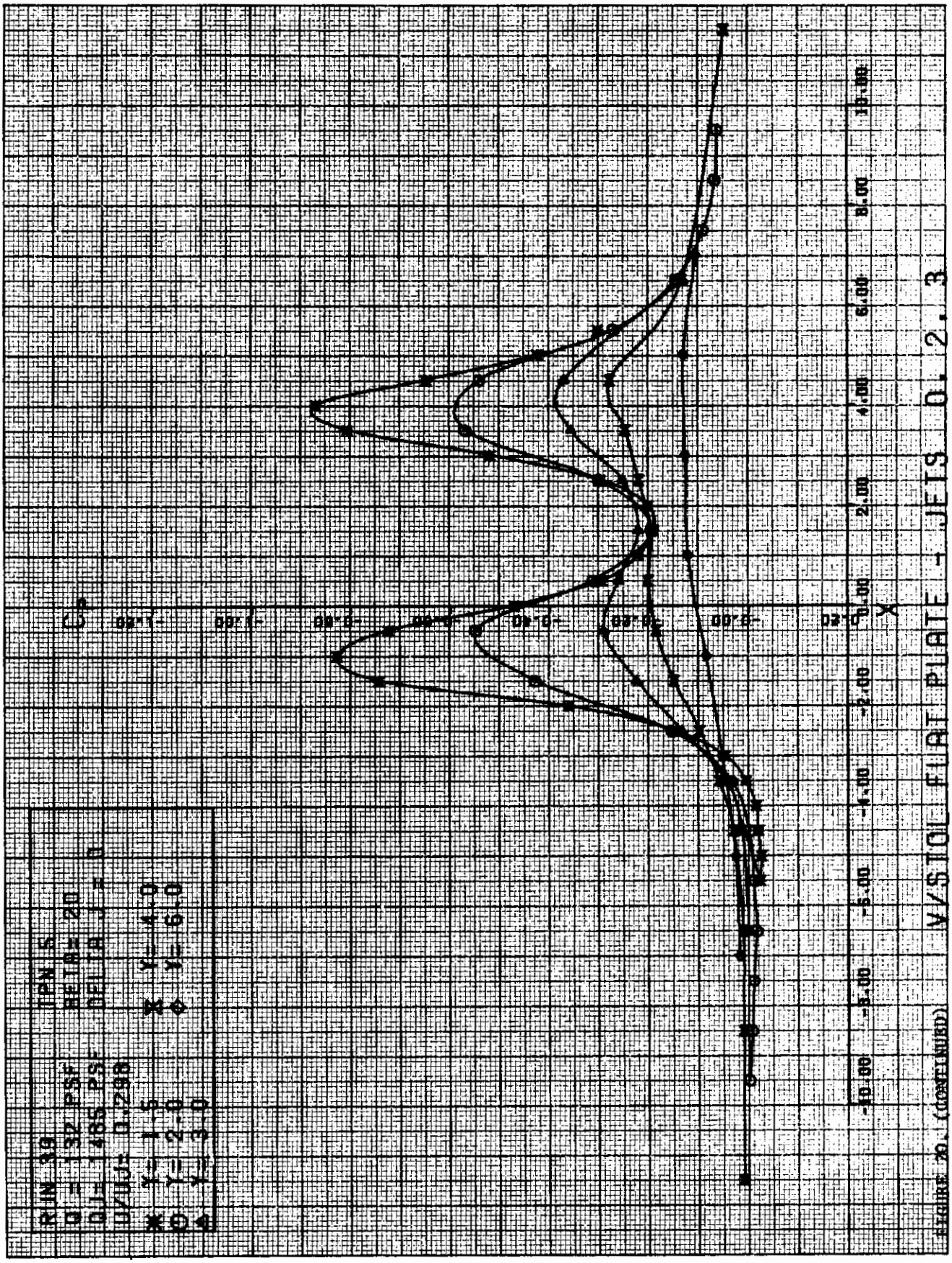

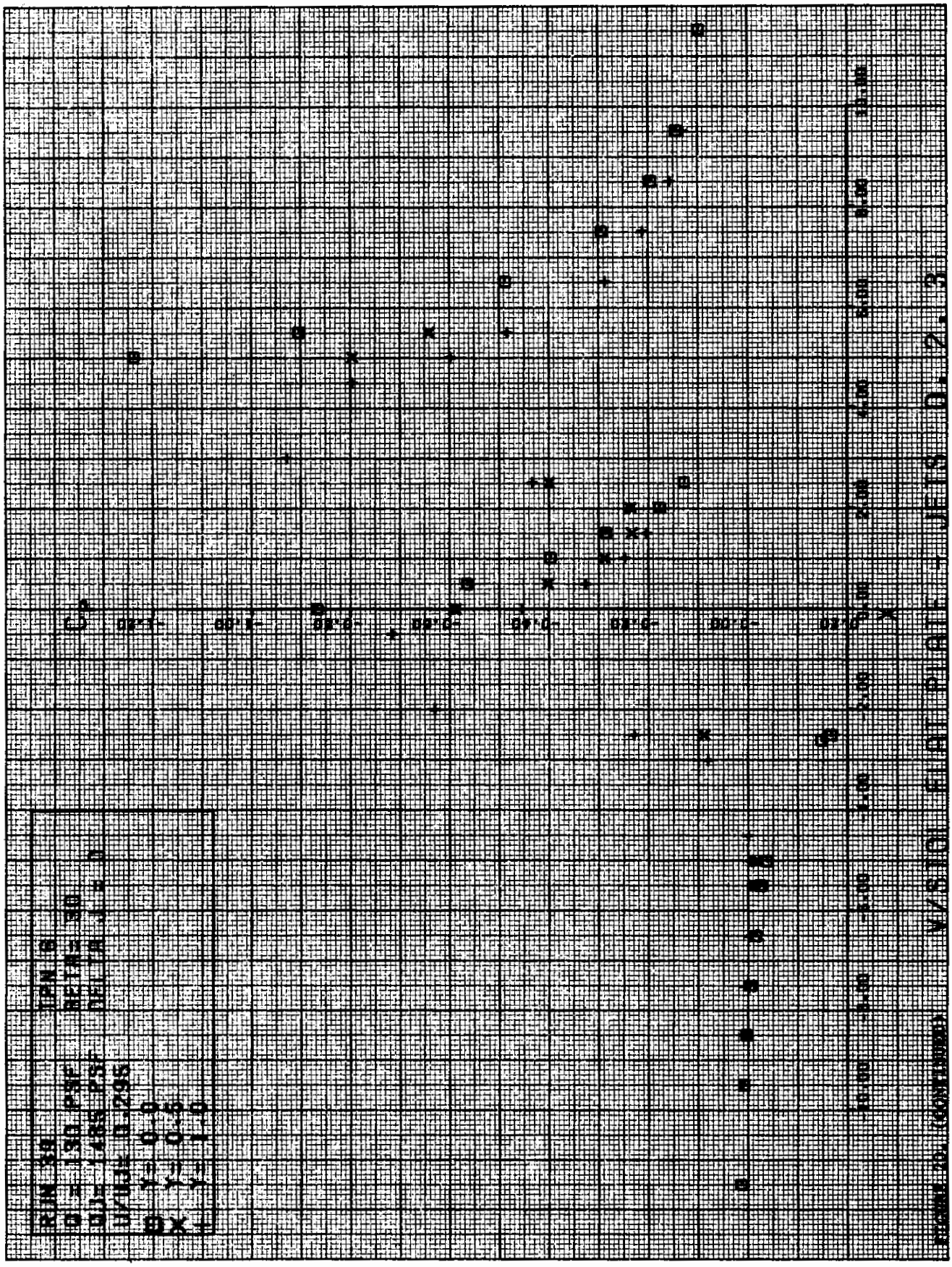

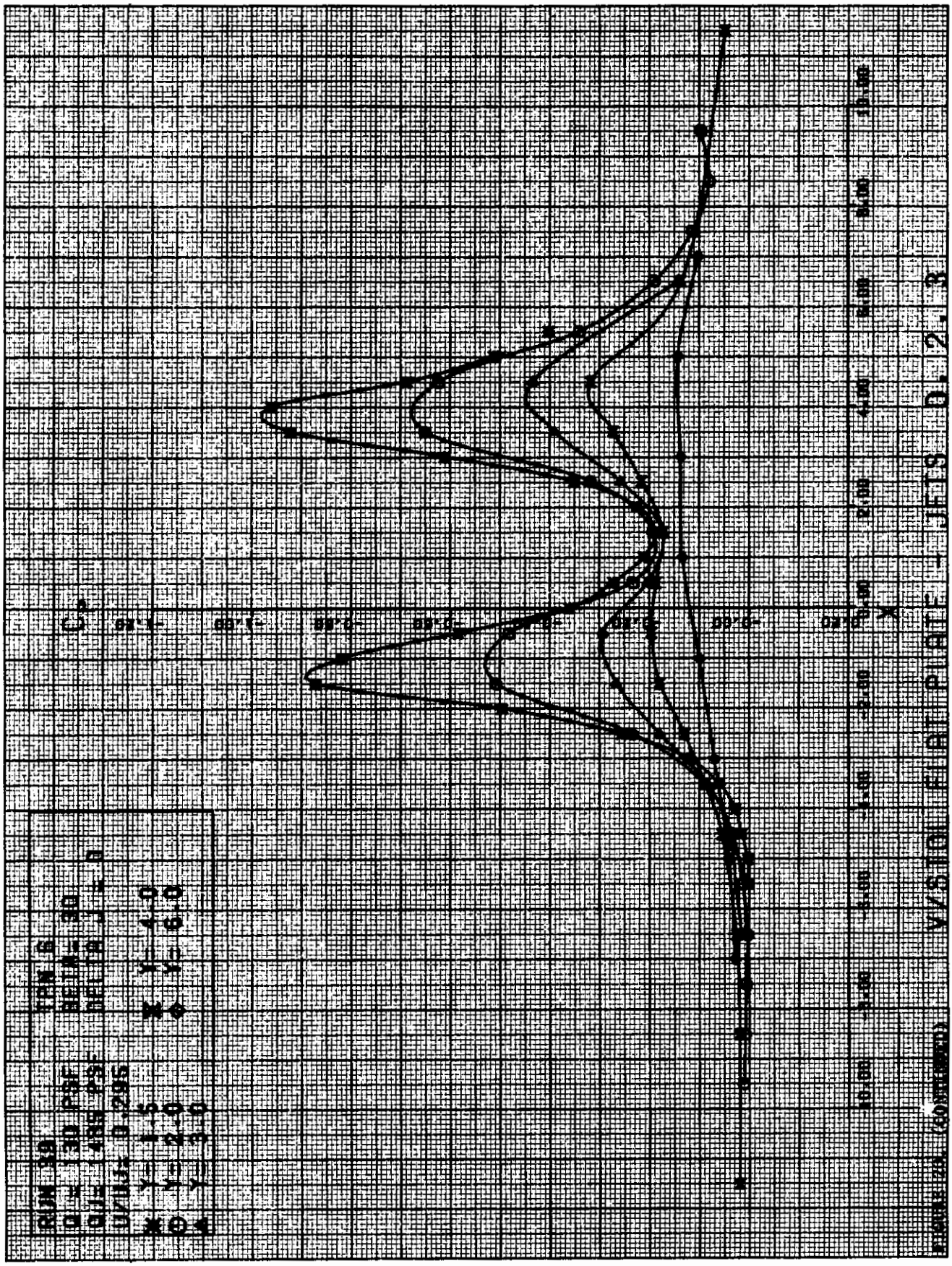

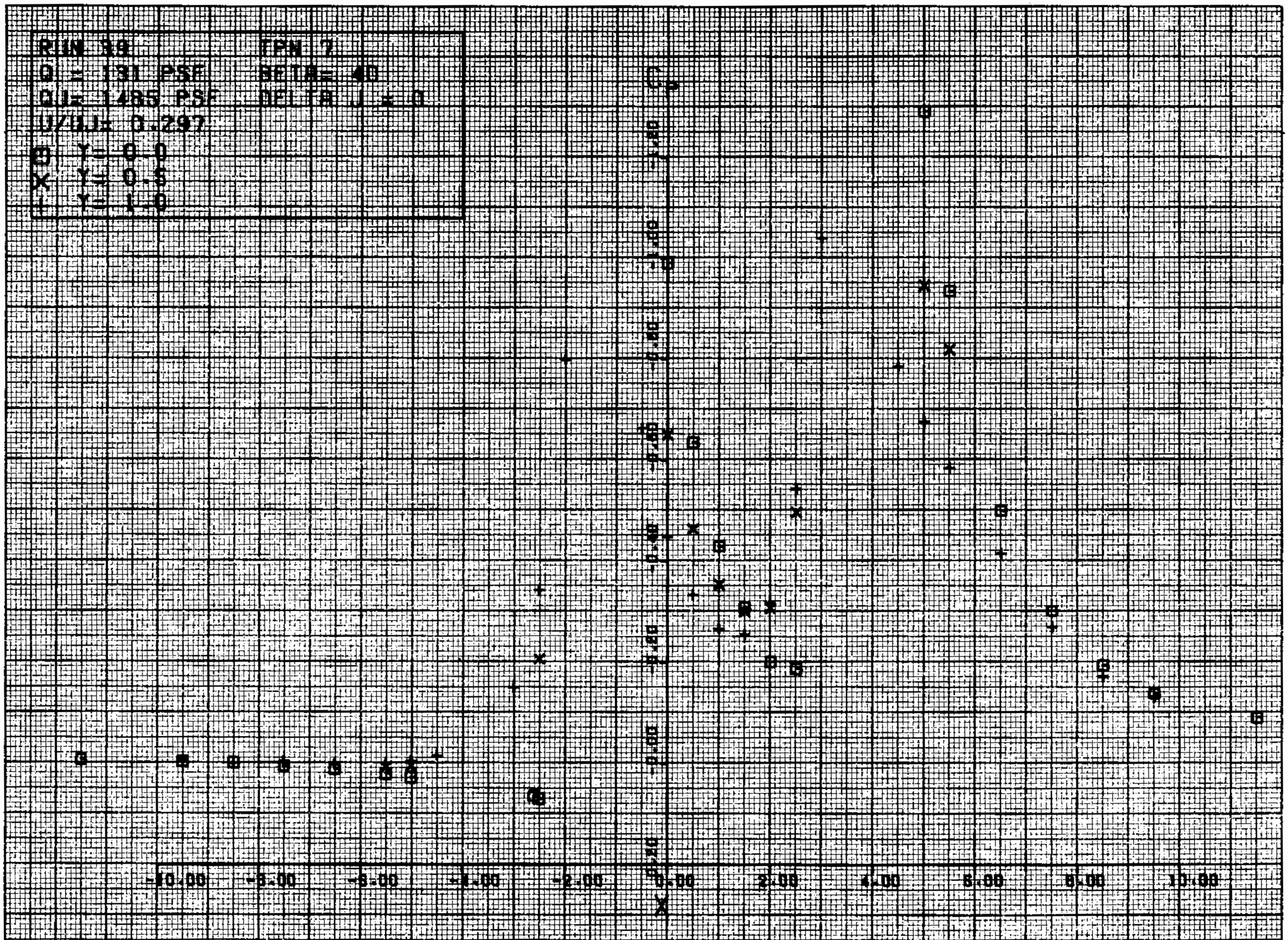

FIGURE [illegible] (CONTINUED) V/STOL FLAT PLATE - JETS 0, 2, 3

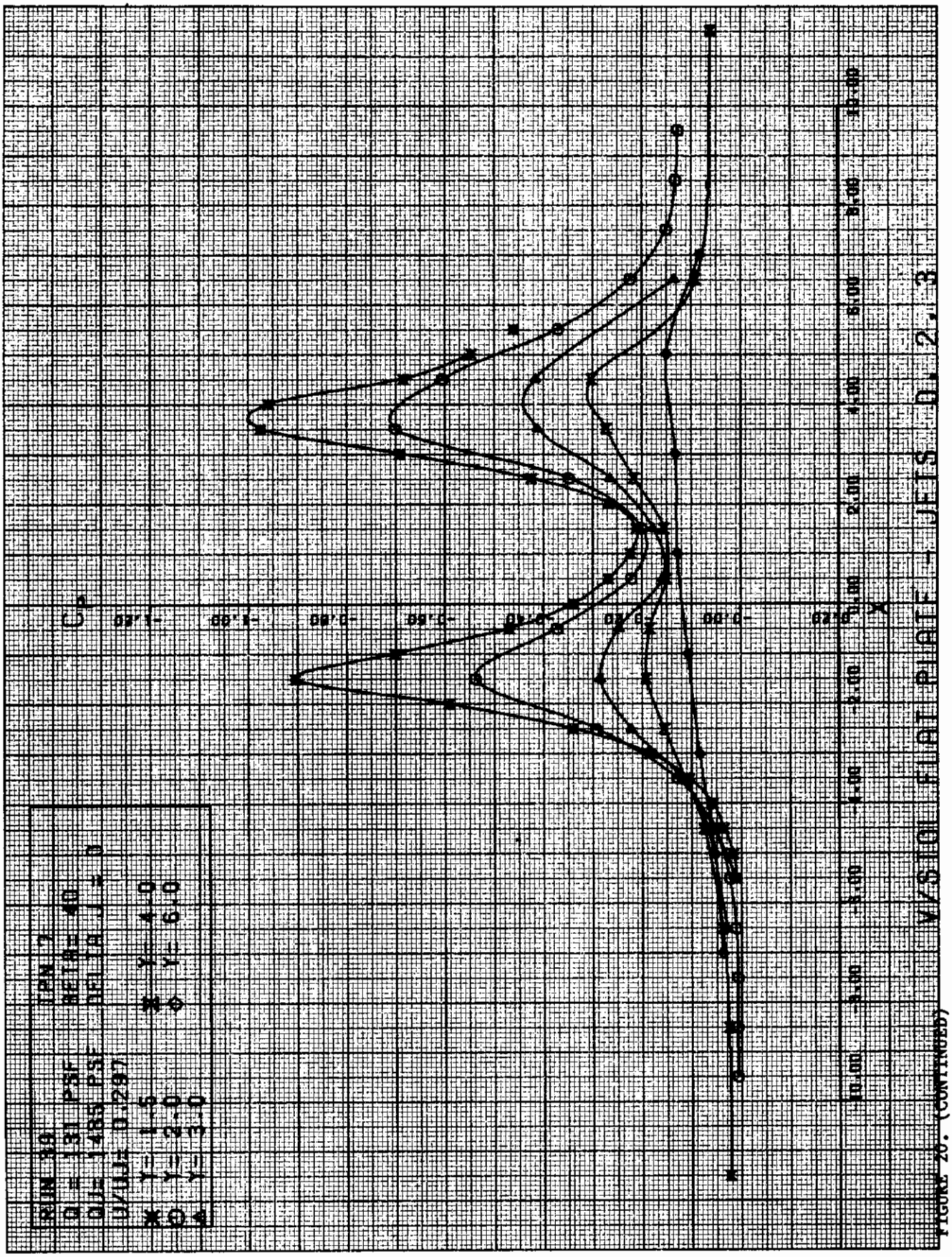

FIGURE 20. (CONTINUED)

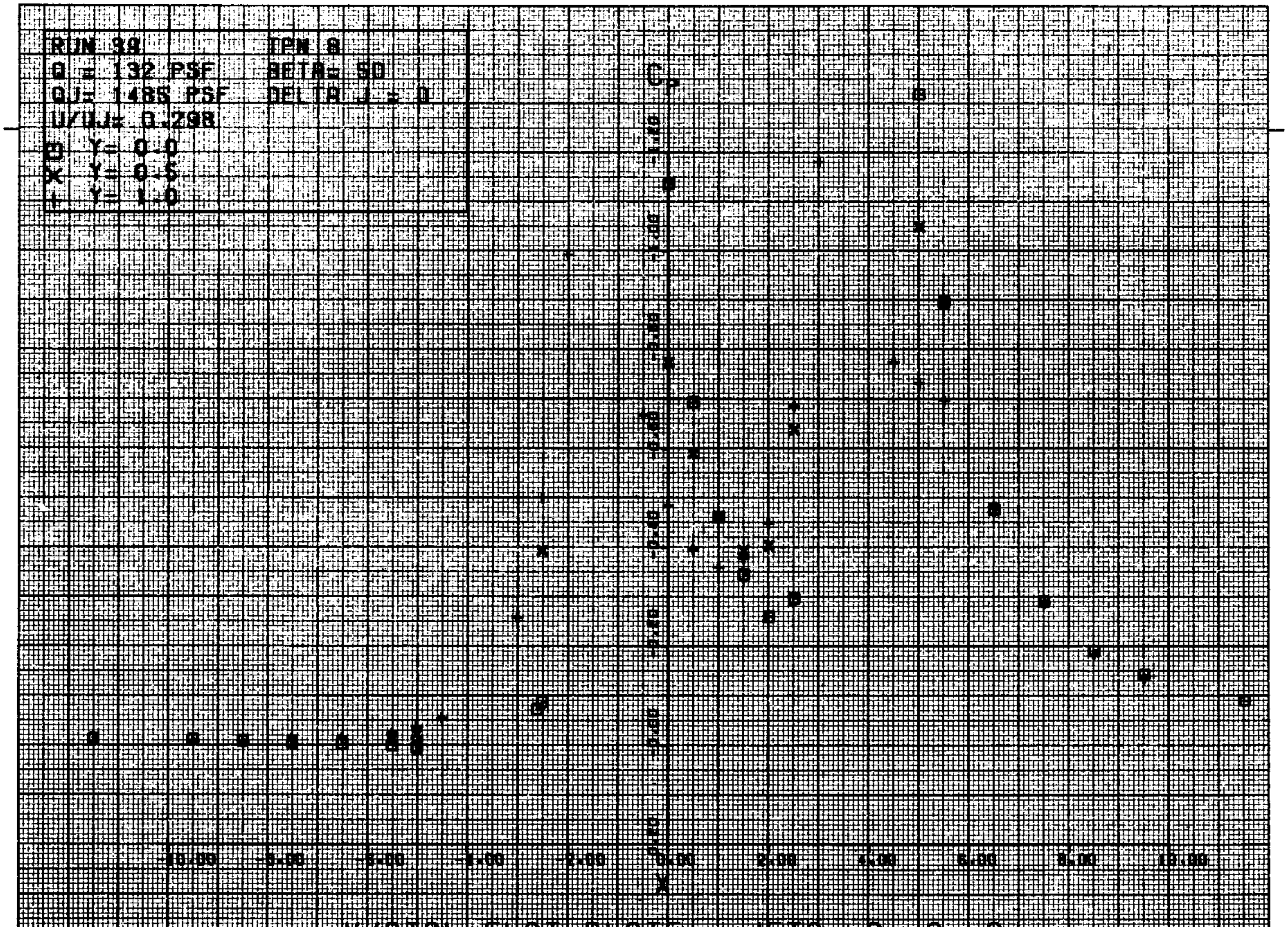

FIGURE 30. (CONTINUED) V/STOL FLAT PLATE - JETS 0. 2. 3

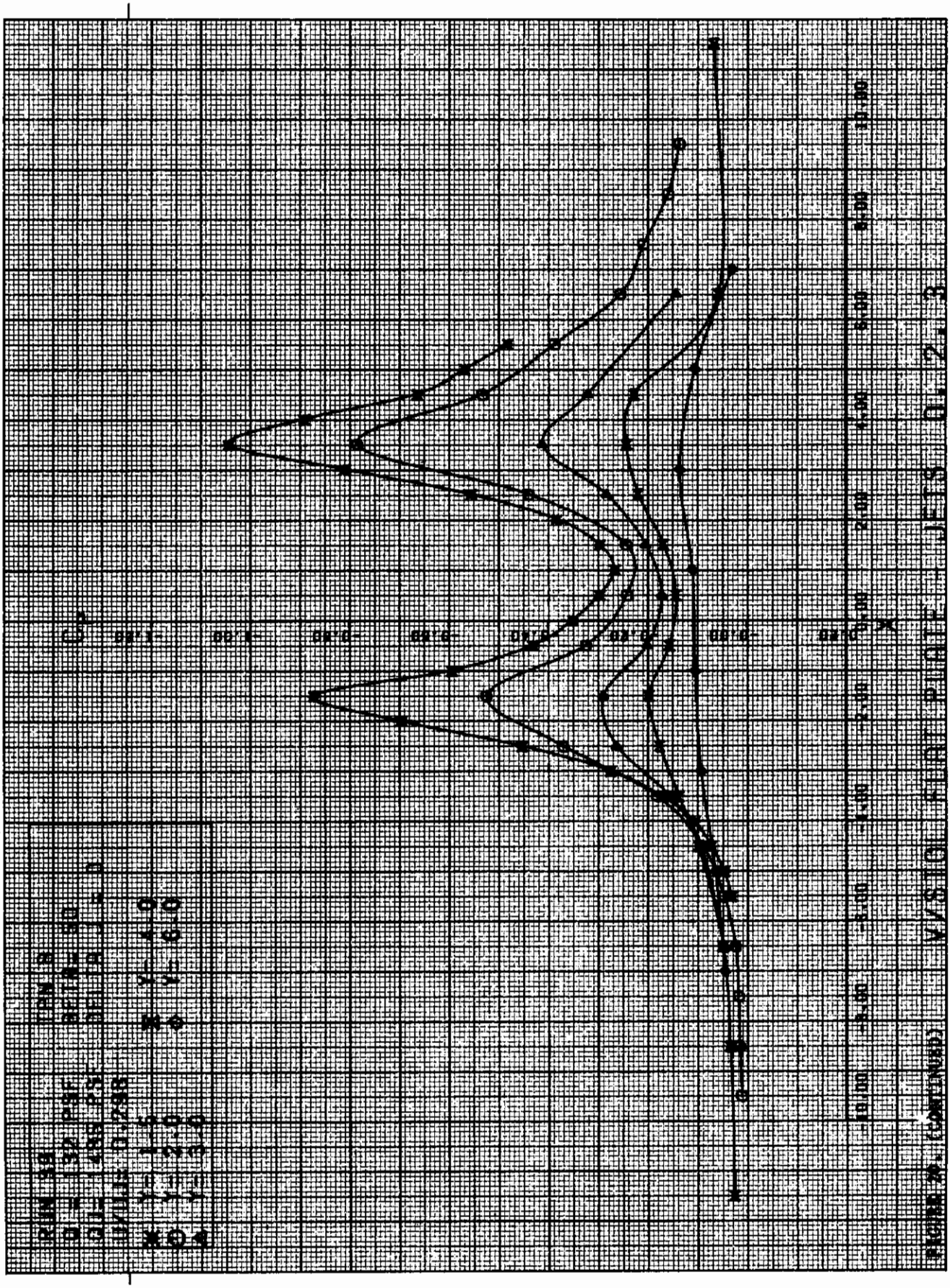

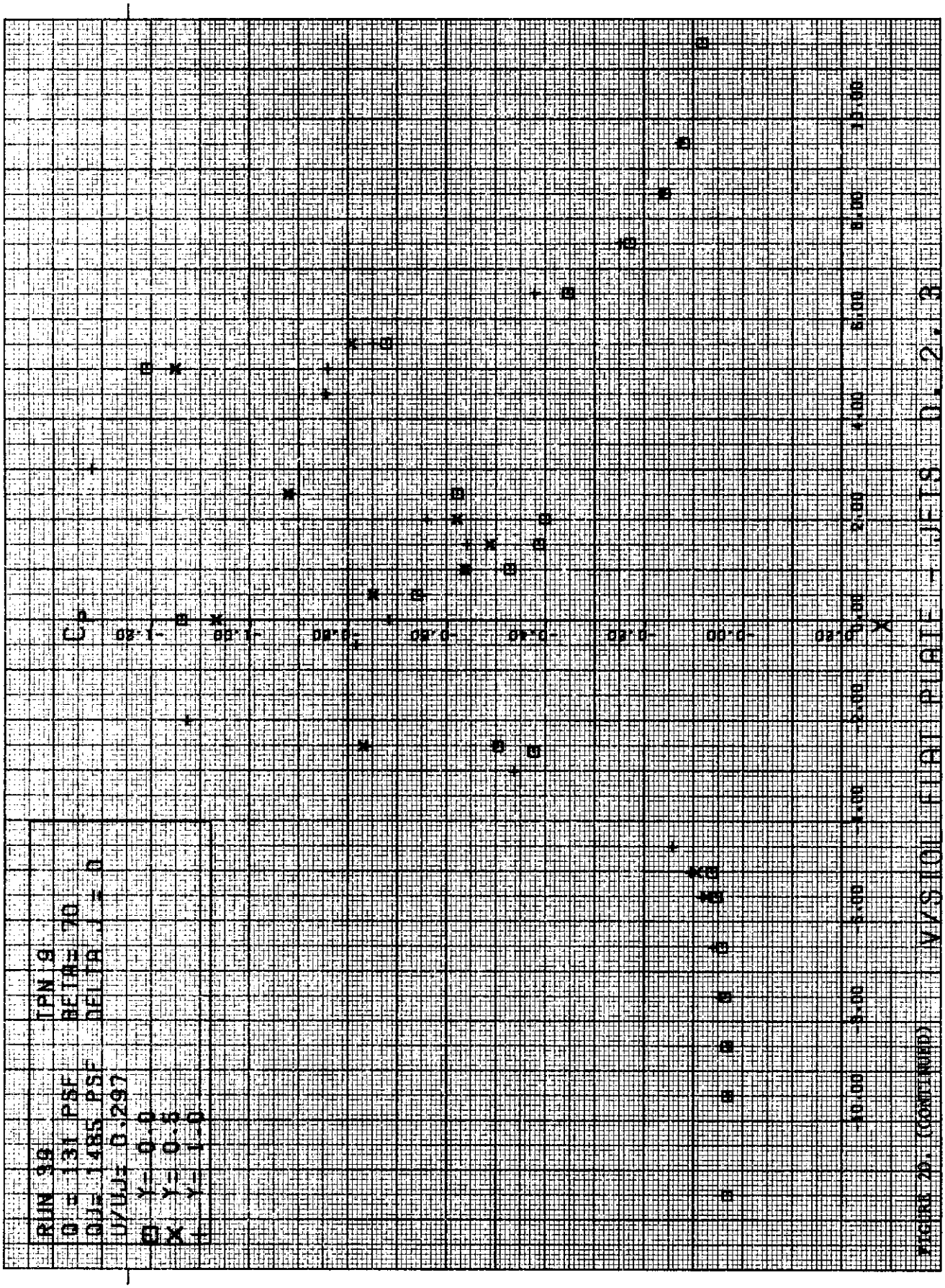

FIGURE 20. (CONTINUED)

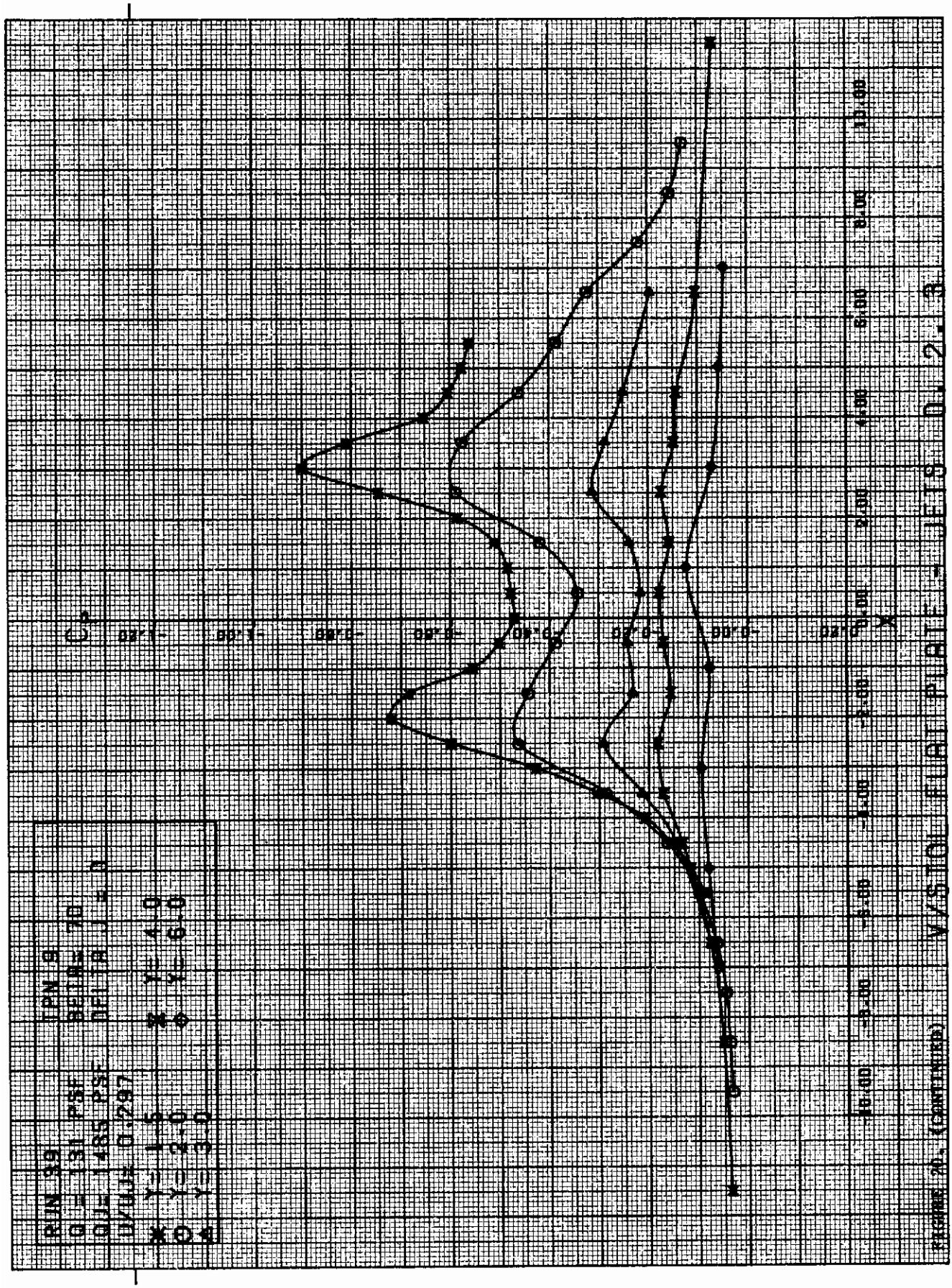

FIGURE 20. (CONTINUED)

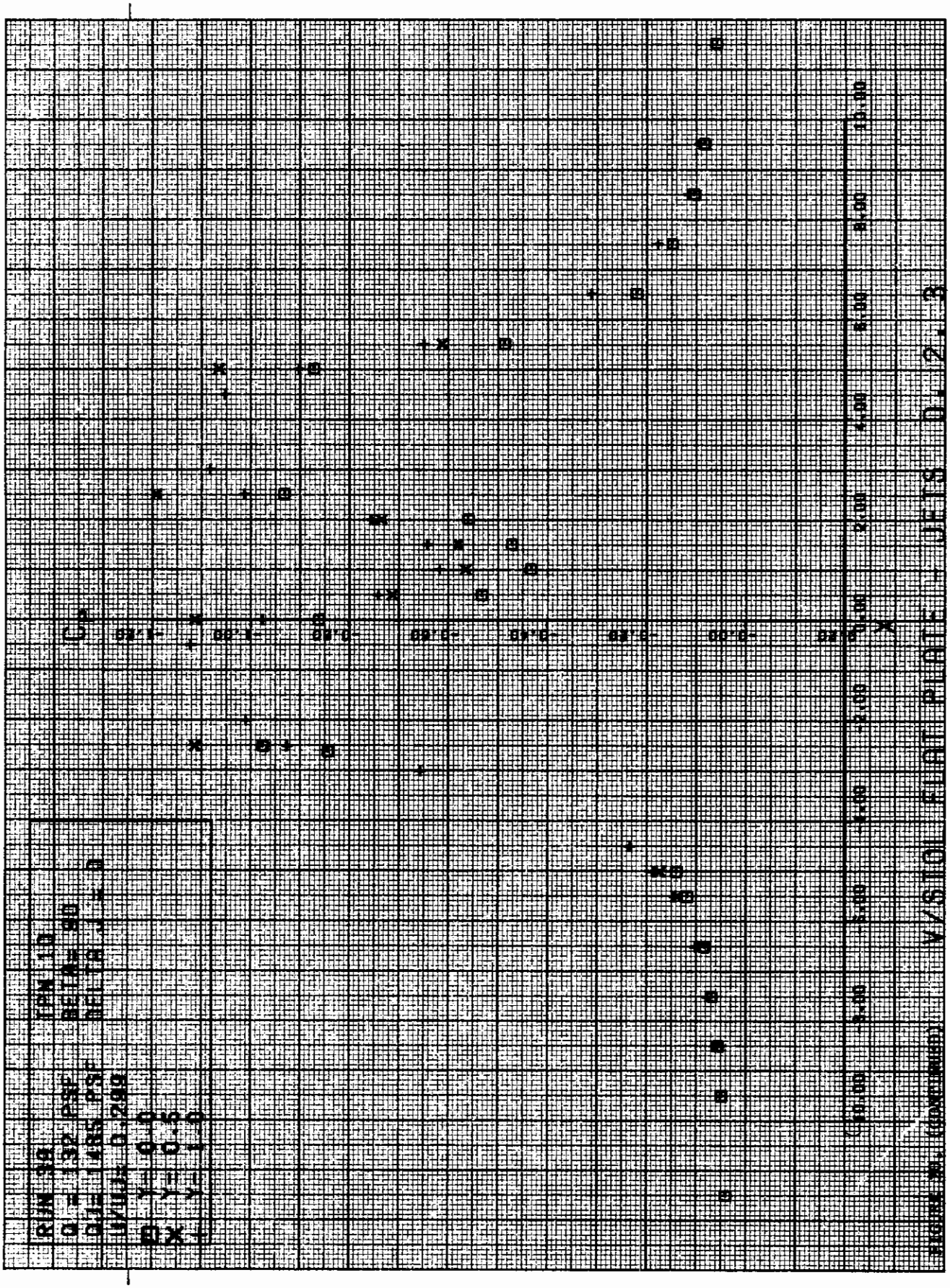

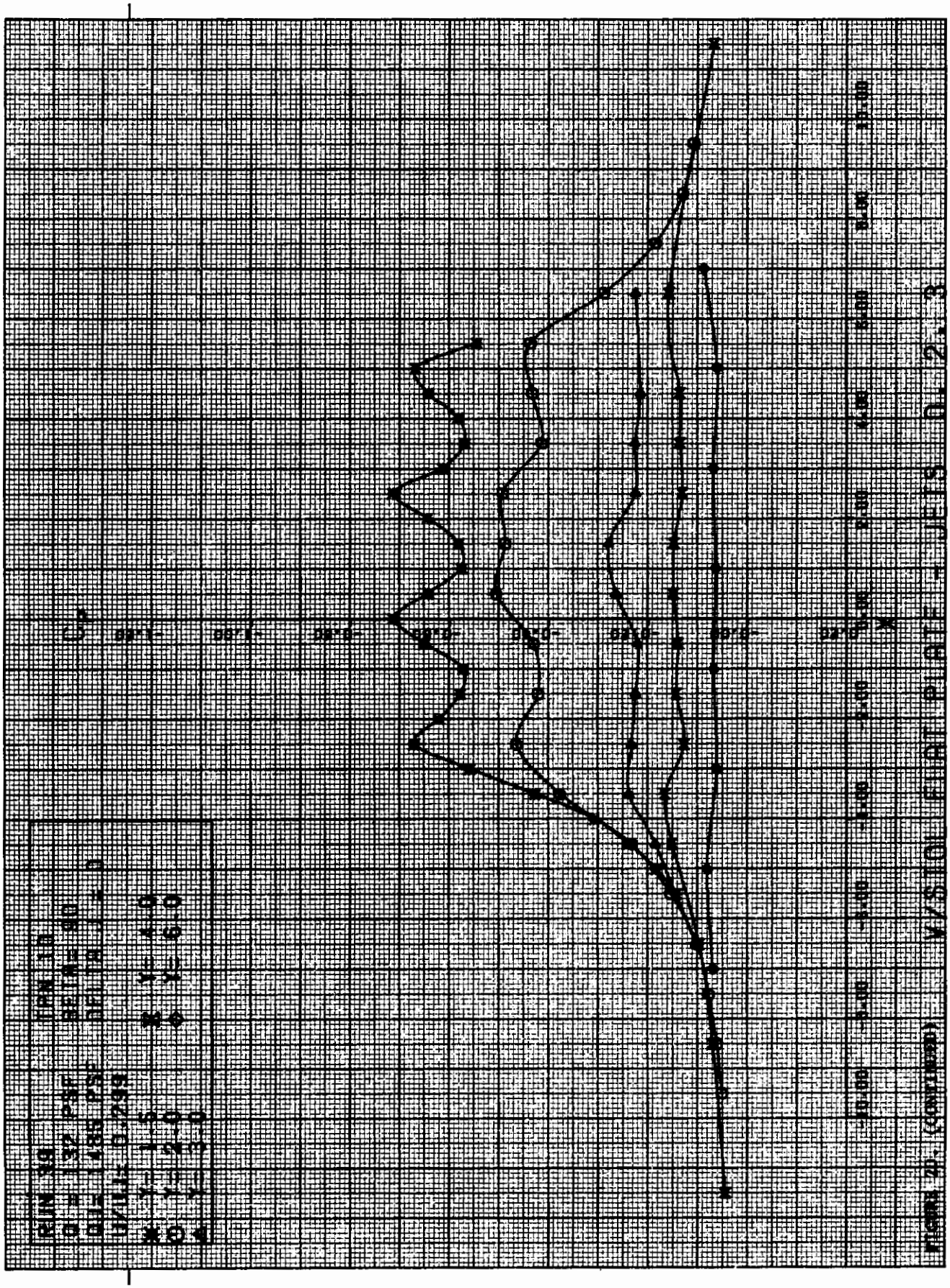

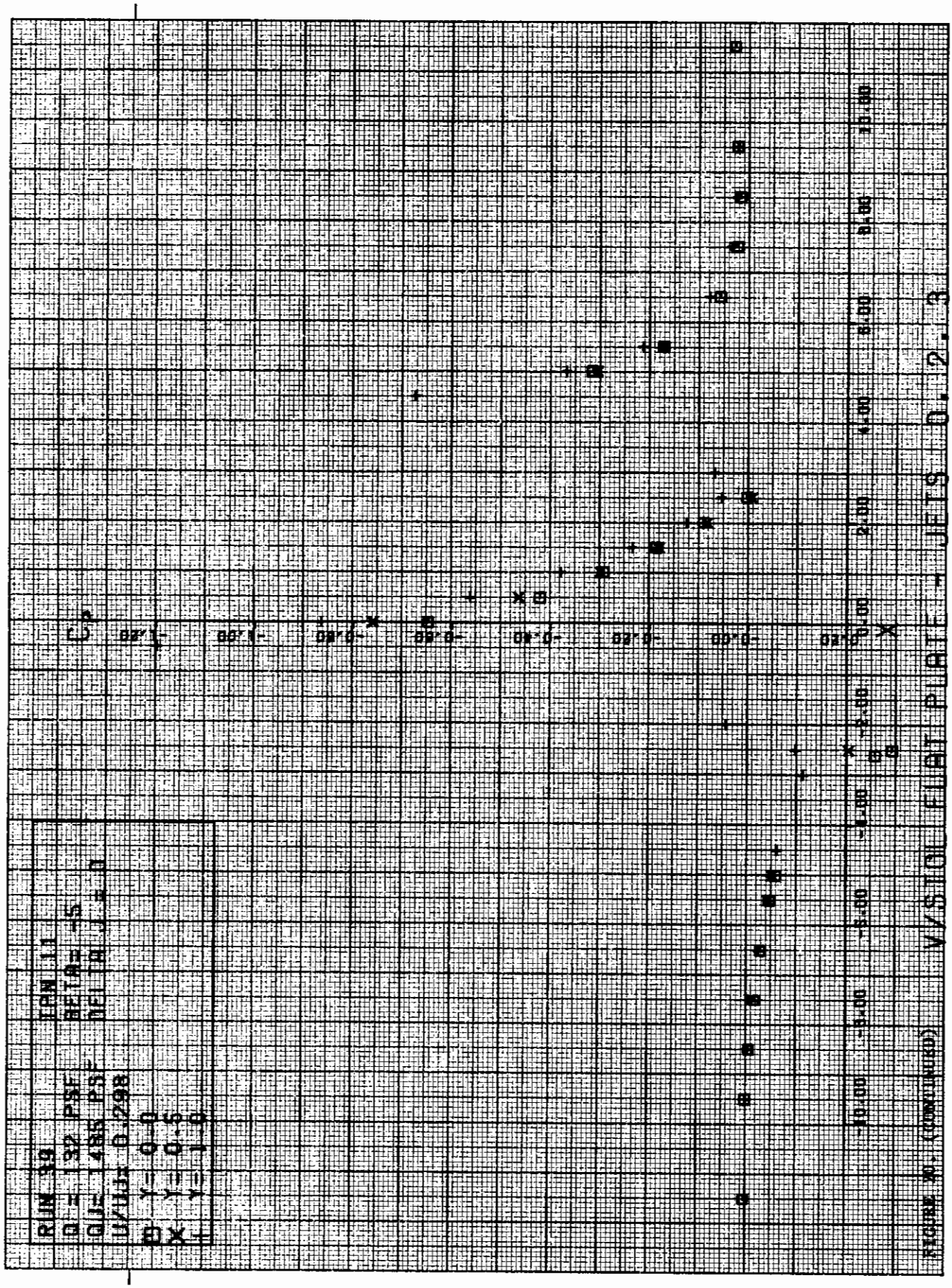

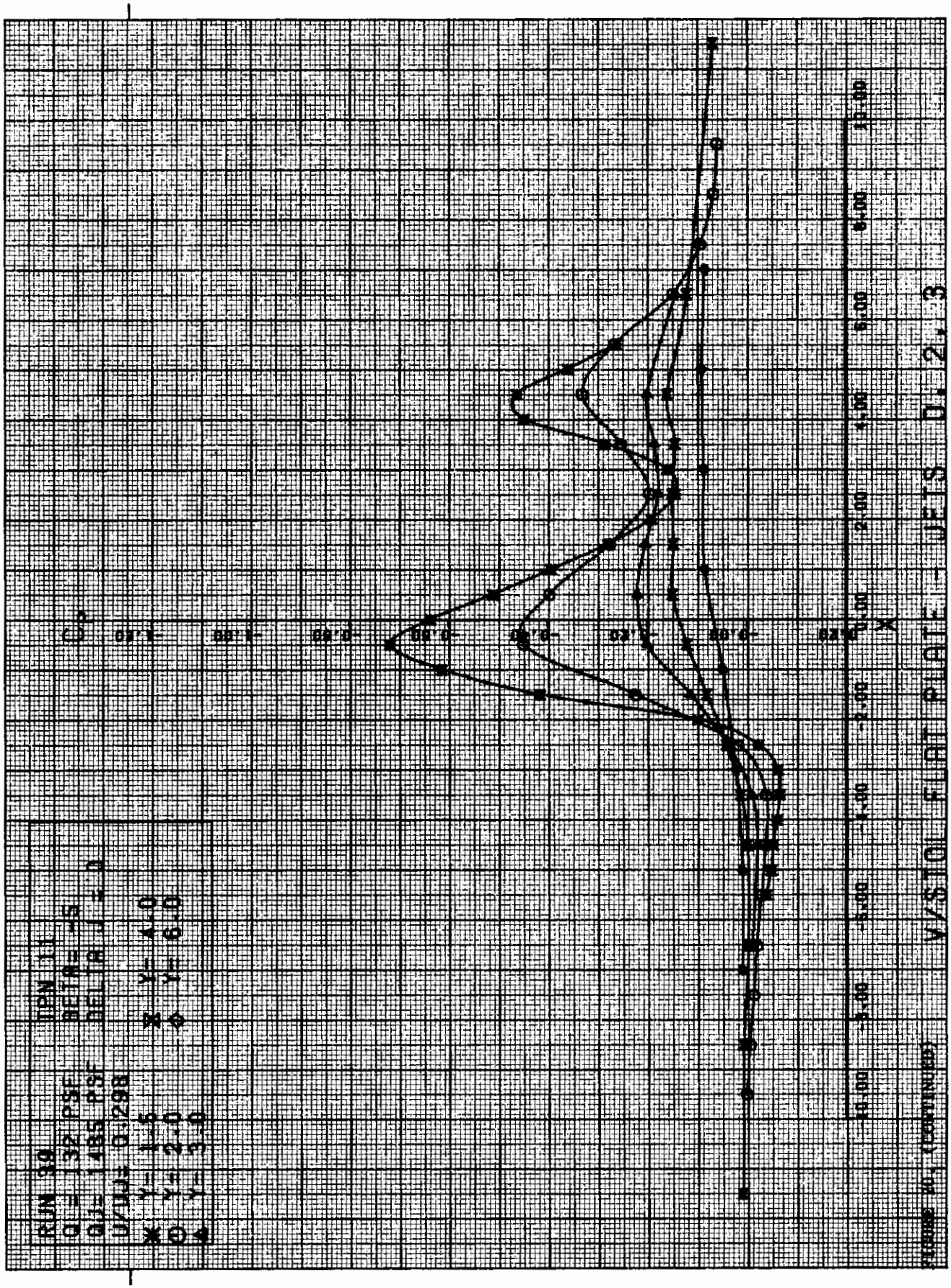

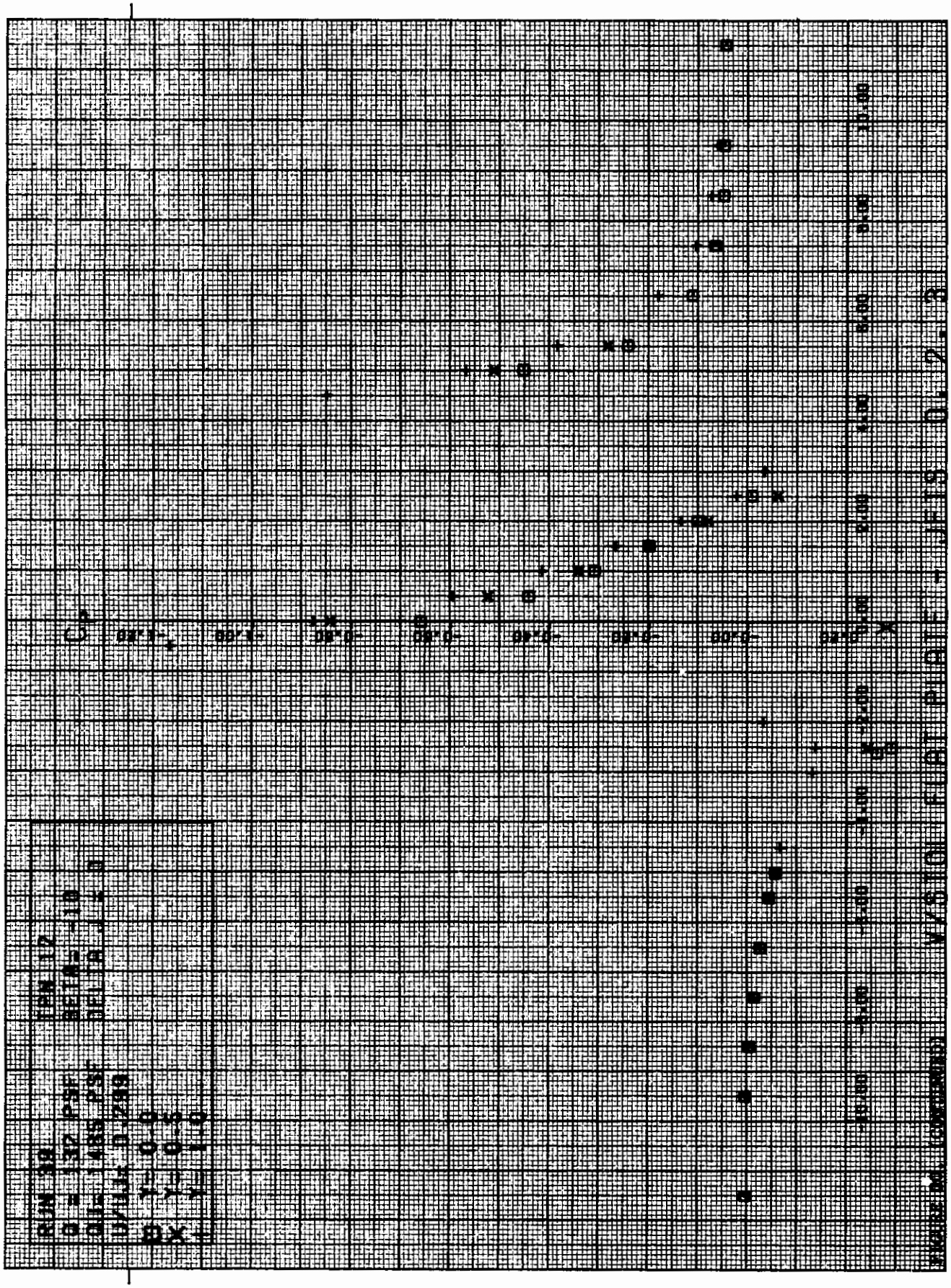

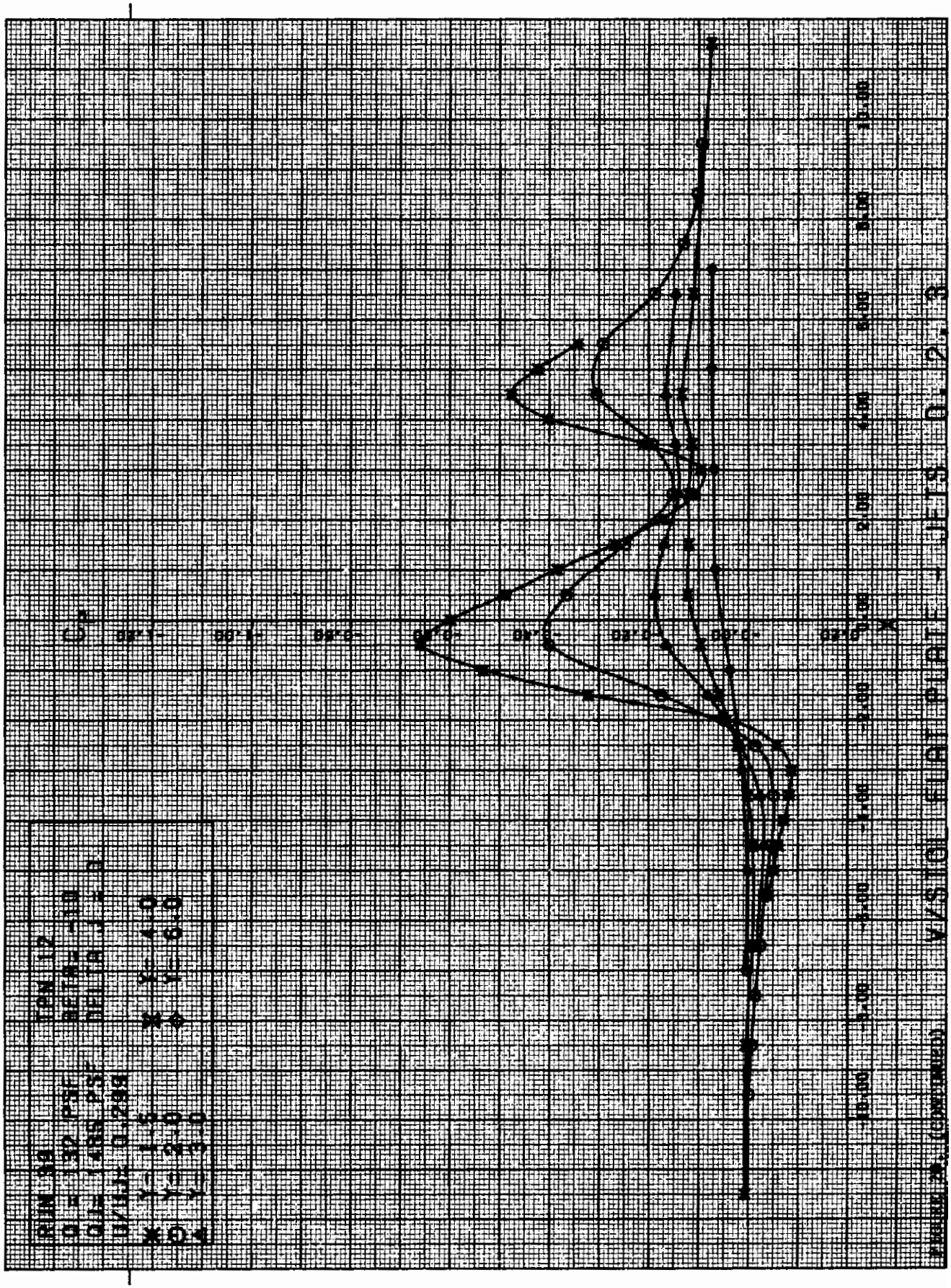

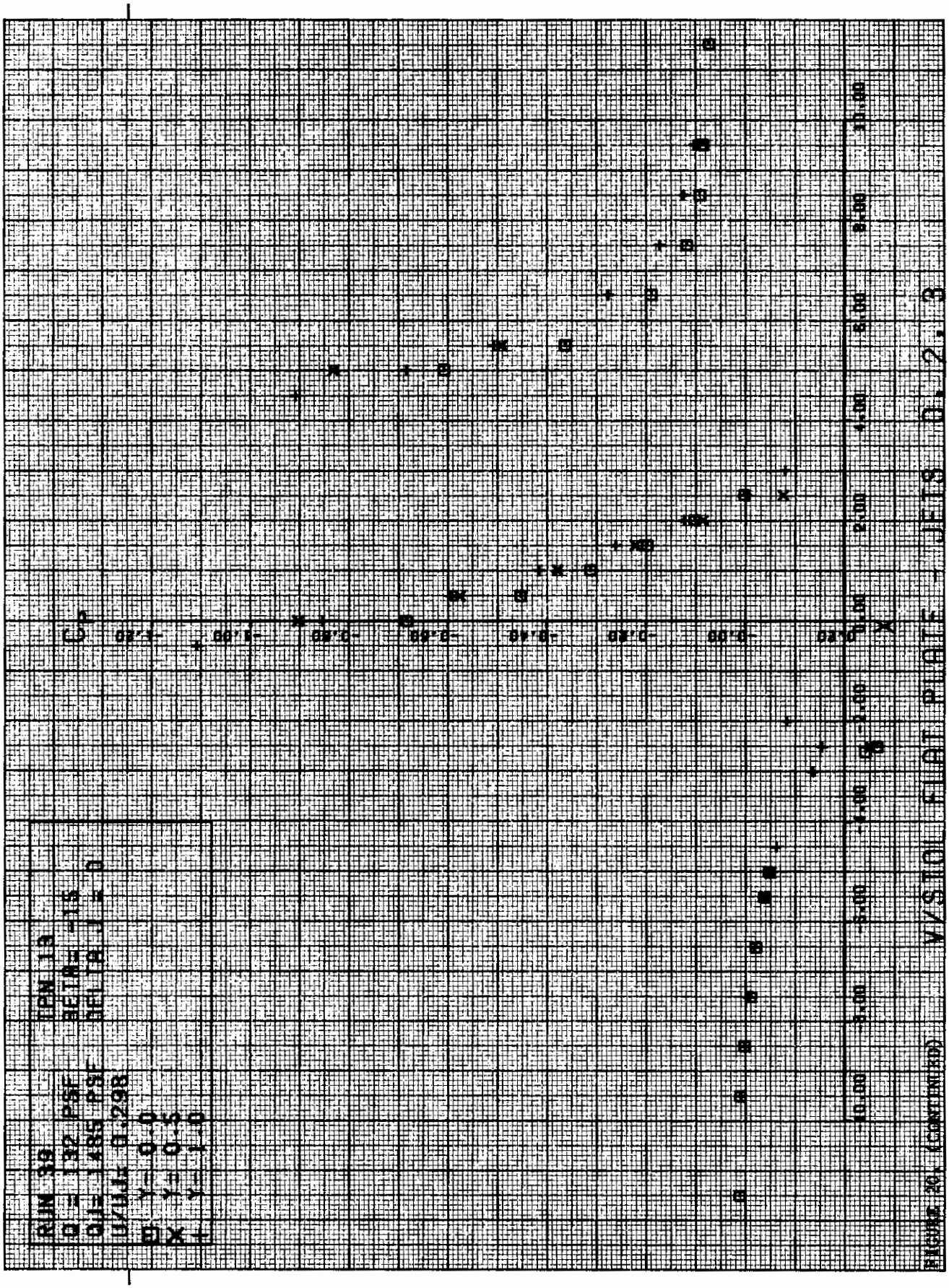

FIGURE 20. (CONCLUDED)

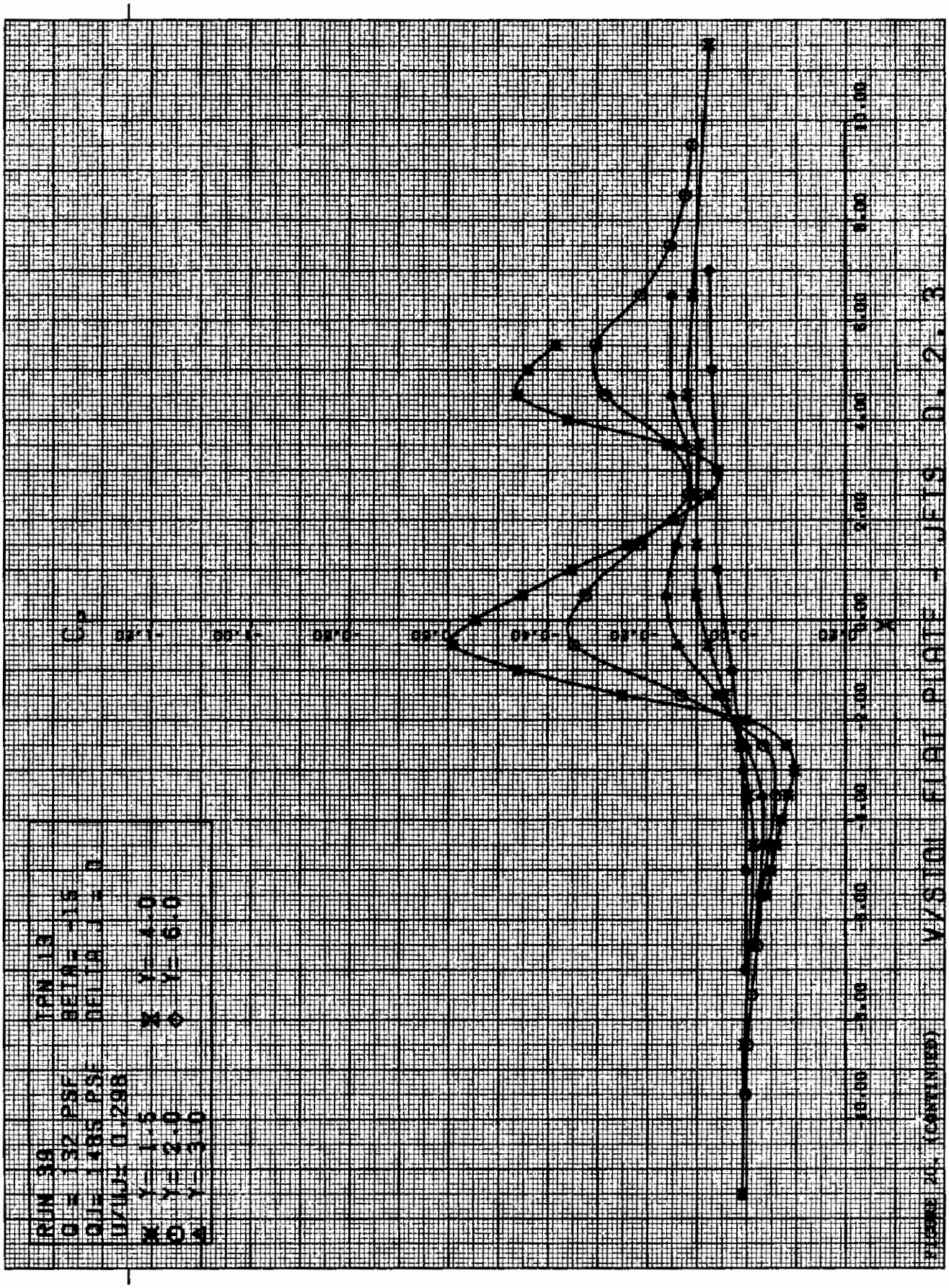

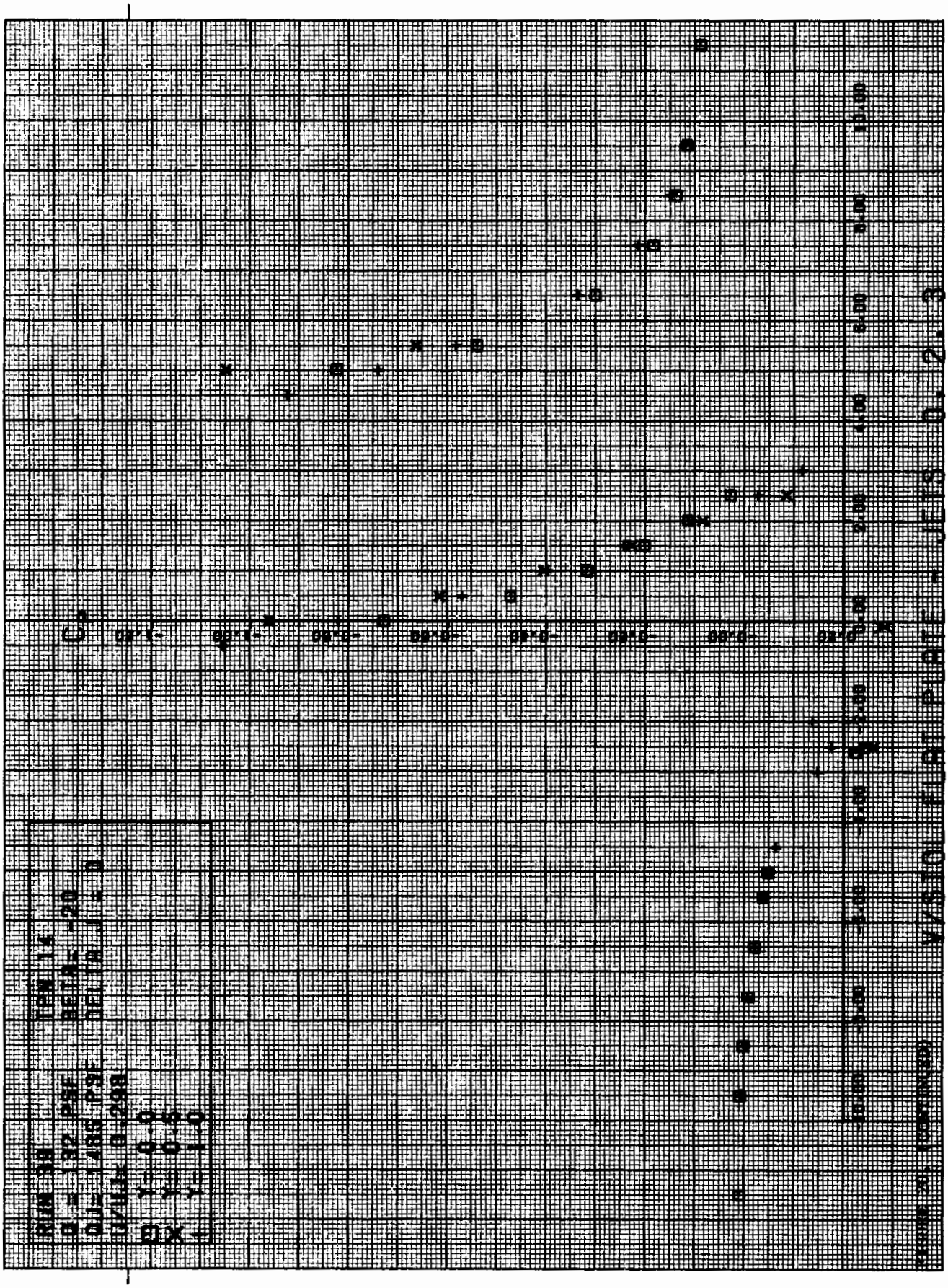

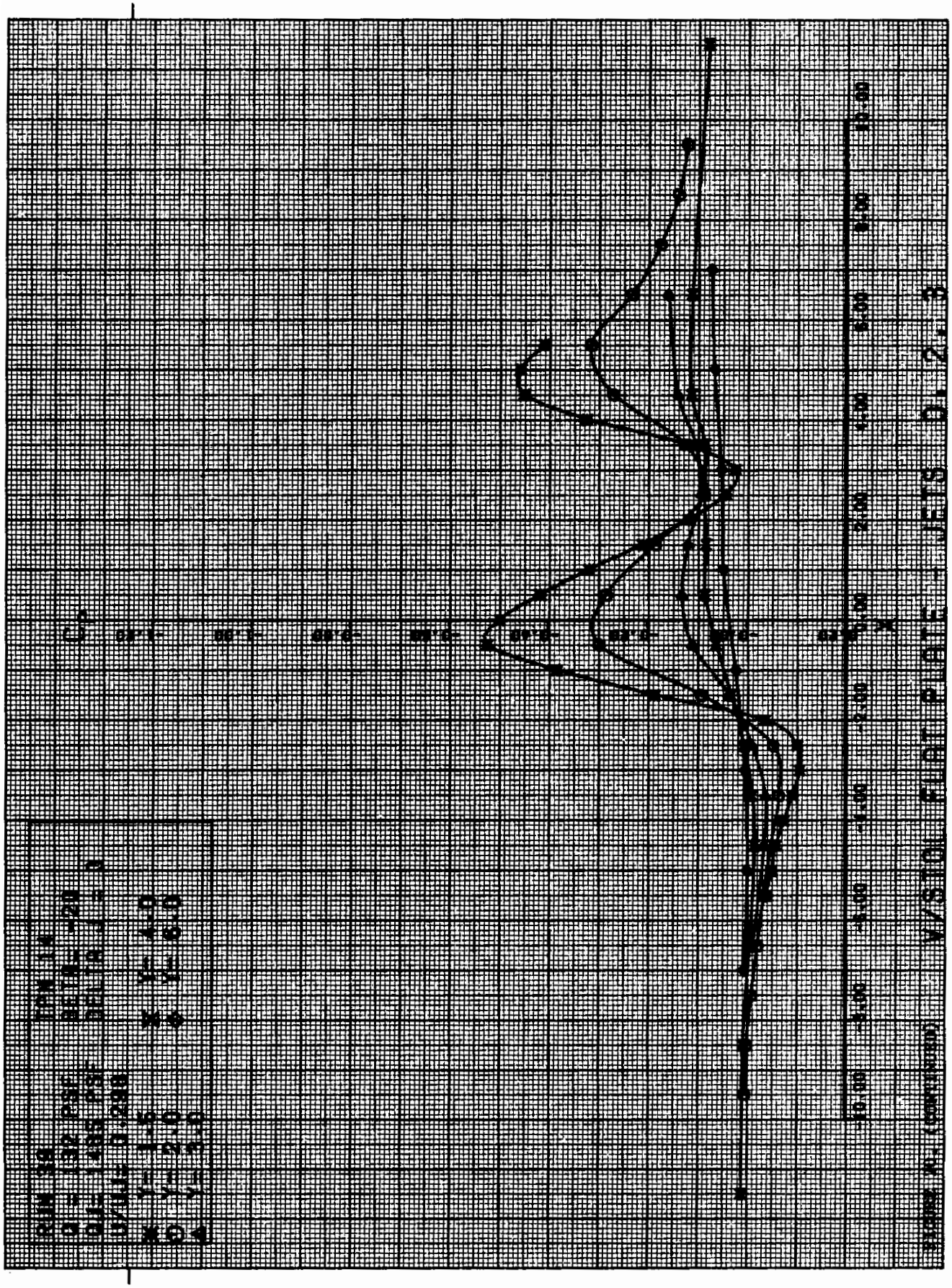

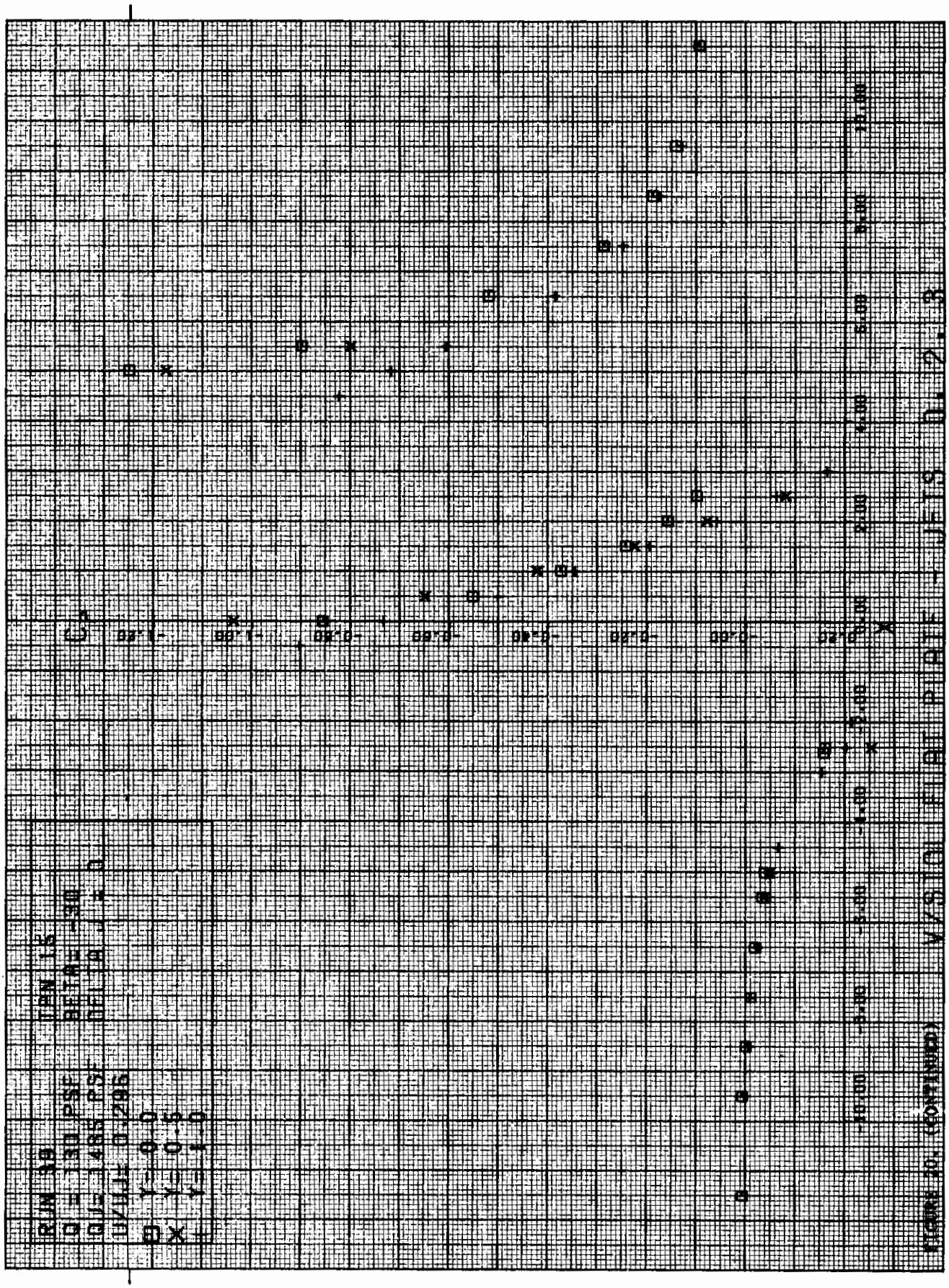

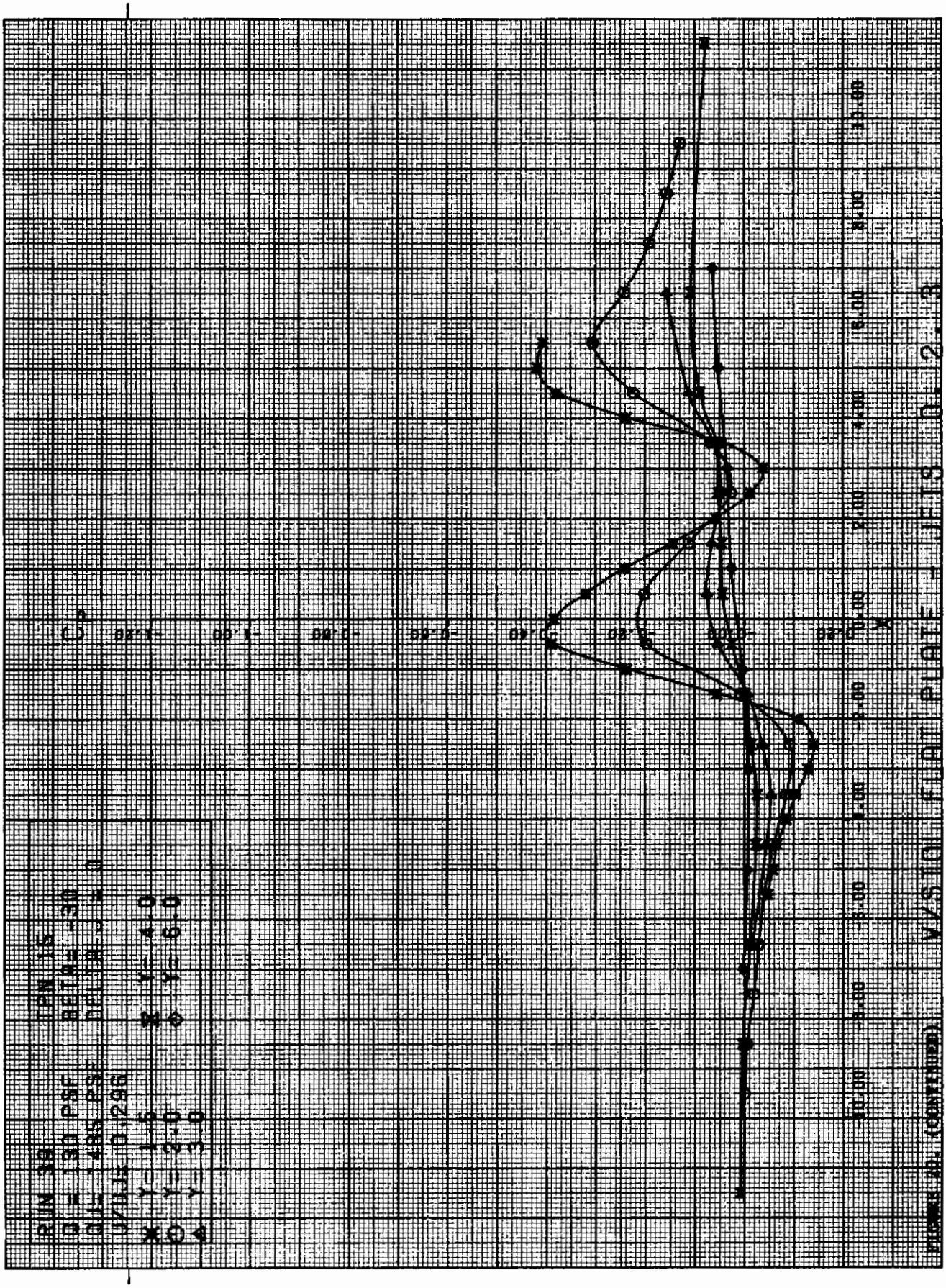

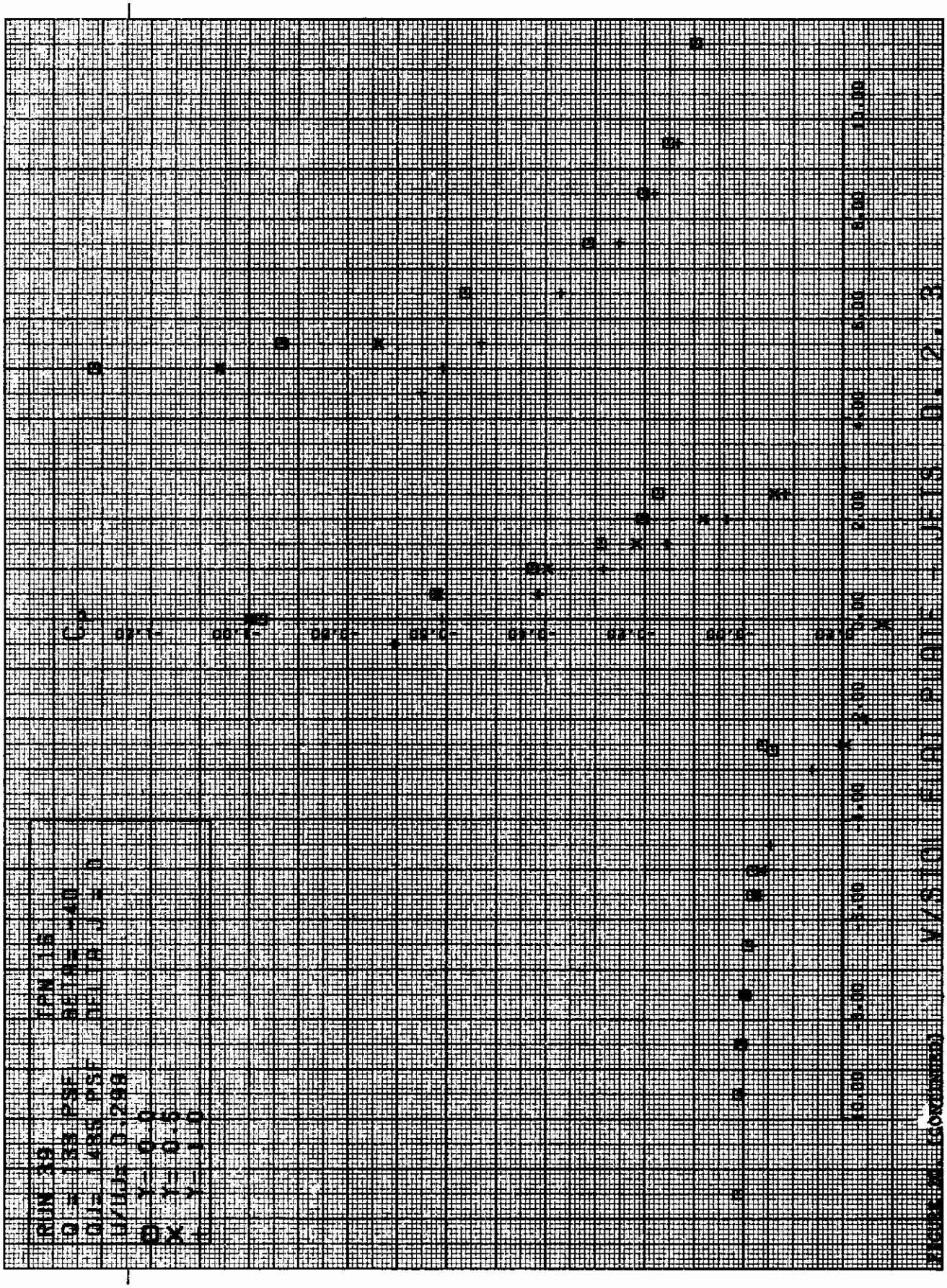

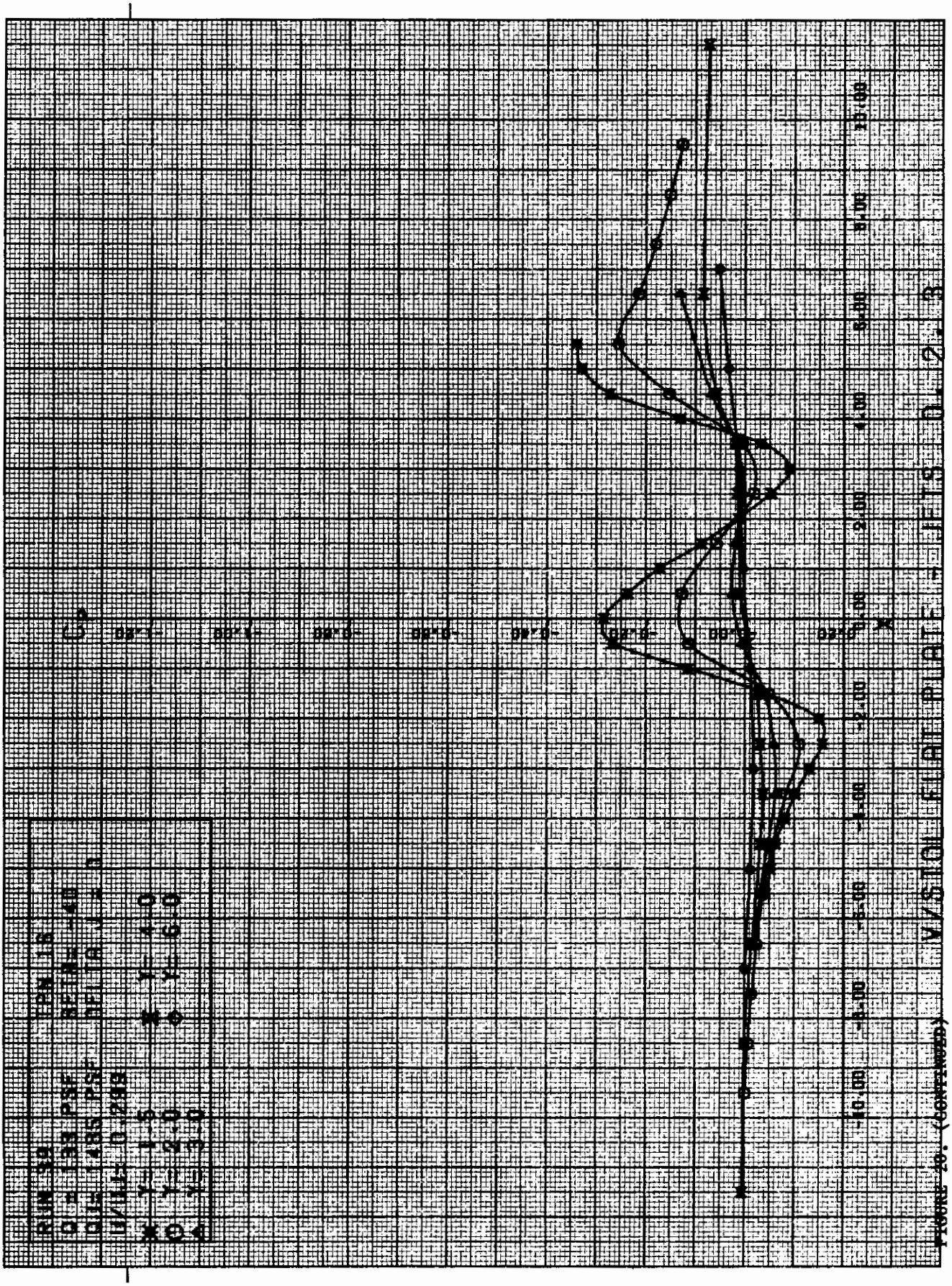

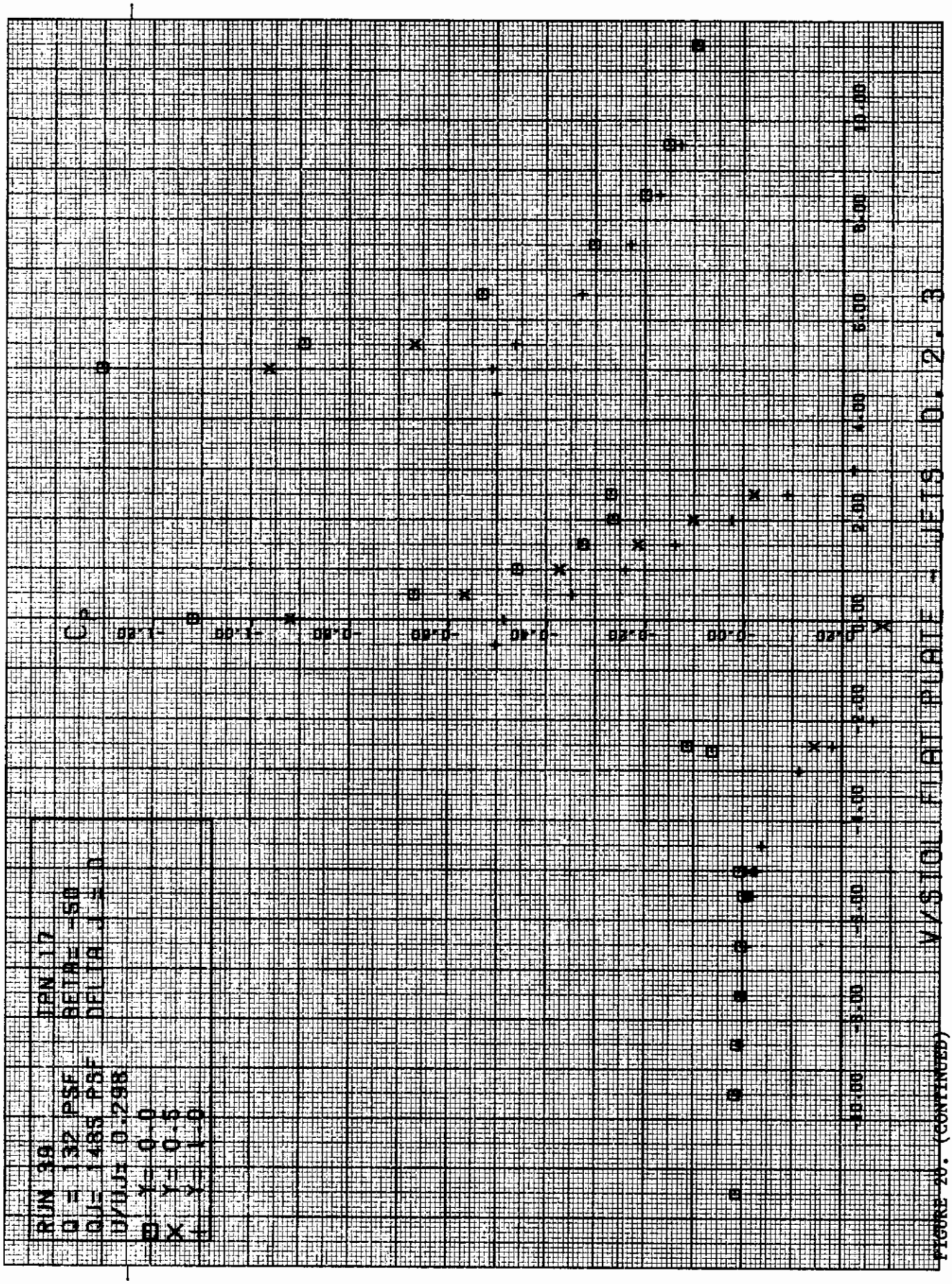

FIGURE 20. (CONTINUED)

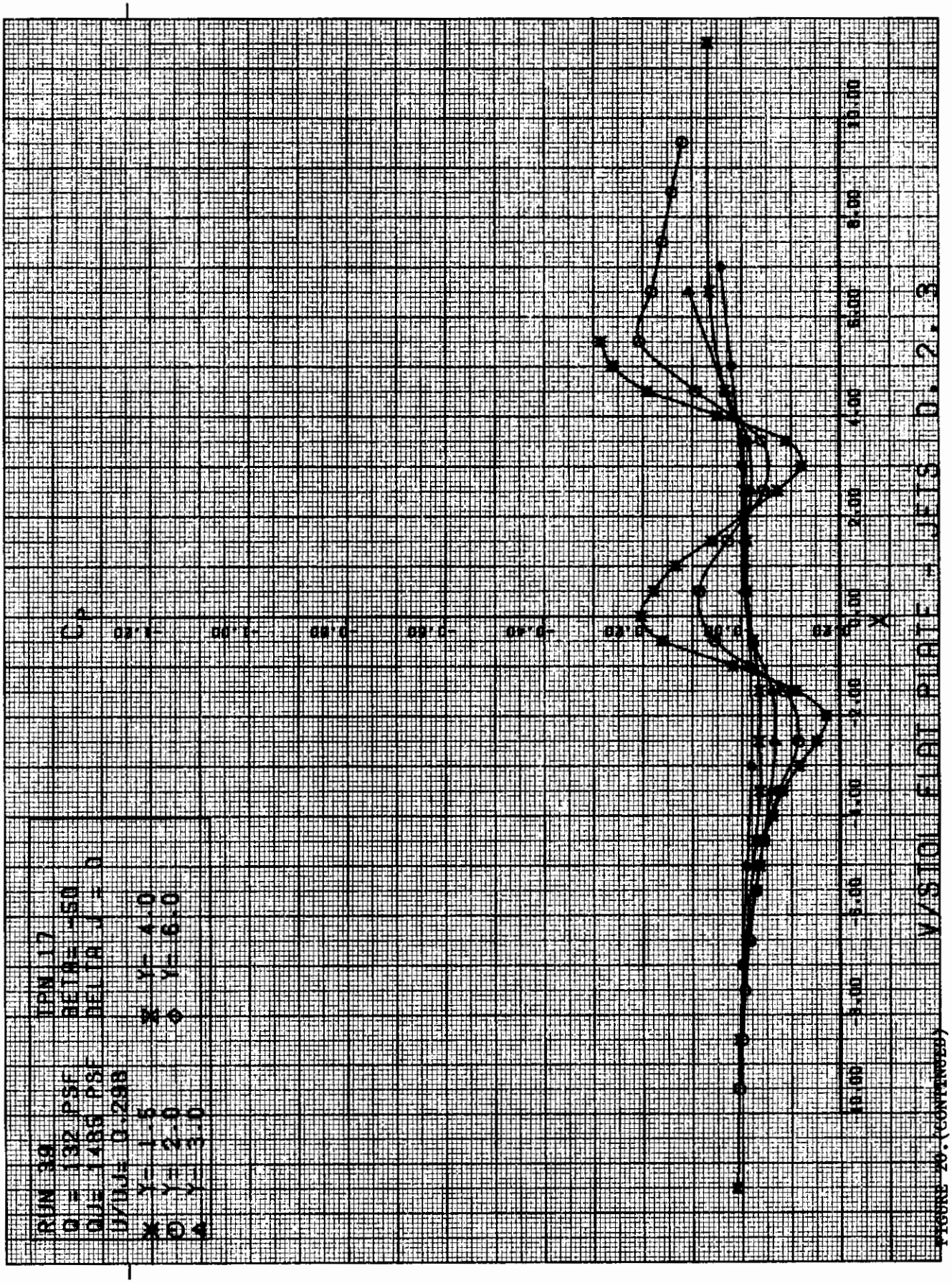

FIGURE 20. (CONTINUED)

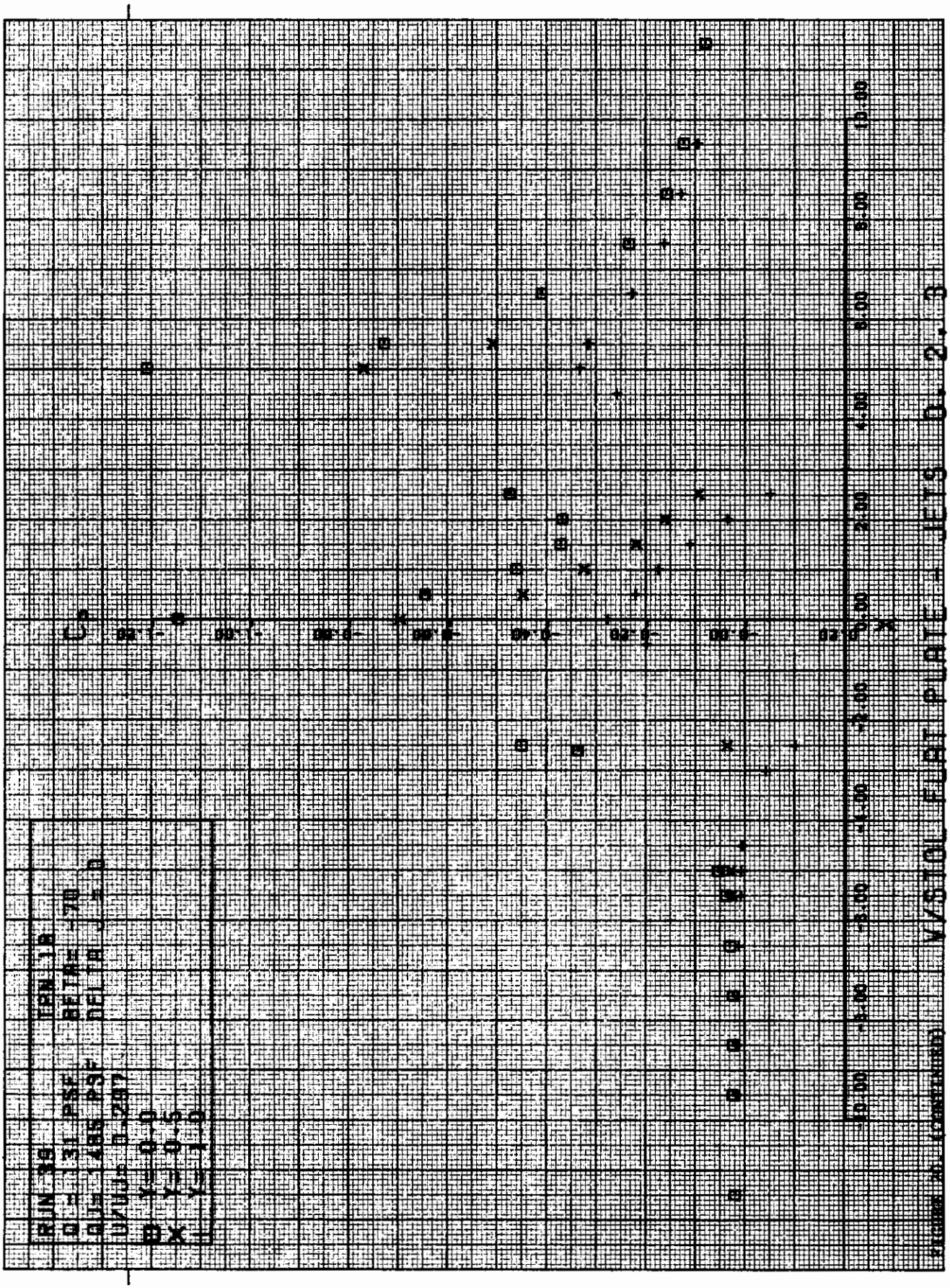

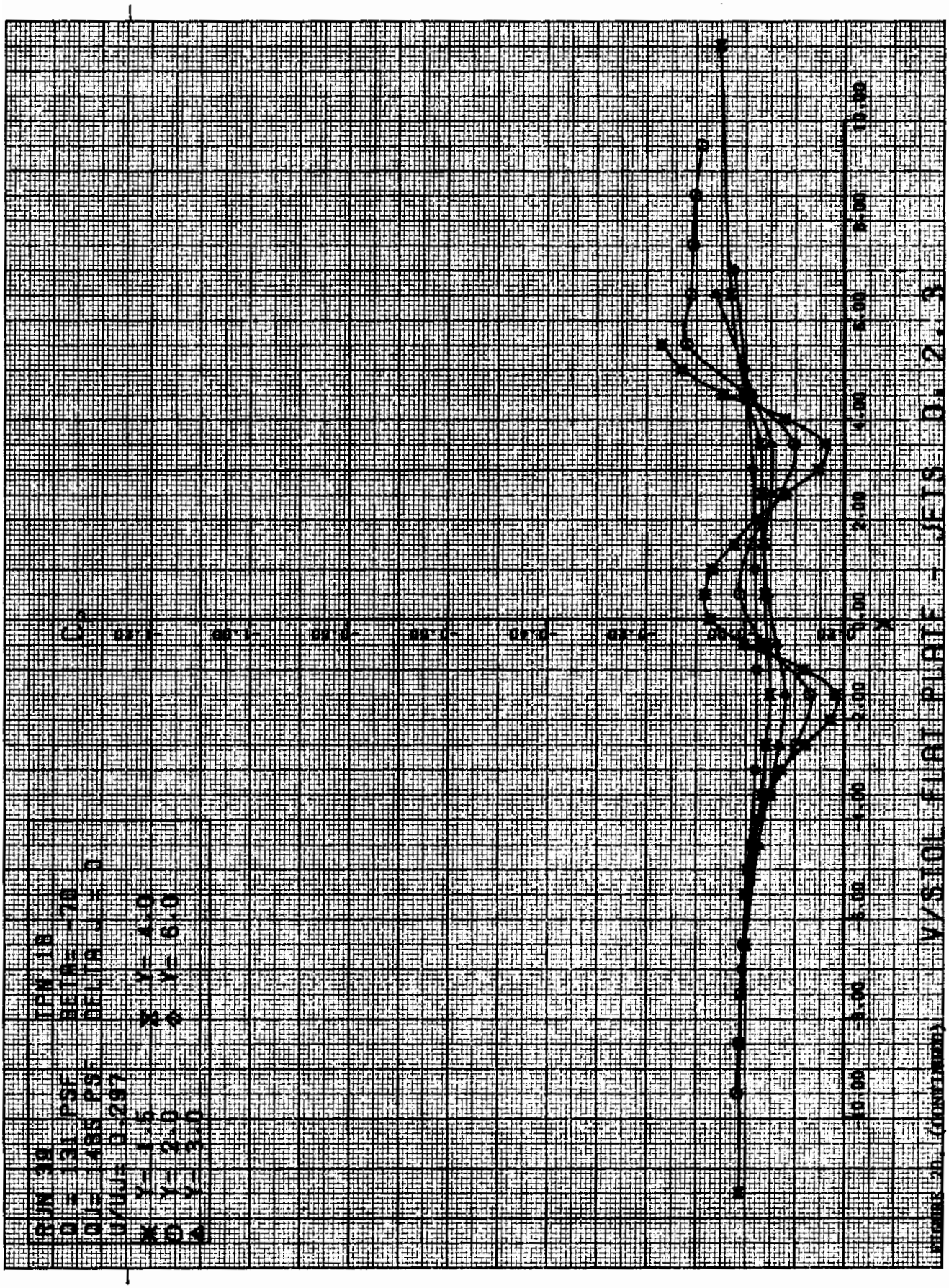

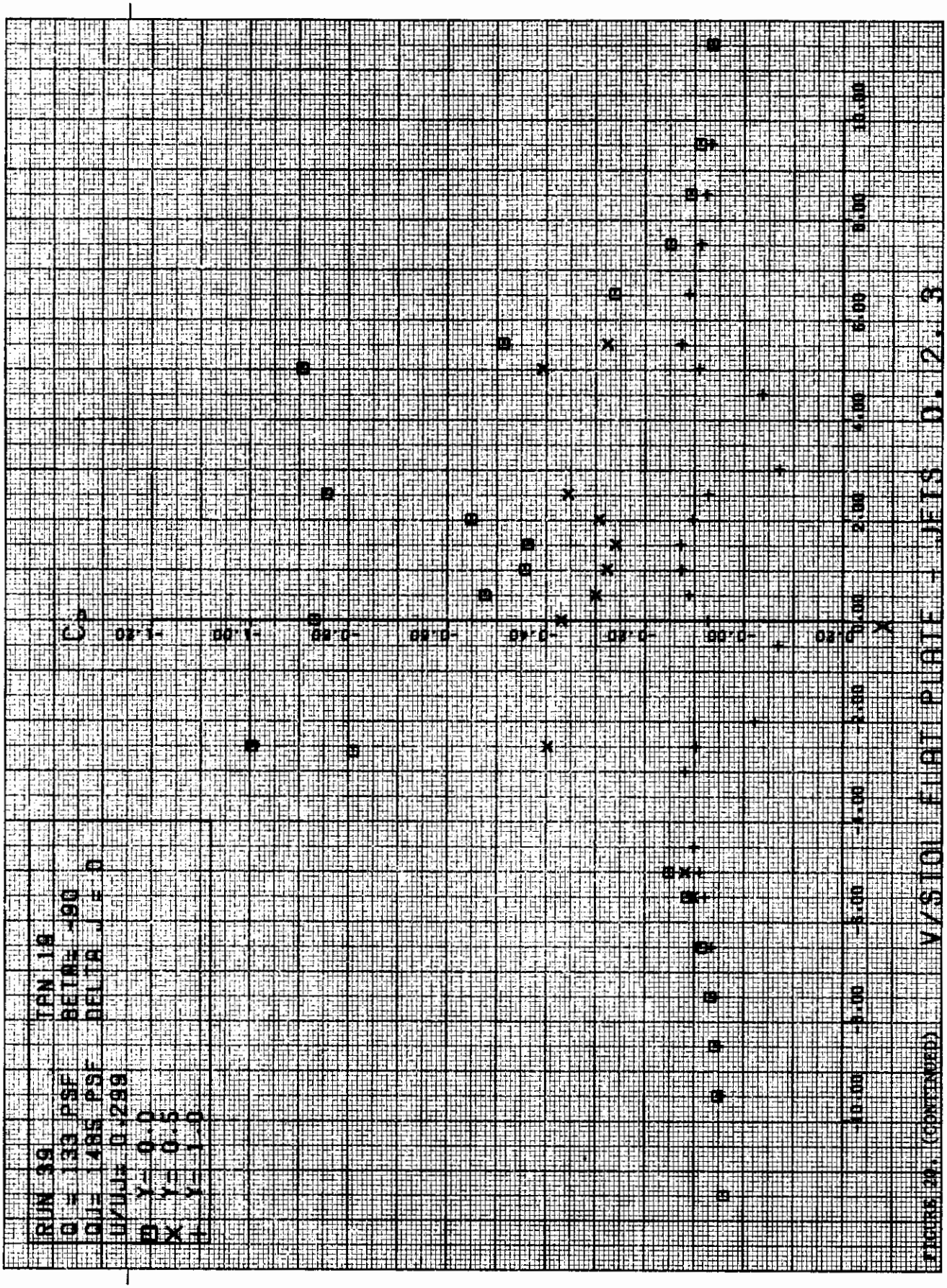

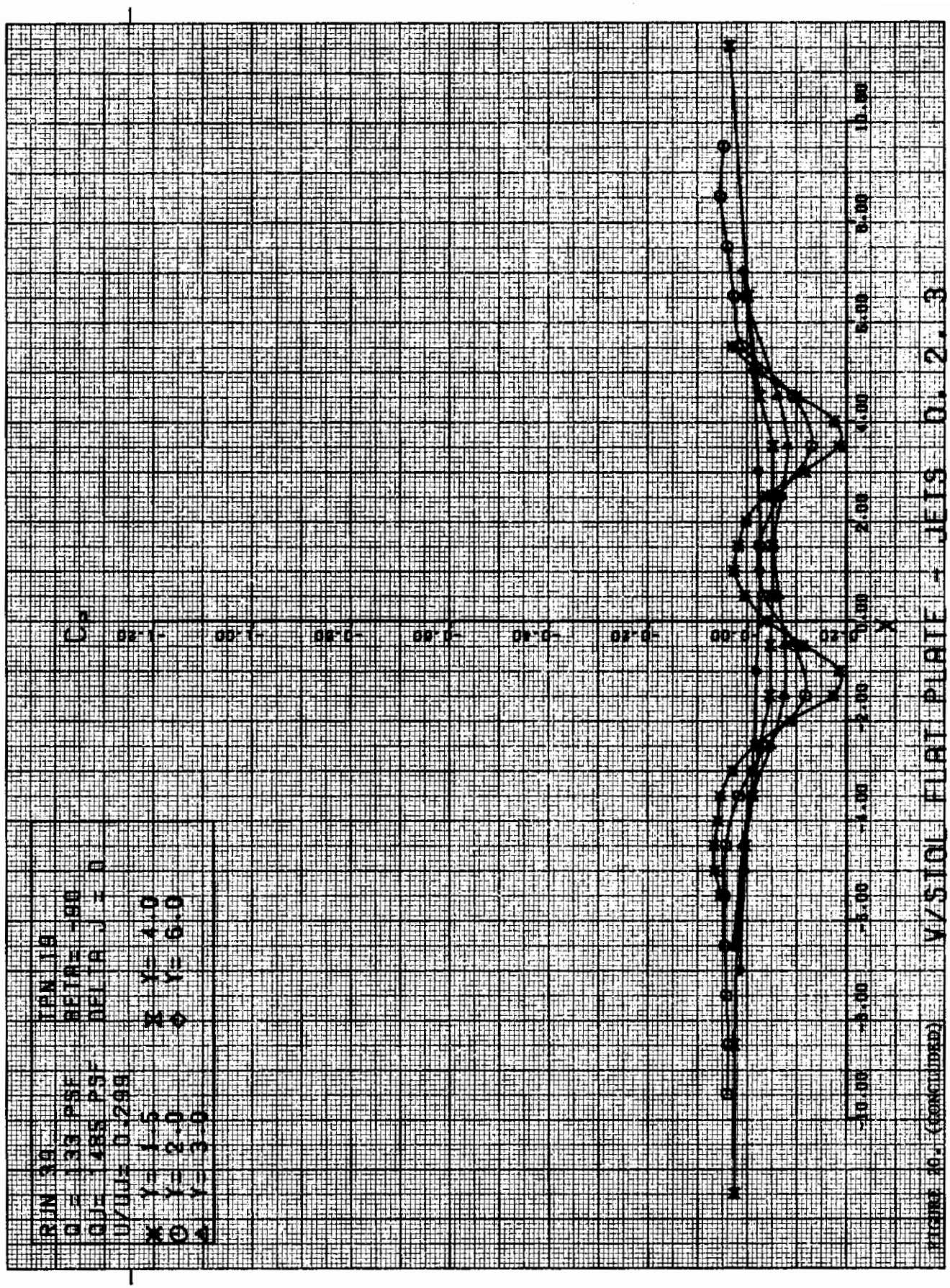

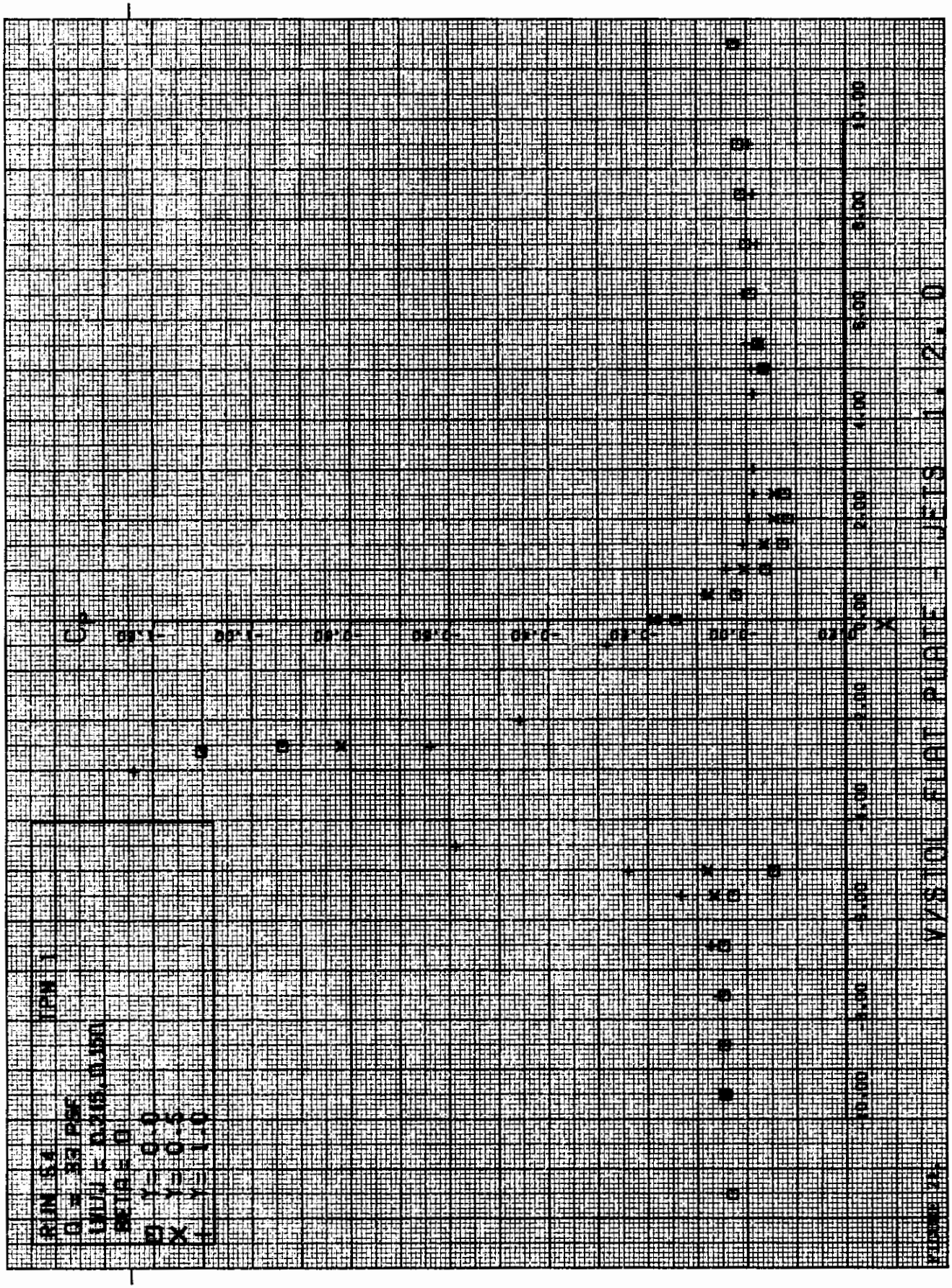

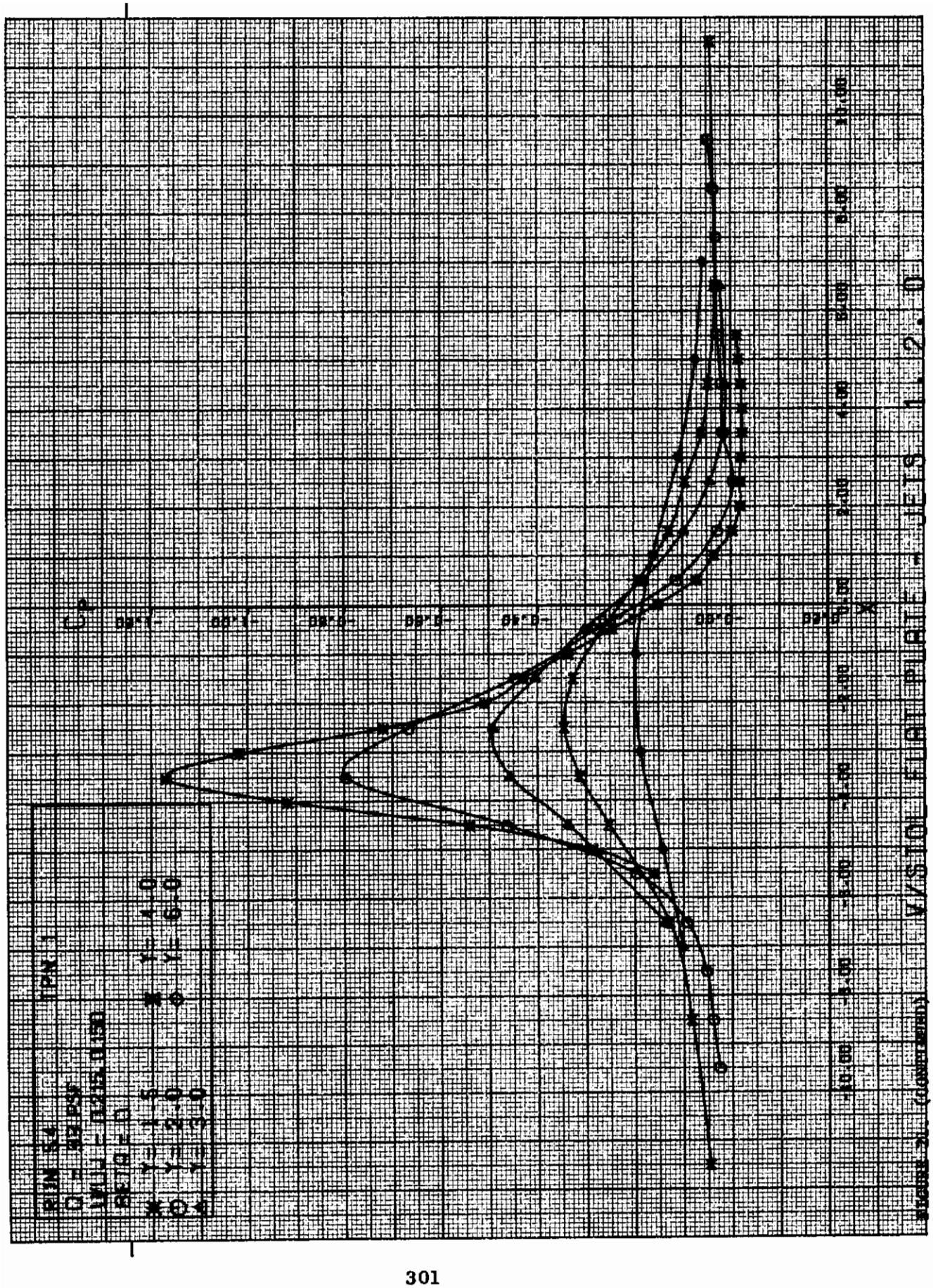

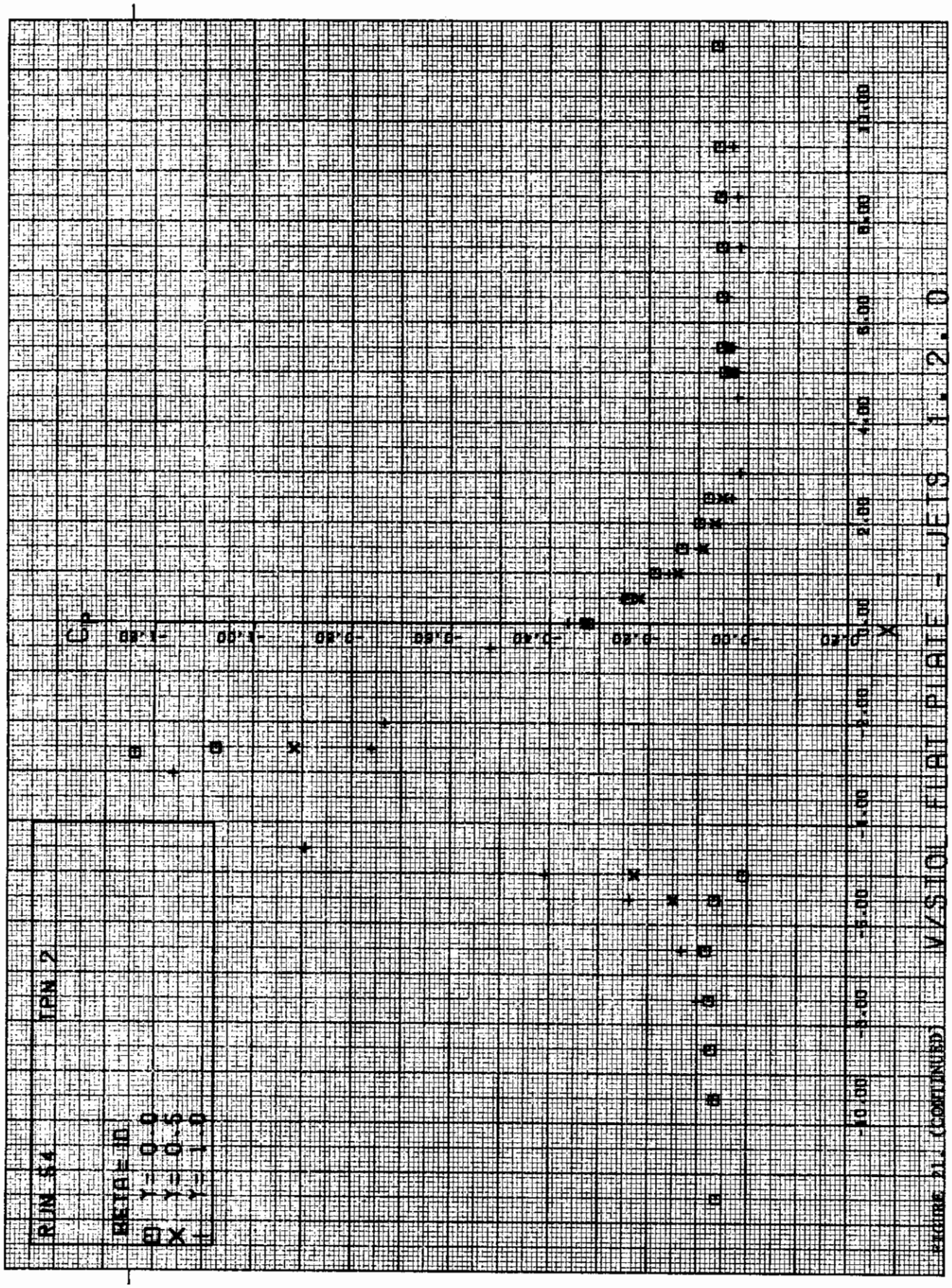

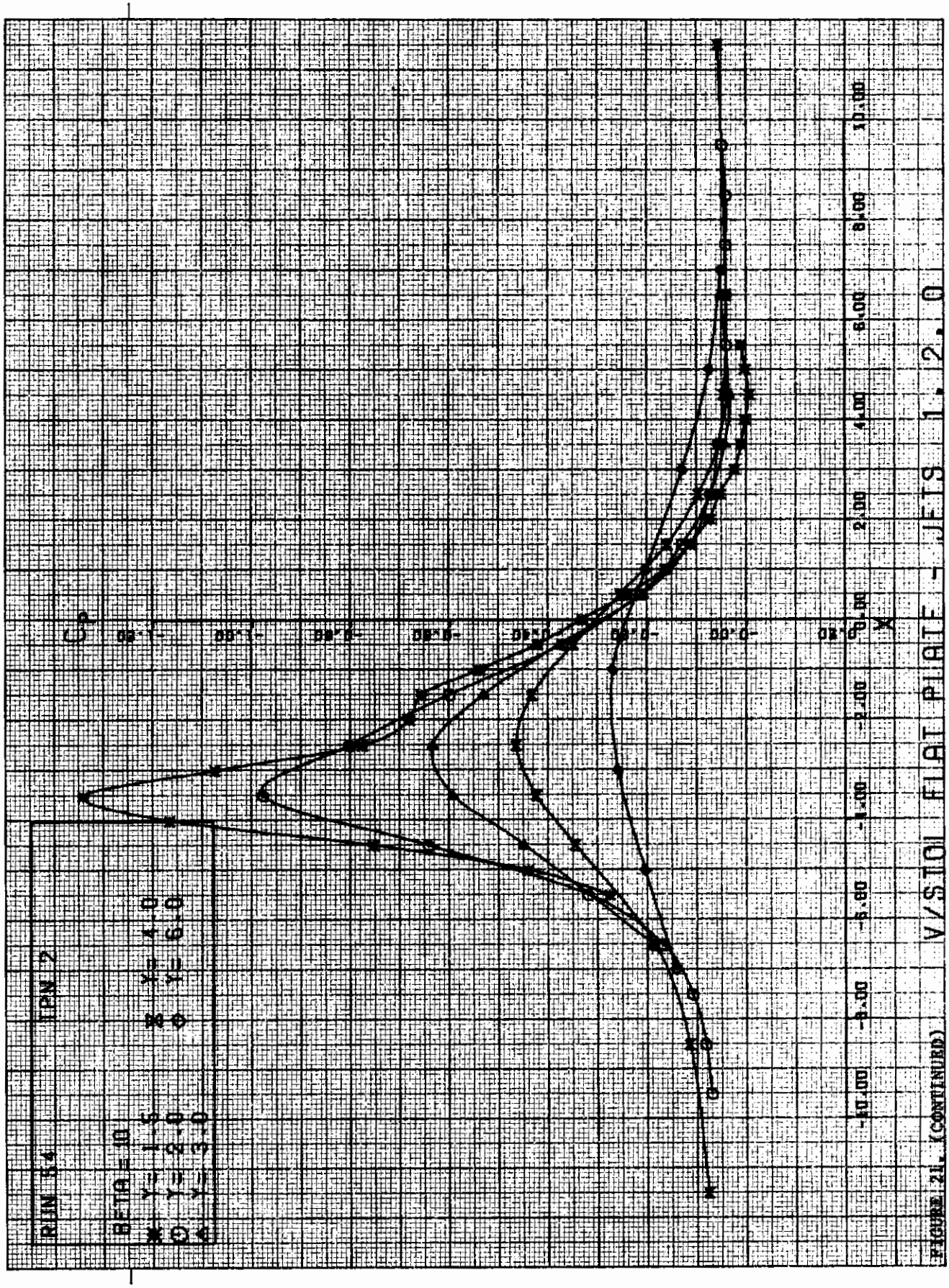

FIGURE 21. (CONTINUED)

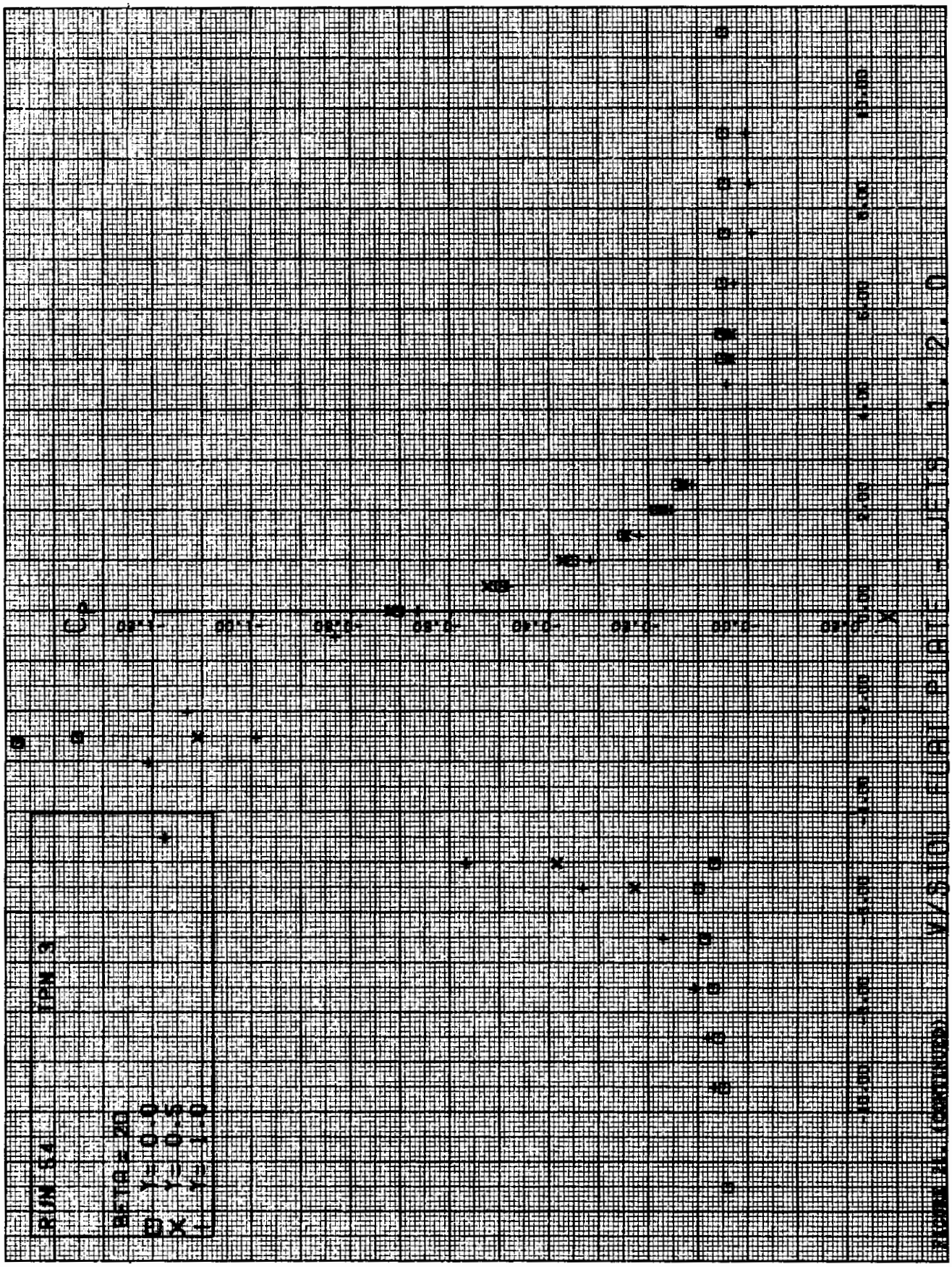

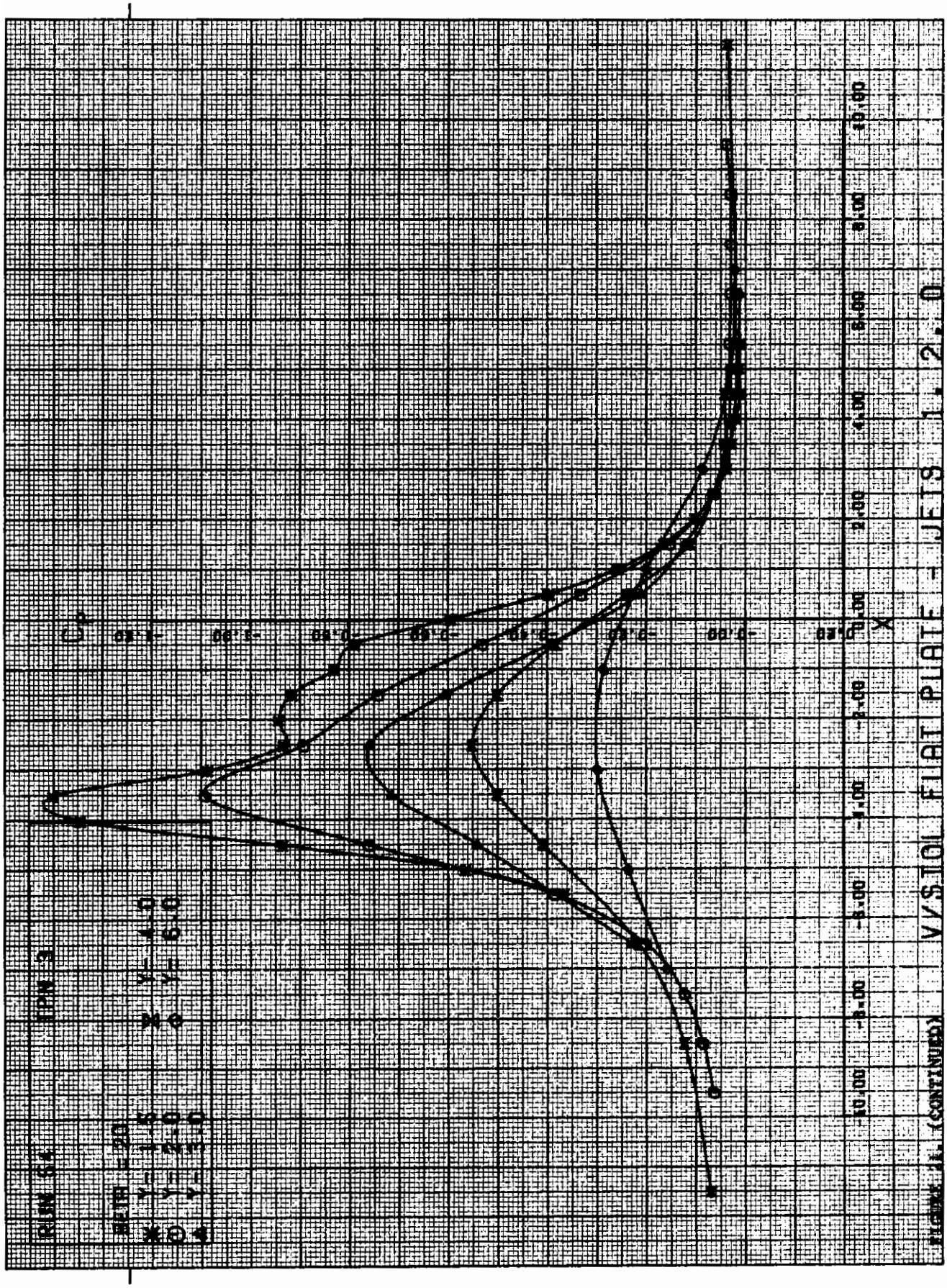

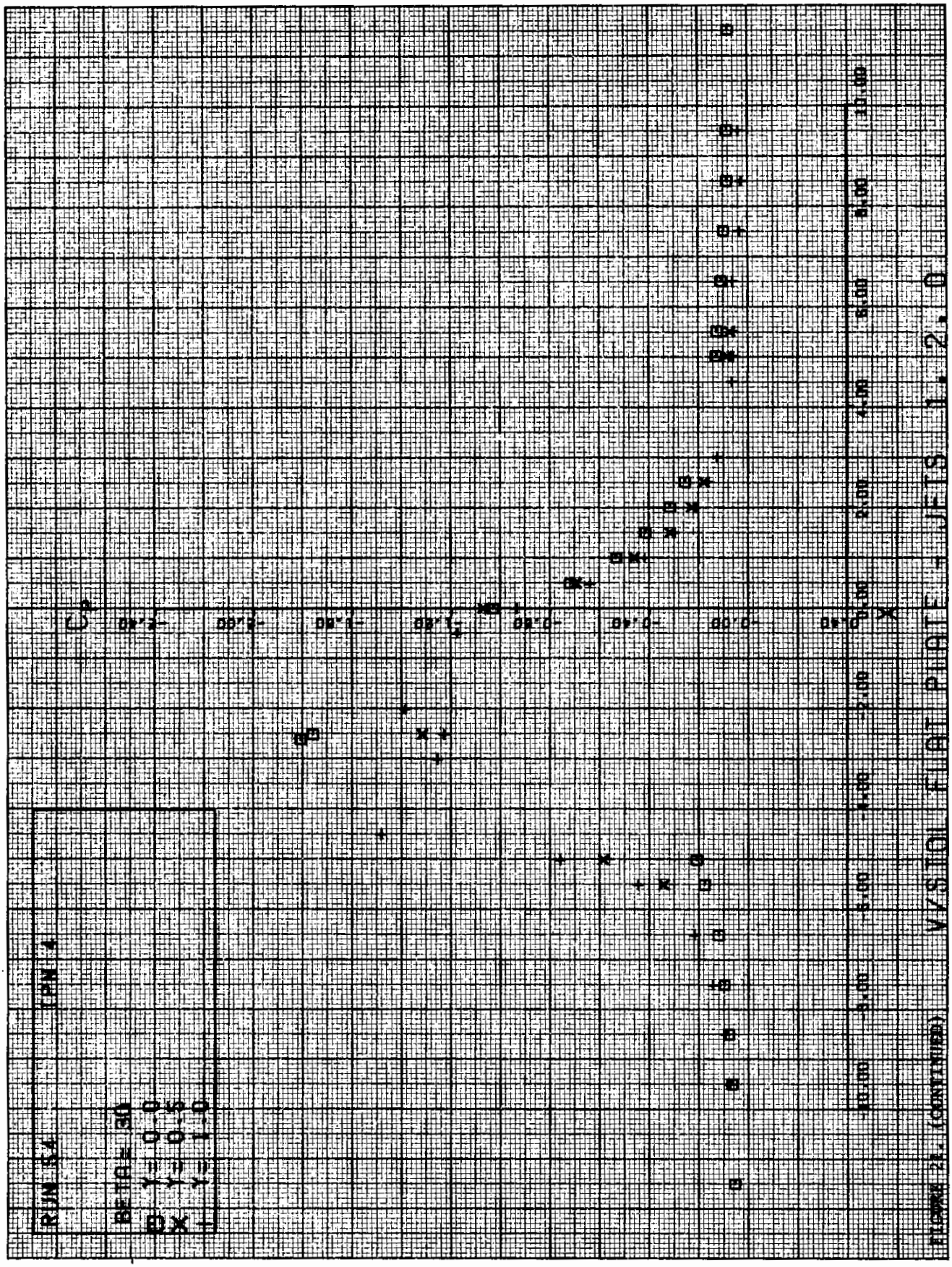

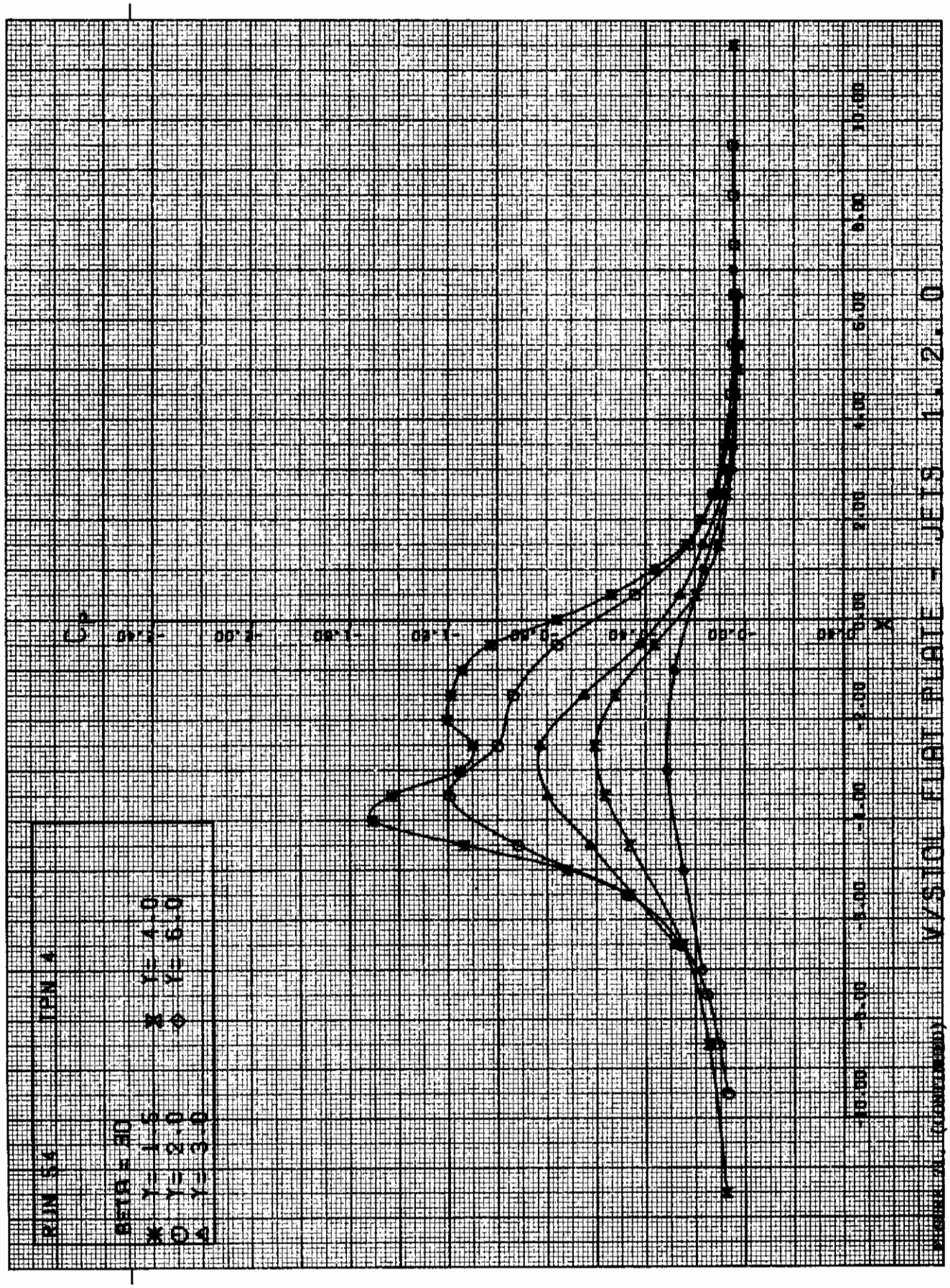

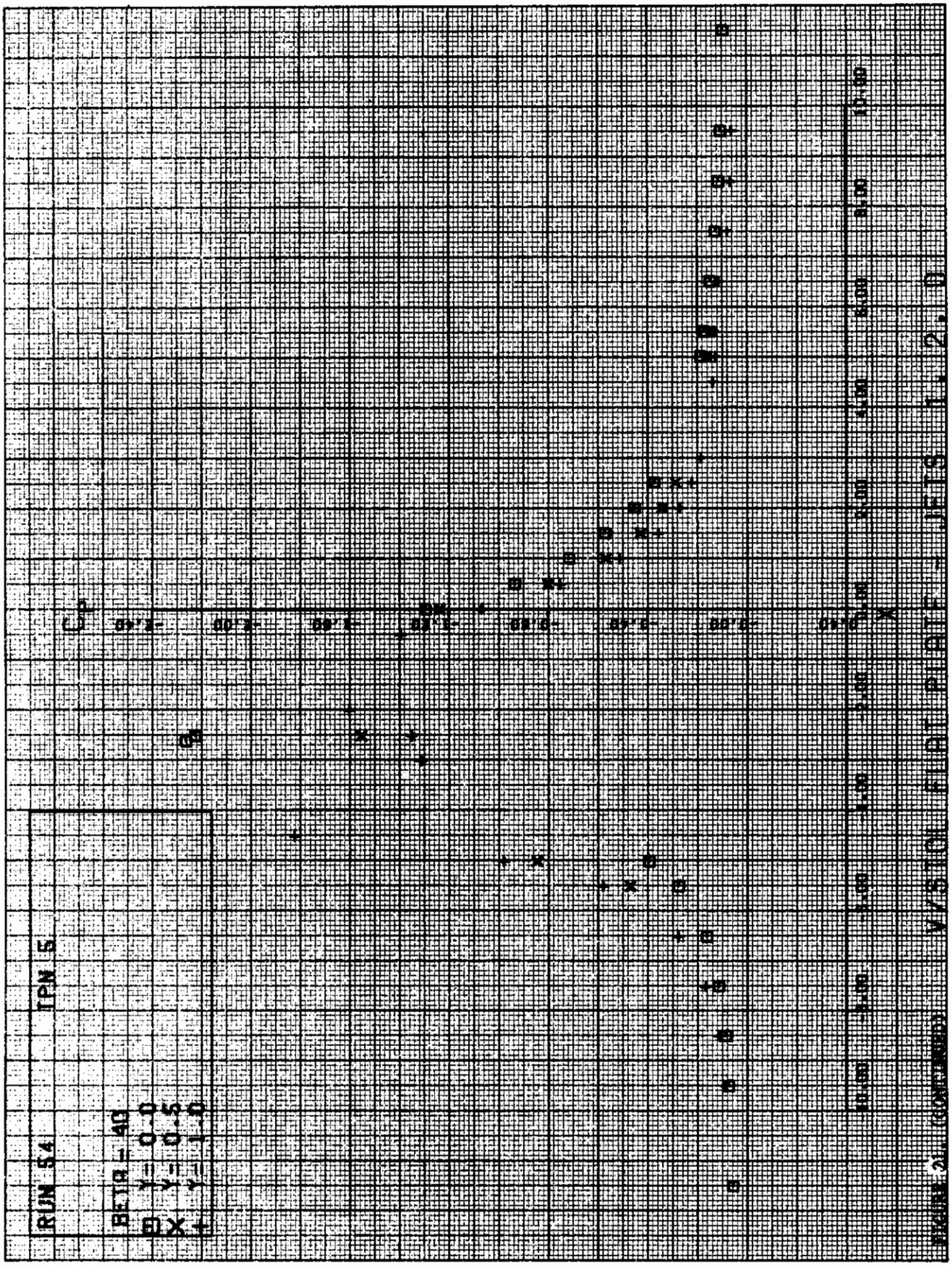

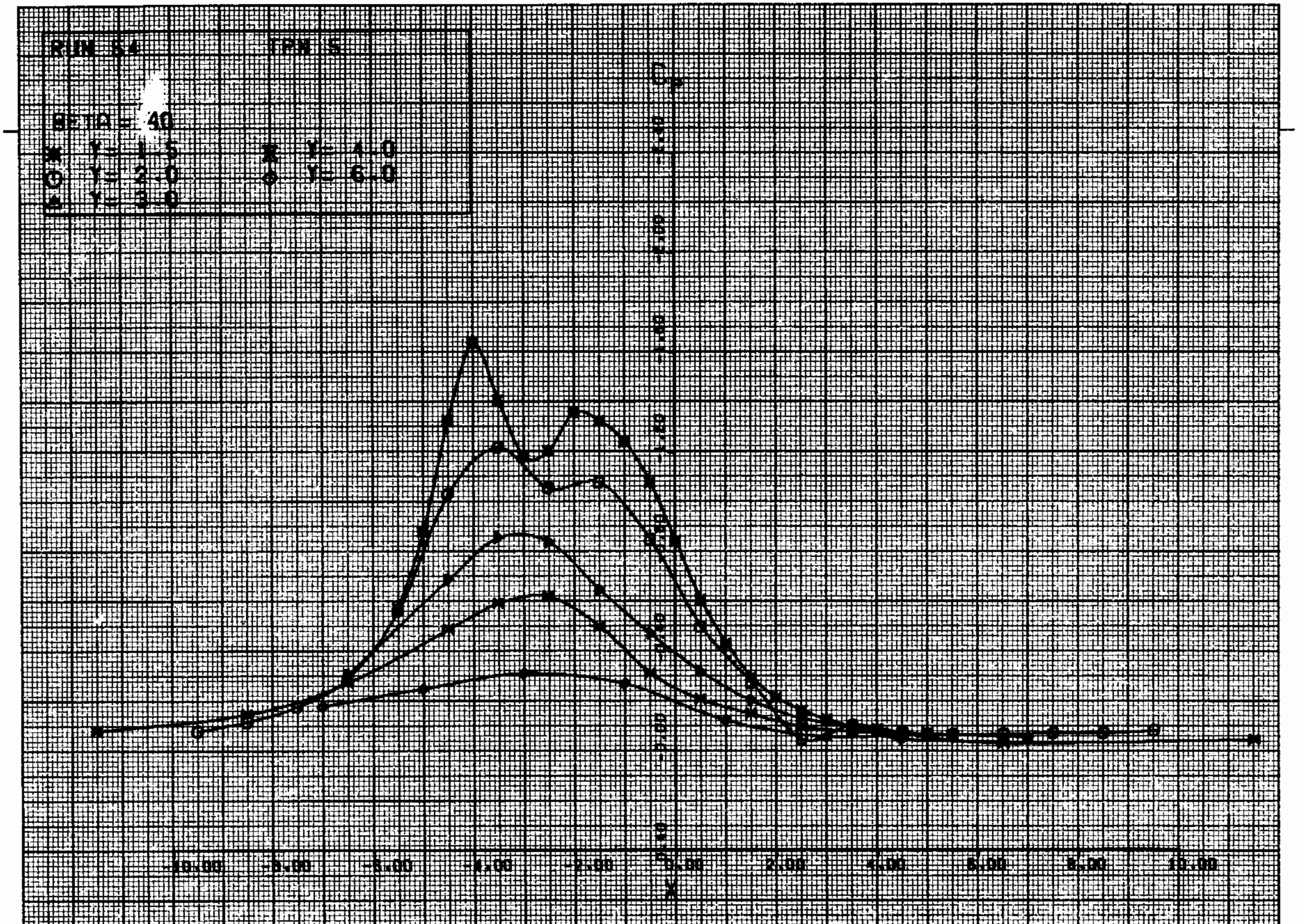

FIGURE [illegible]. (CONTINUED) V/STOL FLAT PLATE - JETS 1, 2, 0

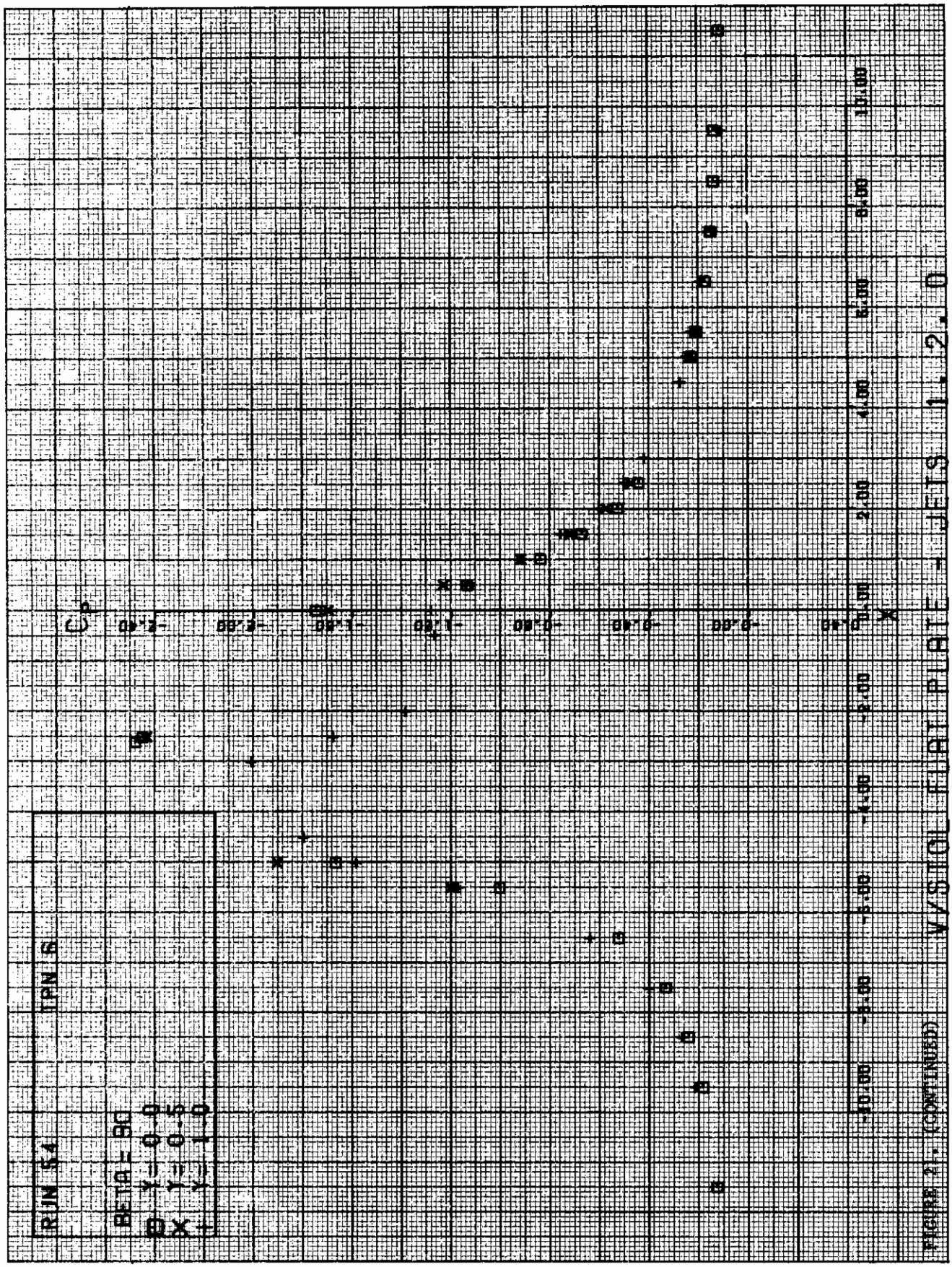

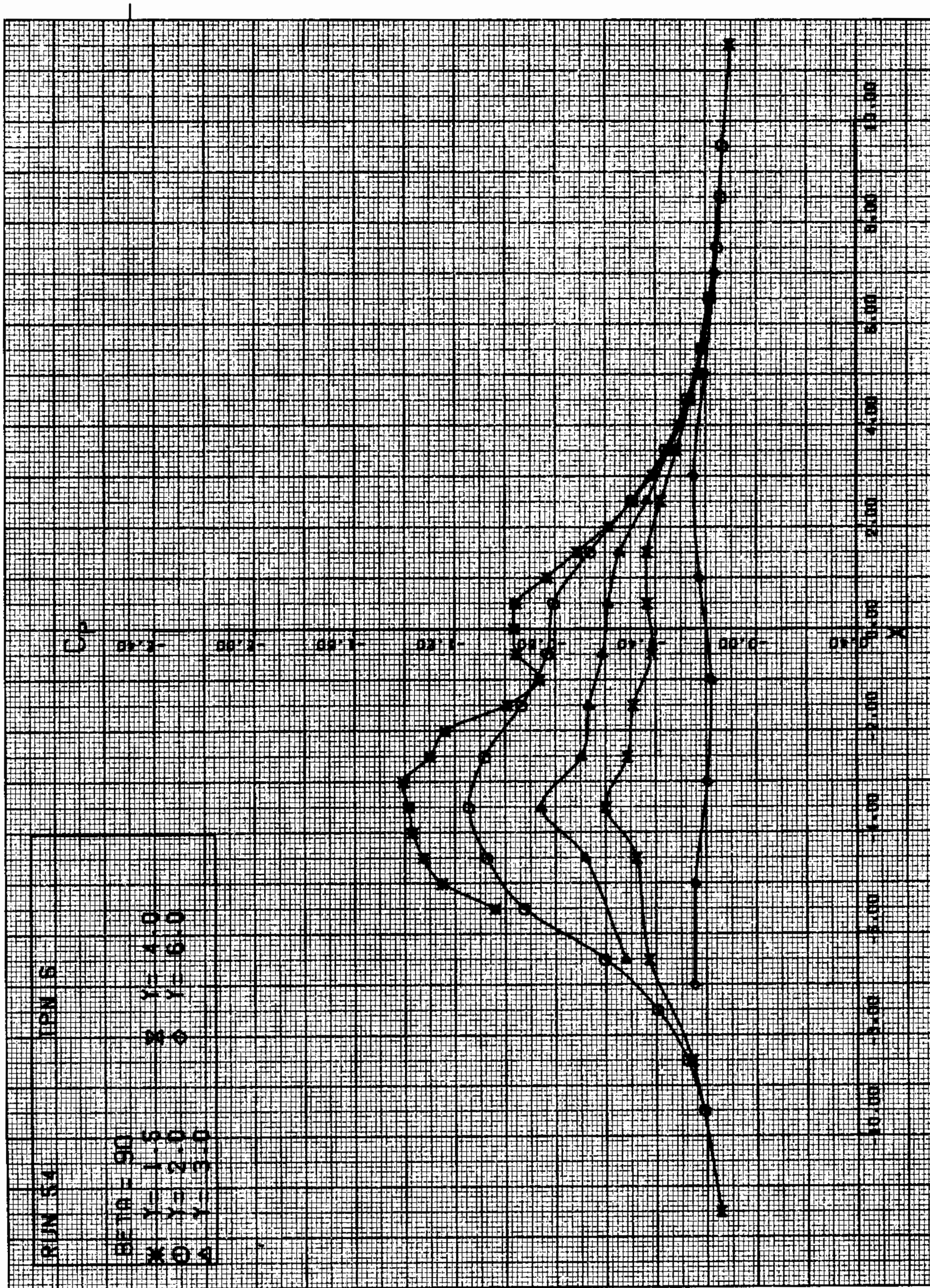

FIGURE 21. (CONTINUED) V/STOL FLAT PLATE - JETS 1, 2, 0

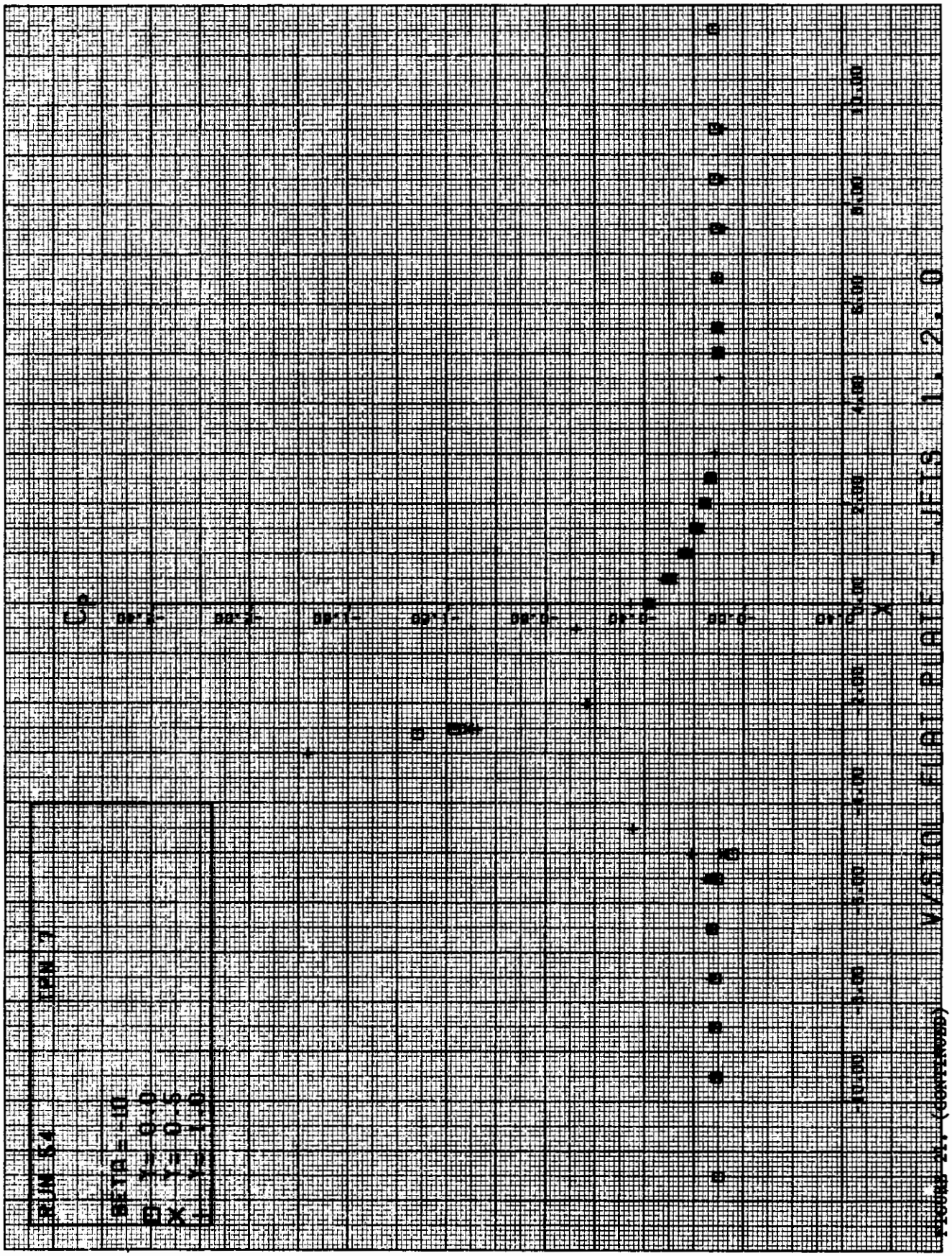

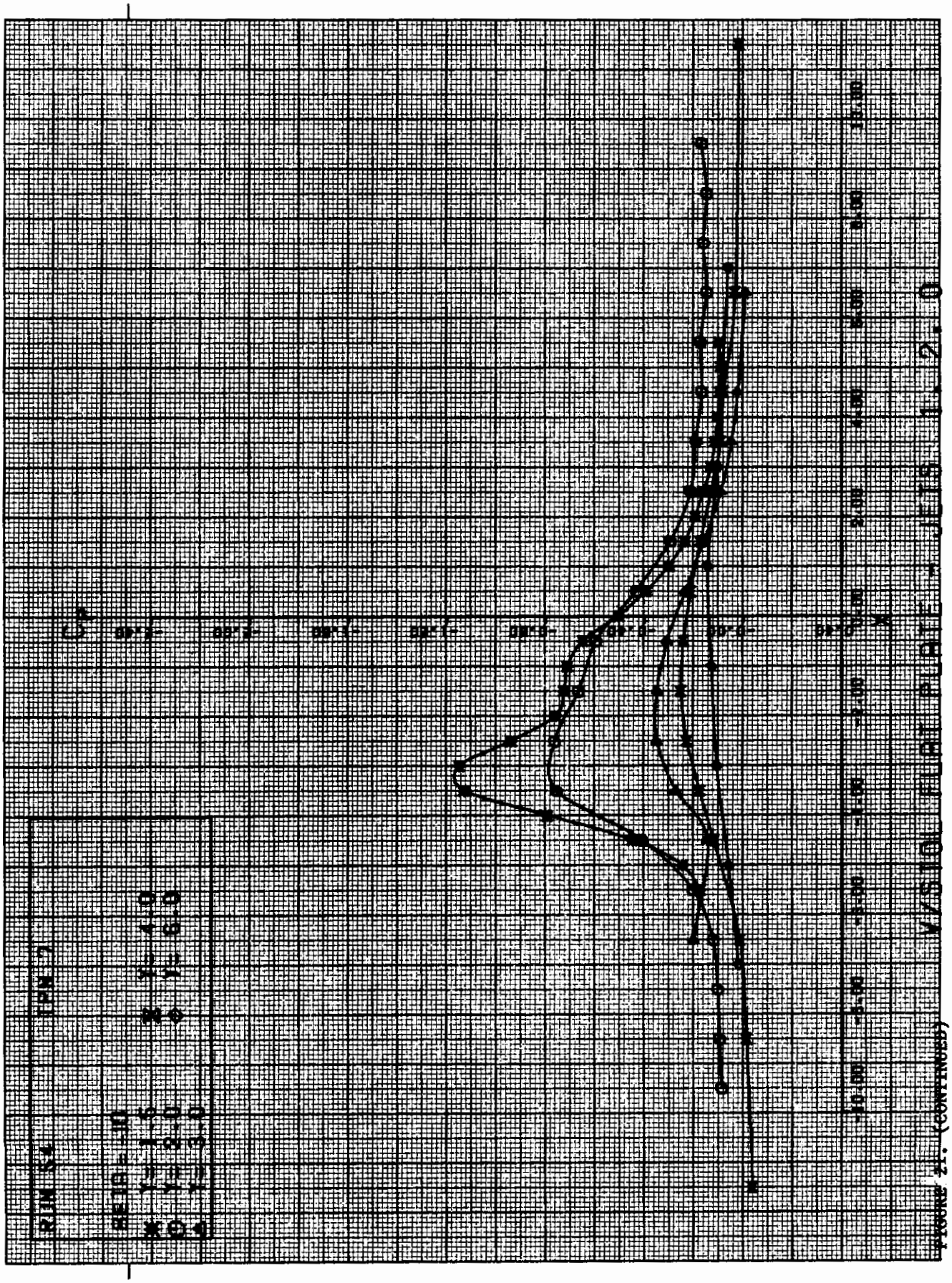

FIGURE 21. (CONTINUED)

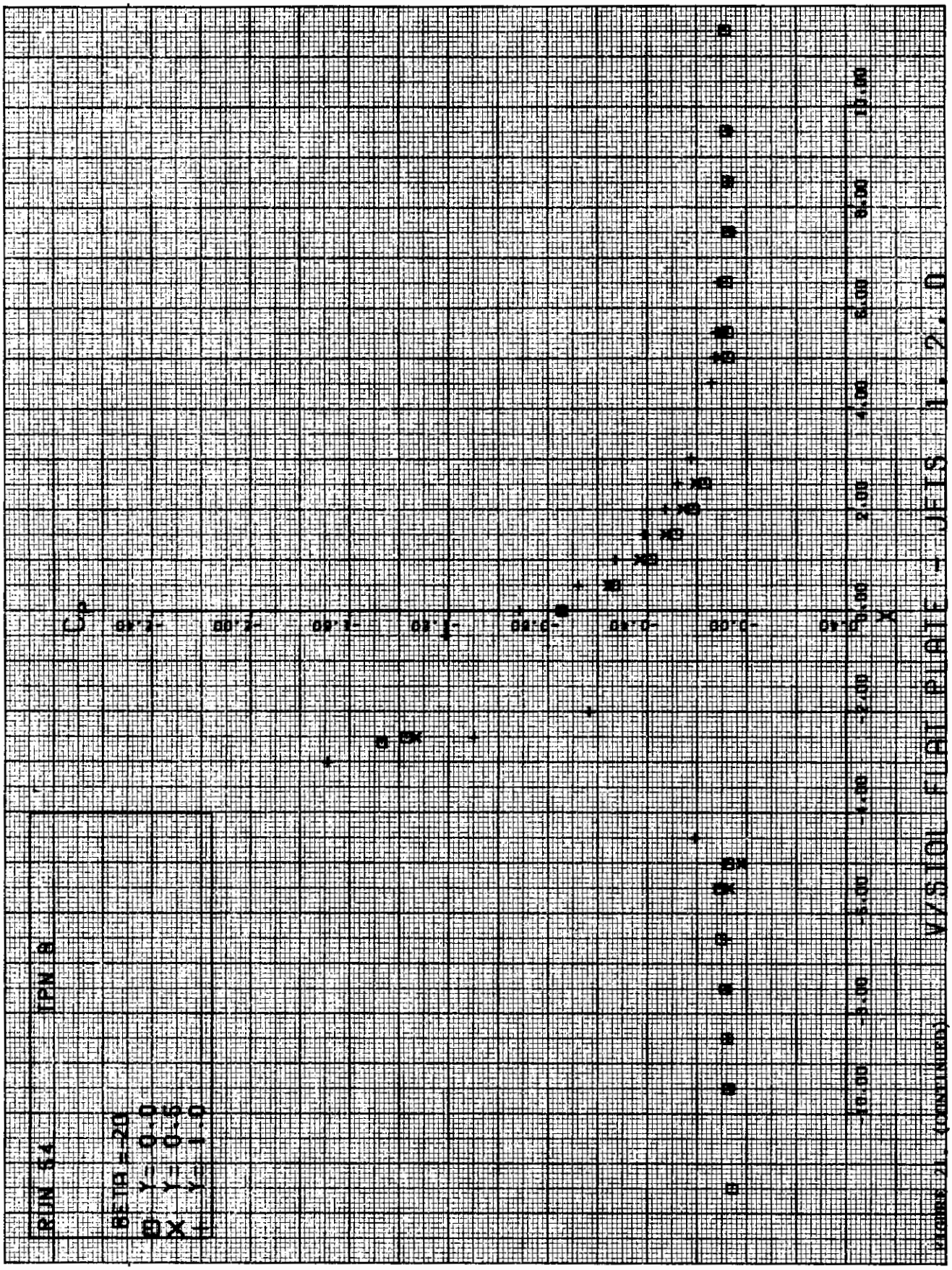

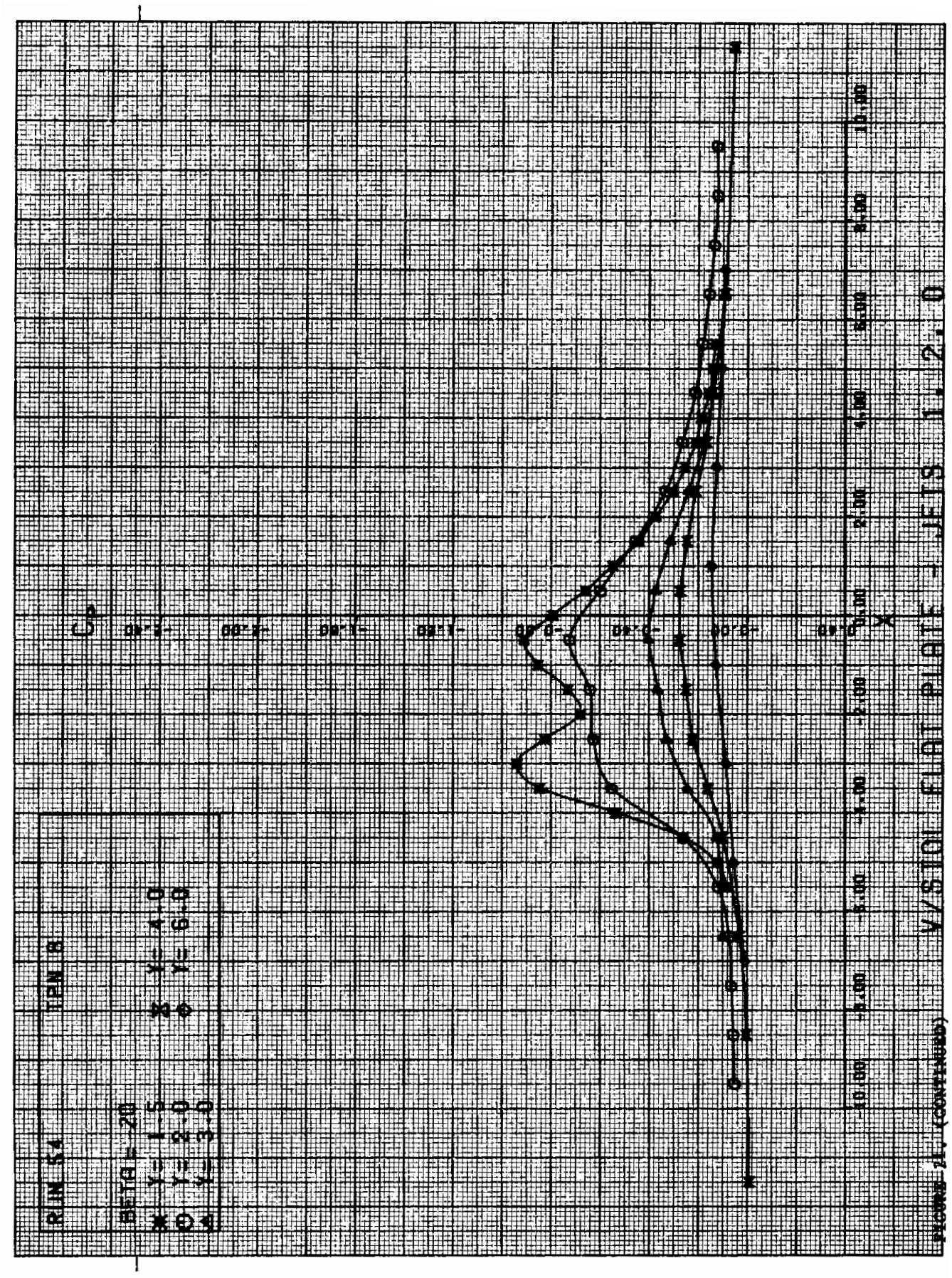

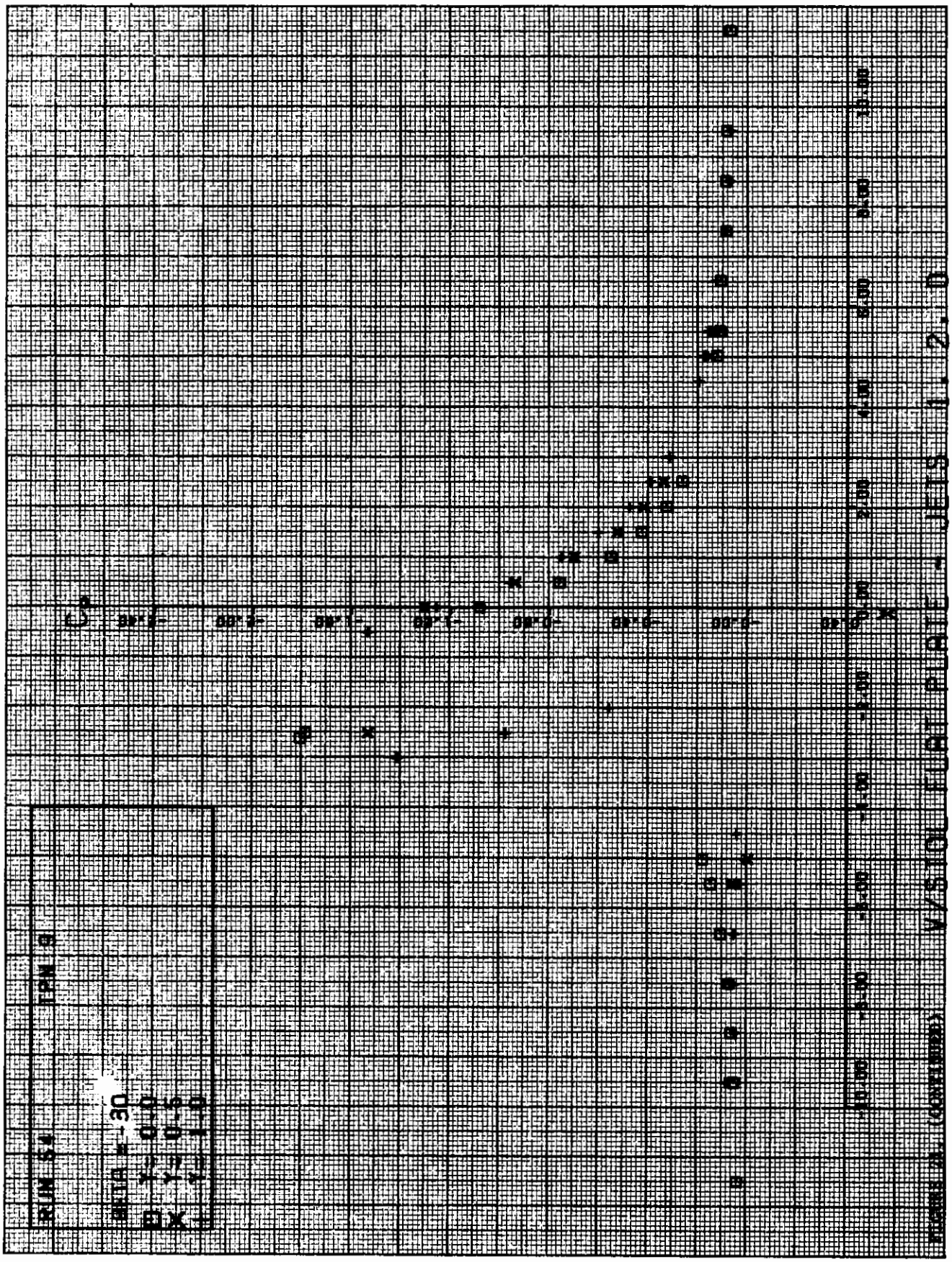

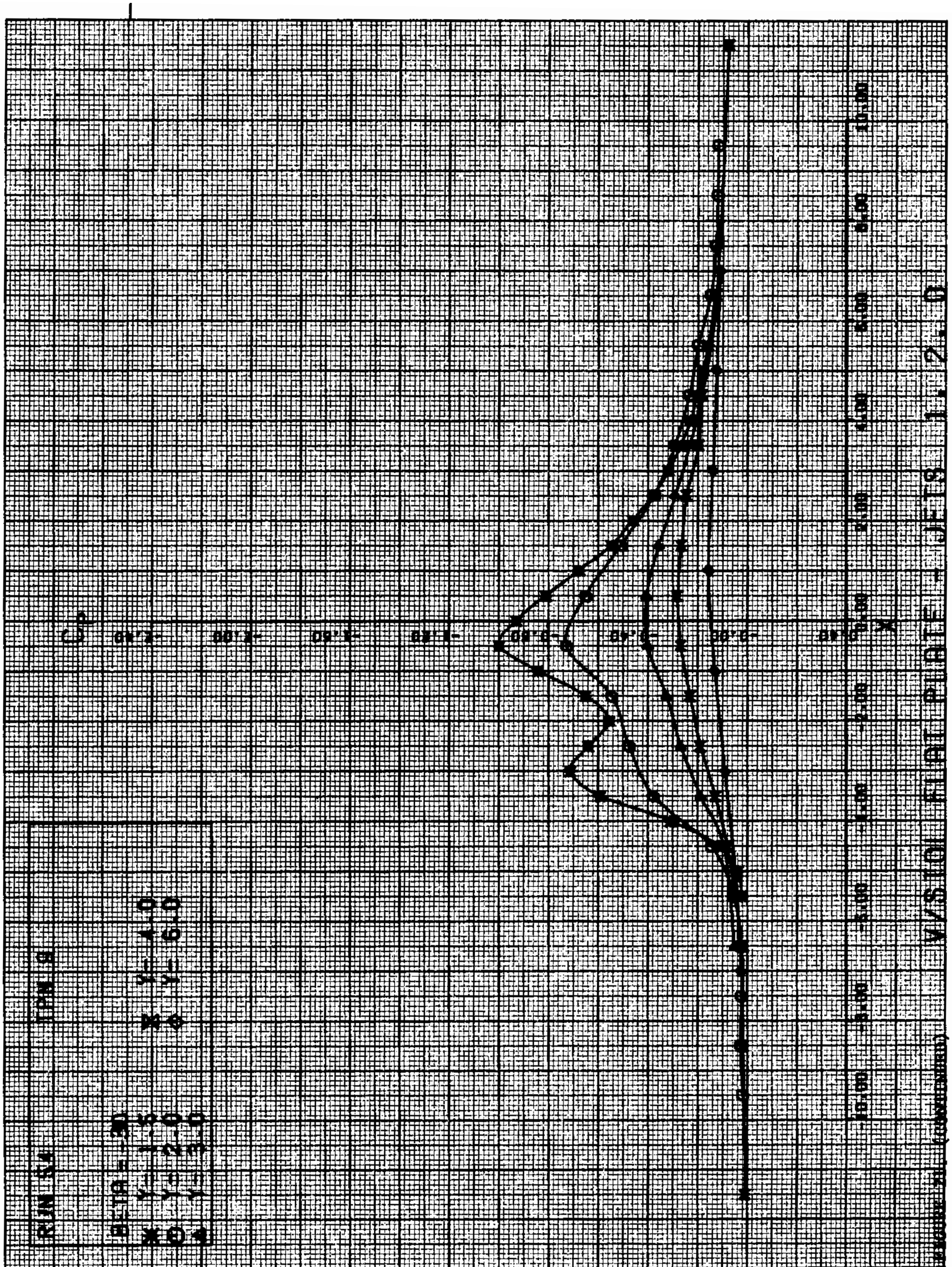

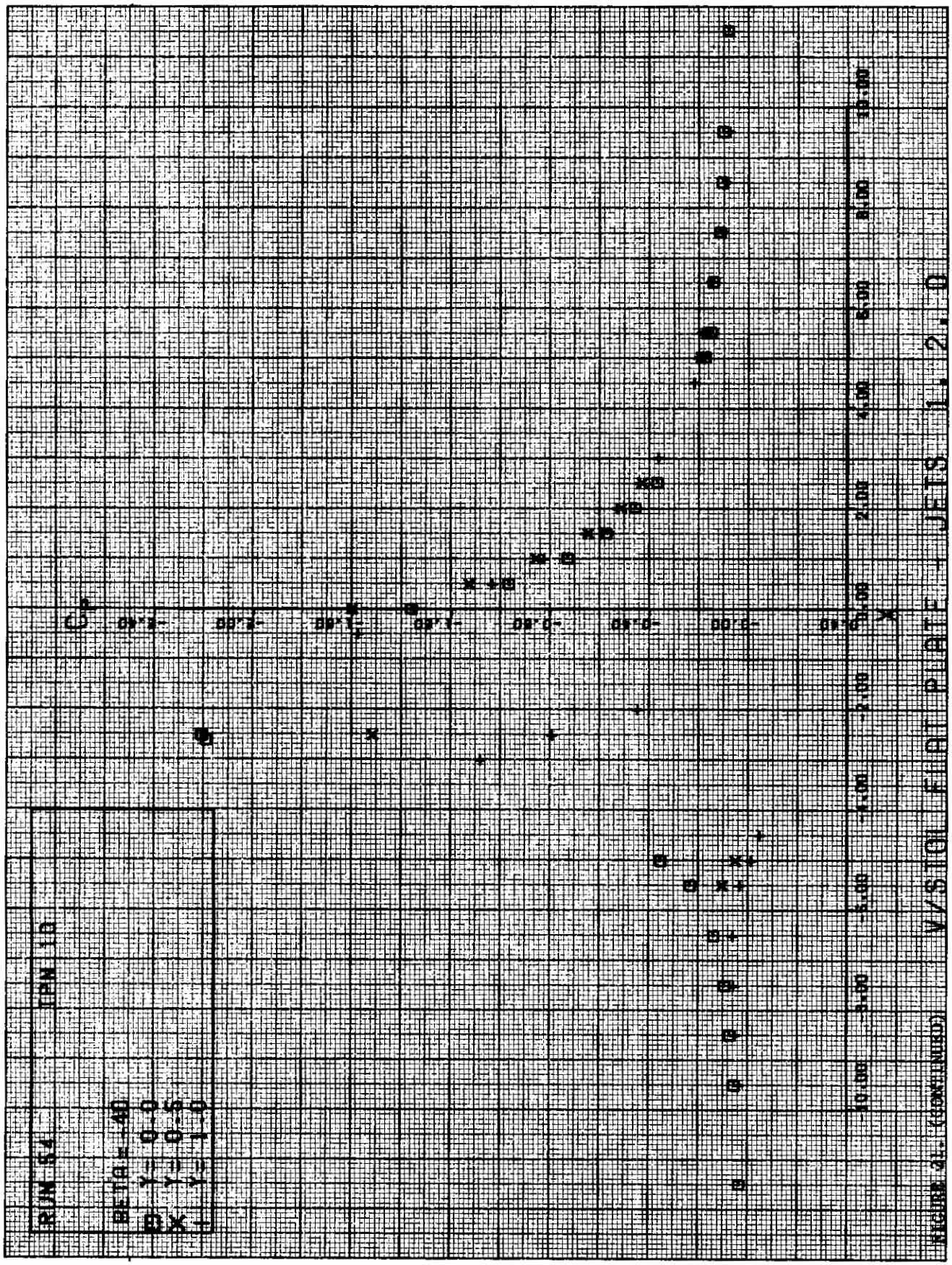

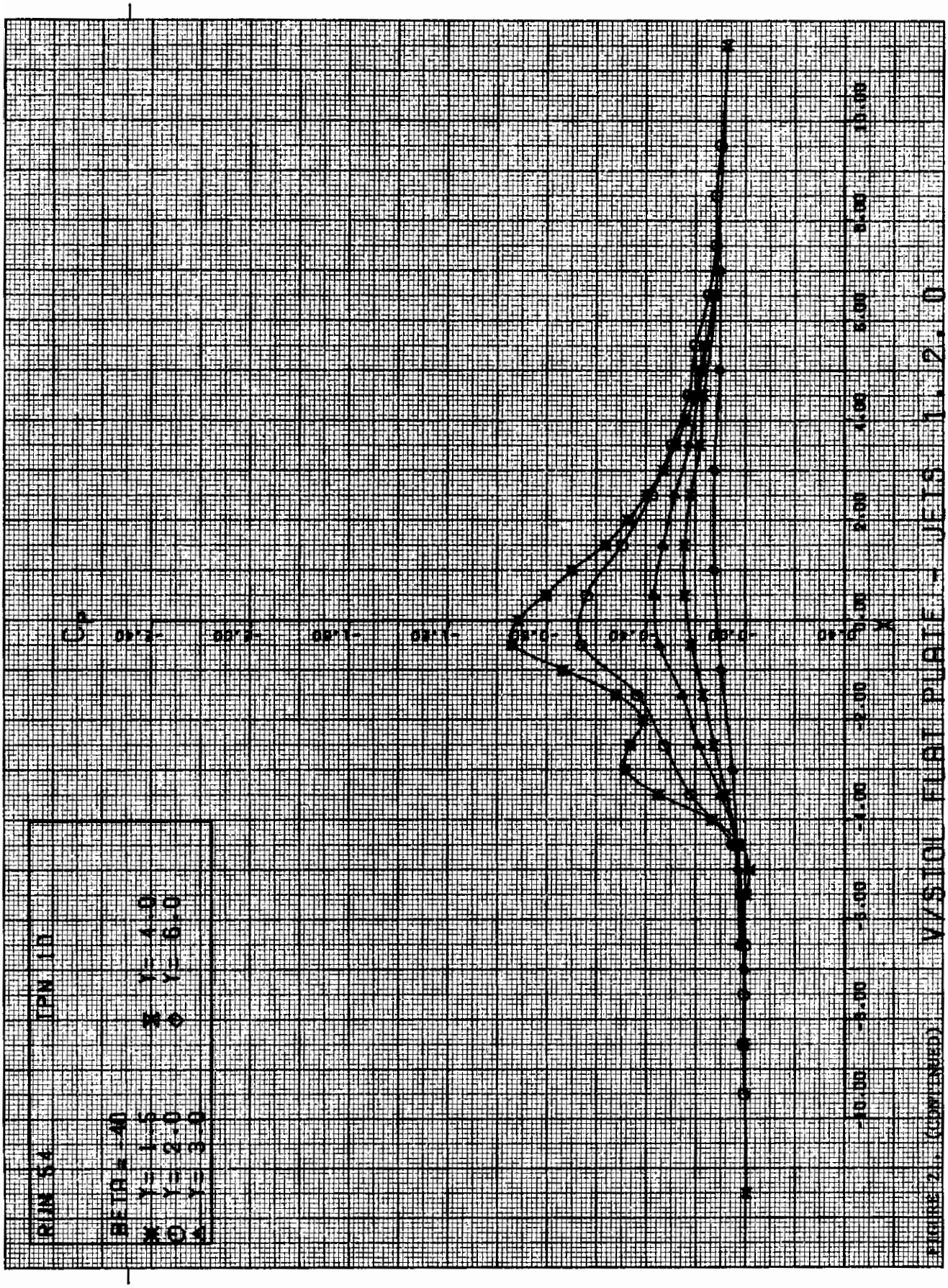

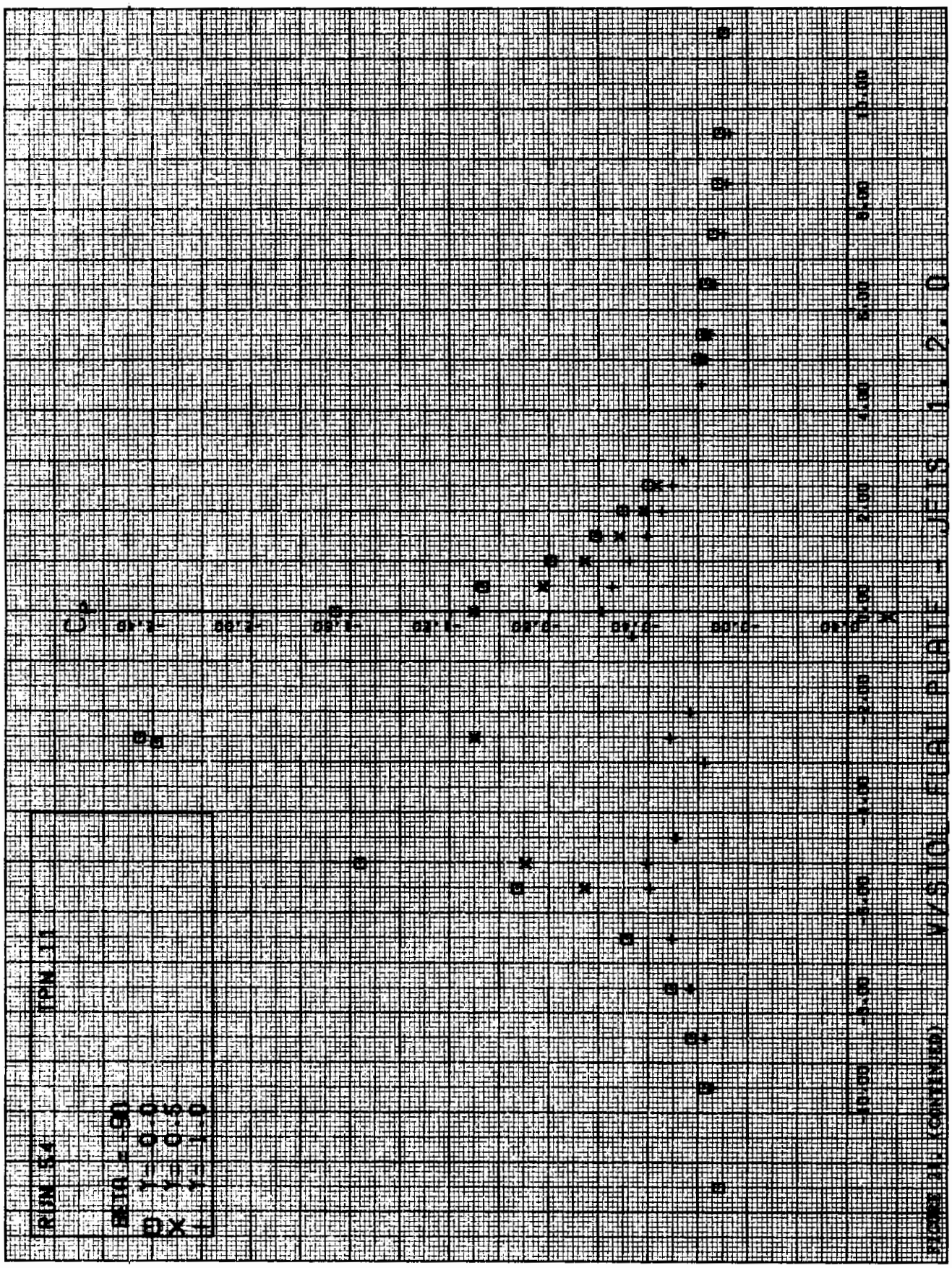

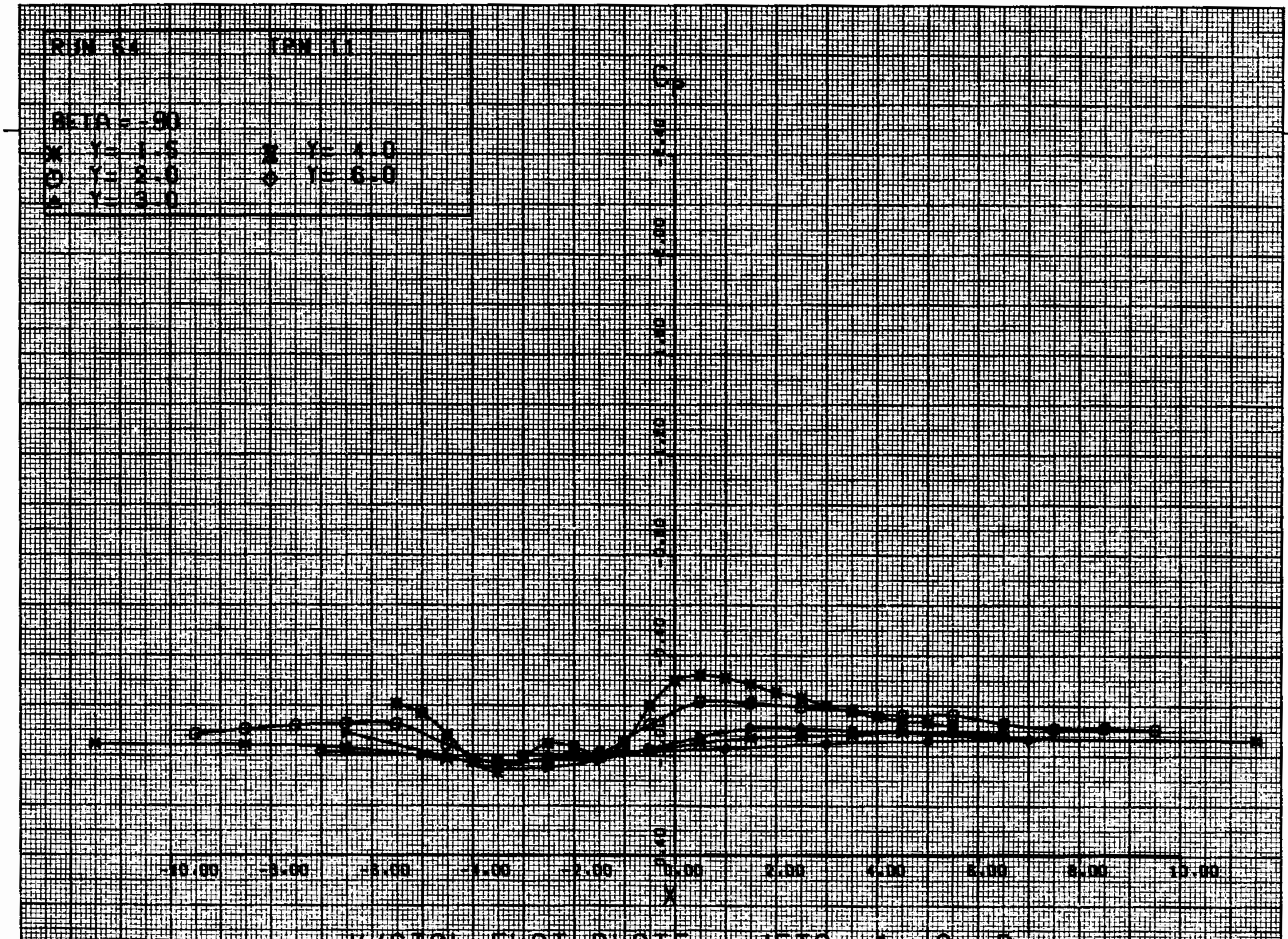

FIGURE 21. (CONCLUDED) V/STOL FLAT PLATE - JETS 1, 2, 0

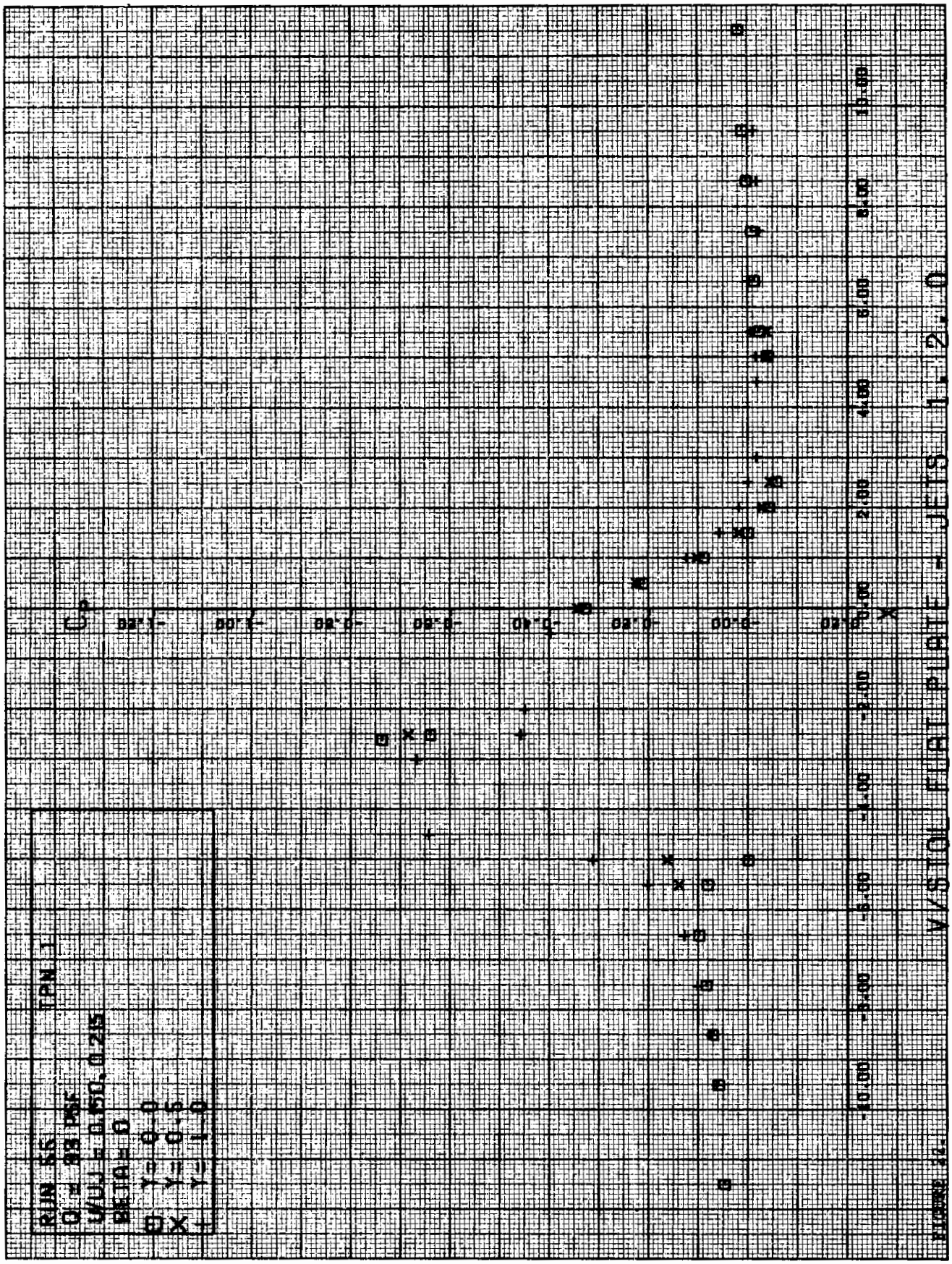

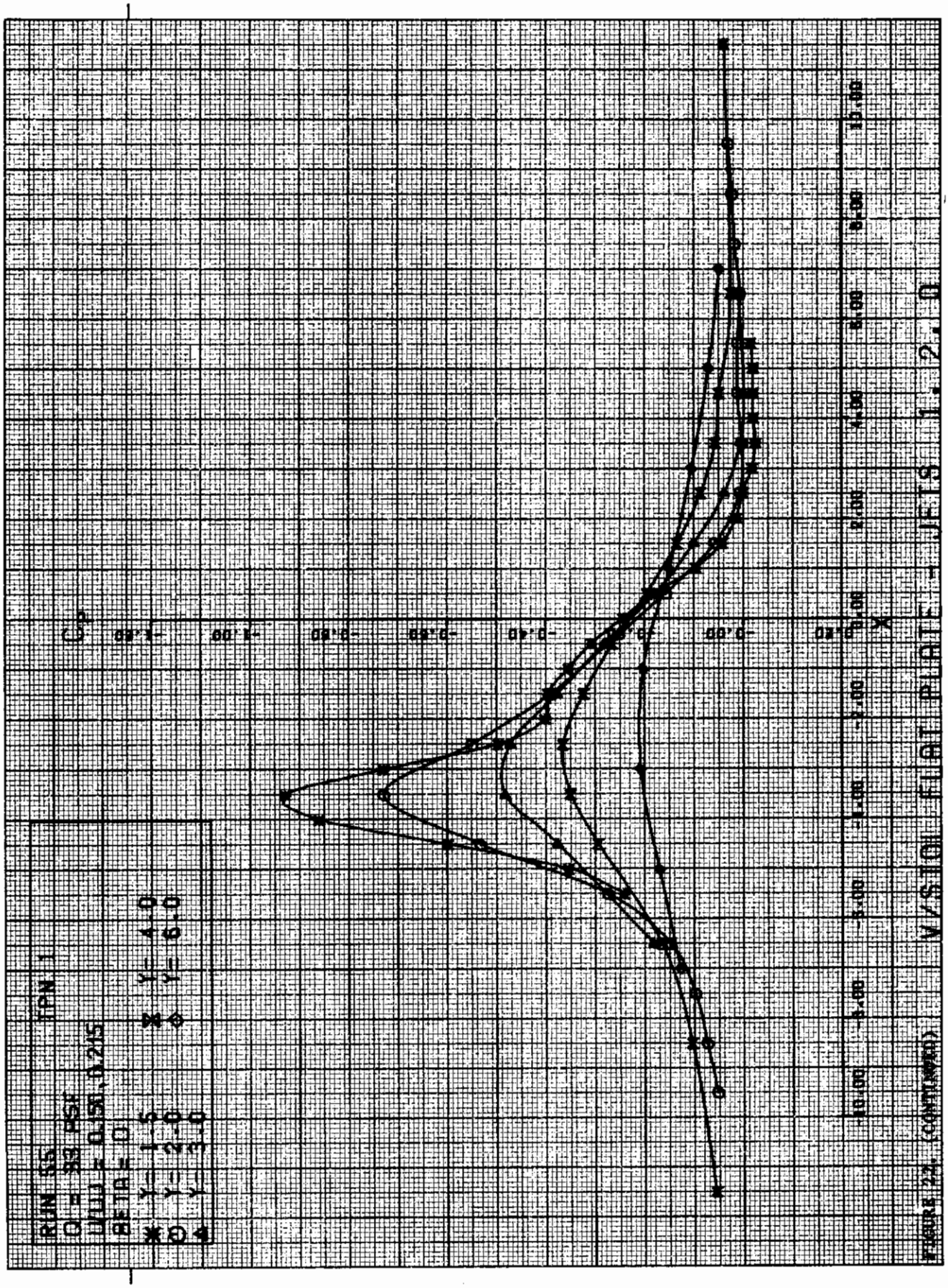

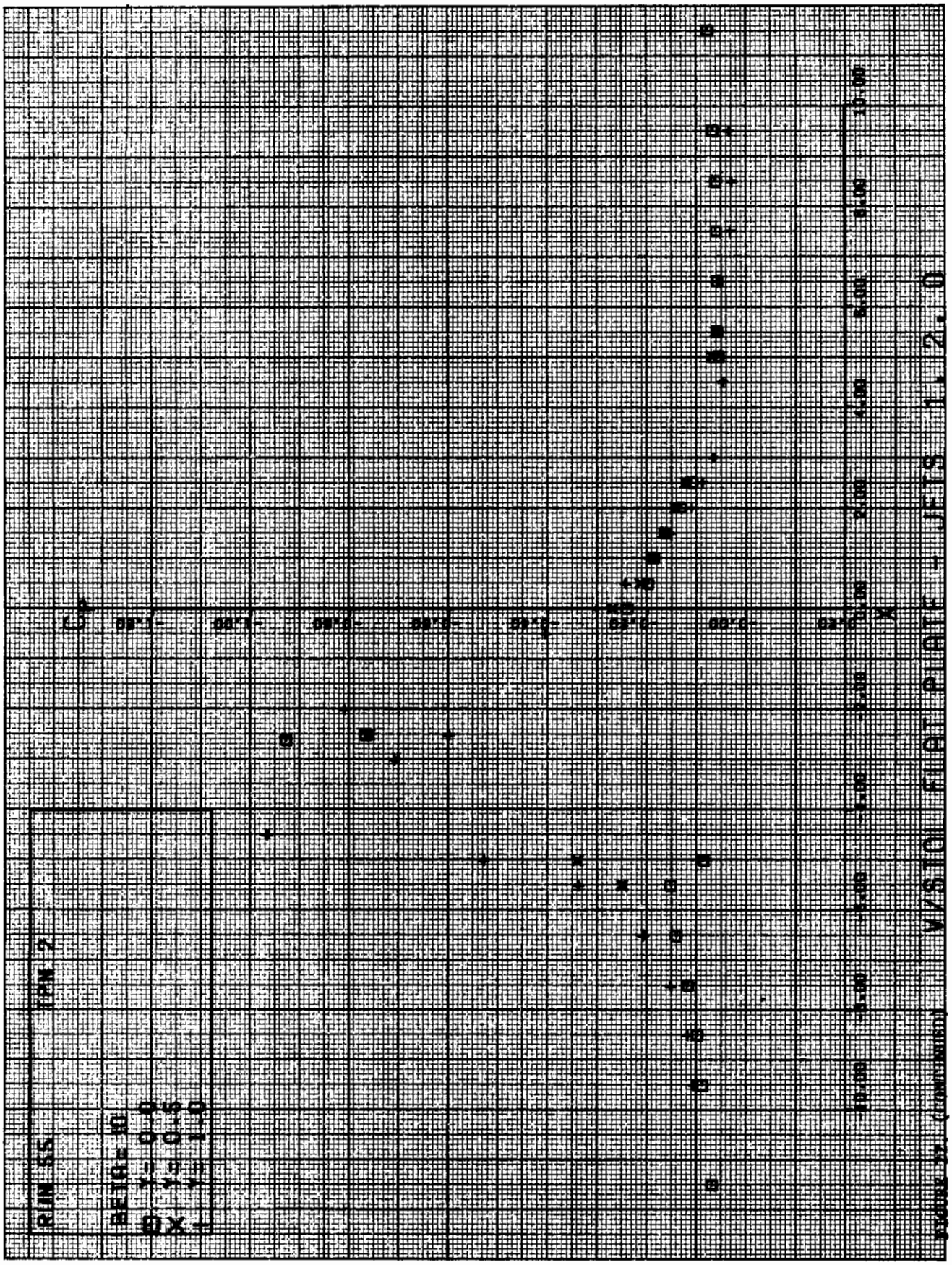

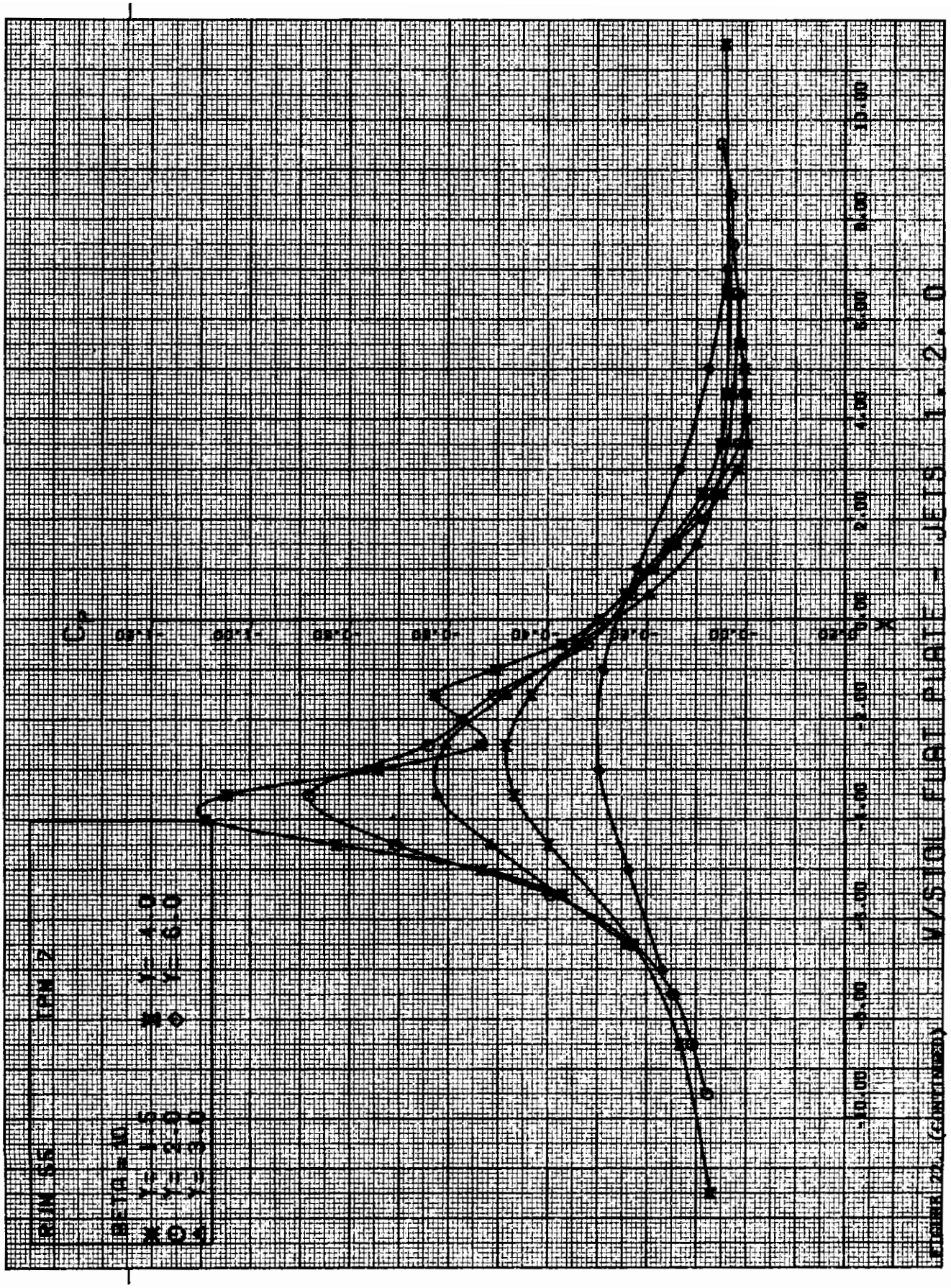

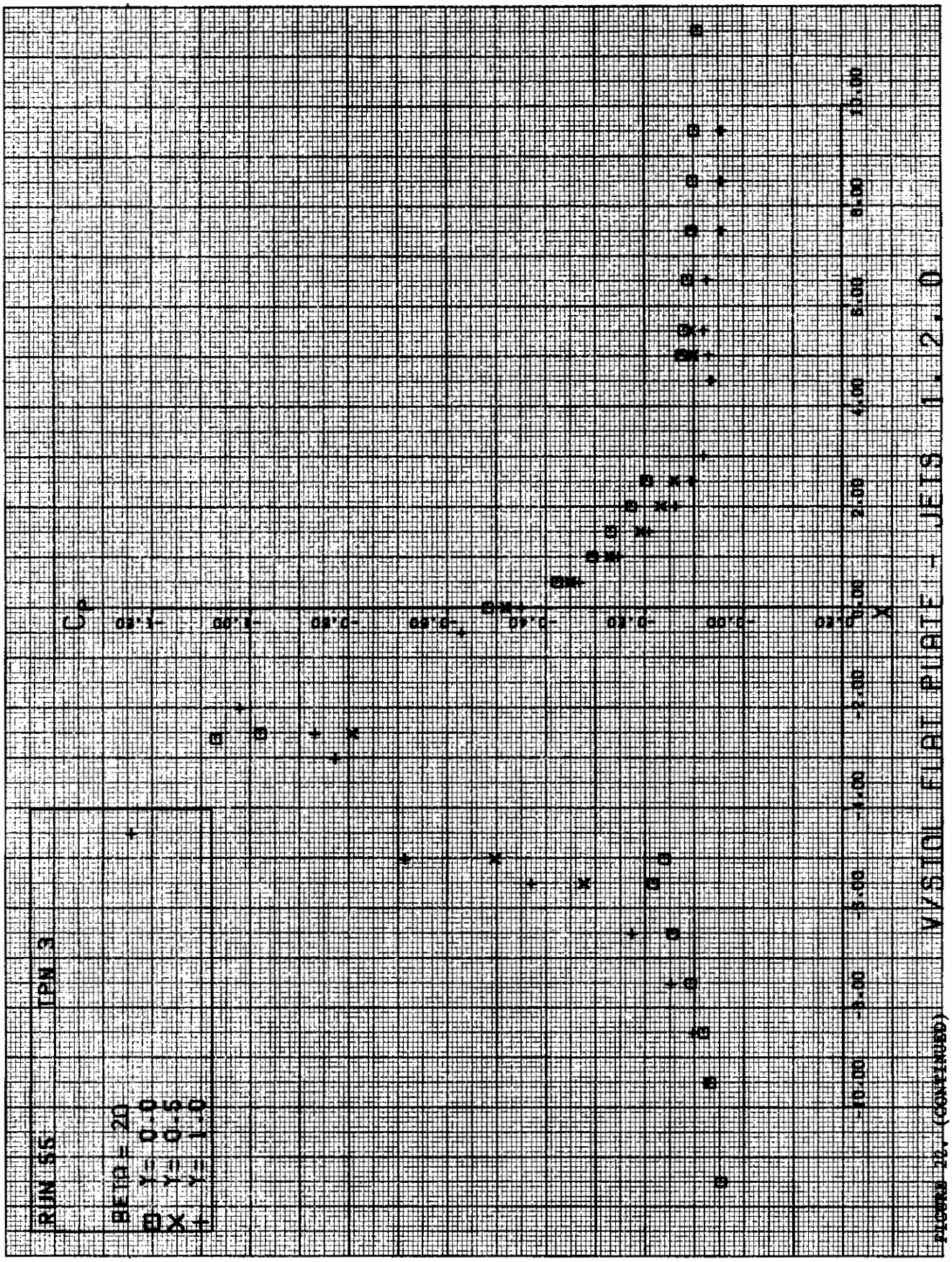

FIGURE 22. (CONTINUED)

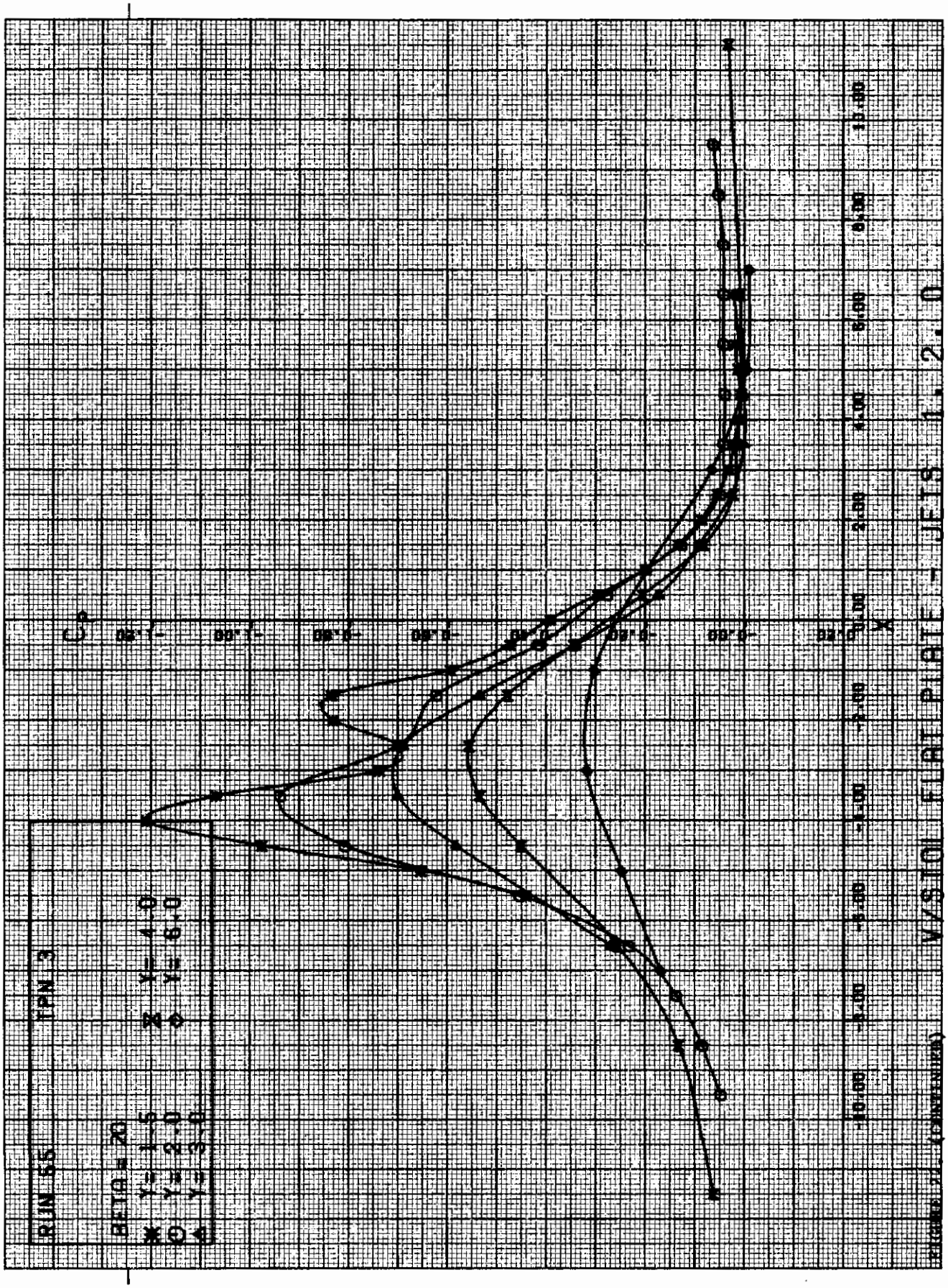

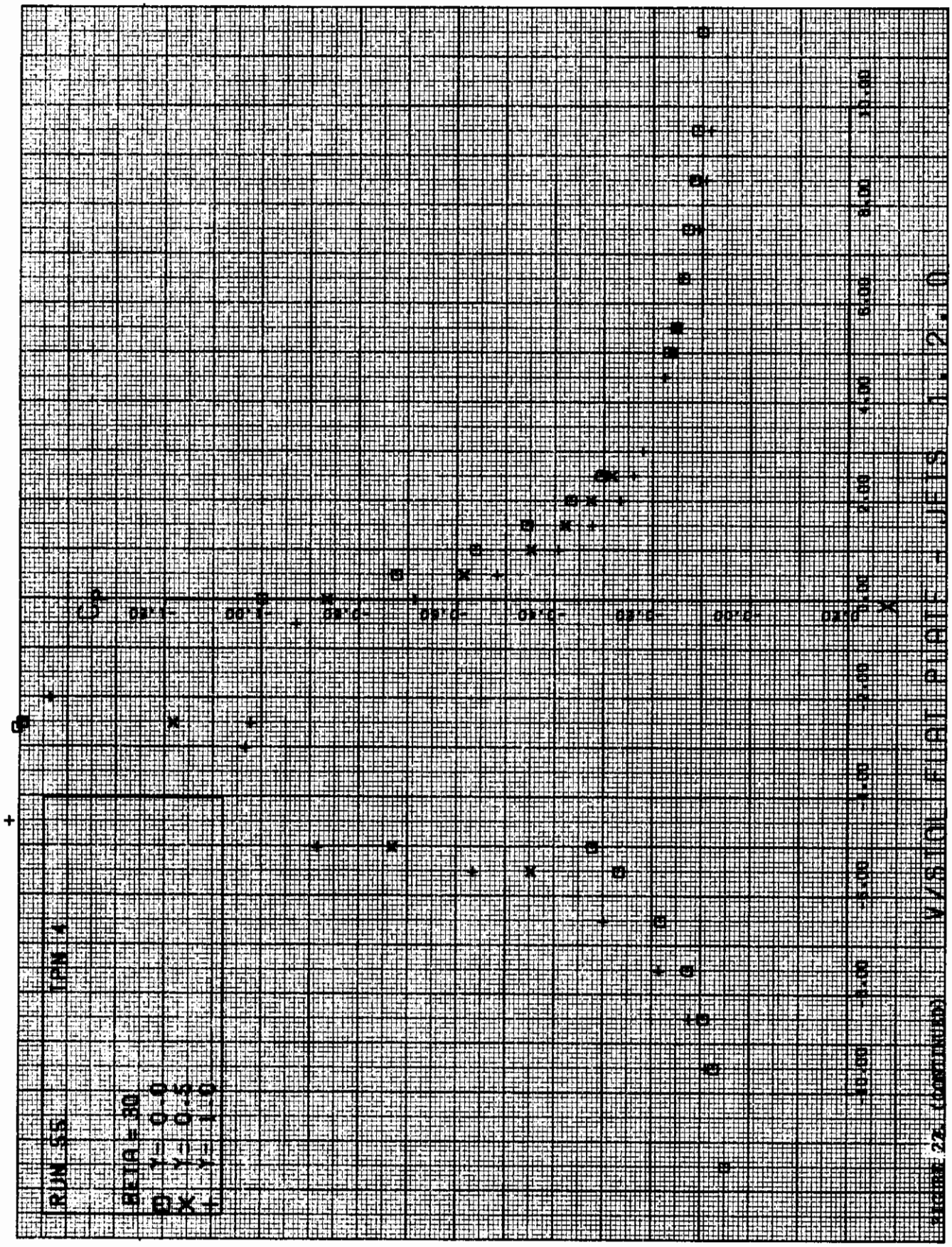

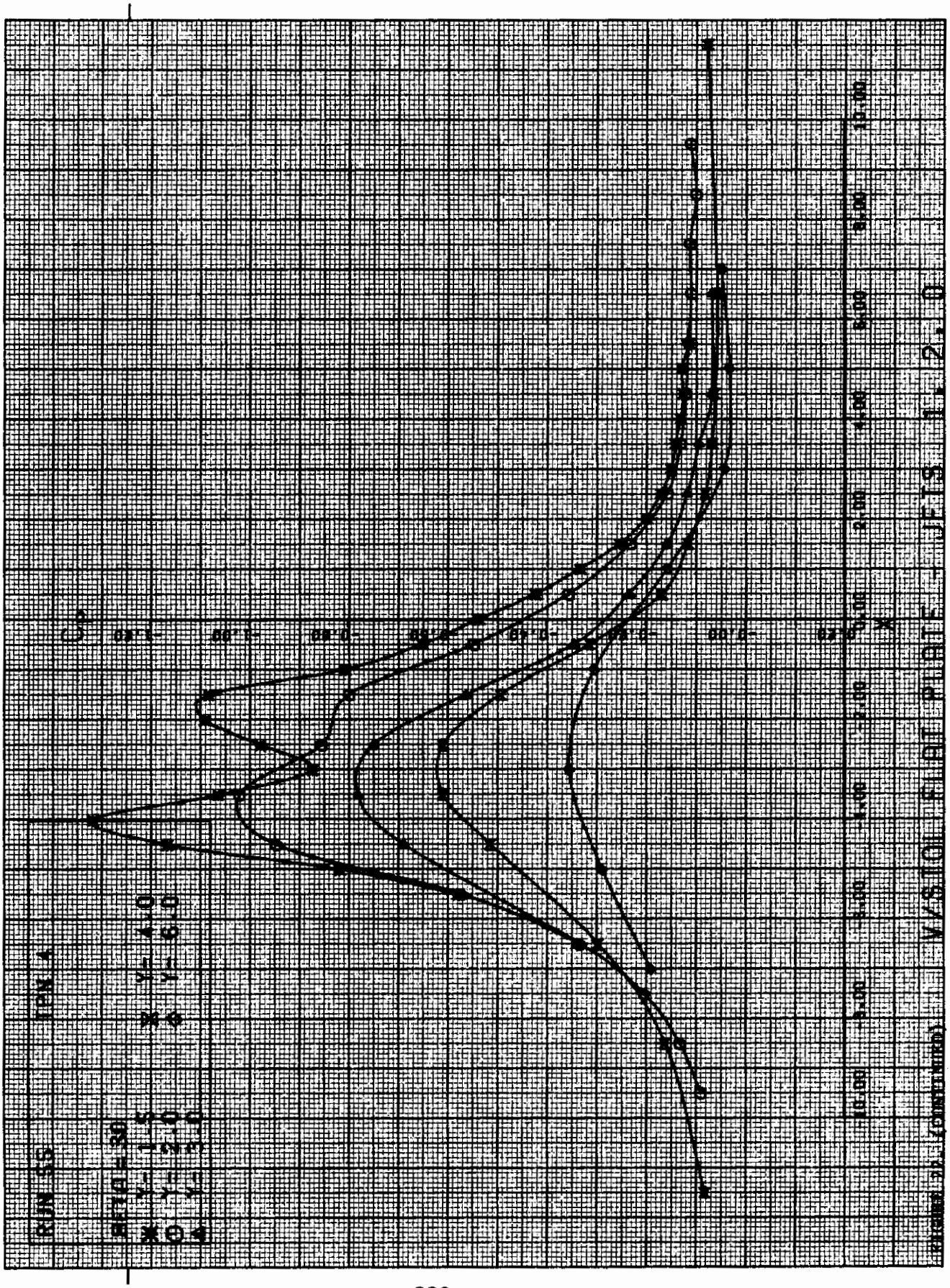

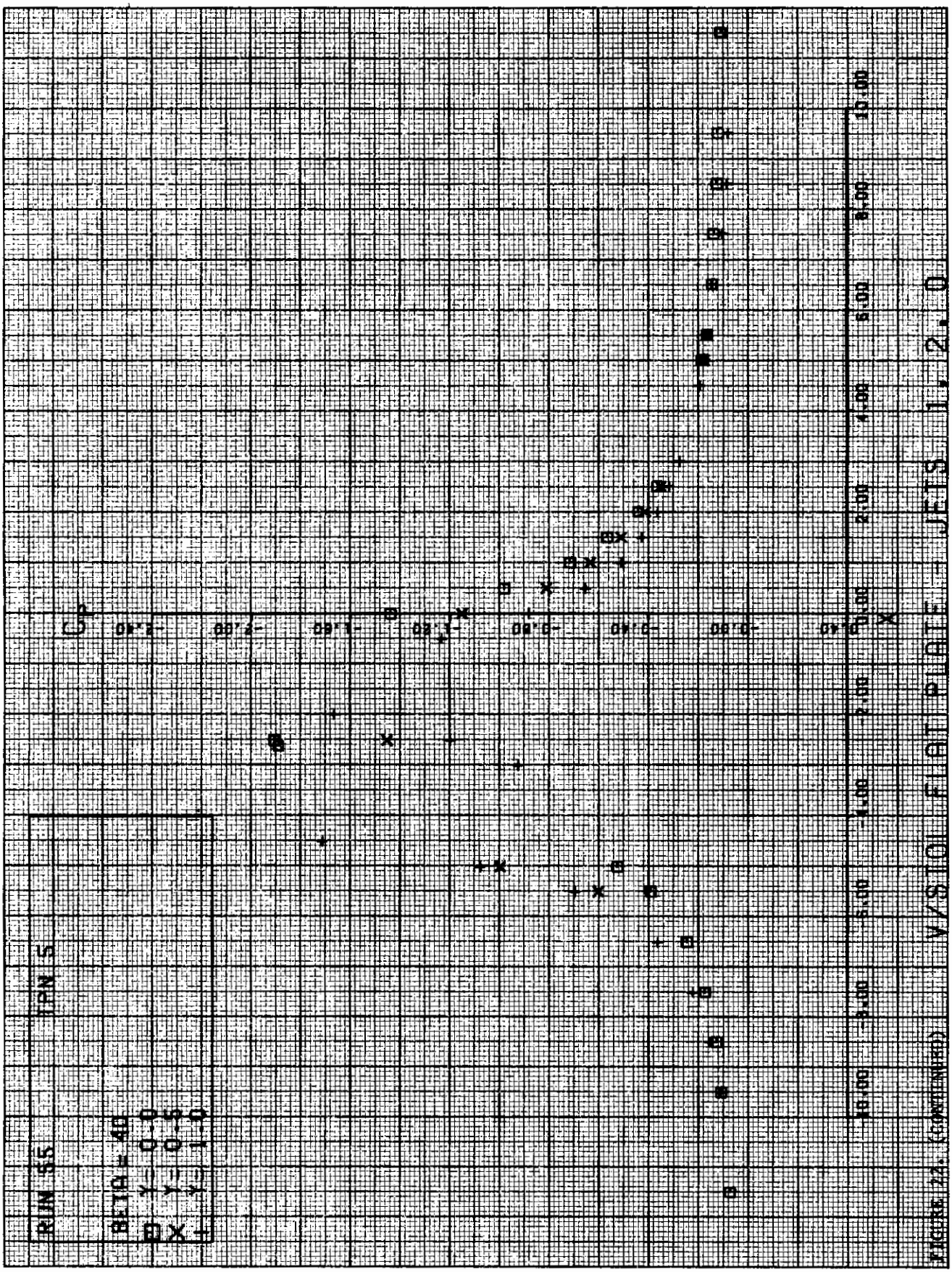

FIGURE 22. (CONTINUED)

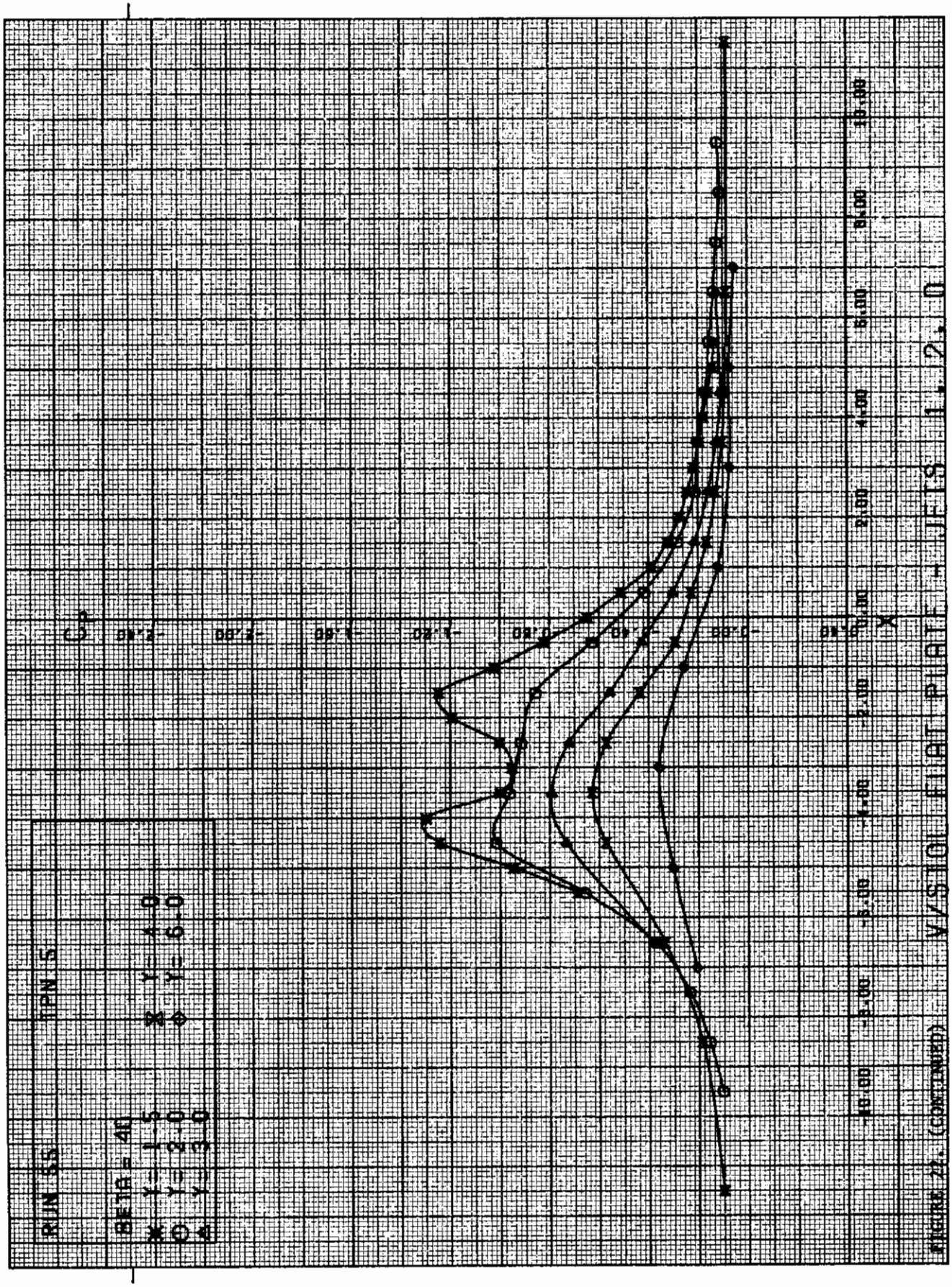

FIGURE 27. (CONTINUED)

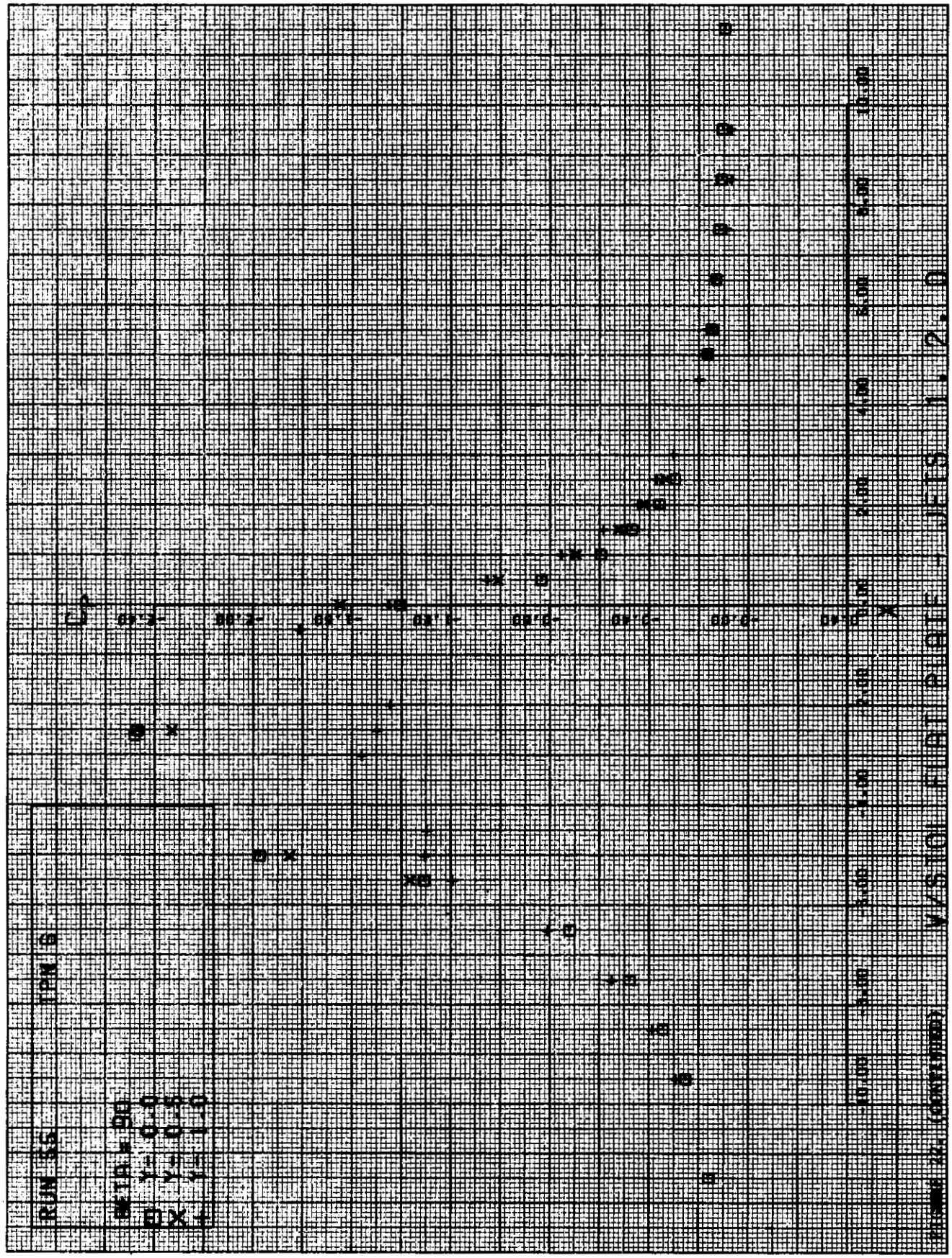

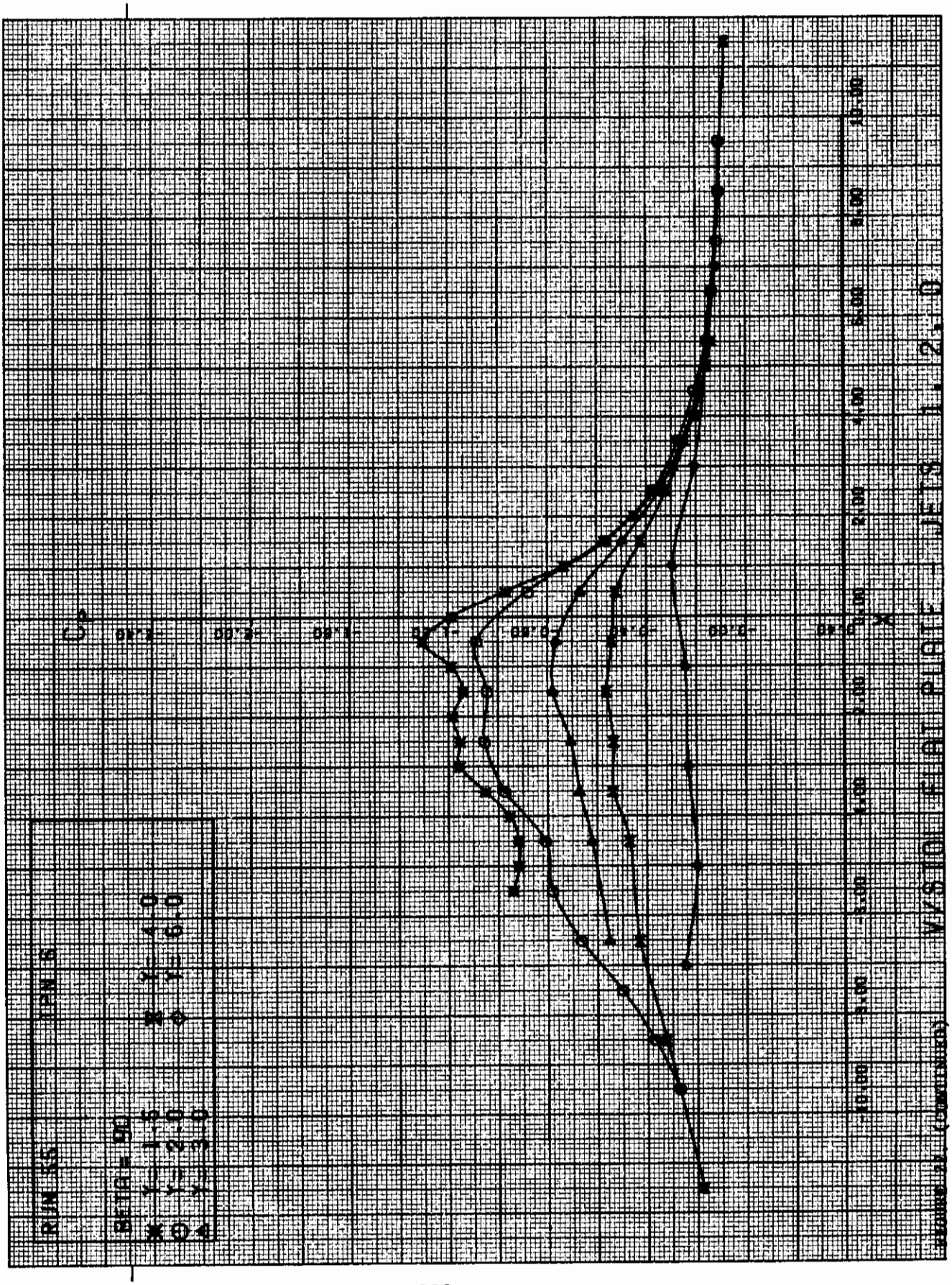

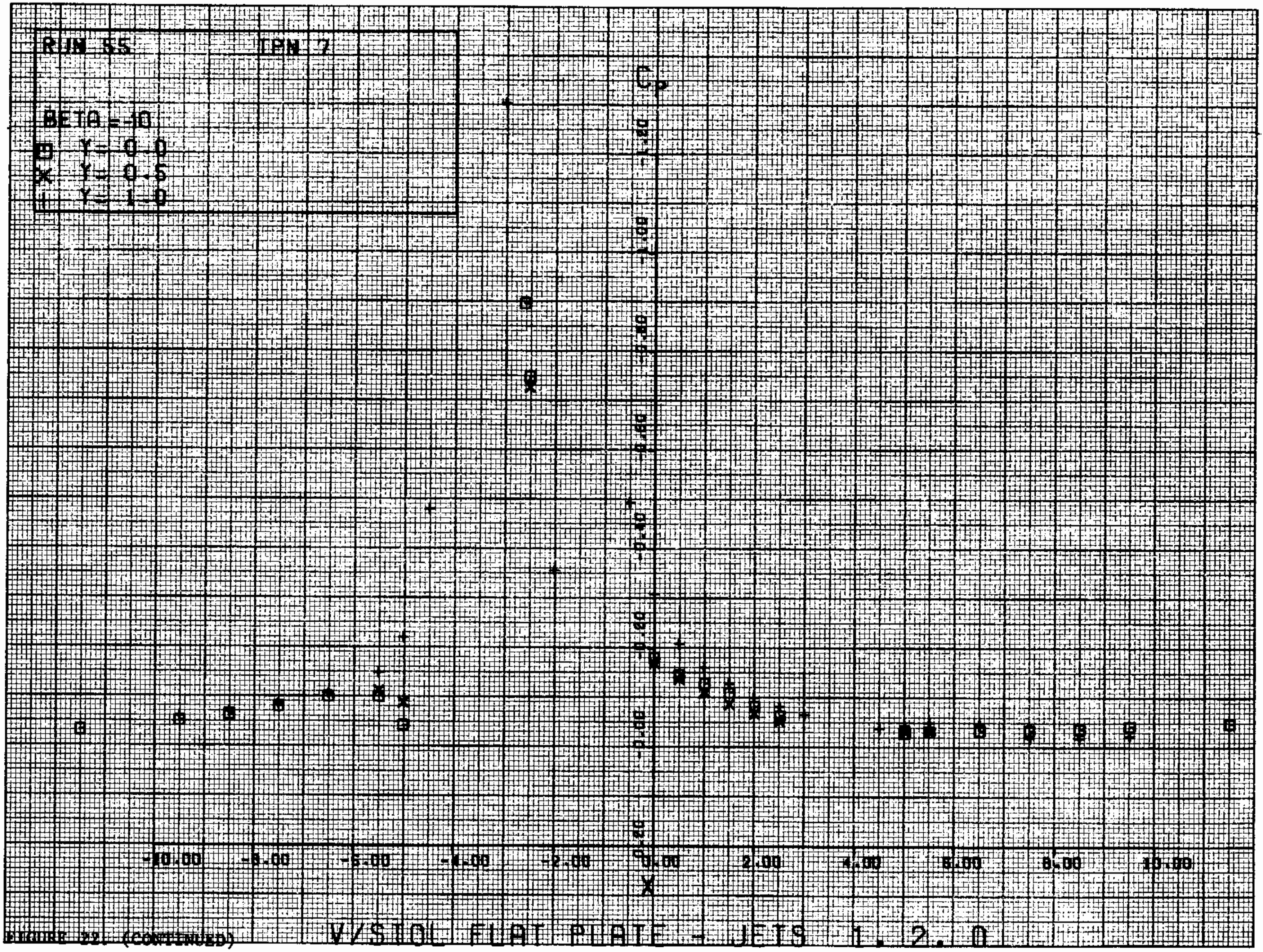

FIGURE 22. (CONTINUED)

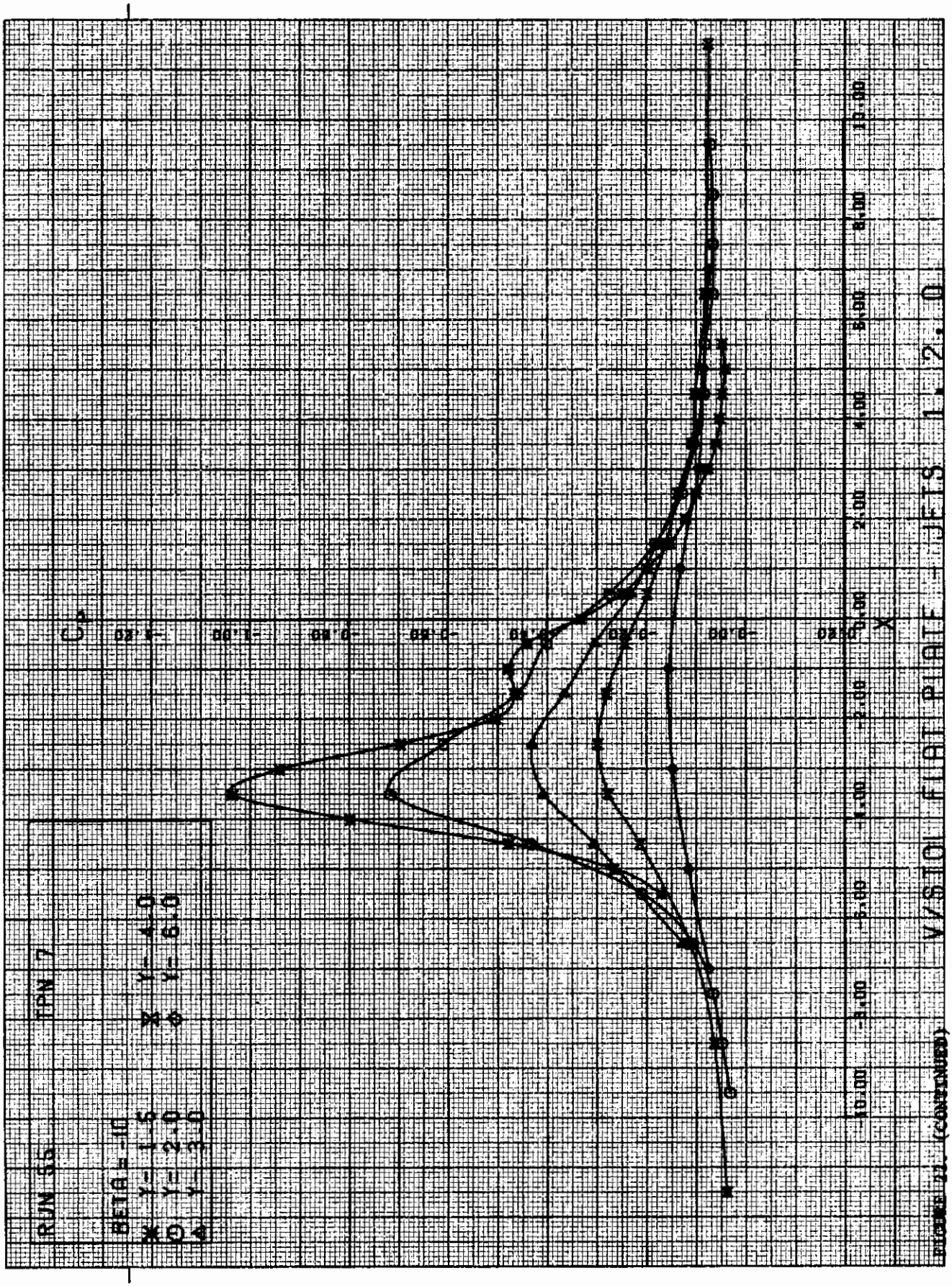

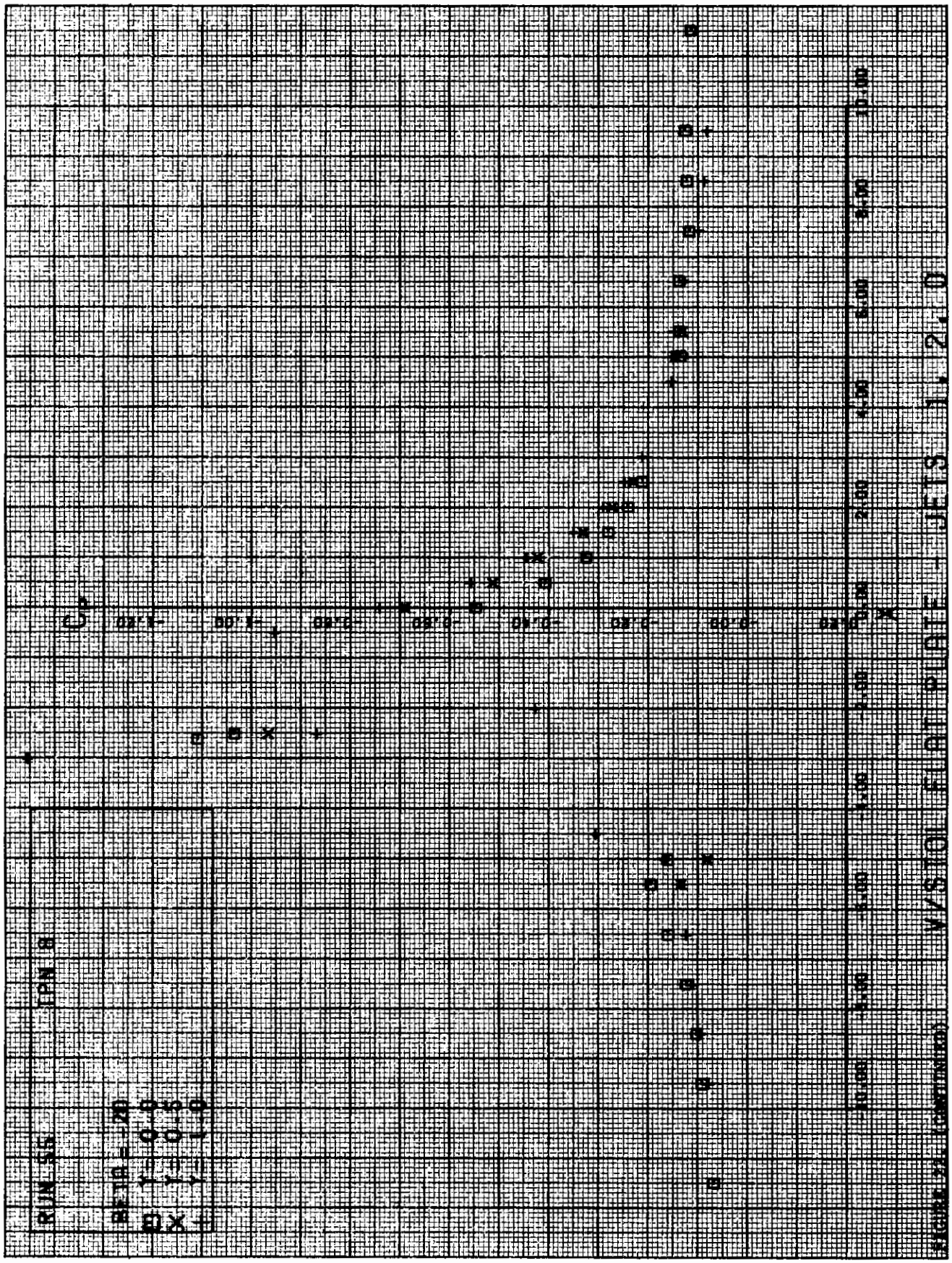

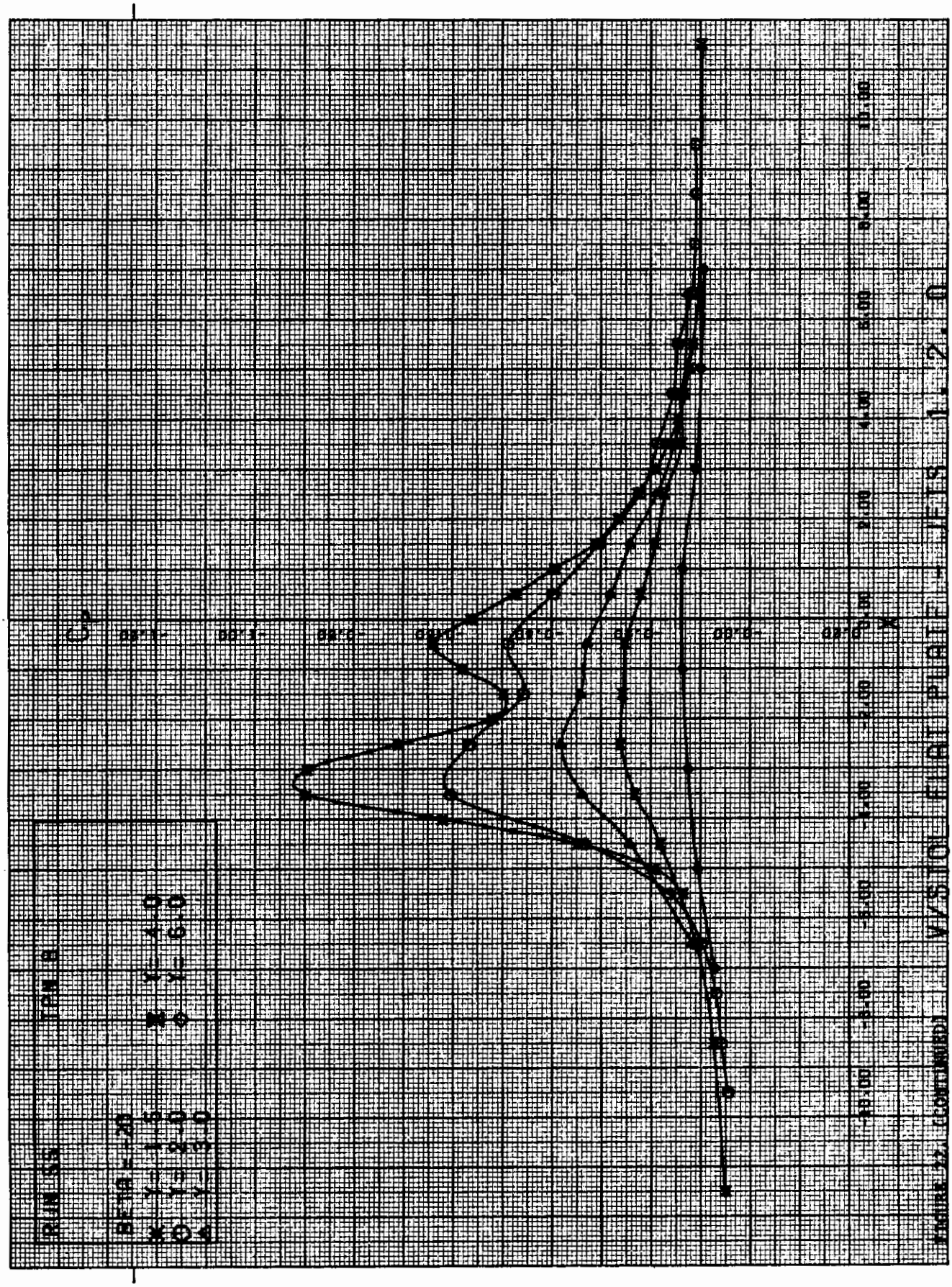

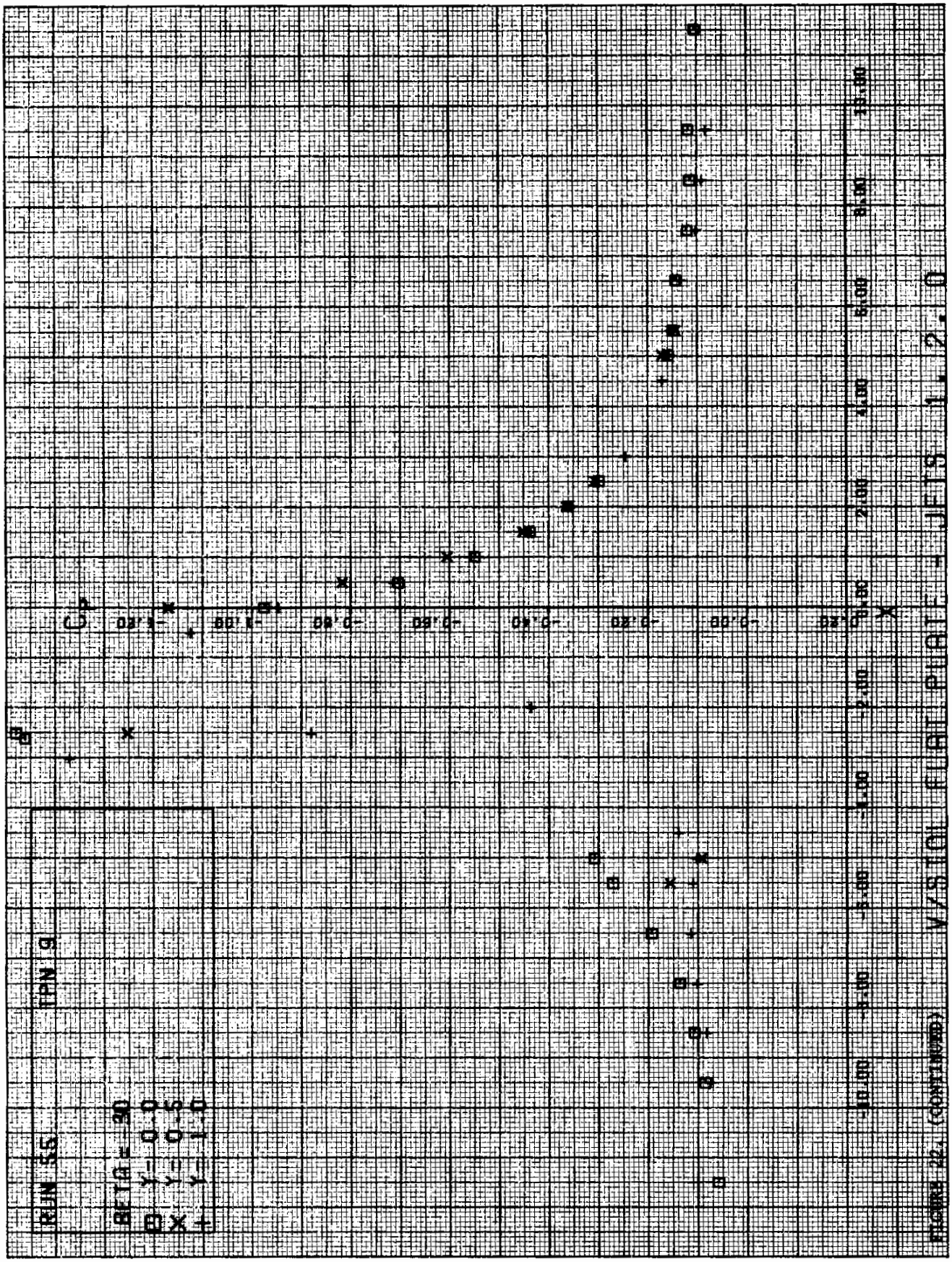

FIGURE 22. (CONTINUED)

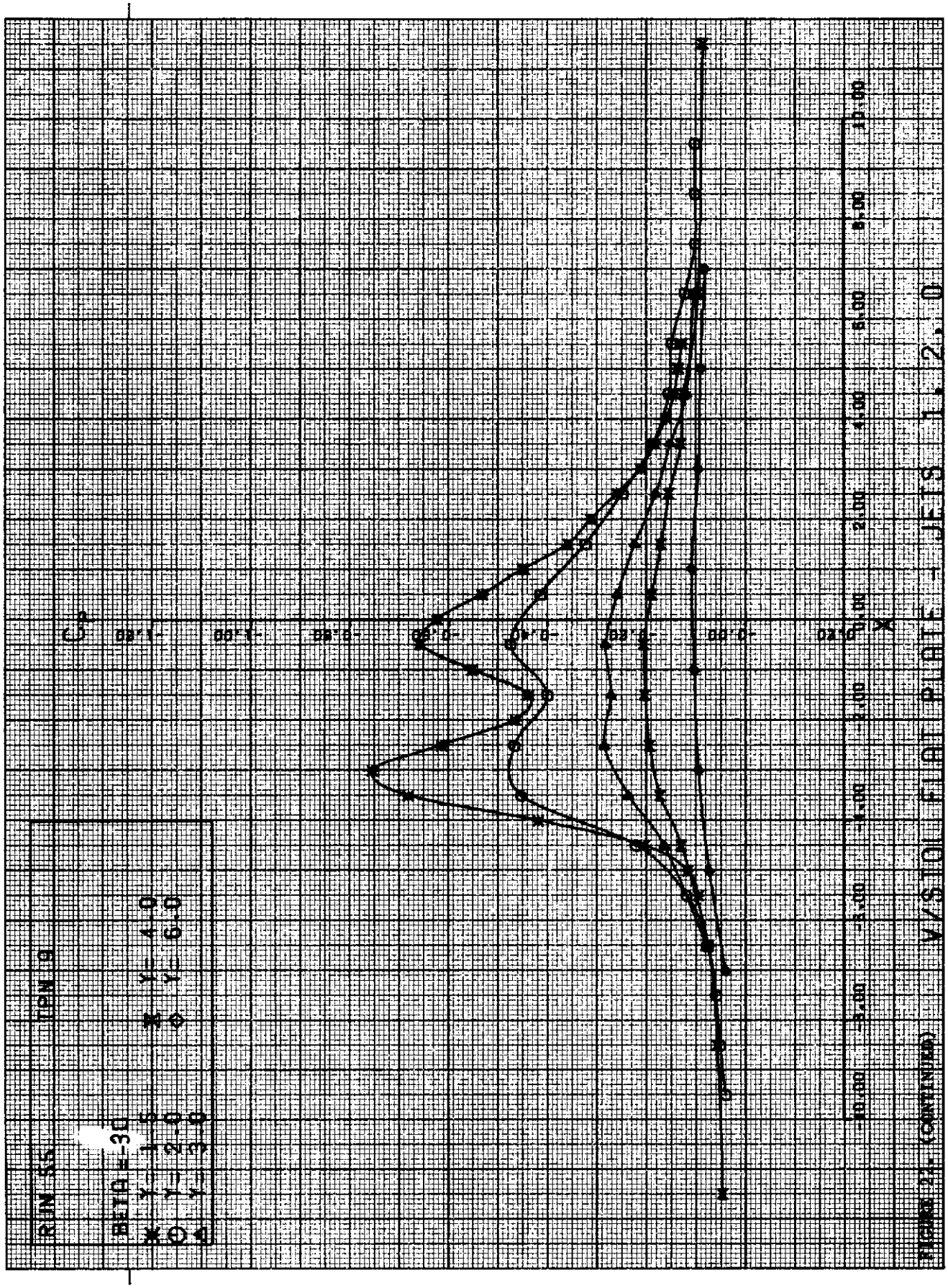

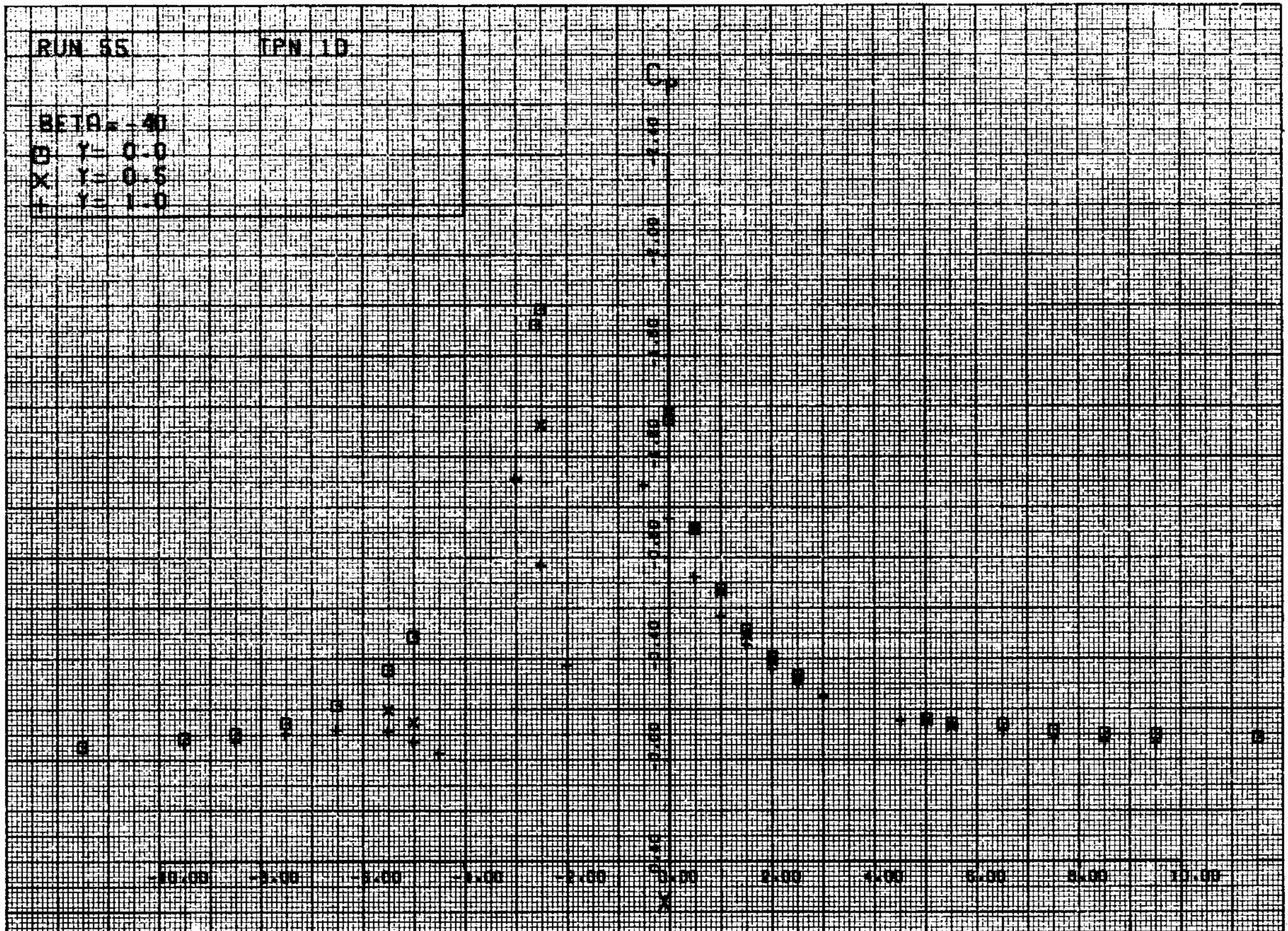

FIGURE 22. (CONTINUED) V/STOL FLAT PLATE - JETS 1, 2, 0

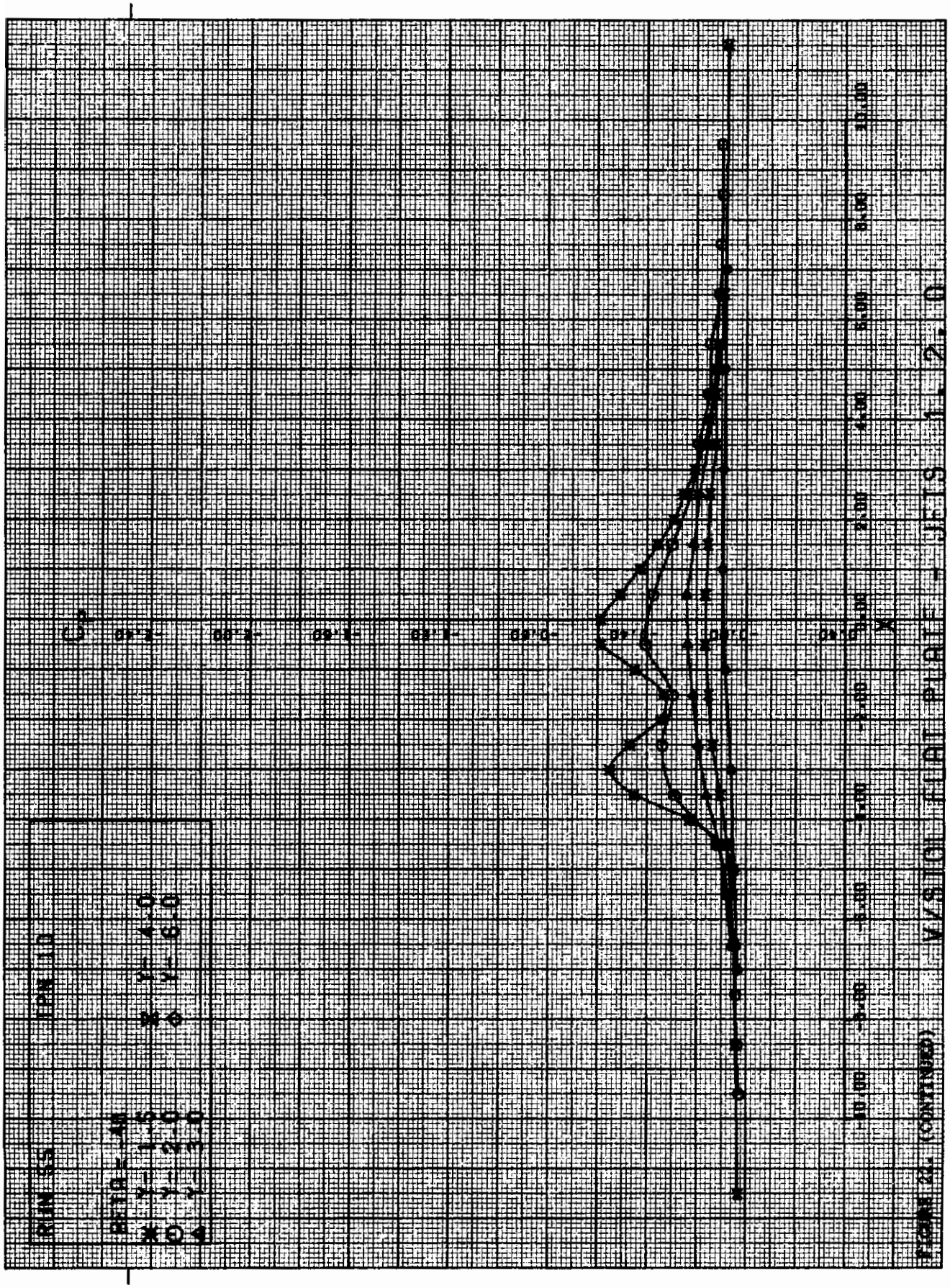

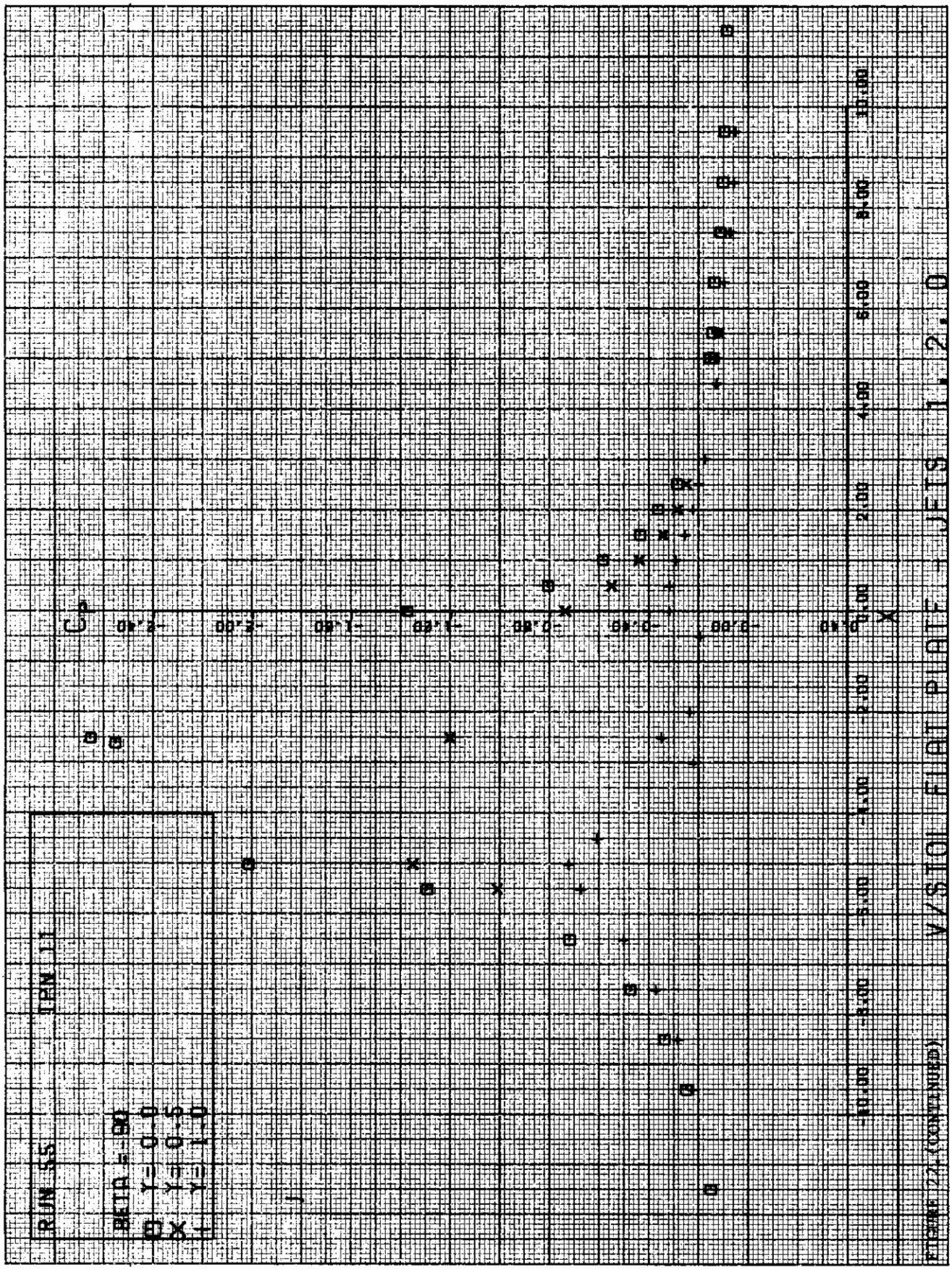

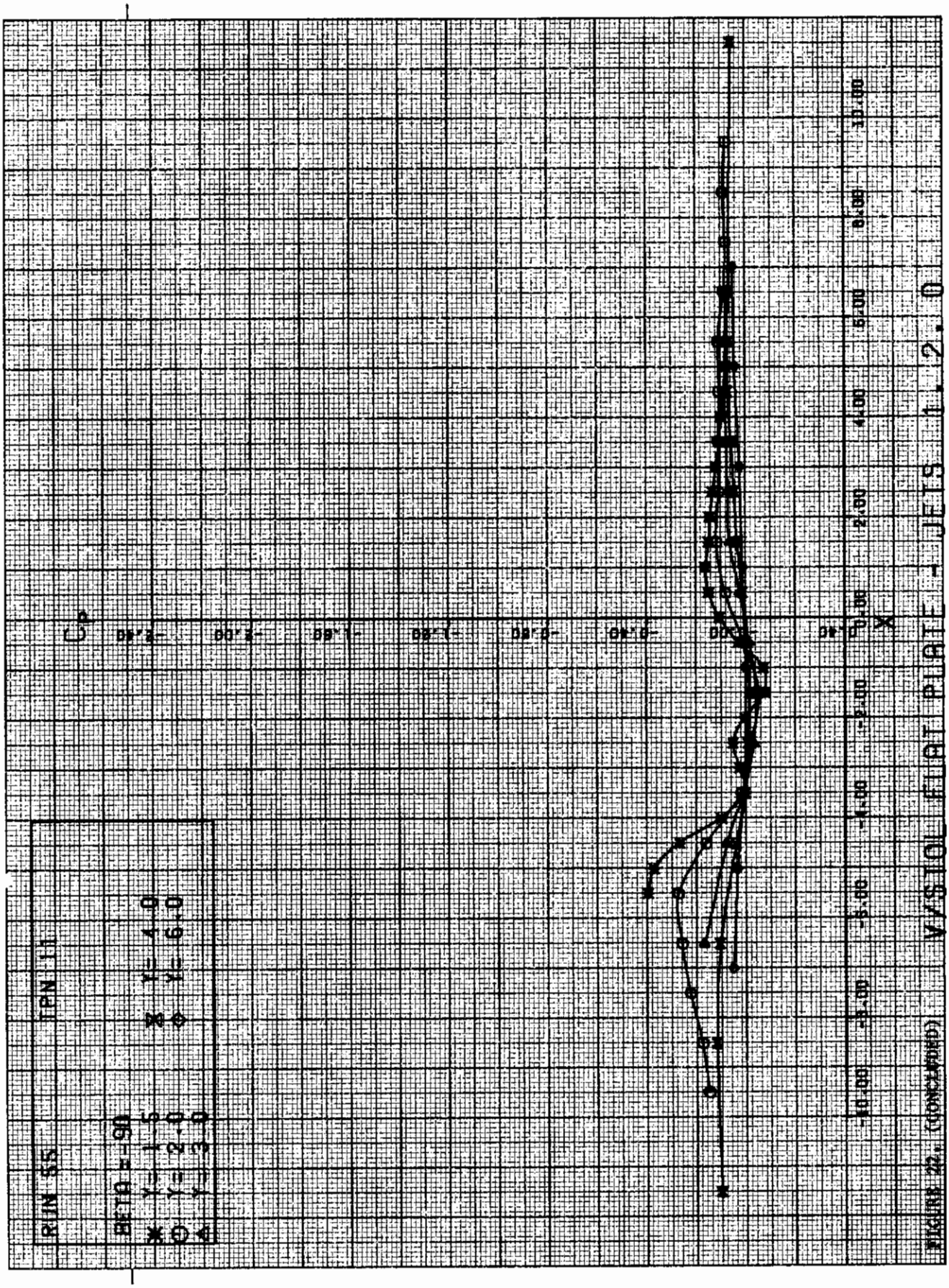

FIGURE 22. (CONCLUDED)

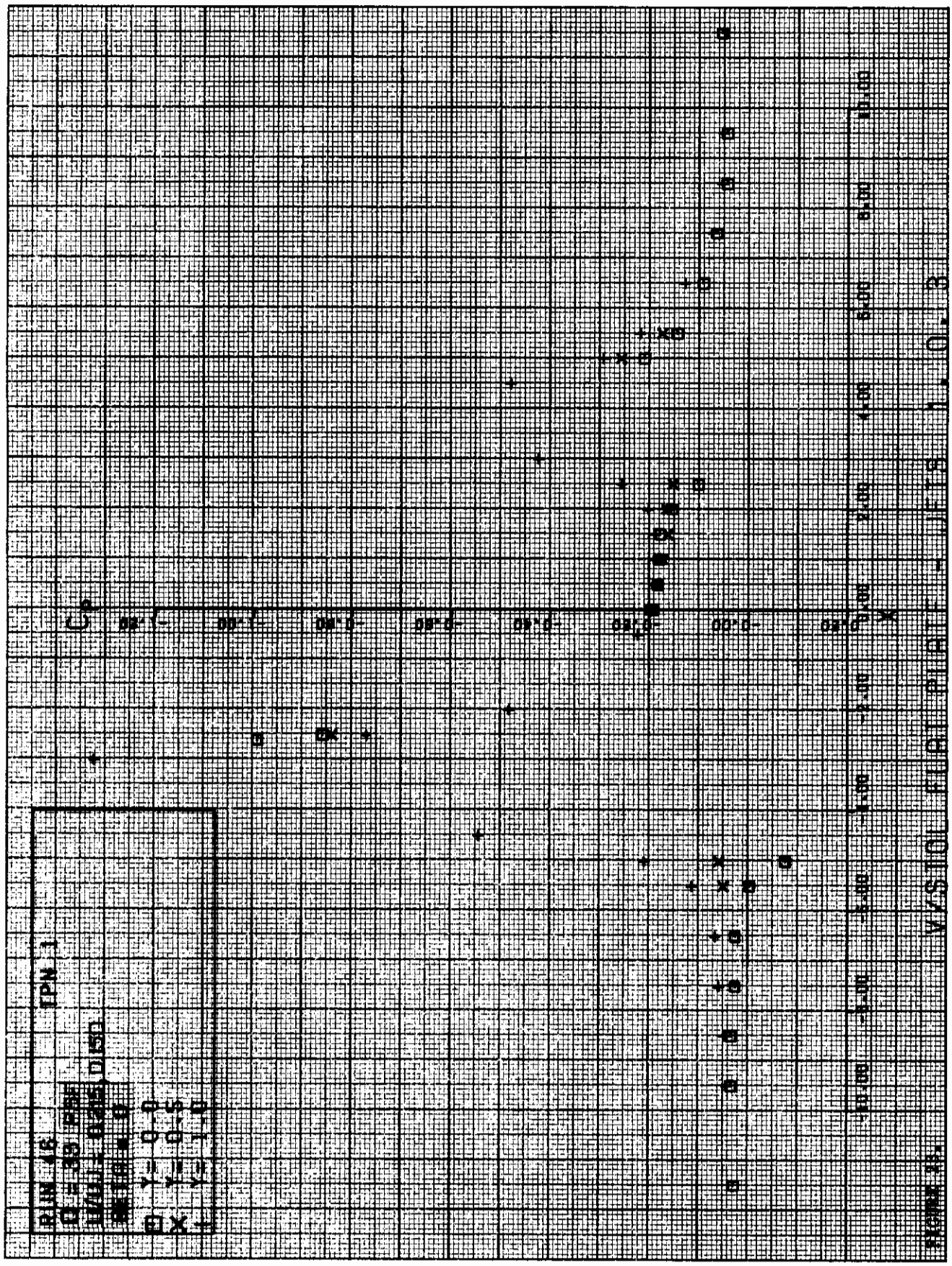

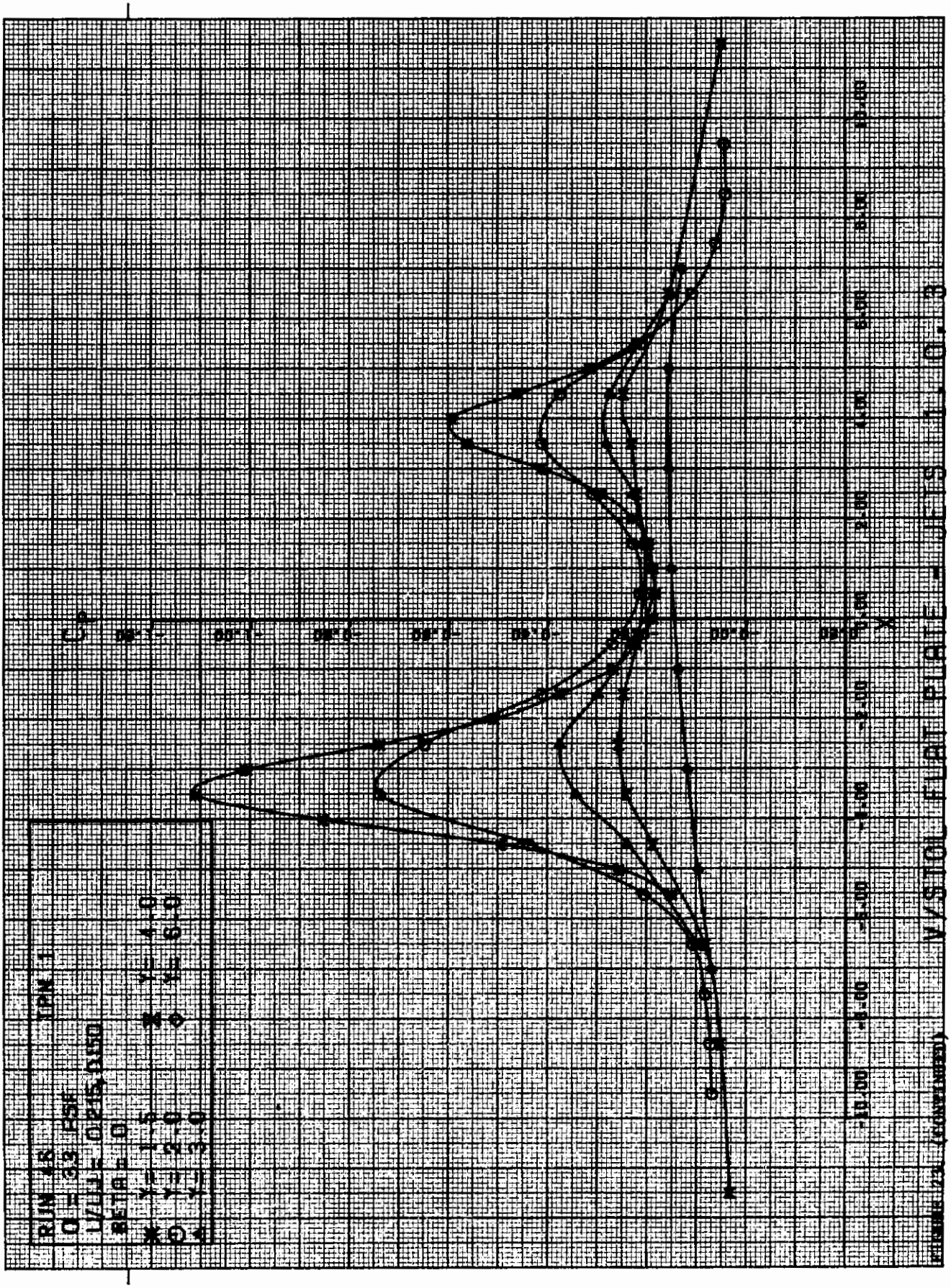

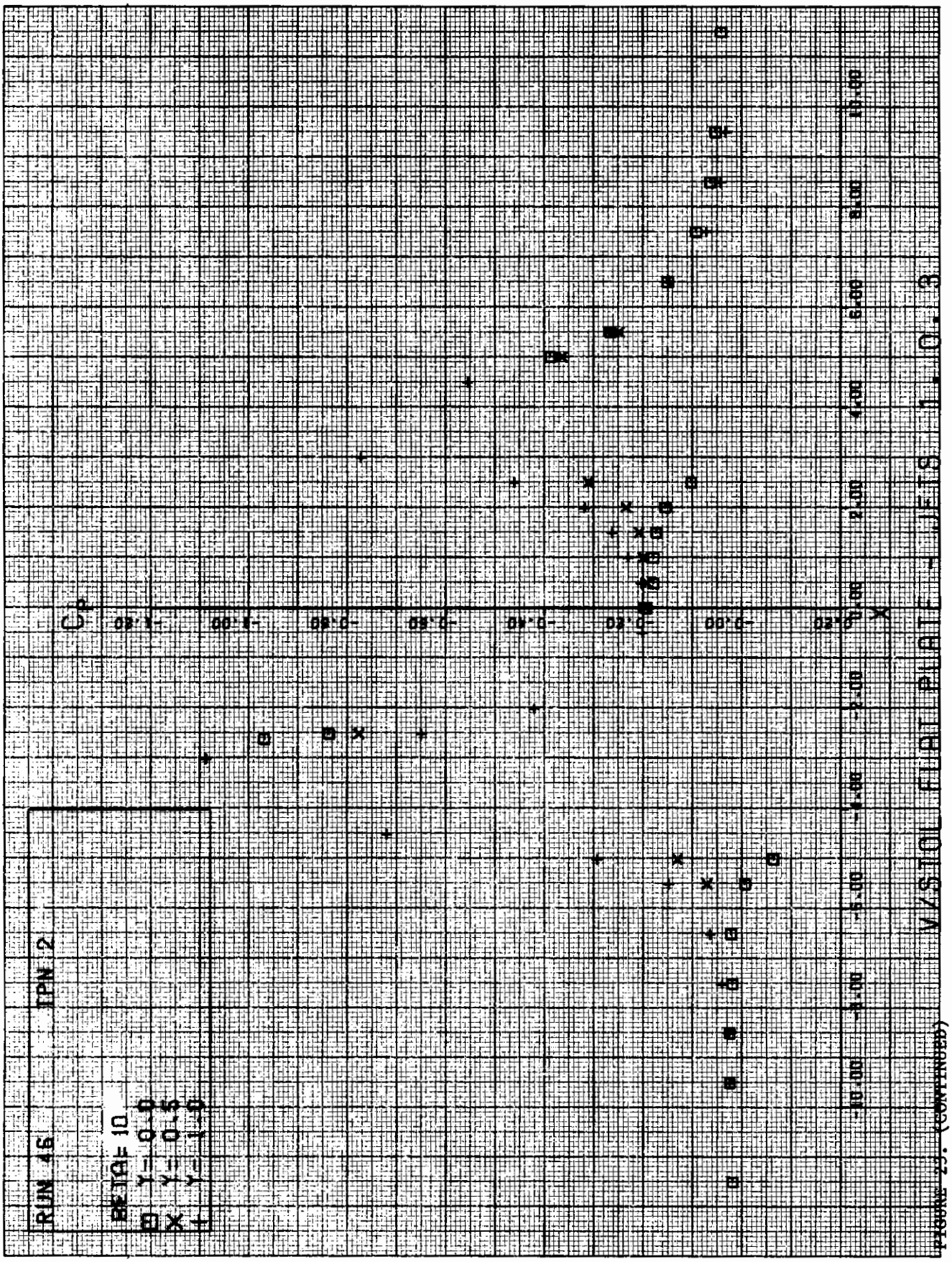

FIGURE 29. (CONTINUED)

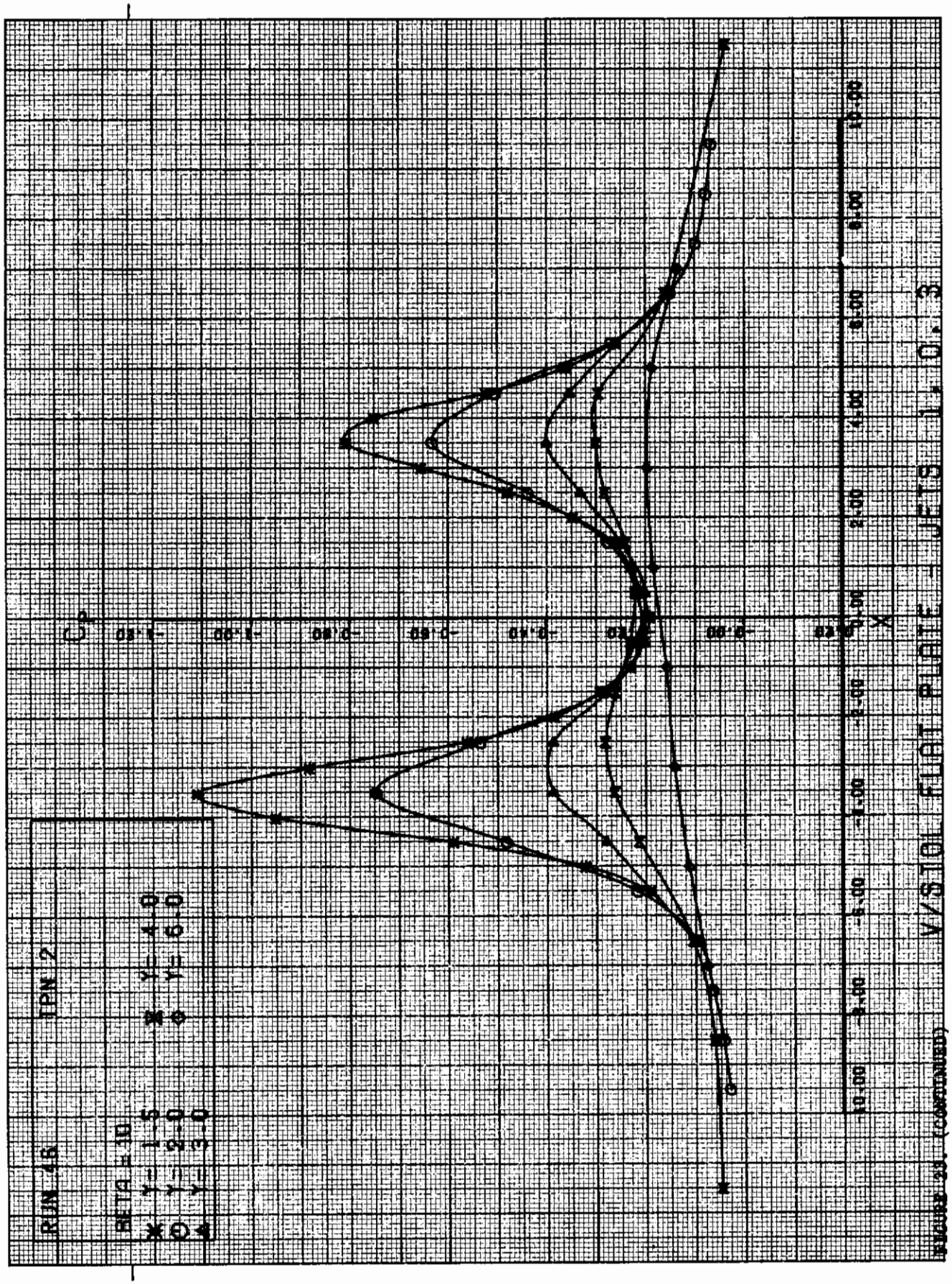

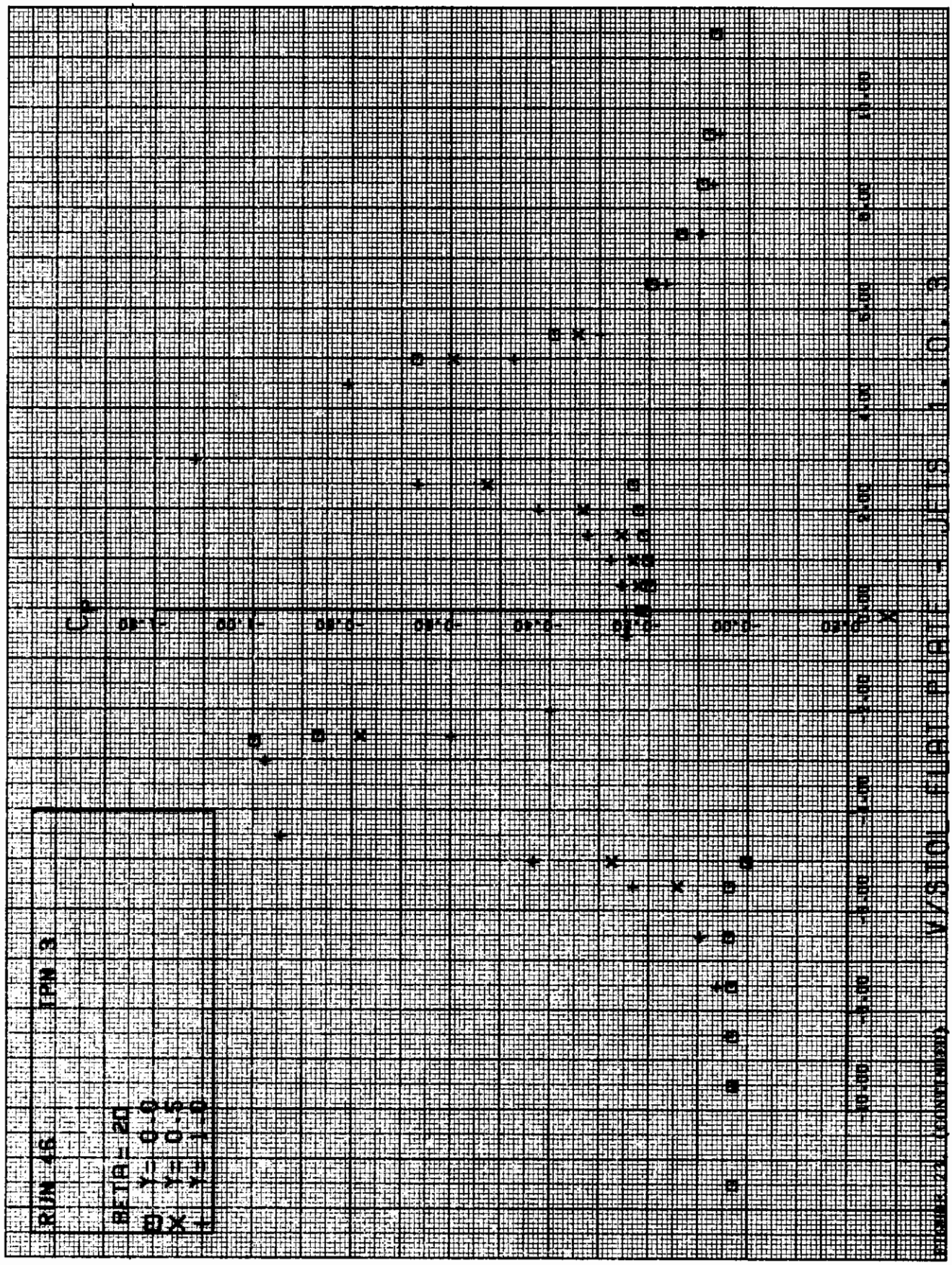

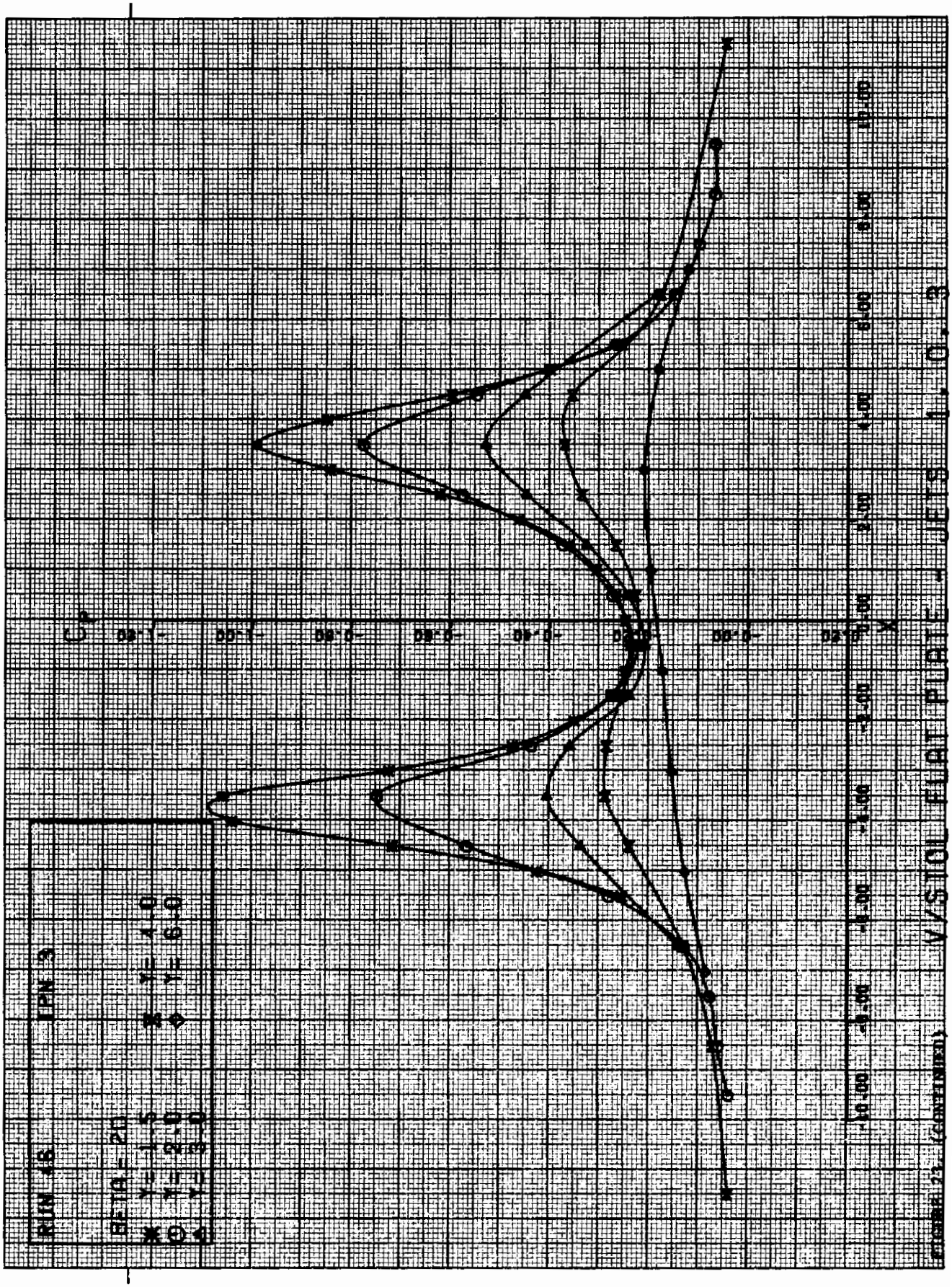

FIGURE 25. (CONTINUED)

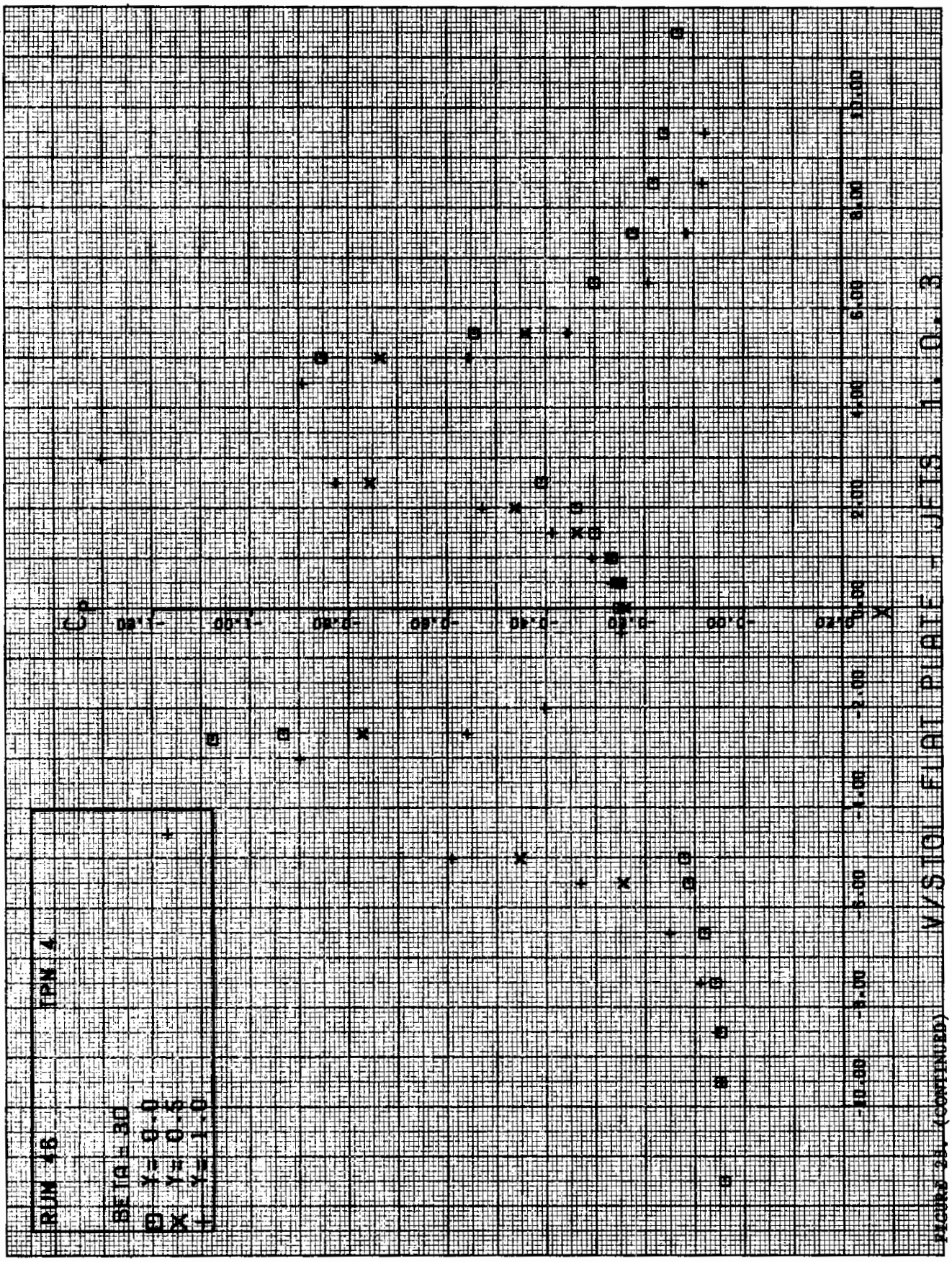

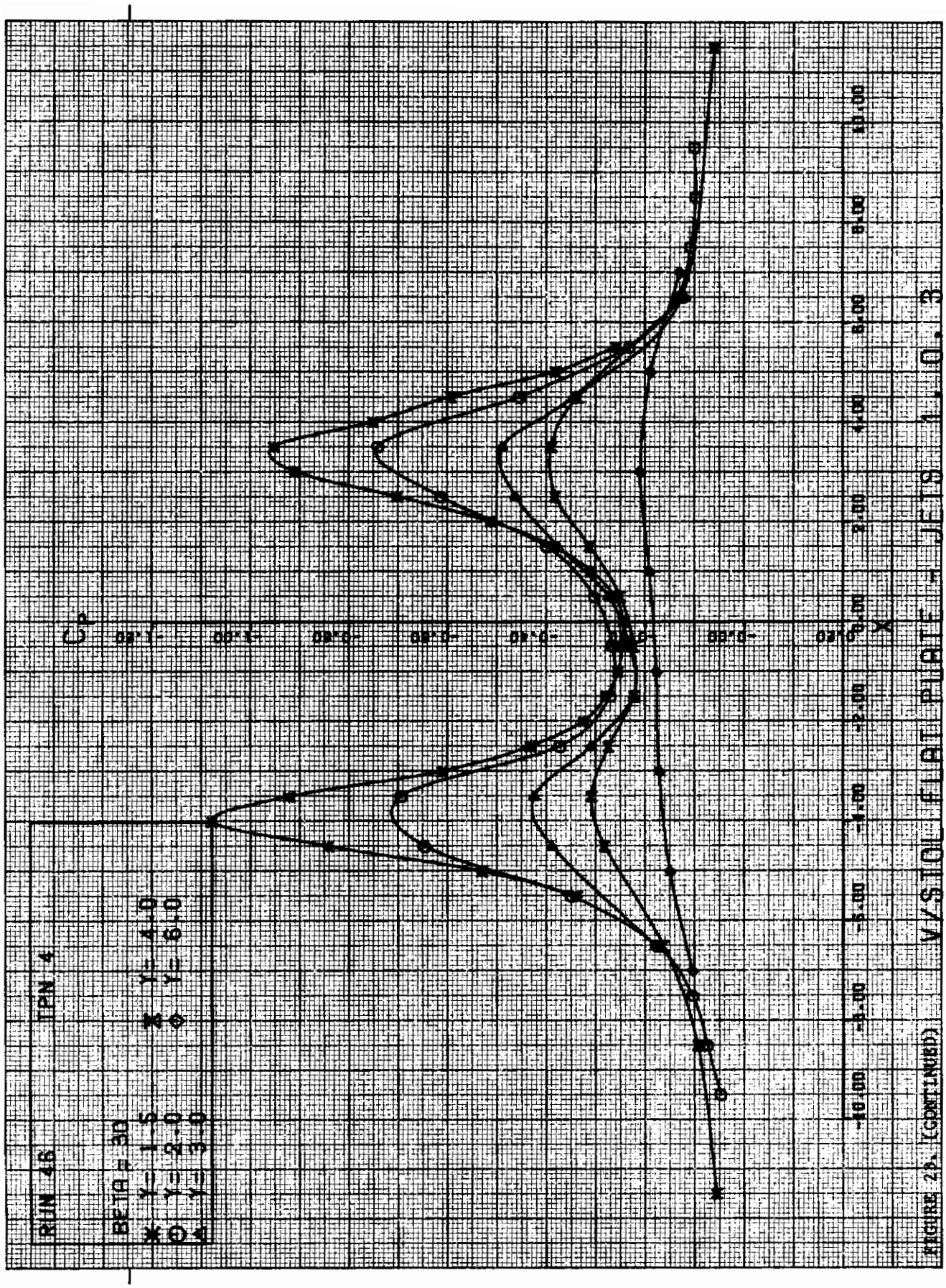

FIGURE 23. (CONTINUED) V/STOL FLAT PLATE JET 1.0, 2

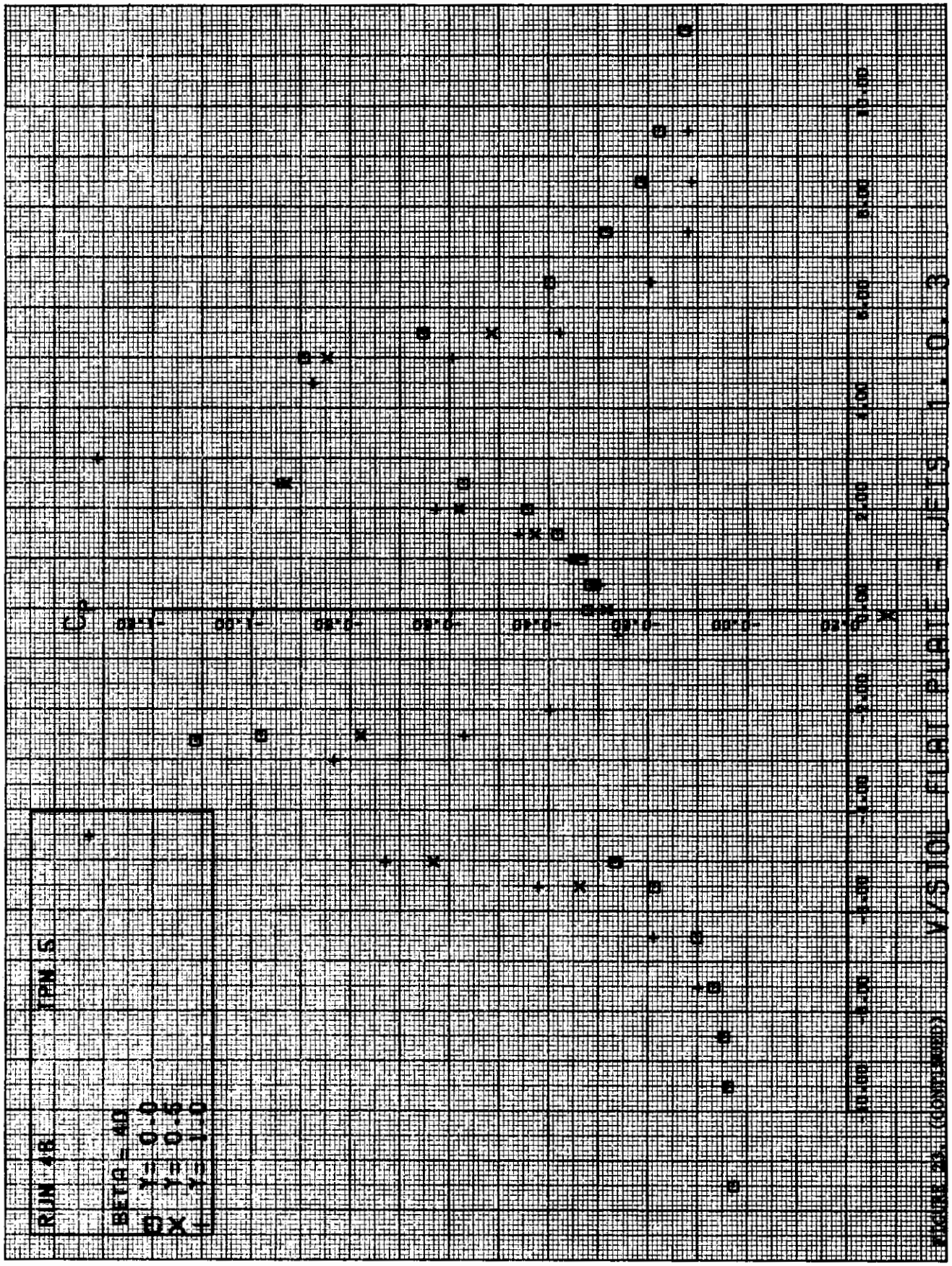

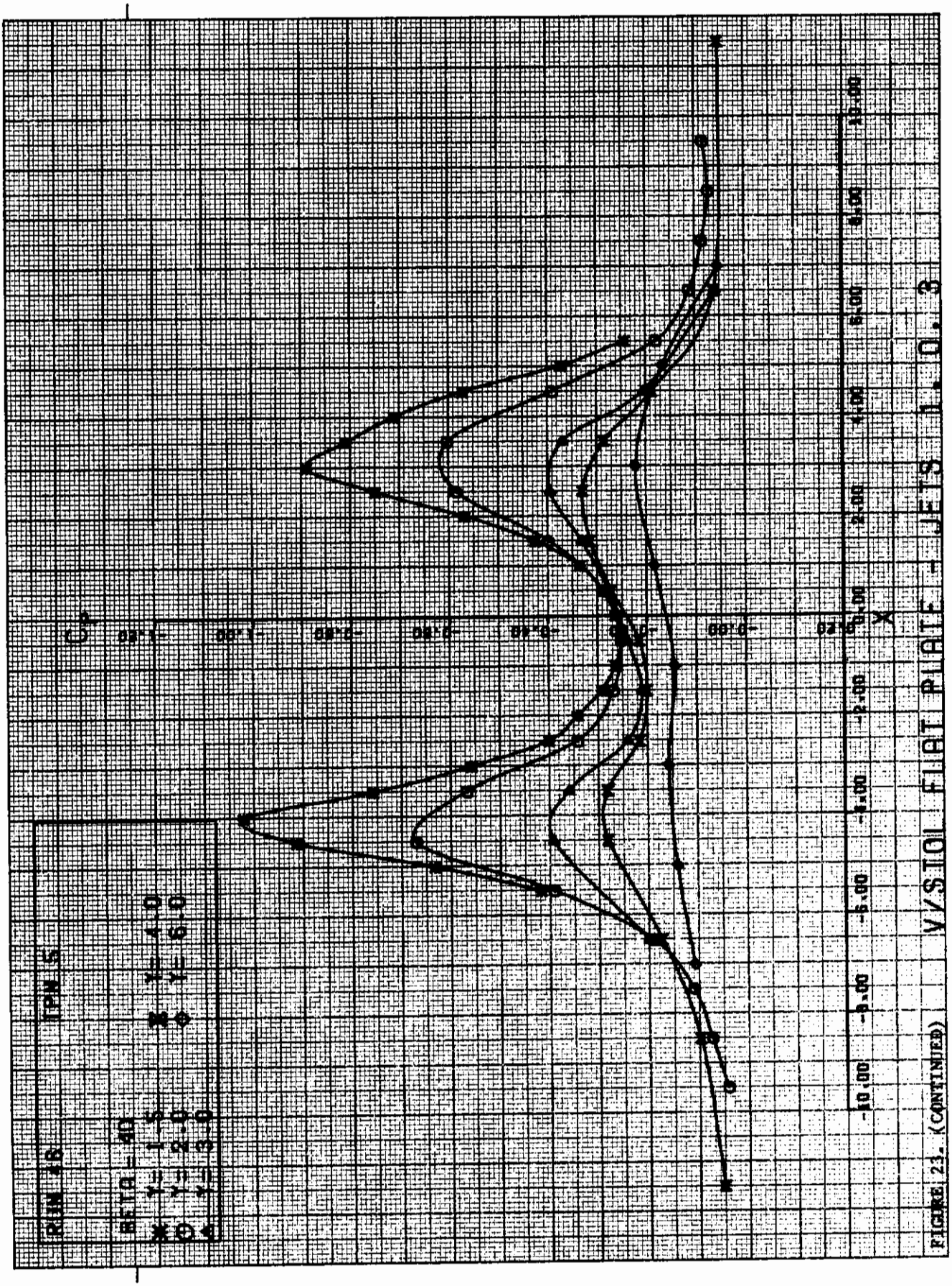

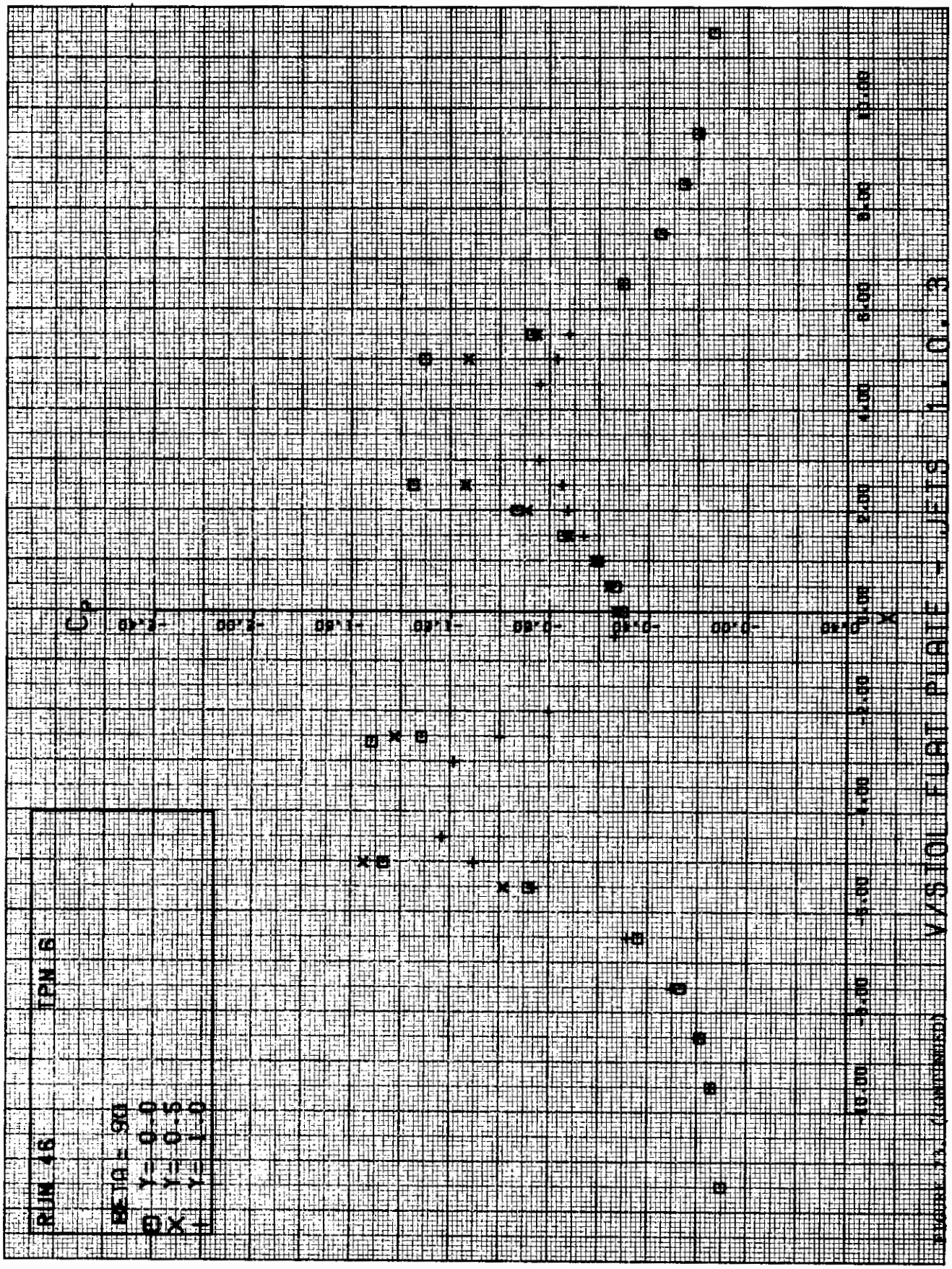

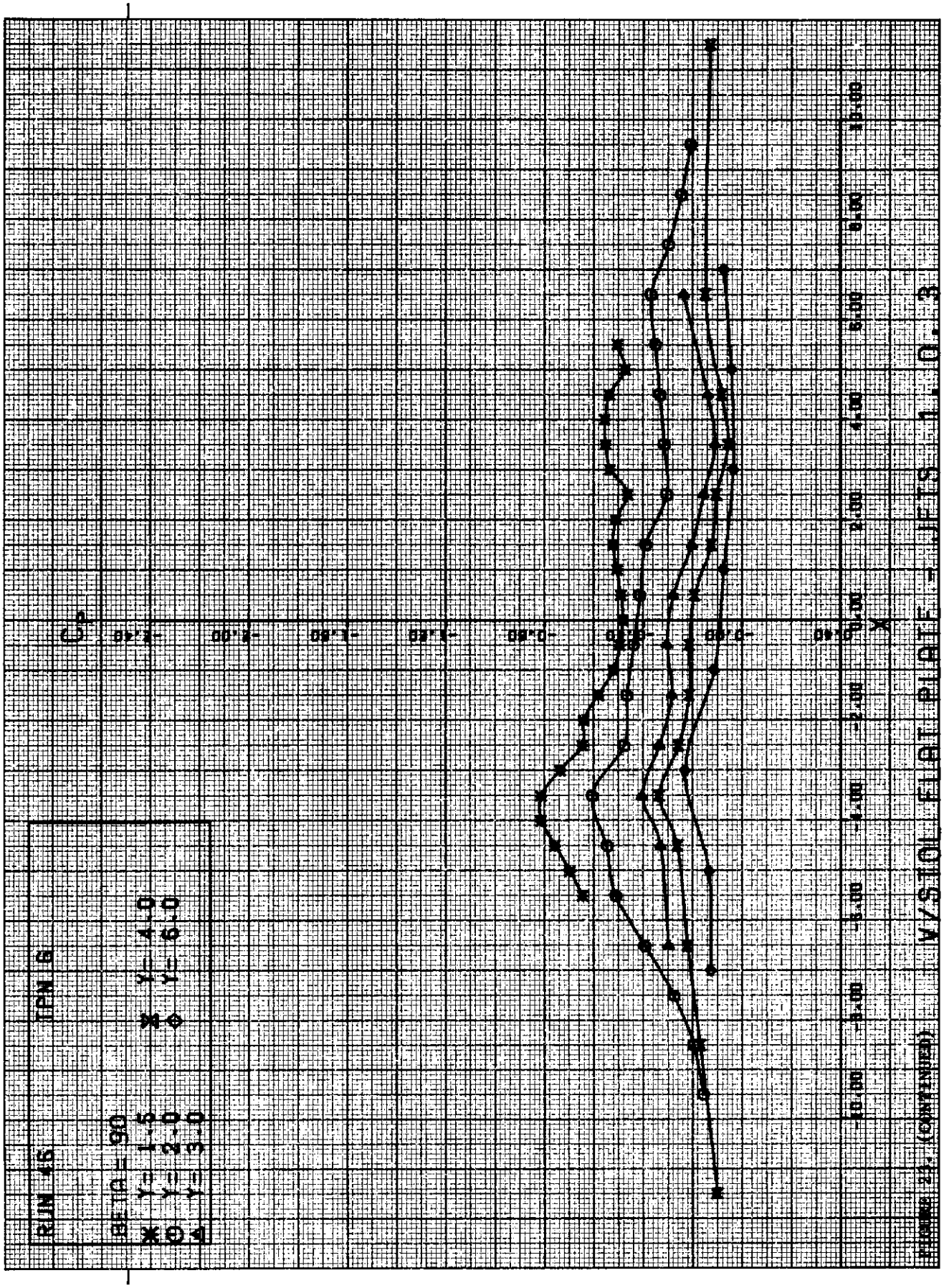

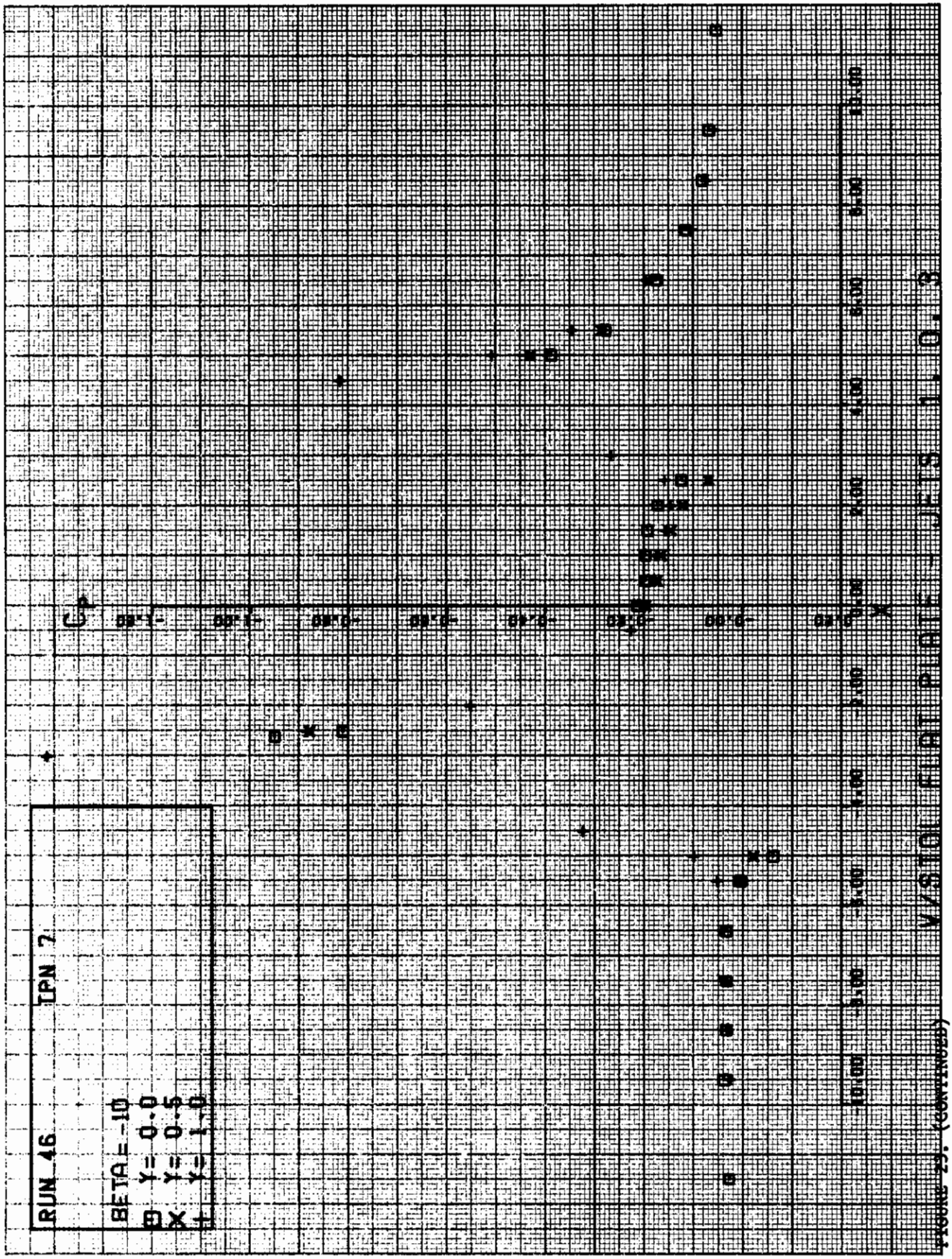

Figure 29. (CONTINUED)

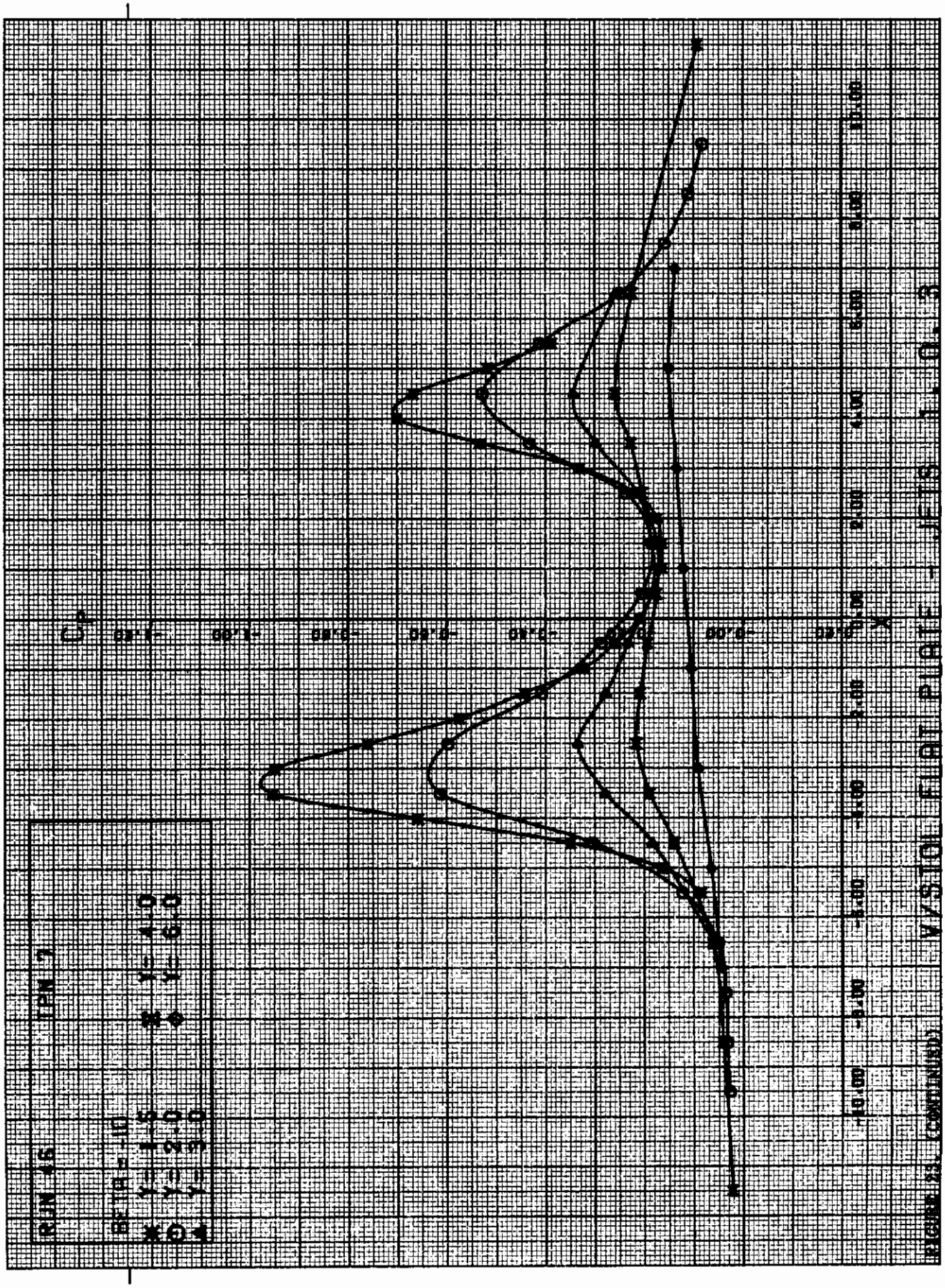

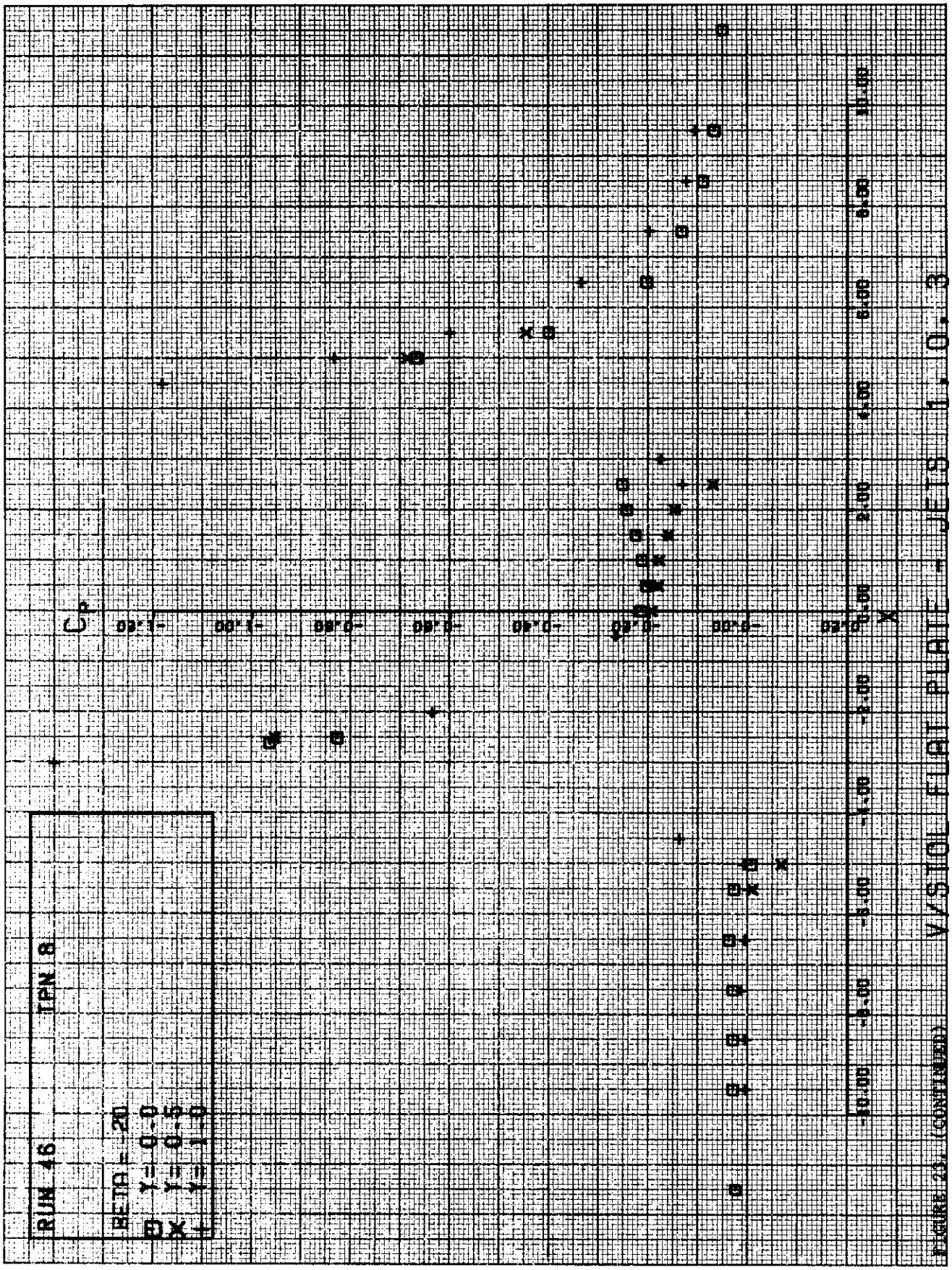

FIGURE 29. (CONTINUED)

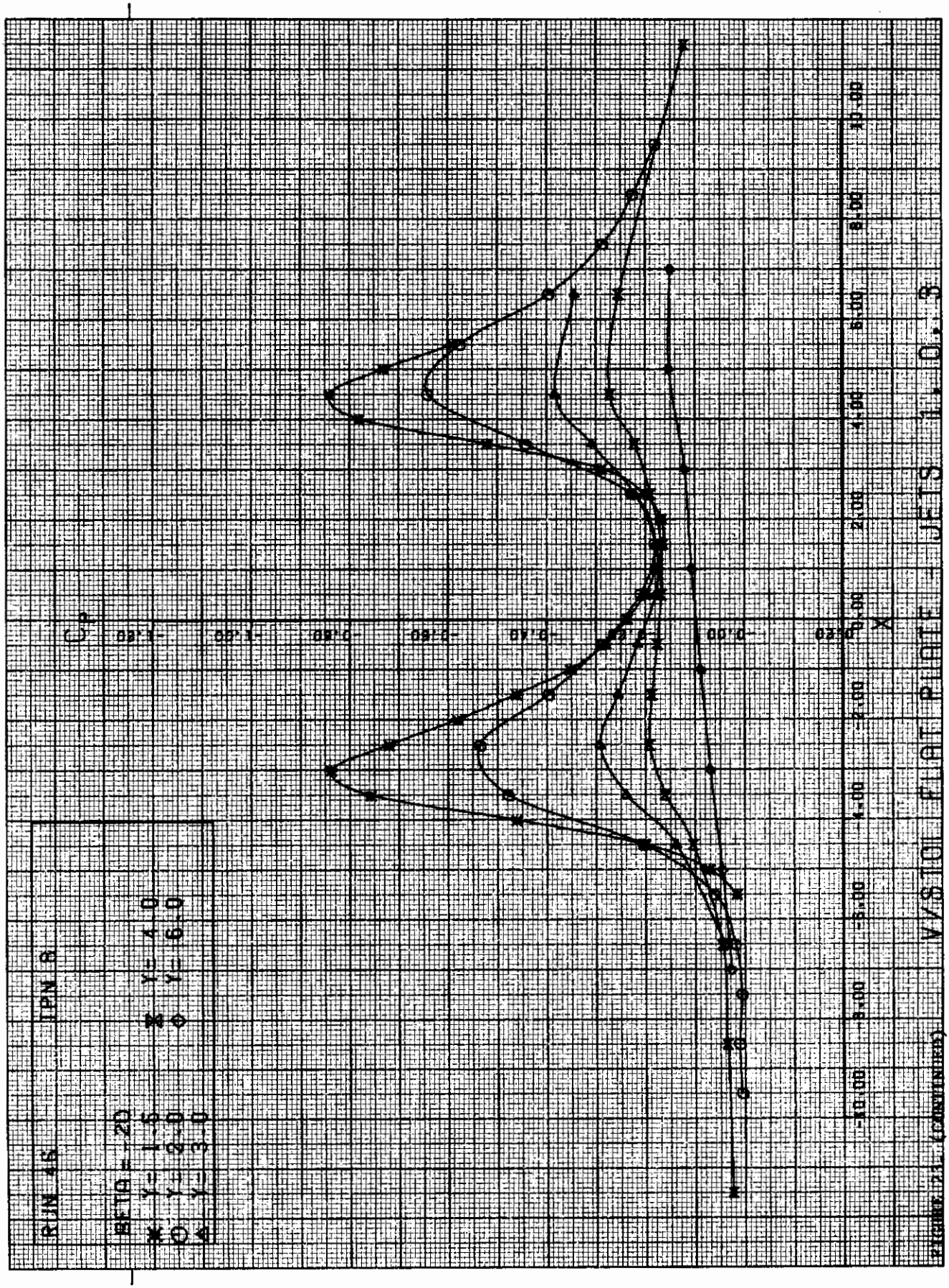

Figure 21. (Continued)

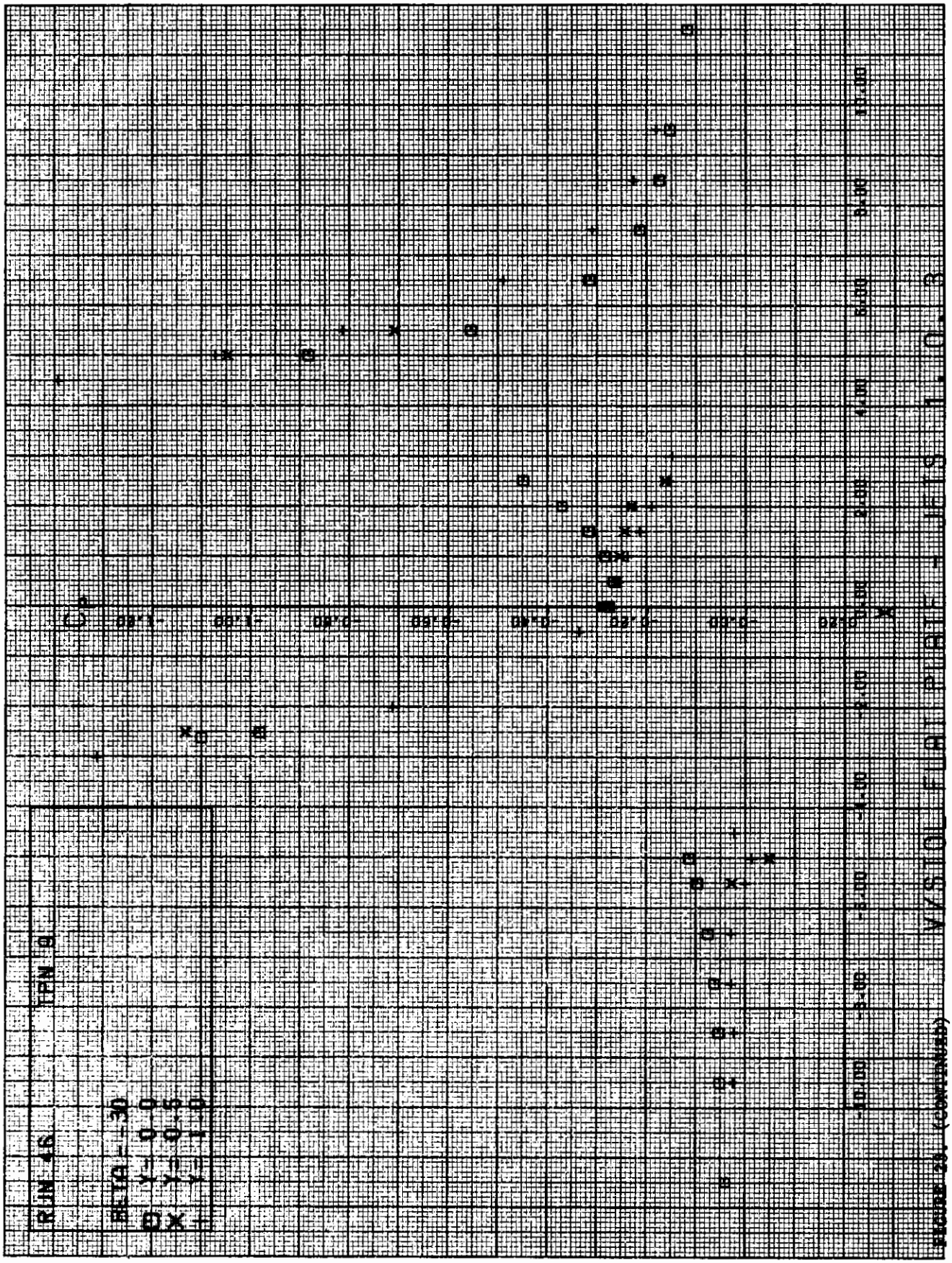

FIGURE 38. (CONTINUED)

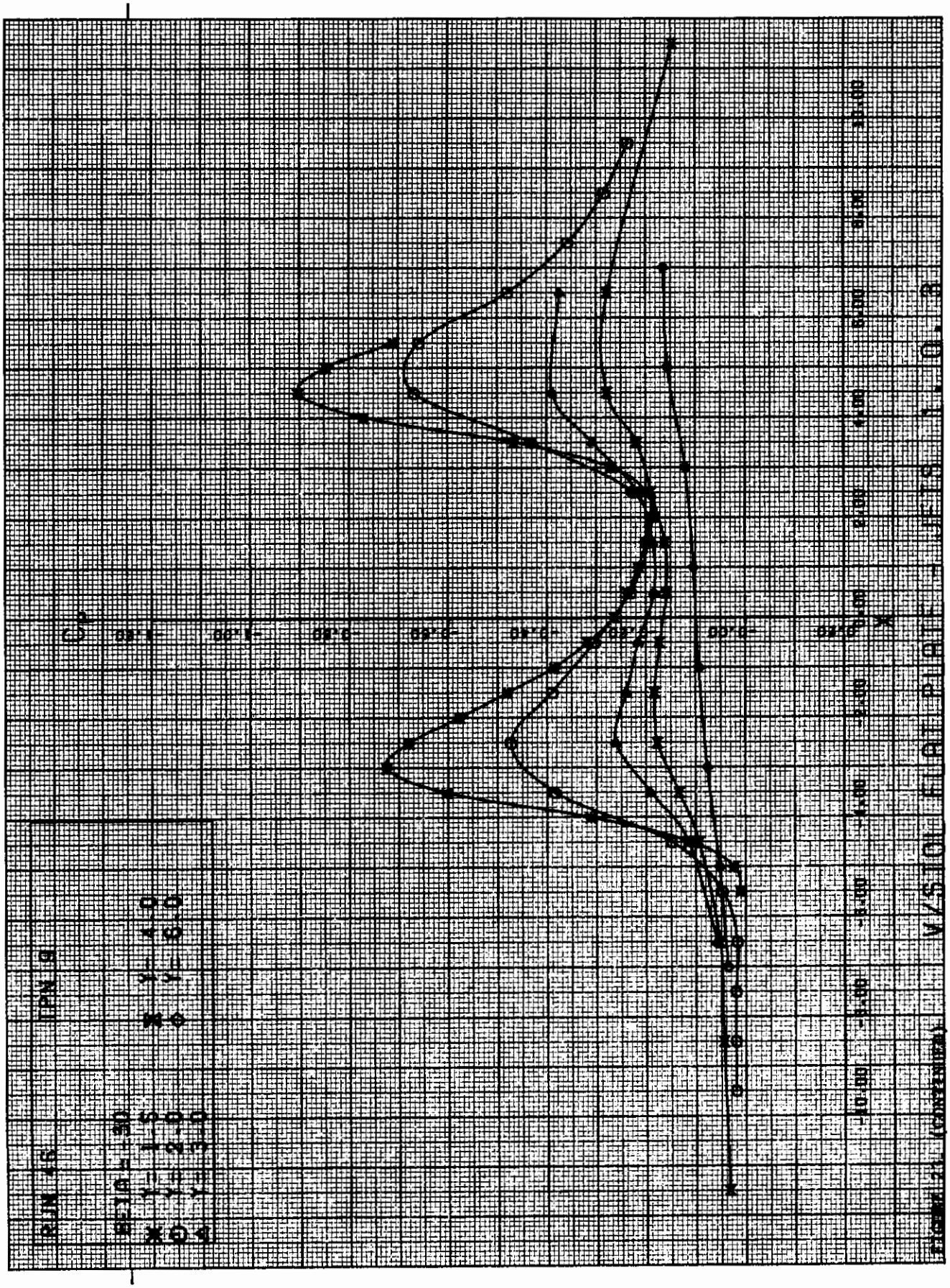

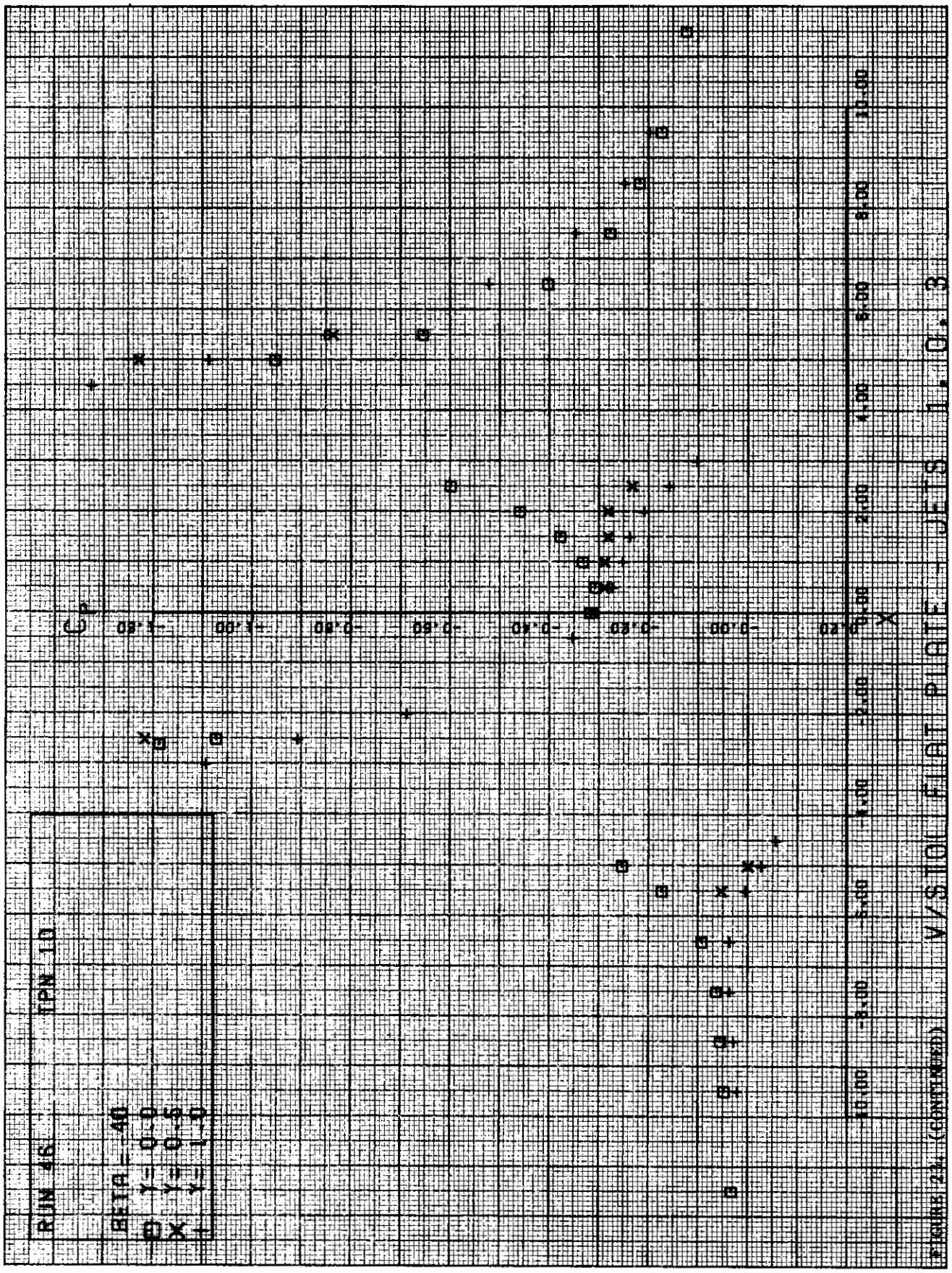

Figure 23. (continued)

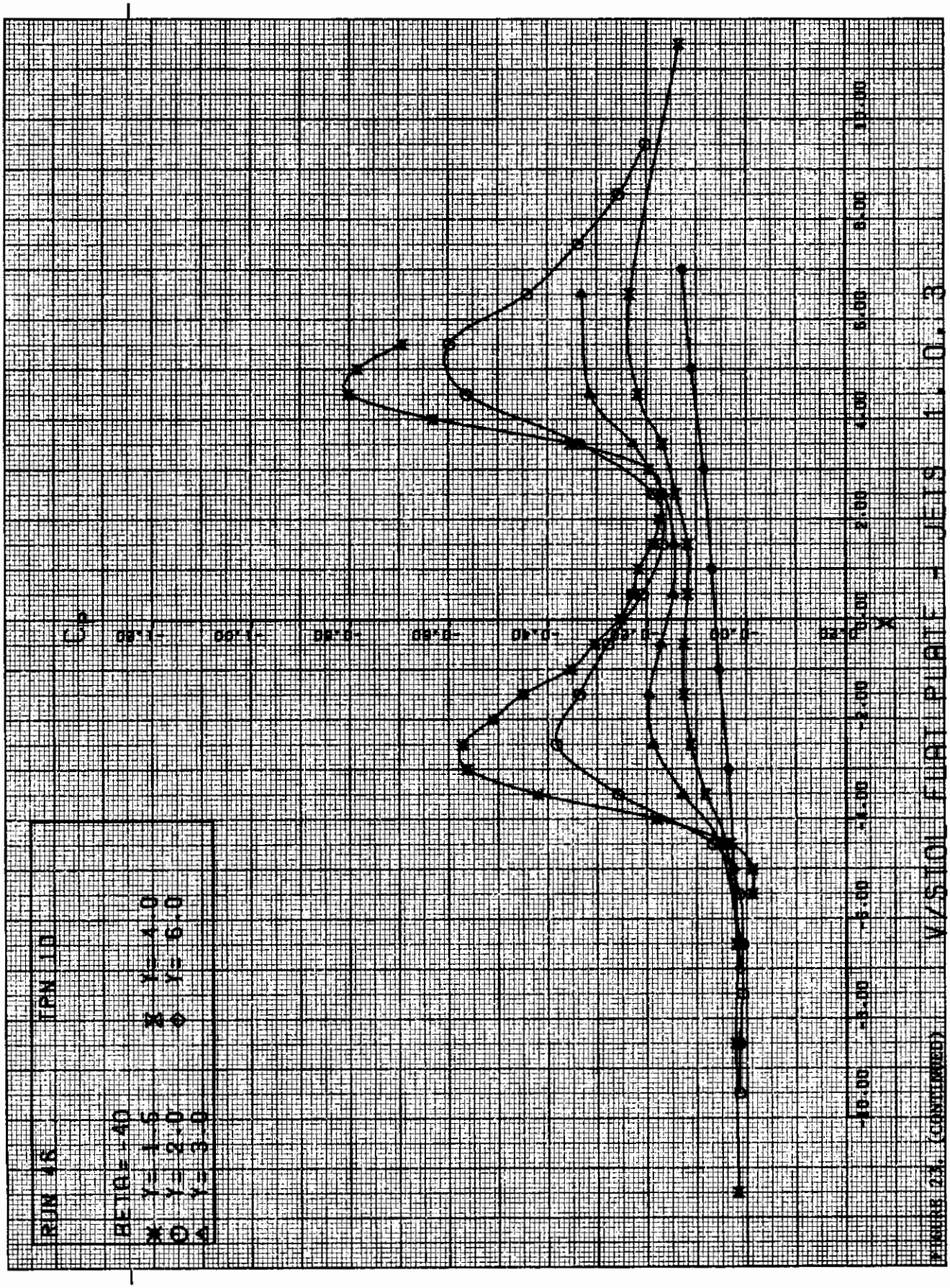

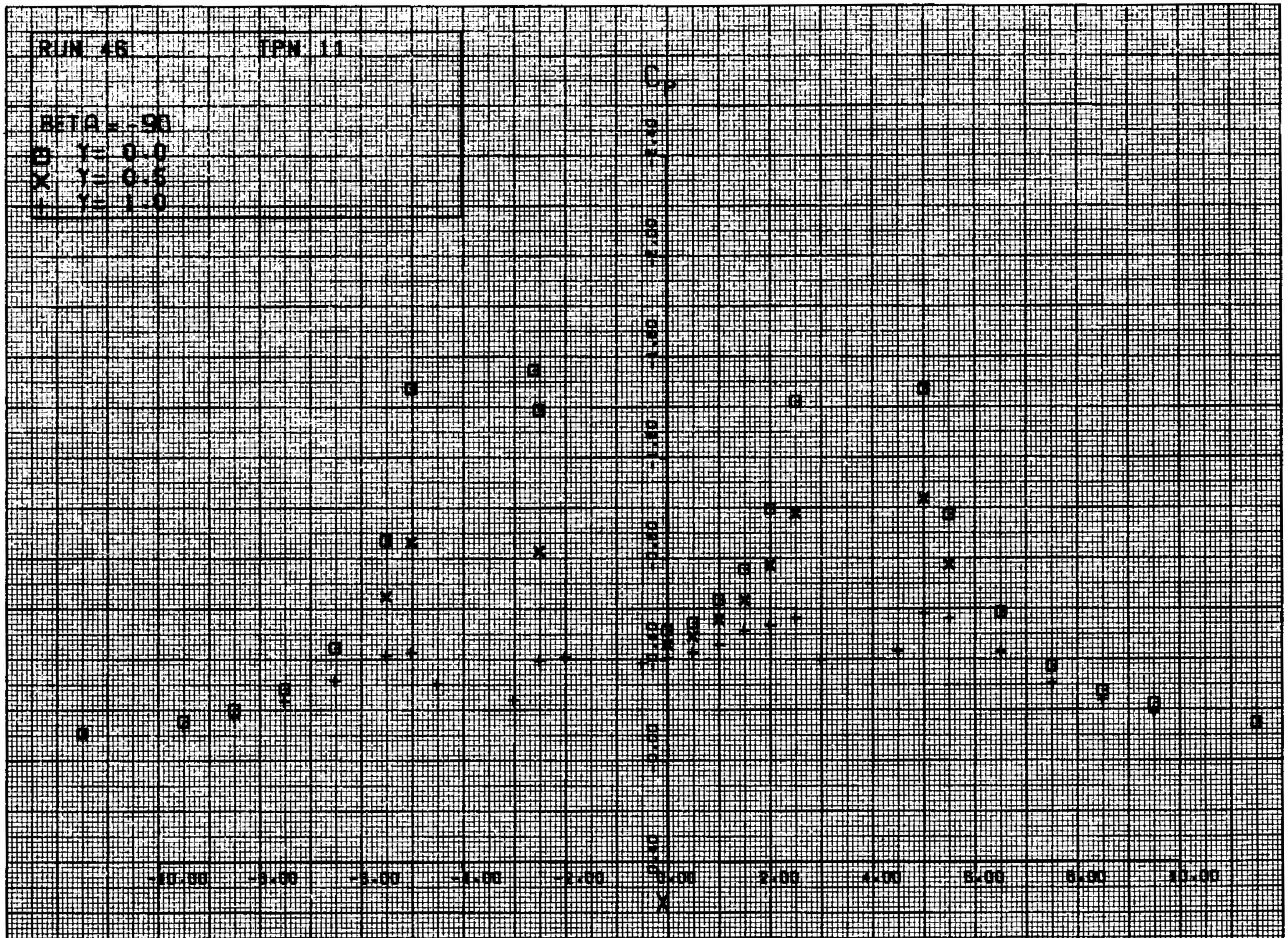

FIGURE [illegible]. (CONTINUED) V/STOL FLAT PLATE - JETS 1, 0.3

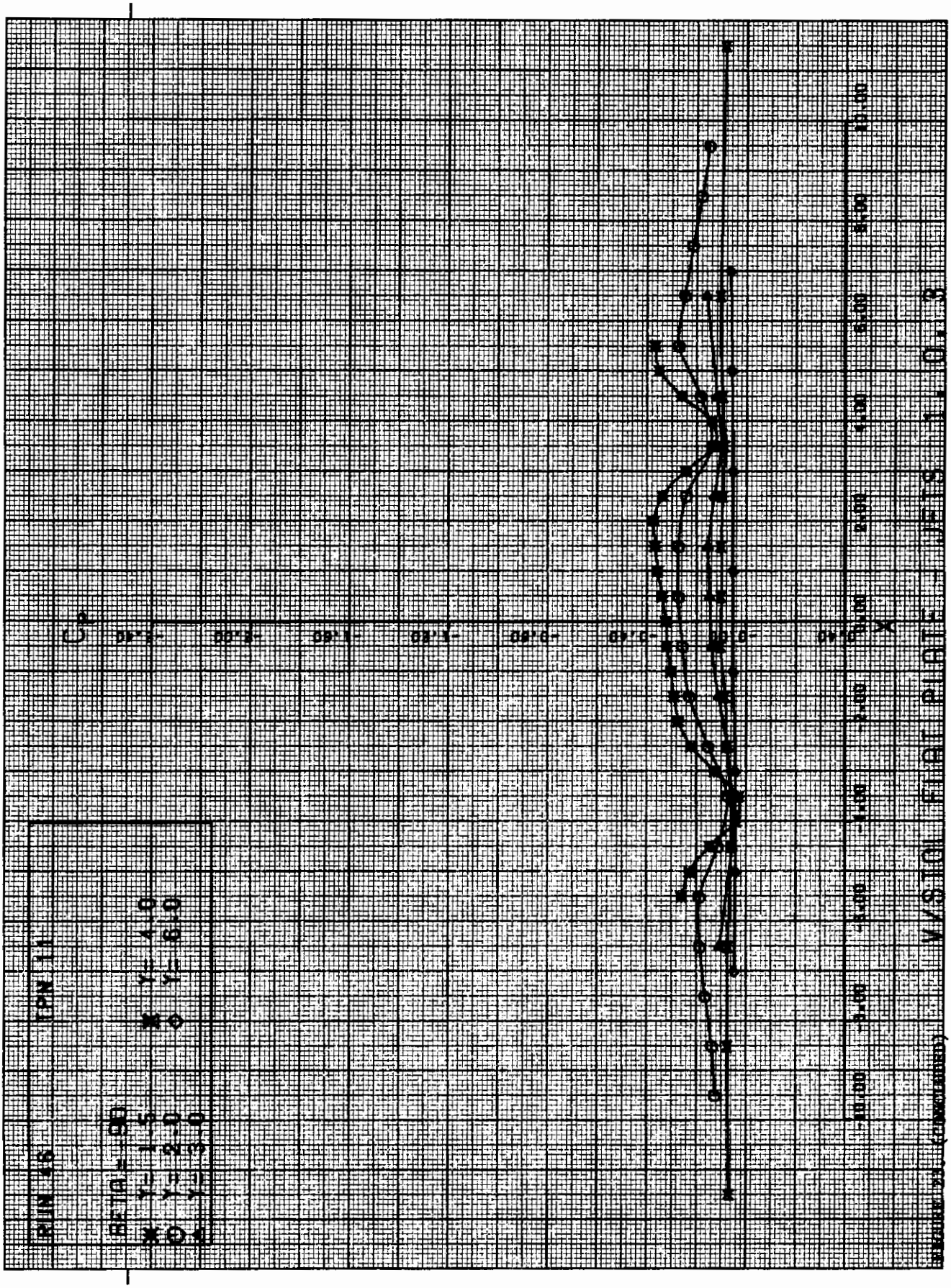

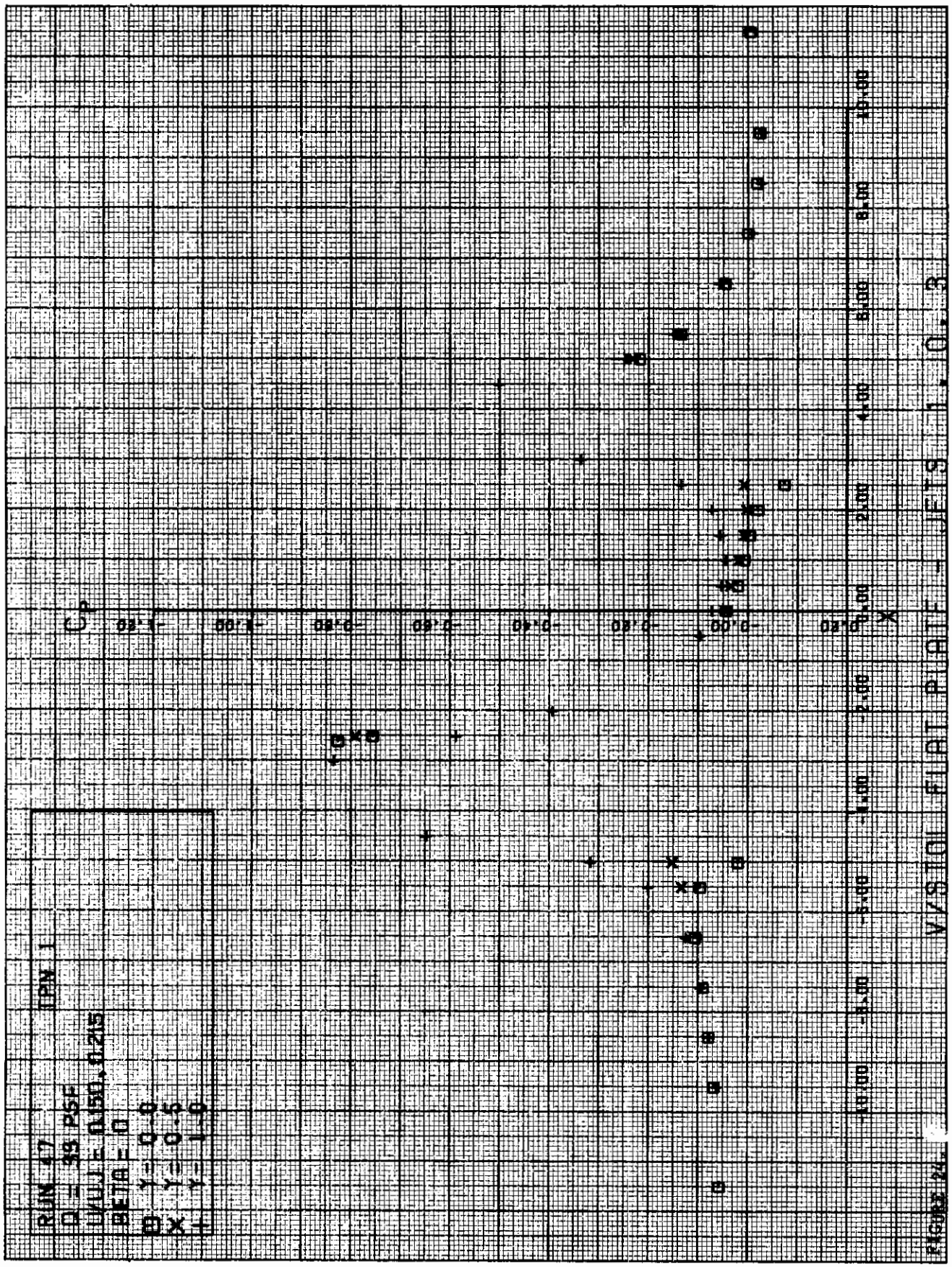

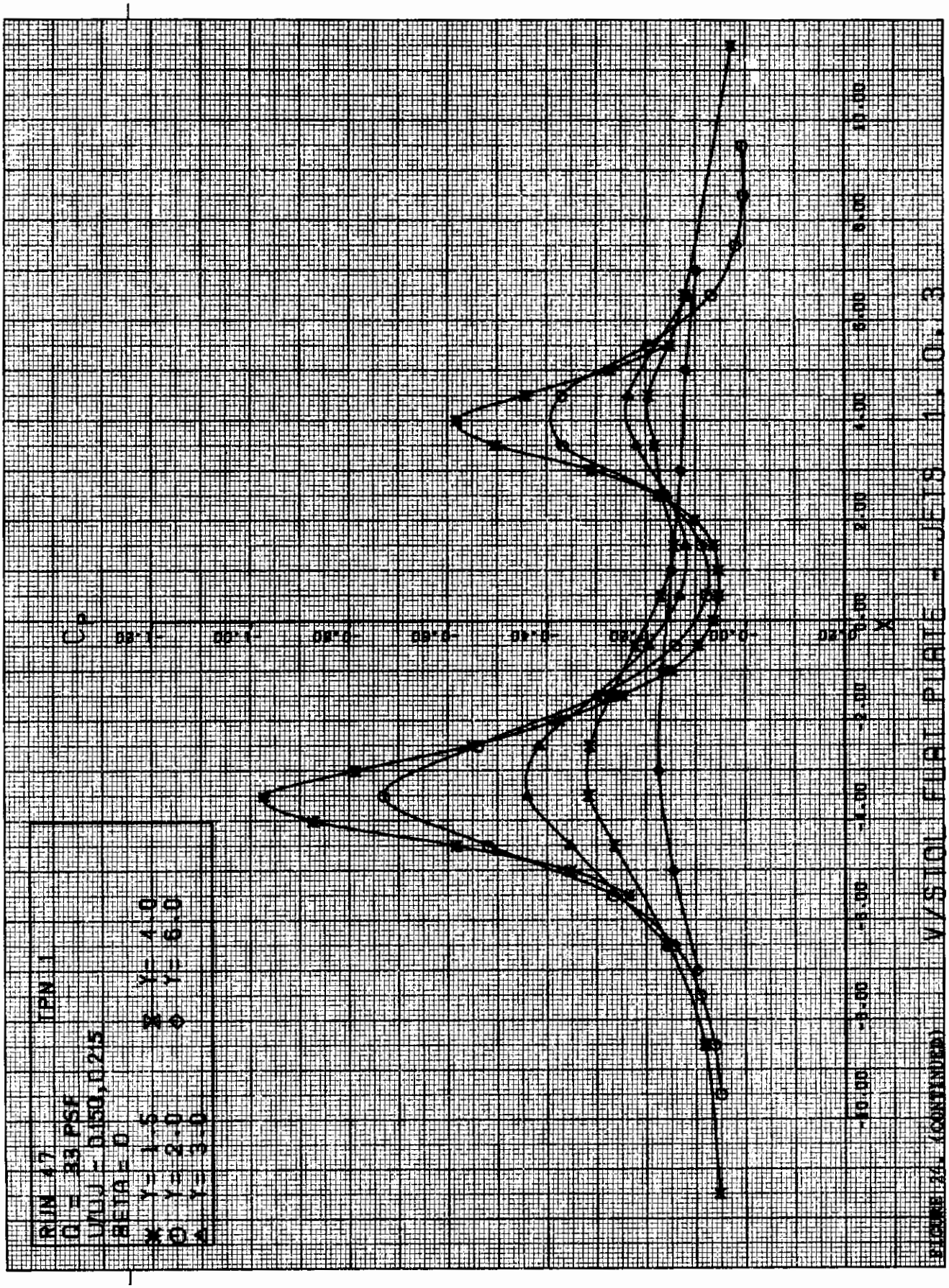

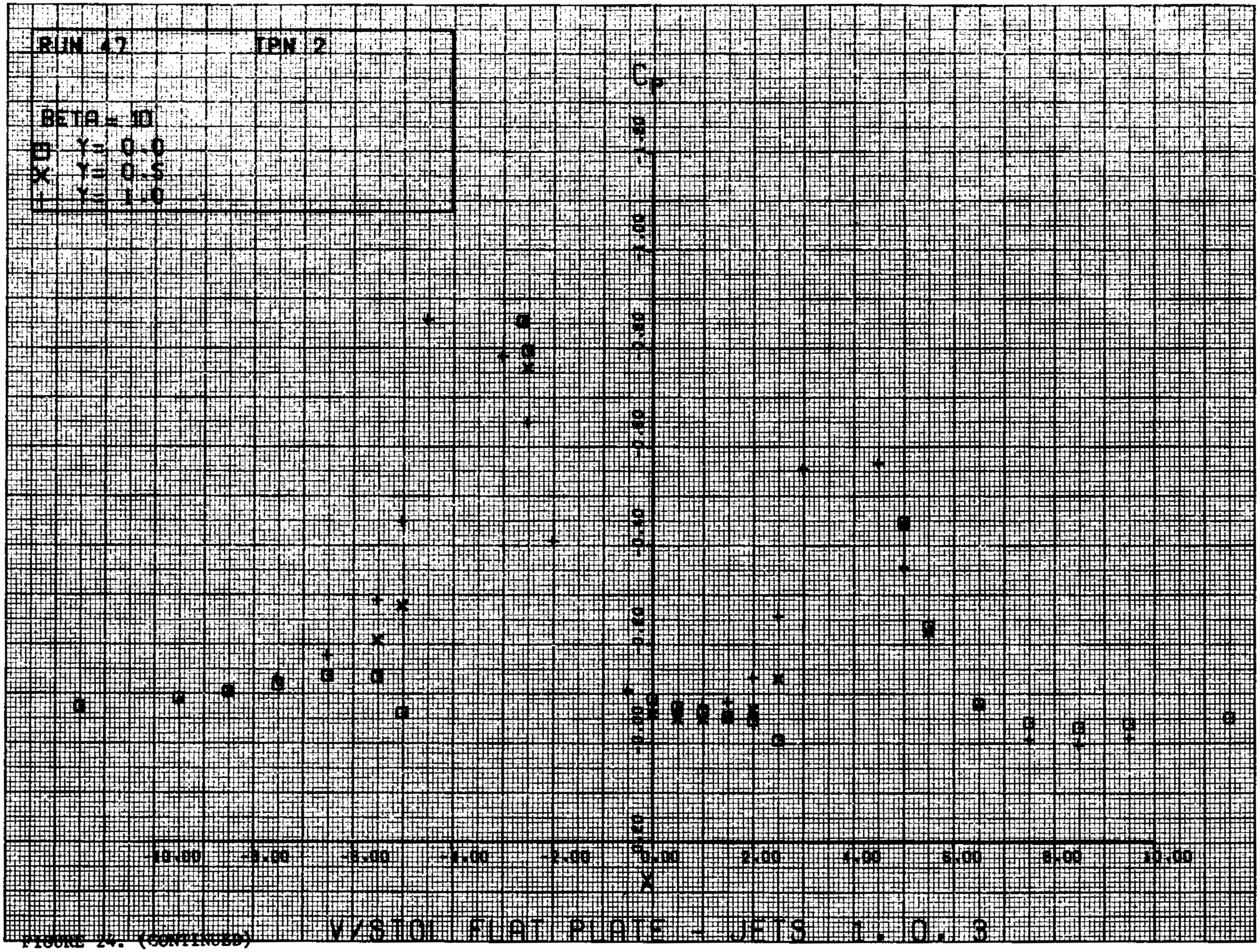

FIGURE 24. (CONTINUED)

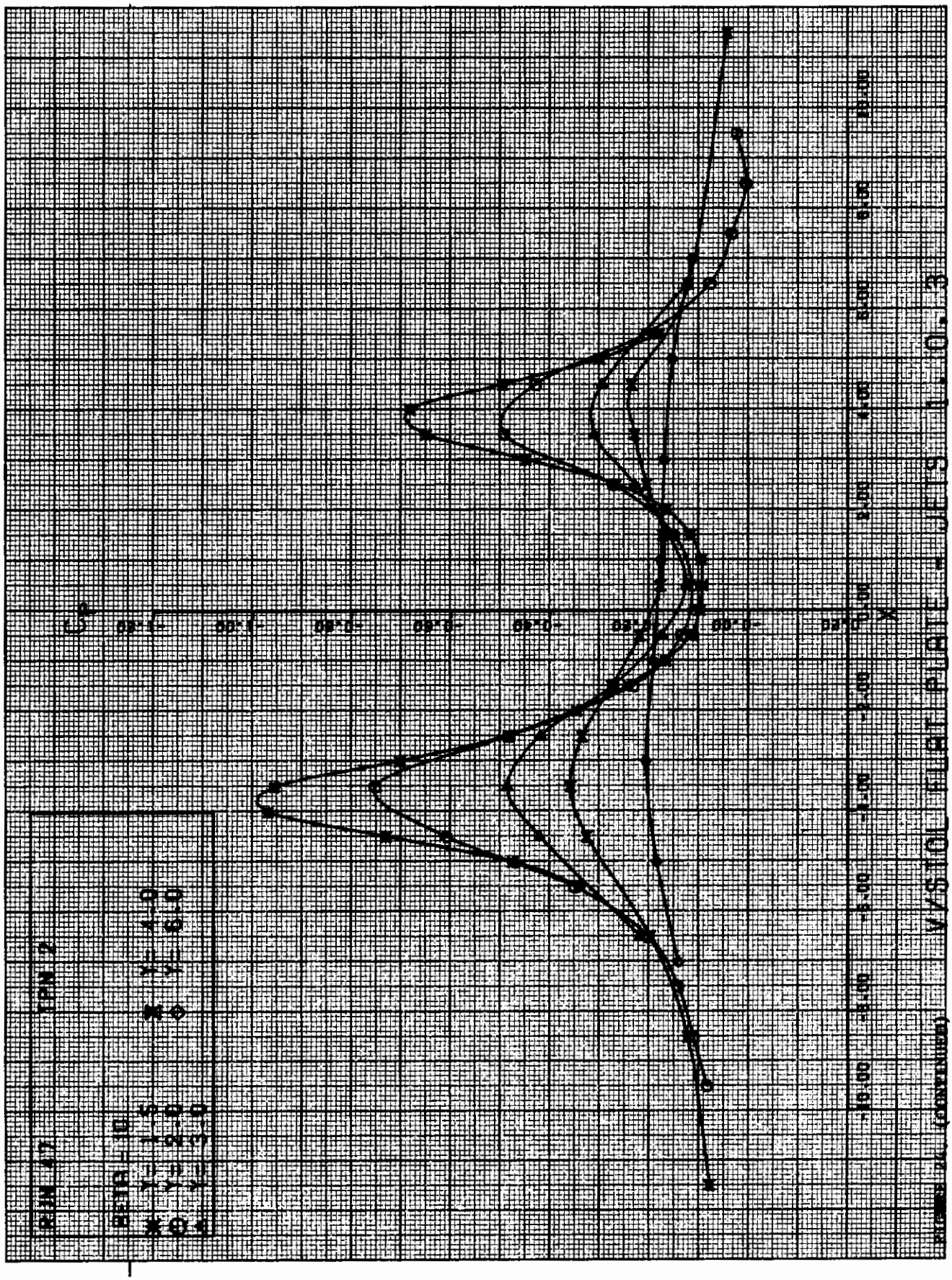

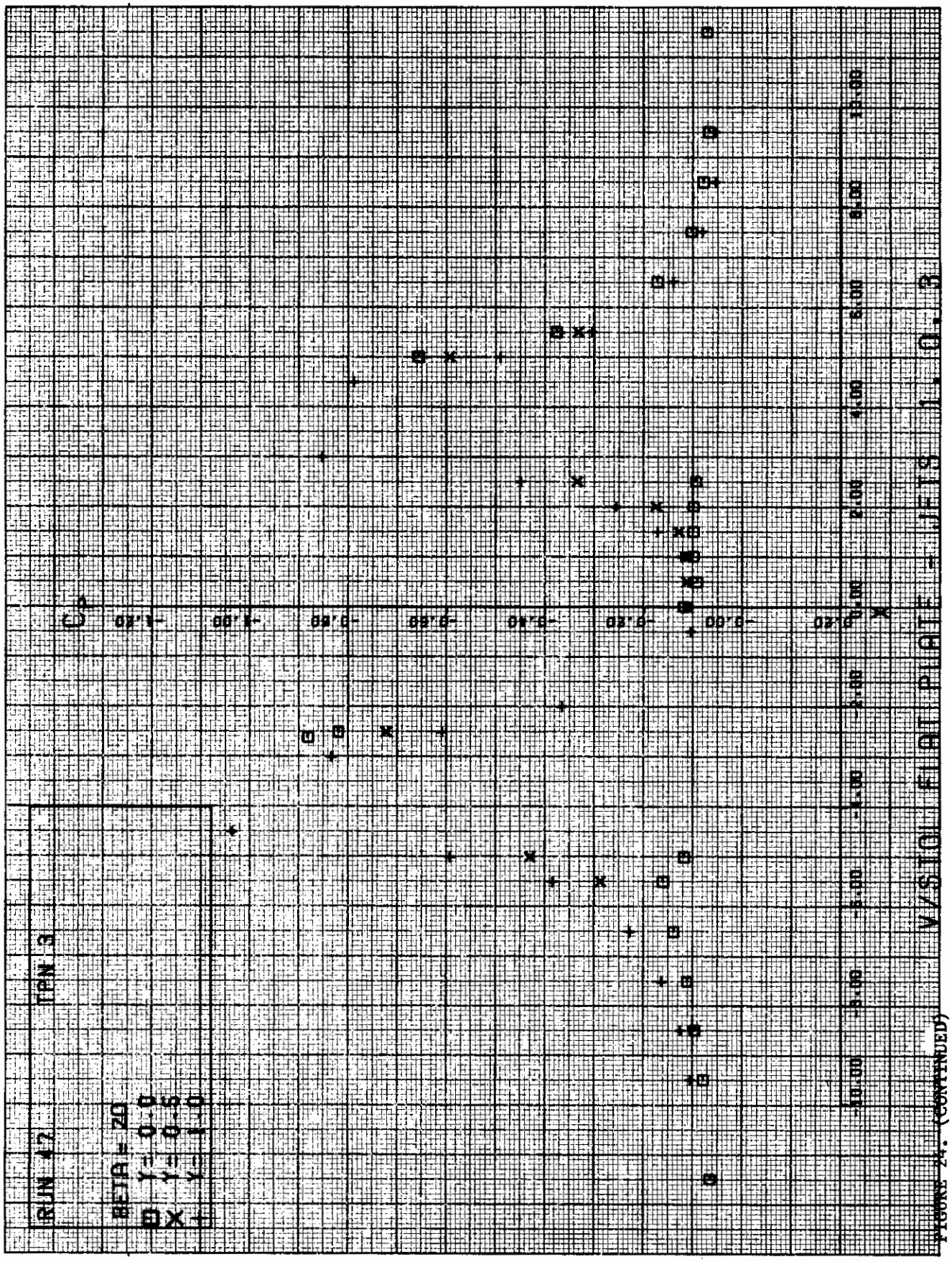

FIGURE 24. (CONTINUED)

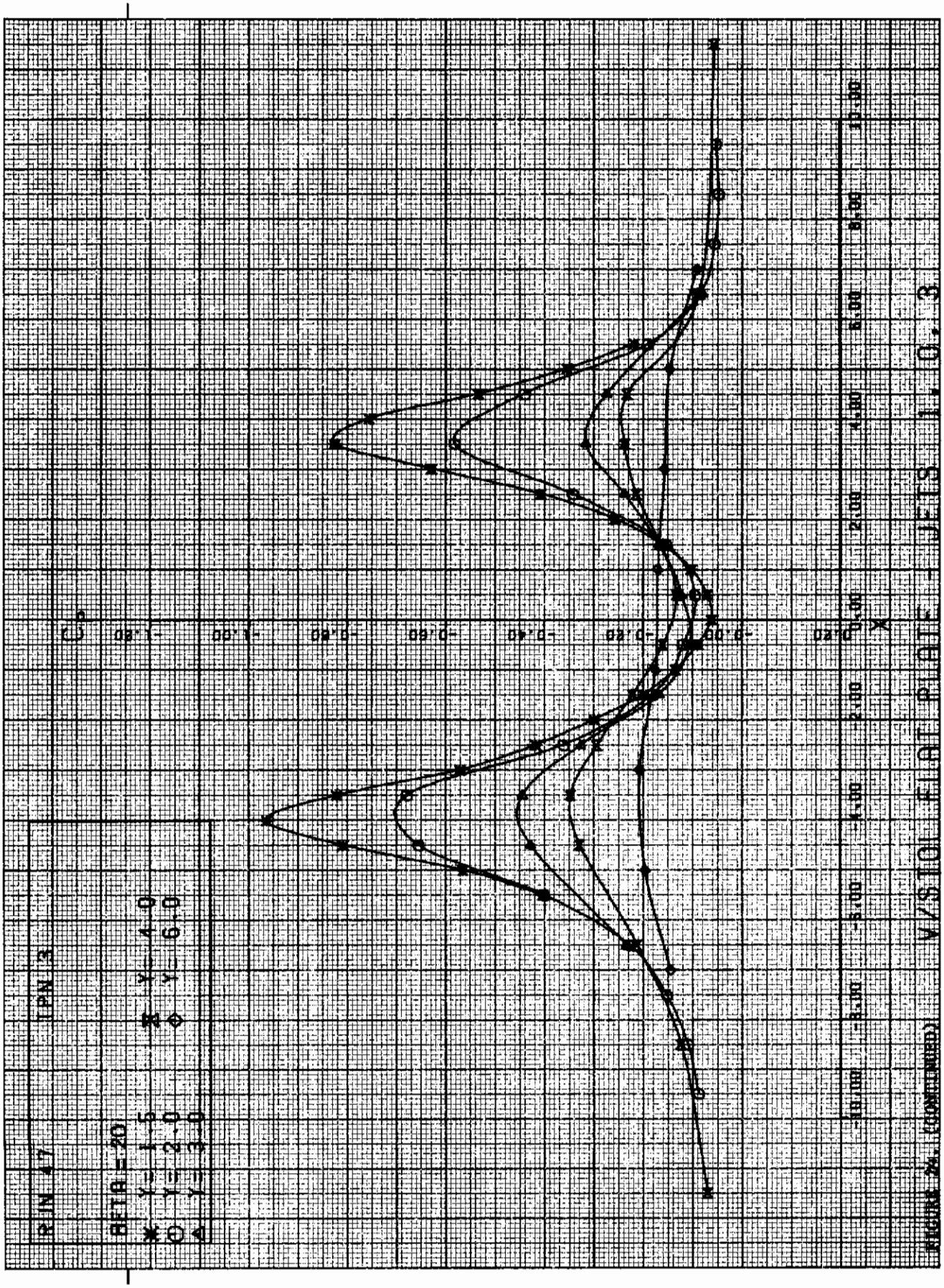

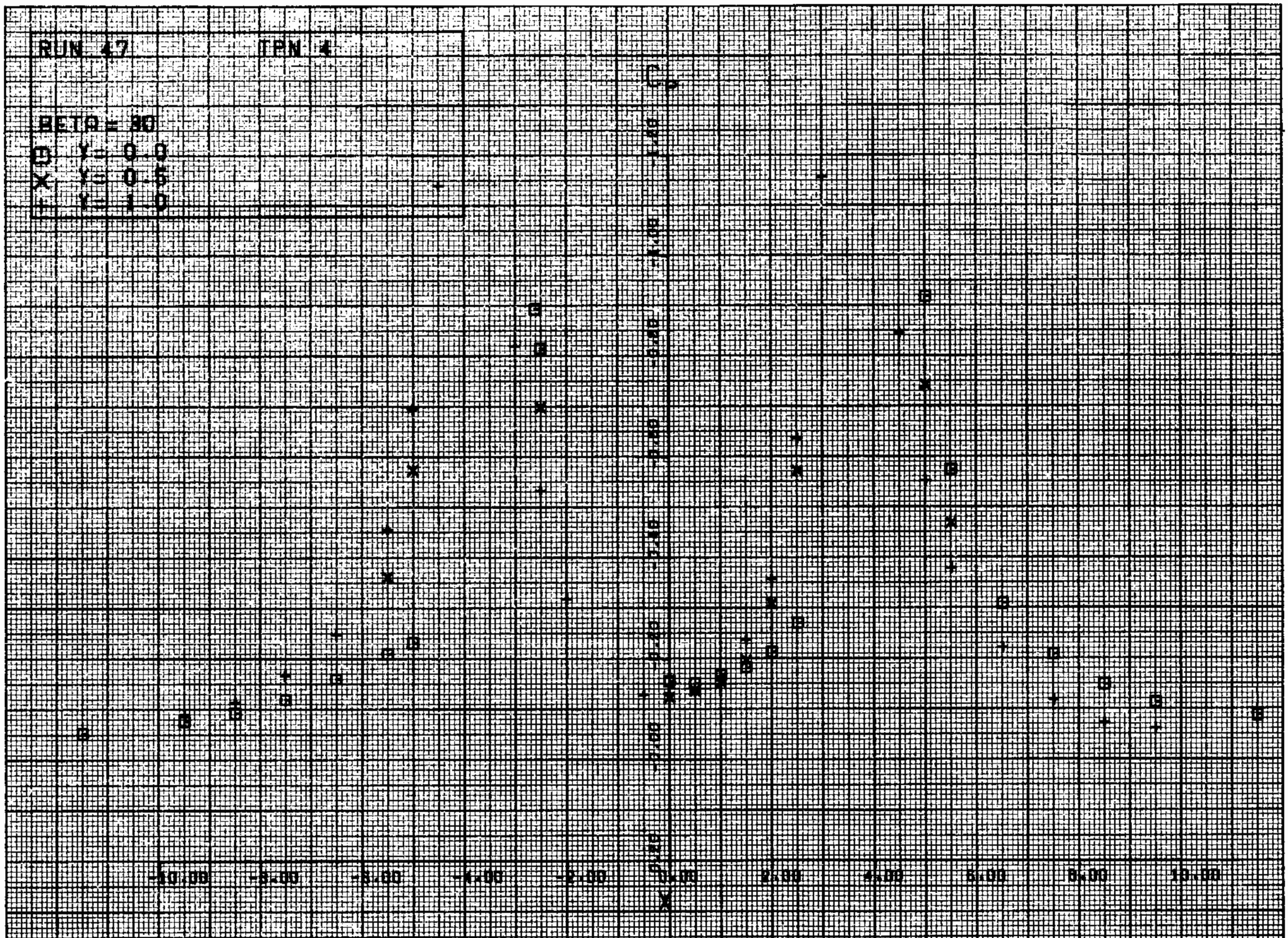

FIGURE 24. (CONTINUED) V/STOL FLAT PLATE - JETS 1. 0. 3

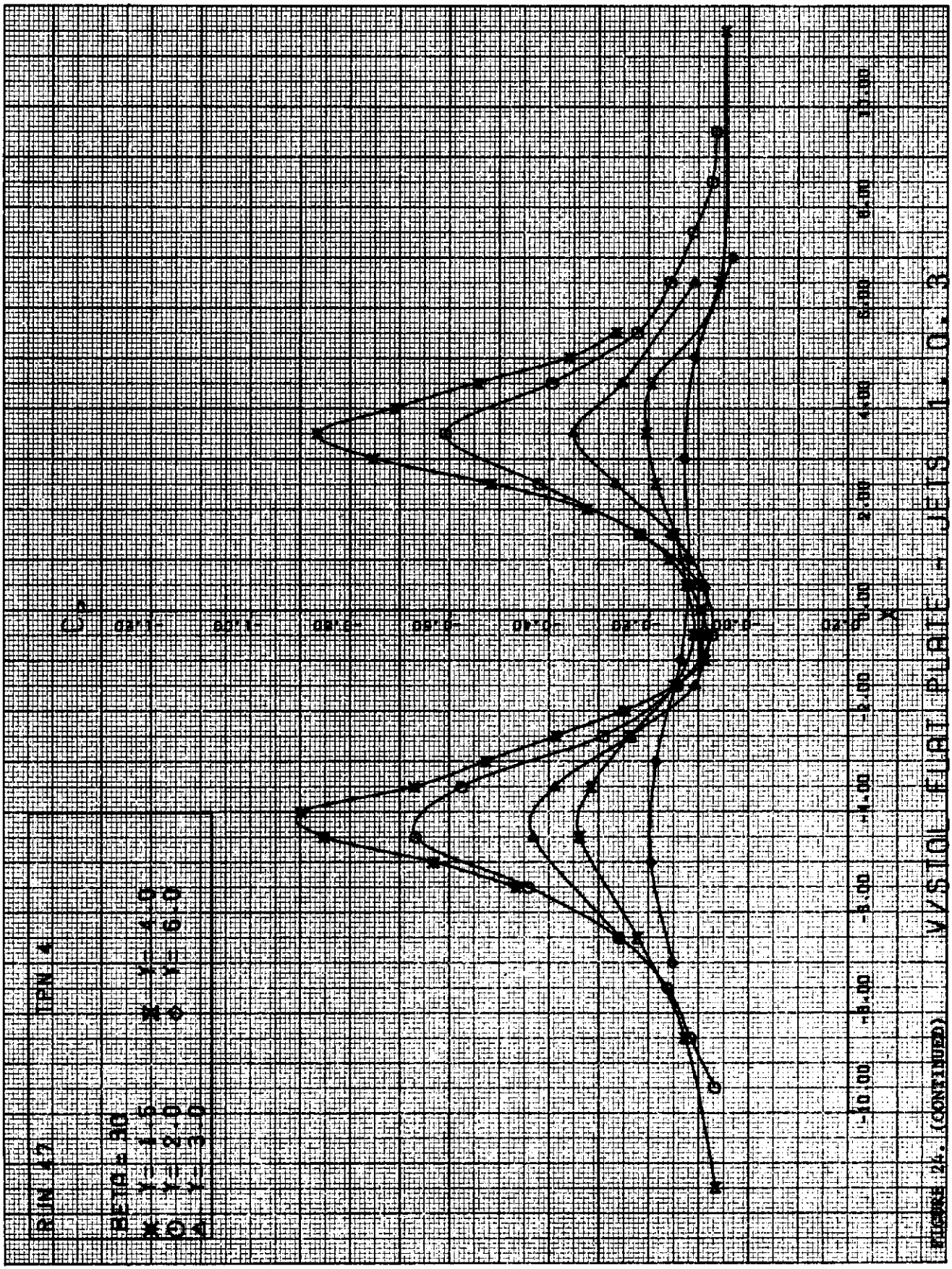

FIGURE 24. (CONTINUED)

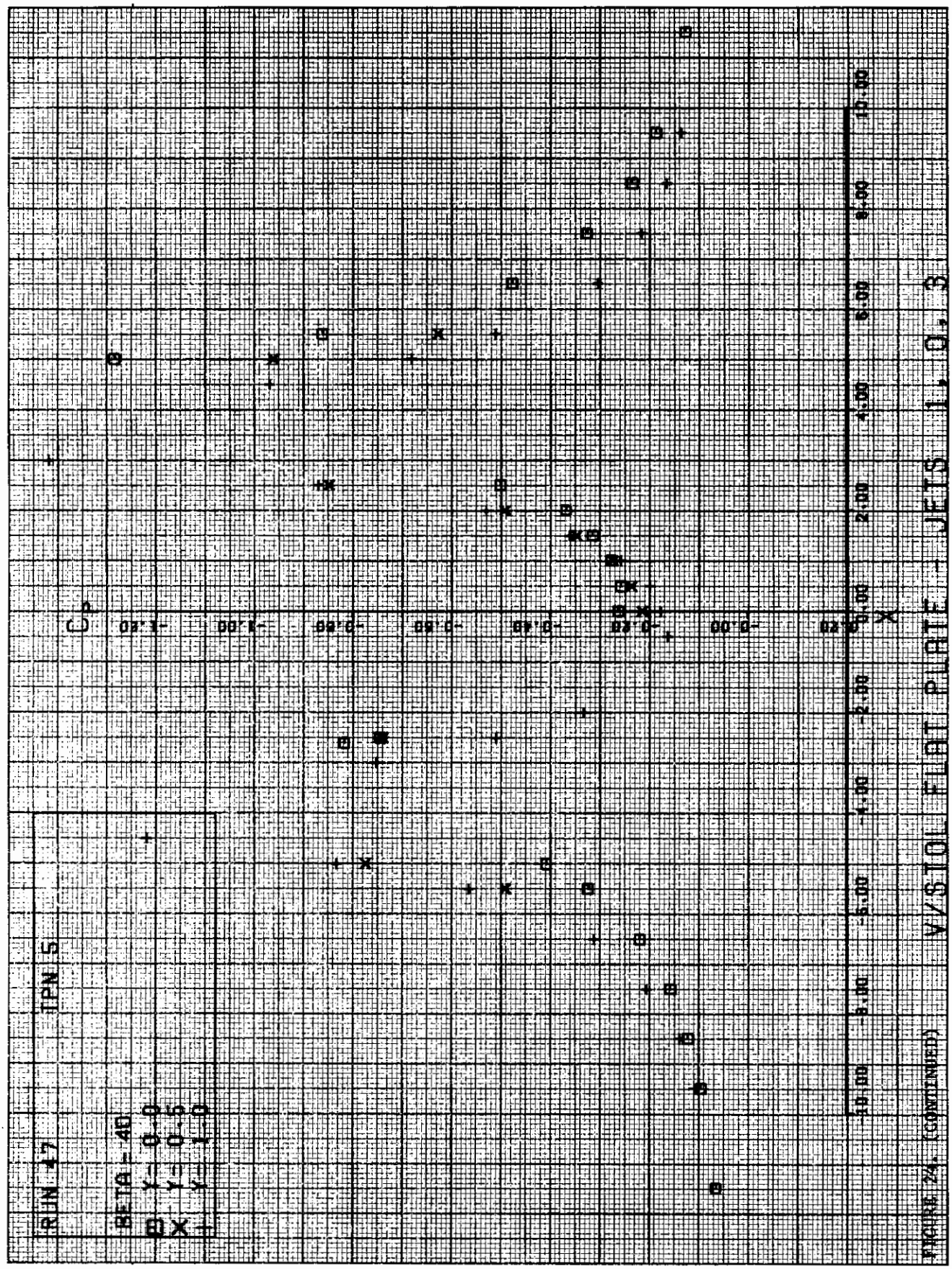

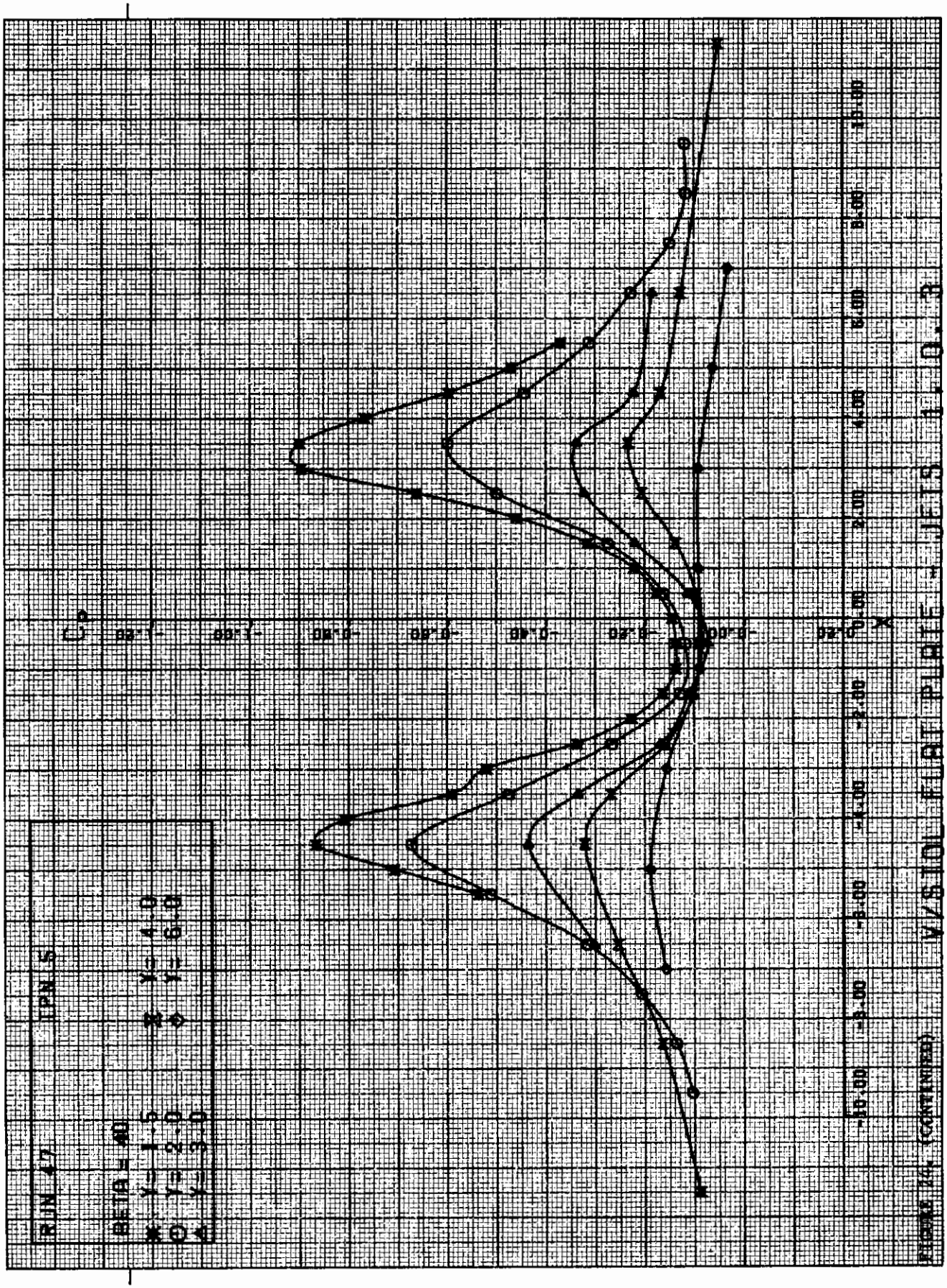

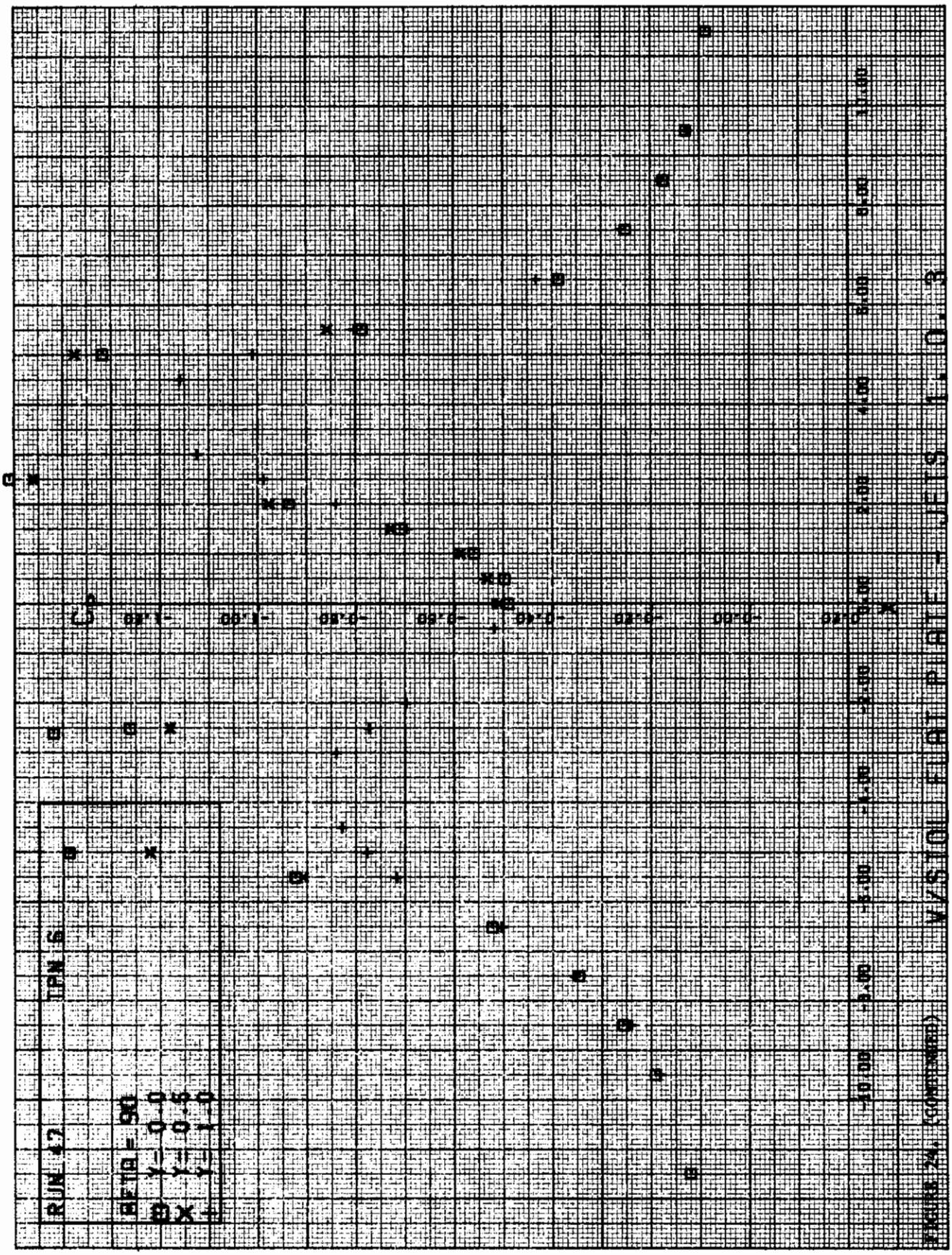

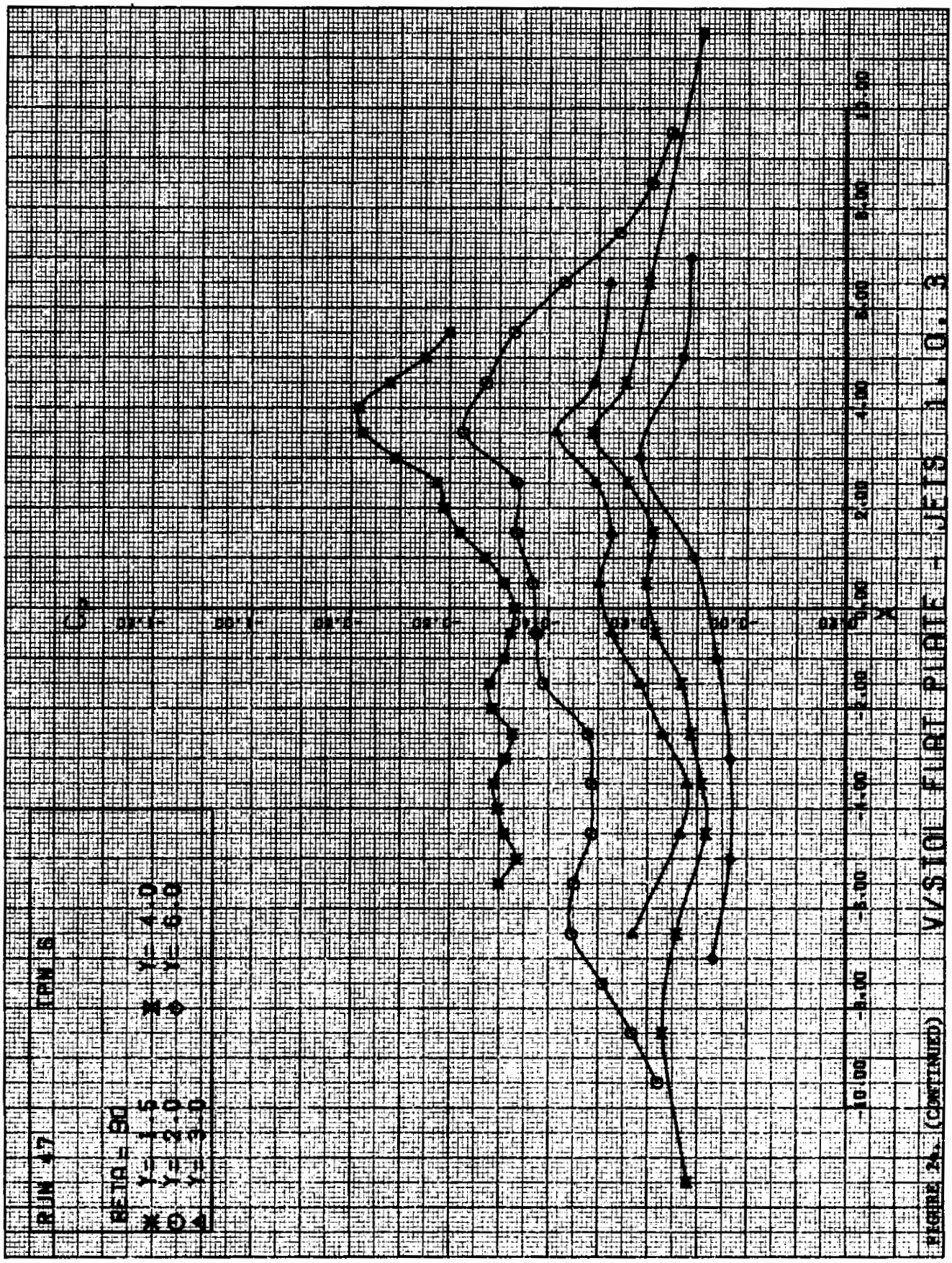

FIGURE 24. (CONTINUED)

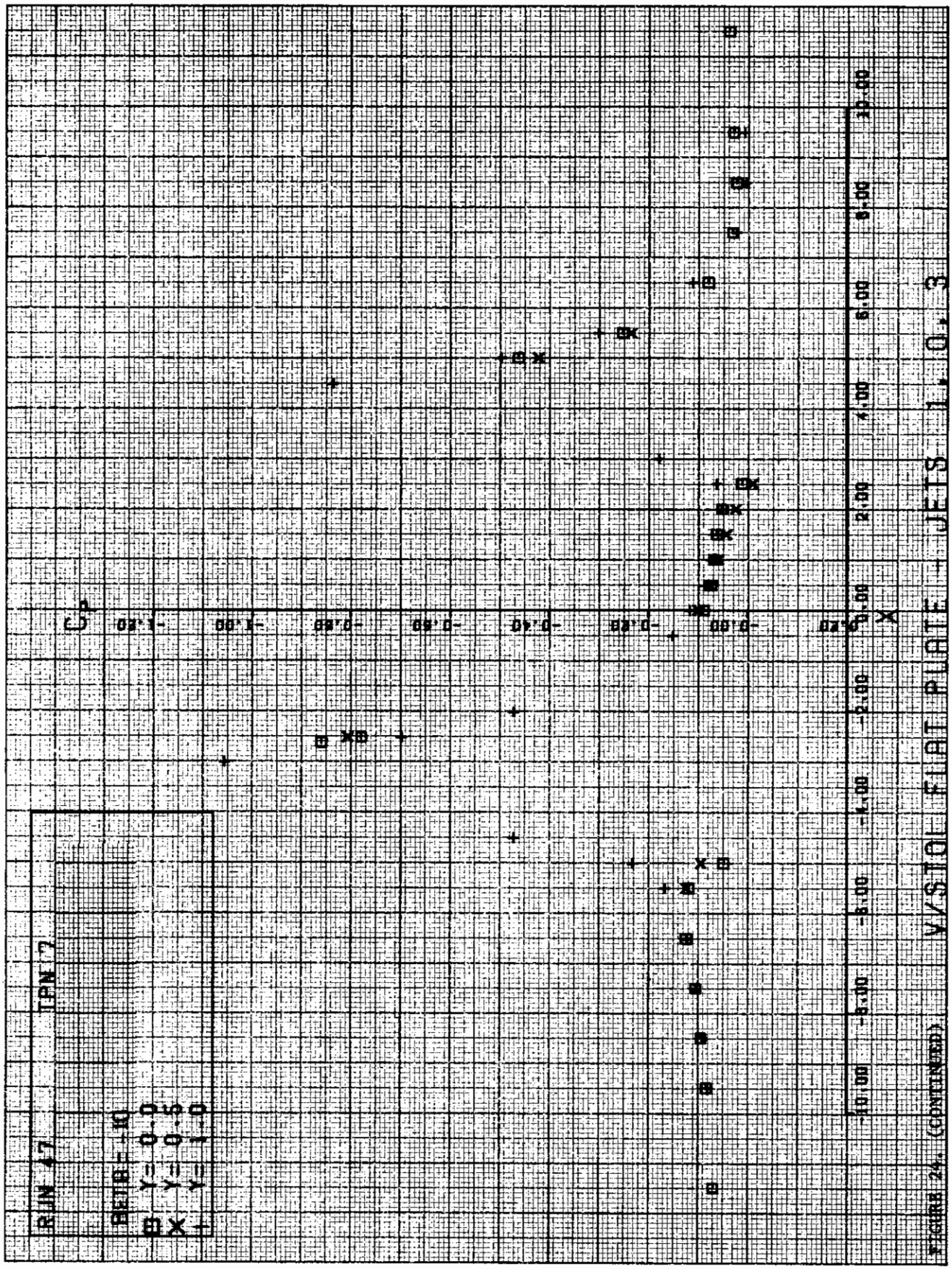

FIGURE 24. (CONTINUED)

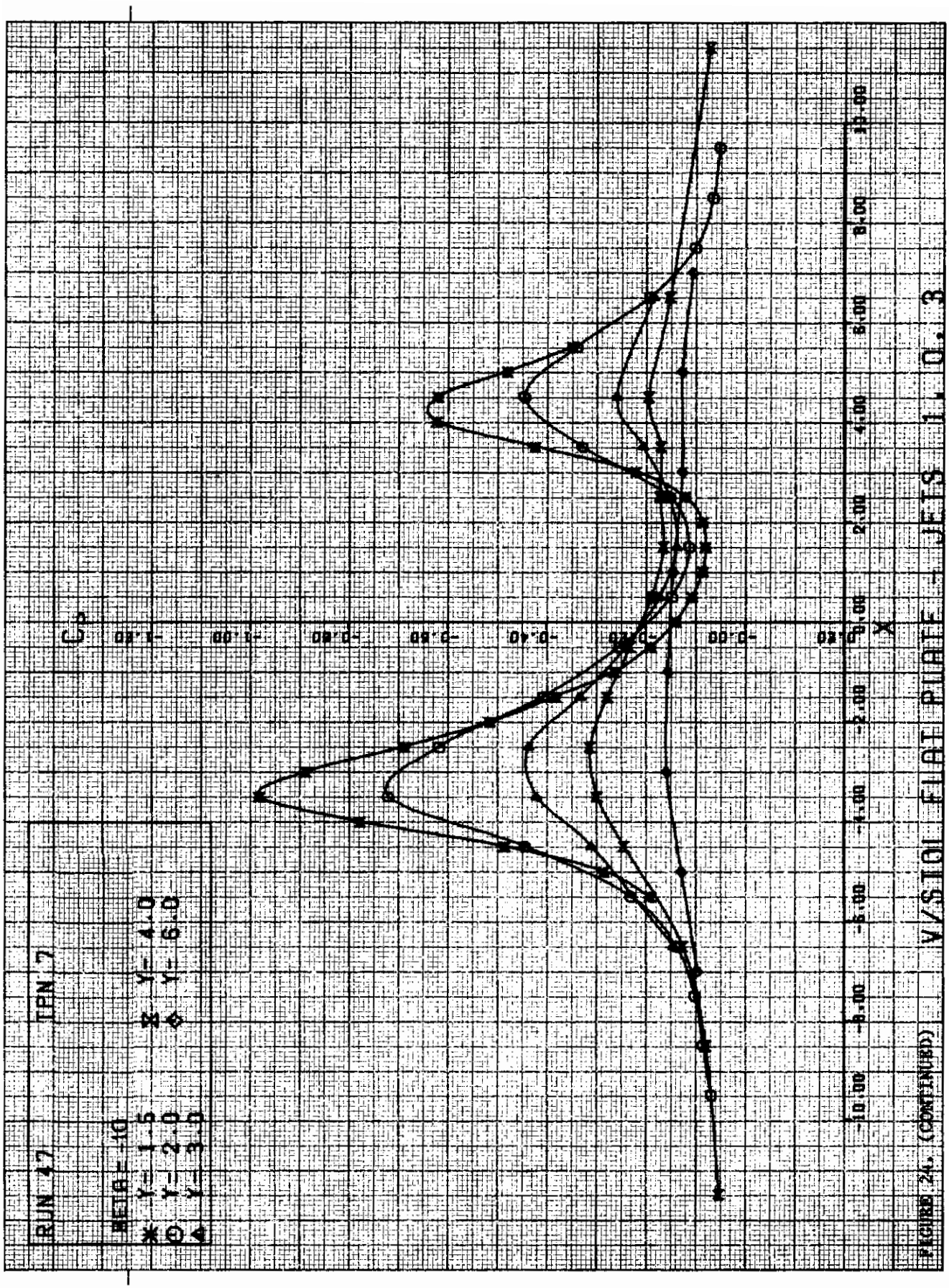

FIGURE 24. (CONTINUED)

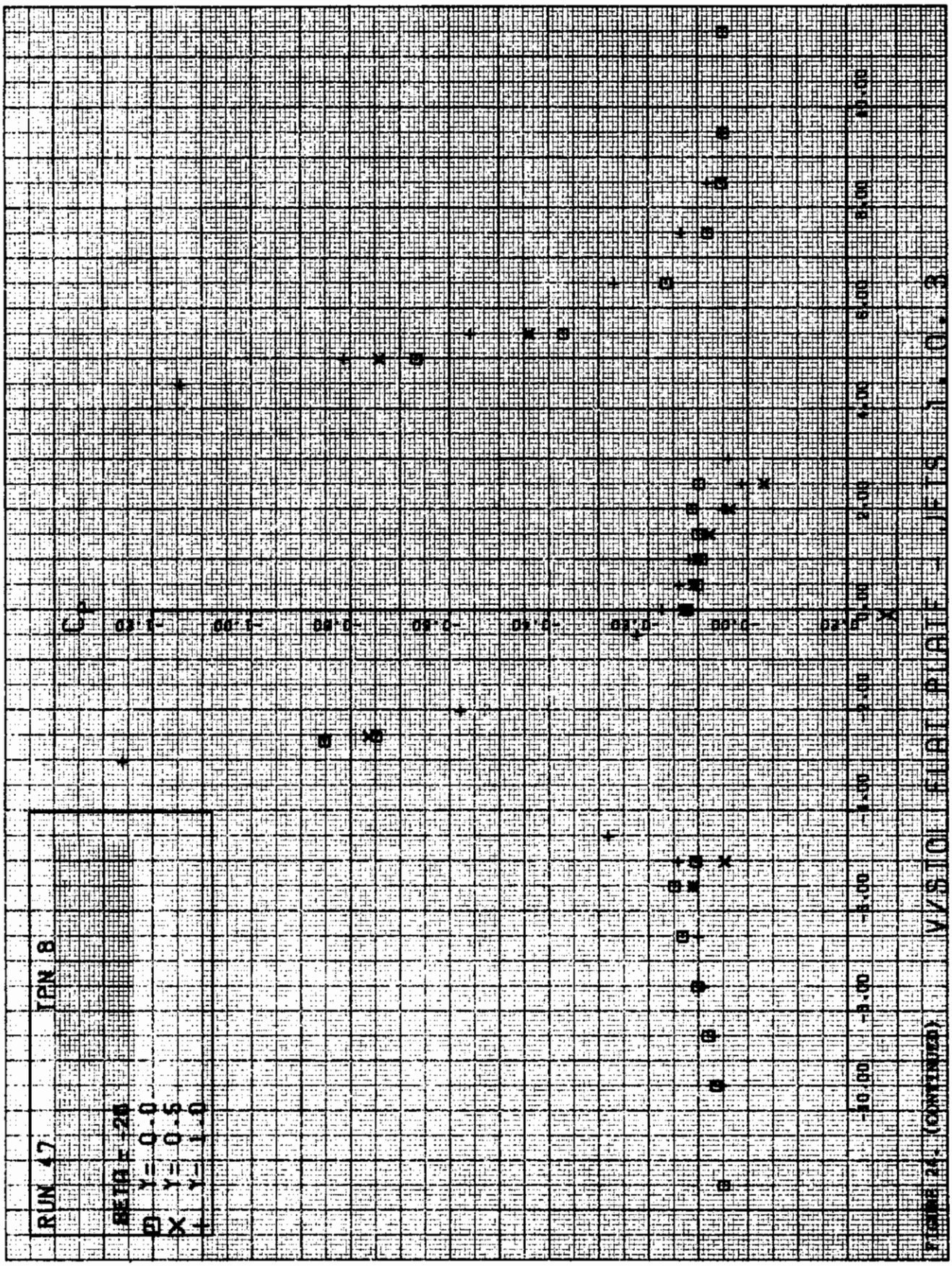

FIGURE 24. (CONTINUED)

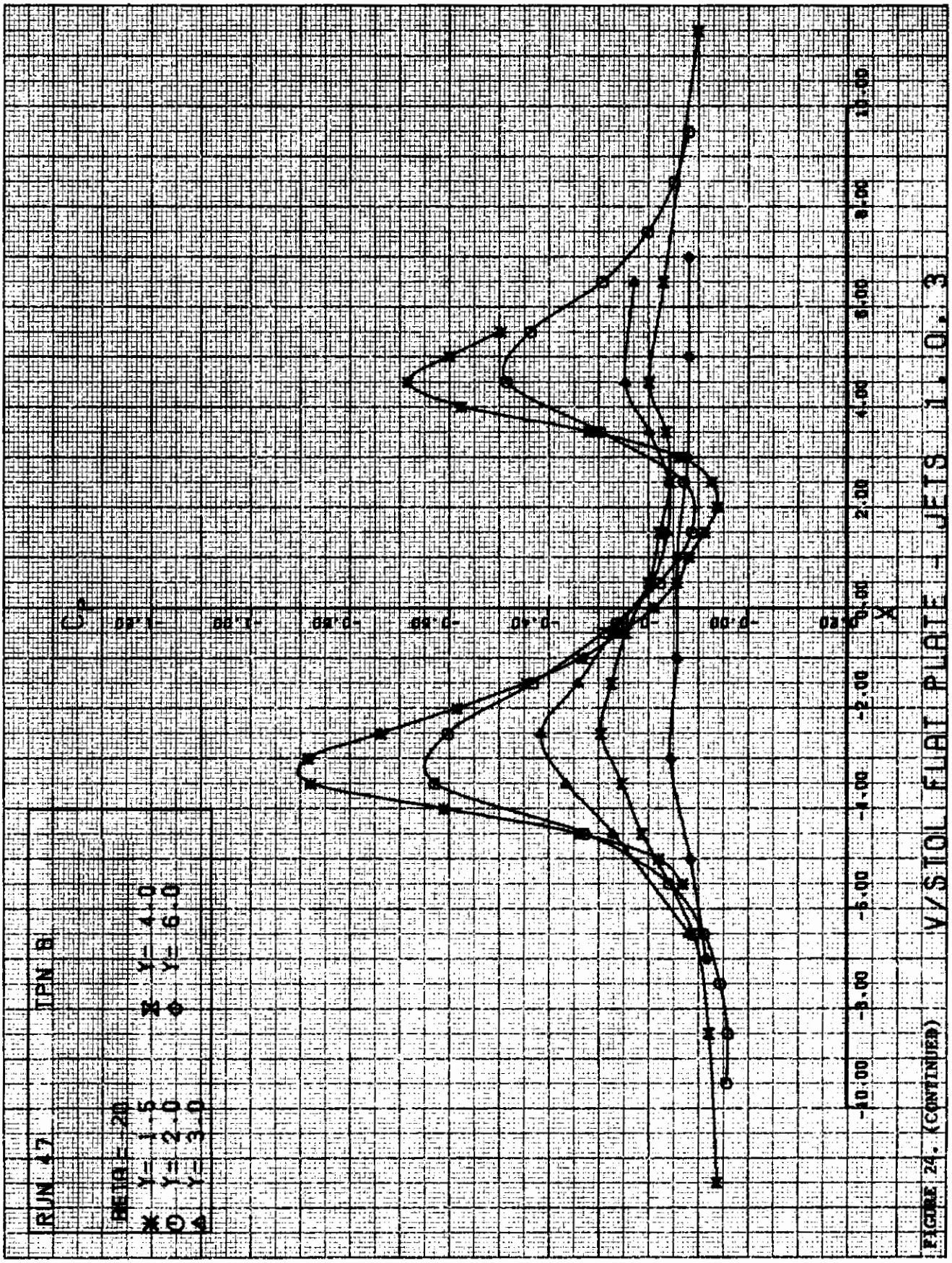

FIGURE 24. (CONTINUED)

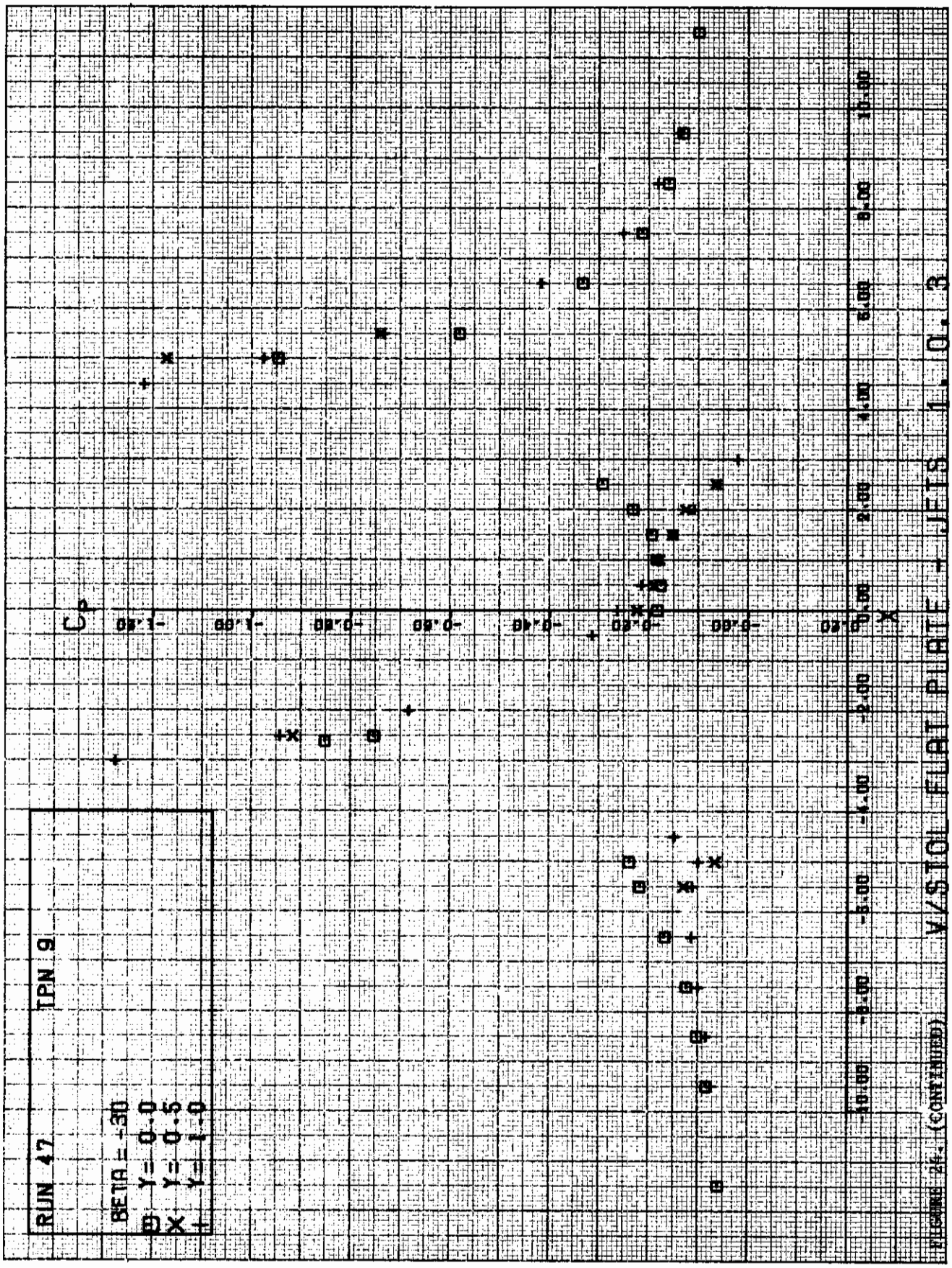

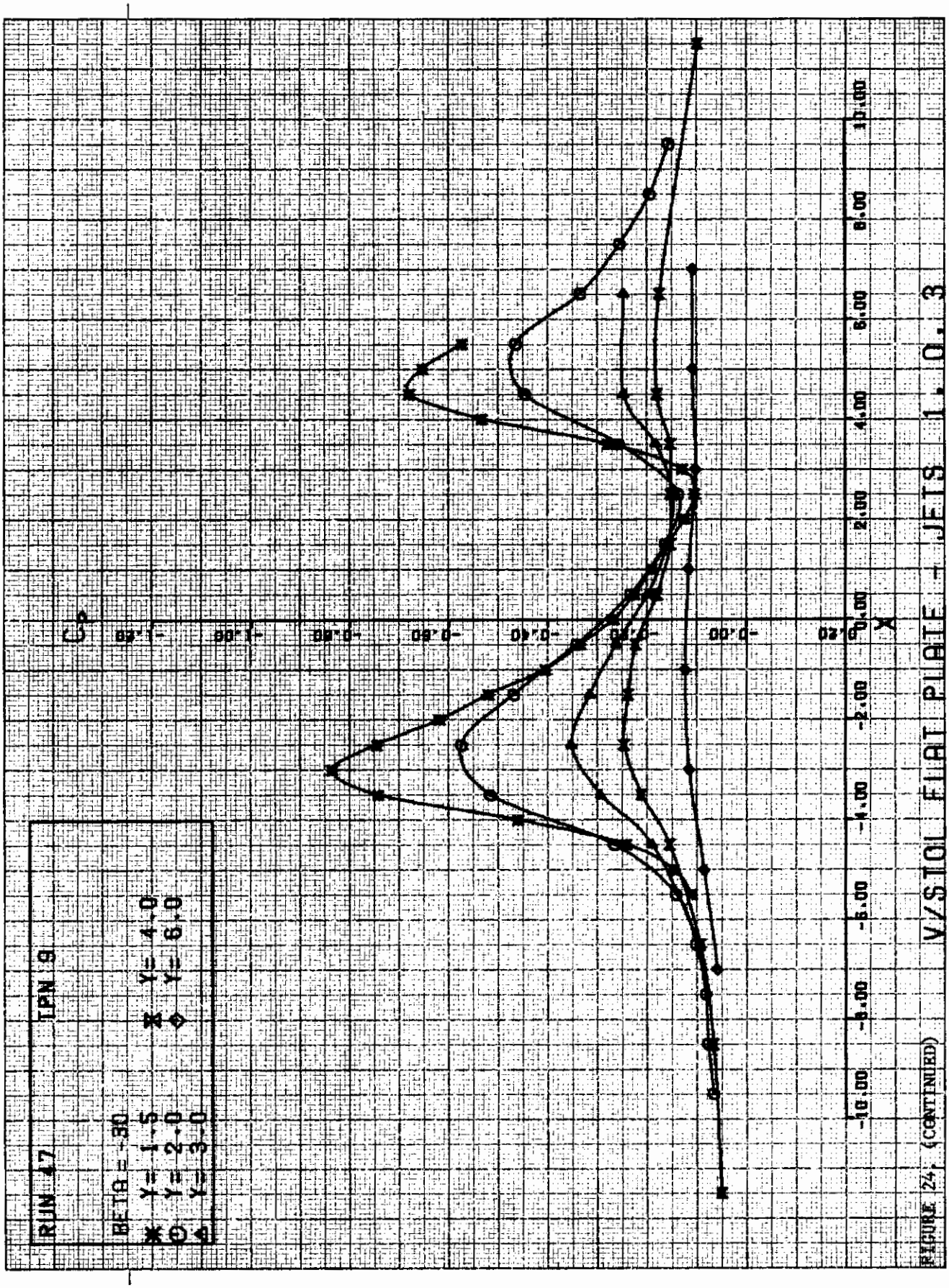

FIGURE 24. (CONTINUED)

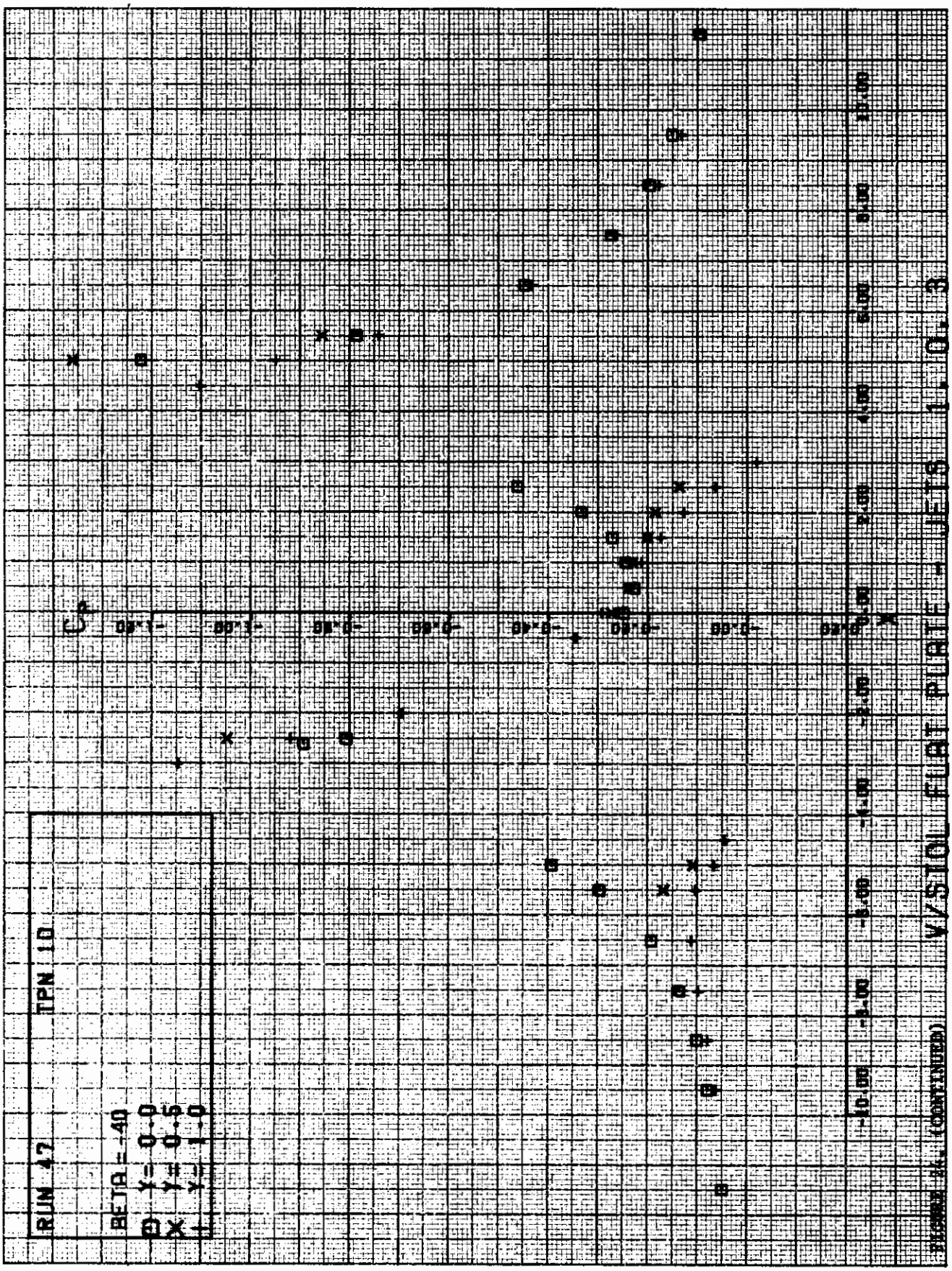

FIGURE 44. (CONTINUED)

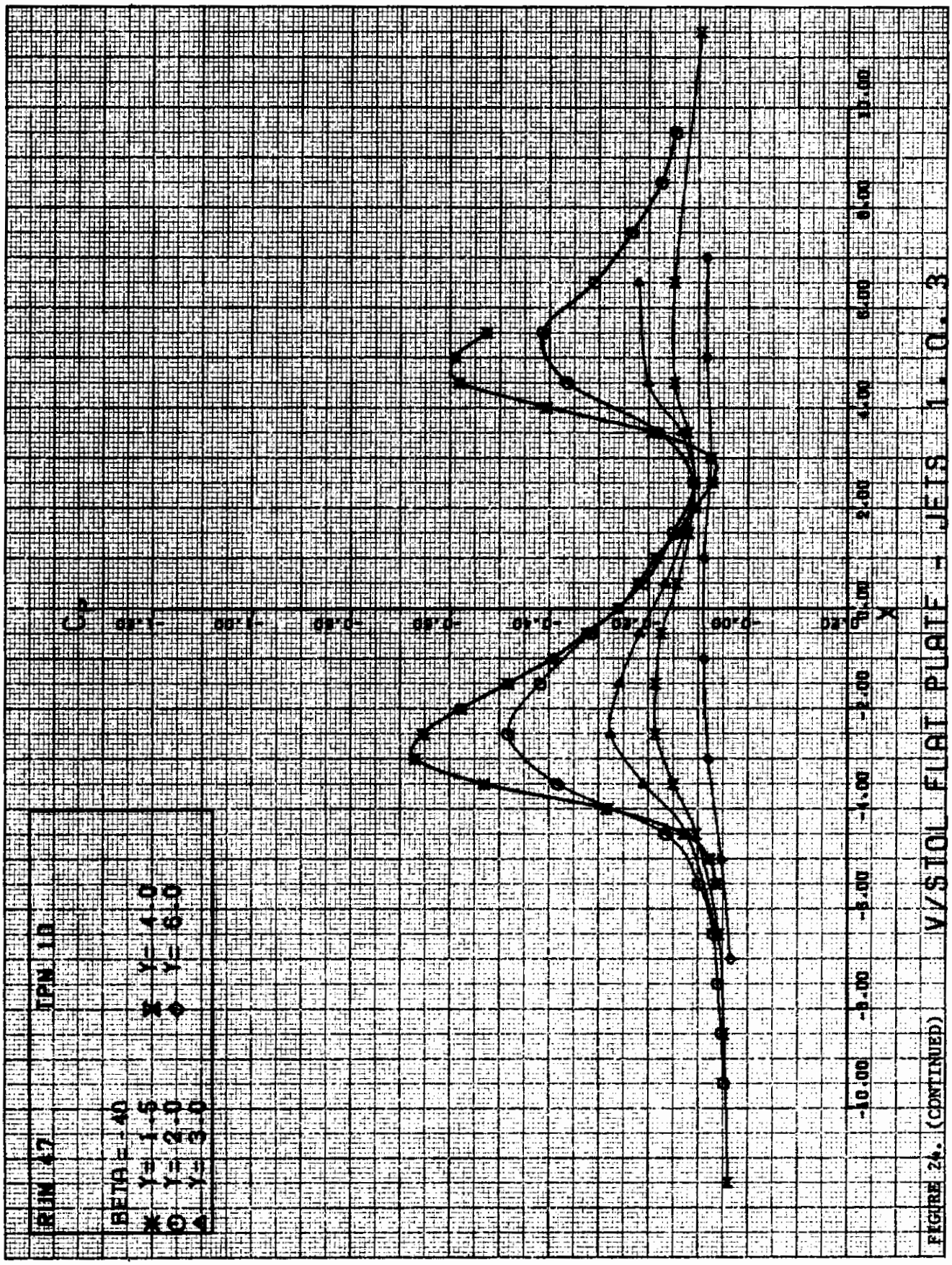

FIGURE 24. (CONTINUED) V/STOL FLAT PLATE - JETS 1.0, 3

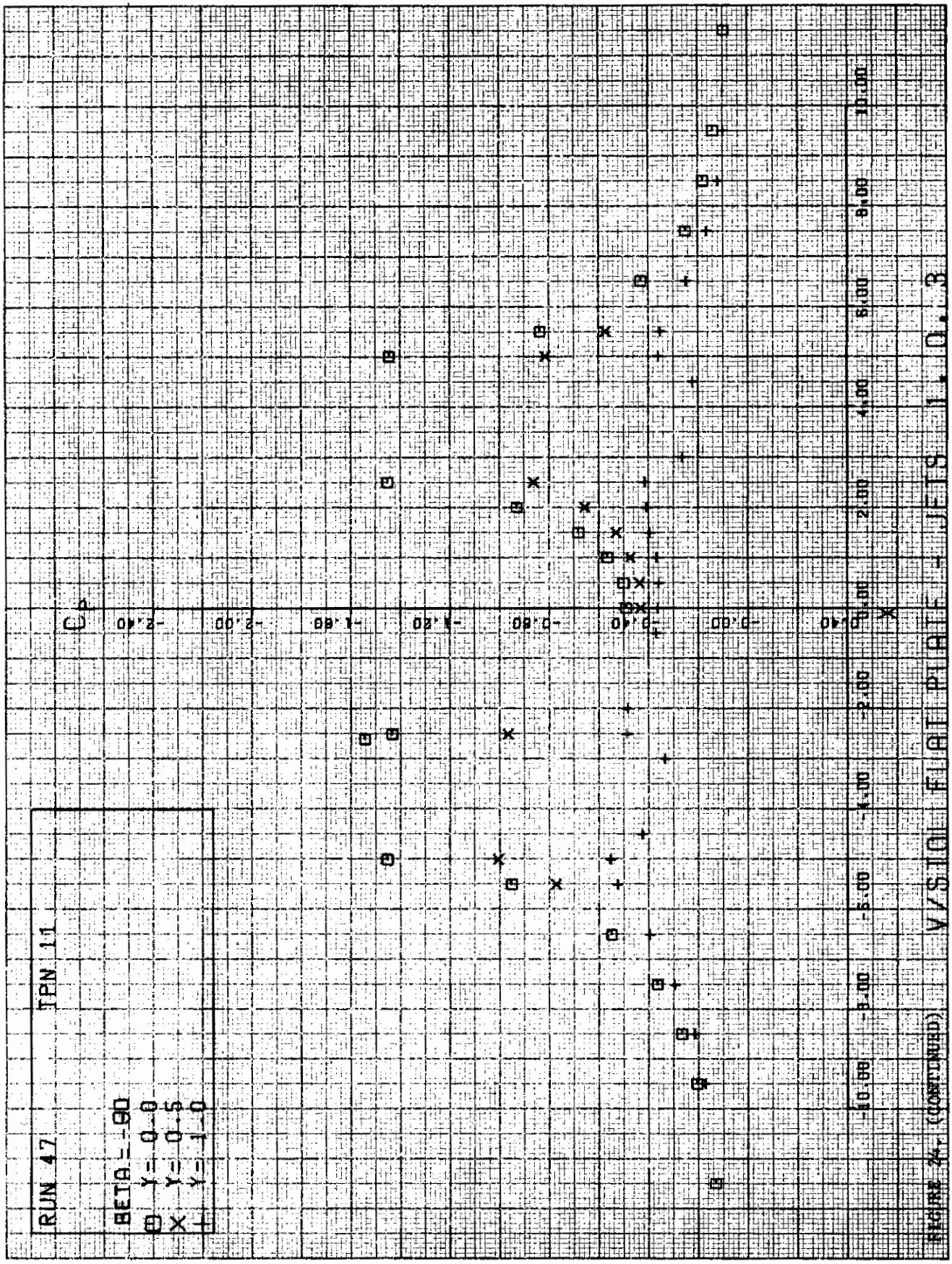

FIGURE 24. (CONTINUED)

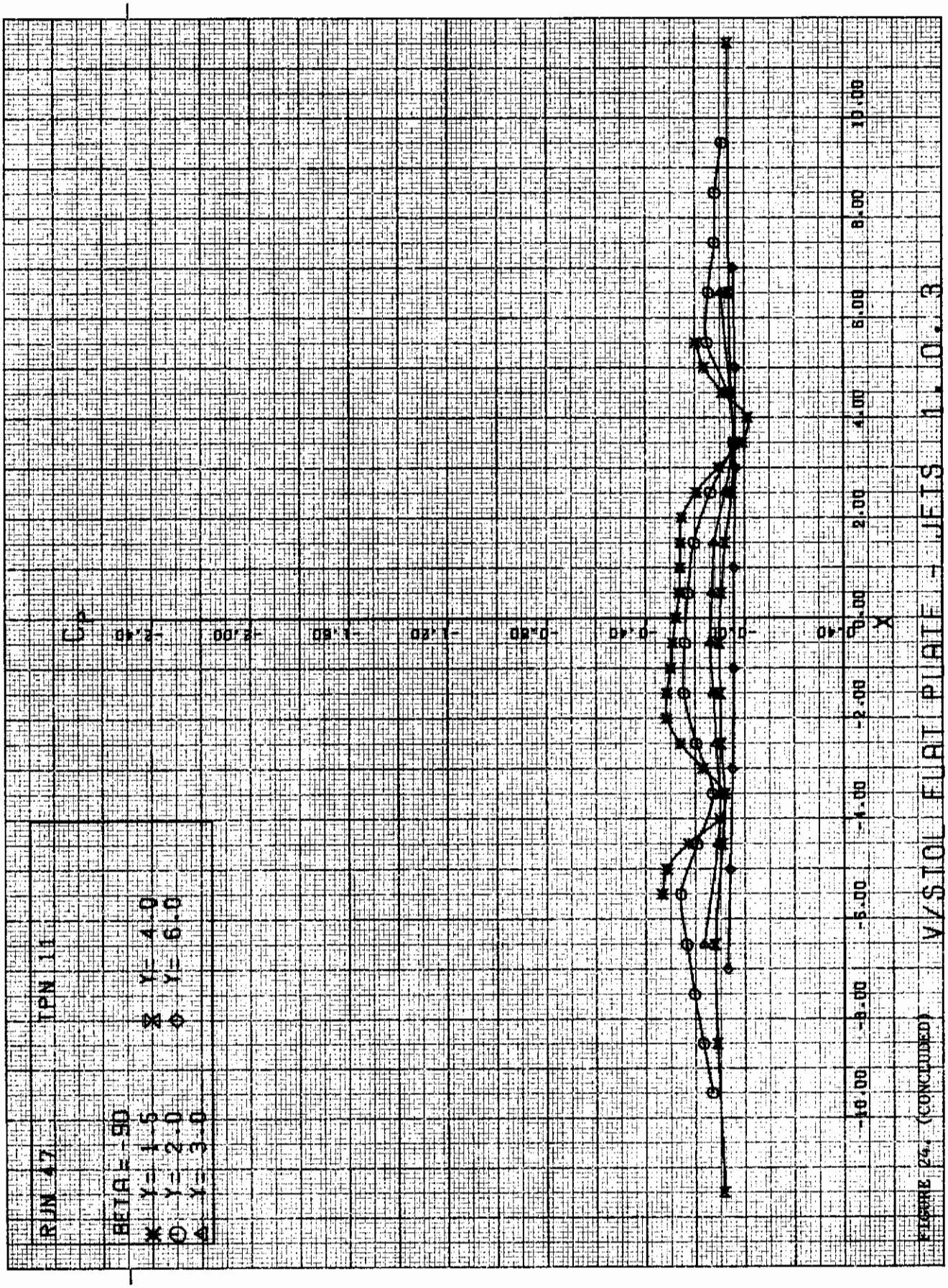

FIGURE 24. (CONCLUDED)

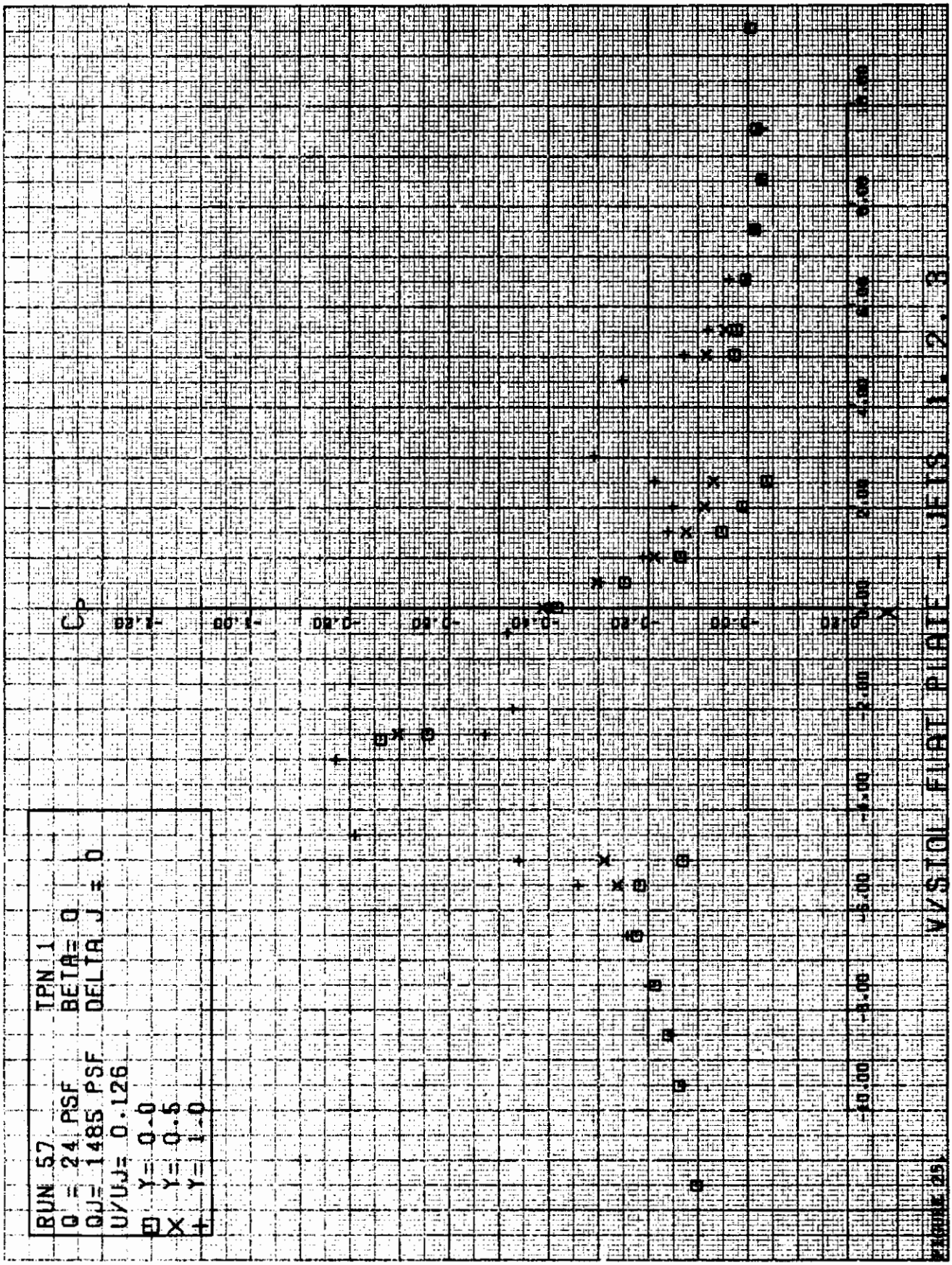

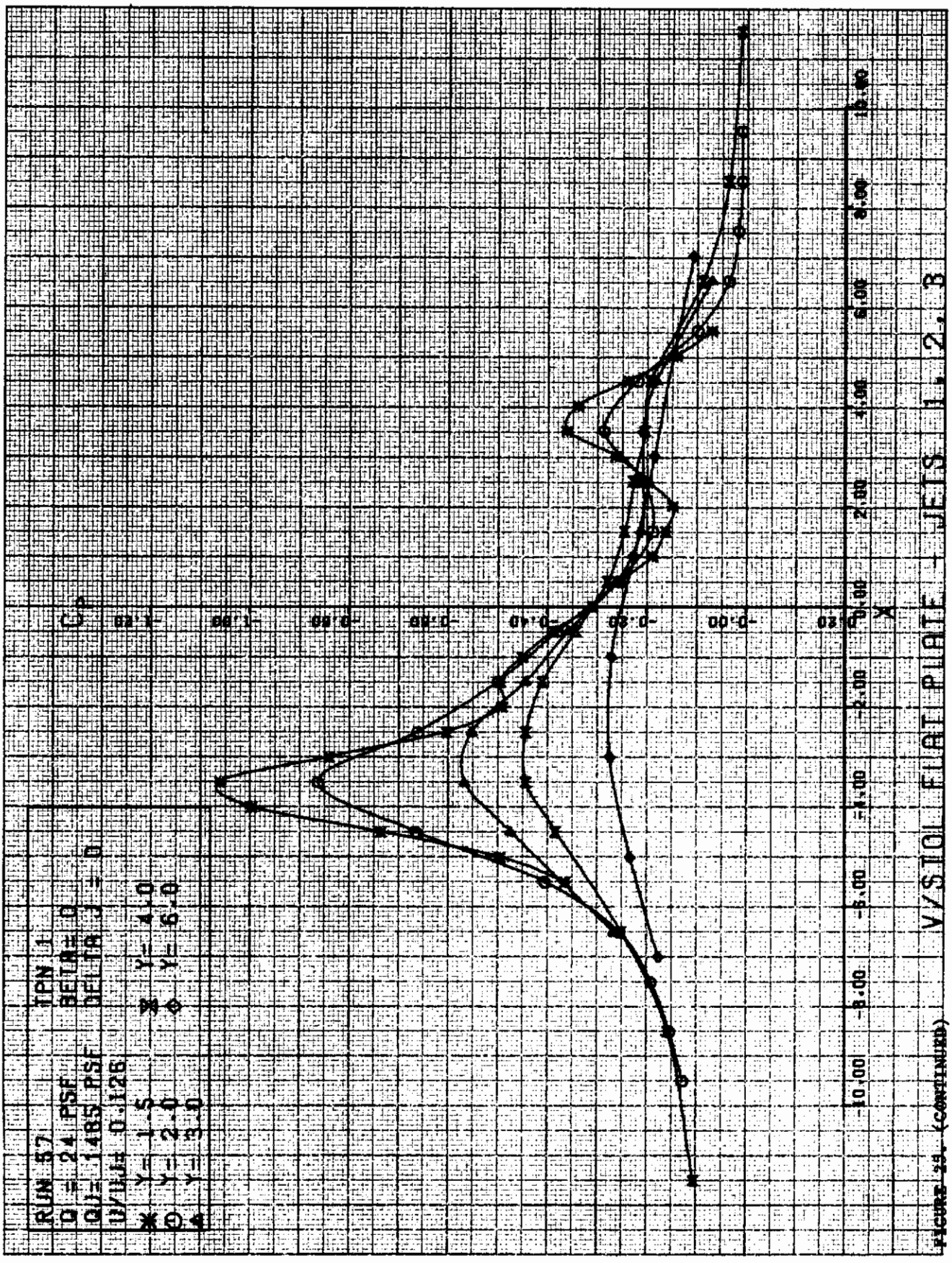

FIGURE 24. (CONTINUED)

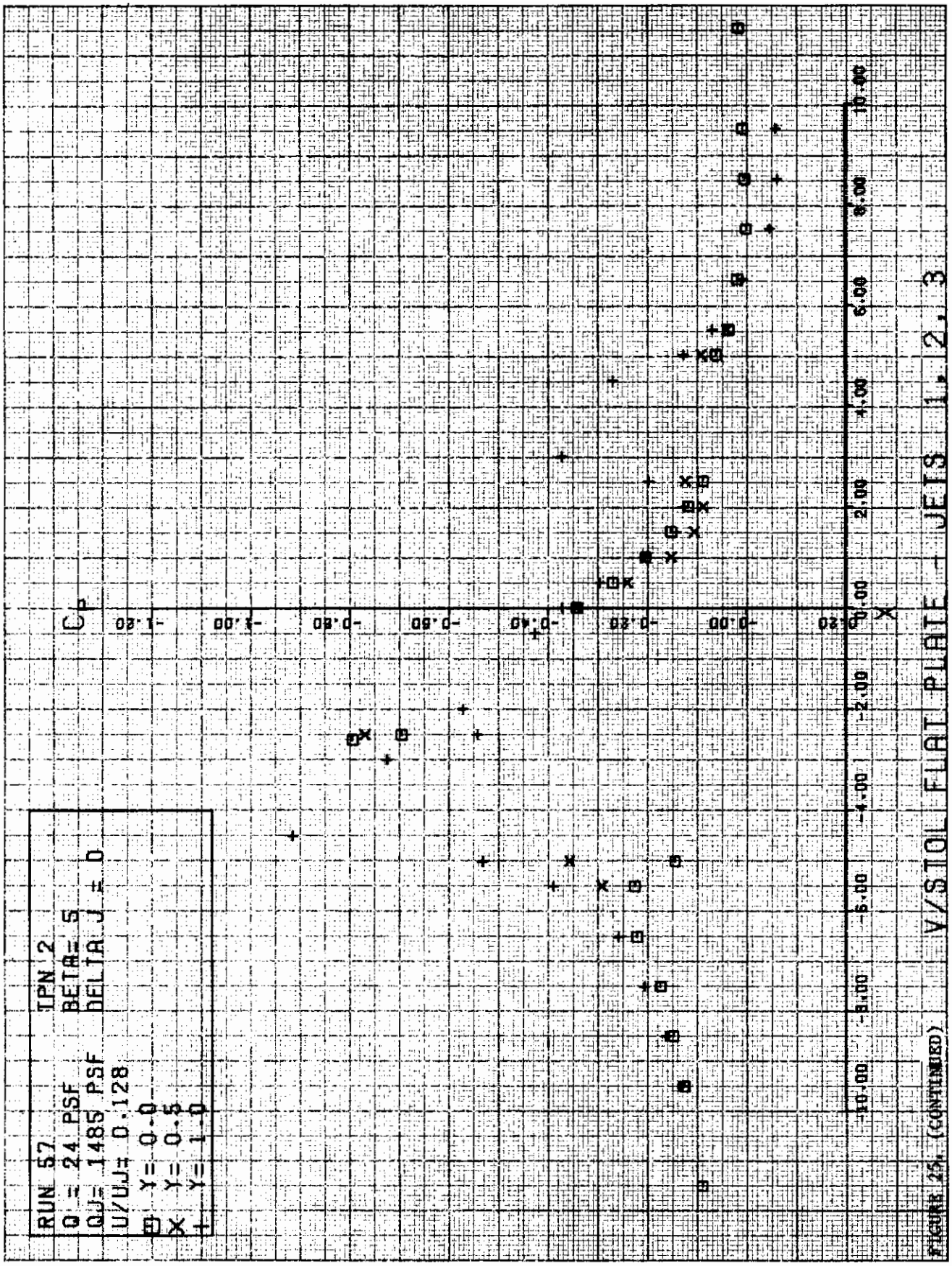

FIGURE 25. (CONTINUED)

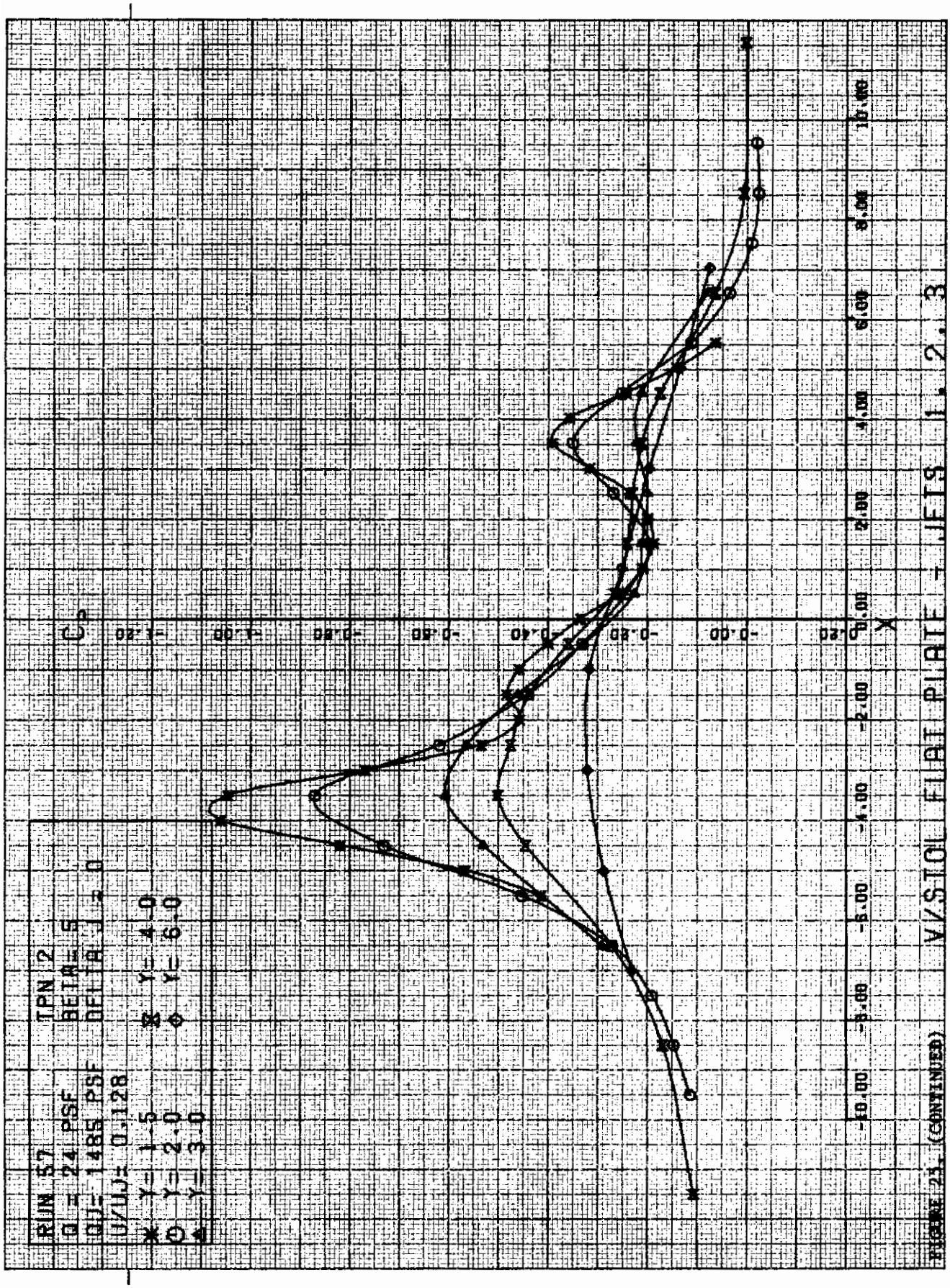

FIGURE 23. (CONTINUED)

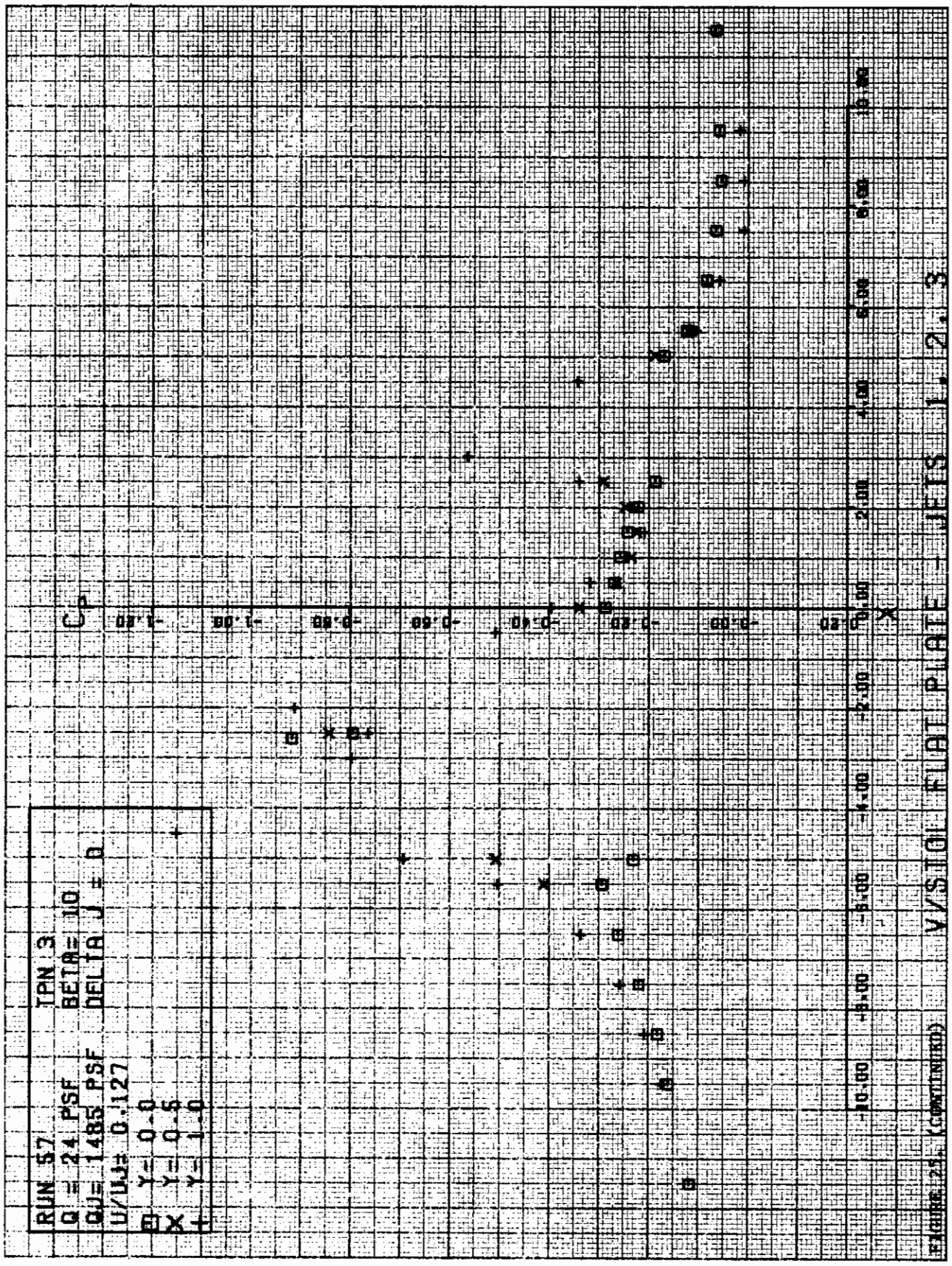

FIGURE 25. (CONTINUED)

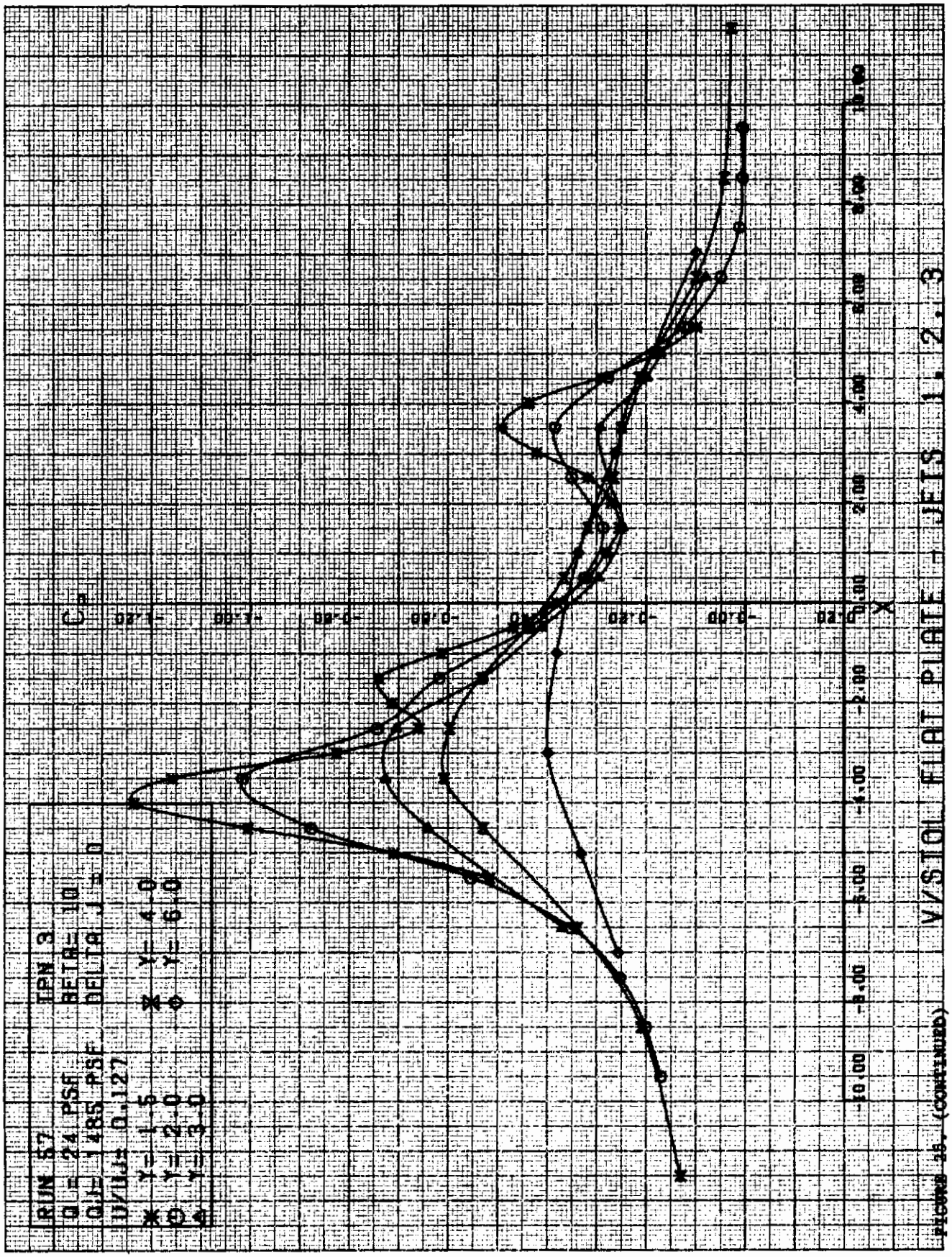

FIGURE 26. (CONTINUED)

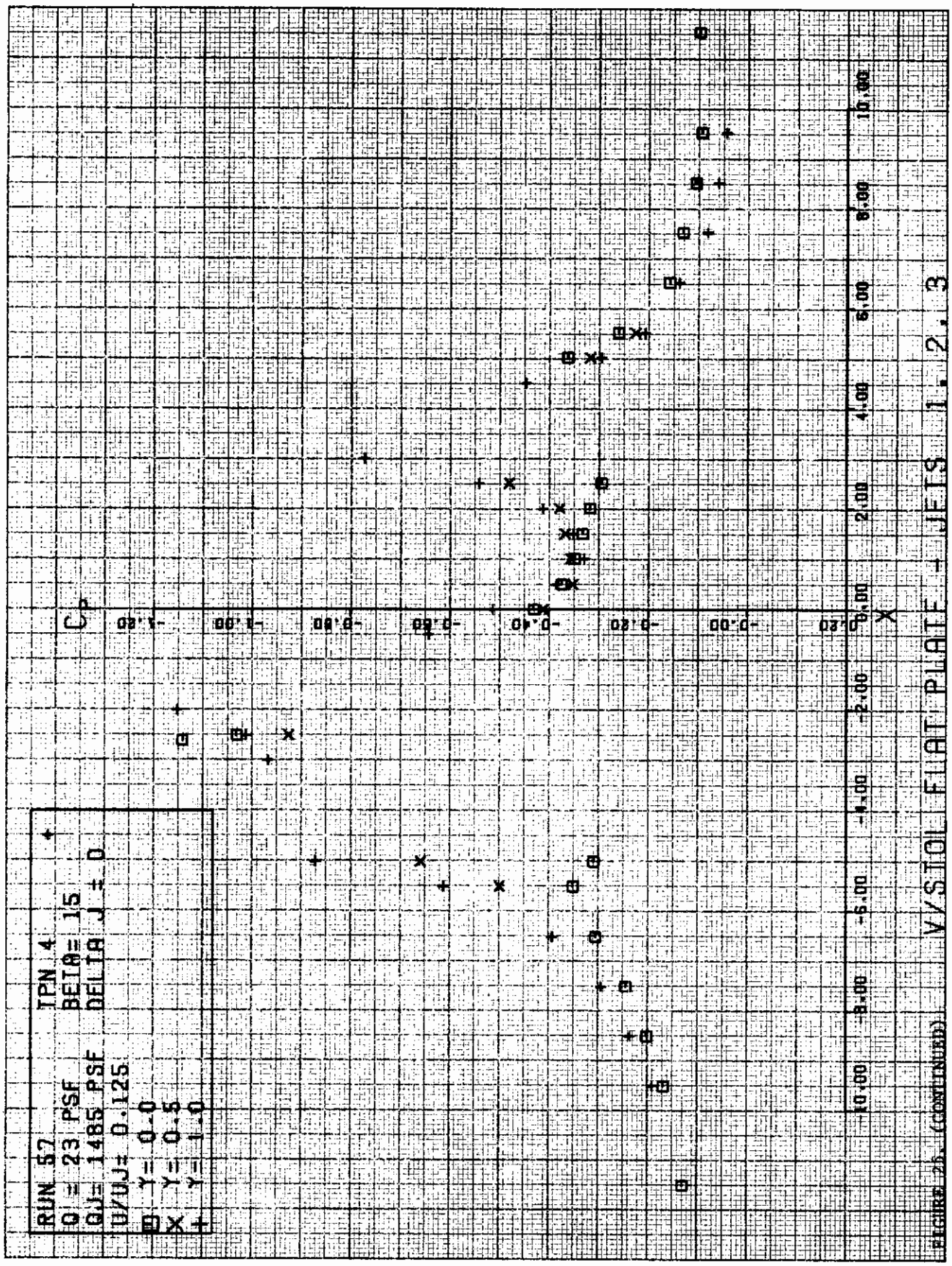

FIGURE 26. (CONTINUED)

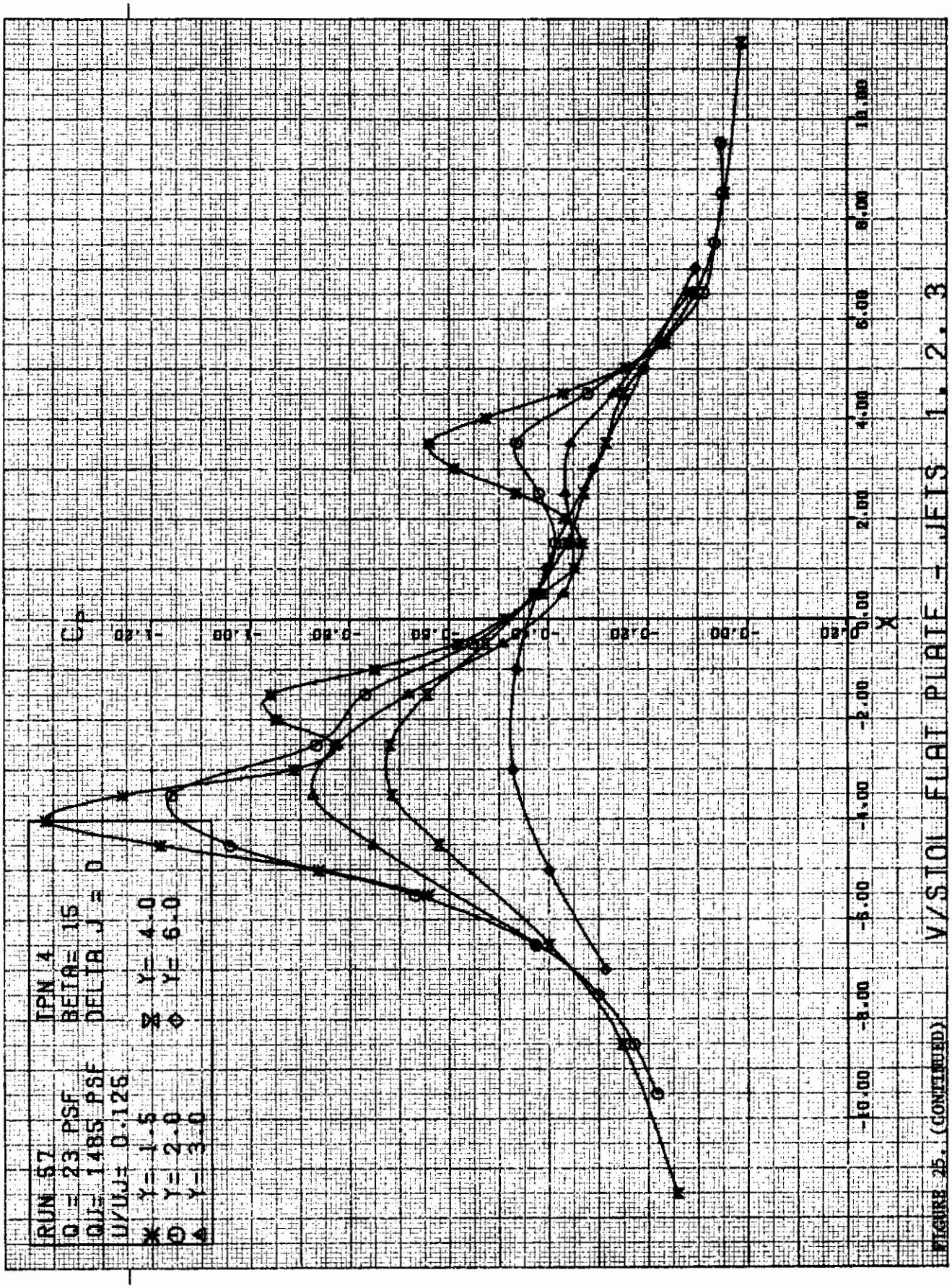

FIGURE 25. (CONTINUED)

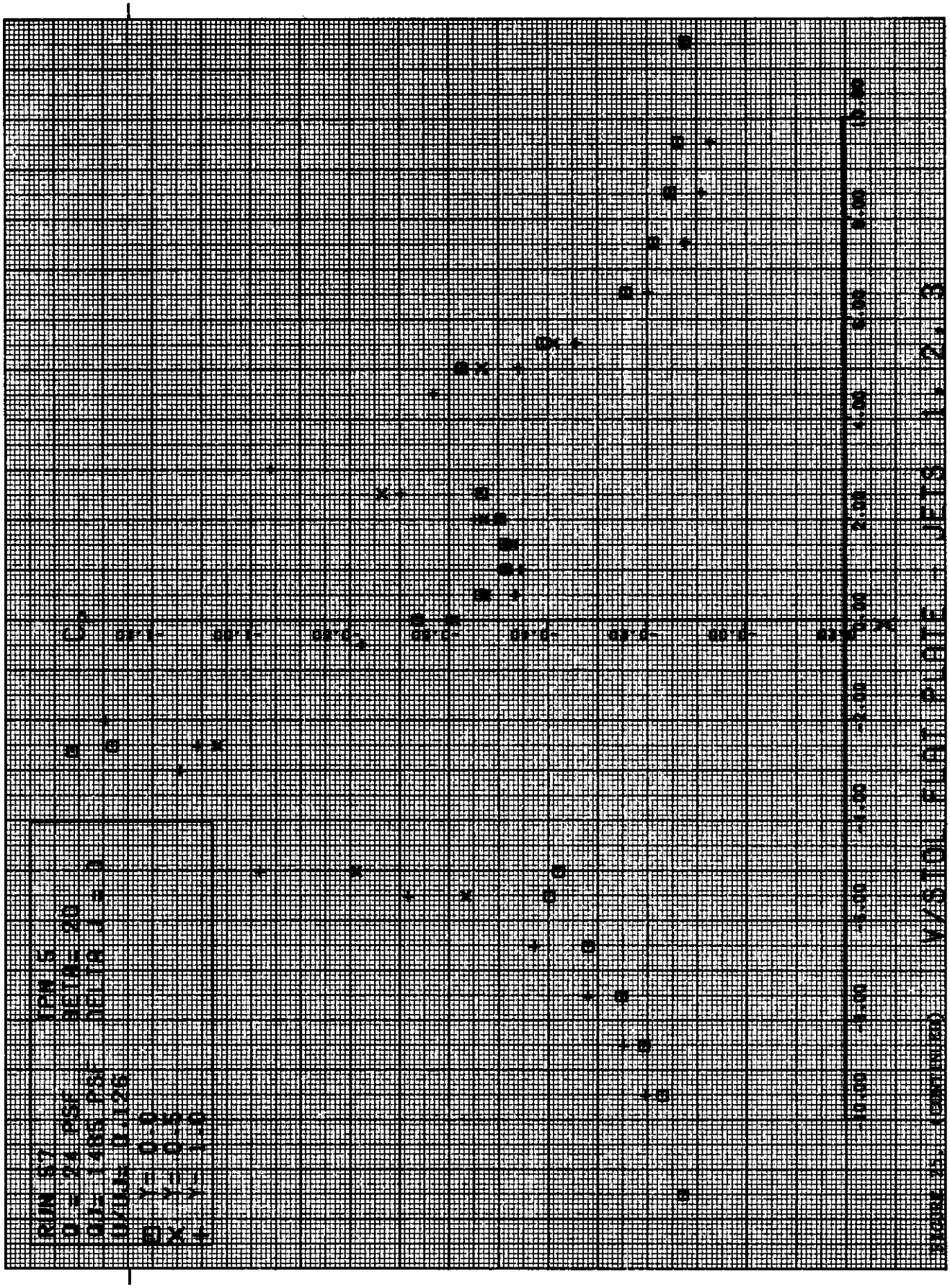

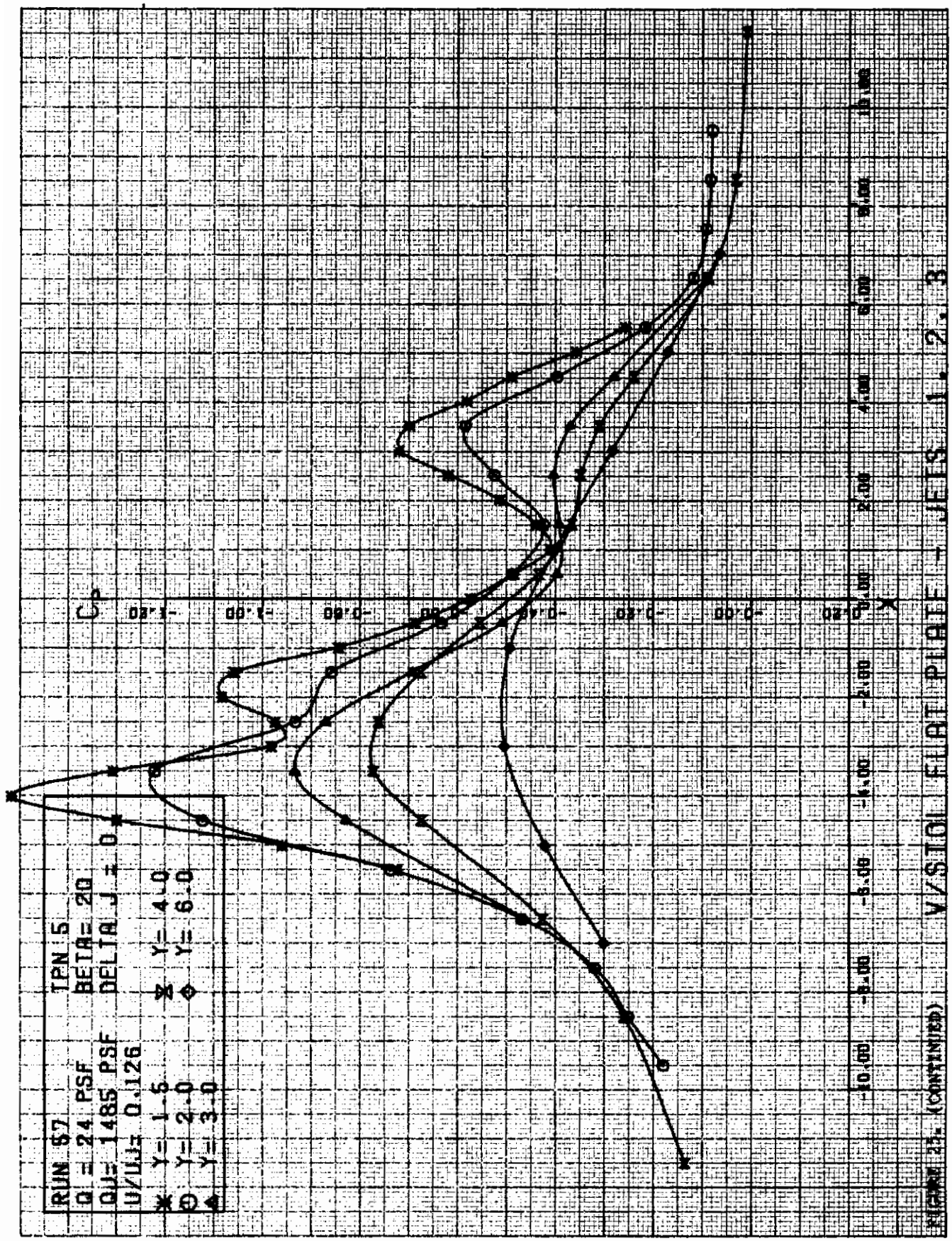

FIGURE 23. (CONTINUED)

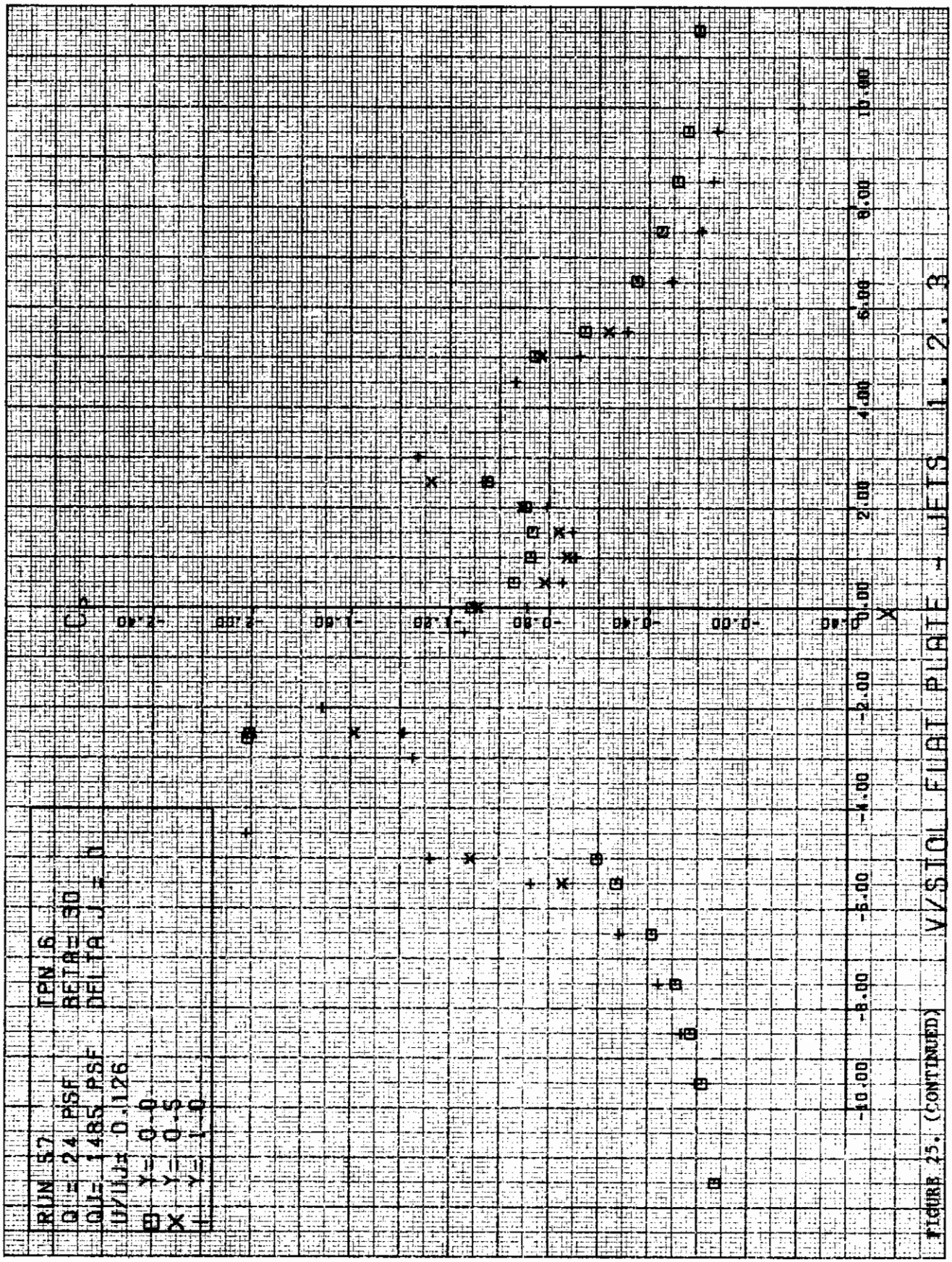

FIGURE 25. (CONTINUED)

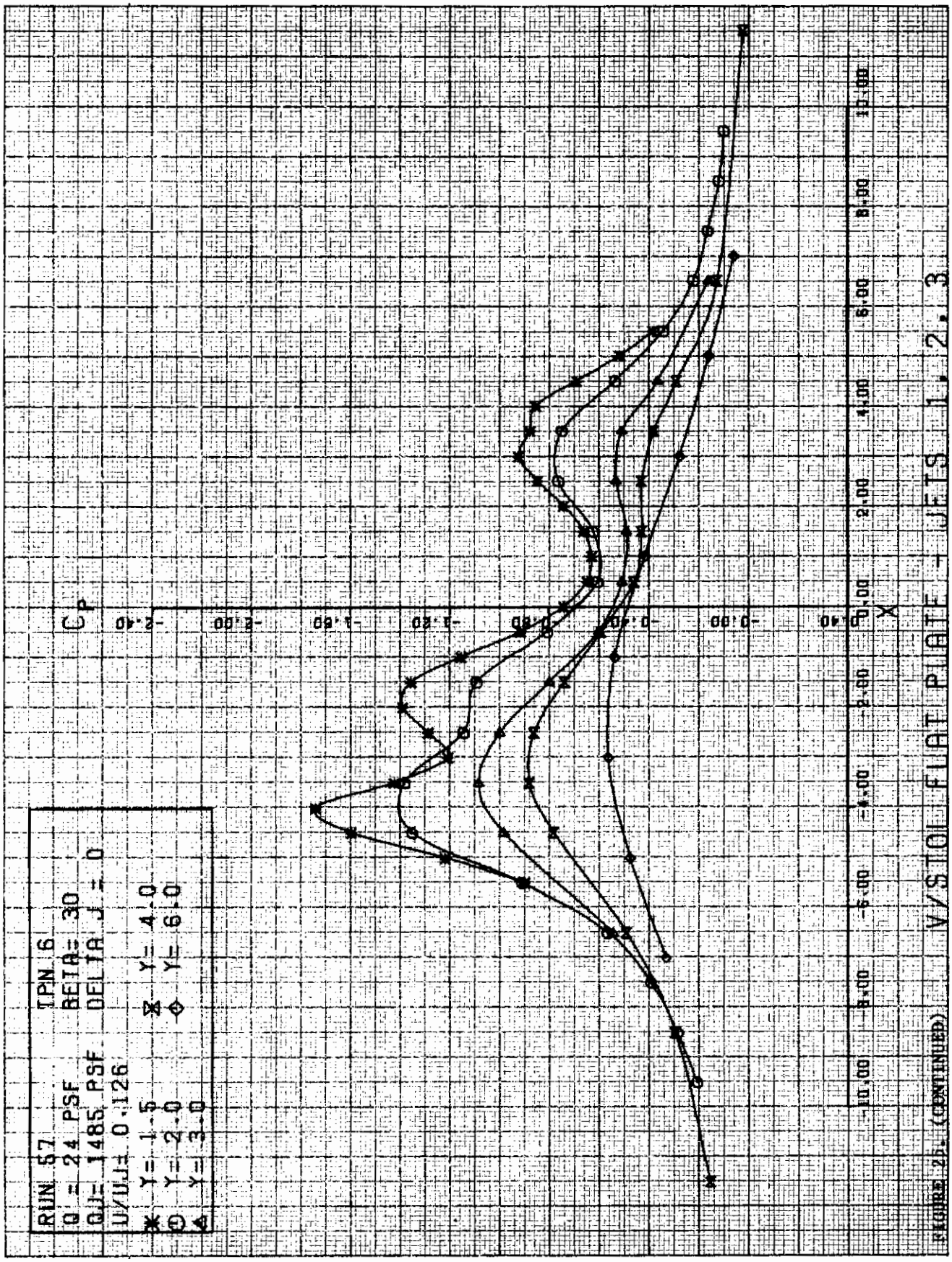

FIGURE 25. (CONTINUED)

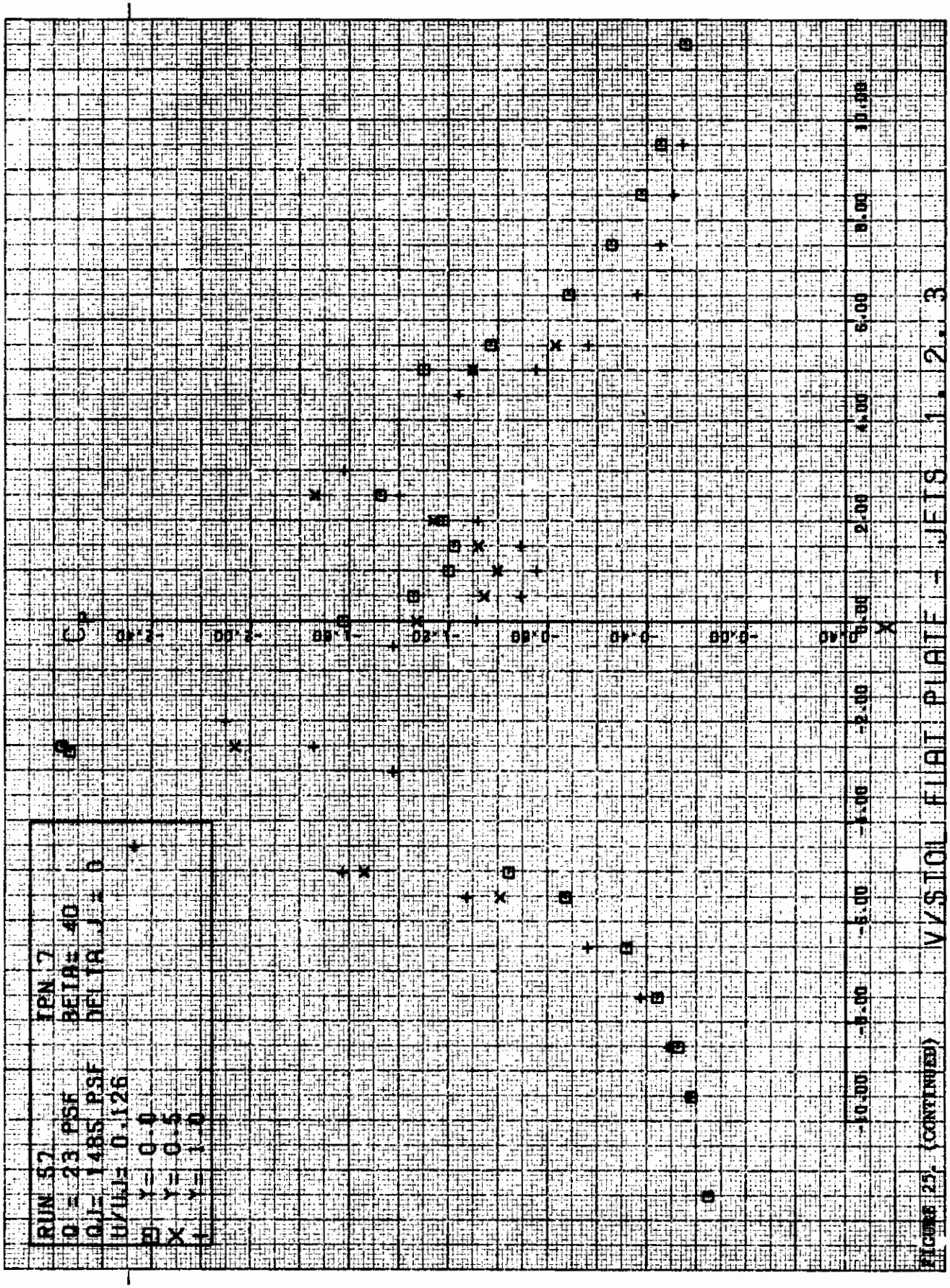

FIGURE 25. (CONTINUED) V/STOL FLAT PLATE - JETS 1, 2, 3

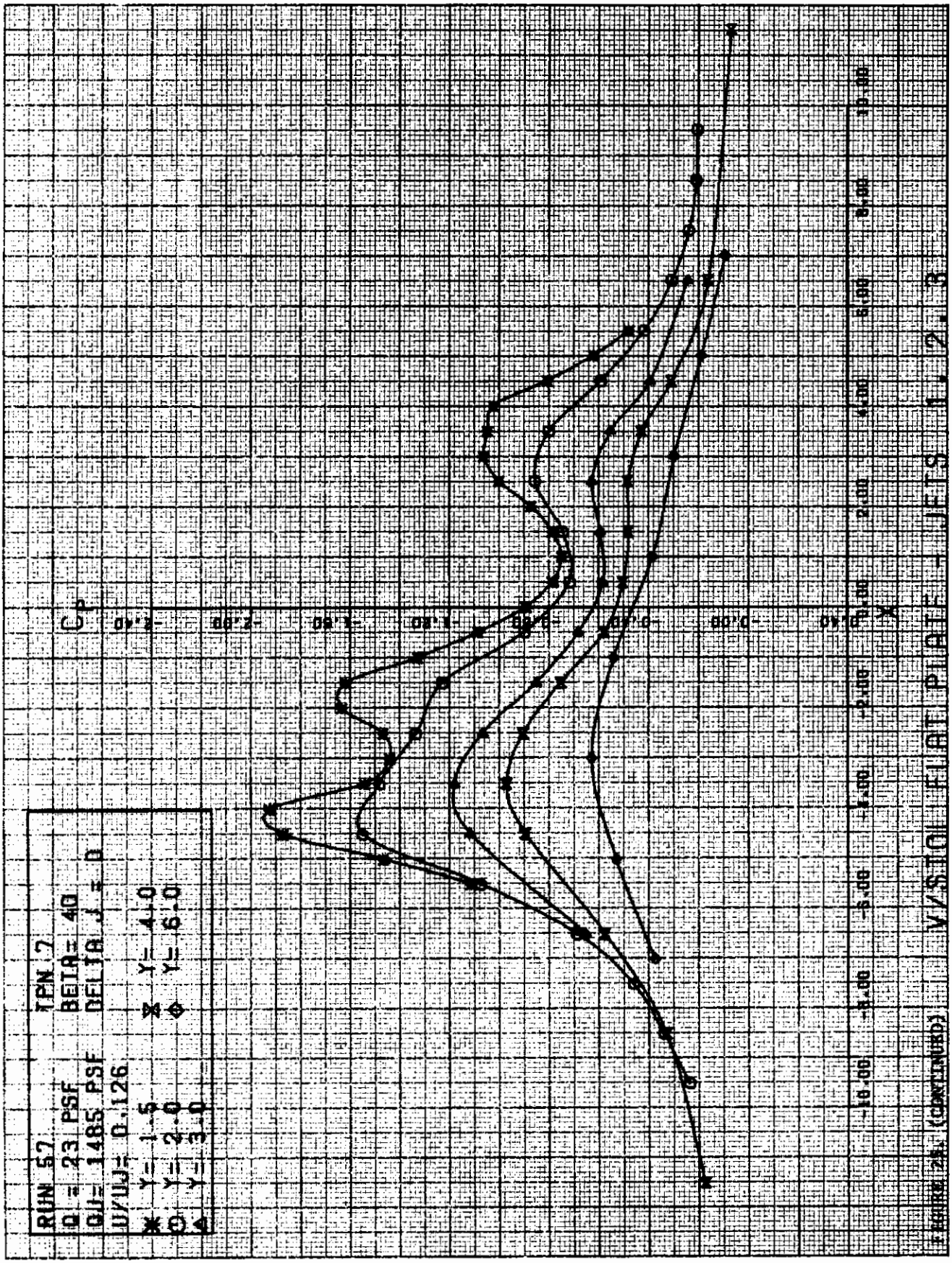

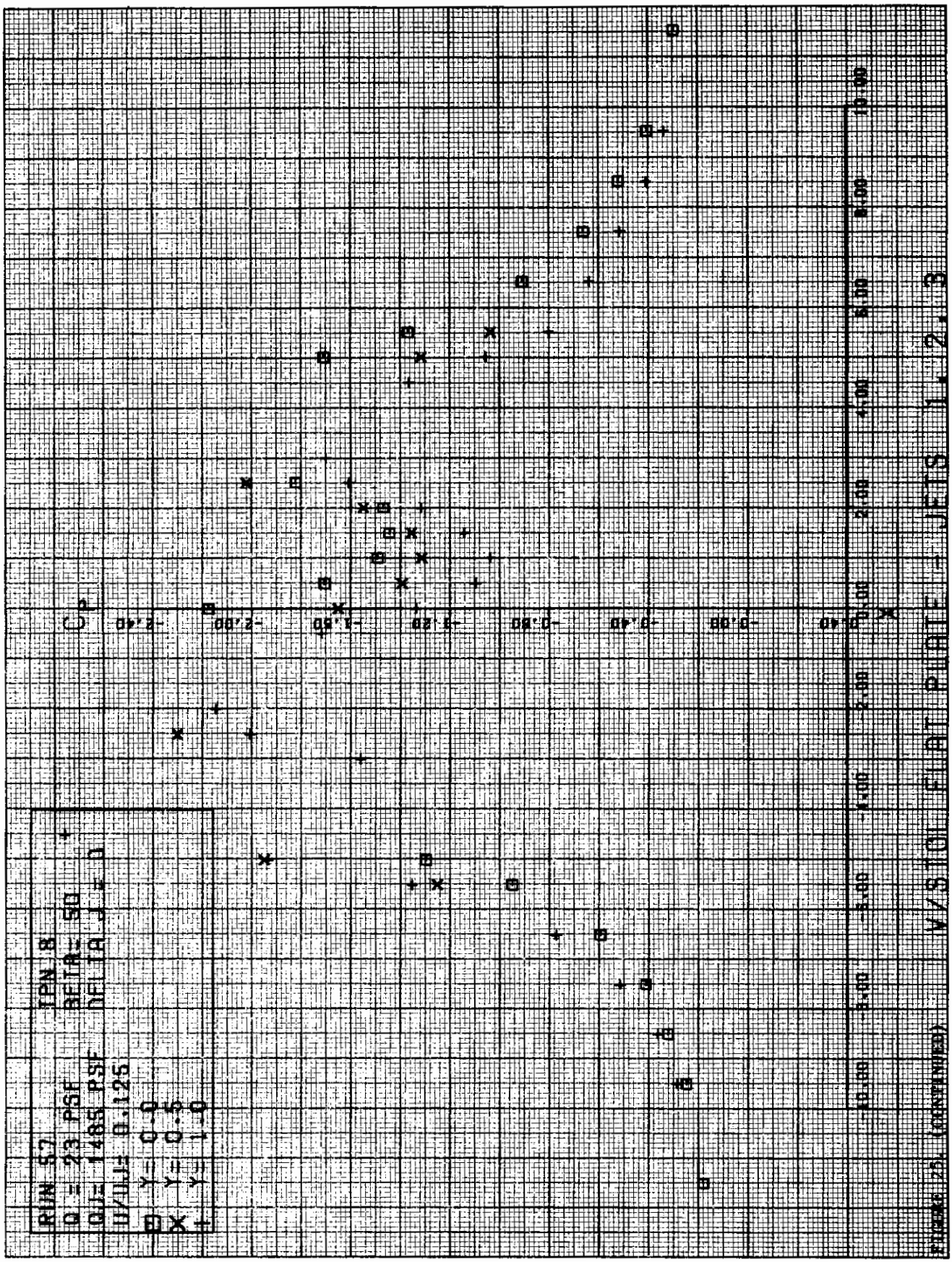

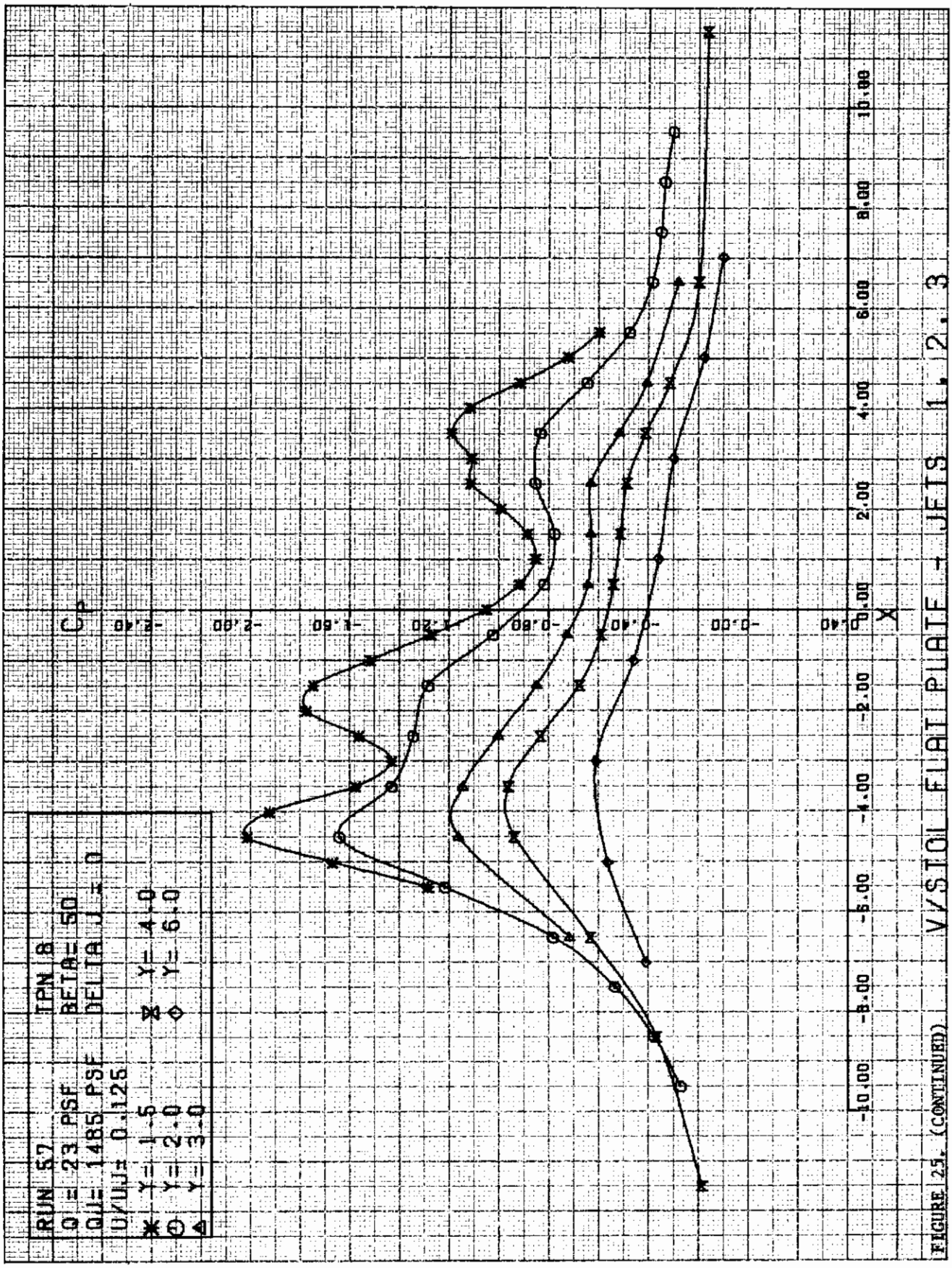

FIGURE 25. (CONTINUED) V/STOL FLAT PLATE + JETS 1, 2, 3

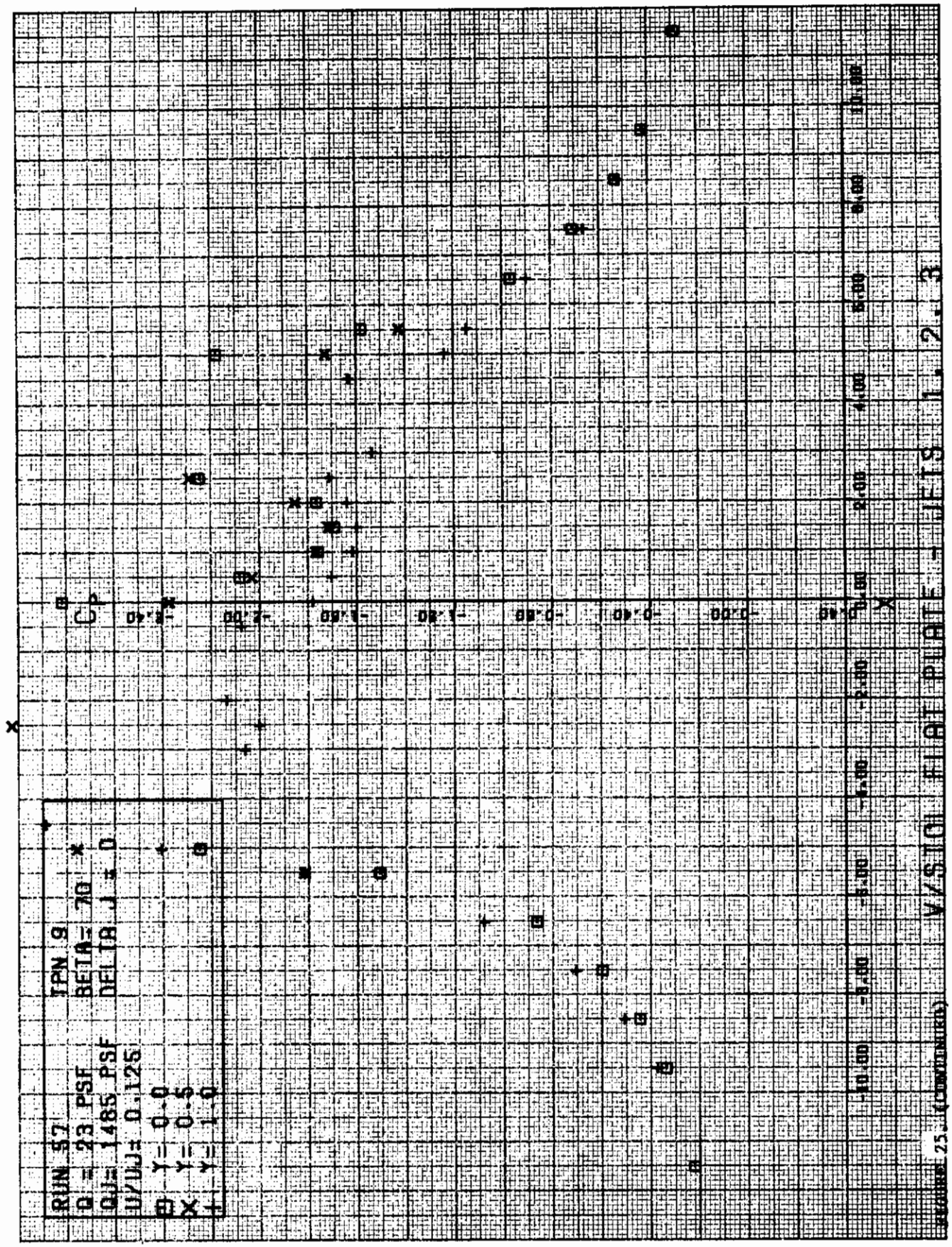

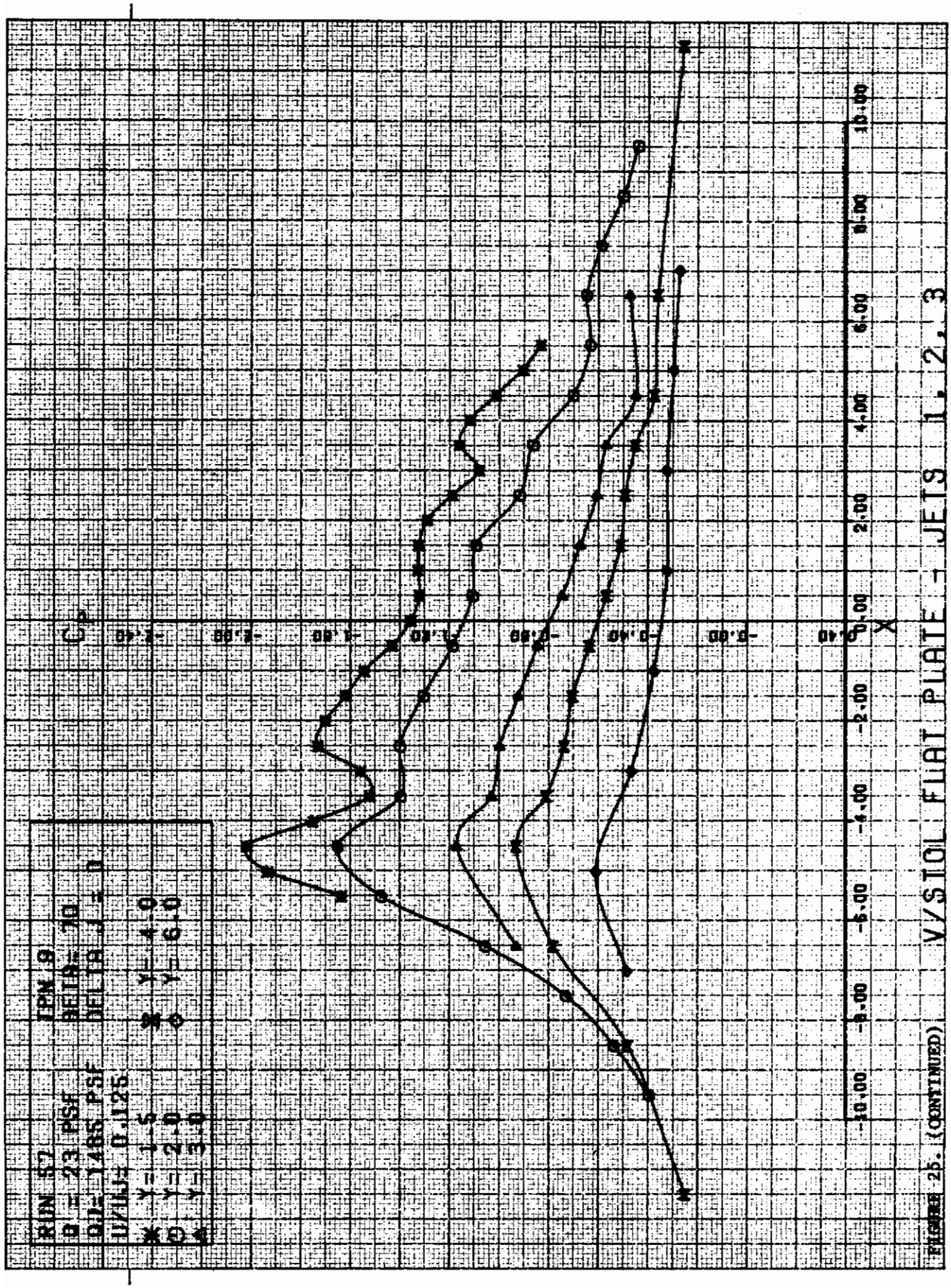

FIGURE 25. (CONTINUED)

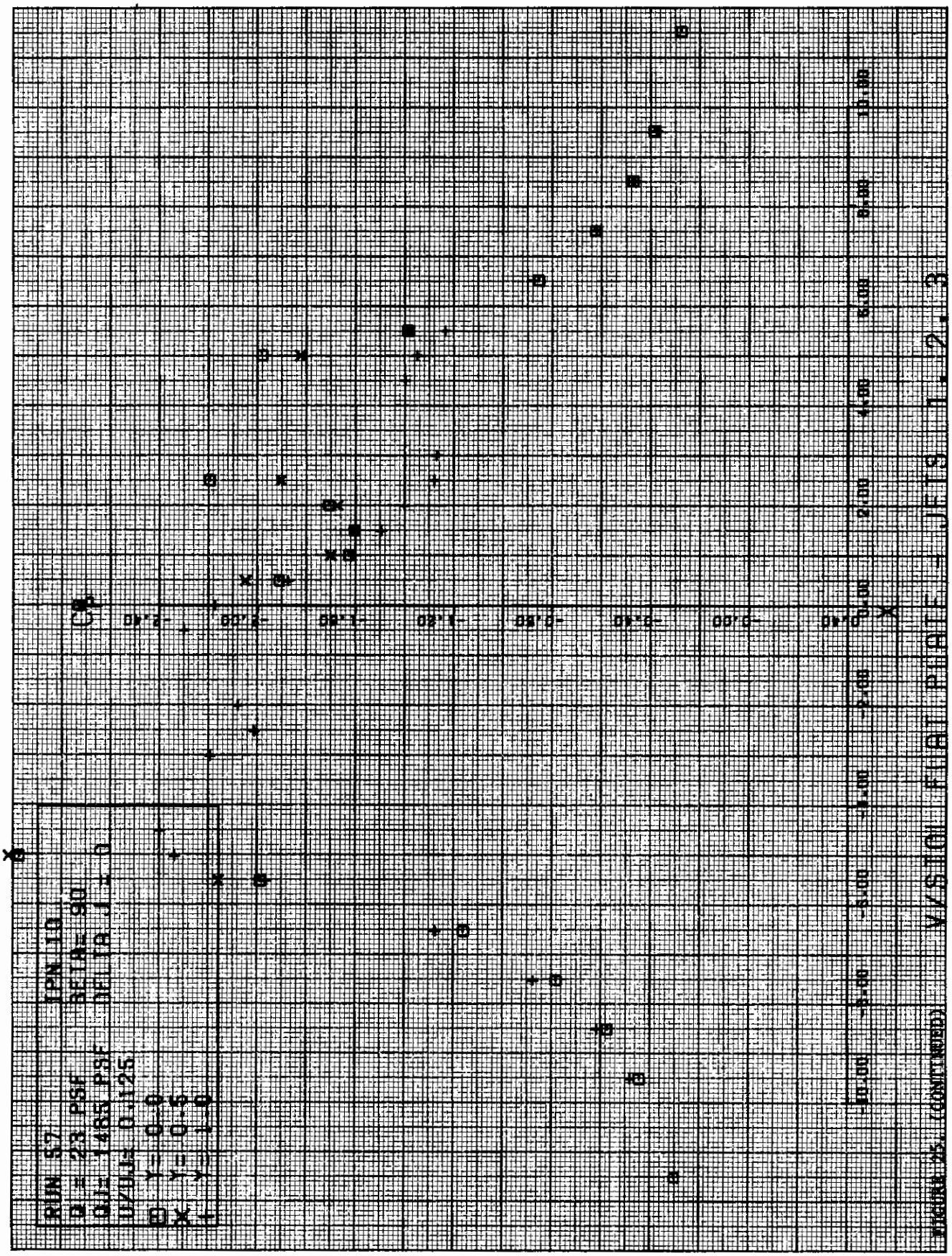

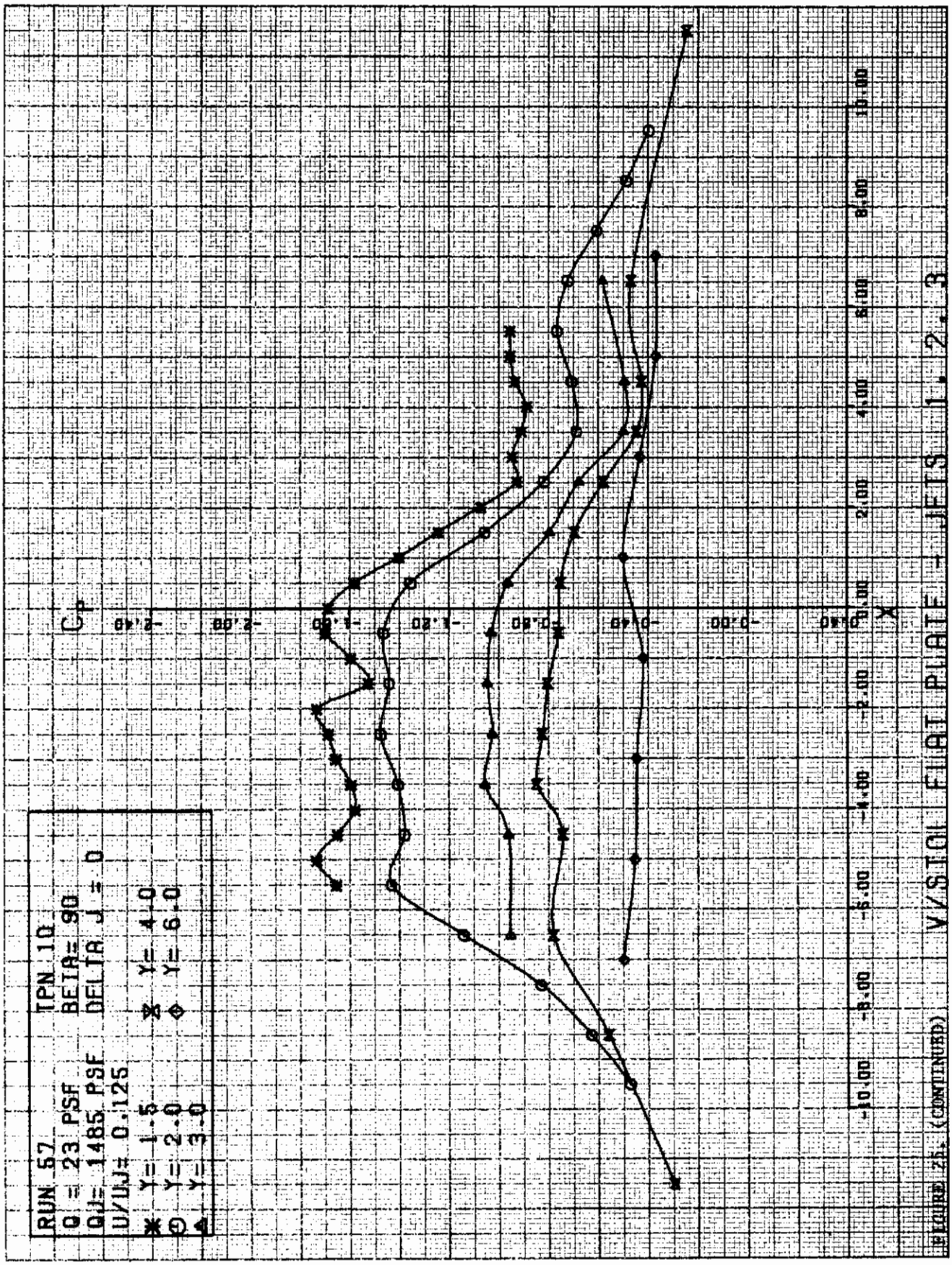

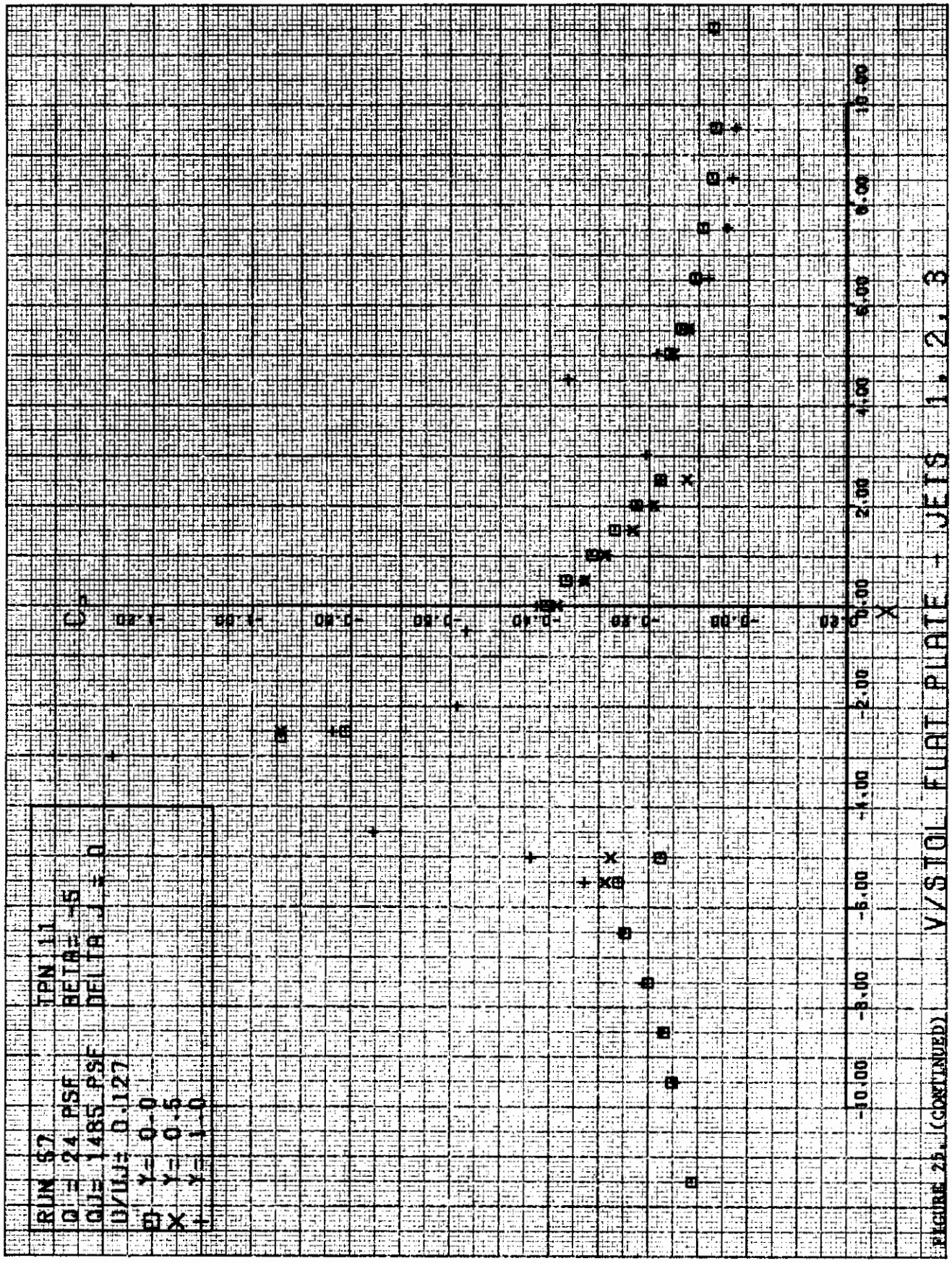

FIGURE 25. (CONTINUED)

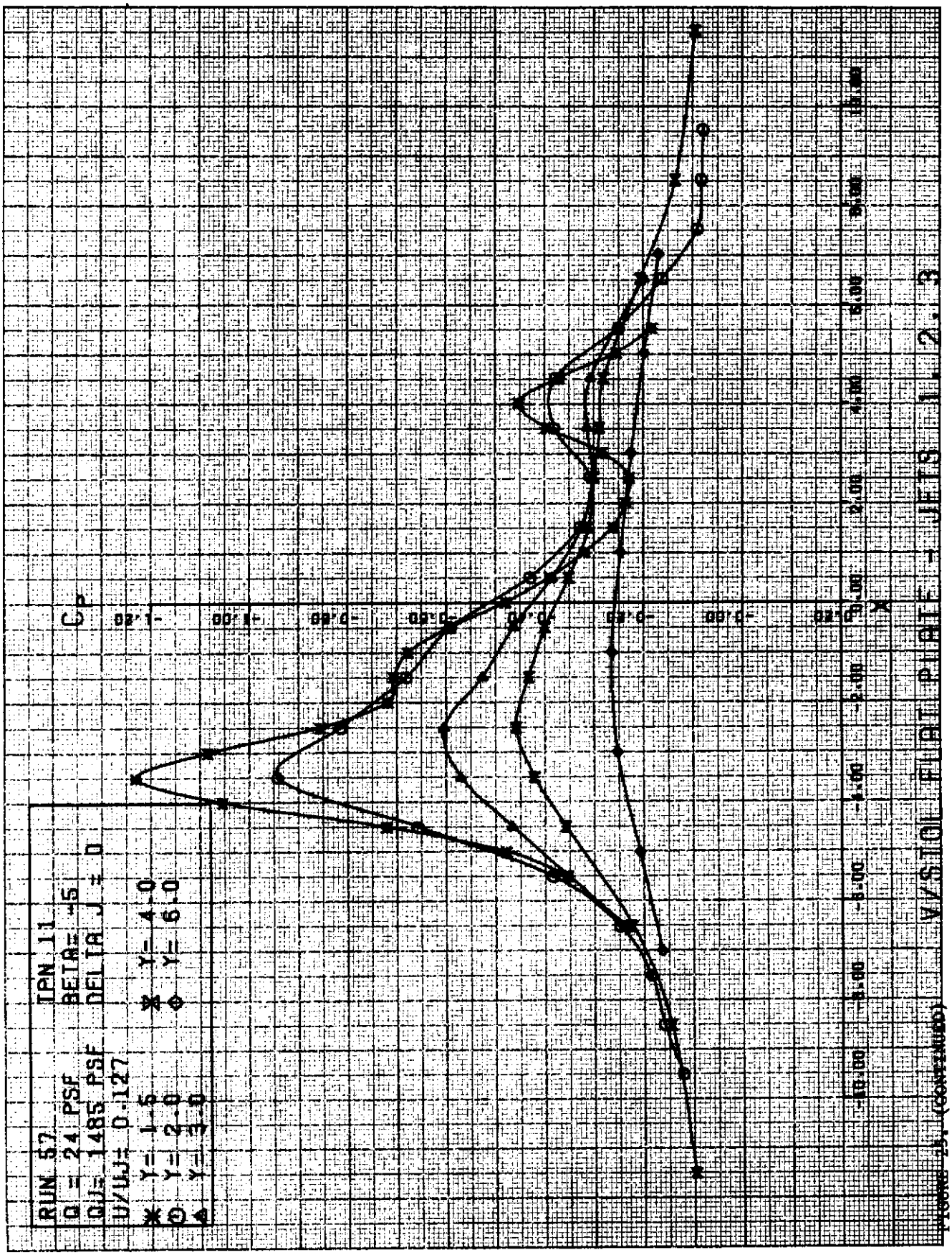

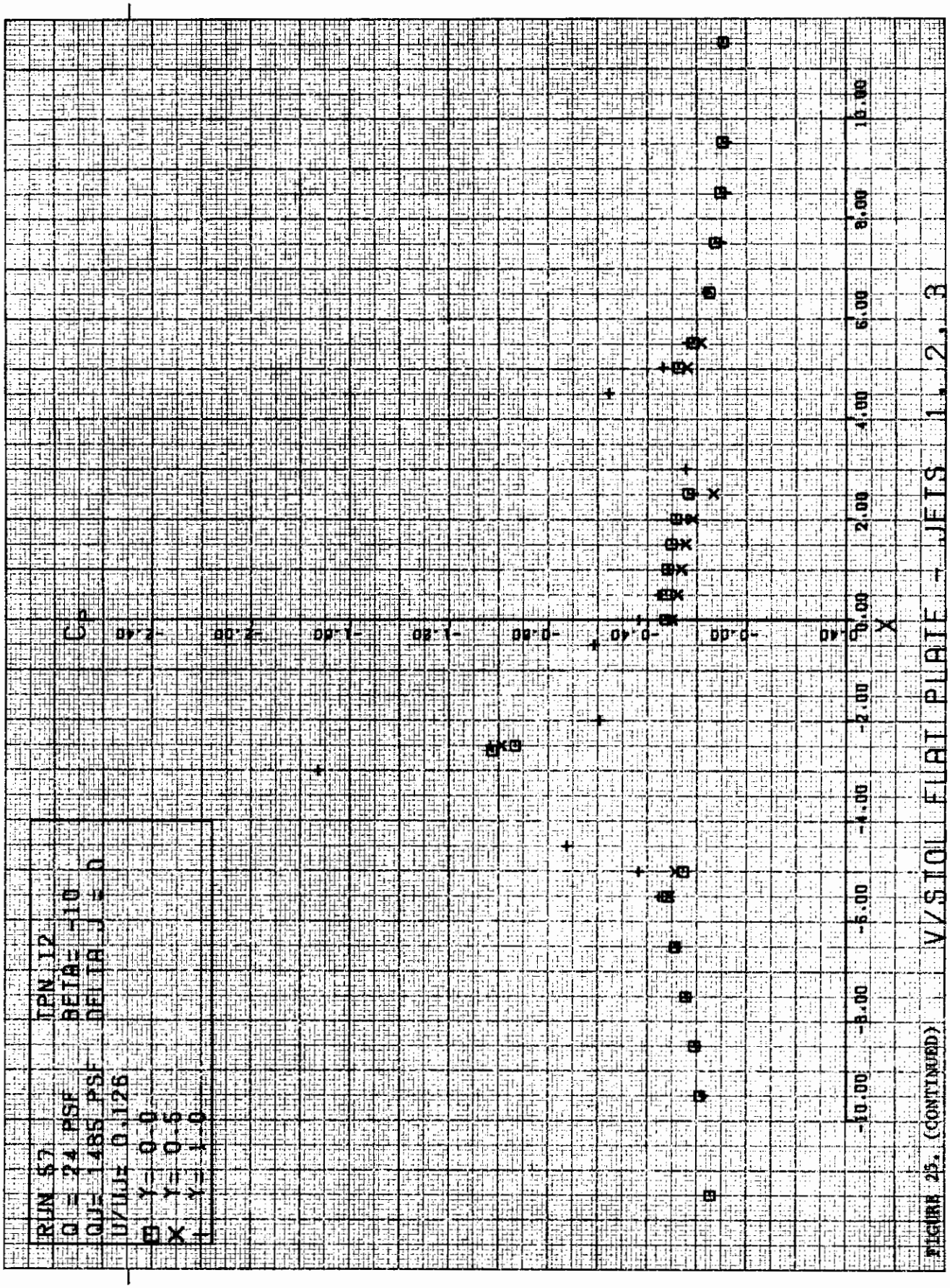

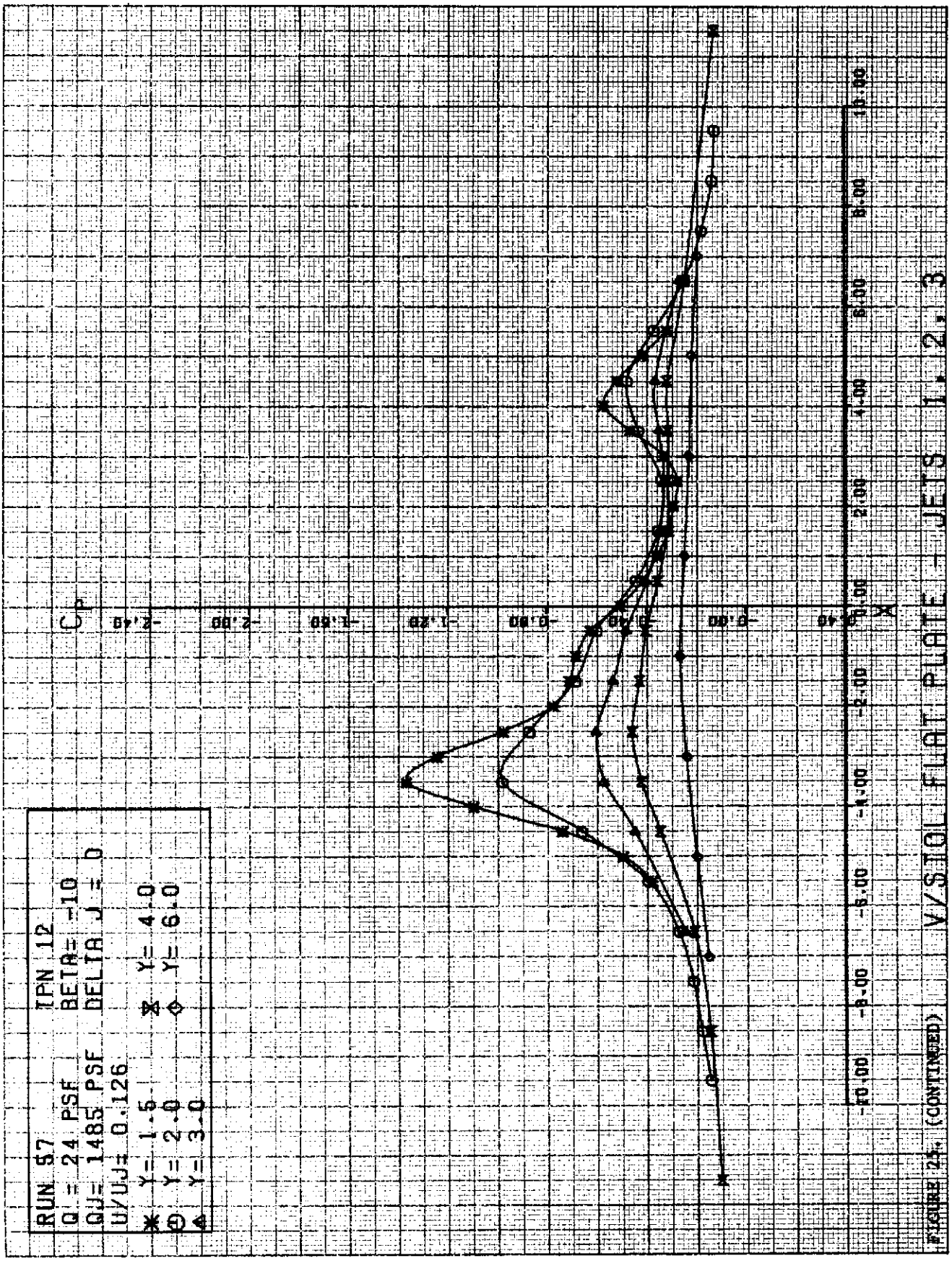

FIGURE 25. (CONTINUED)

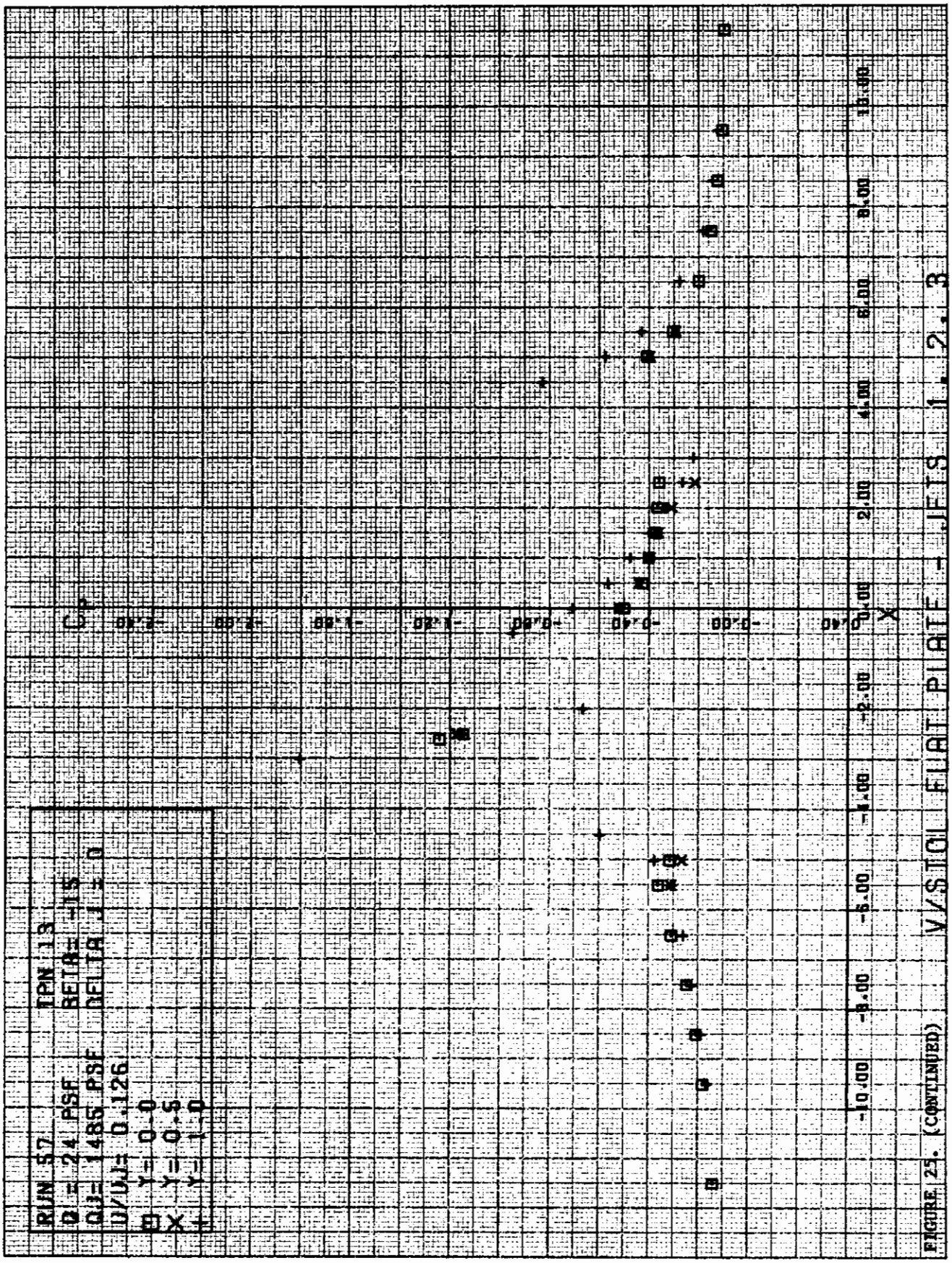

FIGURE 25. (CONTINUED)

FIGURE 25. (CONTINUED) V/STOL FLAT PLATE - JETS 1, 2, 3

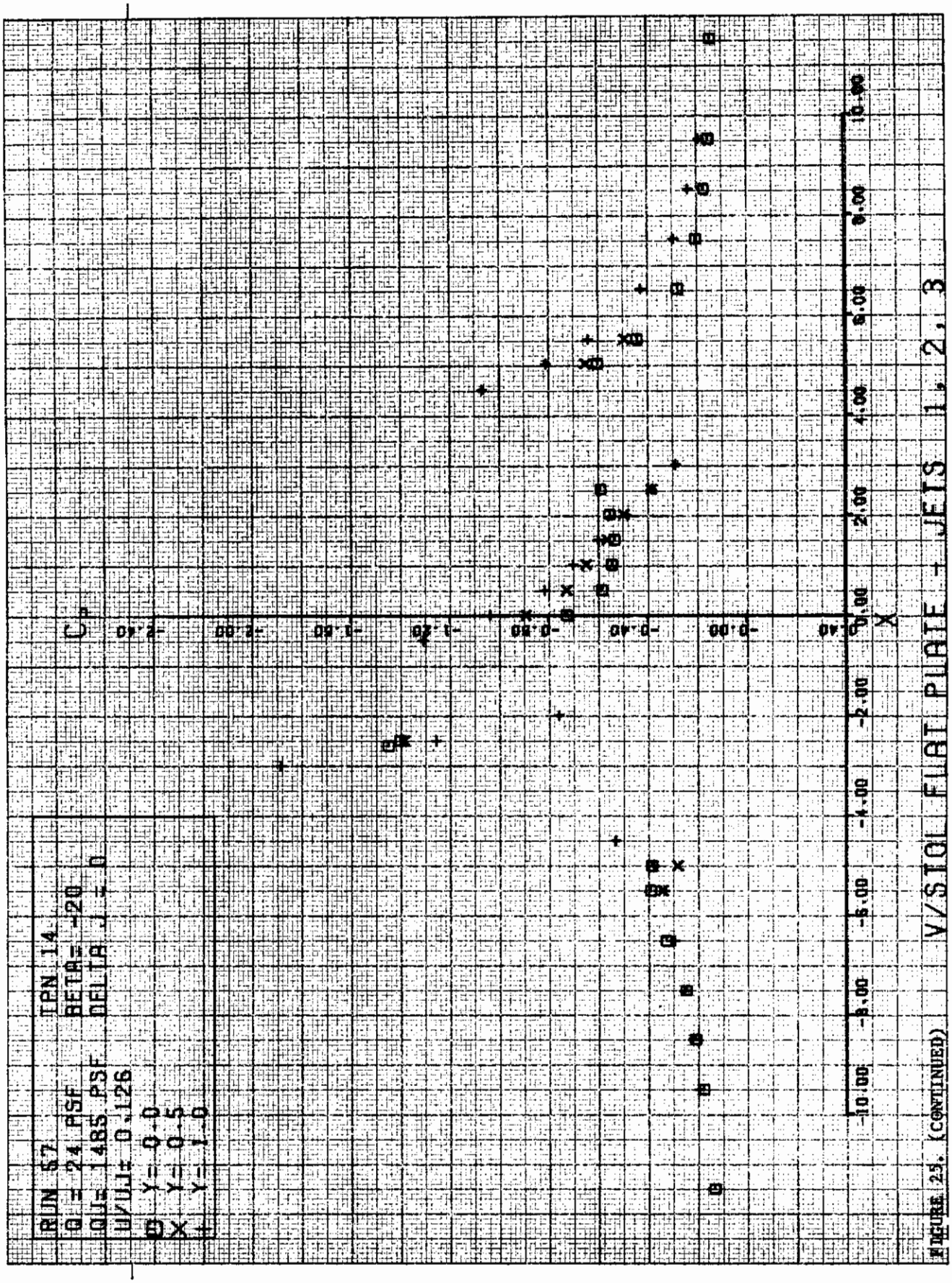

FIGURE 25. (CONTINUED)

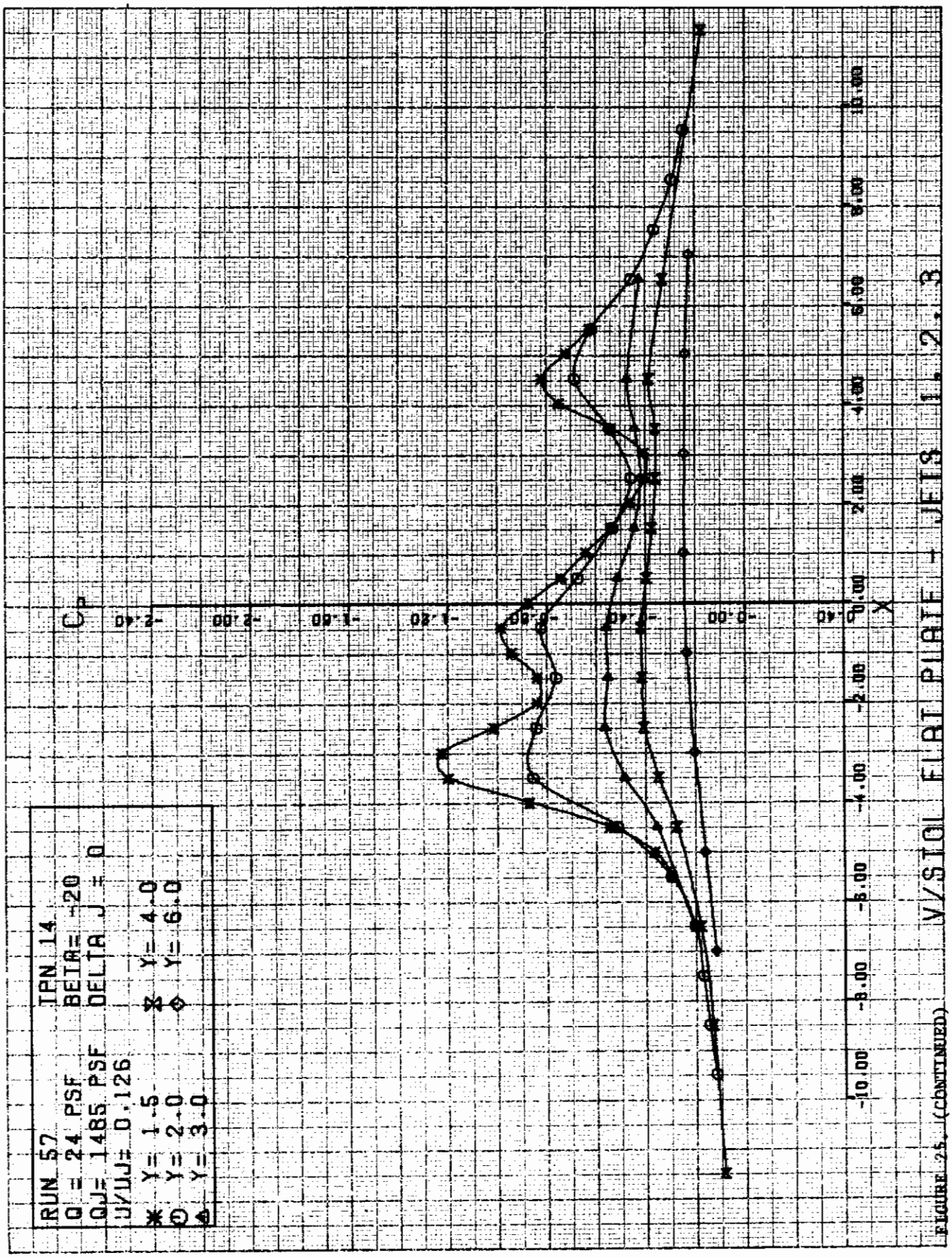

FIGURE 25. (CONTINUED)

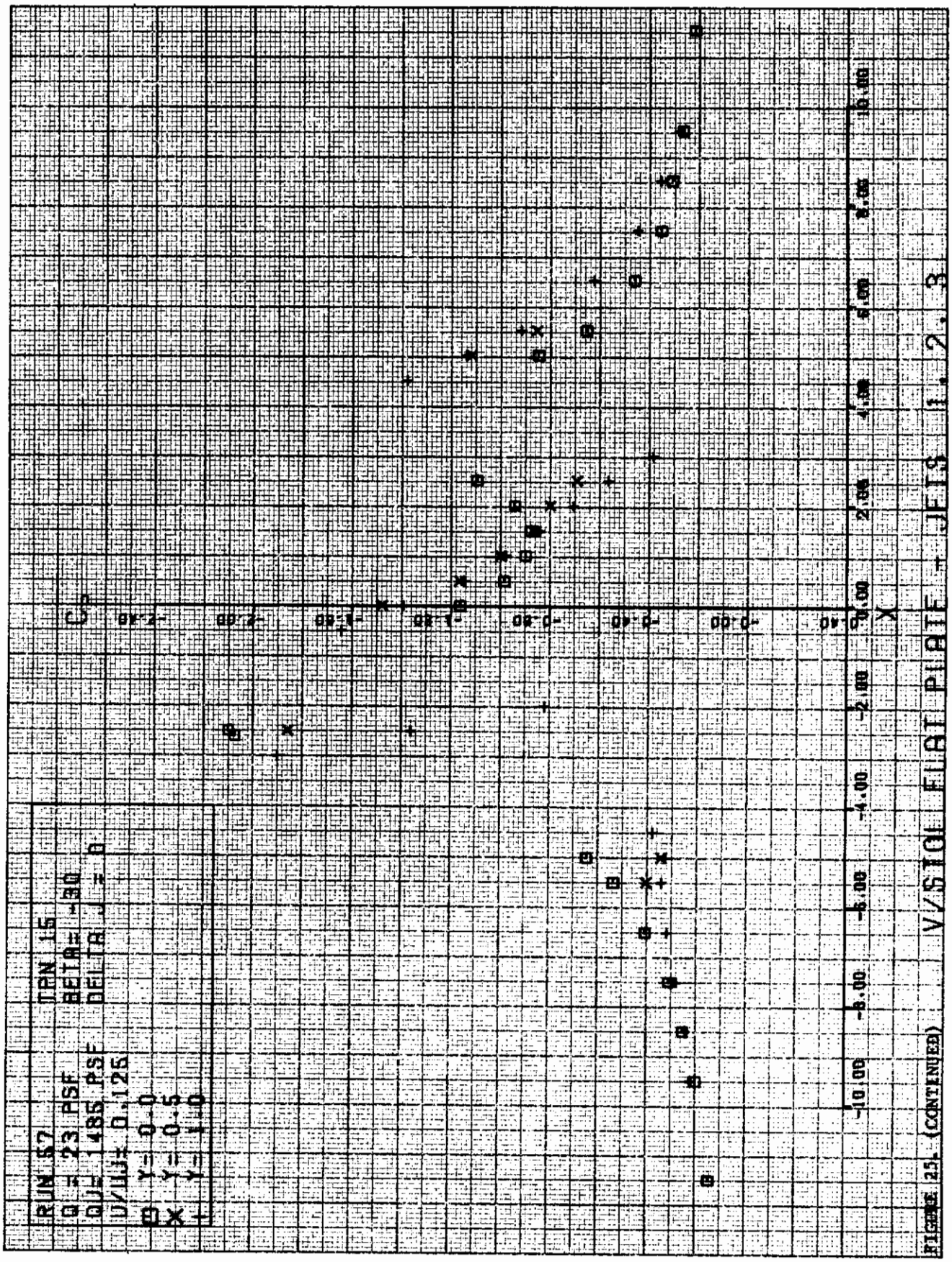

FIGURE 25. (CONTINUED)

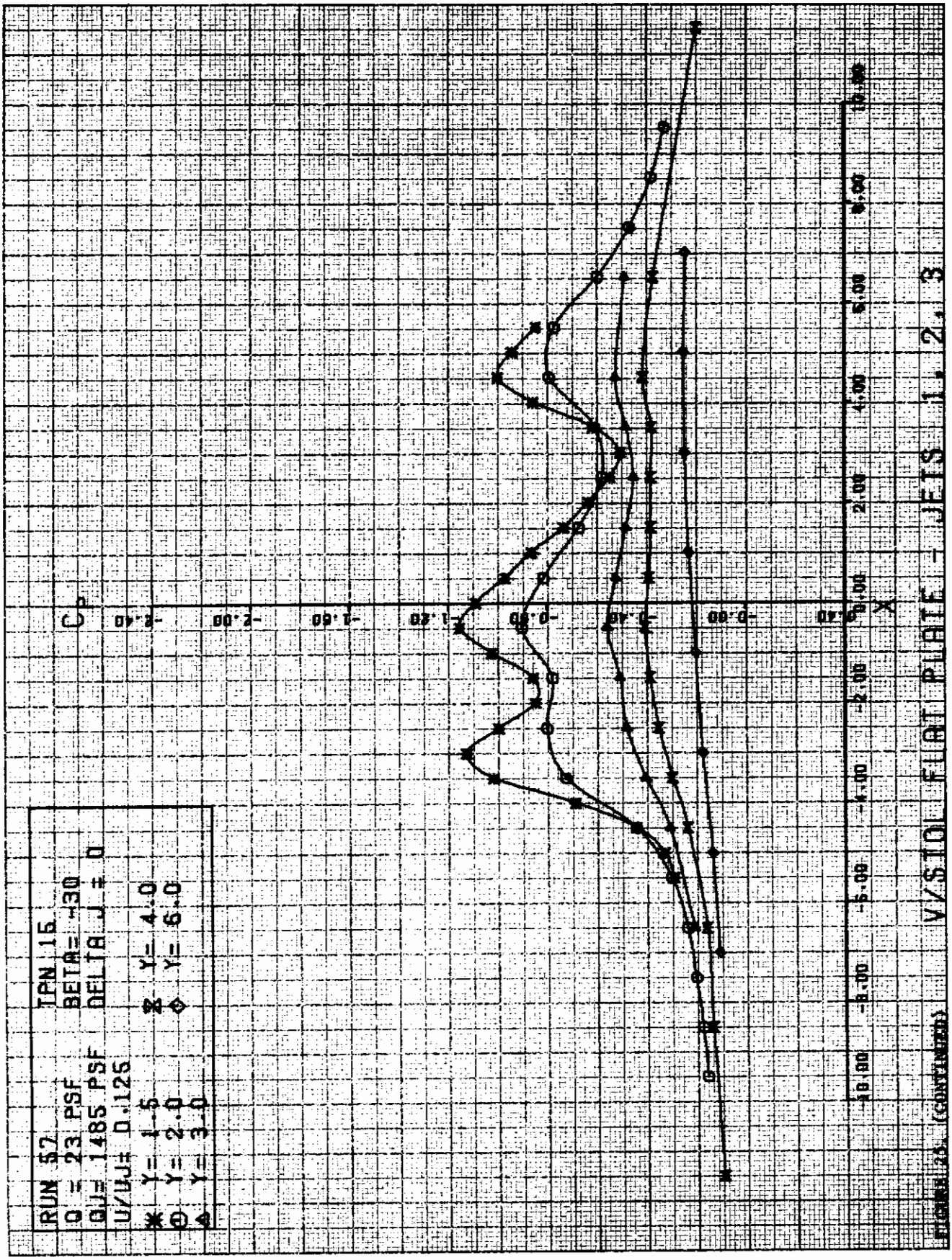

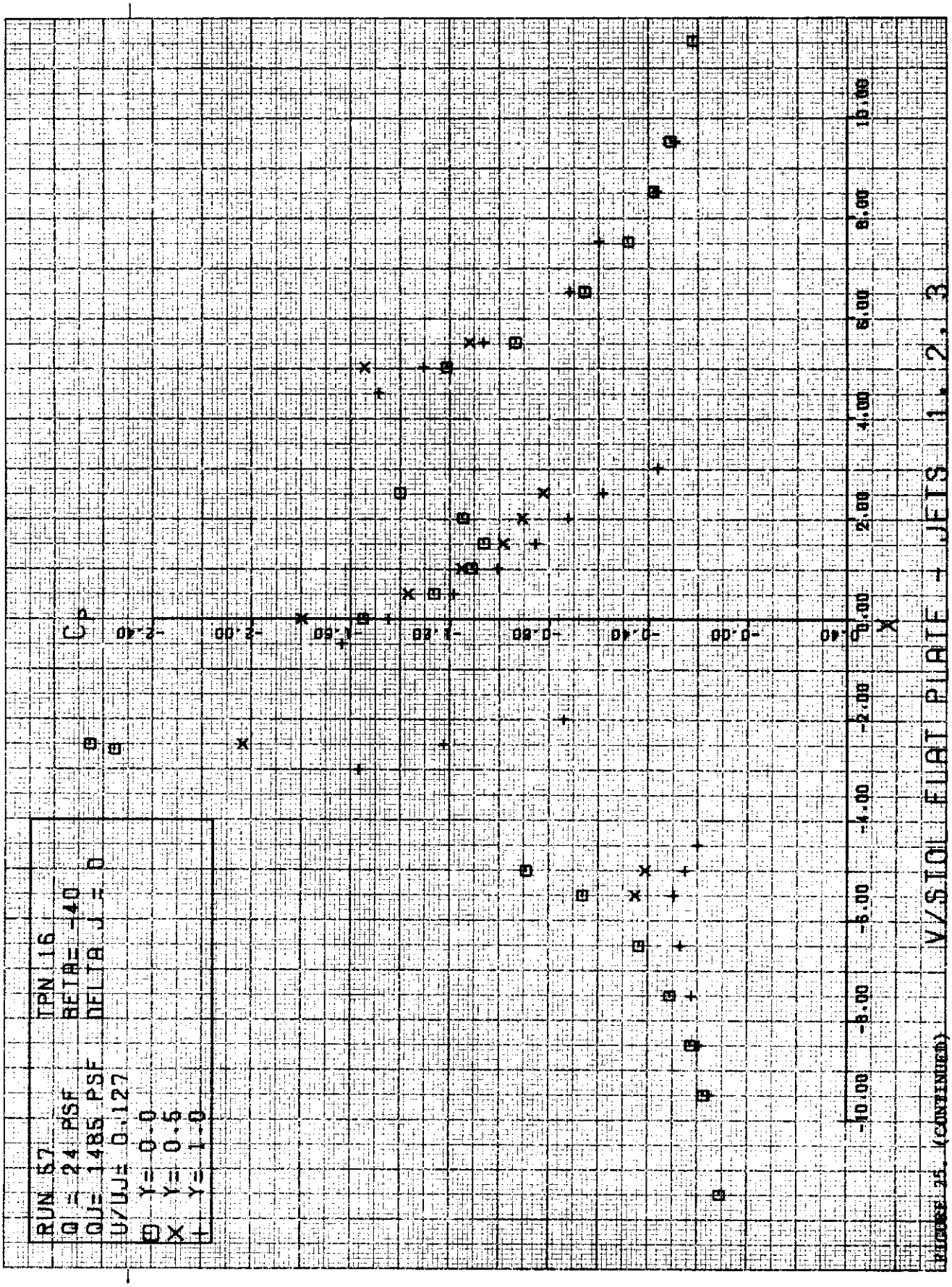

FIGURE 25. (CONTINUED)

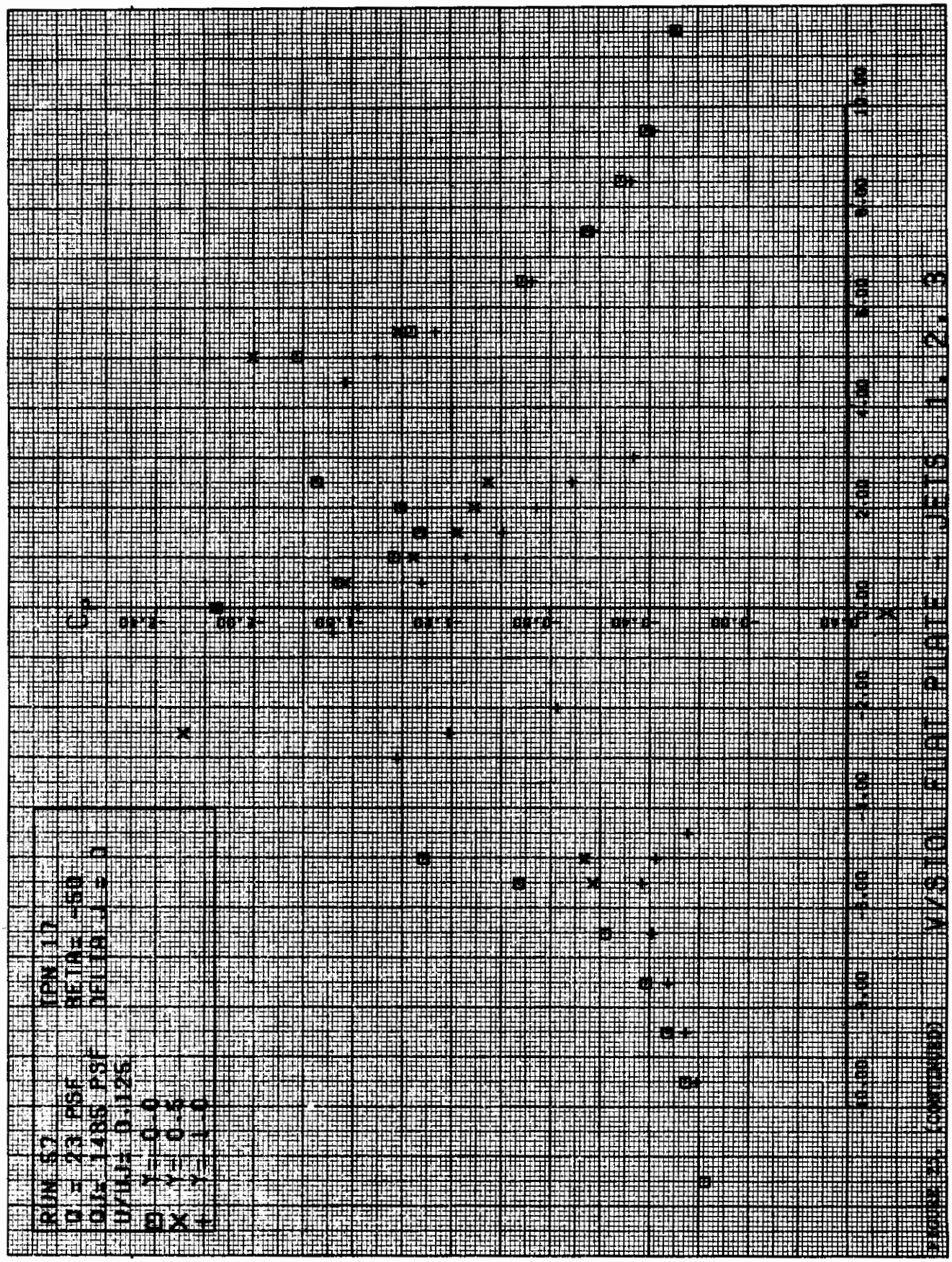

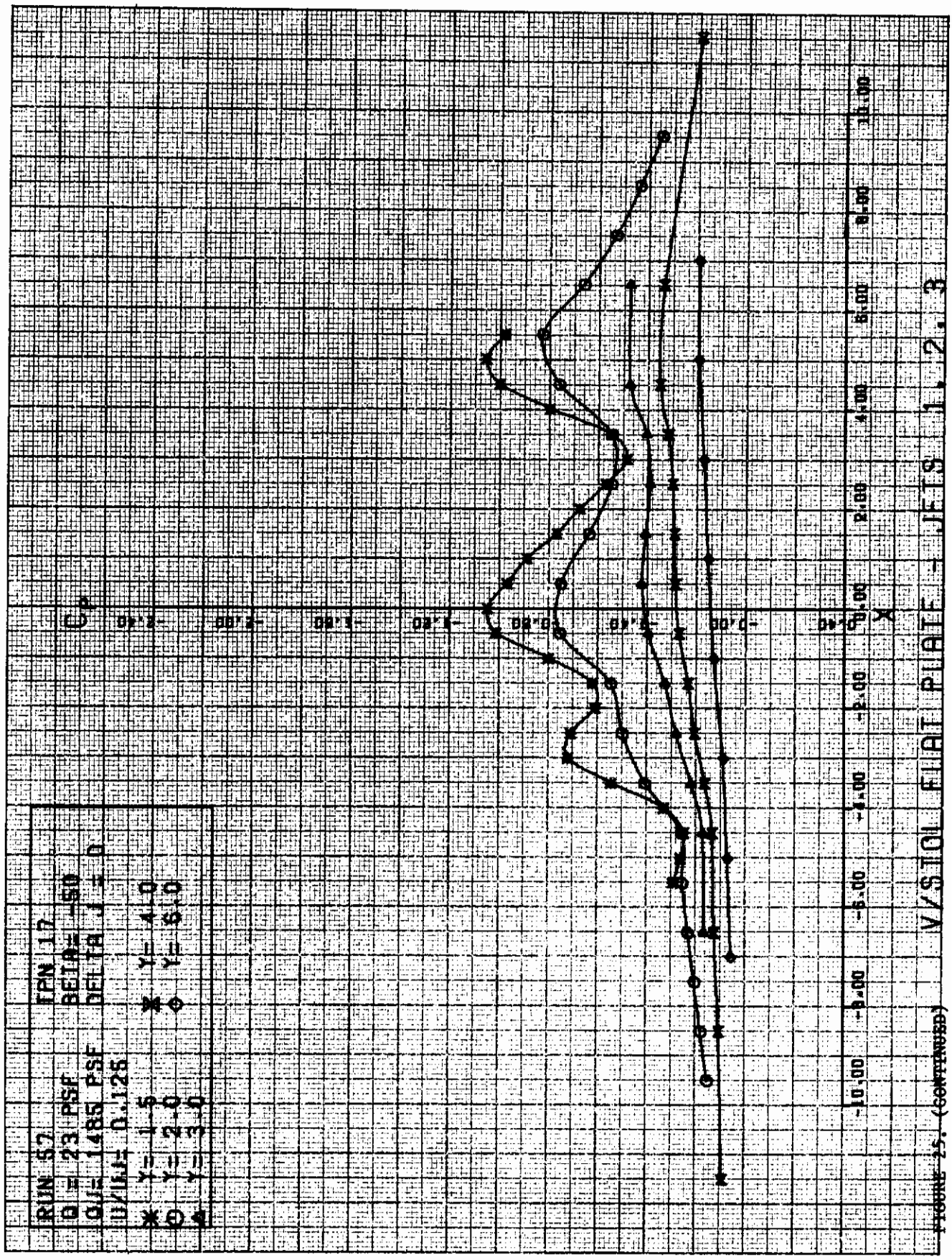

FIGURE 25. (CONTINUED)

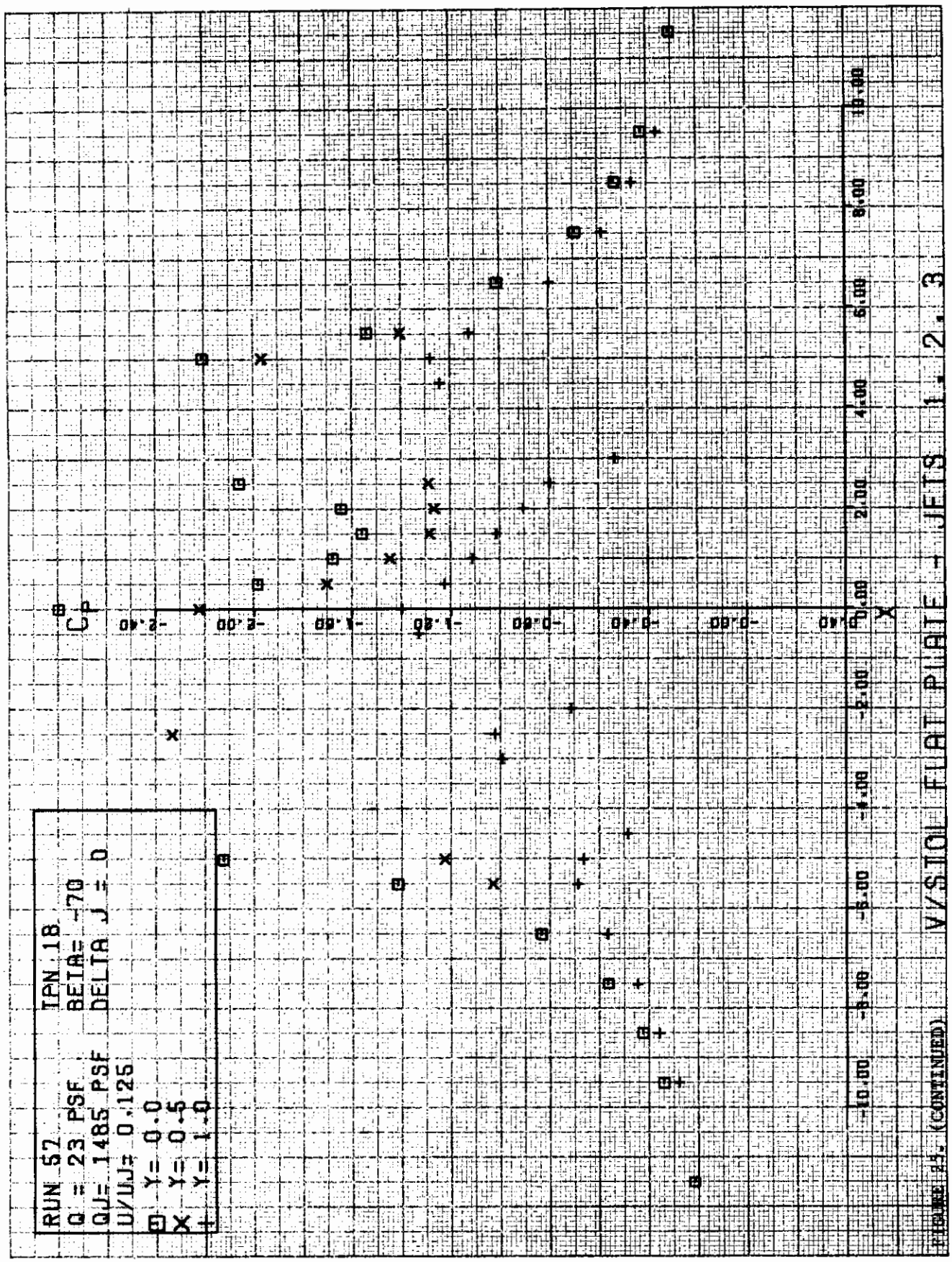

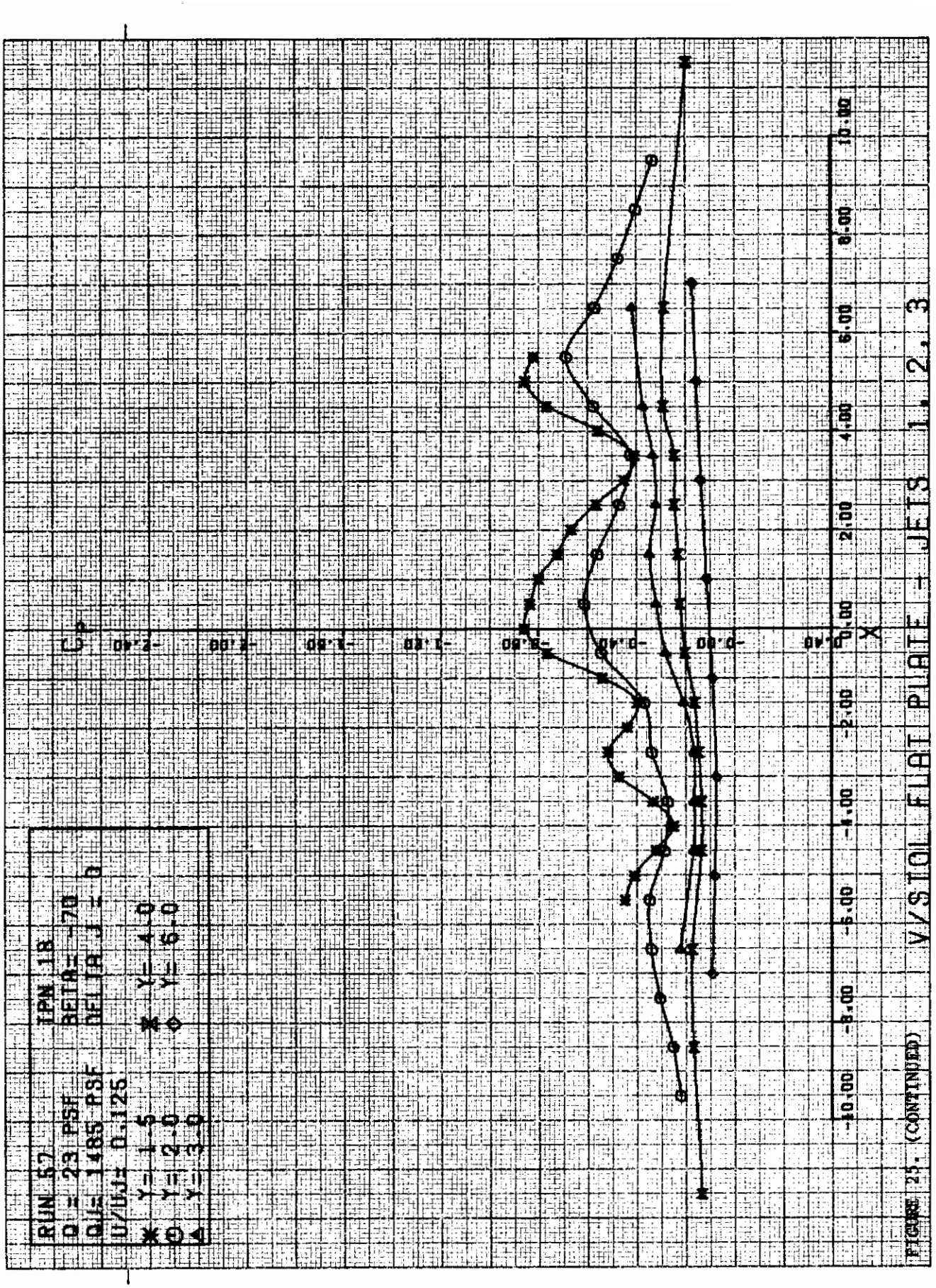

FIGURE 25. (CONTINUED)

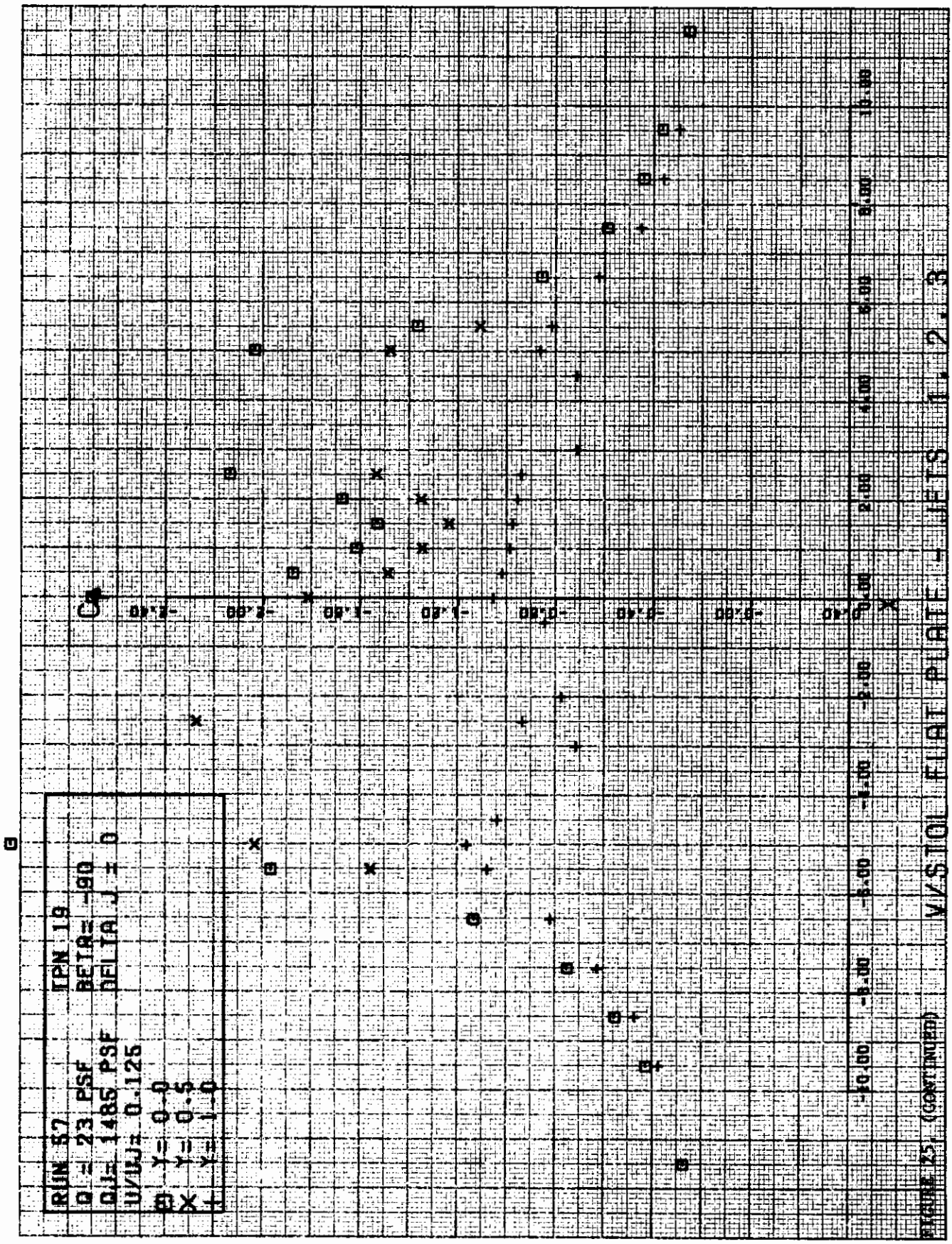

FIGURE 25. (CONTINUED)

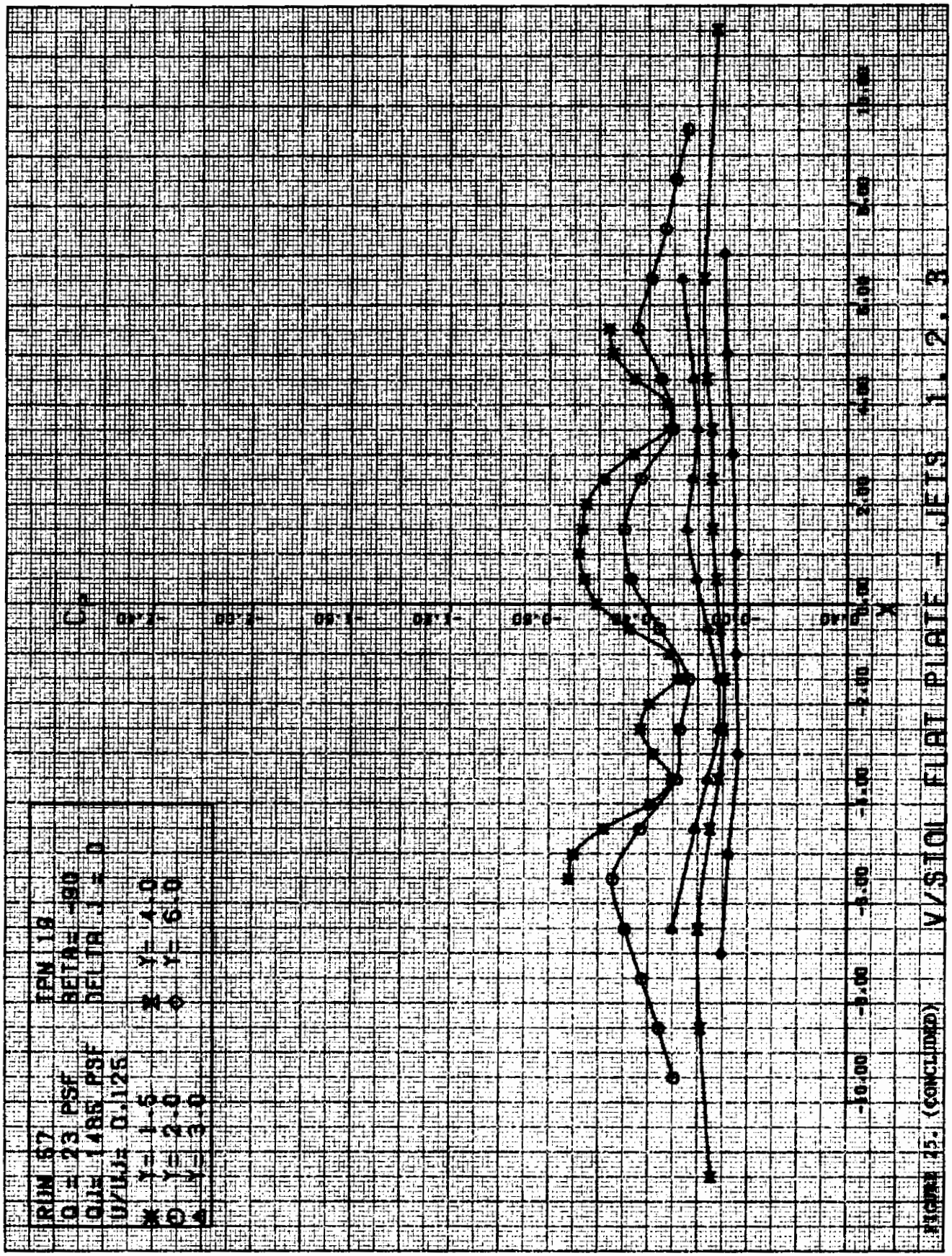

FIGURE 15. (CONCLUDED) V/STOL FLAT PLATE - JETS 1, 2, 3

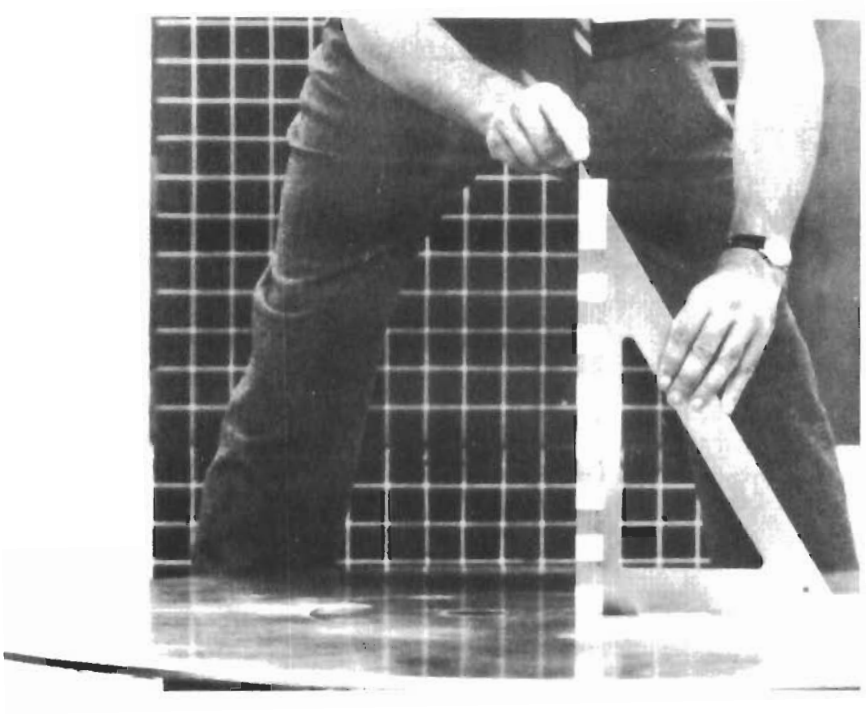

FIGURE 26(a). VERTICAL CALIBRATION FOR FLOW VISUALIZATION

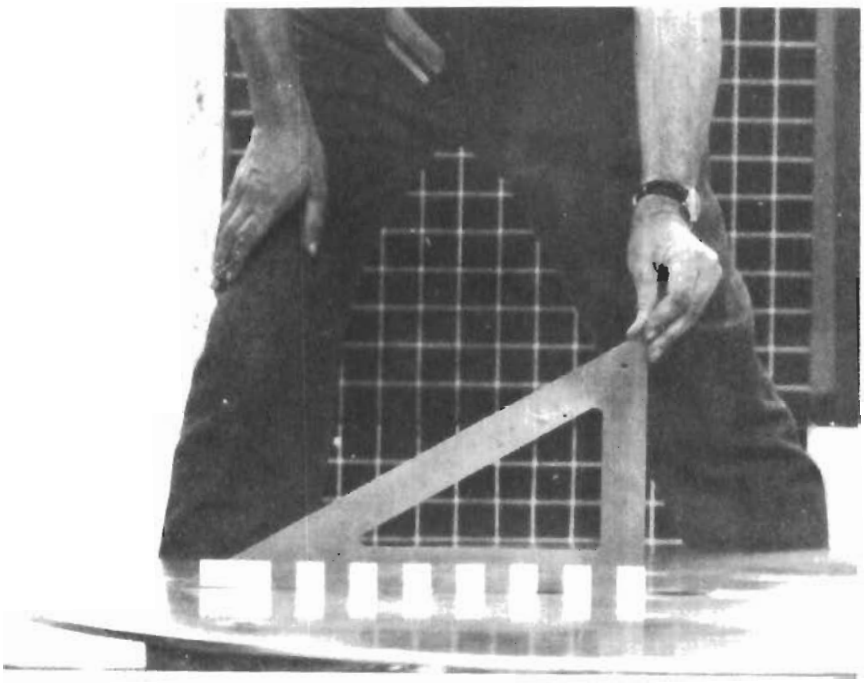

FIGURE 26(b). HORIZONTAL CALIBRATION FOR FLOW VISUALIZATION

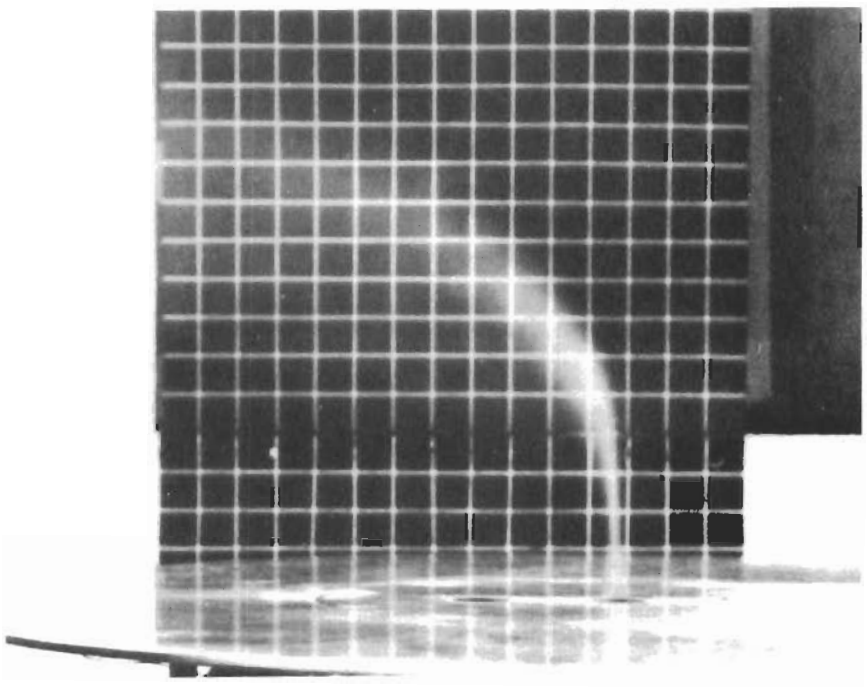

FIGURE 27(a). JET PATH FOR JET 2 AT $U/U_j = .10$

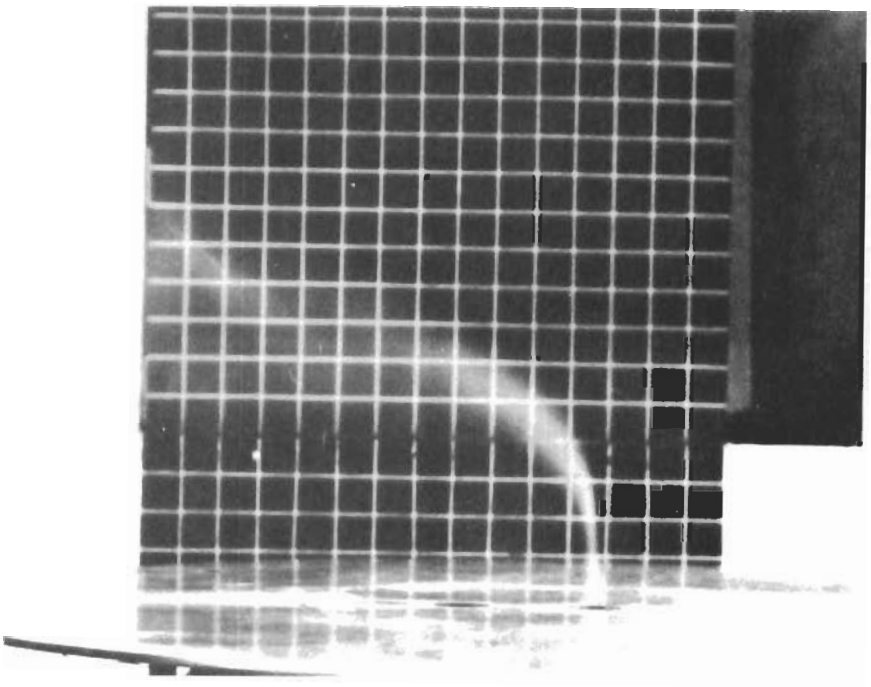

FIGURE 27(b). JET PATH FOR JET 2 AT $U/U_j = .15$

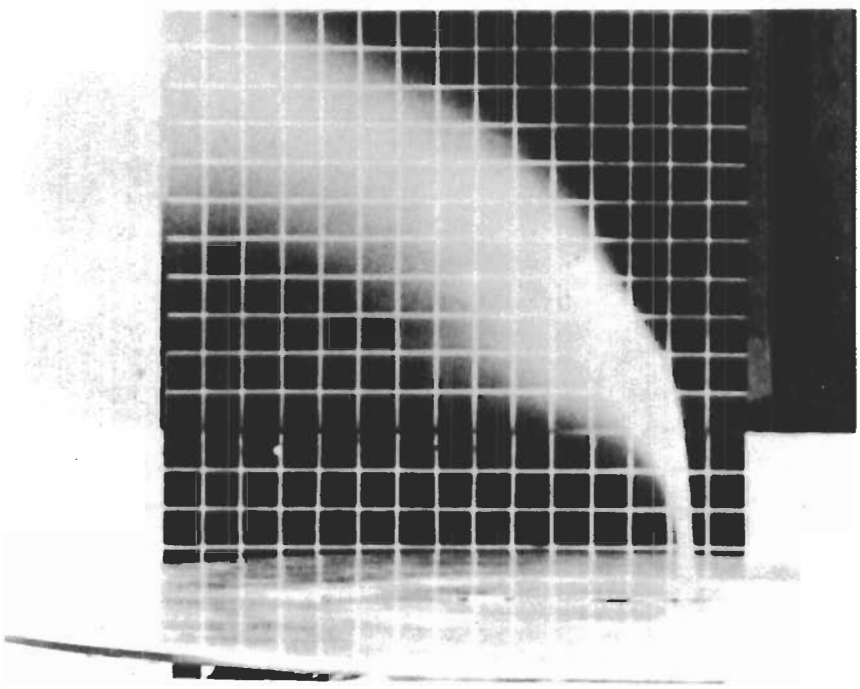

FIGURE 28(a). JET PATH FOR JETS 1, 2 AT $U/U_j = .125$
(WATER INJECTED INTO JET 1)

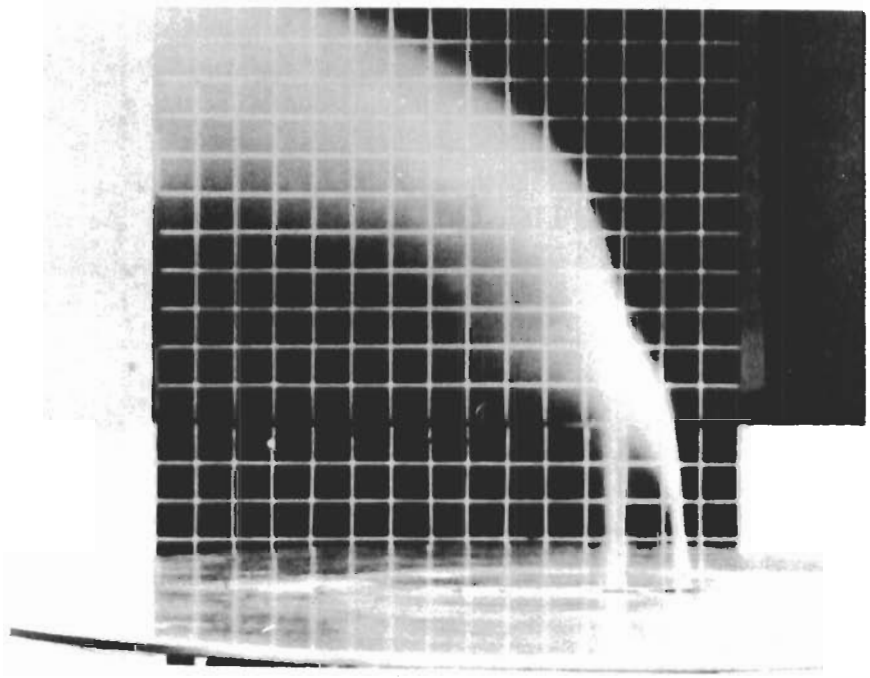

FIGURE 28(b). JET PATH FOR JETS 1, 2 AT $U/U_j = .125$
(WATER INJECTED INTO BOTH JETS)

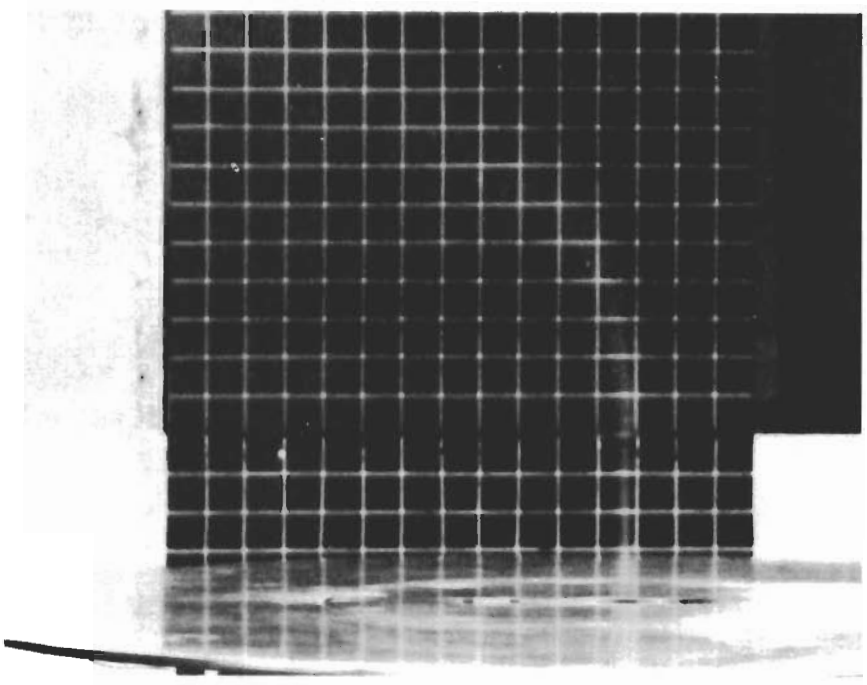

FIGURE 28(c). JET PATH FOR JETS 1, 2 AT $U/U_j = .125$
(WATER INJECTED INTO JET 2)

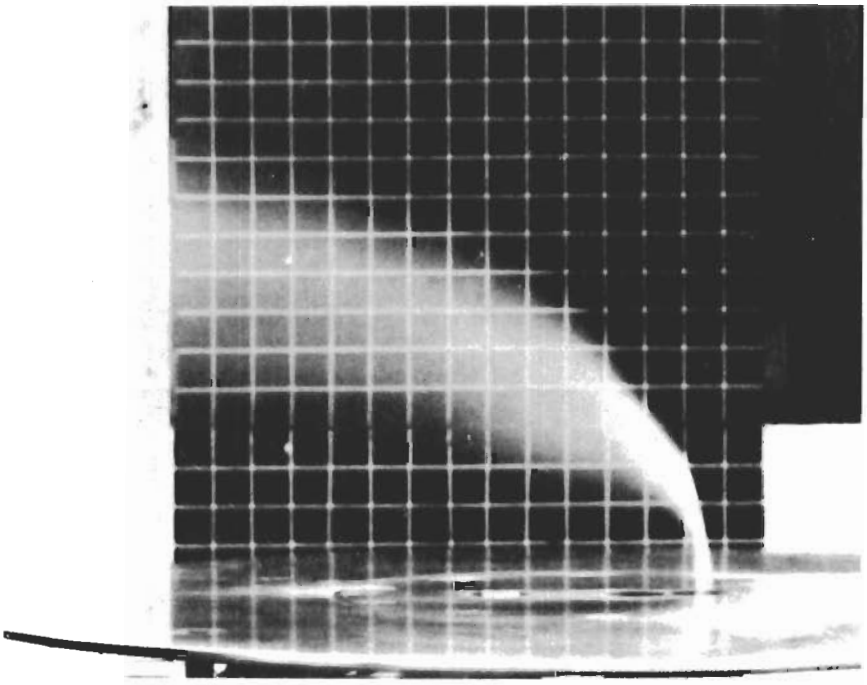

FIGURE 29(a). JET PATH FOR JETS 1, 2 AT $U/U_j = .20$
(WATER INJECTED INTO JET 1)

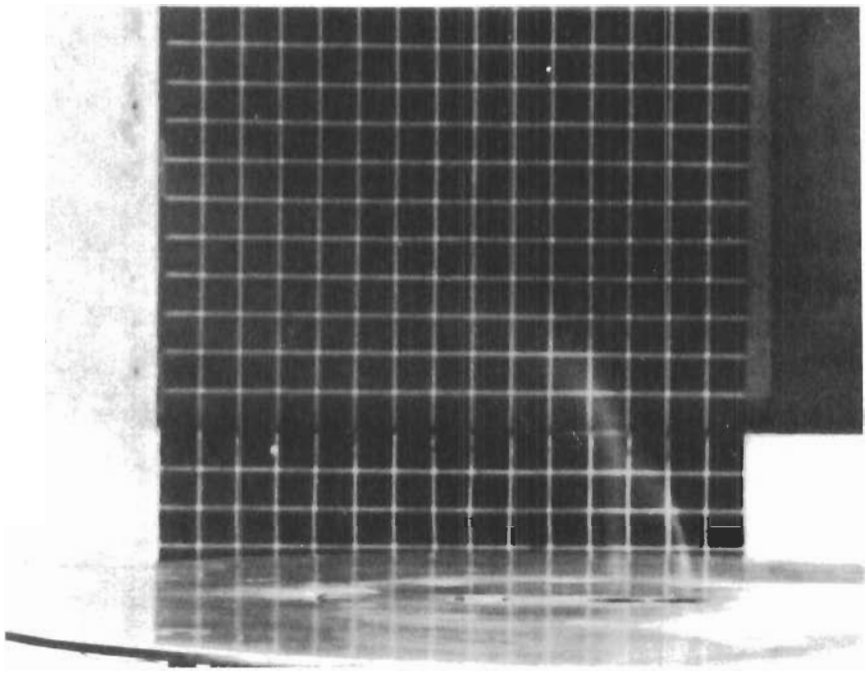

FIGURE 29(b). JET PATH FOR JETS 1, 2 AT $U/U_j = .20$
(WATER INJECTED INTO BOTH JETS)

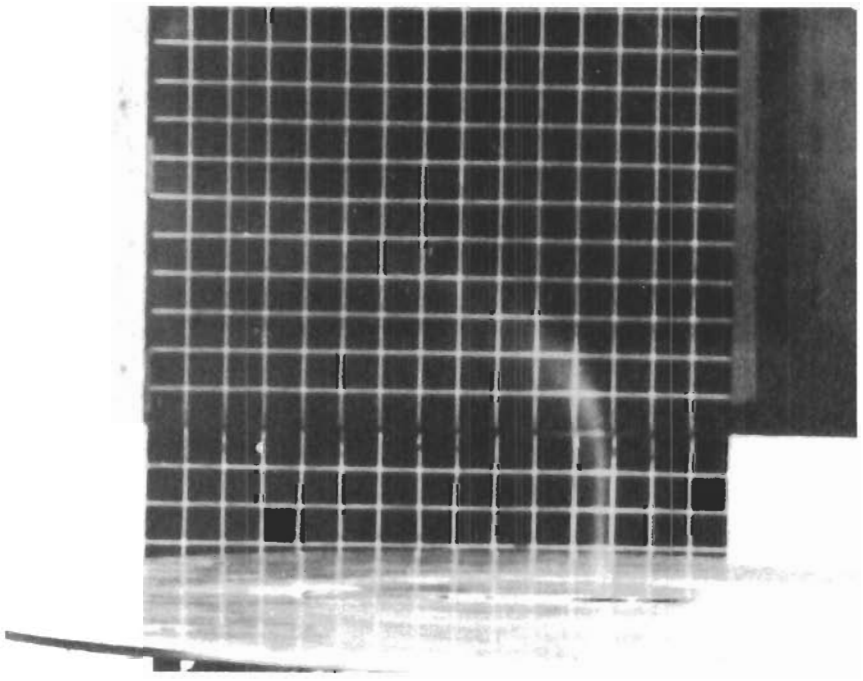

FIGURE 29(c). JET PATH FOR JETS 1, 2 AT $U/U_j = .20$
(WATER INJECTED INTO JET 2)

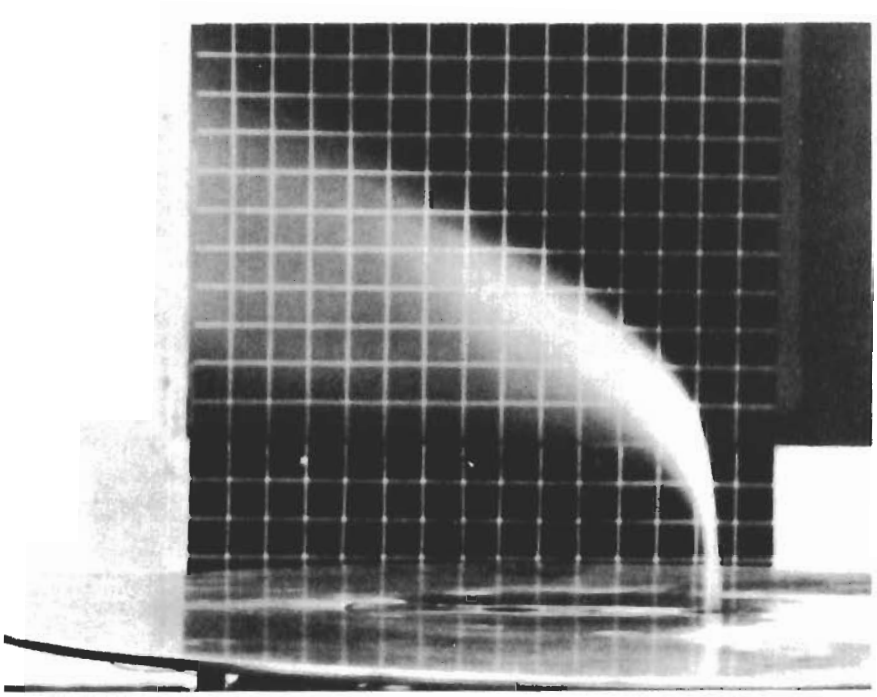

FIGURE 30(a). JET PATH FOR JETS 1, 3 AT $U/U_j = .125$
(WATER INJECTED INTO JET 1)

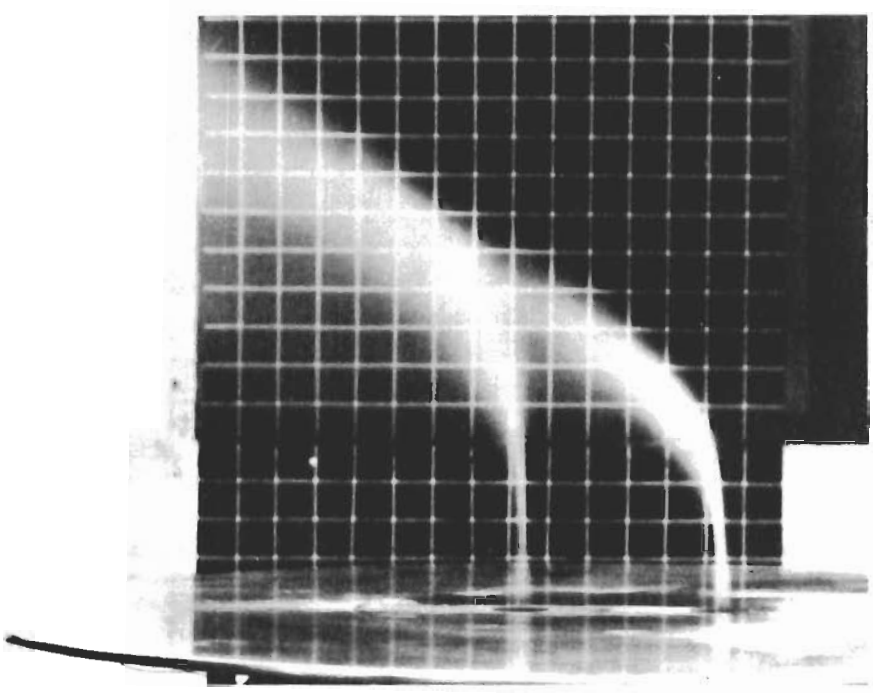

FIGURE 30 (b). JET PATH FOR JETS 1, 3 AT $U/U_j = .125$
(WATER INJECTED INTO BOTH JETS)

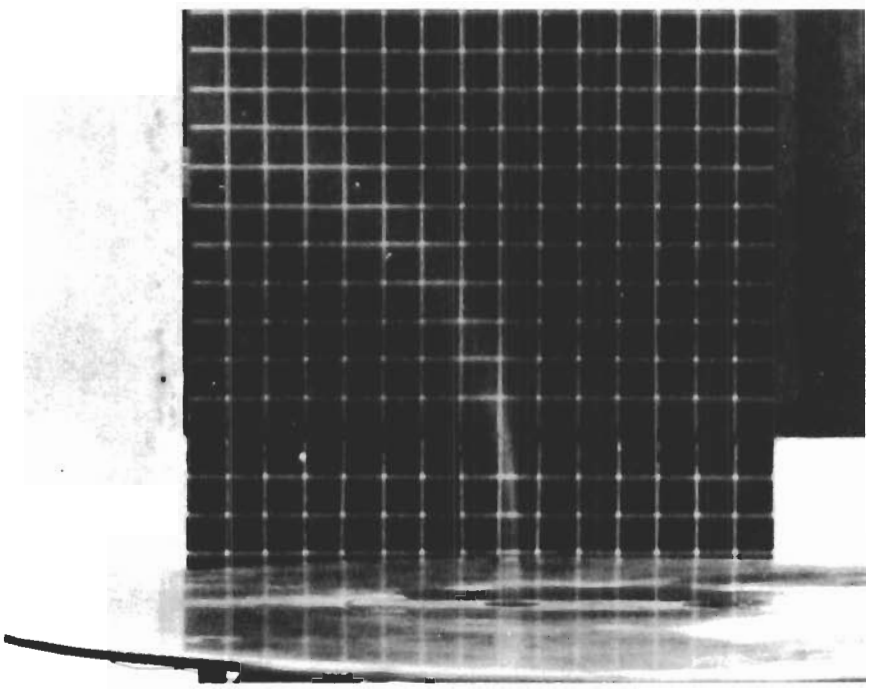

FIGURE 30(c). JET PATH FOR JETS 1, 3 AT $U/U_j = .125$
(WATER INJECTED INTO JET 3)

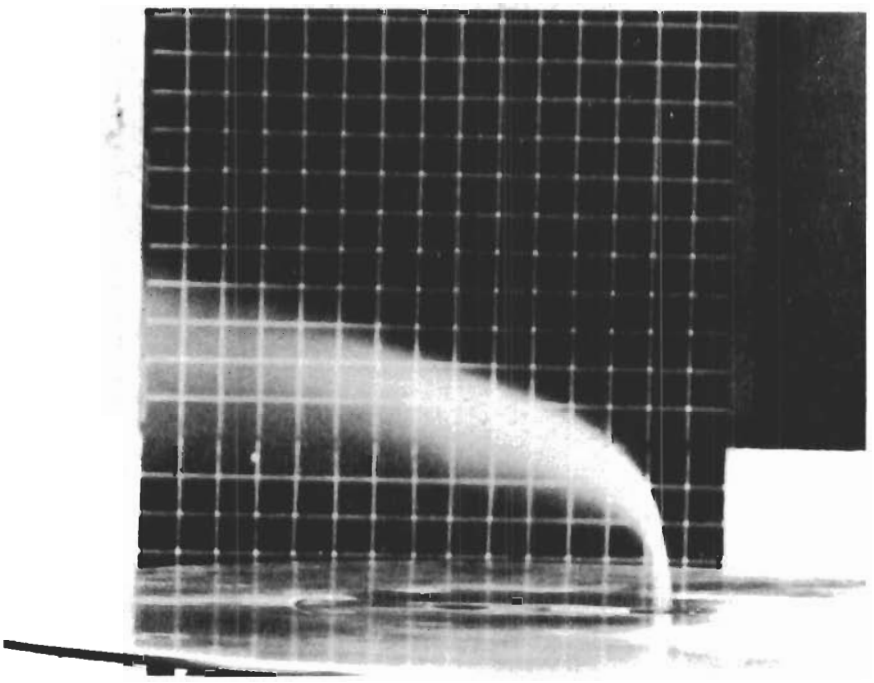

FIGURE 31(a). JET PATH FOR JETS 1, 3 AT $U/U_j = .20$
(WATER INJECTED INTO JET 1)

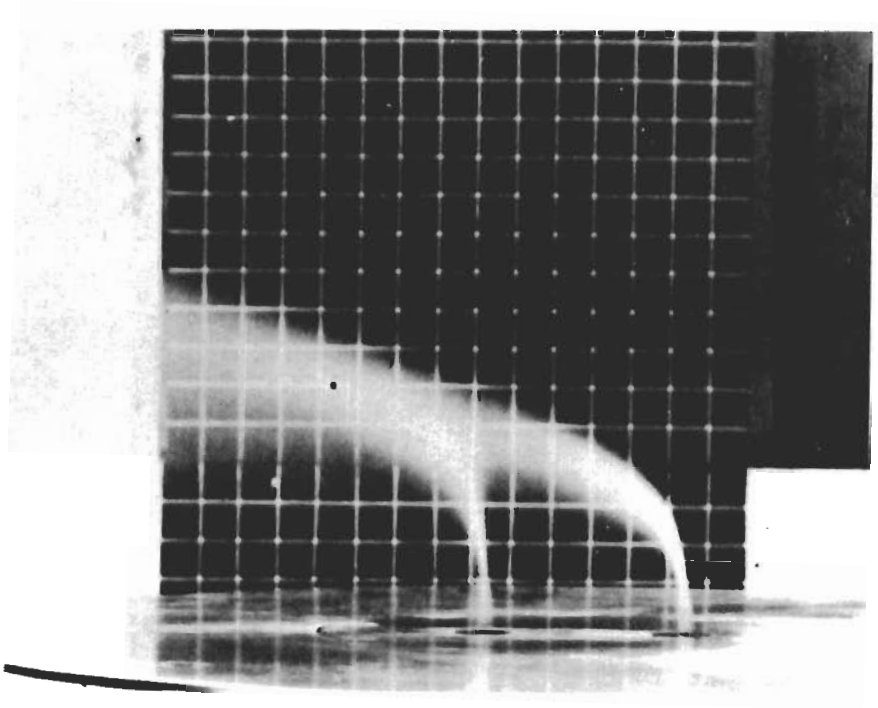

FIGURE 31(b). JET PATH FOR JETS 1, 3 AT $U/U_j = .20$
(WATER INJECTED INTO BOTH JETS)

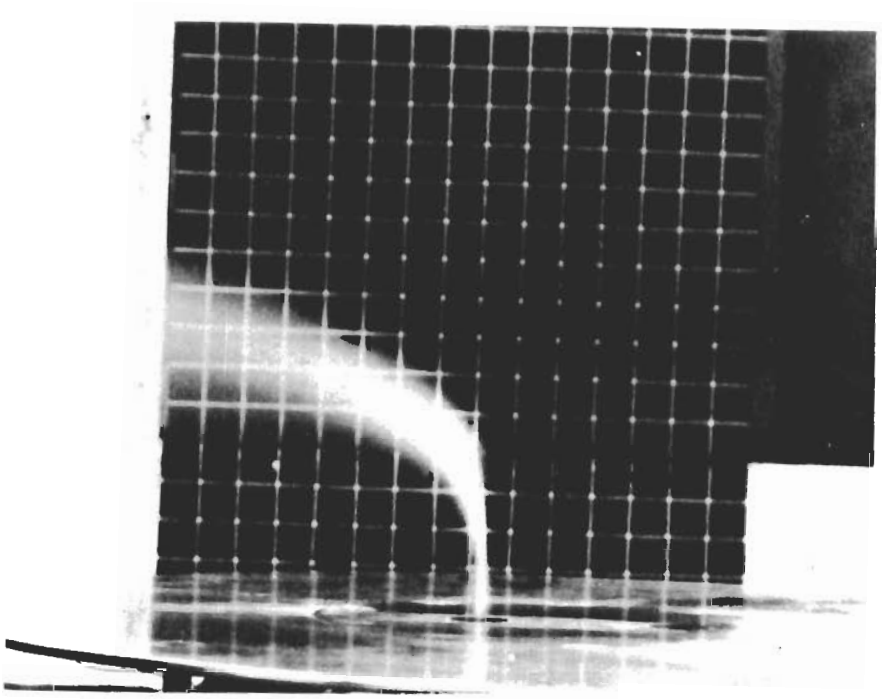

FIGURE 31(c). JET PATH FOR JETS 1, 3 AT $U/U_j = .20$
(WATER INJECTED INTO JET 3).

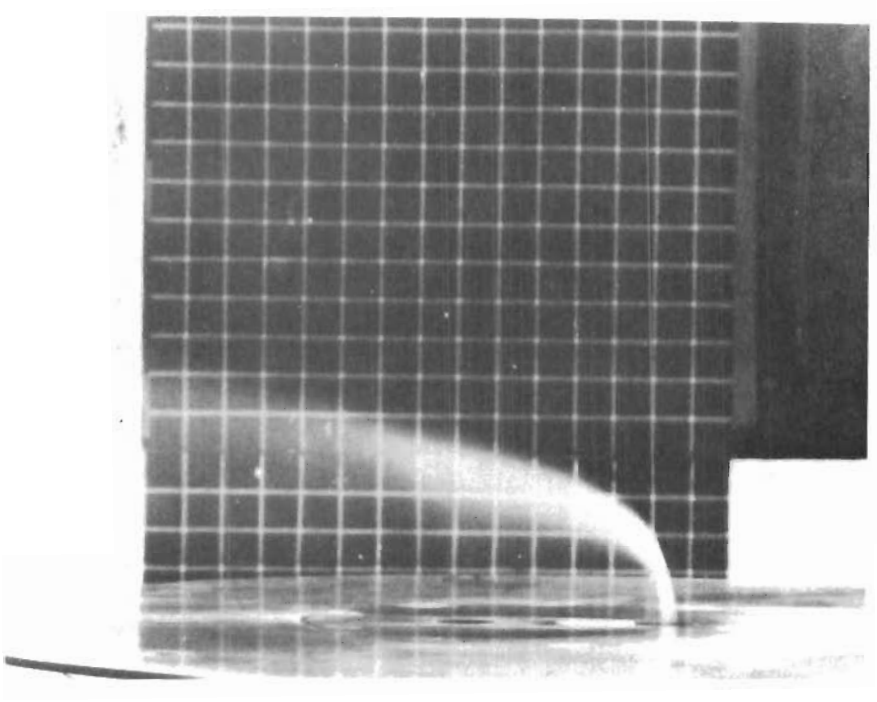

FIGURE 32(a). JET PATH FOR JETS 1, 3 AT $U/U_j = .30$
(WATER INJECTED INTO JET 1)

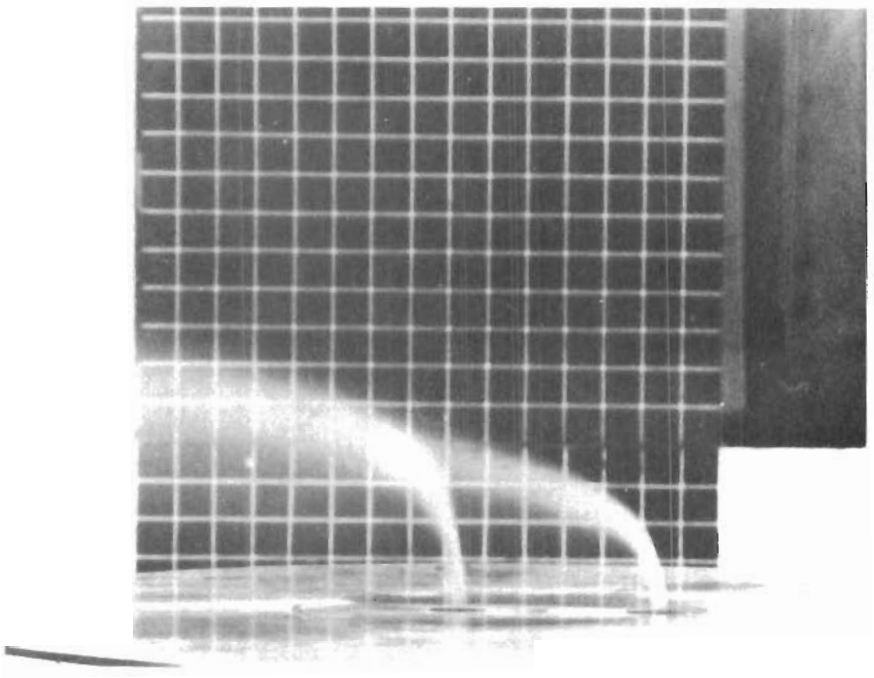

FIGURE 32(b). JET PATH FOR JETS 1, 3 AT $U/U_j = .30$
(WATER INJECTED INTO BOTH JETS)

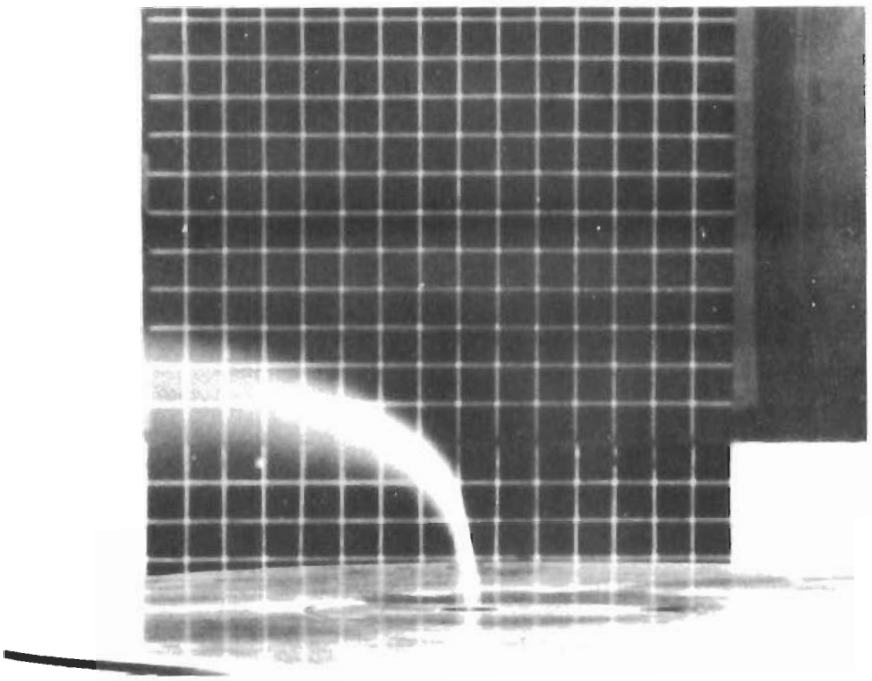

FIGURE 32(c). JET PATH FOR JETS 1, 3 AT $U/U_j = .30$
(WATER INJECTED INTO JET 3)

UNCLASSIFIED

Security Classification

DOCUMENT CONTROL DATA - R & D

(Security classification of title, body of abstract and indexing annotation must be entered when the overall report is classified)

1. ORIGINATING ACTIVITY (Corporate author)	2a. REPORT SECURITY CLASSIFICATION
Northrop Corporation Hawthorne, California 90250	UNCLASSIFIED
	2b. GROUP

3. REPORT TITLE

A Wind Tunnel Investigation of Jets Exhausting into a Crossflow -- Volume I

4. DESCRIPTIVE NOTES (Type of report and inclusive dates)

Data Report

5. AUTHOR(S) (First name, middle initial, last name)

Lynn B. Fricke
Peter T. Wooler
Henry Ziegler

6. REPORT DATE	7a. TOTAL NO. OF PAGES	7b. NO. OF REFS
November 1970	435	10

8a. CONTRACT OR GRANT NO.	9a. ORIGINATOR'S REPORT NUMBER(S)
F33615-69-C-1602	
b. PROJECT NO. 698BT	
c. Task No. 698BT 01	9b. OTHER REPORT NO(S) (Any other numbers that may be assigned this report)
d.	AFFDL-TR-70-154, Volume I

10. DISTRIBUTION STATEMENT

This document has been approved for public release and sale; its distribution is unlimited.

11. SUPPLEMENTARY NOTES	12. SPONSORING MILITARY ACTIVITY
	Air Force Flight Dynamics Laboratory Wright-Patterson AFB, Ohio 45433

13. ABSTRACT

A low speed wind tunnel test of a four-foot diameter circular plate model with up to three exhausting jets was conducted to determine surface static pressure distributions, jet paths, and jet decay characteristics in the presence of a crossflow. Data were obtained for the one-jet configuration with the jet exiting at a number of angles to the plate and at various velocity ratios and sideslip angles. Two-jet arrangements were tested with the jets exiting normal to the plate for three different spacings between the two jets and at a number of velocity ratios and sideslip angles. Three-jet configuration data were obtained with the jets exiting normal to the plate for a number of velocity ratios and sideslip angles. As a result of this investigation, several conclusions are deduced pertaining to the interaction of multiple jets exhausting into a crossflow.

This report consists of four volumes. The test model, instrumentation, test procedure, and reduction and accuracy of the test data are discussed in this volume. A summary and discussion of the test results are also presented herein. Volumes II, III, and IV contain additional data pertaining to the one-, two-, three-jet configurations, respectively.

DD FORM 1 NOV 65 1473

UNCLASSIFIED

Security Classification

14. KEY WORDS	LINK A		LINK B		LINK C	
	ROLE	WT	ROLE	WT	ROLE	WT
V/STOL Aircraft						
Jet Interference Effects						
Jet Exhaust Flow Fields						